

Electronic Thesis and Dissertation Repository

4-20-2018 10:30 AM

Development and applications of polyglyoxylate self-immolative polymers

Bo Fan

The University of Western Ontario

Supervisor

Gillies, Elizabeth R.

The University of Western Ontario

Graduate Program in Chemical and Biochemical Engineering

A thesis submitted in partial fulfillment of the requirements for the degree in Doctor of Philosophy

© Bo Fan 2018

Follow this and additional works at: <https://ir.lib.uwo.ca/etd>

 Part of the [Polymer and Organic Materials Commons](#)

Recommended Citation

Fan, Bo, "Development and applications of polyglyoxylate self-immolative polymers" (2018). *Electronic Thesis and Dissertation Repository*. 5293.

<https://ir.lib.uwo.ca/etd/5293>

This Dissertation/Thesis is brought to you for free and open access by Scholarship@Western. It has been accepted for inclusion in Electronic Thesis and Dissertation Repository by an authorized administrator of Scholarship@Western. For more information, please contact wlsadmin@uwo.ca.

Abstract

Self-immolative polymers (SIPs) are relatively recent class of stimuli-responsive and degradable polymers that have attracted significant attention in the past several years. SIPs consist of polymer backbones and stimuli-responsive end-caps at one or both polymer termini. Upon detection of a stimulus, the decomposition of the end-cap leads to complete end-to-end depolymerization. Polyglyoxylates were introduced as a new class of polyacetal based SIPs by our group in 2014. Compared with other SIPs, polyglyoxylates have two advantages including: 1) readily available monomers and 2) low toxicity depolymerization products. These advantages may allow polyglyoxylates to be used in a wide range of applications. This thesis explored the design, synthesis, and study of a series of responsive end-caps for different potential applications of polyglyoxylates. First, using the previously developed 6-nitroveratryl carbonate end-capped poly(ethyl glyoxylate) (PEtG) that responded to UV light, it was demonstrated that PEtG could depolymerize back to volatile monomer at ambient temperature and pressure. This unusual feature was used to perform a facile polymer reprogramming/recycling sequence as well as polymer patterning by a simple irradiation-evaporation sequence. Moreover, end-caps that allowed polyglyoxylates to respond to oxidizing and reducing conditions, acid, heat, multiple stimuli, and one that enabled cross-linking and UV-triggered depolymerization, were developed. Furthermore, linker end-caps were developed to conjugate PEtG with poly(ethylene glycol) to form amphiphilic block copolymers. These copolymers were self-assembled to form nanoparticles that could load and release payload molecules in response to stimuli. In addition, the hydrophobicity of PEtG was tuned by copolymerization with hydrophobic monomers to improve the nanoparticle drug loading capabilities. Lastly, triphenylmethyl end-capped PEtGs were demonstrated to undergo temperature-dependent depolymerization. Proof-of-concept studies were performed to demonstrate the potential of these polymers for smart packaging applications. Overall, the work presented in this thesis serves to expand the utility of polyglyoxylate-based SIPs for various applications through the design and synthesis of responsive end-caps and new polymer backbones.

Keywords

Self-immolative polymer, stimuli-responsive, degradation, depolymerization, polyglyoxylate, poly(ethyl glyoxylate), traceless, photo-lithography, amphiphilic block copolymer, micelle, vesicle, thermal responsive, drug delivery, self-assembly, sensor.

Co-Authorship Statement

The research described in this thesis is a result of contributions from the author as well as coworkers and supervisor Dr. Elizabeth R. Gillies. The detailed contributions for each chapter are as follows:

Chapter 1 and chapter 2 were written by the author and edited by Dr. Gillies.

Chapter 3 describes a project jointly conceived by the author, Dr. Gillies and postdoctoral fellow Dr. John F. Trant. The author conducted most of the depolymerization studies with assistance from Rebecca E. Yardley and Andrew J. Pickering. The photo-patterning study was conducted with assistance from Dr. François Lagugné-Labarhet and the Western Nanofabrication Facility. The manuscript was prepared by the author and was revised with the assistance of Dr. Gillies and Dr. Trant.

Chapter 4 describes work jointly conceived by the author and Dr. Gillies, with additional acid-sensitive end-caps contributed by Dr. Trant. The author conducted most of synthesis (except for the acid-sensitive end-caps), all characterization, and all depolymerization studies. The manuscript was prepared by the author and was revised with the assistance of Dr. Gillies.

Chapter 5 describes work jointly conceived by the author and Dr. Gillies. The author conducted all the experiments. The manuscript was prepared by the author and was revised with the assistance of Dr. Gillies.

Chapter 6 describes work jointly conceived by the author, Dr. Gillies and Dr. Trant. The author conducted most of the synthesis, characterization, and all depolymerization studies. Dr. Trant contributed the synthesis of menthyl glyoxylate, Rebecca Yardley conducted the synthesis of butyl glyoxylate, and Aneta Borecki conducted the cell studies. The manuscript was prepared by the author and was revised with the assistance of Dr. Gillies.

Chapter 7 describes work jointly conceived of by the author, Dr. Trant, Dr. Gillies, and collaborator Dr. Olivier Sandre. Dr. Trant conducted the synthesis of end-caps while the author conducted the synthesis of polymers and all depolymerization studies. The synthesis of iron oxide particles, incorporation of particles into polymer assemblies and magnetic hyperthermia

studies were conducted by Gauvin Hemery, a PhD student of Dr. Sandre. The manuscript was prepared by the author and Gauvin Hemery and was edited by Dr. Gillies and Dr. Sandre.

Chapter 8 describes work jointly conceived of by the author, Dr. Gillies and Dr. Romulo Salazar. The author conducted all synthesis, characterization, and polymer film colour change studies. The polymer film depolymerization studies were conducted by Dr. Salazar. The manuscript was prepared by the author and was revised with the assistance of Dr. Gillies.

Chapter 9 was written by the author and edited by Dr. Gillies.

Acknowledgments

First of all, I would like to give my sincere appreciation to my supervisor Dr. Gillies. I thank her for accepting me as a member of this caring, mutually helping and creative research group. More importantly, I want to acknowledge Dr. Gillies for her guidance and encouragement along the way, without whom this thesis would not be achievable.

My thanks would also go to all the previous and present members of the Gillies group. Thank you all for creating a caring and mutually helping research environment. You leave me with lots of unforgettable memories during the past several years.

I also would like to thank my thesis examiners, Dr. Xu, Dr. Zhang, Dr. Gilroy and Dr. Gu for taking time to read through my thesis. Many thanks to all the faculty and staff in the Department of Chemical and Biochemical Engineering and the Department of Chemistry for their support in my study and research.

Furthermore, I would like to express heartfelt appreciation to my girlfriend-Jing Wan who has been supportive for my all decisions. I also want to thank her for reading through this thesis.

Lastly but not the least, I want to give the deepest thanks to my parents, without the constant love, supporting and encouragement from both of you, nothing will be possible for me.

Thank all the people who helped me along this way!

Table of Contents

Abstract.....	i
Co-Authorship Statement.....	iii
Acknowledgments.....	v
Table of Contents.....	vi
List of Tables.....	x
List of Figures.....	xi
List of Schemes.....	xix
List of Abbreviations.....	xxi
Chapter 1.....	1
1 Introduction.....	1
1.1 Overview.....	1
1.2 Research objectives.....	3
1.3 Thesis outline.....	4
1.4 References.....	6
Chapter 2.....	9
2 Stimuli-responsive polymers (SRPs).....	9
2.1 General non-degradable SRPs.....	10
2.1.1 Light-responsive polymers.....	10
2.1.2 Thermo-responsive polymers.....	14
2.1.3 pH-responsive polymers.....	15
2.1.4 Gas-responsive polymers.....	17
2.2 Stimuli-responsive and degradable polymers.....	19
2.2.1 Acid-degradable polymers.....	20
2.2.2 Redox-degradable polymers.....	21

2.2.3	Photo-degradable polymers	23
2.2.4	Limitations of conventional stimuli-responsive and degradable polymers	24
2.3	Self-immolative polymers.....	25
2.3.1	SIPs depolymerizing via elimination reactions.....	26
2.3.2	SIPs depolymerizing via cyclization reactions	30
2.3.3	SIPs depolymerizing due to low-ceiling temperature.....	34
2.3.4	Applications of SIPs in drug delivery.....	41
2.4	References.....	45
Chapter 3.....		55
3	Photo-controlled depolymerization of stimuli-responsive poly(ethyl glyoxylate): Differentiating features and traceless ambient depolymerization.....	55
3.1	Introduction.....	55
3.2	Experimental section.....	56
3.3	Results and discussion	61
3.4	Conclusions.....	70
3.5	References.....	71
Chapter 4.....		76
4	End-capping strategies for triggering end-to-end depolymerization of polyglyoxylates	76
4.1	Introduction.....	76
4.2	Experimental section.....	78
4.3	Results and discussion	87
4.3.1	Development of redox-responsive PEtG	87
4.3.2	Development of acid-responsive PEtG.....	94
4.3.3	Development of a multi-responsive end-cap	96
4.3.4	Development of a cross-linkable end-cap.....	99

4.3.5	Mechanically triggered depolymerization of PEtG	102
4.4	Conclusions.....	105
4.5	References.....	106
Chapter 5	114
5	Poly(ethyl glyoxylate)-poly(ethylene glycol) nanoparticles: Stimuli-responsive drug release via end-to-end polyglyoxylate depolymerization	114
5.1	Introduction.....	114
5.2	Experimental section.....	116
5.3	Results and discussion	125
5.3.1	Synthesis of stimuli-responsive PEtG-PEG triblock copolymers.....	125
5.3.2	Self-assembly of PEtG-PEG triblock copolymers in aqueous solution..	131
5.3.3	Stimuli-responsive properties of the nanoparticles.....	132
5.3.4	Encapsulation and triggered release of drugs and model drugs.....	139
5.4	Conclusions.....	144
5.5	References.....	145
Chapter 6	151
6	Tuning the hydrophobic core of self-immolative polyglyoxylate assemblies	151
6.1	Introduction.....	151
6.2	Experimental section.....	152
6.3	Results and discussion	161
6.3.1	Polymer synthesis	161
6.3.2	Celecoxib loading and release	169
6.3.3	<i>In vitro</i> toxicity studies	173
6.4	Conclusions.....	174
6.5	References.....	176
Chapter 7	182

7	Thermo-responsive self-immolative nanoassemblies: Direct and indirect triggering	182
7.1	Introduction.....	182
7.2	Experimental section.....	183
7.3	Results and discussion	192
7.4	Conclusions.....	200
7.5	References.....	201
	Chapter 8.....	204
8	Temperature-dependent depolymerization of trityl end-capped poly(ethyl glyoxylate): potential applications in smart packaging.....	204
8.1	Introduction.....	204
8.2	Experimental section.....	206
8.3	Results and discussion.	211
8.4	Conclusions.....	219
8.5	References.....	220
	Chapter 9.....	224
9	Conclusions and future perspectives.....	224
	Appendix 1: Permission to reuse copyrighted material in Chapter 1	228
	Appendix 2: Permission to reuse copyrighted material in Chapter 2 and published chapters	229
	Appendix 3: Supporting information for Chapter 3.....	235
	Appendix 4: Supporting information for Chapter 4.....	245
	Appendix 5: Supporting information for Chapter 5.....	283
	Appendix 6: Supporting information for Chapter 6.....	307
	Appendix 7: Supporting information for Chapter 7.....	331
	Appendix 8: Supporting information for Chapter 8.....	356
	Curriculum Vitae Bo Fan.....	363

List of Tables

Table 4.1 Molar mass and thermal properties of end-capped PEtGs and measured by SEC, TGA, and DSC.....	90
Table 5.1 Properties of PEtG with different linker end-caps and PEG-PEtG-PEG copolymers. These polymers have been previously reported.....	129
Table 5.2 Hydrophilic mass fractions (f) of the block copolymers and corresponding characterization of self-assembled nanoparticles by DLS and CAC measurement. Errors on the measurements correspond to the standard deviations.	131
Table 6.1 SEC and thermal analysis results for the polymers. From SEC; From TGA; From DSC; From previously published work.	163
Table 6.2 Characterization data for the amphiphilic block copolymers and their resulting assemblies. Previously reported; From SEC; Measured at 1 mg/mL of copolymer.....	166
Table 6.3 Characterization data for the block copolymer assemblies. Previously reported.	168
Table 6.4 Size characterization and celecoxib loading data for the block copolymer assemblies containing drug	170

List of Figures

Figure 1.1 Structure of polyglyoxylates and the depolymerization mechanism after end-cap removal. (Reproduced with permission from reference (29). Copyright 2014 American Chemical Society.).....	3
Figure 2.1 Schematic representations of SRPs: a) General non-degradable SRPs that change in physical properties in response to a stimulus; b) SRPs that can entirely degrade in response to a stimulus stoichiometrically; c) Self-immolative polymers (SIPs) as a sub-class of SRPs that can depolymerize in response to a stimulus in an amplified manner.	9
Figure 2.2 Representative light-responsive molecules applied in stimuli-responsive polymers: a) <i>Cis-trans</i> transformation of aromatic azo compounds, b) hydrophobic spiropyran to hydrophilic merocyanine transformations under different wavelengths of light.....	11
Figure 2.3 a) Synthesis procedure for the azobenzene liquid crystalline polymer network; b) Schematic and c) photographs showing light-driven forward moving of a “vehicle” equipped with a spring-like “motor”. (Reproduced with permission from reference (12). Copyright 2017 WILEY-VCH Verlag GmbH & Co. KGaA, Weinheim.).....	12
Figure 2.4 Photochromic polymersomes exhibiting photo-switchable and reversible bilayer permeability. (Reproduced with permission from reference (14). Copyright 2015 American Chemical Society.).....	13
Figure 2.5 Chemical structures of some typical thermo-responsive polymers.	14
Figure 2.6 a) Temperature dependence of water and oil contact angles for a PMMA- <i>b</i> -PNIPAM film; b) Reversible water and oil contact angle transition of block copolymer film at different temperatures; c) Diagram of reversible formation of intermolecular hydrogen bonding between PNIPAM chains and water below and above the LCST. (Reproduced with permission from reference (23). Copyright 2013 WILEY-VCH Verlag GmbH & Co. KGaA, Weinheim.).....	15
Figure 2.7 Chemical structures of some representative pH-responsive polymers.....	16

Figure 2.8 Structures of a) P2VP-QD and b) PAA-QD; c) Schematic illustration of the conformation and behavior of QD-GO at a given pH value. (Reproduced with permission from reference (24). Copyright 2014 American Chemical Society.).....	17
Figure 2.9 Schematic illustration of: a) Preparation of P(DMAEMA- <i>co</i> -CMA) single-chain nanoparticles through intrachain photo-cross-linking and the gas-switchable size change of nanoparticle in aqueous solution; b) Preparation of tadpole-like PS- <i>b</i> -P(DMAEMA- <i>co</i> -CMA) nanoparticles and their gas-responsive self-assembled micellar assemblies. (Reproduced with permission from reference (35). Copyright 2017 American Chemical Society.).....	19
Figure 2.10 Common acid-degradable functional groups and their degradation products.....	20
Figure 2.11 Polyurethane containing acid-sensitive ketal groups in polymer backbone.....	21
Figure 2.12 Chemical structure of poly(disulfide) with incorporation of paclitaxel via a PEG linker. (Reproduced with permission from reference (48). Copyright 2012 Elsevier Ltd.) ...	22
Figure 2.13 Chemical structure of oxidation-responsive polymer and the particle degradation mechanism in response to H ₂ O ₂ . (Reproduced with permission from reference (52). Copyright 2012 American Chemical Society.).....	23
Figure 2.14 a) Synthesis of a photo-degradable amphiphilic block copolymer containing ortho-nitrobenzyl photolabile groups; b) Schematic illustration of a photo-degradable micelle. (Reproduced with permission from reference (54). Copyright 2011 American Chemical Society.).....	24
Figure 2.15 Synthesis of a poly(benzyl carbamate)-based SIP and its depolymerization mechanism following end-cap removal.....	27
Figure 2.16 Modification of poly(benzyl carbamate) SIP via backbone structures and end-cap design.....	28
Figure 2.17 Chemical structure and depolymerization mechanism of poly(benzyl ether)s, and stimuli-responsive end-caps installed on this category of SIPs.....	30

Figure 2.18 Synthesis of polycarbamate that can depolymerize via a sequence of cyclization, elimination and decarboxylation reactions, and stimuli-responsive end-caps installed on this category of SIPs.	31
Figure 2.19 SIPs that depolymerize via cyclization and elimination reactions: a) Replacement of the carbamate from Figure 2.18 with a carbonate leads to faster depolymerization; b) Replacement of the amine nucleophile in Figure 2.18 with a thiol leads to even faster depolymerization; c) An SIP that depolymerizes entirely through a series of cyclization reactions.	32
Figure 2.20 Depolymerization profile for linear SIPs involving an initial pseudo zero-order domain followed by a gradual transition toward first-order behavior. (Reproduced with permission from reference (60). Copyright 2013 American Chemical Society.)	34
Figure 2.21 General synthesis and depolymerization of polyacetals.	34
Figure 2.22 Synthesis and end-capping of PPA.	35
Figure 2.23 A patterned film that reveals a cylindrical hole when exposed to the corresponding stimulus: a) Patterned plastic film design strategy; b) Photograph of the film before stimulus; c) Photograph of the film after 15 min of exposure to stimulus. (Reproduced with permission from reference (69). Copyright 2010 American Chemical Society.)	36
Figure 2.24 a) Schematic illustration for the preparation of PPA microcapsules by a flow focusing microfluidic technique; b) SEM images of microcapsules before and after exposure to stimulus. (Reproduced with permission from reference (75). Copyright 2013 American Chemical Society.)	38
Figure 2.25 Synthesis and end-capping of PEtG-based SIPs.	41
Figure 2.26 a) Chemical structure of an amphiphilic polycarbamate-b-PEG; b) TEM image of particles formed from this polymer; c) Nile red release from the particles over time as measured by fluorescence spectroscopy. (Reproduced with permission from reference (72). Copyright 2009 American Chemical Society.)	42

Figure 2.27 Synthesis of diblock copolymers containing self-immolative blocks with light- and reduction-responsive linkers and their self-assembly into vesicles. (Reproduced with permission from reference (70). Copyright 2014 American Chemical Society.)	43
Figure 2.28 Chemical structure of an amphiphilic PEG-PEtG-PEG triblock copolymer; b) TEM image of micelles formed from this polymer; c) Micelle disintegration study as measured by ¹ H NMR in response to UV irradiation. (Reproduced with permission from reference (62). Copyright 2014 American Chemical Society.)	44
Figure 3.1 Mass loss profiles for UV light irradiated (I) and non-irradiated (N-I) PEtG-NVOC coatings under different conditions: a) 150 μm thickness immersed at 20 °C in buffers of pH 3-8; b) 150 μm thickness immersed at varying temperatures in pH 7.0 buffer; c) Varying film thicknesses from 25-150 μm immersed in pH 7.0 buffer at 20 °C; d) 150 μm thickness immersed in soil with either 10, 20 or 30 mass % of pH 7.0 buffer at 20 °C; e) Film thicknesses of 50 or 150 μm in air (no aqueous immersion) at either 20 or 30 °C; f) Film thicknesses of 50 or 150 μm in air either exposed or not exposed to sunlight in a greenhouse. In each experiment, the error bars represent the standard deviation of the measurements for three samples.	63
Figure 3.2 a) Number average molar mass (M _n) of polymer remaining on the coating during the mass loss study, as measured by SEC.; b,c) SEM images of the polymer coating after 5 days of immersion in 0.1 M, pH 7.0 phosphate buffer at 20 °C b) control without UV irradiation and c) with UV irradiation.	65
Figure 3.3 Collection of depolymerized ethyl glyoxylate monomer over time after irradiation of PEtG-NVOC and the corresponding experimental set-up.	68
Figure 3.4 Digital optical microscopy of ambient self-developed patterns: The metal masks are shown in a) and b) while the corresponding 500 μm and 20 μm reservoirs fabricated from these masks are shown in c) and d) respectively.	70
Figure 4.1 Schematic illustrating the end-cap cleavage and depolymerization process for PEtG.	78
Figure 4.2 Proposed triggering mechanisms for redox-responsive PEtG end-caps.	88

Figure 4.3 a) ^1H NMR spectra of PEtG-boronate in 9:1 $\text{CD}_3\text{CN}:\text{D}_2\text{O}$ before addition of H_2O_2 and at various time points after H_2O_2 addition (spectra are offset to allow the progression over time to be clearly observed); b-d) Percent depolymerization versus time in the presence and absence of stimuli for b) PEtG-boronate with H_2O_2 , c) PEtG-disulfide-a with DTT, and d) PEtG-azobenzene with DTT. In each case, PEtG-control was also exposed to the stimulus to confirm that the cleavage was specific to the end-cap..... 92

Figure 4.4 Percent depolymerization versus time for a) PEtG-MMT and b) PEtG-DMT in the absence and presence of varying concentrations of acetic acid. 96

Figure 4.5 Depolymerization versus time for PEtG-multi following exposure to UV light, H_2O_2 , Zn/acetic acid, and combinations of these stimuli..... 99

Figure 4.6 ^1H NMR spectrum (400 MHz, 9:1 $\text{CD}_3\text{CN}:\text{D}_2\text{O}$) of PEtG-cross-linked a) before and b) after UV irradiation. Note that peaks corresponding to derivatized cross-linker 16 are not visible because assuming a 1:1 ratio of PEtG:16 in the network, there would be >100 EtGH molecules per derivatized 16. 101

Figure 4.7 a-b) SEC traces (RI detection) for a) PEtG-disulfide-a and b) PEtG-disulfide-b following different sonication times; c) Changes in M_n for PEtG-disulfide-a and PEtG-disulfide-b following different sonication times. 104

Figure 5.1 Depolymerization of PEtG to ethyl glyoxylate (EtG), hydration to form ethyl glyoxylate hydrate (EtGH), and hydrolysis to glyoxylic acid (GA) and ethanol. 116

Figure 5.2 Chemical structures of linker end-caps each containing a chloroformate, one or more stimuli-responsive moieties, and a site for conjugation of PEG..... 126

Figure 5.3 TEM images of nanoparticles formed from a) PEtG-disulfide-PEG, b) PEtG-nitrobenzyl-PEG, c) PEtG-boronate-PEG, and d) PEtG-multi-PEG. 132

Figure 5.4 Stimuli-responsive properties of PEtG-disulfide-PEG nanoparticles: a) % Initial count rate versus time (measured by DLS) for nanoparticles exposed to varying concentrations of DTT, b) % Depolymerization versus time for PEtG-disulfide-PEG nanoparticles in 5:1 pH 7.4, phosphate buffered $\text{D}_2\text{O}:\text{DMSO-d}_6$ in the absence and presence

of 10 mM DTT (measured by NMR spectroscopy). c) ¹H NMR spectra (400 MHz) of PEtG-disulfide-PEG nanoparticles in the same solvent. Peaks corresponding to the depolymerization products EtGH and the DTT adduct appear after the addition of 10 mM DTT..... 135

Figure 5.5 %Initial count rate, measured by DLS, versus time for nanoparticles and their corresponding controls with or without stimuli: a) PEtG-nitrobenzyl-PEG nanoparticles with UV light, b) PEtG-boronate-PEG with H₂O₂, c) PEtG-multi-PEG with H₂O₂, UV light, or both. The study was carried out at pH 7.4, except for b) which was also performed at pH 5.0. The temperature was 37 °C. Error bars represent the standard deviation on 3 samples..... 137

Figure 5.6 Change in Nile red fluorescence intensity as an indicator of its release from nanoparticles composed of a) PEtG-disulfide-PEG, b) PEtG-boronate-PEG, and c) PEtG-nitrobenzyl-PEG in the presence and absence of their corresponding stimuli. Error bars correspond to the standard deviation on three samples. 141

Figure 5.7 Release of Dox from PEtG-nitrobenzyl-PEG nanoparticles with and without UV irradiation at a) pH 7.4 and b) pH 5.0. 142

Figure 5.8 Curcumin retention in a) PEtG-disulfide-PEG and b) PEtG-boronate-PEG nanoparticles in the presence and absence of stimuli as well as their corresponding controls. 143

Figure 6.1 Chemical structure of the monomers used in this chapter..... 161

Figure 6.2 TEM images of particles formed from a) PEtBuG-PEG2000; b) PEtBuG-PEG5000; c) PEtMenG-PEG2000; d) PMenG-PEG750; e) PEtGC-PEG2000; f) PEtGC-PEG5000. 168

Figure 6.3 Depolymerization of particles following UV light irradiation (or no light for controls), monitored by DLS based on count rate. 169

Figure 6.4 Release of celecoxib over time for assemblies irradiated with UV light and for the corresponding systems stored in the dark. 172

Figure 6.5 Metabolic activities, measured by MTT assays of a) particles before UV irradiation and b) after UV irradiation.	173
Figure 7.1 ^1H NMR spectra of PEtG-DA-Bn incubated in 9:1 $\text{CD}_3\text{CN}:\text{D}_2\text{O}$ at 75 °C. Spectra are offset to allow the progression over time to be clearly observed.	195
Figure 7.2 a) Depolymerization of polymers in 9:1 $\text{CD}_3\text{CN}:\text{D}_2\text{O}$ monitored by NMR spectroscopy; Assembly degradation in pH 7.4 phosphate buffer monitored by b) DLS count rate changes, c) Nile red fluorescence changes, and d) NMR spectroscopy.	196
Figure 7.3 TEM images of a) PEtG-DA-PEG750 vesicles, b) PEtG-DA-PEG5000 micelles, c) unloaded IONPs, d) IONP-loaded PEtG-DA-PEG5000 micelles.	197
Figure 7.4 Bulk temperature, particle diameter, and count rate measured before, during, and after magnetic hyperthermia using an in situ DLS for 35 mass% IONP-loaded a) PEtG-DA-PEG5000 micelles and b) Micelle-control.	198
Figure 8.1 Structures of trityl end-capped PEtG.	205
Figure 8.2 Chemical structure of PEtG-control.	213
Figure 8.3 Mass loss profiles for end-capped PEtGs at different temperatures: a) PEtG-DMT; b) PEtG-MMT; c) PEtG-AMT; d) PEtG-AT; d) PEtG-control. In each experiment, the error bars represent the standard deviation of the measurements for three samples.	214
Figure 8.4 Variable temperature ^1H NMR spectra of a) PEtG-AMT and b) PEtG-control at different temperatures (15 min per temperature increment unless otherwise indicated). Spectra are offset to allow the progression over time to be clearly observed.	215
Figure 8.5 Mechanism for temperature dependent depolymerization of trityl-capped PEtG.	216
Figure 8.6 a) and b) Color changes of different PEtG coatings containing either a) 0.1 wt% Nile red or b) 0.5 wt% IR-780 incubated at 22 °C for different time periods. The rectangular color patches are computer generated color samples that were sub-sampled from digital pixels to display color changes of the coating. c) and d) UV-Vis spectra of c) PEtG-AMT and	

d) PEtG-control thin films containing 0.1 wt% Nile red before and after incubation at 37 °C for 24 h, the inserted pictures in c) are polymer coatings before and after incubation..... 218

List of Schemes

Scheme 3.1 Chemical structure of PEtG-NVOC and its UV light-initiated depolymerization. This is followed by hydrate formation and hydrolysis of the resulting ethyl glyoxylate in the presence of water.	62
Scheme 4.1 Synthesis of chloroformate end-caps 4 - 6.	89
Scheme 4.2 Synthesis and end-capping of PEtG.	89
Scheme 4.3 Synthesis of multi-responsive end-cap 11.	97
Scheme 4.4 Synthesis of cross-linkable end-cap 15.	100
Scheme 4.5 Cross-linking of PEtG-trialkene and UV light triggered depolymerization of the resulting PEtG-cross-linked.	101
Scheme 5.1 Synthesis of end-cap 3.	127
Scheme 5.2 Synthesis of end-cap 4.	127
Scheme 5.3 Synthesis of end-capped PEtGs.	128
Scheme 5.4 Synthesis of PEG-PEtG-PEG copolymers a) PEtG-disulfide-PEG, b) PEtG-nitro-PEG, c) PEtG-boronate-PEG, and d) PEtG-multi-PEG.	130
Scheme 6.1 Synthesis of polymers: a) PEtBuG; b) PMenG; c) PEtMenG; d) PEtGC.	163
Scheme 6.2 Synthesis of block copolymers via coupling of PEG-N ₃ with a) PEtBuG; b) PMenG; c) PEtMenG; d) PEtGC.	165
Scheme 7.1 Proposed end-cap cleavage and depolymerization mechanism of PEtG end-capped with a DA adduct (PEtG-DA).	183
Scheme 7.2 Synthesis of end-caps 4a and 4b.	193
Scheme 7.3 Synthesis of end-capped PEtG and its block copolymers.	194

Scheme 8.1 Synthesis of new trityl chloride based end-caps with alkynes and zero or one methoxy groups.....	212
Scheme 8.2 Synthesis of PEtG-AT and PEtG-AMT.	213

List of Abbreviations

AIBN	2,2'azobis(2-methylpropionitrile)
ATR	Attenuated total reflectance
Bu	Butyl
BuG	Butyl glyoxylate
Boc	<i>tert</i> -butyloxycarbonyl
BSA	Bovine serum albumin
C	Chloral
CuAAC	Copper-assisted azide-alkyne cycloaddition
CR	Counter rate
CAC	Critical aggregation concentration
Cur	Curcumin
DBTL	Dibutyltin dilaurate
DA	Diels-Alder
DLS	Dynamic light scattering
DSC	Differential scanning calorimetry
DEG	Di(ethylene glycol)
DMEM	Dulbecco's modified eagle medium
Dox	Doxorubicin
DTT	Dithiothreitol
DMAP	4-Dimethylaminopyridine
DMF	<i>N, N'</i> -Dimethylformamide
DMSO	Dimethyl sulfoxide
<i>D</i>	Dispersity
EDC	1-Ethyl-3-(3-dimethylaminopropyl)carbodiimide
EI	Electron impact
ESI	Electrospray mass spectrometer
Et	Ethyl
EtG	Ethyl glyoxylate
EtGH	Ethyl glyoxylate hydrate
FBS	Fetal bovine serum
FT-IR	Fourier transform infrared spectroscopy

FWR	Feed weight ratios
GA	Glyoxylic acid
GO	Graphene oxide
HRMS	High-resolution mass spectrometry
IONPs	Iron oxide nanoparticles
LCST	Lower critical solution temperature
Me	Methyl
MenG	L-menthyl glyoxylate
MFH	Magnetic field hyperthermia
M_n	Number average molecular weight
M_w	Weight average molecular weight
MWCO	Molecular weight cut-off
MSDS	Material safety data sheets
NMDEA	<i>N</i> -methyldiethanolamine
NEt ₃	Triethyl amine
NMR	Nuclear magnetic resonance
NIR	Near-infrared
NVOC	6-Nitroveratryloxycarbonyl
NVOC-Cl	6-Nitroveratryloxycarbonyl chloride
OPA	<i>o</i> -phthalaldehyde
PAA	Poly(acrylic acid)
PBuG	Poly(butyl glyoxylate)
PDI	Polydispersity index
PDMAEMA	Poly(dimethylaminoethyl methacrylate)
PDMA	Poly(<i>N,N'</i> -dimethylacrylamide)
PE	Polyethylene
PEtG	Poly(ethyl glyoxylate)
PEtBuG	Poly[(ethyl glyoxylate)- <i>co</i> -(butyl glyoxylate)]
PEtGC	Poly[(ethyl glyoxylate)- <i>co</i> -chloral]
PEtMenG	Poly[(ethyl glyoxylate)- <i>co</i> -(menthyl glyoxylate)]
PEG	Poly(ethylene glycol)
PG	Poly(glyoxylate)

PIPOZ	Poly(2-isopropyl-2-oxazoline)
PMeG	Poly(methyl glyoxylate)
PMenG	Poly(menthyl glyoxylate)
PMA	Poly(methyl acrylate)
PMMA	Poly(methyl methacrylate)
PNIPAM	Poly(<i>N</i> -isopropylacrylamide)
PPA	Poly(phthalaldehyde)
PS	Polystyrene
PTEGMA	Poly[tri(ethylene glycol) monoethyl ether methacrylate]
P2VP	Poly(2-vinylpyridine)
PVS	Poly(vinyl sulfone)
QDs	Quantum dots
RAFT	Reversible addition-fragmentation chain transfer
ROS	Reactive oxygen species
SANS	Small angle neutron scattering
SEC	Size exclusion chromatography
SEM	Scanning electron microscopy
SIPs	Self-immolative polymers
SRPs	Stimuli-responsive polymers
TBDMS	<i>tert</i> -butyldimethylsilyl
TGA	Thermogravimetric analysis
THF	Tetrahydrofuran
TEM	Transmission electron microscopy
T _o	On-set degradation temperature
T _c	Ceiling temperatures
T _g	Glass transition temperature
T _m	Melting point temperature
UV	Ultraviolet

Chapter 1

1 Introduction

1.1 Overview

Polymers are large molecules composed of many repeating units linked together via covalent bonds. They can be natural, such as polysaccharides, proteins, and nucleic acids, or synthetic, such as polyethylene (PE), polystyrene (PS), and nylon.¹ Their high molar mass provides polymers with properties that are significantly different from small molecules.² In addition, the physical properties of polymers can be tuned significantly to achieve specific functions by changing the chemical structures of the polymer backbones and side groups, as well as their molecular weight, branching, or tacticity.² For example, PE is one of the most commonly encountered plastics in our daily lives. Depending on the molecular weight or chain branching, its physical properties change dramatically. Ultra-high-molecular-weight polyethylene has a yield strength that is comparable with high-strength steels, therefore it can be used in bulletproof vests.³ However, low-density polyethylene, which contains a high degree of branching, is more frequently used in packaging due to its low tensile strength.⁴

Since the first successful commercialization of the thermoplastic polymer-Nylon,⁵ by Wallace Carothers at Dupont's research facility in 1935, polymeric materials have offered great possibilities for the development of human society in the past century. A series of polymeric materials have been successfully commercialized in 1940s-1980s.⁶ However, since the 1990s, a significant amount of research effort has shifted to polymeric materials that can respond to their environmental conditions or external stimuli. These polymers are usually referred to as stimuli-responsive polymers (SRPs) or "smart" polymers.⁷ SRPs can receive external signals and exhibit responses by changing their physical properties, such as shape, color, solubility, and even chemical structure (e.g., cleavage of side groups or polymer backbone). The chemical or physical property changes associated with SRPs endow them with a series of novel applications that cannot be achieved by traditional materials. Up until now, a diverse range of applications have been explored for SRPs,

including biosensors,⁸ smart coatings,⁹ drug delivery vehicles,¹⁰⁻¹² self-healing,¹³ and shape-memory materials.¹⁴ However, conventional SRPs usually need significant amounts of stimuli for a clear response, and one specific polymer backbone can usually respond to only one stimulus.¹⁵ These limitations create a bottleneck for the applications of many current SRPs.

Self-immolative polymers (SIPs), are a new class of SRPs. They consist of a polymer backbone and a stimuli-responsive end-cap at one (or both) polymer termini.¹⁶⁻¹⁷ Once the end-cap detects an external signal, the decomposition of the end-cap leads to complete collapse of the polymer backbone via end-to-end depolymerization. Therefore, compared with traditional stimuli-responsive polymers, SIPs can easily achieve responsiveness to a series of different stimuli via changes in the end-cap rather than completely re-engineering a new polymer backbone. Via this simple strategy, SIPs that respond to light,¹⁸⁻¹⁹ heat,²⁰ pH,²¹ ultrasound,²² oxidizing and reducing conditions,²³ and chemicals²⁴ have been developed. In addition, the response structure of SIPs allows signal amplification, as one equivalent of stimulus can lead to complete polymer depolymerization and the generation of hundreds and even thousands of monomers or depolymerization products. In the past 10 years, SIPs including polycarbamates, polycarbonates, poly(benzyl ether)s, and polyacetals have been reported.^{15, 25-26} However, many of these SIPs produce toxic depolymerization products such as quinone methides²⁷ or *o*-phthalaldehyde,²⁸ which may hinder their use in some applications.

Polyglyoxylates (PGs) were introduced by our group as a new class of polyacetal-based SIPs in 2014 (Figure 1.1).²⁹ PGs can be readily prepared from inexpensive commercially available glyoxylates such as ethyl glyoxylate or from other simple glyoxylates prepared from readily available starting materials such as maleic or fumaric acid via ozonolysis of the corresponding diesters. Following depolymerization, PGs ultimately degrade to the alcohol and glyoxylic acid, a metabolic intermediate in the important glyoxylate cycle.³⁰ This is an anabolic variant of the tricarboxylic acid cycle that occurs in plants, bacteria, protists, and fungi. Glyoxylic acid is also a metabolic byproduct of mammalian biochemical pathways, such as the biosynthesis of amidated peptides.³¹ There is evidence

suggesting that the depolymerization products of poly(ethyl glyoxylate) (PEtG) are well tolerated in the environment by plants and in mammalian models.³² The innocuousness of these depolymerization products position PGs as ideal materials for applications *in vivo* or in the environment.

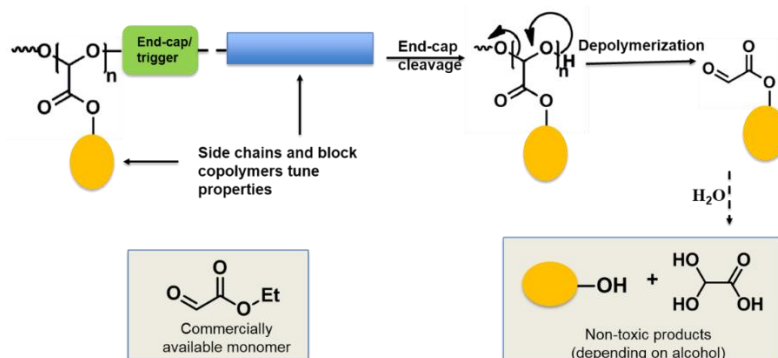


Figure 1.1 Structure of polyglyoxylates and the depolymerization mechanism after end-cap removal. (Reproduced with permission from reference (29). Copyright 2014 American Chemical Society.)

1.2 Research objectives

Our group has previously reported the synthesis of a small number of different alkyl and benzyl polyglyoxylates end-capped with a UV-responsive trigger.²⁹ We also prepared amphiphilic block copolymers of triggerable hydrophobic poly(ethyl glyoxylate) PEtG with hydrophilic poly(ethylene glycol) (PEG) and showed that these materials self-assembled into micelles. Furthermore, when the micelles were exposed to UV light, the hydrophobic block depolymerized, decomposing the micelle.²⁶ This PG-based UV-responsive SIP had a fast depolymerization rate in solution. However, its depolymerization profiles in the solid state under different conditions, such as different pHs, temperatures, coating thicknesses, and even different environmental media, should be explored for practical applications. In addition, the UV-responsive PGs may find application in fields where UV light can be used as a trigger, such as agricultural materials and industrial photolithography. However, for applications such as drug delivery, UV-responsive SIPs may play limited role, due to the detrimental effects of high energy light on human tissue.

Therefore, this thesis aims to expand the applications of polyglyoxylate-based SIPs by increasing the flexibility of the triggering stimuli initiating decomposition by incorporating different end-caps capable of responding to additional environmental cues besides UV light. As an extension of this, the self-assembly of PG-based amphiphilic block copolymers into nano-carriers (such as micelles and vesicles) for on-demand drug release has also been explored.

1.3 Thesis outline

The thesis is divided into 9 chapters. A broad literature review of all classes of SRPs is presented in Chapter 2. Following the review, Chapter 3-8 will describe six projects towards the synthesis, modifications and applications of PG based self-immolative polymers. The projects details are as follows.

Chapter 3 describes the solid-state depolymerization of UV-sensitive PEtG under different conditions. This thesis chapter will explore the effects of different environmental conditions such as pH, temperature, and coating thickness on the depolymerization of PEtG coatings with the aim to fully understand the depolymerization process in the solid state and thus understand potential applications of these materials as coatings.

Chapter 4 includes work aimed at increasing the flexibility of the triggering stimuli initiating decomposition by incorporating different end-caps. New stimuli include biologically relevant signals such as changes in the concentrations of oxidizing or reducing agents. An oxidation-sensitive end-cap incorporating a pinacol borane that cleaves in the presence of hydrogen peroxide and a reduction-sensitive disulfide end-cap that cleaves in the presence of biologically relevant thiols that would be appropriate for targeting the reductive environments of cancer tumors were prepared and studied. Novel multi-responsive end-caps that respond to very different stimuli including combinations of UV light, hydrogen peroxide, and reducing conditions simultaneously will be introduced. Furthermore, a cross-linker end-cap that allows SIPs to form cross-linked networks while at the same time depolymerizing in response to external stimuli, such as UV light will also be developed, further demonstrating the versatility of these materials.

Chapter 5 explores the development and application of PG-based nano-assemblies. New linker end-caps allowed different stimuli-responsive PEtGs to form amphiphilic block copolymers that were capable of self-assembling to form nano-sized particles in aqueous solution. Specifically, based on the multi-responsive PEtGs in Chapter 4, the design, synthesis and self-assembly of H₂O₂, reduction, and dual-responsive (both UV light and H₂O₂) micelles will be described. The signal amplification properties of PEtGs was also explored in this context. Moreover, loading of anti-cancer drugs into PG-based nano-carriers and their release in response to stimuli were examined. This work will expand the applications of PEtG-based SIPs into the biomedical field for the release of drugs and other molecules on demand.

Chapter 6 explores different monomer combinations to increase the hydrophobicity of PG-based particles and thereby improve their hydrophobic drug loading capabilities. Specifically, ethyl glyoxylate was copolymerized with *n*-butyl glyoxylate, choral, and menthol glyoxylate, respectively, and these monomers were also polymerized to form hydrophobic homopolymers. These PGs were further coupled with hydrophilic PEG to form amphiphilic block copolymers. The loading capabilities of the nanoparticles formed from these copolymers were examined by incorporation of the hydrophobic drug-celecoxib.

Chapter 7 introduces the design and synthesis of a new generation of thermo-responsive end-caps based on Diels-Alder adducts that allow SIPs to depolymerize in response to environmental temperature changes. Furthermore, self-assembly and disassembly of thermo-responsive micelles and vesicles formed from these polymers in response to direct and indirect heat were also explored.

Chapter 8: This Chapter explores the temperature dependent depolymerization properties of triphenylmethyl end-capped PEtG films, and their potential applications in smart packaging.

Finally, a general discussion with conclusions outlining the significance, limitations and possible future directions of this research are presented in Chapter 9.

1.4 References

- (1) Gao, Y.; Wei, M.; Li, X.; Xu, W.; Ahiabu, A.; Perdiz, J.; Liu, Z.; Serpe, M. J. Stimuli-responsive polymers: Fundamental considerations and applications. *Macromol. Res.* **2017**, *25*, 513-527.
- (2) Stein, R. S.; Tobolsky, A. V. An investigation of the relationship between polymer structure and mechanical properties: Part I: relationship between structure, mechanical properties, and birefringence. *Text. Res. J.* **1948**, *18*, 201-223.
- (3) Kelly, J. M. Ultra-high molecular weight polyethylene. *J. Macromol. Sci., Polym. Rev.* **2002**, *42*, 355-371.
- (4) Raj, B. Low density polyethylene/starch blend films for food packaging applications. *Adv. Polym. Technol.* **2004**, *23*, 32-45.
- (5) Kauffman, G. B. Wallace Hume Carothers and nylon, the first completely synthetic fiber. *J. Chem. Educ.* **1988**, *65*, 803-808.
- (6) Brandrup, J.; Immergut, E. H.; Grulke, E. A.; Abe, A.; Bloch, D. R., *Polymer Handbook*. Wiley New York etc: **1989**; Vol. 7.
- (7) Stuart, M. A. C.; Huck, W. T.; Genzer, J.; Müller, M.; Ober, C.; Stamm, M.; Sukhorukov, G. B.; Szleifer, I.; Tsukruk, V. V.; Urban, M. Emerging applications of stimuli-responsive polymer materials. *Nat. Mater.* **2010**, *9*, 101-113.
- (8) Hu, J.; Liu, S. Responsive polymers for detection and sensing applications: current status and future developments. *Macromolecules* **2010**, *43*, 8315-8330.
- (9) Nath, N.; Chilkoti, A. Creating “smart” surfaces using stimuli responsive polymers. *Adv. Mater.* **2002**, *14*, 1243-1247.
- (10) Mura, S.; Nicolas, J.; Couvreur, P. Stimuli-responsive nanocarriers for drug delivery. *Nat. Mater.* **2013**, *12*, 991-1003.
- (11) Ganta, S.; Devalapally, H.; Shahiwala, A.; Amiji, M. A review of stimuli-responsive nanocarriers for drug and gene delivery. *J. Controlled Release* **2008**, *126*, 187-204.
- (12) Cabane, E.; Zhang, X.; Langowska, K.; Palivan, C. G.; Meier, W. Stimuli-responsive polymers and their applications in nanomedicine. *Biointerphases* **2012**, *7*:9.
- (13) Habault, D.; Zhang, H.; Zhao, Y. Light-triggered self-healing and shape-memory polymers. *Chem. Soc. Rev.* **2013**, *42*, 7244-7256.

- (14) Meng, H.; Li, G. A review of stimuli-responsive shape memory polymer composites. *Polymer* **2013**, *54*, 2199-2221.
- (15) Fan, B.; Gillies, E. R. Self-Immolative Polymers. *Encycl. Polym. Sci. Technol.* **2015**, 1-35.
- (16) Sagi, A.; Weinstain, R.; Karton, N.; Shabat, D. Self-immolative polymers. *J. Am. Chem. Soc.* **2008**, *130*, 5434-5435.
- (17) Roth, M. E.; Green, O.; Gnaim, S.; Shabat, D. Dendritic, oligomeric, and polymeric self-immolative molecular amplification. *Chem. Rev.* **2015**, *116*, 1309-1352.
- (18) de Gracia Lux, C.; McFearin, C. L.; Joshi-Barr, S.; Sankaranarayanan, J.; Fomina, N.; Almutairi, A. Single UV or Near IR triggering event leads to polymer degradation into small molecules. *ACS Macro Lett.* **2012**, *1*, 922-926.
- (19) Liu, G.; Wang, X.; Hu, J.; Zhang, G.; Liu, S. Self-immolative polymersomes for high-efficiency triggered release and programmed enzymatic reactions. *J. Am. Chem. Soc.* **2014**, *136*, 7492-7497.
- (20) Peterson, G. I.; Church, D. C.; Yakelis, N. A.; Boydston, A. J. 1, 2-oxazine linker as a thermal trigger for self-immolative polymers. *Polymer* **2014**, *55*, 5980-5985.
- (21) Esser-Kahn, A. P.; Sottos, N. R.; White, S. R.; Moore, J. S. Programmable microcapsules from self-immolative polymers. *J. Am. Chem. Soc.* **2010**, *132*, 10266-10268.
- (22) Diesendruck, C. E.; Peterson, G. I.; Kulik, H. J.; Kaitz, J. A.; Mar, B. D.; May, P. A.; White, S. R.; Martínez, T. J.; Boydston, A. J.; Moore, J. S. Mechanically triggered heterolytic unzipping of a low-ceiling-temperature polymer. *Nat. Chem.* **2014**, *6*, 623-628.
- (23) DeWit, M. A.; Beaton, A.; Gillies, E. R. A reduction sensitive cascade biodegradable linear polymer. *J. Polym. Sci., Part A: Polym. Chem.* **2010**, *48*, 3977-3985.
- (24) Zhang, H.; Yeung, K.; Robbins, J. S.; Pavlick, R. A.; Wu, M.; Liu, R.; Sen, A.; Phillips, S. T. Self-powered microscale pumps based on analyte-initiated depolymerization reactions. *Angew. Chem., Int. Ed.* **2012**, *51*, 2400-2404.
- (25) Phillips, S. T.; DiLauro, A. M. Continuous head-to-tail depolymerization: an emerging concept for imparting amplified responses to stimuli-responsive materials. *ACS Macro Lett.* **2014**, *3*, 298-304.

- (26) Fan, B. Polyglyoxylates: a new class of triggerable self-immolative polymers. **2014**. Electronic Thesis and Dissertation Repository. 2568. <https://ir.lib.uwo.ca/etd/2568>.
- (27) Monks, T. J.; Jones, D. C. The metabolism and toxicity of quinones, quinonimines, quinone methides, and quinone-thioethers. *Curr. Drug Metab.* **2002**, *3*, 425-438.
- (28) Peterson, G. I.; Boydston, A. J. Kinetic analysis of mechanochemical chain scission of linear poly (phthalaldehyde). *Macromol. Rapid Commun.* **2014**, *35*, 1611-1614.
- (29) Fan, B.; Trant, J. F.; Wong, A. D.; Gillies, E. R. Polyglyoxylates: a versatile class of triggerable self-immolative polymers from readily accessible monomers. *J. Am. Chem. Soc.* **2014**, *136*, 10116-10123.
- (30) Springsteen, G.; Yerabolu, J. R.; Nelson, J.; Rhea, C. J.; Krishnamurthy, R. Linked cycles of oxidative decarboxylation of glyoxylate as protometabolic analogs of the citric acid cycle. *Nat. Commun.* **2018**, *9*, 91.
- (31) Lorenz, M. C.; Fink, G. R. The glyoxylate cycle is required for fungal virulence. *Nature* **2001**, *412*, 83-86.
- (32) Belloncle, B.; Bunel, C.; Menu-Bouaouiche, L.; Lesouhaitier, O.; Burel, F. Study of the degradation of poly (ethyl glyoxylate): biodegradation, toxicity and ecotoxicity assays. *J. Polym. Environ.* **2012**, *20*, 726-731.

Chapter 2

2 Stimuli-responsive polymers (SRPs)

SRPs are polymers that can detect external signals and respond with changes in physical properties (e.g., shape, color, solubility) or chemical structures (e.g., cleavage of side groups or polymer backbone).¹ The chemical or physical property changes associated with SRPs endow them with a series of novel applications that cannot be achieved by traditional materials.²⁻³ Therefore, SRPs have attracted significant attention from both academia and industry. SRPs can be classified into two main categories according to their physical and chemical property changes. However, depending on their degradability, SRPs can also be separated into 1) general non-degradable SRPs (Figure 2.1a), and 2) stimuli-responsive and degradable polymers (Figure 2.1b, 2.1c).

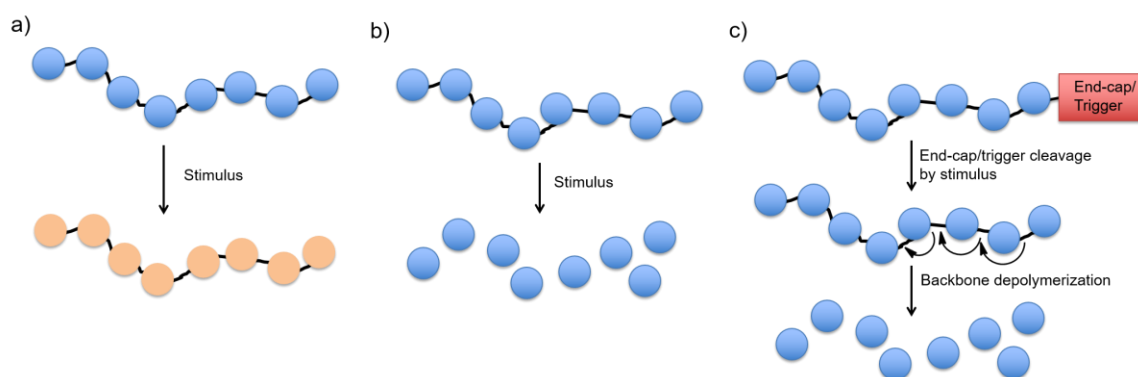


Figure 2.1 Schematic representations of SRPs: a) General non-degradable SRPs that change in physical properties in response to a stimulus; b) SRPs that can entirely degrade in response to a stimulus stoichiometrically; c) Self-immolative polymers (SIPs) as a sub-class of SRPs that can depolymerize in response to a stimulus in an amplified manner.

Over the past decade, stimuli-responsive and degradable polymers have evolved into two different classes. The first class of SRPs can entirely degrade stoichiometrically in response to stimuli (Figure 2.1b). However, a key limitation of these stimuli-responsive and degradable polymers is that multiple stimuli-mediated events are required in order to cause

complete degradation.⁴ In addition, for each different stimulus, a completely new polymer backbone is usually required, which significantly increases the barrier for practical applications. To address the limitations associated with conventional stimuli-responsive and degradable polymers, new efforts have been directed to the amplified degradation of polymeric materials in response to external stimuli in the past 10 years. This new generation of stimuli-responsive and degradable polymers is usually referred as “self-immolative polymers” (SIPs) (Figure 2.1c).⁵

This chapter systematically reviews the development and applications of stimuli-responsive polymers (SRPs) in three main sections: 1) General non-degradable SRPs that undergo changes in physical properties in response to external stimuli; 2) SRPs that can entirely degrade stoichiometrically in response to stimuli; 3) Self-immolative polymers (SIPs) as a sub-class of SRPs that can depolymerize in response to stimuli in an amplified manner.

2.1 General non-degradable SRPs

The general non-degradable SRPs are polymers that can detect external stimuli and respond in form of changes in physical properties such as shape, solubility, or color. The triggering stimuli can be light, heat, specific chemicals or gases, or changes in pH, depending on the responsive sites on polymer structures. Each stimulus has its own advantages and can usually meet the demand for a specific application. For example, light can be applied in a situation that does not require external additives and can be controlled spatiotemporally. Heat can be readily applied from outside of polymer environment. Gases are easy to add and remove, especially, in large volume operations and are of great interest in industrial applications. This section reviews four representative non-degradable SRPs that can respond to light, heat, pH changes, and gases.

2.1.1 Light-responsive polymers

Light has been one of the most extensively investigated stimuli for controlling polymer properties and functions.⁶⁻⁸ It can be easily applied and regulated remotely and possesses advantages such as spatiotemporal precision, wavelength tunability, and does not require

external additives. Reversible light-controllable polymers have been heavily investigated since the 1980s, and the potential applications of these polymers in optical-to-mechanical conversion actuators and polymer nanoparticles for drug delivery have been explored.

In 1980, by incorporating aromatic azo chromophores as cross-linkers for rubbery poly(ethyl acrylate), Eisenbach and coworkers demonstrated that the rubbery network could contract and extend when it was irradiated with different wavelengths of light.⁹ This photomechanical effect was believed to be caused by the conformational change resulting from the *trans-cis* isomerization of the aromatic azo cross-linker. At the same time, Riordan's group observed the same effects when they incorporated the aromatic azo functional group into polyamides, specifically, poly(3,3'-zaodibenzoyl-*trans*-2,5-dimethylpiperazine) and poly(4,4'-azodibenzoyl-*trans*-dimethylpiperazine).¹⁰ The photomechanical effect of aromatic azo compounds is an interesting phenomenon as it allows the direct conversion of light into mechanical energy. Now, it has been well established that aromatic azo compounds can undergo *trans-cis* isomerization when irradiated by light with a wavelength of ~330-380 nm, and that this process is completely reversible.¹¹ The *cis* isomer can convert back to the *trans* isomer when the compound is exposed to light with wavelength of ~420 nm, depending on the specific structure (Figure 2.2a)

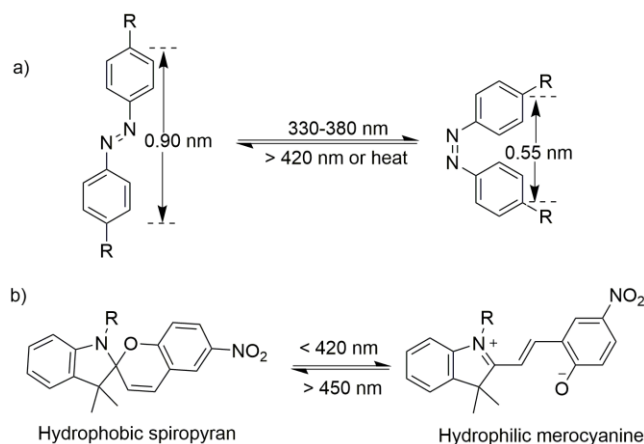


Figure 2.2 Representative light-responsive molecules applied in stimuli-responsive polymers: a) *Cis-trans* transformation of aromatic azo compounds, b) hydrophobic spiropyran to hydrophilic merocyanine transformations under different wavelengths of light.

Following Eisenbach and Riordan's pioneering work, much research was devoted to aromatic azo-containing polymers in order to develop them as light-triggerable actuators. For example, Zhao and coworkers recently reported a light-driven actuator based on an azobenzene-containing liquid crystalline polymer network (Figure 2.3a).¹² In this work, they demonstrated that they could use UV light to generate mechanical force using light to mechanical energy conversion and also light-triggered release of prestored strain energy in a azobenzene-containing liquid crystalline polymer network that was synthesized from 4,4'-diglycidyloxyazobenzene and dodecanedioic acid. They achieved large and tunable photoinduced contractile stress up to 7 MPa, which was much higher than previously reported. Moreover, the azobenzene-containing polymer enabled continuous motions of large rolling objects under irradiation of UV light (Figure 2.3b, c).

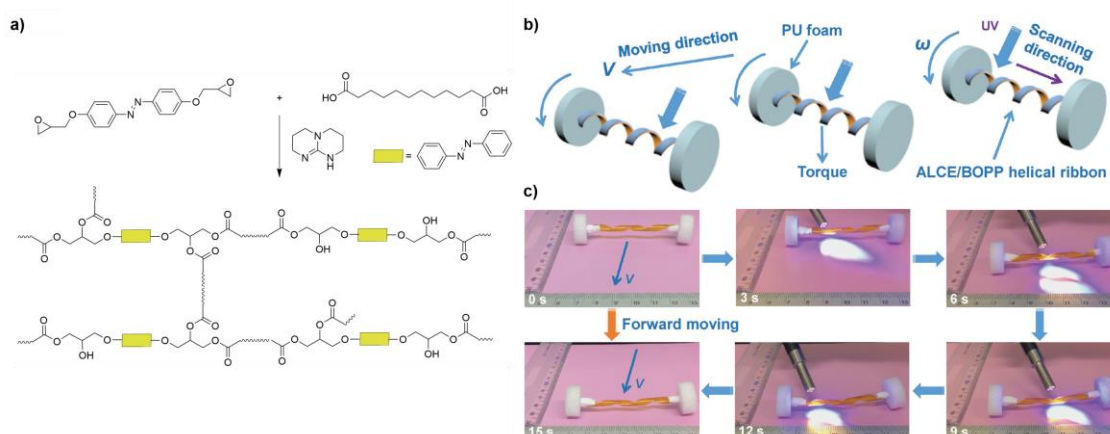


Figure 2.3 a) Synthesis procedure for the azobenzene liquid crystalline polymer network; b) Schematic and c) photographs showing light-driven forward moving of a “vehicle” equipped with a spring-like “motor”. (Reproduced with permission from reference (12). Copyright 2017 WILEY-VCH Verlag GmbH & Co. KGaA, Weinheim.)

In addition to aromatic azo compounds, spiropyran (Figure 2.2b) is another well-known photochromic molecule that has been widely studied in photo-responsive dynamic materials. Spiropyran can respond to light irradiation (wavelength < 420 nm) and undergo reversible isomerization from a colorless hydrophobic spiropyran to a colored hydrophilic merocyanine. This isomerization process can be reversed when merocyanine is irradiated

by light with wavelengths above 450 nm. Recognizing the possible application of this molecule for drug delivery, in 2015 Liu's group reported the fabrication of photochromic vesicles that exhibited reversible changes in bilayer permeability upon triggering by UV-Vis light irradiation (Figure 2.4).¹⁴ The photochromic amphiphilic block copolymer was poly(ethylene glycol)-*b*-PSPA (PEG-*b*-PSPA) diblock copolymer, where SPA was a spiropyran-based monomer containing a carbamate linkage. Upon self-assembly into vesicles, the spiropyran moieties within the vesicle bilayers underwent reversible photo-triggered isomerization between spiropyran and zwitterionic merocyanine states. The microstructures of both vesicles were stabilized by multiple cooperative noncovalent interactions including hydrogen bonding, π - π stacking, and zwitterionic interactions. Interestingly, they found that the UV-actuated merocyanine vesicle possessed both sustained release upon short UV irradiation and on-demand switchable release under alternating UV-Vis light irradiation.

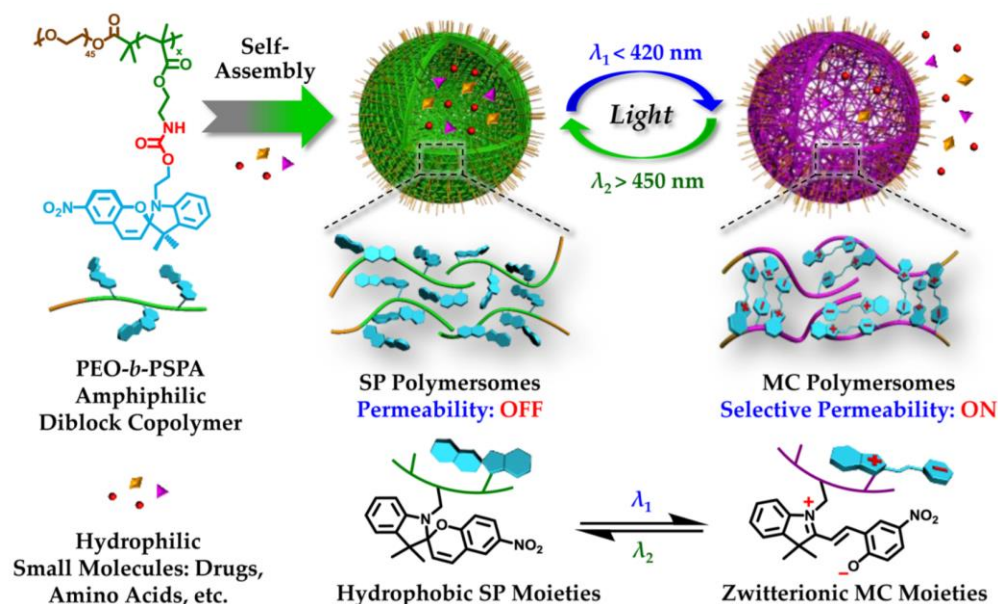


Figure 2.4 Photochromic polymersomes exhibiting photo-switchable and reversible bilayer permeability. (Reproduced with permission from reference (14). Copyright 2015 American Chemical Society.)

2.1.2 Thermo-responsive polymers

Temperature change as a stimulus for polymers has also played a key role among all available stimuli, as it can be readily applied from outside of the polymer environment.¹⁵ In particular, poly(*N*-isopropylacrylamide) (PNIPAM) is one of the most studied thermo-responsive polymers that undergoes a phase transition in solution with temperature changes.¹⁶ Once the temperature is above a certain limit, the polymer chain transforms from a coil state to a globular state to minimize the free energy of the system. This leads to the macroscopic phenomenon of an increase in solution turbidity. This temperature associated phase transition is usually called the lower critical solution temperature (LCST). Besides PNIPAM, there are several other polymers such as, poly[tri(ethylene glycol) monoethyl ether methacrylate] (PTEGMA),¹⁷ poly(dimethylaminoethyl methacrylate) (PDMAEMA),¹⁸ and poly(2-isopropyl-2-oxazoline) (PIPOZ)¹⁹ that have the property of an LCST as well (Figure 2.5). Because of this unique property, thermo-responsive polymers have been widely studied for numerous applications such as drug delivery,²⁰ catalysis,²¹ tissue engineering,²² and surface engineering.²³

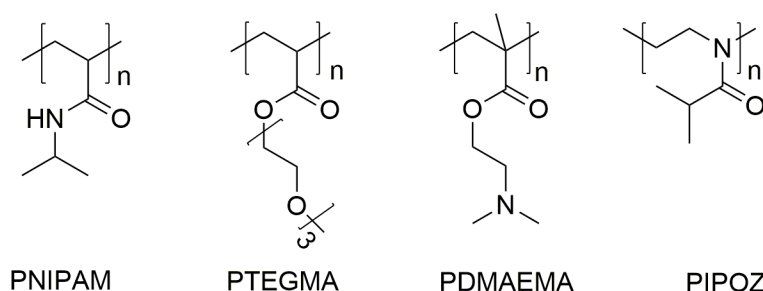


Figure 2.5 Chemical structures of some typical thermo-responsive polymers.

In 2013, Liu and coworkers reported a temperature-controllable dual water/oil on-off switch mesh allowing the separation of water and oil by controlling the temperature.²³ The steel mesh was coated with block copolymer poly(methyl methacrylate) (PMMA)-*b*-PNIPAM. Due to the hydrophilic-hydrophobic transition around the LCST of PNIPAM and the resultant surface roughness change, the mesh could be open to water and closed to oil below the LCST of PNIPAM, or open to oil and closed to water above the LCST (Figure

2.6). This work provided a smart solution to the controllable separation of water and oil mixtures.

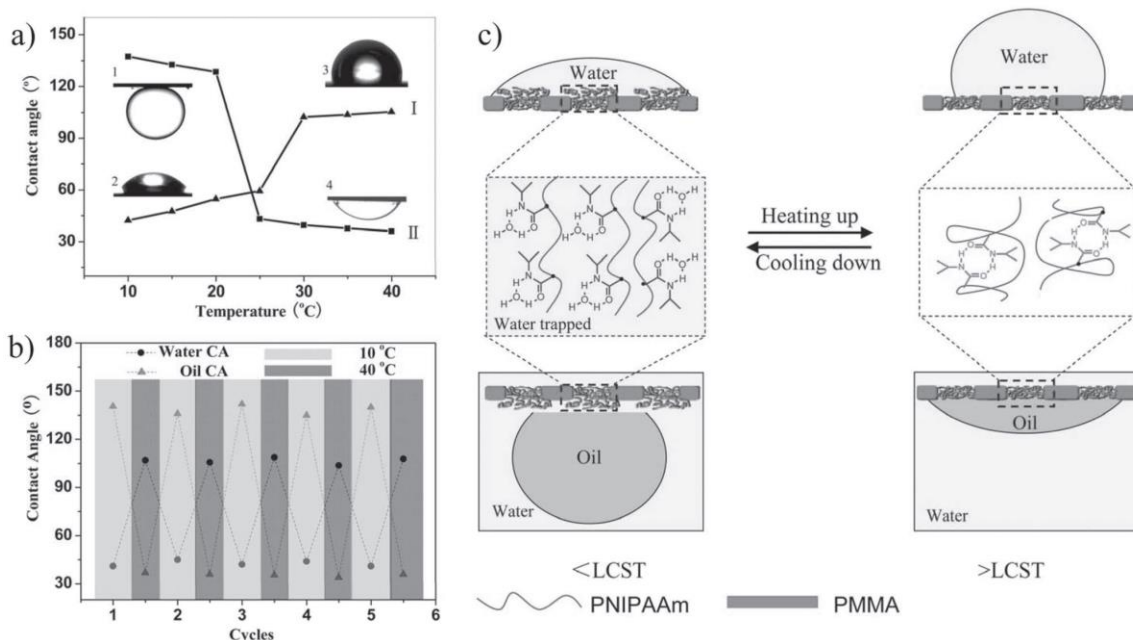


Figure 2.6 a) Temperature dependence of water and oil contact angles for a PMMA-*b*-PNIPAM film; b) Reversible water and oil contact angle transition of block copolymer film at different temperatures; c) Diagram of reversible formation of intermolecular hydrogen bonding between PNIPAM chains and water below and above the LCST. (Reproduced with permission from reference (23). Copyright 2013 WILEY-VCH Verlag GmbH & Co. KGaA, Weinheim.)

2.1.3 pH-responsive polymers

Change in pH is another stimulus that can trigger the change of polymer physical properties. For some organic functional groups, such as organic acids, pyridines, and amines, environmental pH changes lead to the protonation or deprotonation of these functional groups and consequently result in solubility changes of these molecules. Therefore, polymers containing these functional groups also exhibit pH-dependent solubility. Examples of pH-sensitive polymers include poly(acrylic acid) (PAA) ($pK_a = 4.5$), poly(2-

vinylpyridine) (P2VP) ($pK_a = 3.0$), and poly(2-*N,N'*-dimethylaminoethyl methacrylate) (PDMAEMA) ($pK_a = 7.5$) (Figure 2.7).

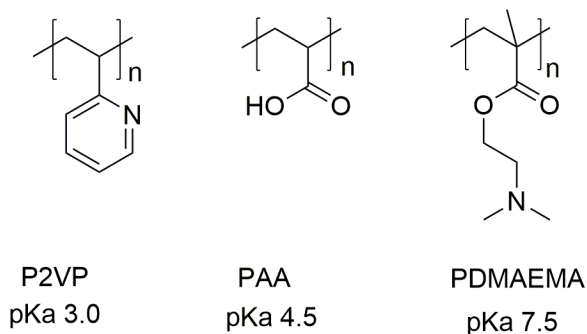


Figure 2.7 Chemical structures of some representative pH-responsive polymers.

Based on the properties of pH-responsive polymers, in 2014 Kim and coworkers reported a versatile platform for a highly stable and wide-range pH sensor that could respond to pH variations from 1 to 7.²⁴ This sensor platform consisted of the pH-responsive polymers PAA and P2VP, and quantum dots (QDs). The PAA chain was grafted onto the surface of blue-colored cadmium sulfide/zinc sulfide QDs, and the P2VP chain was grafted onto the surface of orange-colored cadmium selenide/zinc sulfide QDs. The hybrids were deposited on the surface of single graphene oxide (GO) sheets via π - π stacking interactions between the pyrene functional groups on the polymer termini and the basal plane of the GO surfaces. The distances between the two color-emitting QDs and the GO were controlled by the linker polymers PAA and P2VP. The sensing scheme is shown in Figure 2.8. Specifically, when the pH was lower than 3, the protonation of P2VP led to the swelling and extension of polymer chains, while the PAA chains were protonated and less soluble in water, resulting in their collapse and attachment to the GO. This led to the quenching of blue colored QDs, and consequently the orange colored QDs on P2VP dominated the emission. When the pH was higher than 4.5, the deprotonation of PAA led to the swelling and extension of PAA and the collapse of P2VP, so emission from the blue QDs dominated. When the pH was between these two values, both QDs emitted light and therefore white was observed.

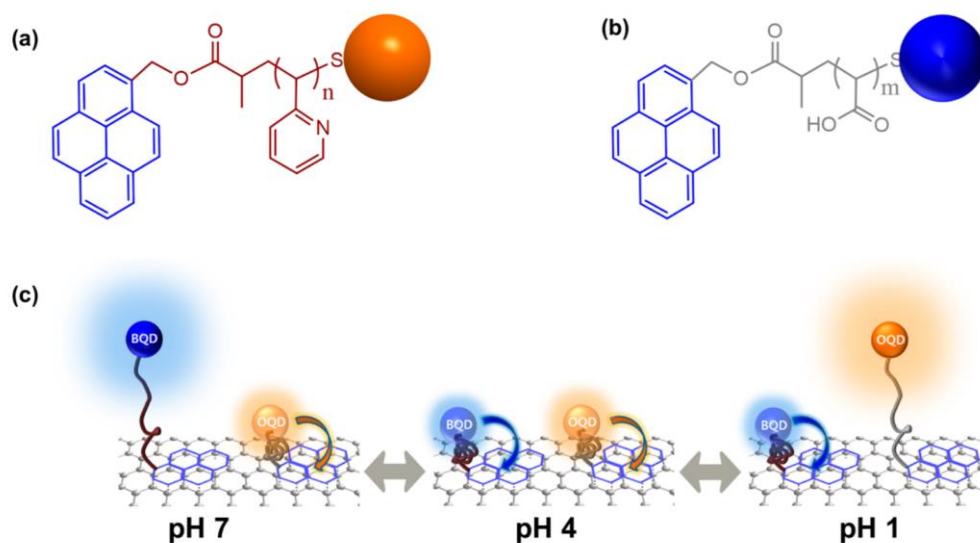


Figure 2.8 Structures of a) P2VP-QD and b) PAA-QD; c) Schematic illustration of the conformation and behavior of QD-GO at a given pH value. (Reproduced with permission from reference (24). Copyright 2014 American Chemical Society.)

In addition to pH sensors, pH-responsive polymers have also been exploited to deliver drugs or genes to specific tissues and trigger the release of payloads at target sites. The basic theory behind this application is that healthy tissues have a pH of 7.4, whereas in inflamed tissues or tumors the environment is slightly acidic. These pH variations can lead to solubility and morphology changes of pH-responsive polymers, enabling the delivery of the payload.²⁵⁻²⁶

2.1.4 Gas-responsive polymers

Gases can be easily added and removed from a system, especially, in large volume operations. Therefore, gaseous triggers are of great interest in industrial applications. Several gaseous triggers have been reported so far including CO₂,²⁷ CO,²⁸ NO,²⁹ and H₂S.³⁰ Numerous applications have been explored for these gas-responsive polymers, such as drug delivery vehicles, cell signaling systems, microgels, and nanoreactors.³¹ As a non-toxic and abundant gas, CO₂ is the most studied gas trigger for gas-responsive polymers. A number of CO₂-reactive functional groups have been explored including tertiary amines, amidines, guanidines, and imidazoles.^{27, 32-33} Of these functional groups, tertiary amine groups such

as those in PDMAEMA (Figure 2.7) are the most frequently explored because the pKa values of polymeric tertiary amines typically range from 6.5 to 8.1.³⁴ The protonation and deprotonation of this class of polymers can readily occur upon the addition or removal of CO₂ through bubbling of CO₂ or an inert gas (nitrogen or argon) respectively, resulting in solubility changes of the polymer.

For example, in 2017 Zhao and coworkers reported CO₂-responsive polymer nanoparticles and micellar aggregates as gas-controlled nanoreactors for gold nanoparticle synthesis with the capability to tune the gold nanoparticle size and formation rate.³⁵ The nanoparticles were prepared from the random copolymer poly{(N,N'-dimethylaminoethyl methacrylate)-*co*-4-methyl-[7-(methacryloyl)oxyl-ethyl-oxyl]coumarin} (P(DMAEMA-*co*-CMA). Tadpole-like single-chain nanoparticles were prepared from an amphiphilic block copolymer of PS-*b*-P(DMAEMA-*co*-CMA). (PS represents polystyrene) (Figure 2.9). Both particles underwent reversible swelling/shrinking with CO₂/N₂ stimulation. In addition, they found the rate of gold nanoparticle formation using these particles as nanoreactors increased under CO₂ stimulation and slowed down by bubbling with N₂. CO₂-induced swelling likely provided easier access of AuCl₄⁻ counterions into the nanoreactors for association with protonated amine groups, and residual non-protonated tertiary amine groups led to AuCl₄⁻ *in-situ* reduction to zerovalent gold. They also demonstrated that the size of the gold nanoparticles could be controlled by the amount of CO₂ in solution *via* the same mechanism.

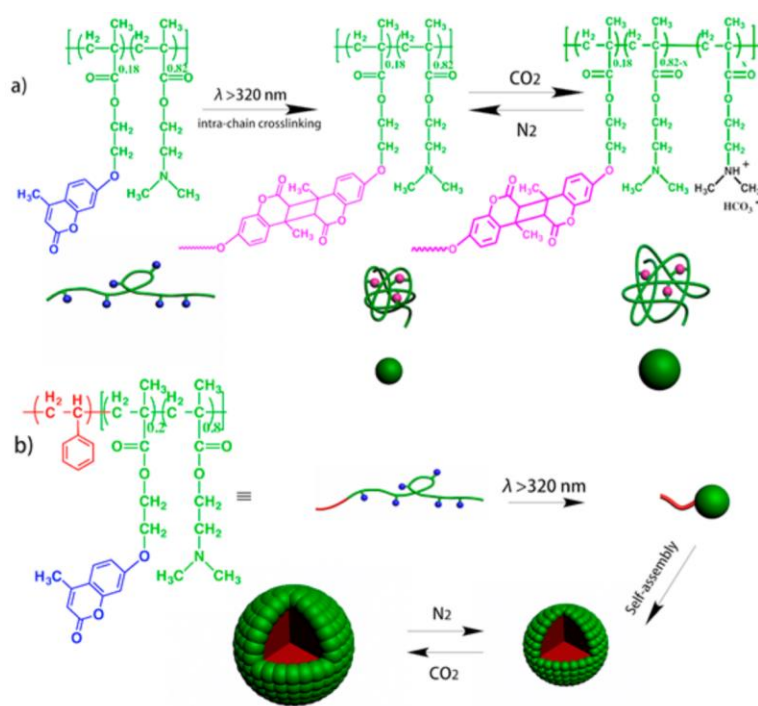


Figure 2.9 Schematic illustration of: a) Preparation of P(DMAEMA-*co*-CMA) single-chain nanoparticles through intrachain photo-cross-linking and the gas-switchable size change of nanoparticle in aqueous solution; b) Preparation of tadpole-like PS-*b*-P(DMAEMA-*co*-CMA) nanoparticles and their gas-responsive self-assembled micellar assemblies. (Reproduced with permission from reference (35). Copyright 2017 American Chemical Society.)

2.2 Stimuli-responsive and degradable polymers

In addition to the physical property changes that occur in non-degradable SRPs as described above, there is another class of SRPs that can undergo complete backbone degradation in response to specific stimuli. In general, there are three major class of stimuli-responsive and degradable polymers including 1) acid-degradable polymers; 2) redox-degradable polymers; 3) photo-degradable polymers. In this section, examples and applications for these three classes of stimuli-responsive and degradable polymers will be described.

2.2.1 Acid-degradable polymers

Acid-responsive and degradable polymers are usually designed with the incorporation of acid-sensitive functional groups such as acetals, ketals, imines, and hydrazones (Figure 2.10).³⁶ Despite the structural diversity of these groups, they all tend to be stable or have slow degradation at neutral pH and are prone to degrade much faster at acidic pH. These acid-responsive and degradable polymers are commonly used to form drug delivery vehicles for the targeted and triggered release of therapeutics, as healthy tissues have a pH around 7.4, whereas inflamed tissues or tumors have mildly acidic pHs ranging from 5.7-7.8. The endosomal and lysosomal compartments of cells also have acidic pHs ranging from 4.5-5.5.^{3,36-37}

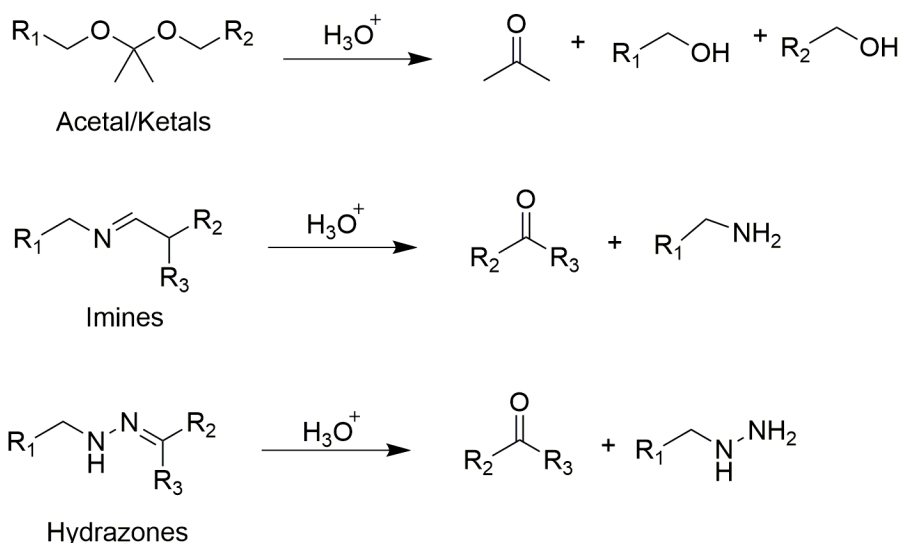


Figure 2.10 Common acid-degradable functional groups and their degradation products.

The degradation of acetals and ketals has been a subject of interest since 1960s,³⁸⁻³⁹ and has attracted significant attention in the past decades, as these moieties yield charge-neutral and potentially non-toxic products upon cleavage.⁴⁰ In addition, the hydrolysis rate is linearly proportional to the H⁺ concentration, ensuring a predictable response to pH changes. Therefore, acetal- and ketal-based polymers have been the most widely studied among all above acid-sensitive polymers. For example, in 2008, Fréchet and coworkers

reported a library of fully acid-degradable polyketals to fabricate microparticles for drug delivery.⁴¹ Specifically, a library of polyurethanes (Figure 2.11) and polyureas containing acid-sensitive dimethyl ketal functional groups incorporated in the polymer backbone were synthesized by reactions of bis(*p*-nitrophenyl carbamate/carbonate) or diisocyanate monomers with ketal-containing diamines via AA-BB type step-growth polymerizations. These polymers could degrade at different rates in acidic conditions to afford small molecules as a function of polymer backbone hydrophobicity. The microparticles formed from these polymers via emulsion techniques degraded significantly faster at an acidic pH of 5.0 than at a physiological pH of 7.4. These acid-sensitive and degradable polymer particles have the potential to find use in the delivery of various therapeutics with the capability to target sites with acidic conditions.

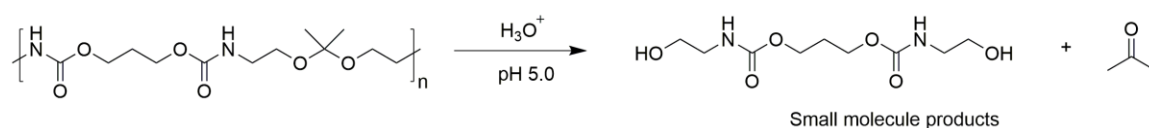


Figure 2.11 Polyurethane containing acid-sensitive ketal groups in polymer backbone.

2.2.2 Redox-degradable polymers

It has been well-established that diseased tissues are usually associated with abnormally high concentrations of redox-active species. For example, cancer cells have high concentrations of reducing glutathione (up to 10 mM)⁴² compared to healthy tissue (1-10 mM), or the extracellular environment (1 μ M).⁴³ Inflammatory tissues produce excessive reactive oxygen species (ROS), including H₂O₂, hydroxyl radicals and singlet oxygen.⁴¹ Therefore, it is attractive to develop polymer systems that can respond to redox changes for targeted drug delivery.

Poly(disulfide)s are a class of polymers with disulfide linkages in their backbones. The disulfide bond is a dynamic covalent bond that can be easily cleaved by reductive stimuli such as dithiothreitol (DTT), or glutathione.⁴⁵ For example, Kim and coworkers developed a paclitaxel-conjugated poly(ethylene glycol) (PEG) and arginine-grafted poly(disulfide amine) (Figure 2.12) micelle.⁴⁸ Because of the disulfide linkages in the polymer backbone,

the micelle could degrade into small molecules in an intracellular environment and release paclitaxel. Moreover, due to the positive charge, the polymeric micelle was also explored for gene delivery with improved gene delivery efficiency.

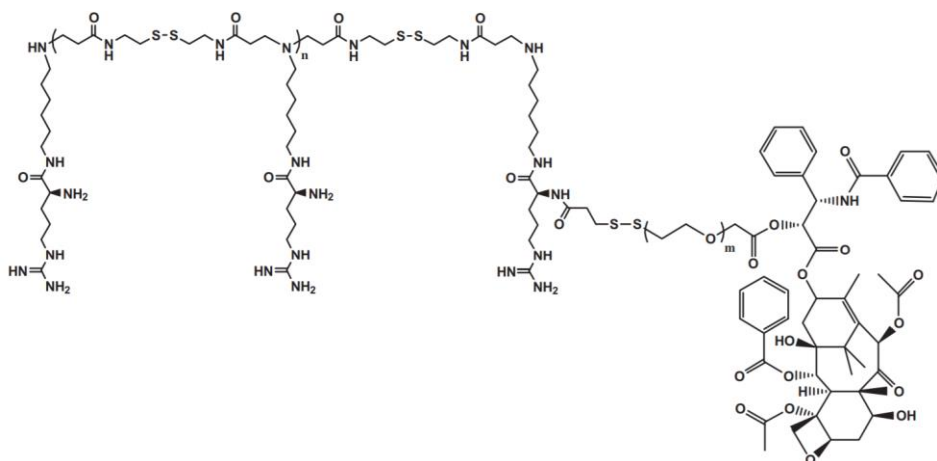


Figure 2.12 Chemical structure of poly(disulfide) with incorporation of paclitaxel via a PEG linker. (Reproduced with permission from reference (48). Copyright 2012 Elsevier Ltd.)

Due to the excessive concentration of ROS associated with diseased tissue, oxidation-responsive polymers have also been developed for targeted drug delivery.⁴⁹ One of the most studied oxidation-responsive polymers is a boronic ester-based system. The responsive moieties are either on the polymer backbone⁵⁰ or incorporated as pendant groups.⁵¹ For example, in 2012 Almutairi and coworkers reported aryl boronic ester-based polymer systems (Figure 2.13) that were capable of undergoing backbone degradation in response to H_2O_2 .⁵² Upon detecting of H_2O_2 , the cleavage of the boronic ester resulted in subsequent 1,6-elimination and 1,4-elimination reactions to break down the polymer backbone. The nanoparticles formulated based on this oxidation-responsive polymer responded to biologically relevant concentration of H_2O_2 (50-100 μM). These particles could potentially be used to deliver small molecules or ROS-quenching enzymes such as catalase and superoxide dismutase to treat chronic inflammatory diseases.

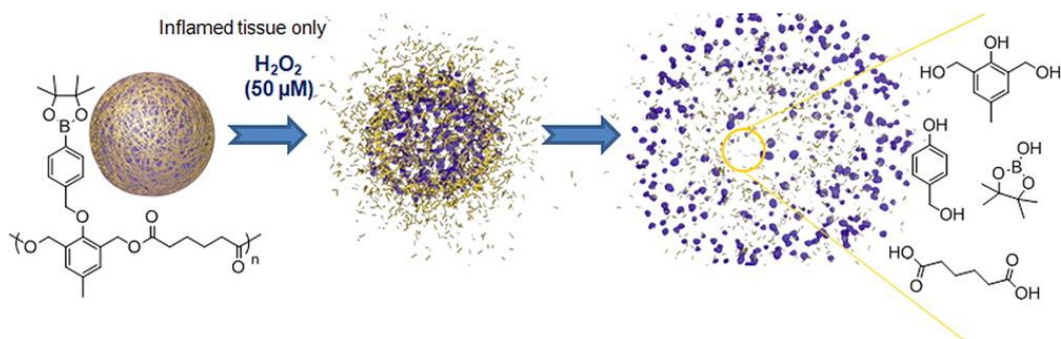


Figure 2.13 Chemical structure of oxidation-responsive polymer and the particle degradation mechanism in response to H_2O_2 . (Reproduced with permission from reference (52). Copyright 2012 American Chemical Society.)

2.2.3 Photo-degradable polymers

The third major class of stimuli-responsive and degradable polymers comprises photo-degradable polymers. As discussed above, light is a stimulus that can be controlled conveniently in both temporal and spatial dimensions. Therefore, photodegradable polymers are also one of the most studied stimuli-responsive and degradable polymers. Photo-degradable polymers are usually designed with incorporation of photolabile groups. Among all the photolabile groups that have been studied, *ortho*-nitrobenzyl alcohol derivatives have gained tremendous attention and have been widely applied in polymeric material design and synthesis.⁵³ For example, in 2011, Zhao and coworkers reported an ABA-style photolabile amphiphilic triblock copolymer, in which B was synthesized by a step-growth reaction between tolylene 2,4-diisocyanate and 2-nitro-1,3-benzenedimethanol.⁵⁴ A represents a hydrophilic block, which was coupled on by directly reacting with PEG monomethyl ether (Figure 2.14). They successfully self-assembled the block copolymer into micelles with diameters of ~60 nm. These micelles underwent fast photoinduced (light wavelength 300 nm) disintegration, triggering the burst release of the hydrophobic payload in aqueous conditions.

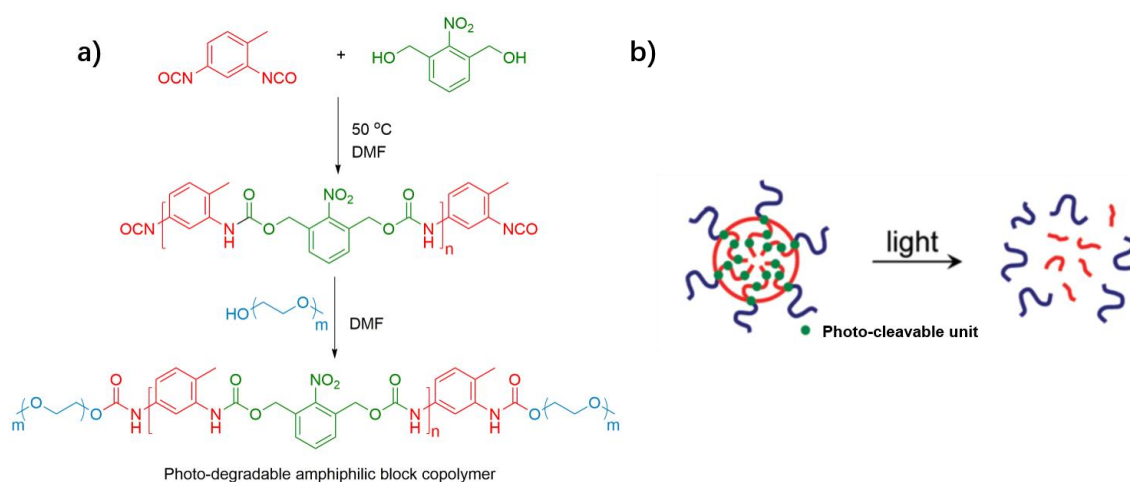


Figure 2.14 a) Synthesis of a photo-degradable amphiphilic block copolymer containing *ortho*-nitrobenzyl photolabile groups; b) Schematic illustration of a photo-degradable micelle. (Reproduced with permission from reference (54). Copyright 2011 American Chemical Society.)

A clear drawback of *ortho*-nitrobenzyl alcohol-based polymer systems is that they can only be degraded under UV light irradiation, which limits their biological applications. Recently, research attention has shifted to biologically benign near-IR light-responsive systems, such as 4-bromo-7-hydroxycoumarin derivatives. However, thus far, these have only been incorporated as pendant groups,⁵⁵⁻⁵⁷ and did not lead to complete polymer degradation. Therefore, detailed examples will not be discussed here.

2.2.4 Limitations of conventional stimuli-responsive and degradable polymers

Stimuli-responsive and degradable polymers degrade completely in response to external stimuli, and circumvent the limitations of conventional non-specifically degradable polyesters. However, a key limitation of these stimuli-responsive and degradable polymers is that multiple stimuli-mediated events are required in order to cause complete degradation. While they perform well in the laboratory, where large changes in the chemical environment or high concentrations of stimuli can be easily achieved, in real applications such as *in vivo*, the gradient of conditions and the stimuli concentrations are usually much

smaller. In addition, for each different stimulus, a completely new polymer backbone is usually required, which significantly increases the barrier for practical applications.

2.3 Self-immolative polymers

To address the limitations associated with conventional stimuli-responsive and degradable polymers, in the past 10 years, new efforts have been directed to the amplified depolymerization of polymeric materials in response to external stimuli. One simple way to achieve this is to install stimuli-responsive molecules on polymer termini. These moieties are usually referred as end-caps. Once the end-cap is cleaved by an external stimulus, a cascade of spontaneous reactions results in polymer backbone depolymerization unit-by-unit in an end-to-end fashion to small molecules (Figure 2.1c). This results in an amplified response as many monomer units can be produced by a single end-cap cleavage. This new class of stimuli-responsive polymers is usually referred as “self-immolative polymers” (SIPs).^{4, 58, 59}

Compared to traditional degradable polymers, the depolymerization rate of SIPs can be easily tuned by adjusting the polymer backbone and the degree of polymerization.⁶⁰ SIPs also afford the advantage that a single polymer backbone can be designed to respond to different external stimuli simply by changing the end-cap rather than requiring a re-engineering of the entire polymer.⁶¹ Thus far, SIPs responsive to light,⁶² heat,⁶³ fluoride ions,⁶⁴ redox change,⁶⁵ enzymes,⁶⁶ and mechanical force⁶⁷ have been reported. This versatility suggests that SIPs are promising polymers for a diverse array of applications including molecular sensors,⁶⁸ responsive films,⁶⁹ micropumps,⁶⁴ responsive drug delivery systems,⁷⁰ and microcapsules⁷¹.

In the past several years, SIPs including polycarbamates,⁶⁸ polycarbonates,⁷² polythiocarbamates,⁷³ polythiocarbonates,⁷³ poly(benzyl ether)s,⁷⁴ and polyacetals^{62, 75} have been reported. Although there are about six different polymer backbones, after end-cap removal the depolymerization of these SIPs mainly occur through three types of processes. The first two types involve sequential spontaneous intramolecular reactions such as an elimination (including polycarbamates, poly(benzyl ether)s) or cyclization

(including polycarbonates, polythiocarbamates, polythiocarbonates) that result in the production of small molecules. The depolymerization of third class of SIPs results from their low ceiling temperatures (T_c), and polyacetals belong to this category. In this section, the design, synthesis and depolymerization mechanisms for each type of SIP will be discussed.

2.3.1 SIPs depolymerizing via elimination reactions

(1) Poly(benzyl carbamate)s

Derived from previous work on self-immolative spacers⁷⁶ and dendrimers,⁷⁷ Shabat and coworkers first reported the design and synthesis of a poly(benzyl carbamate)-based linear SIP in 2008.⁶⁸ Even though several modifications were conducted on benzyl carbamate-based SIPs later, all of the monomers are benzyl alcohols derivatives with caged isocyanate at their *para* positions (Figure 2.15). This caged isocyanate monomer is relatively stable at room temperature, but it can undergo condensation polymerization at high temperature (~100 °C) with dibutyltin dilaurate (DBTL) as a catalyst. Usually, an excess of primary alcohol, which may be a stimuli-responsive molecule, is added with the monomers to cap the polymer terminus. The polymerization degree of this class of SIP can be tuned to some extent via changing of reaction temperature, time, monomer concentration, and the equivalents of the end-cap.

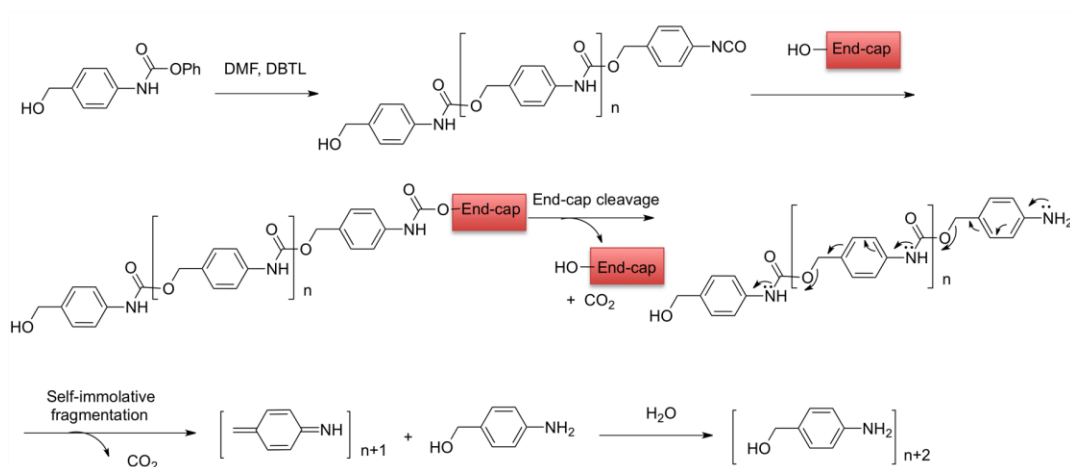


Figure 2.15 Synthesis of a poly(benzyl carbamate)-based SIP and its depolymerization mechanism following end-cap removal.

In Shabat's first example, 4-hydroxy-2-butanone was added to end-cap the polymer.⁶⁸ This served as an enzyme-responsive trigger. When exposed to bovine serum albumin (BSA), the end-cap was removed via β -elimination and led to an unprotected terminal amine. This free amine initiated fast and continuous 1,6-elimination and decarboxylation to decompose the polymer backbone, and simultaneously generated azaquinone methide and carbon dioxide as depolymerization products (Figure 2.15). The released electrophilic azaquinone methide could further react with surrounding nucleophiles, such as water, methanol or even enzymes with nucleophilic groups. Therefore, in 2009 Shabat's group further reported the application of this class of SIPs as active enzyme labeling probes.⁷⁸

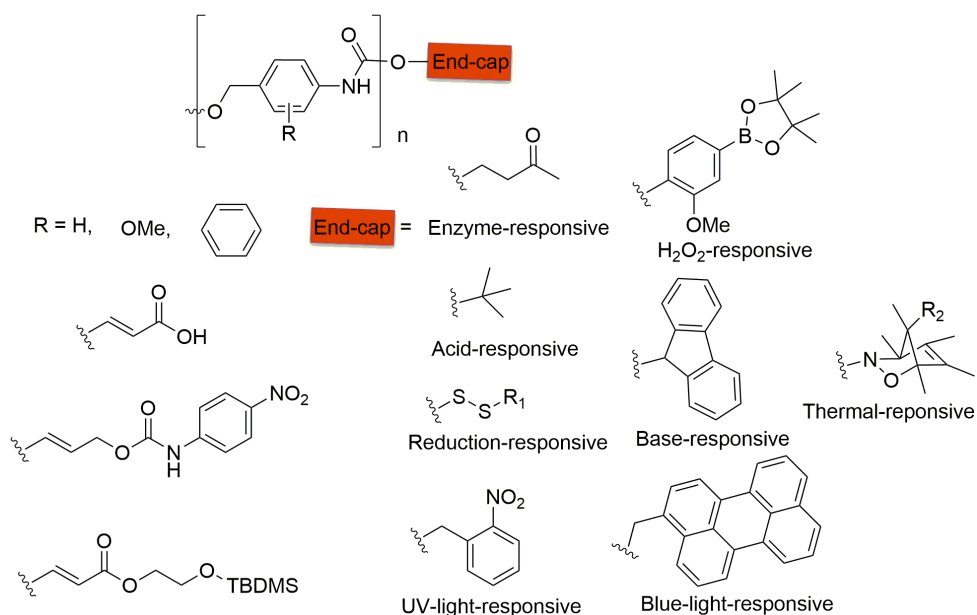


Figure 2.16 Modification of poly(benzyl carbamate) SIP via backbone structures and end-cap design.

In Shabat's subsequent work, monomers with ionized carboxyl group or reporter molecules (4-nitroaniline) on each aromatic building block were designed and synthesized (Figure 2.16).⁷⁹ These monomers endowed the new poly(benzyl carbamate)s with properties such as water solubility, capability to generate reporter molecules upon depolymerization, and also amplified signal to noise ratios for potential sensor applications.

Following the Shabat group's pioneering work, a series of poly(benzyl carbamate)s that could respond to acid, base,⁷¹ H_2O_2 ,⁸⁰ thermal changes,⁶³ redox conditions,⁷⁰ light,⁷⁰ were designed and synthesized with different end-caps (Figure 2.16). These polymers with diverse responsive properties provided proof-of-principle for poly(benzyl carbamate)s in various applications. For example, through the incorporation of *tert*-butyldimethylsilyl (TBDMS) protected hydroxyl group onto the aromatic backbone of this polymer, Moore and coworkers introduced cross-linkable functional groups and used these to prepare cross-linked microcapsules as self-healing components for damaged materials.⁷¹ In 2013 Phillips and coworkers applied poly(benzyl carbamate)s in quantitative time-based assays.⁸⁰ The basic theory behind this application was the quick phase change of the hydrophobic

polymer to hydrophilic depolymerization products due to the cleavage of end-cap upon cleavage by H₂O₂. Following this, they investigated a series of optimization steps for this assay that enabled the measurement of active enzymes⁸¹ and heavy metals (such as, Pb²⁺ and Hg²⁺) in water with a quantitative readout.⁸² Some other applications of poly(benzyl carbamate)s, including self-immolative drug delivery nanoparticles,^{70,83} and self-immolative nanofiber membranes have also been explored.⁸⁴

The depolymerization rate of poly(benzyl carbamate)s based SIPs was found to be greatly limited by the formation of azaquinone methide. This polymer can completely depolymerize into small molecules in polar environment, such as water, in the time scale of hours, but it requires several days or more in a low polarity solvent. To increase the depolymerization rate, Phillips and coworkers investigated the influence of the aromatic character of the benzene ring on the depolymerization rate.⁸⁵ They demonstrated that through the incorporation of electron-donating groups, such as methoxy, on the aromatic ring or reduction of the aromatic character through the use of other ring systems such as naphthalene (Figure 2.16), the depolymerization rate could be greatly enhanced to more than 140 times. This work provided an important guideline on the design of rapidly-degradable SIPs.

(2) Poly(benzyl ether)s

Another SIP that depolymerizes via continuous elimination reactions is the poly(benzyl ether), which was first reported by Phillips and coworkers in 2013 (Figure 2.17).⁷⁴ This polymer was prepared via anionic polymerization, with isopropanol as an initiator and 1-*tert*-butyl-2,2,4,4,4-pentakis (dimethylamino)-2λ⁵,4λ⁵-catenadi-(phosphazene) (P₂-*t*-Bu) as a catalyst at -10 °C for 1 h. Depending on the initiator to monomer ratio, polymerization time, temperature, and purity of the monomer, the molar mass of the final polymer range from 3.6 to 484 kg/mol. After polymerization, they end-capped the polymer with a series of end-caps that were sensitive to fluoride ions, UV light and palladium(0) (Figure 2.17). Similar to poly(benzyl carbamate)s, the depolymerization rate of this polymer depended on the polarity of solvent. For example, after removal of the end-caps, the polymer underwent fast depolymerization in dimethylformamide (DMF) in the time scale of

minutes, but required more than a week in toluene to reach complete depolymerization. So far, poly(benzyl ether)-based SIPs have been explored as on-command debonding adhesives,⁸⁶ depolymerizable and recyclable plastics,⁸⁷ and self-immolative antimicrobial polymers.⁸⁸

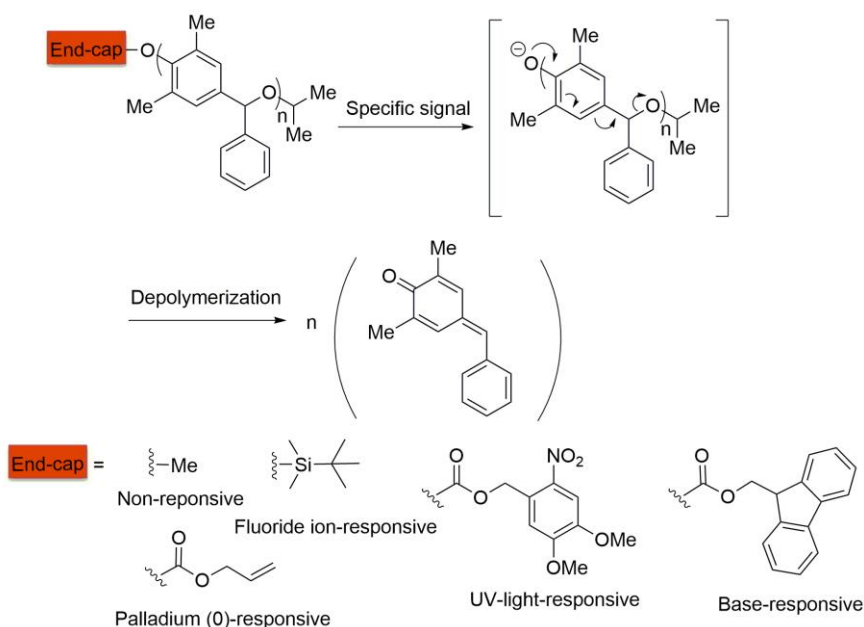


Figure 2.17 Chemical structure and depolymerization mechanism of poly(benzyl ether)s, and stimuli-responsive end-caps installed on this category of SIPs.

2.3.2 SIPs depolymerizing via cyclization reactions

In addition to the poly(benzyl carbamate)-based SIPs, which depolymerize via 1,6-elimination reaction, another important category of SIPs that depolymerizes *via* alternating 1,6-elimination and cyclization reactions was first reported by Gillies and coworkers in 2009.⁷² As it is shown in Figure 2.18, this polymer contained carbamate repeating units in the backbone, and was derived from an activated monomer based on 4-hydroxybenzyl alcohol and *N,N'*-dimethylethylenediamine *via* a condensation-type polymerization. In the presence of base, the activated amine at one end of the monomer reacted with the active carbonate of another monomer to form a carbamate, simultaneously releasing *para*-nitrophenol as byproduct. Triggerable end-caps could be introduced by adding small amounts of monomer protected by a functional group that was sensitive to a stimulus.

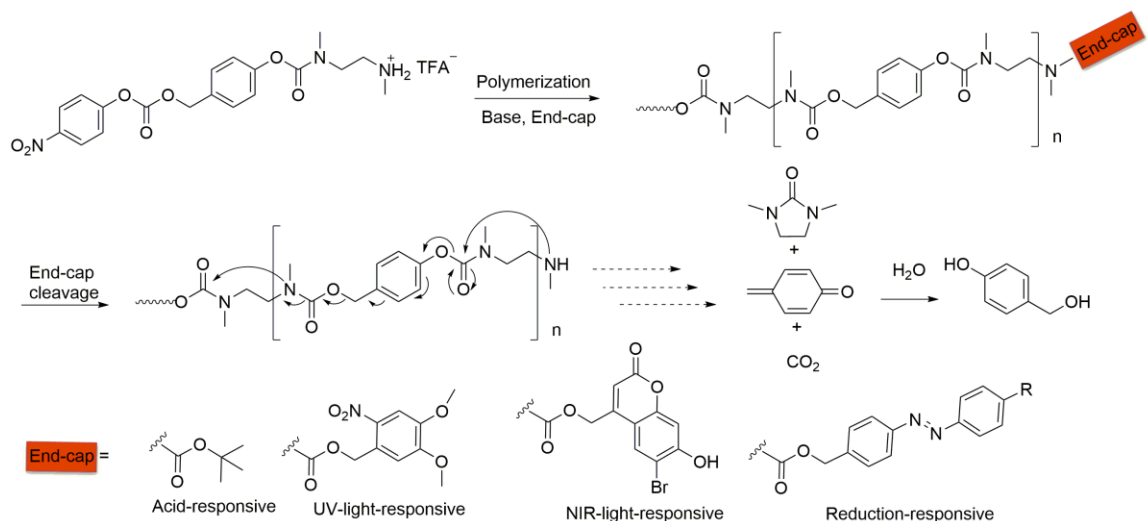


Figure 2.18 Synthesis of polycarbamate that can depolymerize via a sequence of cyclization, elimination and decarboxylation reactions, and stimuli-responsive end-caps installed on this category of SIPs.

In the Gillies group's first example, the *tert*-butyloxycarbonyl (Boc) protected monomer was used as the end-cap, leading to SIP that was sensitive to acid (Figure 2.18). Upon removal of Boc group and incubation in pH 7.4 phosphate buffer:acetone (3:2), the free amine generated at the terminus of polymer could initiate depolymerization by a sequence of cyclization, decarboxylation and 1,6-elimination reactions. Due to the relatively slow rate of cyclization, this backbone required a few days to depolymerize. Other than the acid-responsive end-cap, a series of different end-caps have also been installed on this class of SIPs, including a UV light-responsive *ortho*-nitrobenzyl moiety and a NIR light-responsive 4-bromo-7-hydroxycoumarin by Almutairi and coworkers in 2012,⁸⁹ and a reduction-responsive azobenzene group by Gillies and Wong in 2014.⁹⁰

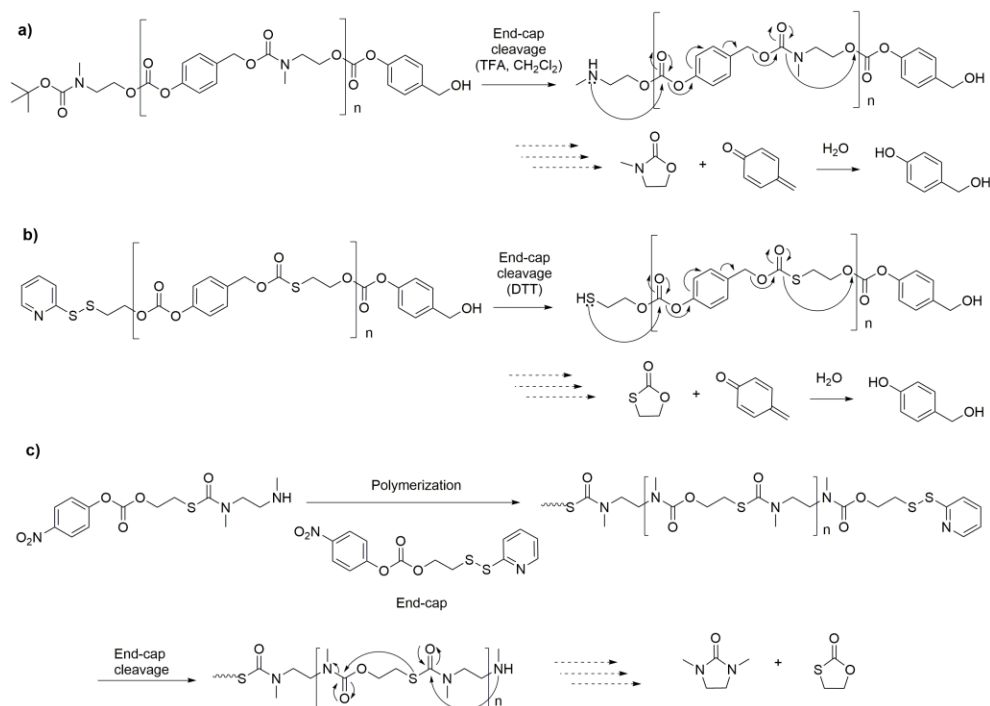


Figure 2.19 SIPs that depolymerize *via* cyclization and elimination reactions: a) Replacement of the carbamate from Figure 2.18 with a carbonate leads to faster depolymerization; b) Replacement of the amine nucleophile in Figure 2.18 with a thiol leads to even faster depolymerization; c) An SIP that depolymerizes entirely through a series of cyclization reactions.

With the purpose of increasing the depolymerization rate of this class of SIPs upon triggering, research has been dedicated to the development of improved self-immolative spacers. For example, Phillips and coworkers have tuned the chemical structures of 1,6-elimination spacers to afford rapid elimination.⁸⁵ Gillies and Dewit developed 4-aminobutyric acid spacers that cyclized in seconds in pH 7.4 buffer.⁹¹ Gillies and coworkers also investigated the incorporation of different cyclization spacers into SIPs.⁷³ As shown in Figure 2.19 a and b, two new polymers were introduced that still depolymerized via alternating cyclization and 1,6-elimination reactions, but in order to increase depolymerization rate, the nucleophilicity or electrophilicity of the reactive sites involving cyclization reactions were altered. Specifically, they replaced one amino group of *N,N'*-dimethylethylenediamine with oxygen to convert the original carbamate backbone

into a carbonate backbone. A carbonate is more electrophilic than a carbamate, so the cyclization reaction was faster and this reduced the depolymerization time from several days to several hours. Furthermore, by replacing another amino group with a thiol to provide a better nucleophile, the cyclization reaction was even faster, and complete depolymerization occurred in 1-2 h.

To eliminate the toxic quinone methide generated during depolymerization of the poly(carbamate)s and poly(carbonate)s described above, Gillies and coworkers developed an SIP derived from *N,N'*-dimethylethylenediamine and 2-mercaptoethanol.⁶⁵ This SIP (Figure 2.19c) depolymerized entirely through intramolecular cyclization reactions, therefore avoiding the generation of quinone methides. In this work, a reduction-sensitive disulfide end-cap, that could potentially be cleaved under physiological conditions was used. As this SIP depolymerized completely *via* cyclization reactions, the depolymerization occurred relatively slowly over a period of about 10-14 days.

In addition to tuning the structures of the SIP backbones, another approach to change the depolymerization time is to tune the polymer chain length. It had been assumed that the depolymerization time of SIPs was proportional to their chain length, due to the requirement for reactions to occur consecutively in an end-to-end manner. However, no conclusive study had been conducted prior to the Gillies group's report in 2013.⁶⁰ Using their previously reported polycarbamate backbone (Figure 2.18), they prepared a series of monodisperse oligomers *via* a convergent synthesis route to study the relationship between chain length and depolymerization time. The results were used to confirm their proposed theoretical model of depolymerization kinetics that involved an initial *pseudo* zero-order domain followed by a first-order domain (Figure 2.20). Moreover, this model was also extended to fit the depolymerization profile of polydisperse polymers.

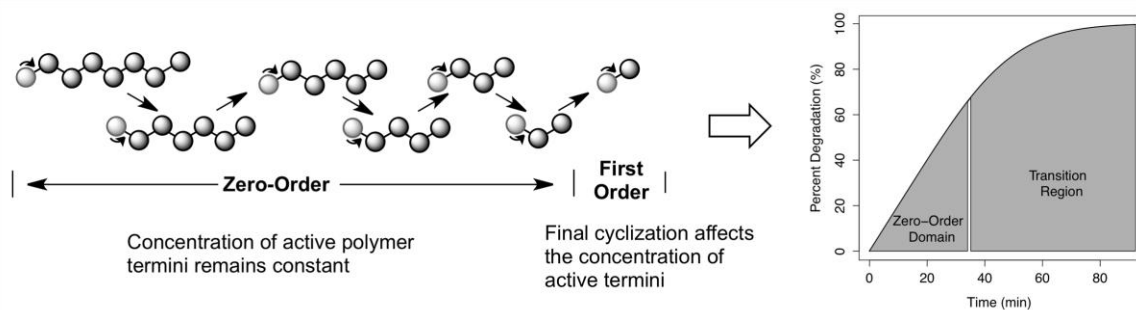


Figure 2.20 Depolymerization profile for linear SIPs involving an initial pseudo zero-order domain followed by a gradual transition toward first-order behavior. (Reproduced with permission from reference (60). Copyright 2013 American Chemical Society.)

2.3.3 SIPs depolymerizing due to low-ceiling temperature

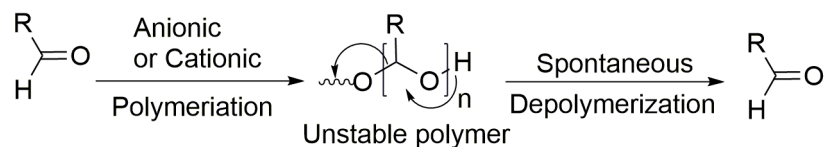


Figure 2.21 General synthesis and depolymerization of polyacetals.

Another important category of SIPs is polyacetals, which includes poly(phthalaldehyde) (PPA) derivatives and poly(glyoxylate) (PG) derivatives. Unlike the previous two categories of SIPs, which depolymerize to products different from the initial monomers from which they are prepared, this class of SIPs depolymerizes back to their original monomers due to their low ceiling temperatures (T_c). T_c , defined as the temperature at which the polymerization rate and depolymerization rate are equal ($\Delta G = 0$; the monomer and polymer are in equilibrium), is a measure of a polymer's tendency to depolymerize to monomers. The T_c s of almost all commercially available polymers are much higher than room temperature, so they can be used as stable materials.⁹² For some polymers, however, the T_c can be much lower. This can occur for polyacetals due to the small negative ΔH for polymerization and an entropic term ($T\Delta S$) that is dependent on temperature (Figure 2.21). For example, polyformaldehyde has a ceiling temperature of ~ 120 °C in its uncapped form,

above which the entropy gained through depolymerization overrides the relatively small enthalpic gain of polymerization.⁹³ However, its T_c can be increased to >200 °C through end-capping. Non-end-capped PPA and PG have ceiling temperatures of approximately -40 °C and 30 °C respectively, and therefore depolymerize spontaneously at room temperature.^{69, 94} However, *via* proper end-capping techniques, the thermal depolymerization temperature can be increased to about 150 °C for both polymers. Therefore, the end-capped polymers can be used as stable materials at room temperature. The synthesis of this type of SIPs occurs by addition polymerization via chain growth.

(1) Poly(phthalaldehyde) (PPA) derivatives

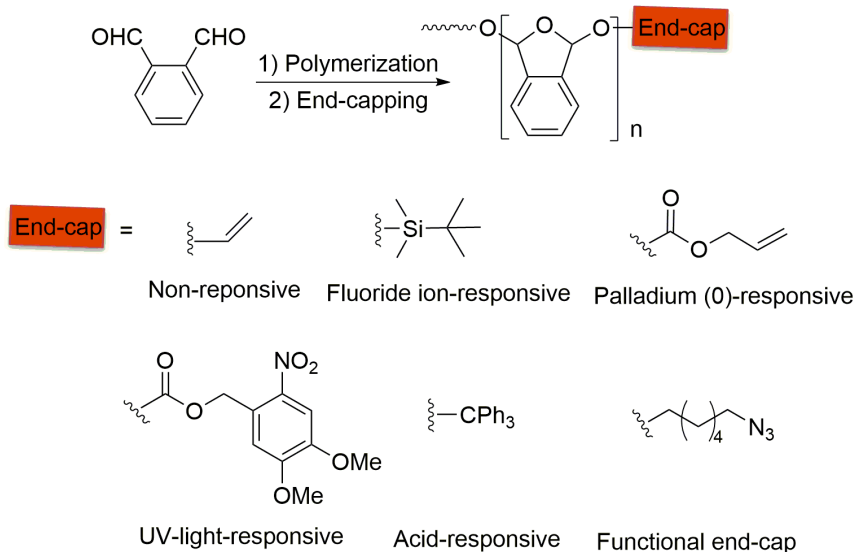


Figure 2.22 Synthesis and end-capping of PPA.

PPA was first synthesized in the 1960s, and was of interest as a potential degradable film for lithography due to its backbone being highly sensitive to acid, radiation and heat.⁹⁵ Its development and application as an SIP began in 2010, when PPA with stimuli-responsive end-caps was introduced.⁶⁹ Polymerization of phthalaldehyde was performed by Phillips and coworkers at -80 °C for about 10 days and the resulting polymer was end-capped with different functional moieties that could respond to specific stimuli. The PPAs they obtained had number average molar masses ranging from 20 kDa to 33 kDa, and dispersities (D) from 1.11 to 1.28. End-capping reactions were performed by reaction with allyl

chloroformate and TBDMS-Cl, which are sensitive to Pd(0) and fluoride ions respectively. After end-capping, the PPAs were stable for at least 15 h, but once the end-caps were removed by stimuli, the polymers completely depolymerized in less than 1 min. Because of the fast depolymerization rate in the solid state, which could not be achieved with previous SIPs, they found that this polymer could be used as a stimuli-responsive plastic for patterning purposes. As shown in Figure 2.23, the PPA end-capped with allyl alcohol was patterned into a square plastic sheet with the central circle filled with TBDMS end-capped PPA. When this plastic sheet was exposed to fluoride ion solution, the TBDMS end-capped area depolymerized immediately to produce a cylindrical hole at the center of plastic.

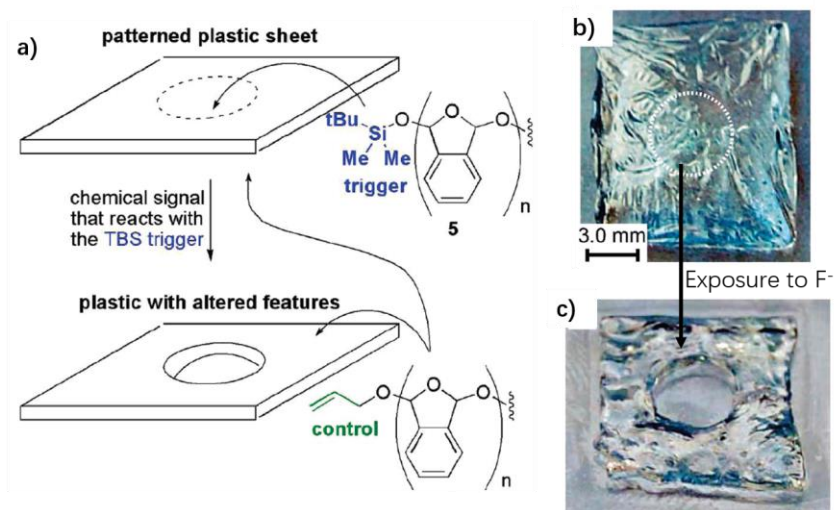


Figure 2.23 A patterned film that reveals a cylindrical hole when exposed to the corresponding stimulus: a) Patterned plastic film design strategy; b) Photograph of the film before stimulus; c) Photograph of the film after 15 min of exposure to stimulus. (Reproduced with permission from reference (69). Copyright 2010 American Chemical Society.)

One limitation for PPA-based SIP was the long polymerization time. However, in 2011, Hedrick and coworkers found that with the addition of the strong base catalyst P_2-t-Bu , the polymerization was decreased to less than 3 h.⁹⁶ Using this approach, in 2013 Phillips and coworkers reported additional end-capping strategies for PPA, which allowed this SIP to

respond to stimuli including UV light and acid.⁶¹ They also reported a functional end-cap having an azide group that allowed for a coupling reaction with another polymer (Figure 2.22). This work made PPA a more accessible and versatile SIP and facilitated subsequent applications.

In their subsequent work, the Phillips group explored the application of PPA in single-use self-powdered microscale pumps that could be turned on by external stimuli.⁶⁴ The core part of the micropump was insoluble PPA end-capped by TBDMS. Upon exposure of this polymer film to fluoride ion solution, the cleavage of the TBDMS end-cap led to fast depolymerization of PPA, which released numerous of monomers into the solution and forced surrounding water to move away due to a diffusio-phoretic mechanism. The pumping speed of this micropump ranged from $0.1\text{--}11\ \mu\text{m s}^{-1}$, depending on the concentration of the analyte. Furthermore, through the incorporation of a β -D-glucuronidase sensitive self-immolative spacer that was capable of releasing fluoride ion, the micropump could be turned on by an enzyme as well.

The amplification effect afforded by SIPs also promoted the exploration of PPA in stimuli-responsive microcapsules. For example, via a flow-focusing microfluidic technique, microcapsules were fabricated by Phillips and coworkers in 2013 using TBDMS end-capped PPA (Figure 2.24).⁷⁵ These microcapsules could selectively release their contents due to the fast depolymerization of PPA upon exposure to fluoride ions. The diameters of the microcapsules were $\sim 150\ \mu\text{m}$, and their release rate could be tuned either by adjusting the thickness of the membrane or the chain length of the polymer. Using the same technique, Moore and coworkers reported the fabrication of PPA microcapsules with diameters $\sim 100\ \mu\text{m}$ that degraded in response to acid environments, as the polymer backbone is highly sensitive to acid.⁹⁷ In addition, in 2017 the Moore group reported another technique called rapid emulsion-solvent evaporation to prepare microcapsules with hydrophobic core materials and PPA shells that allowed high core loading as well as controlled size and morphology.⁹⁸

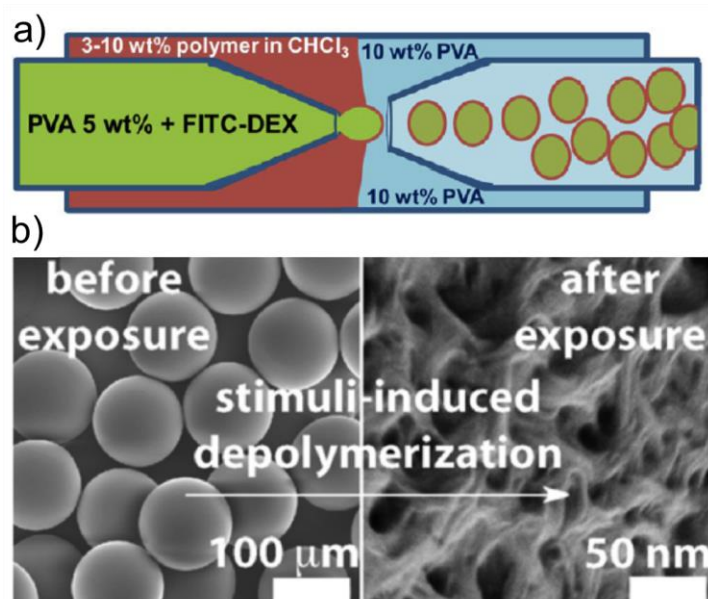


Figure 2.24 a) Schematic illustration for the preparation of PPA microcapsules by a flow focusing microfluidic technique; b) SEM images of microcapsules before and after exposure to stimulus. (Reproduced with permission from reference (75). Copyright 2013 American Chemical Society.)

As described above, PPA is a promising SIP that can quickly depolymerize in response to stimuli both when dissolved in solution and in the solid state. Equally importantly, PPA was the only SIP that could be synthesized from a commercially available monomer. However, the chemical modifications that had been performed on this polymer were limited. One reason for the limited chemical diversity was the acid-sensitivity of the PPA backbone, which made it challenging to work with. However, another important reason was that functionalizable monomers were difficult to access synthetically and not available commercially. In order to address this limitation and further expand the applications of PPA, in 2013 Moore's group explored the copolymerization of phthalaldehyde with substituted benzaldehydes to introduce functional groups for chemical modification of this polymer.⁹⁹ Through a series of copolymerization experiments, they found that benzylaldehydes with Hammett values higher than 0.92 could be incorporated into PPA. In this way, copolymerizations of phthalaldehyde and benzylaldehydes with bromides or extra aldehyde groups on the *meta* position were performed, and a series of further modifications

of the resulting polymers were possible. Moreover, based on this work, the cross-linking of PPA and selective depolymerization of the resulting polymer network were achieved. Meanwhile, with the purpose to improve PPA backbone stability, in 2015 Phillips and coworkers reported another PPA derivative with two electron-withdrawing chloro groups placed *para* to the benzylic acetals-poly(4,5-dichlorophthalaldehyde) (PCl₂PA).¹⁰⁰⁻¹⁰¹ This polymer exhibited the same self-immolative behaviors as PPA, but had improved thermal stability, which enabled selective laser sintering to create macroscopic three-dimensional materials. The mechanistic hypothesis for the improved stability was that the electron-withdrawing groups on the benzylic acetals disfavored the formation of oxocarbenium ion intermediates that were involved in nonspecific degradation. This made PPA more attractive and further expanded its application as a versatile SIP.

In addition to anionic polymerization, cationic polymerization is another possible route for the synthesis of PPA as reported by Ribitsch and coworkers in 2009.¹⁰² In addition, cationic polymerization can produce polymers at a much faster rate, on the time scale of minutes, compared to hours or longer for anionic polymerization. In 2013 Moore's group demonstrated that the cationic polymerization of phthalaldehyde with boron trifluoride as an initiator led to cyclic rather than linear PPA.¹⁰³ Furthermore, they found that this polymerization process showed living character, meaning that the cyclic polymer could open and close its ring reversibly, making it possible to control the ring size. Based on this discovery, they further demonstrated that the mixture of cyclic homopolymers of PPA derivatives could open their rings, depolymerize, and exchange their monomers to form new block copolymers and random copolymers under the cationic polymerization condition.¹⁰⁴ Later, they found that the copolymerization of ethyl glyoxylate with phthalaldehyde could also form cyclic polymers by cationic polymerization.¹⁰⁵ In addition, because of the low glass transition temperature (T_g) of poly(ethyl glyoxylate), the copolymerization could greatly decrease the T_g of copolymers, providing soft rather than brittle materials.

In addition to the PPA stimuli as described above, in 2014 Moore's group found that high molar mass linear or cyclic PPAs could depolymerize to monomers in response to a

mechanochemical signal applied by ultrasound.⁶⁷ Moreover, the resulting monomers could be repolymerized back to polymers under the polymerization conditions to complete the depolymerization-repolymerization cycle. This may have great application in self-healing for damaged materials. However, due to the low-ceiling temperature of PPA, the polymerization process requires a very low temperature, so it cannot be performed at room temperature after mechanical damage of PPA.

(2) Poly(glyoxylate)s (PGs)

PGs such as poly(methyl glyoxylate) (PMeG),⁹⁴ poly(ethyl glyoxylate) (PEtG)¹⁰⁶ and poly(glyoxylic acid) (PGA) are another class of polyacetals with low ceiling temperatures, meaning that they depolymerize at room temperature. To prevent random degradation and obtain stable materials, Bunel and others explored a series of end-capping agents, such as vinyl ethers, anhydrides and isocyanates.^{94, 106} They found that isocyanates afforded polymers that were stable up to 150 °C. In 2014 Gillies and coworkers demonstrated PGs as a new versatile class of SIPs.⁶² Poly(ethyl glyoxylate) (PEtG) with UV-sensitive end-cap (6-nitroveratryl chloroformate) on both termini of the polymer were synthesized. Once the end-caps were removed by UV irradiation, the PEtG depolymerized spontaneously back to monomers in solution. Compared with previous SIPs, there are three advantages for PGs. First, the monomer ethyl glyoxylate is commercially available, facilitating the synthesis and potential scale-up of the polymers for applications. Second, the glyoxylic acid depolymerization product of PEtG is a metabolic intermediate, which means that it should exhibit low toxicity and has potential for biological applications. Furthermore, the ester side group of PEtG can be readily replaced with other alcohols to produce materials with functional groups and different physical properties. In their work, Gillies and coworkers used a UV-sensitive linker molecule (Figure 2.25), to couple the hydrophobic PEtG with hydrophilic PEG to achieve an amphiphilic block copolymer and self-assembled it into micelles. After UV irradiation, the micelles rapidly disintegrated in buffer solution. Moreover, Gillies and coworkers expanded the family of PGs to include poly(butyl glyoxylate), poly(benzyl glyoxylate) and their copolymers, and found all of them showed the properties of SIPs but with different physical properties such as T_g s. This research

therefore expanded the SIP library, and facilitated fast access to SIP materials with different properties.

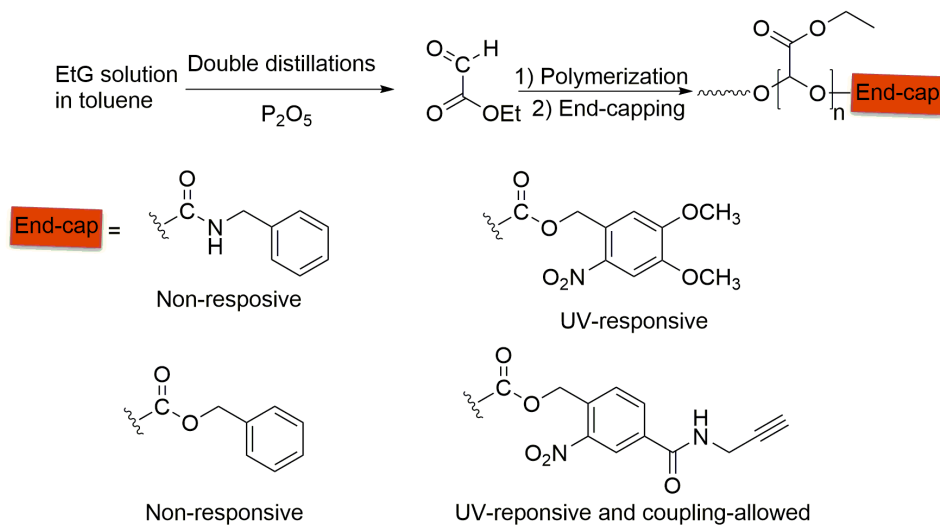


Figure 2.25 Synthesis and end-capping of PETG-based SIPs.

2.3.4 Applications of SIPs in drug delivery

Polymer-based nano-sized drug delivery systems have attracted significant attention in the past 20 years, as they can enhance the water-dispersibility and stability of drugs, especially for hydrophobic drugs.²⁻³ More recently, the introduction of SRPs into drug delivery furthered the field as they have the potential to deliver drug at target sites in response to stimuli, thereby decreasing the toxic effects of the drug on healthy tissue. However, as noted above, a limitation of conventional SRPs is that multiple stimuli-mediated events are required to change the polymer properties or degrade the polymers. While they perform well in the laboratory, where large changes in the environment can be easily induced, they may perform less well in real environments such as *in vivo*, where stimuli are present at lower concentrations and the changes in environment such as pH are more subtle.

Due to the signal amplification effect that results from the depolymerization of SIPs in response to stimuli, they have excellent potential to be applied in the field of drug delivery. In 2009, Gillies and coworkers first explored the formation of nano-sized particles by sonication of amphiphilic polycarbamate-*b*-PEG (Figure 2.26).⁷² Moreover, the

hydrophobic and fluorescent dye Nile red was used as a model drug and incorporated into the particles to study their release properties. However, in this first example the initiation of the self-immolative block depolymerization relied on the random hydrolysis of an ester linkage between the two blocks. In 2012, Almutairi and coworkers introduced UV light and NIR light sensitive molecules, *o*-nitrobenzyl alcohol and bromo-coumarin (Figure 2.18),⁸⁹ as end-caps for the same SIP, and Nile red was also incorporated into the SIP-based nanoparticles formed by emulsification with poly(vinyl alcohol). Upon irradiation with the appropriate wavelength of light, Nile red was released from the particles. These two studies demonstrated the great potential of SIPs as drug delivery vehicles to target the release of drugs in response to external stimuli. However, in both of their cases, no loading and release of real drugs were conducted.

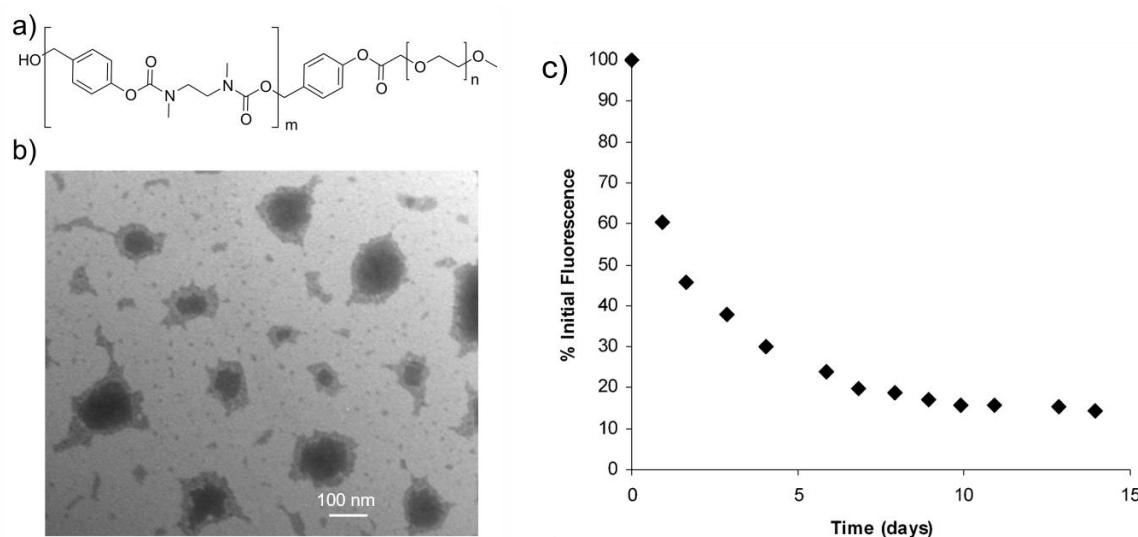


Figure 2.26 a) Chemical structure of an amphiphilic polycarbamate-*b*-PEG; b) TEM image of particles formed from this polymer; c) Nile red release from the particles over time as measured by fluorescence spectroscopy. (Reproduced with permission from reference (72). Copyright 2009 American Chemical Society.)

In addition to micelles, which can only carry hydrophobic molecules, vesicles can also be obtained through block copolymer self-assembly and can encapsulate both hydrophobic and hydrophilic molecules. In 2014, Liu and coworkers reported the formation of vesicles from poly(benzyl carbamate)s, with one polymer terminus incorporating a perylen-3-yl

methanol, 2-nitrobenzyl alcohol, or diethanol disulfide end-cap that was responsive to blue light, UV light, and reduction conditions respectively (Figure 2.27).⁷⁰ The other termini of these polymers were functionalized with a reversible addition-fragmentation chain transfer (RAFT) agent, which could initiate the growth of a hydrophilic block poly(*N,N'*-dimethyl acrylamide) (PDMA) to result in amphiphilic block copolymers with hydrophilic mass fractions of ~60-70 wt%. Vesicles with diameters ranging from 200 nm to 580 nm were obtained via nanoprecipitation, as confirmed by dynamic light scattering (DLS), confocal laser scanning microscopy, transmission electron microscopy (TEM), and scanning electron microscopy (SEM). With proper stimuli corresponding to the end-cap cleavage conditions, these vesicles were successfully disintegrated and released both hydrophilic and hydrophobic molecules. Furthermore, with these different stimuli responsiveness vesicles they constructed OR, AND and XOR logic gate-type programmed enzymatic reactions.

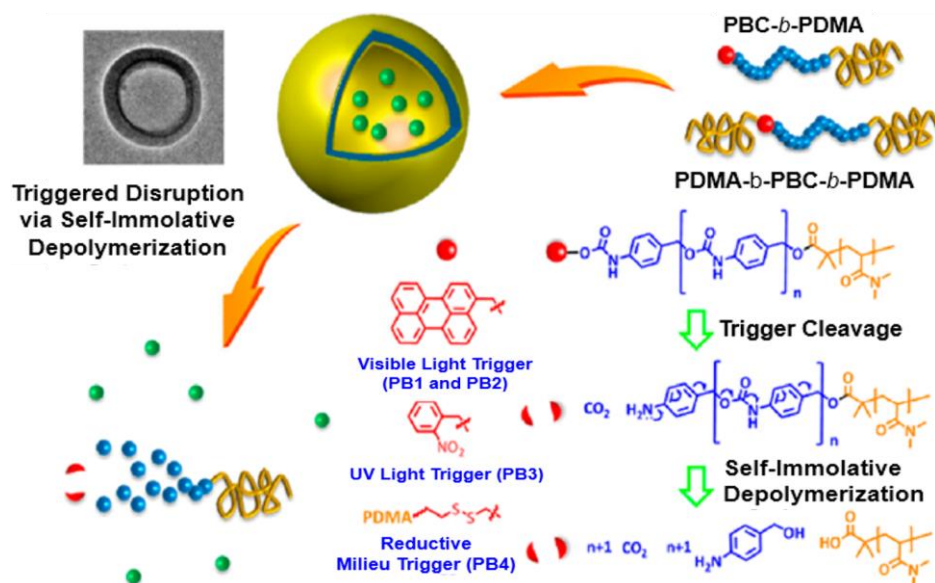


Figure 2.27 Synthesis of diblock copolymers containing self-immolative blocks with light- and reduction-responsive linkers and their self-assembly into vesicles. (Reproduced with permission from reference (70). Copyright 2014 American Chemical Society.)

In the same year, Gillies and coworkers reported the formation of SIP-based micelles from PEG-*b*-PEtG-*b*-PEG amphiphilic triblock copolymer (Figure 2.28).⁶² The micelles had

diameters of ~50 nm and rapidly disintegrated in response to UV light. However, no drug loading or triggerable release studies were conducted at that point.

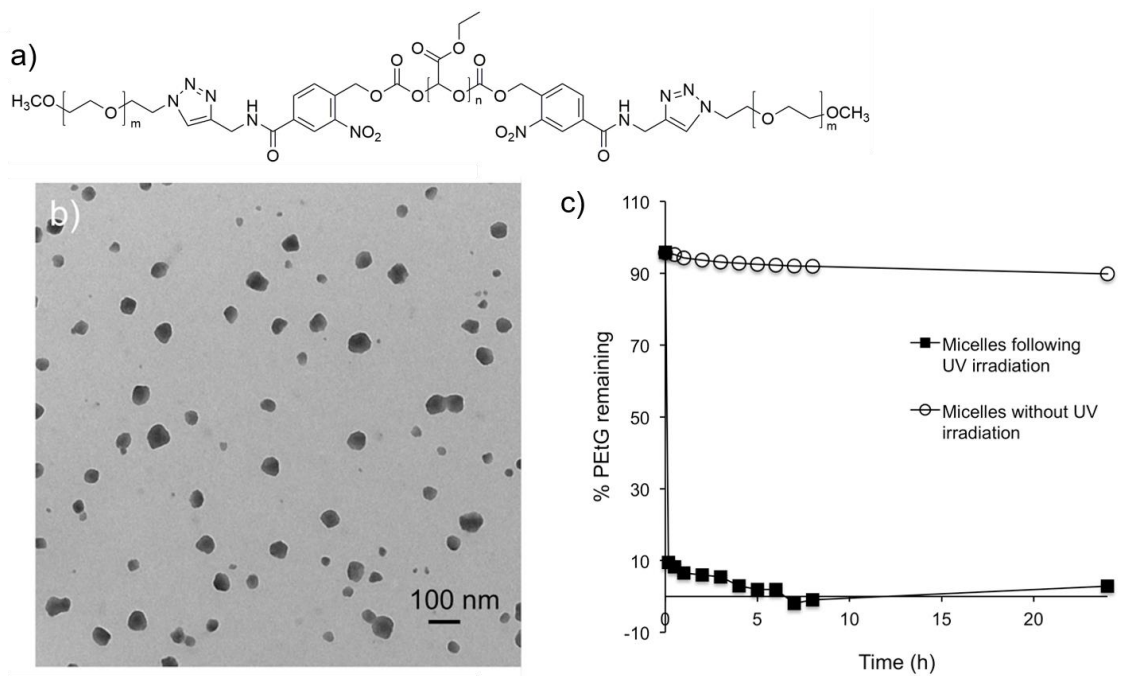


Figure 2.28 Chemical structure of an amphiphilic PEG-PEtG-PEG triblock copolymer; b) TEM image of micelles formed from this polymer; c) Micelle disintegration study as measured by ^1H NMR in response to UV irradiation. (Reproduced with permission from reference (62). Copyright 2014 American Chemical Society.)

2.4 References

- (1) Gao, Y.; Wei, M.; Li, X.; Xu, W.; Ahiabu, A.; Perdiz, J.; Liu, Z.; Serpe, M. J. Stimuli-responsive polymers: Fundamental considerations and applications. *Macromol. Res.* **2017**, *25*, 513-527.
- (2) Cabane, E.; Zhang, X.; Langowska, K.; Palivan, C. G.; Meier, W. Stimuli-responsive polymers and their applications in nanomedicine. *Biointerphases* **2012**, *7*:9.
- (3) Mura, S.; Nicolas, J.; Couvreur, P. Stimuli-responsive nanocarriers for drug delivery. *Nat. Mater.* **2013**, *12*, 991-1003.
- (4) Fan, B.; Gillies, E. R. Self-Immolative Polymers. *Encycl. Polym. Sci. Technol.* **2015**, 1-35.
- (5) Wong, A. D.; DeWit, M. A.; Gillies, E. R. Amplified release through the stimulus triggered degradation of self-immolative oligomers, dendrimers, and linear polymers. *Adv. Drug Delivery Rev.* **2012**, *64*, 1031-1045.
- (6) Olejniczak, J.; Huu, V. A. N.; Lux, J.; Grossman, M.; He, S.; Almutairi, A. Light-triggered chemical amplification to accelerate degradation and release from polymeric particles. *Chem. Commun.* **2015**, *51*, 16980-16983.
- (7) Katz, J. S.; Burdick, J. A. Light-responsive biomaterials: development and applications. *Macromol. Biosci.* **2010**, *10*, 339-348.
- (8) Zeng, H.; Wasylczyk, P.; Wiersma, D. S.; Priimagi, A. Light robots: bridging the gap between microrobotics and photomechanics in soft materials. *Adv. Mater.* **2017**, 1703554-1703563.
- (9) Eisenbach, C. D. Isomerization of aromatic azo chromophores in poly (ethyl acrylate) networks and photomechanical effect. *Polymer* **1980**, *21*, 1175-1179.
- (10) Blair, H. S.; Pague, H. I.; Riordan, J. E. Photoresponsive effects in azo polymers. *Polymer* **1980**, *21*, 1195-1198.
- (11) Cembran, A.; Bernardi, F.; Garavelli, M.; Gagliardi, L.; Orlandi, G. On the mechanism of the *cis-trans* isomerization in the lowest electronic states of azobenzene: S0, S1, and T1. *J. Am. Chem. Soc.* **2004**, *126*, 3234-3243.

- (12) Lu, X.; Guo, S.; Tong, X.; Xia, H.; Zhao, Y. Tunable photocontrolled motions using stored strain energy in malleable azobenzene liquid crystalline polymer actuators. *Adv. Mater.* **2017**, *29*, 1606467.
- (13) Klajn, R. Spiropyran-based dynamic materials. *Chem. Soc. Rev.* **2014**, *43*, 148-184.
- (14) Wang, X.; Hu, J.; Liu, G.; Tian, J.; Wang, H.; Gong, M.; Liu, S. Reversibly switching bilayer permeability and release modules of photochromic polymersomes stabilized by cooperative noncovalent interactions. *J. Am. Chem. Soc.* **2015**, *137*, 15262-15275.
- (15) De las Heras Alarcón, C.; Pennadam, S.; Alexander, C. Stimuli responsive polymers for biomedical applications. *Chem. Soc. Rev.* **2005**, *34*, 276-285.
- (16) Zhang, Y.; Furyk, S.; Bergbreiter, D. E.; Cremer, P. S. Specific ion effects on the water solubility of macromolecules: PNIPAM and the Hofmeister series. *J. Am. Chem. Soc.* **2005**, *127*, 14505-14510.
- (17) Adamus, A.; Komasa, J.; Kadłubowski, S.; Ulański, P.; Rosiak, J.; Kawecki, M.; Klama-Baryła, A.; Dworak, A.; Trzebicka, B.; Szweda, R. Thermoresponsive poly[tri(ethylene glycol) monoethyl ether methacrylate]-peptide surfaces obtained by radiation grafting-synthesis and characterisation. *Colloids Surf., B* **2016**, *145*, 185-193.
- (18) Xiong, Z.; Peng, B.; Han, X.; Peng, C.; Liu, H.; Hu, Y. Dual-stimuli responsive behaviors of diblock polyampholyte PDMAEMA-*b*-PAA in aqueous solution. *J. Colloid Interface Sci.* **2011**, *356*, 557-565.
- (19) Park, J.-S.; Kataoka, K. Precise control of lower critical solution temperature of thermosensitive poly(2-isopropyl-2-oxazoline) via gradient copolymerization with 2-ethyl-2-oxazoline as a hydrophilic comonomer. *Macromolecules* **2006**, *39*, 6622-6630.
- (20) Schmaljohann, D. Thermo- and pH-responsive polymers in drug delivery. *Adv. Drug Delivery Rev.* **2006**, *58*, 1655-1670.
- (21) Liu, X.-Y.; Cheng, F.; Liu, Y.; Liu, H.-J.; Chen, Y. Preparation and characterization of novel thermoresponsive gold nanoparticles and their responsive catalysis properties. *J. Mater. Chem.* **2010**, *20*, 360-368.
- (22) Jeong, B.; Gutowska, A. Lessons from nature: stimuli-responsive polymers and their biomedical applications. *Trends Biotechnol.* **2002**, *20*, 305-311.

- (23) Xue, B.; Gao, L.; Hou, Y.; Liu, Z.; Jiang, L. Temperature controlled water/oil wettability of a surface fabricated by a block copolymer: application as a dual water/oil on-off switch. *Adv. Mater.* **2013**, *25*, 273-277.
- (24) Paek, K.; Yang, H.; Lee, J.; Park, J.; Kim, B. J. Efficient colorimetric pH sensor based on responsive polymer-quantum dot integrated graphene oxide. *ACS Nano* **2014**, *8*, 2848-2856.
- (25) Cheng, Q.; Du, L.; Meng, L.; Han, S.; Wei, T.; Wang, X.; Wu, Y.; Song, X.; Zhou, J.; Zheng, S. The promising nanocarrier for doxorubicin and siRNA co-delivery by PDMAEMA-based amphiphilic nanomicelles. *ACS Appl. Mater. Interfaces* **2016**, *8*, 4347-4356.
- (26) Huh, K. M.; Kang, H. C.; Lee, Y. J.; Bae, Y. H. pH-sensitive polymers for drug delivery. *Macromol. Res.* **2012**, *20*, 224-233.
- (27) Lin, S.; Theato, P. CO₂-responsive polymers. *Macromol. Rapid Commun.* **2013**, *34*, 1118-1133.
- (28) Xu, M.; Liu, L.; Hu, J.; Zhao, Y.; Yan, Q. CO-Signaling Molecule-responsive nanoparticles formed from palladium-containing block copolymers. *ACS Macro Lett.* **2017**, *6*, 458-462.
- (29) Hu, J.; Whittaker, M. R.; Duong, H.; Li, Y.; Boyer, C.; Davis, T. P. Biomimetic polymers responsive to a biological signaling molecule: Nitric oxide triggered reversible self-assembly of single macromolecular chains into nanoparticles. *Angew. Chem., Int. Ed.* **2014**, *53*, 7779-7784.
- (30) Liu, B.; Chen, Y. Responsive lanthanide coordination polymer for hydrogen sulfide. *Anal. Chem.* **2013**, *85*, 11020-11025.
- (31) Zhang, Q.; Lei, L.; Zhu, S. Gas-responsive polymers. *ACS Macro Lett.* **2017**, *6*, 515-522.
- (32) Yan, Q.; Zhou, R.; Fu, C.; Zhang, H.; Yin, Y.; Yuan, J. CO₂-responsive polymeric vesicles that breathe. *Angew. Chem., Int. Ed.* **2011**, *123*, 5025-5029.
- (33) Schattling, P.; Pollmann, I.; Theato, P. Synthesis of CO₂-responsive polymers by post-polymerization modification. *React. Funct. Polym.* **2014**, *75*, 16-21.

- (34) Song, Z.; Wang, K.; Gao, C.; Wang, S.; Zhang, W. A new thermo-, pH-, and CO₂-responsive homopolymer of poly[N-[2-(diethylamino) ethyl] acrylamide]: is the diethylamino group underestimated? *Macromolecules* **2015**, *49*, 162-171.
- (35) Fan, W.; Tong, X.; Farnia, F.; Yu, B.; Zhao, Y. CO₂-responsive polymer single-chain nanoparticles and self-assembly for gas-tunable nanoreactors. *Chem. Mater.* **2017**, *29*, 5693-5701.
- (36) Hefferman, M. J.; Murthy, N. Polyketal nanoparticles: a new pH-sensitive biodegradable drug delivery vehicle. *Bioconjugate Chem.* **2005**, *16*, 1340-1342.
- (37) Liu, J.; Huang, Y.; Kumar, A.; Tan, A.; Jin, S.; Mozhi, A.; Liang, X. J. pH-sensitive nano-systems for drug delivery in cancer therapy. *Biotechnol. Adv.* **2014**, *32*, 693-710.
- (38) Cordes, E.; Bull, H. Mechanism and catalysis for hydrolysis of acetals, ketals, and ortho esters. *Chem. Rev.* **1974**, *74*, 581-603.
- (39) Kreevoy, M. M.; Morgan, C. R.; Taft Jr, R. W. Steric and ring-size effects on ketal hydrolysis rates. *J. Am. Chem. Soc.* **1960**, *82*, 3064-3066.
- (40) Liu, B.; Thayumanavan, S. Substituent effects on the pH sensitivity of acetals and ketals and their correlation with encapsulation stability in polymeric nanogels. *J. Am. Chem. Soc.* **2017**, *139*, 2306-2317.
- (41) Paramonov, S. E.; Bachelder, E. M.; Beaudette, T. T.; Standley, S. M.; Lee, C. C.; Dashe, J.; Fréchet, J. M. Fully acid-degradable biocompatible polyacetal microparticles for drug delivery. *Bioconjugate Chem.* **2008**, *19*, 911-919.
- (42) Gamcsik, M. P.; Kasibhatla, M. S.; Teeter, S. D.; Colvin, O. M. Glutathione levels in human tumors. *Biomarkers* **2012**, *17*, 671-691.
- (43) Cheng, R.; Feng, F.; Meng, F.; Deng, C.; Feijen, J.; Zhong, Z. Glutathione-responsive nano-vehicles as a promising platform for targeted intracellular drug and gene delivery. *J. Controlled Release* **2011**, *152*, 2-12.
- (44) Waris, G.; Ahsan, H. Reactive oxygen species: role in the development of cancer and various chronic conditions. *J. Carcinog.* **2006**, *5*, 14.
- (45) Bang, E.-K.; Lista, M.; Sforazzini, G.; Sakai, N.; Matile, S. Poly (disulfide) s. *Chem. Sci.* **2012**, *3*, 1752-1763.

- (46) Lee, Y.; Mo, H.; Koo, H.; Park, J.-Y.; Cho, M. Y.; Jin, G.-W.; Park, J.-S. Visualization of the degradation of a disulfide polymer, linear poly (ethylenimine sulfide), for gene delivery. *Bioconjugate Chem.* **2007**, *18*, 13-18.
- (47) Ou, M.; Wang, X.-L.; Xu, R.; Chang, C.-W.; Bull, D. A.; Kim, S. W. Novel biodegradable poly(disulfide amine) s for gene delivery with high efficiency and low cytotoxicity. *Bioconjugate Chem.* **2008**, *19*, 626-633.
- (48) Nam, K.; Nam, H. Y.; Kim, P.-H.; Kim, S. W. Paclitaxel-conjugated PEG and arginine-grafted bio-reducible poly(disulfide amine) micelles for co-delivery of drug and gene. *Biomaterials* **2012**, *33*, 8122-8130.
- (49) Kim, A.; Ha, J. H.; Park, S. N. Selective release system for antioxidative and anti-inflammatory activities using H₂O₂-responsive therapeutic nanoparticles. *Biomacromolecules* **2017**, *18*, 3197-3206.
- (50) Song, C.-C.; Ji, R.; Du, F.-S.; Li, Z.-C. Oxidation-responsive poly(amino ester) s containing arylboronic ester and self-immolative motif: synthesis and degradation study. *Macromolecules* **2013**, *46*, 8416-8425.
- (51) Broaders, K. E.; Grandhe, S.; Fréchet, J. M. A biocompatible oxidation-triggered carrier polymer with potential in therapeutics. *J. Am. Chem. Soc.* **2010**, *133*, 756-758.
- (52) de Gracia Lux, C.; Joshi-Barr, S.; Nguyen, T.; Mahmoud, E.; Schopf, E.; Fomina, N.; Almutairi, A. Biocompatible polymeric nanoparticles degrade and release cargo in response to biologically relevant levels of hydrogen peroxide. *J. Am. Chem. Soc.* **2012**, *134*, 15758-15764.
- (53) Zhao, H.; Sterner, E. S.; Coughlin, E. B.; Theato, P. *o*-Nitrobenzyl alcohol derivatives: Opportunities in polymer and materials science. *Macromolecules* **2012**, *45*, 1723-1736.
- (54) Han, D.; Tong, X.; Zhao, Y. Fast photodegradable block copolymer micelles for burst release. *Macromolecules* **2011**, *44*, 437-439.
- (55) Goodwin, A. P.; Mynar, J. L.; Ma, Y.; Fleming, G. R.; Fréchet, J. M. Synthetic micelle sensitive to IR light via a two-photon process. *J. Am. Chem. Soc.* **2005**, *127*, 9952-9953.
- (56) Babin, J.; Pelletier, M.; Lepage, M.; Allard, J. F.; Morris, D.; Zhao, Y. A new two-photon-sensitive block copolymer nanocarrier. *Angew. Chem., Int. Ed.* **2009**, *48*, 3329-3332.

- (57) Fomina, N.; McFearin, C. L.; Almutairi, A. Increasing materials' response to two-photon NIR light via self-immolative dendritic scaffolds. *Chem. Commun.* **2012**, *48*, 9138-9140.
- (58) Roth, M. E.; Green, O.; Gnaim, S.; Shabat, D. Dendritic, oligomeric, and polymeric self-immolative molecular amplification. *Chem. Rev.* **2015**, *116*, 1309-1352.
- (59) Phillips, S. T.; Robbins, J. S.; DiLauro, A. M.; Olah, M. G. Amplified responses in materials using linear polymers that depolymerize from end-to-end when exposed to specific stimuli. *J. Appl. Polym. Sci.* **2014**, *131*, 40992.
- (60) McBride, R. A.; Gillies, E. R. Kinetics of self-immolative degradation in a linear polymeric system: demonstrating the effect of chain length. *Macromolecules* **2013**, *46*, 5157-5166.
- (61) DiLauro, A. M.; Robbins, J. S.; Phillips, S. T. Reproducible and scalable synthesis of end-cap-functionalized depolymerizable poly(phthalaldehydes). *Macromolecules* **2013**, *46*, 2963-2968.
- (62) Fan, B.; Trant, J. F.; Wong, A. D.; Gillies, E. R. Polyglyoxylates: a versatile class of triggerable self-immolative polymers from readily accessible monomers. *J. Am. Chem. Soc.* **2014**, *136*, 10116-10123.
- (63) Peterson, G. I.; Church, D. C.; Yakelis, N. A.; Boydston, A. J. 1, 2-oxazine linker as a thermal trigger for self-immolative polymers. *Polymer* **2014**, *55*, 5980-5985.
- (64) Zhang, H.; Yeung, K.; Robbins, J. S.; Pavlick, R. A.; Wu, M.; Liu, R.; Sen, A.; Phillips, S. T. Self-powered microscale pumps based on analyte-initiated depolymerization reactions. *Angew. Chem., Int. Ed.* **2012**, *51*, 2400-2404.
- (65) DeWit, M. A.; Beaton, A.; Gillies, E. R. A reduction sensitive cascade biodegradable linear polymer. *J. Polym. Sci., Part A: Polym. Chem.* **2010**, *48*, 3977-3985.
- (66) Yeung, K.; Schmid, K. M.; Phillips, S. T. A Thermally-stable enzyme detection assay that amplifies signal autonomously in water without assistance from biological reagents. *Chem. Commun.* **2013**, *49*, 394-396.
- (67) Diesendruck, C. E.; Peterson, G. I.; Kulik, H. J.; Kaitz, J. A.; Mar, B. D.; May, P. A.; White, S. R.; Martínez, T. J.; Boydston, A. J.; Moore, J. S. Mechanically triggered heterolytic unzipping of a low-ceiling-temperature polymer. *Nat. Chem.* **2014**, *6*, 623-628.

- (68) Sagi, A.; Weinstain, R.; Karton, N.; Shabat, D. Self-immolative polymers. *J. Am. Chem. Soc.* **2008**, *130*, 5434-5435.
- (69) Seo, W.; Phillips, S. T. Patterned plastics that change physical structure in response to applied chemical signals. *J. Am. Chem. Soc.* **2010**, *132*, 9234-9235.
- (70) Liu, G.; Wang, X.; Hu, J.; Zhang, G.; Liu, S. Self-immolative polymersomes for high-efficiency triggered release and programmed enzymatic reactions. *J. Am. Chem. Soc.* **2014**, *136*, 7492-7497.
- (71) Esser-Kahn, A. P.; Sottos, N. R.; White, S. R.; Moore, J. S. Programmable microcapsules from self-immolative polymers. *J. Am. Chem. Soc.* **2010**, *132*, 10266-10268.
- (72) DeWit, M. A.; Gillies, E. R. A cascade biodegradable polymer based on alternating cyclization and elimination reactions. *J. Am. Chem. Soc.* **2009**, *131*, 18327-18334.
- (73) Chen, E. K.; McBride, R. A.; Gillies, E. R. Self-immolative polymers containing rapidly cyclizing spacers: toward rapid depolymerization rates. *Macromolecules* **2012**, *45*, 7364-7374.
- (74) Olah, M. G.; Robbins, J. S.; Baker, M. S.; Phillips, S. T. End-capped poly(benzyl ethers): acid and base stable polymers that depolymerize rapidly from head-to-tail in response to specific applied signals. *Macromolecules* **2013**, *46*, 5924-5928.
- (75) DiLauro, A. M.; Abbaspourrad, A.; Weitz, D. A.; Phillips, S. T. Stimuli-responsive core-shell microcapsules with tunable rates of release by using a depolymerizable poly (phthalaldehyde) membrane. *Macromolecules* **2013**, *46*, 3309-3313.
- (76) Kratz, F.; Müller, I. A.; Ryppa, C.; Warnecke, A. Prodrug strategies in anticancer chemotherapy. *ChemMedChem* **2008**, *3*, 20-53.
- (77) Sella, E.; Shabat, D. Self-immolative dendritic probe for direct detection of triacetone triperoxide. *Chem. Commun.* **2008**, *44*, 5701-5703.
- (78) Weinstain, R.; Baran, P. S.; Shabat, D. Activity-linked labeling of enzymes by self-immolative polymers. *Bioconjugate Chem.* **2009**, *20*, 1783-1791.
- (79) Weinstain, R.; Sagi, A.; Karton, N.; Shabat, D. Self-immolative comb-polymers: multiple-release of side-reporters by a single stimulus event. *Chem. Eur. J.* **2008**, *14*, 6857-6861.

- (80) Lewis, G. G.; Robbins, J. S.; Phillips, S. T. Phase-switching depolymerizable poly (carbamate) oligomers for signal amplification in quantitative time-based assays. *Macromolecules* **2013**, *46*, 5177-5183.
- (81) Lewis, G. G.; Robbins, J. S.; Phillips, S. T. Point-of-care assay platform for quantifying active enzymes to femtomolar levels using measurements of time as the readout. *Anal. Chem.* **2013**, *85*, 10432-10439.
- (82) Lewis, G. G.; Robbins, J. S.; Phillips, S. T. A prototype point-of-use assay for measuring heavy metal contamination in water using time as a quantitative readout. *Chem. Commun.* **2014**, *50*, 5352-5354.
- (83) Liu, G.; Zhang, G.; Hu, J.; Wang, X.; Zhu, M.; Liu, S. Hyperbranched self-immolative polymers (h-SIPs) for programmed payload delivery and ultrasensitive detection. *J. Am. Chem. Soc.* **2015**, *137*, 11645-11655.
- (84) Han, D.; Yu, X.; Chai, Q.; Ayres, N.; Steckl, A. J. Stimuli-responsive self-immolative polymer nanofiber membranes formed by coaxial electrospinning. *ACS Appl. Mater. Interfaces* **2017**, *9*, 11858-11865.
- (85) Robbins, J. S.; Schmid, K. M.; Phillips, S. T. Effects of electronics, aromaticity, and solvent polarity on the rate of azaquinone-methide-mediated depolymerization of aromatic carbamate oligomers. *J. Org. Chem.* **2013**, *78*, 3159-3169.
- (86) Kim, H.; Mohapatra, H.; Phillips, S. T. Rapid, On-command debonding of stimuli-responsive cross-linked adhesives by continuous, sequential quinone methide elimination reactions. *Angew. Chem., Int. Ed.* **2015**, *54*, 13063-13067.
- (87) Baker, M. S.; Kim, H.; Olah, M. G.; Lewis, G. G.; Phillips, S. T. Depolymerizable poly(benzyl ether)-based materials for selective room temperature recycling. *Green Chem.* **2015**, *17*, 4541-4545.
- (88) Ergene, C.; Palermo, E. F. Cationic Poly(benzyl ether)s as self-immolative antimicrobial polymers. *Biomacromolecules* **2017**, *18*, 3400-3409.
- (89) de Gracia Lux, C.; McFearin, C. L.; Joshi-Barr, S.; Sankaranarayanan, J.; Fomina, N.; Almutairi, A. Single UV or Near IR triggering event leads to polymer degradation into small molecules. *ACS Macro Lett.* **2012**, *1*, 922-926.

- (90) Wong, A. D.; Güngör, T. M.; Gillies, E. R. Multiresponsive Azobenzene end-cap for self-immolative polymers. *ACS Macro Lett.* **2014**, *3*, 1191-1195.
- (91) DeWit, M. A.; Gillies, E. R. Design, synthesis, and cyclization of 4-aminobutyric acid derivatives: potential candidates as self-immolative spacers. *Org. Biomol. Chem.* **2011**, *9*, 1846-1854.
- (92) Ryan, B.; McCann, G. Novel sub-ceiling temperature rapid depolymerization-repolymerization reactions of cyanoacrylate polymers. *Macromol. Rapid Commun.* **1996**, *17*, 217-227.
- (93) Stansbury, J.; Dickens, B.; Liu, D.-W. Preparation and characterization of cyclopolymerizable resin formulations. *J. Dent. Res.* **1995**, *74*, 1110-1115.
- (94) Brachais, C.; Huguet, J.; Bunel, C. Synthesis, characterization and stabilization of poly(methyl glyoxylate). *Polymer* **1997**, *38*, 4959-4964.
- (95) Ito, H.; Willson, C. G. Chemical amplification in the design of dry developing resist materials. *Polym. Eng. Sci.* **1983**, *23*, 1012-1018.
- (96) Boileau, S.; Illy, N. Activation in anionic polymerization: Why phosphazene bases are very exciting promoters. *Prog. Polym. Sci.* **2011**, *36*, 1132-1151.
- (97) Grolman, J. M.; Inci, B.; Moore, J. S. pH-dependent switchable permeability from core-shell microcapsules. *ACS Macro Lett.* **2015**, *4*, 441-445.
- (98) Tang, S.; Yourdkhani, M.; Possanza Casey, C. M.; Sottos, N. R.; White, S. R.; Moore, J. S. Low ceiling temperature polymer microcapsules with hydrophobic payloads via rapid emulsion-solvent evaporation. *ACS Appl. Mater. Interfaces* **2017**, *9*, 20115-20123.
- (99) Kaitz, J. A.; Moore, J. S. Functional phthalaldehyde polymers by copolymerization with substituted benzaldehydes. *Macromolecules* **2013**, *46*, 608-612.
- (100) DiLauro, A. M.; Lewis, G. G.; Phillips, S. T. Self-immolative poly(4,5-dichlorophthalaldehyde) and its applications in multi-stimuli-responsive macroscopic plastics. *Angew. Chem., Int. Ed.* **2015**, *127*, 6298-6303.
- (101) DiLauro, A. M.; Phillips, S. T. End-capped poly(4, 5-dichlorophthalaldehyde): a stable self-immolative poly(aldehyde) for translating specific inputs into amplified outputs, both in solution and the solid state. *Polym. Chem.* **2015**, *6*, 3252-3258.

- (102) Köstler, S.; Zechner, B.; Trathnigg, B.; Fasl, H.; Kern, W.; Ribitsch, V. Amphiphilic block copolymers containing thermally degradable poly(phthalaldehyde) blocks. *J. Polym. Sci., Part A: Polym. Chem.* **2009**, *47*, 1499-1509.
- (103) Kaitz, J. A.; Diesendruck, C. E.; Moore, J. S. End group characterization of poly(phthalaldehyde): surprising discovery of a reversible, cationic macrocyclization mechanism. *J. Am. Chem. Soc.* **2013**, *135*, 12755-12761.
- (104) Kaitz, J. A.; Diesendruck, C. E.; Moore, J. S. Dynamic covalent macrocyclic poly(phthalaldehyde)s: scrambling cyclic homopolymer mixtures produces multi-block and random cyclic copolymers. *Macromolecules* **2013**, *46*, 8121-8128.
- (105) Kaitz, J. A.; Moore, J. S. Copolymerization of *o*-phthalaldehyde and ethyl glyoxylate: cyclic macromolecules with alternating sequence and tunable thermal properties. *Macromolecules* **2014**, *47*, 5509-5513.
- (106) Burel, F.; Rossignol, L.; Pontvianne, P.; Hartman, J.; Couesnon, N.; Bunel, C. Synthesis and characterization of poly(ethyl glyoxylate)-a new potentially biodegradable polymer. *e-Polym.* **2003**, *3*, 407-418.
- (107) Duncan, R. The dawning era of polymer therapeutics. *Nat. Rev. Drug Discovery* **2003**, *2*, 347-360.

Chapter 3

3 Photo-controlled depolymerization of stimuli-responsive poly(ethyl glyoxylate): Differentiating features and traceless ambient depolymerization

The content of this chapter has been published in “B. Fan, J. F. Trant, R. E. Yardley, A. J. Pickering, F. Laguné-Labarhet, E. R. Gillies, *Macromolecules*, **2016**, *49*, 7196–7203”

3.1 Introduction

In recent years, there has been increasing interest in the development of degradable polymers for a wide range of applications from packaging to biomedical devices.¹⁻³ At present, polyesters are widely used, as they can be broken down to nontoxic products.^{4,5} However, their degradation cannot be easily controlled, as random backbone scission occurs gradually in a wide range of environments, and cannot be turned on or off as desired for a given application. To address this limitation, significant efforts have been directed towards the development of stimuli-responsive polymers. Polymers responsive to light,^{6,7} heat,⁸ changes in pH⁹ and many other stimuli have been developed.^{10,11} These polymers require many stimuli-mediated events to completely degrade the polymer backbones. While they perform well in the laboratory, where large changes in conditions can easily be introduced, the gradient of conditions and the concentrations of stimuli in real environments are typically much smaller, presenting a challenge.

To address the above limitations, molecules that depolymerize from end-to-end in response to the cleavage of stimuli-responsive end-caps from the polymer termini, were developed.^{12,13} These polymers, often referred to as “self-immolative polymers” (SIPs), afford amplification of stimuli-mediated events as an entire polymer chain can depolymerize in response to a single end-cap cleavage. In addition, because of their end-to-end depolymerization mechanism, they exhibit predictable depolymerization times that are dependent on their length and backbone composition.¹⁴ Backbones including polycarbamates,¹⁵⁻¹⁸ polycarbonates,¹⁹ polyethers,²⁰ polyphthalaldehydes,^{21,22} and polyglyoxylates²³ have been synthesized and studied over the last several years and end-

caps responsive to stimuli including light,²⁴ heat,²⁵ fluoride ions,²⁶ redox change,^{16,27} enzymes,²⁸ and mechanical force²⁹ have been reported. The unique features of these polymers have made them attractive for potential applications in molecular sensors,^{15,30} responsive films,^{31,32} micropumps,²⁶ drug delivery systems,^{17,24} and microcapsules.^{33,34}

Polyglyoxylates are an attractive class of polymers that can undergo depolymerization upon end-cap cleavage due to their low ceiling temperatures (T_c).²³ Glyoxylate monomers such as ethyl glyoxylate (EtG) are commercially available or can be prepared from readily available starting materials such as maleic or fumaric acid.²³ In addition, they ultimately degrade to glyoxylic acid,³⁵⁻³⁷ a metabolite found in some mammalian biochemical pathways³⁸ and an intermediate in the glyoxylate cycle, an anaerobic variant of the tricarboxylic acid cycle that occurs in plants, bacteria, protists, and fungi.³⁷ This chapter explored in detail the depolymerization of end-capped self-immolative poly(ethyl glyoxylate) (PEtG). In particular, the solid-state depolymerization of PEtG demonstrates several important novel and unusual aspects of the end-to-end depolymerization and also reveals that upon end-cap cleavage, PEtG undergoes depolymerization under ambient conditions to afford volatile products. This offers new opportunities for one-step traceless patterning and for simple polymer recycling or reprogramming.

3.2 Experimental section

General procedures and materials. All chemicals were purchased from commercial suppliers and used without further purification unless otherwise noted. Et₃N and CH₂Cl₂ were distilled from calcium hydride before use. 6-Nitroveratryl carbonate end-capped PEtG (**PEtG-NVOC**) and benzyl carbonate end-capped PEtG were prepared as previously reported.²³ **PEtG-NVOC** used in the current studies had a number average molar mass (M_n) of 35 kg/mol and a dispersity (D) of 1.4. The benzyl carbonate end-capped PEtG had an M_n of 42 kg/mol and a D of 1.4. Characterization data for these specific batches are included in Figures A3.1-A3.6. The soil was standard potting soil from Premier Tech (Rivière-du-Loup, Canada). Nylon bags were made from a Nylon 6/6 woven mesh sheet with 80 μ m mesh size purchased from Small Parts, Inc. (Logansport, IN, USA). The size exclusion chromatography (SEC) instrument was equipped with a Viscotek GPC Max

VE2001 solvent module (Malvern Instruments Ltd., Malvern, UK). Samples were analyzed using the Viscotek VE3580 RI detector operating at 30 °C. The separation technique employed two Agilent Polypore (300 x 7.5 mm) columns connected in series and to a Polypore guard column (50 x 7.5 mm) (Agilent Technologies, Santa Clara, CA, USA). Samples were dissolved in tetrahydrofuran (THF) (glass distilled grade) at a concentration of approximately 5.0 mg/mL and filtered through 0.22 μm syringe filters, then injected using a 100.0 μL loop. The THF eluent was filtered and eluted at 1.0 mL/min for a total of 30 min. A calibration curve was obtained from poly(methyl methacrylate) standards with molar masses from 1540-1126000 g/mol (Agilent Technologies, Santa Clara, CA, USA). ^1H NMR spectra were obtained at 600 MHz on a Varian Inova instrument (Varian, Palo Alto, CA, USA). The scanning electron microscopy (SEM) images of polymer films were taken on a Hitachi S-3400N instrument at a voltage of 2 kV (Hitachi, Tokyo, Japan). The samples were mounted on carbon-taped aluminum stubs and sputtered with gold at a rate of 5 nm/min for 4 min (Hummer-6 sputtering system, Anatech, Union City, CA, USA).

Preparation of PEtG coatings. PEtG was dissolved in CH_2Cl_2 at a concentration of 90.0 mg/mL. This solution was drop-cast onto glass microscope slides and the solvent was evaporated in vacuo for 48 h to afford coatings. The coating thickness was measured using a caliper. 330.0 μL cast over 2 cm^2 afforded a thickness of ~ 150 μm . For thinner coatings, 1 mL of 30.0 mg/mL polymer solution cast over 6 cm^2 afforded ~ 50 μm , or 2 mL of 15 mg/mL polymer solution cast over 12 cm^2 afforded ~ 25 μm . Each coating had a total mass of ~ 30 mg.

Depolymerization studies of PEtG films in aqueous buffer solutions at varying pH and temperature. The initial masses of coatings were measured and recorded. Irradiated coatings were placed into an ACE Glass photochemistry cabinet containing a mercury light source (450 W bulb, 2.8 mW/cm^2 measured for UVA radiation at the sample position) for 5 h to cleave the NVOC end-cap. A coating of PEtG with a benzyl carbonate (non-photo-responsive end-cap) was also irradiated to verify that the polymer backbone was stable to UV irradiation and that it was specifically the NVOC end-cap that was susceptible to cleavage by UV light (Figure A3.7). Non-irradiated coatings were stored in the dark. Next,

all of the slides (3 per time point, per condition) were immersed into a 0.1 M aqueous buffer solution (citrate buffer for pH 3.0, 4.0, 5.0; phosphate buffer for pH 6.0, 7.0 and 8.0) at a given temperature. 10 °C was obtained by placing the samples into a refrigerator set to this temperature. 20 °C corresponded to ambient temperature of a temperature-controlled room. In this case, protection from light was afforded by storing the samples in a cabinet. 30 °C was obtained by placing samples into an oven set to this temperature. At selected times, 3 coatings from each treatment were removed from the buffer solution, rinsed with distilled water, dried under house vacuum for 48 h, and then weighed. The percent of initial mass of the coating at a given time point was calculated as (mass at time point/initial mass) x 100%. In each case, the error bars correspond to the standard deviation of the measurements of 3 different samples. At pH 7.0 and 20 °C, the samples were also analyzed by SEC, samples at t = 0 and t = 5 days were analyzed by SEM, and the residual coatings at selected time points were dissolved in CDCl₃ and ¹H NMR spectra were obtained (Figures A3.8-A3.11).

Depolymerization of PEtG coatings in soil with varying water content. The soil was autoclaved, dried in an oven (120 °C), and weighed. The soil was then used dry or rehydrated with 0.1 M pH 7.0 phosphate buffer to 10, 20, or 30 mass percent. The irradiated and non-irradiated coatings with a thickness of 150 μm were prepared as described above for the studies in buffer except that instead of immersing the coatings into buffer solution, they were placed into nylon bags, and immersed in soil (350.0 g dry soil per 30 slides). The box was sealed to prevent the evaporation of water. At different time points, the nylon bags were removed from the soil, and both the slides and nylon bags were washed with CH₂Cl₂, filtered and the solvent was evaporated. The remaining material was weighed to determine the mass of remaining polymer and the percent of initial mass of the coating was calculated as described above. Error bars correspond to the standard deviation of the measurements of 3 different samples.

Depolymerization of PEtG coatings in air. Coatings were prepared and weighed as described above. Irradiated coatings were placed into the photochemistry cabinet described above for 4 h to remove the end-cap. During this time the non-irradiated coatings were

stored in the dark. All coatings were then stored at either 20 °C (ambient, thermostat-controlled) or at 30 °C (oven). Protection from light was afforded by storing samples in either a cabinet or the oven. At selected time points, the masses of the slides were measured and then the slides were returned to their depolymerization conditions. The percent of initial mass of the coating was calculated as described above. Error bars correspond to the standard deviation on the measurements of 3 different samples.

Sunlight-triggered coating depolymerization. Coatings were prepared and weighed as described above. All coatings were then placed in a greenhouse, with half protected from sunlight with aluminum foil, and the other half exposed to sunlight through the greenhouse glass. The temperature of the environment varied over the experiment from approximately 9 to 37 °C over the day-night cycle in a Southwestern Ontario, Canada, Spring (May-June). At selected time points, the masses of the slides were measured and then they were returned to their depolymerization conditions. The percent of initial mass of the coating remaining was calculated as described above. Error bars correspond to the standard deviation of on the measurements of 3 different samples.

Collection of depolymerized ethyl glyoxylate monomer. 600.0 mg of **PEtG-NVOC** was dissolved in 5.0 mL of CH_2Cl_2 , then the CH_2Cl_2 was evaporated in vacuo to coat the walls of a round bottom flask (A). Then the polymer film was dried under high vacuum. Flask A was then placed in the photochemistry cabinet described above for 4 h. It was then immersed in an oil bath at 50 °C, and connected to a vacuum (240 mTorr) and to Flask B, which was cooled in a liquid nitrogen bath to trap the volatile ethyl glyoxylate depolymerization product (Figure A3.13). The mass of flask B was measured every 1 or 2 h over a period of 9 h to determine the mass of collected ethyl glyoxylate. The identity of the collected product was determined by ^1H NMR spectroscopy to be ethyl glyoxylate, by comparison with the known spectrum of the commercial product (Figure A3.14). A control experiment was also performed under identical conditions but without UV irradiation. No conversion to liquid monomer was observed and no monomer transferred to the collection flask.

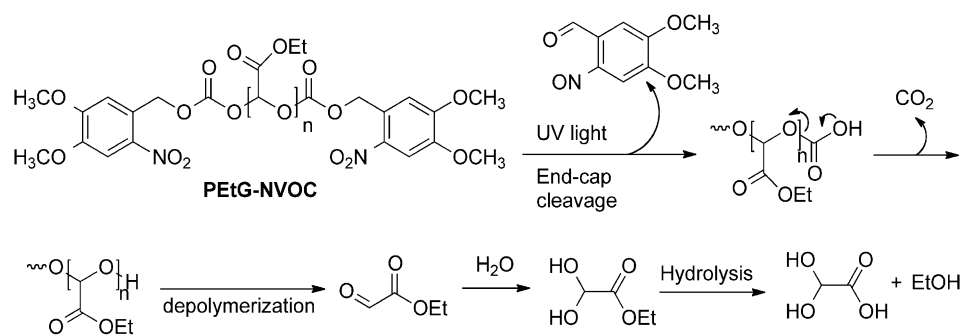
Repolymerization of collected monomer. The collected ethyl glyoxylate (0.5 g, 5.0 mmol, 1.0 equiv.) was dissolved in CH₂Cl₂ (0.5 mL) and Et₃N (0.4 μL, 2.5 μmol, 0.0005 equiv.) was added. The solution was stirred for 1 h at -20 °C. 6-Nitrovertryloxycarbonyl chloride (NVOC-Cl) (22.0 mg, 73.0 μmol, 0.014 equiv.) and Et₃N (10.0 μL, 73.0 μmol, 0.014 equiv.) were then added at 0 °C to end-cap the polymer. The solution was stirred for 24 h at room temperature. Purification was achieved by dialysis against 1:1 acetone: methanol using a regenerated cellulose membrane with a molecular weight cut-off of 2000 g/mol. The yield was 12%. This is an unoptimized yield as the aim of the experiment was to demonstrate proof of principle. It is likely low as the polymer has a low M_n, making the standard precipitation procedure impossible and much material was likely lost through the dialysis. It can likely be improved through optimization of the set-up (such as decreasing exposure of the ethyl glyoxylate to air during the weighing procedure that was used to generate (Figure 3.3) and also certainly through distillation of the recycled ethyl glyoxylate if required (high purity is very important for achieving high degrees of polymerization). ¹H NMR (600 MHz, CDCl₃): δ 7.69-7.76 (m, 2H), 7.12-7.21 (m, 2H), 5.46-5.78 (m, 18H), 4.10-4.33 (m, 32H), 4.00-4.06 (m, 6H), 3.94-3.98 (m, 6H), 1.21-1.44 (m, 50H). SEC: M_n = 1.7 kg/mol, M_w = 2.8 kg/mol, Đ = 1.65.

Pattern fabrication. For Figure 3.4c, **PEtG-NVOC** (15.0 mg) was dissolved in CH₂Cl₂ (1.0 mL) and was drop-cast onto a glass slide over a surface area of 6.6 cm² to provide a ~20 μm-thick film. For Figure 3.4d, **PEtG-NVOC** (100.0 mg) was dissolved in CH₂Cl₂ (4.0 mL) and 1.0 mL was spin-coated (Laurell Technologies Corporation, Model WS-400BZ-6NPP/LITE) at speed of 2000 rpm for 90 s onto a glass slide over a surface area of 20 cm² to provide a 13 μm-thick film. After the solvent was evaporated in vacuo for 48 h, the coatings were covered with metal mask patterns shown in Fig. 3.3a and 3.3b, for the 20 μm and the 13 μm-thick coatings respectively. The mask with 500 μm diameter holes was a meshed aluminum grid while the mask with 20 μm diameter holes was a chromium mask engraved over a borosilicate glass. Irradiation through the masks was performed using a mask-aligner (Neutronix-Quintel NXQ 4006) to ensure spatial uniformity of the irradiation. The thinner film was irradiated for 0.5 h while the thicker film was irradiated for 1 h using an irradiance of 35 mW/cm² from a mercury light source. After the irradiation,

the films were stored in the dark at ambient temperature (~ 20 °C) for 6 days. The images of polymer patterns were taken on an optical microscope (Zeiss Axioskop2 MAT Microscope equipped with 1300 CCD Digital Camera) on the 6th day after irradiation.

3.3 Results and discussion

PEtG with a UV light-sensitive 6-nitroveratryl carbonate end-cap (**PEtG-NVOC**) was synthesized as previously reported via the low temperature polymerization of EtG, following by end-capping with 6-nitroveratryl chloroformate.²³ Irradiation of **PEtG-NVOC** with UV light results in cleavage of the NVOC moiety from the polymer terminus (Scheme 3.1). This is followed by decarboxylation, revealing hemiacetal-terminated PEtG, which undergoes depolymerization. In the presence of water, the resulting ethyl glyoxylate (EtG) is rapidly converted to ethyl glyoxylate hydrate (EtGH), then gradually hydrolyzed to glyoxylic acid hydrate and ethanol.²³ It was previously demonstrated that the degradation of PEtG by backbone cleavage in the absence of UV light was much slower than UV-triggered depolymerization and that UV irradiation of PEtG with a non-responsive benzyl carbonate end-cap did not lead to degradation.²³ For the current study, unless otherwise indicated, coatings of **PEtG-NVOC** were prepared by drop-casting the polymer onto glass slides to provide coatings ~ 150 μm thick. Samples treated with UV light were irradiated with a mercury lamp having an intensity of ~ 2.8 mW/cm^2 in the UVA range. Control coatings were kept in the dark. The slides were then immersed in aqueous solution. At each time point, irradiated and control films were removed from the solution, rinsed, dried, and their masses were measured. As the polymers are insoluble in water beyond the oligomer form and the films remained intact and adhered to the glass slides until greater than 90% mass loss had occurred, this measurement provided a good indication of the extent of depolymerization that had occurred.



Scheme 3.1 Chemical structure of PEtG-NVOC and its UV light-initiated depolymerization. This is followed by hydrate formation and hydrolysis of the resulting ethyl glyoxylate in the presence of water.

To investigate the effect of pH, coatings were immersed in buffer solutions of pH 3 - 8 and stored at 20 °C. As shown in Figure 3.1a, at pH 6 - 8 the irradiated coatings behaved similarly, eroding to ~50% of their initial mass over 5 days. At pH 5, the erosion of the irradiated polymer was significantly slower, requiring more than 20 days to reach 50% mass loss. Then, at pH 3-4 the erosion again became more rapid, reaching a rate intermediate between that of pH 5 and pH 6-8. This highlights the first key difference between the end-to-end depolymerization and random backbone cleavage mechanism for polyglyoxylates. Random backbone cleavage of PEtG would involve the hydrolysis of an acetal linkage. This is well known to be an acid-catalyzed process, with a rate directly dependent on the concentration of H^+ (Scheme A3.1).³⁹ Based on the stability of the non-irradiated control coatings, this reaction is very slow at 20 °C from pH 3-8. This can likely be attributed to the electron-withdrawing ester moiety, which would destabilize the adjacent carbocation intermediate involved in the hydrolysis mechanism. On the other hand, end-to-end depolymerization of the triggered PEtG involves the sequential breakdown of terminal hemiacetals. In aqueous solution, hemiacetal hydrolysis can be catalyzed by acid (Scheme A3.2) or base (Scheme A3.3).^{40,41} It has been reported that hemiacetal decomposition is generally faster than acetal decomposition and that a rate minimum for hemiacetal cleavage occurs at mildly acidic pH.^{40,41} Both of these observations are consistent with the results of the current study, where more rapid mass loss was observed for the irradiated polymer coatings at all pHs, and a minimum rate of

mass loss was observed at pH 5. Overall, these differences in mechanisms and rates between of the backbone cleavage and end-to-end depolymerization demonstrate an effective decoupling of these processes.

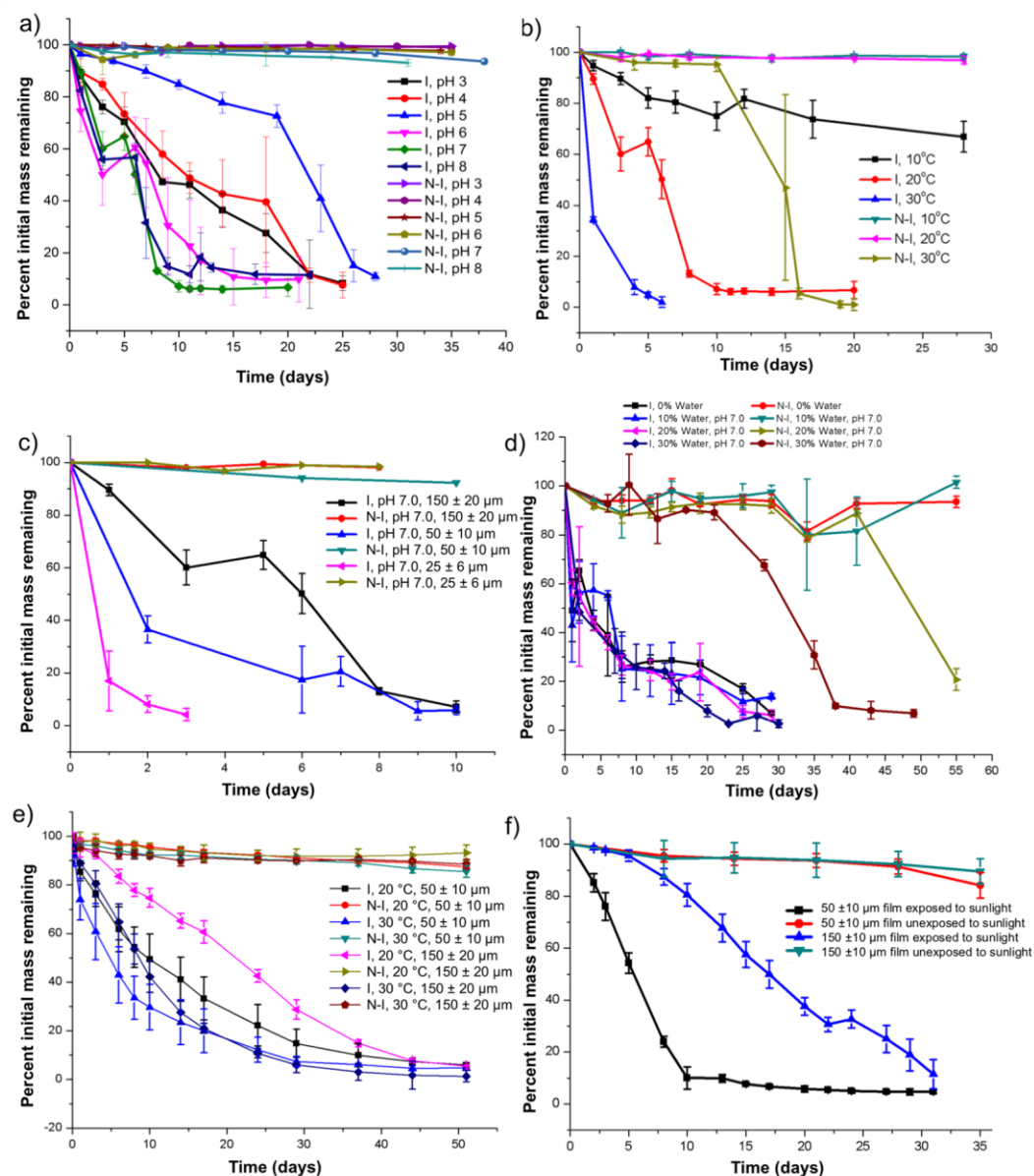


Figure 3.1 Mass loss profiles for UV light irradiated (I) and non-irradiated (N-I) PEtG-NVOC coatings under different conditions: a) 150 μm thickness immersed at 20 $^{\circ}\text{C}$ in buffers of pH 3-8; b) 150 μm thickness immersed at varying temperatures in pH 7.0 buffer; c) Varying film thicknesses from 25-150 μm immersed in pH 7.0 buffer at 20 $^{\circ}\text{C}$; d) 150 μm thickness immersed in soil with either 10, 20 or 30 mass % of pH

7.0 buffer at 20 °C; e) Film thicknesses of 50 or 150 μm in air (no aqueous immersion) at either 20 or 30 °C; f) Film thicknesses of 50 or 150 μm in air either exposed or not exposed to sunlight in a greenhouse. In each experiment, the error bars represent the standard deviation of the measurements for three samples.

The effect of temperature on the depolymerization rate was also explored by incubating irradiated and non-irradiated coatings in pH 7 buffer at temperatures of 10, 20, or 30 °C. As expected on the basis of kinetics as well as entropic contributions to ΔG , temperature had a significant effect on the rate of coating erosion, with the irradiated coating at 30 °C requiring less than 1 day for 50% mass loss while more than 28 days was required at 10 °C (Figure 3.1b). The non-irradiated coatings were stable at 10 °C and 20 °C while at 30 °C degradation began at \sim 12 days. At this temperature, the rate of backbone cleavage reactions in the presence of water becomes sufficient to cleave chains and initiate depolymerization.

A notable and unusual feature of the mass loss profiles in Figure 3.1a-b was a distinct plateau or even increase at \sim 40 % mass loss. We hypothesized that this was related to the surface accessibility of the polymers and resulting depolymerization products. It was proposed that the apparent mass increase might have arisen from the production and temporary trapping of EtGH as depolymerization occurred and water slowly penetrated into the coating, subsequently reacting to form this hydrate within the coating. Indeed ^1H NMR spectra of the residual coating material at 3 day and 6 days (pH 7, 20 °C) contained peaks assignable to EtGH (Figures A3.8-A3.9). To further evaluate this phenomenon, coatings of different thicknesses were prepared and studied. As shown in Figure 3.1c, the plateau for a \sim 50 μm thick coating was at \sim 80% mass loss while no plateau was observed for an even thinner film of \sim 25 μm . This confirms that accessibility of depolymerizing polymers to the coating surface is indeed important for coating erosion. This can likely be attributed to the fact that released EtG can potentially re-add to the polymer terminus if it is not rapidly released from the coating or trapped by water to form the hydrate. This presents an opportunity to tune the coating erosion time by simply changing the coating thickness for various applications. It should be noted however that upon increasing the coating thickness to 300 μm , the mass loss did not proceed beyond \sim 60% (Figure A3.12).

This presumably results from incomplete end-cap cleavage due to the inability of sufficient UV light to penetrate these thicker coatings using our experimental set-up. ^1H NMR spectra of the 150 μm -thick coatings did not show any end-cap, confirming complete cleavage (Figures A3.8-A3.9), whereas intact end-cap could be clearly observed for non-irradiated coatings (Figure A3.10-A3.11).

Conditions of pH 7.0 and 20 $^\circ\text{C}$ and a coating thickness of 150 μm were selected to further probe the erosion mechanism. Water-insoluble degradable polymers can undergo surface erosion or bulk erosion. Which process dominates for a given polymer is generally dependent on the relative rates of bond cleavage, diffusion of water into the polymer and the dimensions of a given polymer specimen.⁴² As shown in Figure 3.1a-c, the depolymerization profiles for the irradiated polymers suggest a surface erosion process, as mass loss began immediately. This was supported by minimal changes in the molar mass characteristics of the bulk polymer as determined by size exclusion chromatography (Figure 3.2a). The initial small drop in M_n can likely be attributed to some depolymerization that occurred in the THF SEC solvent after sample dissolution of each of the irradiated samples as depolymerization can occur slowly in THF.

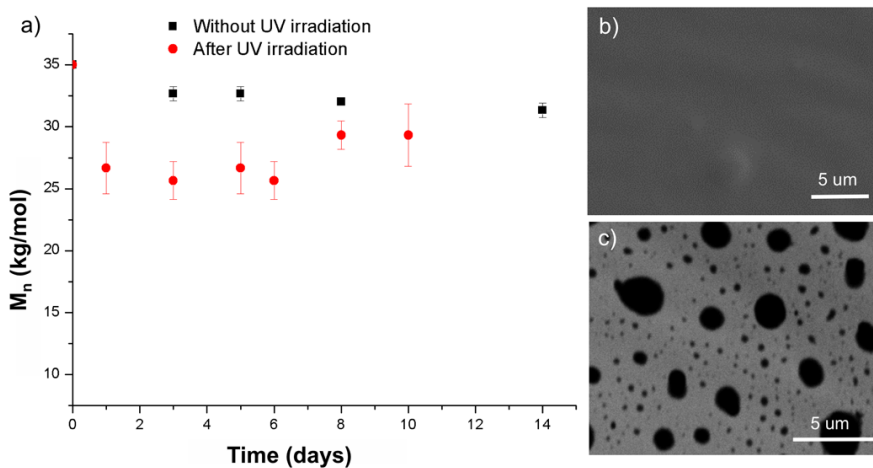


Figure 3.2 a) Number average molar mass (M_n) of polymer remaining on the coating during the mass loss study, as measured by SEC.; b,c) SEM images of the polymer coating after 5 days of immersion in 0.1 M, pH 7.0 phosphate buffer at 20 $^\circ\text{C}$ b) control without UV irradiation and c) with UV irradiation.

The surfaces were also imaged by SEM. The non-irradiated coating retained a smooth and intact surface (Figure 3.2b) while the irradiated coating developed holes (Figure 3.2c). The smooth appearance of these surfaces can be attributed to the amorphous nature and low T_g ($-5\text{ }^\circ\text{C}$) of PEtG.²³ The surface erosion mechanism can be explained by the rapid decomposition of hemiacetals, combined with the importance of surface accessibility for diffusion of the depolymerization products out of the coating. In contrast, the delayed mass loss of the non-irradiated coating is more characteristic of a bulk degradation mechanism, where water diffuses through the polymer, resulting in slow bond cleavage.⁴² In this case bond cleavage would involve slow, non-specific hydrolysis of the polymer backbone. However, unlike polyesters such as poly(lactic acid) that commonly undergo bulk erosion,⁴³ non-irradiated PEtG does not undergo changes in molar mass prior to the onset of mass loss (Figure 3.2a). Polyesters can undergo multiple bond cleavages in the polymer backbone throughout the bulk polymer matrix prior to the loss of mass, as shorter polymer chains remain insoluble. In contrast, even a non-irradiated PEtG undergoes complete backbone depolymerization to water-soluble small molecules following a single backbone scission event. This highlights another key difference between the end-to-end depolymerization mechanism of PEtG and the random backbone hydrolysis that occurs in conventional degradable polymers.

It was also of interest to investigate the erosion of PEtG in the natural environment, so mass loss was investigated in soil-like conditions with varying water content (Figure 3.1d). A significant dependence on the water content was observed for the non-irradiated coatings. This can be attributed to the requirement for water to participate in any cleavage reaction of the end-capped polymer, including ester, acetal, or carbonate hydrolysis. On the other hand, the erosion rate of irradiated coatings exhibited no significant dependence on water, suggesting that water was not required for end-to-end depolymerization. This led to the discovery that irradiated PEtG coatings readily depolymerized under ambient conditions with the depolymerization time dependent on temperature and coating thickness (Figure 3.1e). In the absence of water, the polymer matrix is presumed to serve as a proton transfer agent and EtG is the final depolymerization product (Scheme A3.4). Having a boiling point of $110\text{ }^\circ\text{C}$, similar to toluene, it readily evaporates from the surface. No

plateau in the mass loss was observed in these studies, consistent with the above explanation relating to the trapping of EtGH in coatings that were immersed in aqueous conditions. It was also found that sunlight could trigger depolymerization under ambient conditions resulting in a coating erosion time that was dependent on its thickness (Figure 3.1f). This thickness dependence can arise from the decreased penetration of the light through the thicker coating and also from the inherent dependence of the coating depolymerization time on thickness that was observed in Figure 3.1c and 3.1e. Combined, these data demonstrate that solid-state **PEtG-NVOC** has the ability to depolymerize in an essentially traceless manner under ambient conditions in response to a specific external stimulus and that the coating depolymerization time can be tuned by adjusting parameters such as coating thickness.

The depolymerization of polymers back to volatile monomers under ambient conditions is very rare. “Traceless” depolymerization has been reported using poly(vinyl sulfone)s (PVS) and it has been shown that these polymers undergo depolymerization in the presence of ionizing radiation, UV light, heat, or mechanical force.⁴⁴⁻⁴⁸ However, a key limitation is that the overall stability of PVS is directly correlated with their susceptibility to undergo depolymerization as it is backbone cleavage itself that triggers depolymerization. Consequently, their inherent instability may limit their application. In contrast, end-to-end depolymerization of PEtG is initiated by end-cap cleavage and this is triggered by different stimuli and conditions than backbone cleavage, as demonstrated above. Effectively, the end-cap affords a removable barrier to the otherwise thermodynamically favorable depolymerization process, allowing the polymer to be utilized above its inherent ceiling temperature. Among the other backbones that undergo end-to-end depolymerization, polyphthalaldehyde has also been demonstrated to depolymerize in the solid state.^{21,22} However, the *o*-phthalaldehyde depolymerization product is a solid at room temperature with a melting point of 55 – 58 °C and a boiling point of 266 °C. High vacuum is required to volatilize it, making the recollection of monomer difficult, and it tends to sublime rather than distill.

To demonstrate the proof-of-concept for a potential application of the unusual behavior of **PEtG-NVOC**, a full cycle of material depolymerization and regeneration at the molecular level was performed. **PEtG-NVOC** was irradiated with UV light, and then moderate heating (50 °C) and modest vacuum (240 mTorr) were used to accelerate the depolymerization and transfer of EtG monomer to a second flask (Figure 3.3). More than 85% of the material could be collected over less than 10 h and the identity of the product was confirmed to be ethyl glyoxylate by ^1H NMR spectroscopy (Figure A3.14). Without further processing, this monomer could be repolymerized and end-capped to afford again **PEtG-NVOC** (Figure A3.15-A3.16). In contrast, applying the same conditions without UV irradiation did not result in any conversion of the polymer to liquid monomer and no monomer was transferred to the collection flask, confirming the end-capped polymer's stability under the experimental conditions.

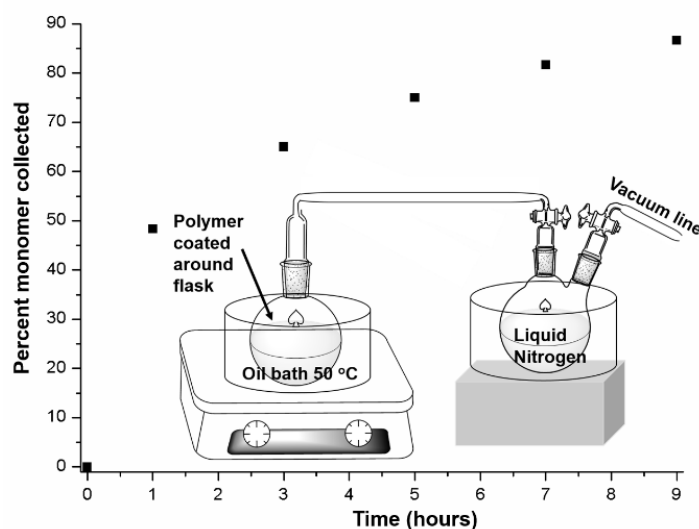


Figure 3.3 Collection of depolymerized ethyl glyoxylate monomer over time after irradiation of PEtG-NVOC and the corresponding experimental set-up.

Recently, depolymerization as a means of potentially recycling polymers has been a topic of increasing interest. For example, it was shown that polycarbonates that were prepared from epoxides and CO_2 could be depolymerized in solution to either their monomers or cyclic carbonates depending on the particular polymer backbone and the depolymerization

conditions.⁴⁹⁻⁵¹ It was also recently demonstrated that poly(γ -butyrolactone) could be depolymerized to monomers due to the thermodynamically favorable generation of the 5-membered lactone ring.⁵² However, high temperatures of 220 °C and 300 °C were required to achieve depolymerization for the linear and cyclic forms of the polymer respectively. Poly(aromatic ester)s derived from benzodioxepinones were also found to undergo reversible polymerization and depolymerization using Al catalysts in solution depending on the temperature and concentration of the material.⁵³ Furthermore, poly(benzyl ether)s could be selectively depolymerized in the presence of polystyrene or polypropylene and then the monomers could be selectively dissolved, purified by extraction, and then repolymerized.⁵⁴ To the best of our knowledge, in comparison with PEtG, there is no other polymer that has been depolymerized and repolymerized through such a simple process under mild conditions.

To further demonstrate the utility of the ambient depolymerization, **PEtG-NVOC** was investigated as a material for traceless one-step patterning. Metal masks with 500 μm or 20 μm holes were placed over **PEtG-NVOC** films and they were then irradiated with UV light. Over a period of 6 days, the corresponding features appeared in the polymer films without any further intervention or treatment under ambient conditions. Shown in Figure 3.4 are the masks and the optical images of the resulting microscale features. The irradiated areas show holes while the integrity of the surrounding thin film is preserved. These results highlight the possibility of using such an approach for micro or nanofabrication processes. All photopolymers used for standardized micro- (UV lithography) and nano-scale (electron beam lithography) production require a wet chemical processing step for both the developing and lift off steps. With our approach we envision the possibility of reducing the use of developing chemicals for lithography processes. Nevertheless, further work will be needed to investigate and optimize the aspect ratio of the obtained structures and their compatibility with other microfabrication steps. In addition, it would be ideal to increase the rate of pattern formation. This might be achieved by increasing the temperature or using a more volatile glyoxylate such as methyl glyoxylate.

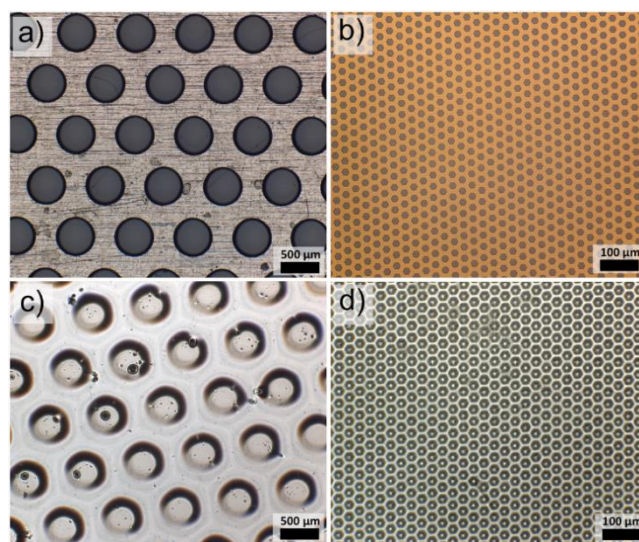


Figure 3.4 Digital optical microscopy of ambient self-developed patterns: The metal masks are shown in a) and b) while the corresponding 500 μm and 20 μm reservoirs fabricated from these masks are shown in c) and d) respectively.

3.4 Conclusions

In conclusion, this study of PEtG depolymerization in the solid state has demonstrated several unique features of PEtG depolymerization that clearly differentiate it from conventional polymer degradation processes. Through studies of the pH dependence, it was shown that the mildly acidic conditions that accelerate backbone cleavage of conventional polyacetals actually slow the depolymerization process as the hemiacetals cleave more readily under neutral conditions. It was also shown that the rapid end-to-end depolymerization combined with the surface erosion mechanism results in an unusual plateau in the mass loss, while the transfer of depolymerization products out of the film catch up with depolymerization. In addition, while the time required for depolymerization depended in a predictable way on temperature and coating thickness, it was not dependent on water, leading to the discovery that after end-cap cleavage, PEtG exhibits a rare ability to undergo depolymerization to volatile products under ambient temperature and pressure. This was demonstrated to offer unique capabilities for the direct reprogramming or recycling of polymers under mild conditions as well as for the preparation of self-developing patternable coatings.

3.5 References

- (1) Tschan, M. J.-L.; Brulé, E.; Haquette, P.; Thomas, C. M. Synthesis of biodegradable polymers from renewable resources. *Polym. Chem.* **2012**, *3*, 836-851.
- (2) Hwang, S.-W.; Song, J.-K.; Huang, X.; Cheng, H.; Kang, S.-K.; Kim, B.-H.; Kim, J.-H.; Yu, S.; Huang, Y.; Rogers, J. A. High-performance biodegradable/transient electronics on biodegradable polymers. *Adv. Mater.* **2014**, *26*, 3905-3911.
- (3) Delplace, V.; Nicolas, J. Degradable vinyl polymers for biomedical applications. *Nat. Chem.* **2015**, *7*, 771-784.
- (4) Tian, H.; Tang, Z.; Zhuang, X.; Chen, X.; Jing, X. Biodegradable synthetic polymers: preparation, functionalization and biomedical application. *Prog. Polym. Sci.* **2012**, *37*, 237-280.
- (5) Yin, Q.; Yin, L.; Wang, H.; Cheng, J. Synthesis and biomedical applications of functional poly(α -hydroxy acids) via ring-opening polymerization of *o*-carboxyanhydrides. *Acc. Chem. Res.* **2015**, *48*, 1777-1787.
- (6) Rwei, A. Y.; Wang, W.; Kohane, D. S. Photoresponsive nanoparticles for drug delivery. *Nano Today* **2015**, *10*, 451-467.
- (7) Gohy, J.-F.; Zhao, Y. Photo-responsive block copolymer micelles: design and behavior. *Chem. Soc. Rev.* **2013**, *42*, 7117.
- (8) Roy, D.; Brooks, W. L.; Summerlin, B. S. New directions in thermoresponsive polymers. *Chem. Soc. Rev.* **2013**, *42*, 7214-7243.
- (9) Binauld, S.; Stenzel, M. H. Acid-degradable polymers for drug delivery: A decade of innovation. *Chem. Commun.* **2013**, *49*, 2082-2012.
- (10) Cohen Stuart, M.; Huck, W. T. S.; Genzer, J.; Muller, M.; Ober, C.; Stamm, M.; Sukhorukov, G. B.; Sziefel, I.; Trukruk, V. V.; Urban, M.; Winnik, F.; Zauscher, S.; Luzinov, I.; Minko, S. Emerging applications of stimuli-responsive polymer materials. *Nat. Mater.* **2010**, *9*, 101-113.
- (11) Schattling, P.; Florian, D. J.; Theato, P. Multi-stimuli responsive polymers—the all-in-one talents. *Polym. Chem.* **2014**, *5*, 25-36.

- (12) Wong, A. D.; DeWit, M. A.; Gillies, E. R. Amplified release through the stimulus triggered degradation of self-immolative oligomers, dendrimers, and linear polymers. *Adv. Drug Delivery Rev.* **2012**, *64*, 1031-1045.
- (13) Phillips, S. T.; DiLauro, A. M. Continuous Head-to-tail depolymerization: an emerging concept for imparting amplified responses to stimuli-responsive materials. *ACS Macro Lett.* **2014**, *3*, 298-304.
- (14) McBride, R. A.; Gillies, E. R. Kinetics of self-immolative degradation in a linear polymeric system: demonstrating the effect of chain length. *Macromolecules* **2013**, *46*, 5157-5166.
- (15) Sagi, A.; Weinstain, R.; Karton, N.; Shabat, D. Self-immolative polymers. *J. Am. Chem. Soc.* **2008**, *130*, 5434-5435.
- (16) DeWit, M. A.; Beaton, A.; Gillies, E. R. A reduction sensitive cascade biodegradable linear polymer. *J. Polym. Sci., Part A: Polym. Chem.* **2010**, *48*, 3977-3985.
- (17) Liu, G.; Wang, X.; Hu, J.; Zhang, G.; Liu, S. Self-immolative polymersomes for high-efficiency triggered release and programmed enzymatic reactions. *J. Am. Chem. Soc.* **2014**, *136*, 7492-7497.
- (18) Liu, G.; Zhang, G.; Hu, J.; Wang, X.; Zhu, M.; Liu, S. Hyperbranched self-immolative polymers (h-SIPs) for programmed payload delivery and ultrasensitive detection. *J. Am. Chem. Soc.* **2015**, *137*, 11645-11655.
- (19) Chen, E. K. Y.; McBride, R. A.; Gillies, E. R. Self-immolative polymers containing rapidly cyclizing spacers: Toward rapid depolymerization rates. *Macromolecules* **2012**, *45*, 7364-7374.
- (20) Olah, M. G.; Robbins, J. S.; Baker, M. S.; Phillips, S. T. End-capped poly(benzyl ethers): acid and base stable polymers that depolymerize rapidly from head-to-tail in response to specific applied signals. *Macromolecules* **2013**, *46*, 5924-5928.
- (21) DiLauro, A. M.; Robbins, J. S.; Phillips, S. T. Reproducible and scalable synthesis of end-cap-functionalized depolymerizable poly(phthalaldehydes). *Macromolecules* **2013**, *46*, 2963-2968.

- (22) DiLauro, A. M.; Lewis, G. G.; Phillips, S. T. Self-immolative poly(4,5-dichlorophthalaldehyde) and its applications in multi-stimuli-responsive macroscopic plastics. *Angew. Chem., Int. Ed.* **2015**, *127*, 6298-6303.
- (23) Fan, B.; Trant, J. F.; Wong, A. D.; Gillies, E. R. Polyglyoxylates: A versatile class of triggerable self-immolative polymers from readily accessible monomers. *J. Am. Chem. Soc.* **2014**, *136*, 10116-10123.
- (24) de Gracia Lux, C.; L. McFearin, C.; Joshi-Barr, S.; Sankaranarayanan, J; Fomina N, Almutairi, A. A Single UV or Near-IR triggering event leads to polymer degradation into small molecules. *ACS Macro Lett.* **2012**, *1*, 922-926.
- (25) Peterson, G. I.; Church, D. C.; , N. A. Y.; Boydston, A. J. 1,2-Oxazine linker as a thermal trigger for self-immolative polymers. *Polymer* **2014**, *09*, 048.
- (26) Zhang, H.; Yeung, K.; Robbins, J. S.; Pavlick, R. A.; Wu, M.; Liu, R.; Sen, A.; Phillips, S. T. Self-powered microscale pumps based on analyte-initiated depolymerization reactions. *Angew. Chem., Int. Ed.* **2012**, *51*, 2400-2404.
- (27) Wong, A. D.; GÜngör, T. M.; Gillies, E. R. Multiresponsive azobenzene end-cap for self-immolative polymers. *ACS Macro Letters* **2014**, *3*, 1191-1195.
- (28) Weinstain, R.; Sagi, A.; Karton, N.; Shabat, D. Self-immolative comb-polymers: Multiple-release of side-reporters by a single stimulus event. *Chem. Eur. J.* **2008**, *14*, 6857-6861.
- (29) Diesendruck, C. E.; Peterson, G. I.; Kulik, H. J.; Kaitz, J. A.; Mar, B. D.; May, P. A.; White, S. R.; Martinez, T. J.; Boydston, A. J.; Moore, J. S. Mechanically triggered heterolytic unzipping of a low-ceiling-temperature polymer. *Nat. Chem.* **2014**, *6*, 623-628.
- (30) Lewis, G. G.; Robbins, J. S.; Phillips, S. T. Phase-switching depolymerizable poly(carbamate) oligomers for signal amplification in quantitative time-based assays. *Macromolecules* **2013**, *46*, 5177-5183.
- (31) Mohapatra, M.; Kim, H.; Phillips, S. T. Stimuli-responsive polymer film that autonomously translates a molecular detection event into a macroscopic change in its optical properties via a continuous, thiol-mediated self-propagating reaction. *J. Am. Chem. Soc.* **2015**, *137*, 12498-12501.

- (32) Kim, H.; Mohapatra, H.; Phillips, S. T. Rapid, On-command debonding of stimuli-responsive cross-linked adhesives by continuous, sequential quinone methide elimination reactions. *Angew. Chem., Int. Ed.* **2015**, *54*, 13063-13067.
- (33) Esser-Kahn, A. P.; Sottos, N. R.; White, S. R.; Moore, J. S. Programmable microcapsules from self-immolative polymers. *J. Am. Chem. Soc.* **2010**, *132*, 10266-10268.
- (34) DiLauro, A. M.; Abbaspourrad, A.; Weitz, D. A.; Phillips, S. T. Stimuli-responsive core-shell microcapsules with tunable rates of release by using a depolymerizable poly(phthalaldehyde) membrane. *Macromolecules* **2013**, *46*, 3309-3313.
- (35) Brachais, C. H.; Huguet, J.; Bunel, C.; Brachais, L. *In Vitro* Degradation of poly(methyl glyoxylate) in water. *Polymer* **1998**, *39*, 883-890.
- (36) Belloncle, B.; Burel, F.; Bunel, C. Synthesis and (bio)degradation of poly(ethyl glyoxylate). *Polym. Prepr.* **2007**, *48*, 633-634.
- (37) Belloncle, B.; Burel, F.; Oulyadi H.; Bunel, C. Study of the *in vitro* degradation of poly(ethyl glyoxylate). *Polym. Deg. Stab.* **2008**, *93*, 1151-1157.
- (38) Funai, T.; Ichiyama, A. High-performance liquid chromatographic determination of glyoxylate in rat liver *J. Biochem.* **1986**, *99*, 579-589.
- (39) Fife, T.; Jao, L. Substituent effects in acetal hydrolysis. *J. Org. Chem.* **1965**, *30*, 1492-1495.
- (40) Przystas, T. J.; Fife, T. H. The mechanism of hemiacetal decomposition, substituent effects in breakdown of substituted benzaldehyde ethyl hemiacetals. *J. Am. Chem. Soc.* **1981**, *103*, 4884-4890.
- (41) Funderburk, L. H.; Aldwin, L.; Jencks, W. P. Mechanisms of general acid and base catalysis of the reactions of water and alcohols with formaldehyde. *J. Am. Chem. Soc.* **1978**, *100*, 5444-5459.
- (42) von Burkersroda, F.; Schedl, L.; Göpferich, A. Why degradable polymers undergo surface erosion or bulk erosion. *Biomaterials* **2002**, *23*, 4221-4231.
- (43) Göpferich, A. Polymer bulk erosion. *Macromolecules* **1997**, *30*, 2598-2604.
- (44) Bowden, M. J.; O'Donnell, J. H. *Developments in Polymer Degradation*, Elsevier: Barking, 1985; Vol. 6, p 21-61.

- (45) Jiang, Y.; Fréchet, J. M. J. Design and synthesis of thermally labile polymers for microelectronics: Poly(vinyl *tert*-butyl carbonate-sulfone). *Macromolecules* **1991**, *24*, 3528-3532.
- (46) Lobez, J. M.; Swager, T. M. Radiation detection: resistivity in functional poly(olefin sulfone)/carbon nanotube composites. *Angew. Chem., Int. Ed.* **2010**, *49*, 95-98.
- (47) Lee, O. P.; Hernandez, H. L.; Moore, J. S. Tunable thermal degradation of poly(vinyl butyl carbonate sulfone)s via side chain branching. *ACS Macro Lett.* **2015**, *4*, 665-668.
- (48) Kumar, K.; Goodwin, A. P. Alternating sulfone copolymers that depolymerize in response to both chemical and mechanical stimuli. *ACS Macro Lett.* **2015**, *4*, 907-911.
- (49) Darensbourg, D. J.; Wei, S.-H. Depolymerization of polycarbonates derived from carbon dioxide and epoxides to provide cyclic carbonates. A kinetic study. *Macromolecules* **2012**, *45*, 5916-5922.
- (50) Darensbourg, D. J.; Wei, S.-H.; Yeung, A. D.; Ellis, W. C. An efficient method of depolymerization of poly(cyclopentene carbonate) to its comonomers: Cyclopentene oxide and carbon dioxide. *Macromolecules* **2013**, *46*, 5850-5855.
- (51) Darensbourg, D. J.; Yeung, A. D.; Wei, S.-H. Base initiated depolymerization of polycarbonates to epoxide and carbon dioxide co-monomers: A computational study. *Green Chem.* **2013**, *15*, 1578-1583.
- (52) Hong, M.; Chen, E. Y.-X. Completely recyclable biopolymers with linear and cyclic topologies via ring-opening polymerization of γ -butyrolactone. *Nat. Chem.* **2016**, *8*, 42-49.
- (53) MacDonald, J. P.; Shaver, M. P. An aromatic/aliphatic polyester prepared via ring-opening polymerisation and its remarkably selective and cycable depolymerisation to monomer. *Polym. Chem.* **2016**, *7*, 553-559.
- (54) Baker, M. S.; Kim, H.; Olah, M. G.; Lewis, G. G.; Phillips, S. T. Depolymerizable poly(benzyl ether)-based materials for selective room temperature recycling. *Green Chem.* **2015**, *17*, 4541-4545.

Chapter 4

4 End-capping strategies for triggering end-to-end depolymerization of polyglyoxylates

The content of this chapter has been published in “B. Fan, J. F. Trant, E. R. Gillies, *Macromolecules*, **2016**, *49*, 9309–9319”

4.1 Introduction

Degradable polymers are of significant interest, both as environmentally-friendly replacements for traditional non-degradable polymers and for wide range of biomedical applications from tissue engineering to drug delivery.¹⁻⁴ Biodegradable polyesters such as poly(lactic acid), poly(glycolic acid), polycaprolactone, and polyhydroxybutyrate have been extensively investigated and show promise in many applications.^{5,6} However, their tendency to undergo slow degradation in a variety of environments is a potential limitation as they may decompose prematurely while still in use or may decompose more slowly than desired in other cases.^{7,8} While their degradation rate can be tuned to some extent based on their chemical structure, molar mass and through formulation adjustments,^{9,10} the ability to “turn on” their degradation at the desired time and place is still quite limited.

Over the past decade, a new class of degradable polymers that depolymerize in an end-to-end manner upon the cleavage of a stimuli-responsive end-cap from the polymer terminus was introduced.¹¹⁻¹⁴ These have often been referred to as “self-immolative” polymers as they were initially inspired by the analogous dendritic structures composed of “self-immolative spacers” that were developed for pro-drug chemistry.¹⁵ Following cleavage of the stabilizing end-cap, the mechanism of depolymerization can involve sequential elimination or cyclization reactions that result in conversion of the polymer to small molecules that are different than the monomers from which they were prepared. Alternatively, it can involve sequential loss of monomer units from the polymer terminus due to the low ceiling temperature of the polymer. Thus far, a number of depolymerizable backbones have been introduced including polycarbamates,^{16,17 18,19} polycarbonates,²⁰ polythiocarbamates,²¹ polythiocarbonates,²⁰ poly(benzyl ether)s²² and polyacetals.²³⁻²⁹

For end-to-end depolymerizable polymers, a single end-cap cleavage reaction is theoretically sufficient to trigger depolymerization of the entire polymer backbone, potentially providing higher sensitivity to stimuli than traditional stimuli-responsive polymers that require many stimuli-mediated events to degrade the backbone. This has made these polymers attractive for a variety of applications and proof-of-concept studies have been performed to demonstrate their potential utility as drug delivery systems,^{18,30-32} molecular sensors,^{16,18,33-36} micropumps,³⁷ responsive films or plastics,^{23,38-40} stimuli-responsive microcapsules,^{41,42} and for simple polymer reprogramming or recycling.^{29,39,43} A key aspect determining the potential of the polymer for a given application is the ability to match the polymer end-cap with suitable triggering conditions that are relevant to that application. For example, end-caps responsive to ultraviolet (UV),⁴⁴ visible,³⁰ and near-infrared (NIR)³¹ light as well as enzymes³² and reducing conditions^{21,30} have been used to trigger release from proof of concept drug delivery systems. End-caps sensitive to fluoride ions have been used in responsive adhesives,³⁸ plastics.^{23,36,40} Furthermore, end-caps responsive to H₂O₂ have been used in sensors.³³⁻³⁵

Polyglyoxylates were reported by our group as a class of end-to-end depolymerizable polymers with attractive features such as ease of synthesis from readily available monomers, depolymerization to non-toxic products,⁴⁵ and the ability to undergo depolymerization in the solid state to volatile products (Figure 4.1).³⁹ In comparison with earlier polyglyoxylates that were not responsive to stimuli,^{46,47} the development of stimuli-responsive polyglyoxylates was made possible through end-capping with chloroformates. This was possible because of the high reactivity of chloroformates, which allows the reaction to be performed at low temperature (-20 °C), below the ceiling temperature of the polyglyoxylate. While this was anticipated to be a versatile end-capping strategy, it was only demonstrated using 6-nitroveratyl chloroformate to afford UV light-responsive polyglyoxylates and benzyl chloroformate to provide analogous non-stimuli-responsive controls.²⁶ In this chapter, using poly(ethyl glyoxylate) (PEtG) we demonstrate that this end-capping strategy can be extended to other end-caps responsive to oxidizing and reducing conditions. In addition, we describe the development of new end-caps responsive to mildly acidic conditions. We further show a versatile design of an end-cap that is

responsive to multiple stimuli, as well as one that enables subsequent cross-linking of the polyglyoxylate to afford a depolymerizable gel. It is also demonstrated that mechanical force can be used to selectively depolymerize high molar mass PEtG.

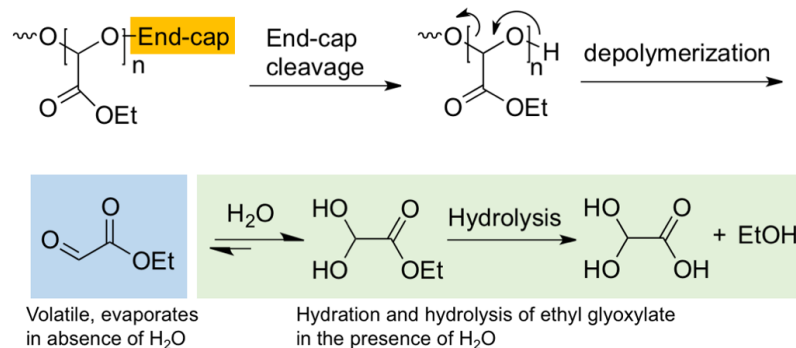


Figure 4.1 Schematic illustrating the end-cap cleavage and depolymerization process for PEtG.

4.2 Experimental section

General procedures and materials. Compounds **2**,⁴⁸ **3**,⁴⁹ **9**,⁵⁰ **12**,⁵¹ **13**⁵² were prepared as previously reported. NEt₃, pyridine, and CH₂Cl₂ were distilled from calcium hydride before use. Anhydrous tetrahydrofuran (THF) was obtained from a solvent purification system using aluminum oxide columns. All the other chemicals were purchased from chemical supplies and used without further purification. ¹H NMR spectra were obtained at 400 MHz or 600 MHz on Varian Inova instruments. NMR chemical shifts (δ) are reported in ppm and are calibrated against residual solvent signals of CDCl₃ (δ 7.27), CD₃CN (δ 1.94), *d*₆-DMSO (δ 2.50) or D₂O (δ 4.75). Fourier transform infrared (FT-IR) spectra were obtained using a Bruker Tensor 27 instrument using thin films of the molecules drop cast from CH₂Cl₂ on KBr plates. High-resolution mass spectrometry (HRMS) was performed using a Finnigan MAT 8400 electron impact (EI) mass spectrometer or Bruker microOTOF 11 electrospray mass spectrometer (ESI). The SEC instrument was equipped with a Viscotek GPC Max VE2001 solvent module. Samples were analyzed using the Viscotek VE3580 RI detector operating at 30 °C. The separation technique employed two Agilent Polypore (300 x 7.5mm) columns connected in series and to a Polypore guard column (50 x 7.5mm). Samples were dissolved in THF (glass distilled grade) at 5.0 mg/mL and filtered through 0.22 μm syringe

filters. Samples were injected using a 100.0 μ L loop. The THF eluent was filtered and eluted at 1.0 mL/min for a total of 30 min. A calibration curve was obtained from poly(methyl methacrylate) (PMMA) standards with molar masses from 1540–1126000 g/mol. Differential scanning calorimetry (DSC) was performed using a Q2000 from TA Instruments (New Castle, DE, USA) and thermogravimetric analysis (TGA) was performed on Q50 from TA Instruments. For TGA the heating rate was 10 $^{\circ}$ C/min between 35–500 $^{\circ}$ C under nitrogen. For DSC, the heating/cooling rate was 10 $^{\circ}$ C/min from -75 to +120 $^{\circ}$ C. Glass transition temperatures (T_g) were obtained from the second heating cycle.

Synthesis of chloroformate 4. 4-(Hydroxymethyl)phenylboronic acid pinacol ester (**1**) (800.0 mg, 3.4 mmol, 1.0 equiv.) was dissolved in THF (7.0 mL). The resulting solution was then added dropwise into a phosgene solution (15 wt% in toluene, 7.5 mL, 10.3 mmol, 3.0 equiv.) under an argon atmosphere at room temperature and was stirred for 24 h. The residual phosgene and solvent were then removed by high vacuum to yield chloroformate **4** (920.0 mg, 91%) as a pale brown liquid. Phosgene collected in the liquid nitrogen-cooled trap was then quenched with methanol (20.0 mL) and saturated sodium hydroxide solution (20 mL) (**Caution! phosgene is toxic**). ^1H NMR (400 MHz, CDCl_3): δ 7.86 (d, J = 8.2 Hz, 2H), 7.39 (d, J = 8.2 Hz, 2H), 5.32 (s, 2H), 1.36 (s, 12H). Spectral data are consistent with published values.⁷⁹

Synthesis of chloroformate 5. Compound **2**⁴⁸ (500.0 mg, 2.7 mmol, 1.0 equiv.) was dissolved in THF (10.0 mL). The resulting solution was then added dropwise into a phosgene solution (15wt% in toluene, 5.8 mL, 8.1 mmol, 3.0 equiv.) under an argon atmosphere at room temperature and the resulting solution was stirred for 24 h. The residual phosgene and solvent were then removed by high vacuum to yield chloroformate **5** (750.0 mg, 98%) as a pale brown solid. Phosgene collected in the liquid nitrogen-cooled trap was then quenched with methanol (20.0 mL) and saturated sodium hydroxide solution (20.0 mL) (**Caution! phosgene is toxic**). ^1H NMR (400 MHz, CDCl_3): δ 8.81 (s, 1H), 8.26 (t, J = 7.0 Hz, 1H), 8.17 (d, J = 8.2 Hz, 1H) 7.69 (t, J = 7.0 Hz, 1H), 4.61 (t, J = 5.9 Hz, 2H), 3.34 (t, J = 5.9 Hz, 2H). ^{13}C NMR (150 MHz, CDCl_3): δ 156.9, 150.5, 145.2, 142.9, 125.0, 123.9, 68.8, 37.8. HRMS (EI) calc'd. for $[\text{M}]^+$ $\text{C}_8\text{H}_8\text{ClNO}_2\text{S}_2$: 248.9685; found: 248.9689.

Synthesis of chloroformate 6. Compound **3**⁸⁰ (230.0 mg, 0.9 mmol, 1.0 equiv.) was dissolved in THF (8.0 mL). The resulting solution was then added dropwise into a phosgene solution (15 wt% in toluene, 1.3 mL, 1.9 mmol, 2.0 equiv.) under an argon atmosphere at room temperature and was stirred for 24 h. The residual phosgene and solvent were then removed by high vacuum to yield chloroformate **6** (255.0 mg, 89%) as a red solid. Phosgene collected in the liquid nitrogen-cooled trap was then quenched with methanol (20.0 mL) and saturated sodium hydroxide solution (20 mL) (**Caution! phosgene is toxic**). ¹H NMR (400 MHz, CDCl₃): δ 8.01 (d, *J* = 8.6 Hz, 2H), 7.72 (dd, *J* = 1.6, 7.8 Hz, 1H), 7.58 (dd, *J* = 1.6, 7.8 Hz, 1H), 7.56 (d, *J* = 8.6 Hz, 2H), 7.33-7.46 (m, 2H), 5.39 (s, 2H). ¹³C NMR (150 MHz, CDCl₃): δ 152.8, 150.4, 148.3, 136.1, 135.4, 131.8, 130.5, 129.2, 127.0, 123.4, 117.3, 72.3. HRMS (EI) calc'd. for [M]⁺ C₁₄H₁₀Cl₂N₂O₂: 308.0120; found: 308.0128.

Synthesis of PEtG-boronate. Ethyl glyoxylate in toluene solution (20.0 mL) was distilled under vacuum (55 °C, 125 mbar) over P₂O₅ to remove toluene and trace water in the first, discarded fraction. The residue was then distilled twice successively over P₂O₅ at atmospheric pressure under argon at 130 °C to obtain the highly pure monomer. Purified ethyl glyoxylate (5.0 mL, 50.0 mmol, 1.0 equiv.) was dissolved in CH₂Cl₂ (5.0 mL) and Et₃N (3.5 μL, 25.0 μmol, 0.0005 equiv.) was added. The solution was stirred for 1 h at -20 °C. Chloroformate **4** (0.2 g, 730.0 μmol, 0.014 equiv.) and Et₃N (100.0 μL, 730.0 μmol, 0.014 equiv.) were added. The solution was allowed to warm to room temperature over a few hours, then stirred overnight. The resulting polymer was purified by precipitation into methanol. After decanting the excess methanol, the residue was dried *in vacuo* to provide 3.3 g of a white, sticky polymer in 63% yield. ¹H NMR (400 MHz, CDCl₃): δ 7.80 (d, *J* = 8.6 Hz, 2H), 7.53 (d, *J* = 8.6 Hz, 2H), 5.46-5.78 (m, 675H), 4.10-4.33 (m, 1367H), 1.34 (s, 12H), 1.21-1.44 (m, 2000H). ¹³C NMR (150 MHz, CDCl₃): δ 164.6-166.5, 90.0-93.9, 61.7, 13.5. IR (KBr, thin film): 2986, 2943, 2908, 1759, 1469, 1446, 1377, 1302, 858, 735, 702 cm⁻¹. SEC: M_n = 131 kg/mol, M_w = 304 kg/mol, Đ = 2.3. T_g = -1 °C.

Synthesis of PEtG-disulfide-a. The procedure and scale described above for the synthesis of PEtG-boronate was used except that chloroformate **5** was used as an end-cap. Yield =

60%. ^1H NMR (400 MHz, CDCl_3): δ 5.48-5.75 (m, 2500H), 4.12-4.33 (m, 5164H), 1.20-1.37 (m, 7624H). ^{13}C NMR (150 MHz, CDCl_3): δ 165.4-166.1, 91.0-94.43, 62.4, 14.2. FT-IR (KBr, thin film): 2986, 2939, 2367, 1765, 1468, 1385, 1302, 1229, 1146, 1020, 966, 8568 cm^{-1} . SEC: $M_n = 250$ kg/mol, $M_w = 425$ kg/mol, $D = 1.7$. $T_g = -7$ °C.

Synthesis of PEtG-disulfide-b. The same procedure described above for the synthesis of **PEtG-disulfide-a** was used except that a different batch of distilled ethyl glyoxylate monomer was used. Yield = 52%. ^1H NMR (400 MHz, CDCl_3): δ 8.56 (s, 3H), 7.93 (s, 4H), 5.44-5.76 (m, 405H), 4.85 (s, 4H), 4.12-4.33 (m, 819H), 3.15 (s, 4H), 1.20-1.37 (m, 1226H). FT-IR (KBr, thin film): 2985, 2942, 1748, 1447, 1376, 1214, 1137, 1016, 959, 856 cm^{-1} . SEC: $M_n = 26$ kg/mol, $M_w = 37$ kg/mol, $D = 1.4$. $T_g = -11$ °C.

Synthesis of PEtG-azobenzene. The procedure and scale described above for the synthesis of **PEtG-boronate** was used except that chloroformate **6** was used as an end-cap. Yield = 63%. ^1H NMR (600 MHz, CDCl_3): δ 7.96 (d, $J = 7.6$ Hz 4H), 7.71 (d, $J = 6.5$ Hz, 2H), 7.53-7.59 (m, 6H), 7.35-7.45 (m, 4H), 5.47-5.76 (m, 524H), 5.29 (s, 4H), 4.09-4.31 (m, 1113H), 1.25-1.42 (m, 1677H). FT-IR (KBr, thin film): 2995, 2948, 1757, 1477, 1384, 1223, 1135, 1020 cm^{-1} . SEC: $M_n = 30$ kg/mol, $M_w = 44$ kg/mol, $D = 1.4$. $T_g = -1$ °C.

Synthesis of PEtG-control. The procedure and scale described above for the synthesis of **PEtG-boronate** was used except that benzyl chloroformate was used as an end-cap. Yield = 58%. ^1H NMR (600 MHz, CDCl_3): δ 7.32-7.41 (m, 10H), 5.48-5.75 (m, 66 3H), 5.20 (s, 4H), 4.07-4.34 (m, 1394H), 1.23-1.45 (m, 2101H). FT-IR (KBr, thin film): 2982, 1762, 1448, 1379, 1020 cm^{-1} . SEC: $M_n = 35$ kg/mol, $M_w = 47$ kg/mol, $D = 1.4$. $T_g = -3$ °C.

Synthesis of PEtG-MMT. Purified ethyl glyoxylate (3.0 mL, 29.7 mmol, 1.0 equiv.) was dissolved in CH_2Cl_2 (3.0 mL) and Et_3N (2.0 μL , 15.0 μmol , 0.0005 equiv.). The solution was stirred for 1 h at -20 °C. 4-Monomethoxytrityl chloride (**7**) (120.0 mg, 375.0 μmol , 0.013 equiv.) and Et_3N (160.0 μL , 1125.0 μmol , 0.037 equiv.) were added at -20 °C to end-cap the polymer. The solution was allowed to warm back to room temperature and stirred for 24 h. Purification was achieved by precipitation of the crude reaction mixture into methanol containing 2 vol% NEt_3 . After decanting the excess methanol, the residue was

dried *in vacuo* for 48 h to provide 1.8 g of a white, sticky polymer. Yield = 58%. ^1H NMR (400 MHz, CDCl_3): δ 7.27-7.56 (m, 22H), 6.77-6.89 (m, 4H), 5.48-5.79 (m, 379H), 4.15-4.39 (m, 762H), 3.67-3.87 (m, 6H), 1.10-1.40 (m, 1150H). FT-IR (KBr, thin film): 2985, 1752, 1447, 1376, 1298, 1216, 1139, 1094, 1018, 963, 856, 734, 702 cm^{-1} . SEC: $M_n = 29$ kg/mol, $M_w = 44$ kg/mol, $D = 1.5$. $T_g = -1$ $^\circ\text{C}$.

Synthesis of PEtG-DMT. The procedure and scale described above for the synthesis of PEtG-MMT was used except that 4,4'-dimethoxytrityl chloride (**8**) was used as an end-cap. Yield = 53%. ^1H NMR (400 MHz, CDCl_3): δ 7.27-7.52 (m, 14H), 7.03-7.19 (m, 4H), 6.74-6.87 (m, 8H), 5.42-5.73 (m, 278H), 4.05-4.41 (m, 573H), 3.67-3.83 (m, 12H), 1.13-1.44 (m, 865H). FT-IR (KBr, thin film): 2985, 2942, 1750, 1468, 1447, 1376, 1298, 1216, 1139, 1095, 1018, 965, 856 cm^{-1} . SEC: $M_n = 21$ kg/mol, $M_w = 27$ kg/mol, $D = 1.3$. $T_g = -10$ $^\circ\text{C}$.

Synthesis of compound 10. Compound **9**⁸³ (1.0 g, 5.9 mmol, 1.0 equiv.) was dissolved in THF (30.0 mL) in a 3-necked round bottom flask. 18.0 mL of saturated Na_2CO_3 solution was then added and the resulting mixture was cooled to 0 $^\circ\text{C}$. Chloroformate **4** (1.8 g, 5.9 mmol, 1.0 equiv.) in 60.0 mL CH_2Cl_2 was added dropwise into the above mixture at the same time as 30.0 mL of saturated Na_2CO_3 solution. After stirring at room temperature for 1 h, the mixture was diluted with 200.0 mL of ethyl acetate. The resulting organic phase was washed with brine once, dried over anhydrous MgSO_4 , filtered and the solvent was removed under reduced pressure. The product was purified by silica gel chromatography using 1:3 ethyl acetate:hexanes as the eluent to yield compound **10** (1.9 g, 76%) as a pale yellow solid. ^1H NMR (600 MHz, CDCl_3): δ 8.25 (d, $J = 8.2$ Hz, 1H), 7.99 (s, 1H), 7.84 (d, $J = 7.6$ Hz, 2H), 7.55 (dd, $J = 1.2$ Hz, 8.2 Hz, 1H), 7.45 (d, $J = 8.2$ Hz, 1H), 7.42 (d, $J = 7.6$ Hz, 2H), 5.25 (s, 2H), 4.77 (s, 2H), 1.36 (s, 12H). ^{13}C NMR (150 MHz, CDCl_3): δ 153.8, 150.4, 140.0, 138.8, 135.4, 135.3, 129.4, 128.0, 127.7, 126.0, 123.0, 118.9, 84.1, 67.6, 57.9, 25.0. HRMS (ESI) calc'd. for $[\text{M}+\text{Na}]^+$ $\text{C}_{21}\text{H}_{25}\text{BN}_2\text{O}_7\text{Na}$: 451.1653; found: 451.1657.

Synthesis of chloroformate 11. Compound **10** (1.8 g, 4.2 mmol, 1.0 equiv.) was dissolved in THF (18.0 mL). The resulting solution was then added dropwise into a phosgene solution (15 wt% in toluene, 9.1 mL, 2.5 mmol, 3.0 equiv.) under an argon atmosphere at room

temperature and was stirred for 24 h. The residual phosgene and solvent were then removed by high vacuum to yield chloroformate **11** (1.9 g, 96%) as a pale yellow solid. Phosgene collected in the liquid nitrogen-cooled trap was then quenched with methanol (20.0 mL) and saturated sodium hydroxide solution (20.0 mL) (**Caution! phosgene is toxic**). ^1H NMR (600 MHz, CDCl_3): δ 8.07 (d, $J = 8.2$ Hz, 1H), 7.84 (d, $J = 7.6$ Hz, 2H), 7.77 (dd, $J = 1.2$ Hz, 8.2 Hz, 1H), 7.58 (t, $J = 8.2$ Hz, 1 H), 7.42 (d, $J = 7.6$ Hz, 2 H), 7.29 (s, 1H), 5.59 (s, 2H), 5.26 (s, 2H), 1.36 (s, 12H). ^{13}C NMR (150 MHz, CDCl_3): δ 153.9, 151.6, 150.9, 139.0, 138.5, 135.3, 131.2, 129.2, 128.4, 127.7, 125.5, 121.4, 84.1, 68.0, 64.5, 25.0. HRMS (ESI) calc'd. for $[\text{M}+\text{Na}]^+$ $\text{C}_{22}\text{H}_{24}\text{BClN}_2\text{O}_8\text{Na}$: 513.1212; found: 513.1207.

Synthesis of PEtG-multi. The procedure and scale described above for the synthesis of **PEtG-boronate** was used except that chloroformate **11** was used as an end-cap. Yield = 50%. ^1H NMR (400 MHz, CDCl_3): δ 7.78-7.84 (m, 2H), 7.65-7.73 (m, 2H), 5.46-5.78 (m, 372H), 5.20-5.32 (m, 4H), 4.10-4.33 (m, 771H), 1.34 (s, 24H), 1.21-1.44 (m, 1199H). FT-IR (KBr, thin film): 2981, 2939, 1754, 1376, 1297, 1140, 1095, 966, 856 cm^{-1} . SEC: $M_n = 41$ kg/mol, $M_w = 66$ kg/mol, $D = 1.6$. $T_g = -4$ °C.

Synthesis of Compound 14. Compound **12**⁸¹ (700.0 mg, 3.6 mmol, 1.0 equiv.) was dissolved in 5:1 CH_2Cl_2 :pyridine (36.0 mL), and then 1-Ethyl-3-(3-dimethylaminopropyl) carbodiimide hydrochloride (EDC·HCl) (814.0 mg, 4.3 mmol, 1.2 equiv.), compound **13**⁸² (3.5 g, 21.3 mmol, 6.0 equiv.), and 4-Dimethylaminopyridine (DMAP) (520 mg, 4.3 mmol, 1.2 equiv.) were added into the stirring mixture under argon. After stirring for 16 h, the reaction mixture was diluted with ethyl acetate (100.0 mL) and washed with saturated Na_2CO_3 solution (1× 50.0 mL), 2 M HCl (3 × 30.0 mL), and brine (1× 30.0 mL) successively. The organic phase was dried over anhydrous MgSO_4 , filtered, and the solvent was then removed under reduced pressure. The product was purified by silica gel chromatography using 2:1 hexane:ethyl acetate as the eluent to yield a pale yellow solid compound **14** (400.0 mg, 33%). ^1H NMR (600 MHz, $\text{DMSO}-d_6$): δ 8.47 (d, $J = 2.4$ Hz, 1H), 8.42 (t, $J = 6.5$ Hz, 1H), 8.20 (dd, $J = 2.4, 8.2$ Hz, 1H), 7.92 (d, $J = 8.2$ Hz, 1 H), 5.90 (m, 3 H), 5.65 (t, $J = 5.3$ Hz, 1H), 5.06 (m, 6H), 4.87 (d, $J = 5.3$ Hz, 2H), 3.26 (d, $J = 6.5$ Hz, 2H), 2.03 (d, $J = 7.6$ Hz, 6H). ^{13}C NMR (150 MHz, $\text{DMSO}-d_6$): δ 165.1, 146.6, 141.3,

134.8, 134.3, 132.5, 128.5, 123.4, 117.9, 60.0, 44.8, 40.3, 39.23. HIMS (EI) calc'd. for $[M]^+C_{19}H_{24}N_2O_4$: 344.1736, $[M-H]^+C_{19}H_{23}N_2O_4$: 343.1663; found: 343.1656.

Synthesis of chloroformate 15. Compound **14** (400.0 mg, 1.2 mmol, 1.0 equiv.) was dissolved in THF (4 mL). The resulting solution was then added dropwise into a phosgene solution (15 wt% in toluene, 1.7 mL, 2.4 mmol, 2.0 equiv.) under an argon atmosphere at room temperature and was stirred for 24 h. The residual phosgene and solvent were then removed by high vacuum to yield chloroformate **15** (450.0 mg, 96%) as a pale yellow solid. Phosgene collected in the liquid nitrogen-cooled trap was then quenched with methanol (20.0 mL) and saturated sodium hydroxide solution (20.0 mL) (**Caution! phosgene is toxic**). 1H NMR (600 MHz, $CDCl_3$): δ 8.52 (d, $J = 1.6$ Hz, 1H), 8.12 (dd, $J = 1.6, 8.2$ Hz, 1H), 7.78 (d, $J = 8.2$ Hz, 1H), 6.53 (s, 1H), 5.95 (m, 3H), 5.80 (s, 2H), 5.21 (m, 6H), 3.47 (d, $J = 6.3$ Hz, 2H), 2.15 (d, $J = 7.4$ Hz, 6H). ^{13}C NMR (150 MHz, $CDCl_3$): δ 163.9, 150.5, 146.9, 136.3, 134.2, 132.7, 132.3, 123.6, 118.6, 68.9, 46.7, 40.4, 29.7. HRMS (EI) calc'd. for $[M]^+C_{20}H_{23}ClN_2O_5$: 406.1296; found: 406.1294.

Synthesis of PEtG-trialkene. The polymer is synthesized using the procedure described above for the synthesis of **PEtG-boronate**, except that chloroformate **15** was used as the end-cap and after the end-cap was added, the solution was kept at -20 °C for 6 h, it was then allowed to reach room temperature and stirred overnight. The polymer was purified by dialysis against 1:1 acetone:methanol using a regenerated cellulose membrane with a molecular weight cut-off of 6000-8000 g/mol. Yield = 25%. 1H NMR (600 MHz, $CDCl_3$): δ 8.52 (s, 2H), 8.08 (d, $J = 9.4$ Hz, 2H), 5.90-5.99 (m, 6H), 5.46-5.78 (m, 168H), 5.14-5.20 (m, 12H) 4.10-4.33 (m, 1367H), 3.75-3.80 (s, 4H), 2.18 (s, 12H), 1.21-1.44 (m, 525H). FT-IR (KBr, thin film): 2980, 2947, 2905, 1746, 1661, 1543, 1462, 1450, 1378, 1213, 1023, 959 cm^{-1} . SEC: $M_n = 11$ kg/mol, $M_w = 19$ kg/mol, $D = 1.7$. $T_g = -7$ °C.

Procedure for the study of PEtG-boronate depolymerization by 1H NMR spectroscopy. **PEtG-boronate** (15.0 mg) was dissolved in a 9:1 $CD_3CN:D_2O$ (1.2 mL). The solution was then divided between two NMR tubes and 4.0 μL of H_2O_2 (50 wt% in water solution) was added to one tube to provide an H_2O_2 concentration of ~ 100 mM. The

tubes were sealed, maintained at ambient temperature (20 °C), and ^1H NMR spectra were obtained at time points over 48 h for both the triggered polymer and the control. At the same time, a non-stimuli-responsive **PEtG-control** with a benzyl carbonate end-cap was also exposed to the same concentration of H_2O_2 following the same procedure as above and its depolymerization was also monitored by ^1H NMR spectroscopy as an additional control. The extent of depolymerization was calculated as: % Depolymerization = $100 - \frac{\text{integration of the peak at 5.5 ppm}}{\text{integration of the peak at 4.2 ppm}} \times 100$, which remained constant as it corresponds to the $\text{CH}_3\text{CH}_2\text{-O-}$ in both the polymer and the depolymerization products.

Procedure for the study of PEtG-disulfide-a and PEtG-azobenzene depolymerization by ^1H NMR spectroscopy. Polymer (15.0 mg) was dissolved in a 9:1 mixture of $\text{CD}_3\text{CN}:\text{D}_2\text{O}$ (1.2 mL). The solution was then divided between two NMR tubes and dithiothreitol (DTT) (10.0 mg, 6.4 μmol) was added to one tube (final DTT concentration ~ 110 mM) to initiate the removal of the end-cap, then the tubes were promptly sealed and maintained at ambient temperature (20 °C). ^1H NMR spectra were obtained at defined time points to monitor the depolymerization. At the same time, a non-stimuli-responsive **PEtG-control** with a benzyl carbonate end-cap was also exposed to the same concentration of DTT following the same procedure as above and its depolymerization was also monitored by ^1H NMR spectroscopy.

Procedure for the study of PEtG-MMT and PEtG-DMT depolymerization by ^1H NMR spectroscopy. Polymer was dissolved in a 9:1 mixture of $\text{CD}_3\text{CN}:\text{D}_2\text{O}$ to achieve a concentration of 7.0 mg/mL of polymer. The solution was then transferred into NMR tubes (0.6 mL/tube). For 170 mM, 340 mM, and 510 mM concentration of acetic acid, 10.0 μL , 20.0 μL and 30.0 μL of acetic acid were added respectively. Then all the tubes were promptly sealed and maintained at ambient temperature (20 °C). ^1H NMR spectra were obtained at defined time points to monitor the depolymerization.

Study of PEtG-multi depolymerization in solution. Polymer (35.0 mg) was dissolved in a 9:1 mixture of $\text{CD}_3\text{CN}:\text{D}_2\text{O}$ (3.0 mL) at ambient temperature (20 °C). The solution was

then divided between five NMR tubes (0.6 mL/tube). One tube was irradiated in an ACE Glass photochemistry cabinet containing a mercury light source (450 W bulb, 2.8 mW/cm² measured for UVA radiation at the sample position) for 20 min and then 4.0 μ L of H₂O₂ (50 wt% in water solution) was also added to the same tube (final H₂O₂ concentration \sim 100 mM). One tube was just irradiated by the same UV lamp for 20 min. One tube only received 4.0 μ L of H₂O₂ (50 wt% in water solution). To one tube were added zinc powder (250 mM) and acetic acid (700 mM). To one tube no stimuli were added. The tubes were promptly sealed and maintained at ambient temperature (20 °C). ¹H NMR spectra were obtained at defined time points to monitor the depolymerization.

Cross-linking of PEG-trialkene. PEG-trialkene (20.0 mg, 1.8 μ mol, 1.0 equiv.) was dissolved in 0.5 mL of toluene, then 3.0 mg of the thiol cross-linker **16** (6.1 μ mol, 3.4 equiv.) followed by 2.0 mg of 2,2'-azobis(2-methylpropionitrile) (AIBN) (8 wt.%) were added. The reaction vial was sealed and then the mixture was then stored in an oven at 60 °C for 2 days, resulting in the formation of a gel.

Determination of the gel content of PEG-cross-linked. PEG-cross-linked was immersed in 10.0 mL CH₂Cl₂, stirred for 10 min, then centrifuged to separate the gel from solution. The solution was decanted. This procedure was conducted 3 times to completely remove any uncross-linked polymer and small molecules. After drying the gel, the gel content was calculated as: (mass of material after washing)/ (mass of dry material prior to washing) *100% = 72%.

Triggered depolymerization of PEG-cross-linked. 7.0 mg of PEG-cross-linked was immersed in 0.6 mL of 9:1 CD₃CN:D₂O in a glass vial equipped with a magnetic stir bar. The vial was sealed, then irradiated in an ACE Glass photochemistry cabinet containing a mercury light source (450 W bulb, 2.8 mW/cm² measured for UVA radiation at the sample position) for 5 h with continuous stirring. After removing the sample from the light source a ¹H NMR spectrum was obtained.

Mechanically triggered depolymerization of PEG. 60.0 mg PEG-disulfide-a and PEG-disulfide-b were each dissolved separately in 60.0 mL of THF. Each solution was

then equally divided between 6 different glass test tubes. The tubes were treated with pulsed ultrasound (Branson 450 Digital Sonifier equipped with a 3.18 mm probe tip diameter, operating at an amplitude of 50%, 8 W, pulse cycle: 1 s on, 0.5 s off) for different time periods from 5 min to 60 min in a bath at -20 °C. Following sonication, the solution was concentrated 5-fold and then analyzed by SEC.

Mechanically triggered depolymerization of PEtG in the presence of TBDMS-Cl. 40 mg of **PEtG-disulfide-a** was dissolved in 40.0 mL of THF (distilled in glass) to prepare a 1.0 mg/mL polymer solution, then *tert*-butyldimethylsilyl chloride (TBDMS-Cl) (12.0 mg, 0.08 mmol, 500.0 equiv. relative to polymer) and pyridine (6.8 μ L, 0.08 mmol, 500.0 equiv. to polymer) were added. The polymer solution was then equally divided between 4 glass test tubes. The tubes were treated with pulsed ultrasound as described above for different time periods from 5 min to 20 min in a bath at -20 °C. Following sonication, the solution was concentrated 5-fold and then analyzed by SEC.

4.3 Results and discussion

4.3.1 Development of redox-responsive PEtG

Polymer systems that respond to oxidizing or reducing conditions have been actively sought for the past several years due to the practical interest in these stimuli.⁵³⁻⁵⁵ For example, increased concentrations of the reducing agent glutathione are associated with the intracellular environment as well as with hypoxic tumor tissue, potentially allowing drug molecules to be selectively released from reduction-sensitive polymers in these environments.^{56,57} Reactive oxygen species are also associated with a wide range of pathologies including inflammation and tissue injury.⁵⁸ While end-to-end depolymerization has previously been initiated by these stimuli,^{21,30,33-35} oxidation- and reduction-sensitive PEtGs were sought as initial targets to explore the versatility of the chloroformate end-capping strategy for PEtG and the response of PEtG to these stimuli.

A phenylboronic acid pinacol ester was selected as the H₂O₂-sensitive end-cap.⁵⁹ As shown in Figure 4.2a, in the presence of H₂O₂ this end-cap undergoes cleavage to the corresponding phenol, which can then undergo a 1,6-elimination followed by loss of CO₂,

releasing the PEtG hemiacetal terminus and triggering depolymerization. The thiol-responsive pyridyl disulfide was selected based on its well-established sensitivity to reduction by thiols as well as its successful use as an end-cap for end-to-end depolymerizable polycarbonates and poly(carbamate-thiocarbamate)s.⁶⁰ Reductive cleavage of the disulfide reveals a thiol that can subsequently cyclize to form either a cyclic thiocarbonate (Figure 4.2b) or a thiirane ring followed by loss of CO₂, releasing the PEtG terminus.⁶¹ Finally, an azobenzene moiety was also explored as a reduction-sensitive end-cap. Recent work from our group has shown that the reduction of azobenzene end-caps with hydrazine can trigger end-to-end depolymerization of polycarbonates⁶² while the reduction of azobenzene pendant groups can trigger backbone cleavage of poly(ester amide)s.⁴⁹ Studies on small molecule model compounds suggested that the reduction should also be possible with thiols, but this was not explicitly demonstrated for the polymers.⁶² As shown in Figure 4.2c, reduction leads an electron-rich hydrazobenzene that can undergo a 1,6-elimination, followed by loss of CO₂ to release the polymer terminus.

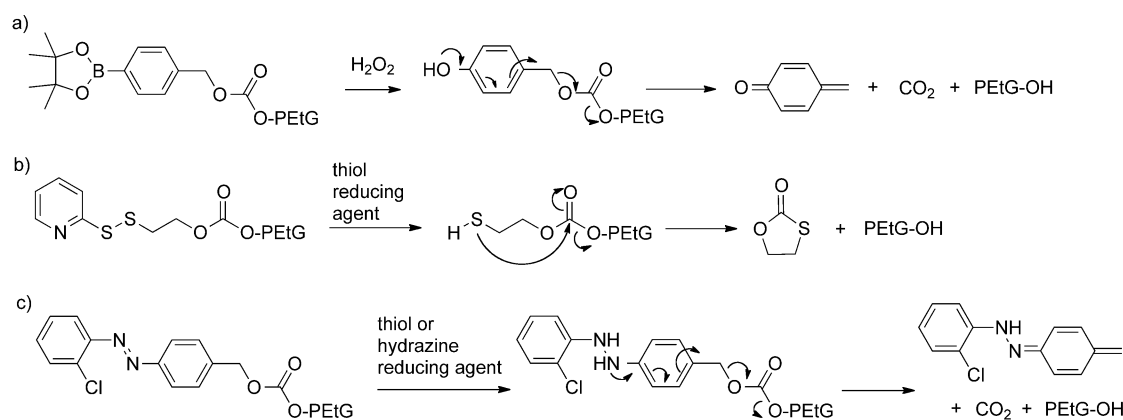
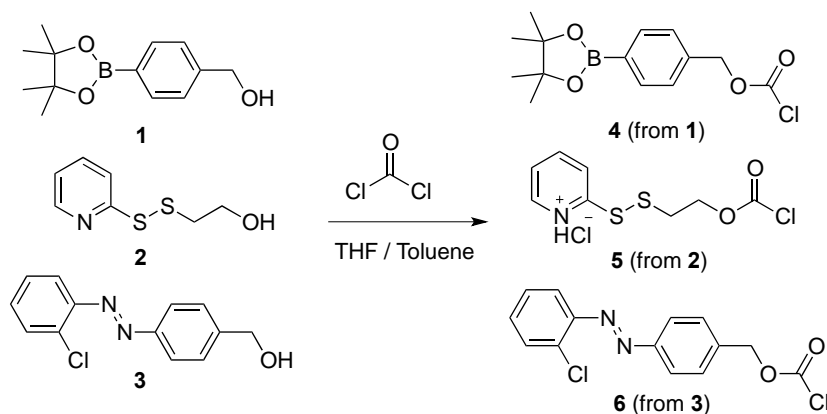


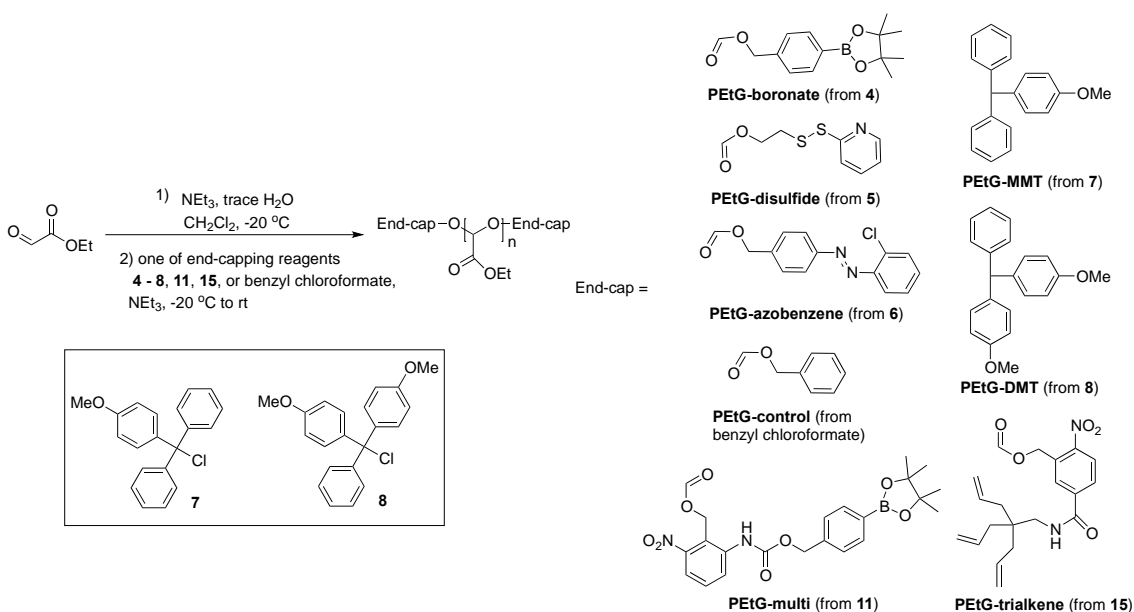
Figure 4.2 Proposed triggering mechanisms for redox-responsive PEtG end-caps.

As shown in Scheme 4.1, alcohol derivatives of the boronate (**1**), disulfide (**2**)⁴⁸ and azobenzene (**3**)⁶² were reacted with phosgene in THF/toluene to afford the corresponding chloroformates **4** - **6**. The disulfide end-cap was isolated as its HCl salt. Polymerization of freshly distilled ethyl glyoxylate was initiated by the addition of NEt₃ and was conducted at -20 °C as previously reported (Scheme 4.2).²⁶ The resulting PEtG was end-capped *in situ* by the addition of the chloroformate and additional NEt₃ at -20 °C and the reaction was

allowed to reach ambient temperature and stirred overnight, affording **PEtG-boronate**, **PEtG-disulfide**, and **PEtG-azobenzene** from chloroformates **4**, **5**, and **6** respectively. In addition to the chloroformates **4** - **6**, benzyl chloroformate was used to provide a non-responsive control carbonate end-capped PEtG (**PEtG-control**) as previously reported.²⁶



Scheme 4.1 Synthesis of chloroformate end-caps **4** - **6**.



Scheme 4.2 Synthesis and end-capping of PEtG.

The end-capped polymers were characterized by size exclusion chromatography (SEC), NMR spectroscopy, and thermal analysis. As shown in Table 4.1, based on SEC the number

average molar masses (M_n) of these polymers ranged from 24 kg/mol to 250 kg/mol and their dispersities (D) ranged from 1.3-2.3. The variation in M_n between the different polymers likely results from the strong dependency of M_n on the purity of monomer prepared for a given polymerization as the polymerization is believed to be initiated by adventitious water or ethyl glyoxylate hydrate (EtGH) that is present in the distilled monomer. Although it is in principle possible to initiate the ethyl glyoxylate polymerization from an alkoxide or *n*-butyllithium this has not yet been successful. NMR spectroscopy showed very small peaks consistent with the presence of the appropriate end-caps on the polymers, however, given the high degrees of polymerization (DP) suggested by the SEC analyses (Table 4.1), these peaks were challenging to detect and accurately integrate, so DP was not estimated by NMR spectroscopy. It was previously demonstrated that TGA provides an excellent indicator of successful end-capping as uncapped polymer is thermally unstable and depolymerizes below 100 °C in the solid state.²⁶ Even fractions of uncapped polymer can be detected. As shown in Table 4.1 and Figures A4.43, based on TGA the polymers had onset degradation temperatures (T_o) from 183 to 255 °C, confirming that they were well end-capped. In addition, through the preparation and analysis of two different batches of **PEtG-disulfide (a and b)** with a ~10-fold difference in M_n , it was confirmed that the PEtG molar mass did not have a significant effect on its thermal stability. Based on DSC, the T_g values were very similar for the different end-capped PEtGs, ranging from -7 to -1 °C.

Table 4.1 Molar mass and thermal properties of end-capped PEtGs and measured by SEC, TGA, and DSC.

Polymer	M_n (SEC) (kg/mol)	Dispersity (D)	T_o (°C)	T_g (°C)
PEtG-boronate	131	2.3	226	-1
PEtG-disulfide-a	250	1.7	183	-7
PEtG-disulfide-b	26	1.4	191	-7
PEtG-azobenzene	30	1.4	255	-1
PEtG-control	35	1.4	247	-3
PEtG-DMT	21	1.3	131	-10

PEtG-MMT	29	1.5	168	-1
PEtG-multi	41	1.6	164	-4
PEtG-trialkene	11	1.7	225	-7
PEtG-crosslinked	N/A	N/A	191	5

The depolymerization of the redox-responsive polymers and **PEtG-control** was then studied in the presence and absence of the corresponding stimuli. PEtG is not soluble in water, but it was possible to dissolve the polymers in 9:1 CD₃CN:D₂O in order to study the depolymerization by ¹H NMR spectroscopy. First, the response of **PEtG-boronate** to H₂O₂ was studied. Prior to the addition of H₂O₂, the ¹H NMR spectrum had three broad peaks corresponding to the protons on the PEtG backbone and pendant ester groups (Figure 4.3a). However, following the addition of H₂O₂, the broad peak at 5.5 ppm corresponding to the acetal hydrogens along the polymer backbone rapidly decreased in intensity while two new sharp peaks at 5.3 ppm and 5.1 ppm emerged. The sharp peak at 5.1 ppm can be assigned to the depolymerization product EtGH as described previously.²⁶ The new peak at 5.3 ppm can be attributed to a peroxy hydrate of ethyl glyoxylate due to the increased nucleophilicity of H₂O₂ compared to water due to the α -effect.⁶³ The same product could be formed by the direct addition of ethyl glyoxylate into the above depolymerization conditions, and was fully characterized by ¹H and ¹³C NMR spectroscopy and high resolution mass spectrometry (Figures A4.23-A4.25). A sharpening of the peaks corresponding to the ethyl group was also consistent with depolymerization to small molecules.

The percent depolymerization, defined as the percentage of the monomer released as small molecule from the polymer, versus time for **PEtG-boronate** is Figure 4.3b. It was noted that depolymerization was more rapid than previously observed following the cleavage of the UV light-sensitive 6-nitroveratryl end-cap from our previous work.²⁶ For example, 80% depolymerization had occurred in 10 min for **PEtG-boronate**, while 70% was observed after 24 h for the previous system. This difference can likely be attributed to the rapid trapping of the ethyl glyoxylate depolymerization product as the peroxy hydrate. However, the drawback of this trapping reaction is that high concentrations of H₂O₂ (~100 mM for ~0.1 mM of polymer) were required in order to achieve complete depolymerization, whereas

lower concentrations led to a plateau in the depolymerization percentage as peroxide that was removed through hydrate formation was no longer available to cleave the end-cap. The required equivalents of H_2O_2 was similar to the DP based on SEC analysis (~ 1000). Control experiments showed that in the absence of H_2O_2 , **PEtG-boronate** was stable, undergoing less than 3% depolymerization over 3 days in 9:1 $\text{CD}_3\text{CN}:\text{D}_2\text{O}$ (Figure 4.3b and A4.29a). Furthermore, **PEtG-control** did not undergo any detectable depolymerization when treated with 100 mM H_2O_2 under the same conditions for 7 days (Figure 4.3b and A4.29b). These results confirm the specificity of H_2O_2 for end-cap cleavage rather than random backbone cleavage or side reactions, even at high concentrations.

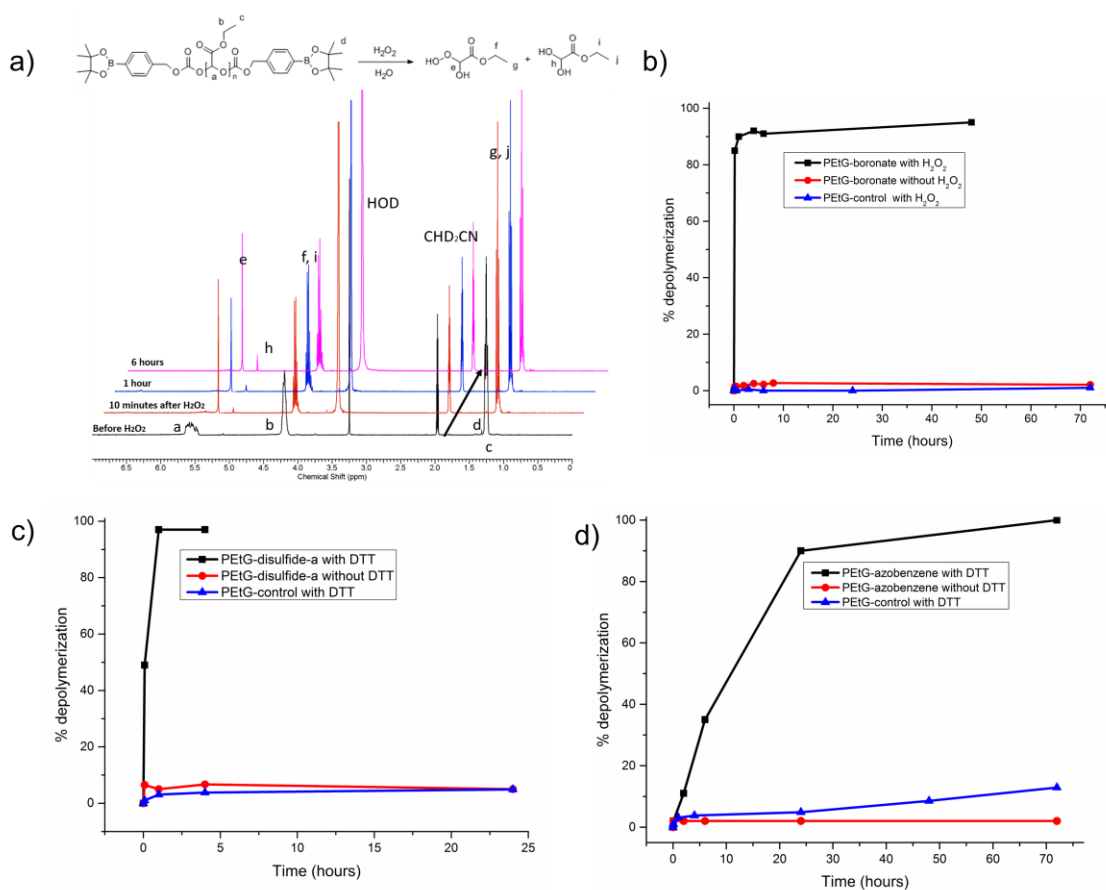


Figure 4.3 a) ^1H NMR spectra of PEtG-boronate in 9:1 $\text{CD}_3\text{CN}:\text{D}_2\text{O}$ before addition of H_2O_2 and at various time points after H_2O_2 addition (spectra are offset to allow the progression over time to be clearly observed); **b-d)** Percent depolymerization versus time in the presence and absence of stimuli for **b)** PEtG-boronate with H_2O_2 , **c)** PEtG-

disulfide-a with DTT, and d) PEtG-azobenzene with DTT. In each case, PEtG-control was also exposed to the stimulus to confirm that the cleavage was specific to the end-cap.

The same procedure was used to study the depolymerization of **PEtG-disulfide-a**, except that the reducing agent dithiothreitol (DTT) was used instead of H₂O₂. As shown in Figure 3c, depolymerization occurred rapidly following DTT addition, with more than 95% depolymerization observed over 1 h. Like H₂O₂, DTT is also a strong nucleophile, and reacted rapidly with ethyl glyoxylate (Figure A4.26-A4.28), resulting in the requirement for high (~110 mM) concentrations of DTT in order to achieve complete end-cap cleavage and depolymerization. **PEtG-disulfide** without DTT and **PEtG-control** in the presence of 110 mM DTT underwent only ~5% depolymerization over 24 h (Figure 4.3c and A4.30-31), again showing that DTT could selectively trigger depolymerization through end-cap cleavage.

Hydrazine was initially investigated as a trigger for **PEtG-azobenzene** as it was successfully used as a trigger in our previous work.⁶² When 100 mM hydrazine was added to **PEtG-azobenzene** in 9:1 CD₃CN:D₂O solution, rapid depolymerization was observed. However, these conditions also resulted in complete depolymerization of **PEtG-control**, suggesting that hydrazine was capable of inducing non-specific cleavage of the terminal carbonate or the pendant esters, which could subsequently trigger backbone cleavage and depolymerization.⁶⁴ With preliminary data suggesting that a thiol-based reduction may be possible,⁶² DTT was investigated as a trigger. As shown in Figures 4.3d and A4.32, 110 mM DTT could indeed induce depolymerization of **PEtG-azobenzene**, albeit at a slower rate than that of **PEtG-disulfide**. For example, ~35% depolymerization was observed after 6 h, whereas more than 95% of **PEtG-disulfide** was depolymerized in the 1 h. Complete depolymerization required ~3 days, suggesting that end-cap cleavage was the rate-limiting step in this process. In the absence of DTT only ~2% depolymerization of **PEtG-azobenzene** was observed over 3 days (Figure 4.3d and A4.33) and ~14% of **PEtG-control** depolymerized over this time period in the presence of 110 mM DTT (Figure 4.3d and A4.31b). This suggests that high concentrations of DTT can induce non-specific backbone

or terminal carbonate cleavage reactions over a period of days. Thus, the azobenzene moiety provides an additional reduction-sensitive end-cap with slower cleavage kinetics that may be useful for some applications, but it is not as selective a trigger as the boronate or carbonate.

4.3.2 Development of acid-responsive PEtG

In addition to reductive and oxidative stimuli, change in pH is a stimulus of significant interest for a number of applications. For example, tumor tissue, as well as the endosomes and lysosome of cells are well known to have mildly acid pHs (e.g., pH 5-7) relative to the normal neutral physiological pH of 7.4, thereby providing a potential mechanism for selectively releasing therapies in these locations.^{55,65} To the best of our knowledge, the use of mildly acidic conditions to trigger end-to-end depolymerization has not yet been reported. Alcohol protecting groups that are sensitive to mildly acidic conditions provide an ideal starting point for the development of acid-sensitive end-caps and our studies began by investigating linkages such as acetals that have been widely exploited in the context of stimuli-responsive polymers.⁶⁶⁻⁶⁸ However, the direct end-capping of PEtG with acetal precursors such as vinyl ethers was unsuccessful and the insertion of spacers that would enable chloroformate preparation resulted in poor initiation of the depolymerization due to the requirement for a subsequent slow cyclization of a hydroxyl nucleophile to release the PEtG hemiacetal terminus. In addition, the formation of chloroformates was particularly challenging in the presence of acid-sensitive moieties.

Fortunately, it was found that triphenylmethyl (trityl) chlorides could be used to directly end-cap PEtG under the same conditions described above. As shown in Scheme 4.3, the use of monomethoxytrityl chloride (**7**) and dimethoxytrityl chloride (**8**) as end-capping reagents led to **PEtG-MMT** and **PEtG-DMT** respectively. Both of these terminal triphenylmethyl ethers are commonly used as acid-labile protecting groups in organic synthesis.⁶⁹ As shown in Table 4.1, **PEtG-MMT** and **PEtG-DMT** had M_n values of 29 and 21 kg/mol and D value of 1.5 and 1.3 respectively. ¹H NMR spectroscopic data were consistent with the incorporation of the end-caps at the PEtG terminus (Figures A4.11, A4.12). TGA confirmed complete end-capping, but while **PEtG-MMT** had a T_o of ~168

°C, **PEtG-DMT** had a T_o of only ~131 °C, which is much lower than all of the other end-capped PEtGs. Analysis of **8** suggested that this can be attributed to the relatively poor thermal stability of the end-cap itself as **8** undergoes degradation with a T_o of 78 °C (Figure A4.45). This T_o is enhanced by ~50°C through its incorporation via an ether linkage at the polymer terminus.

The acid triggered depolymerizations of **PEtG-MMT** and **PEtG-DMT** were studied in 9:1 CD₃CN:D₂O. Normally it is ideal to adjust the pH using buffers, but the high acetonitrile content of the solvent mixture makes buffer salts insoluble, so instead varying concentrations of acetic acid were added to the CD₃CN:D₂O solutions of the polymers. As shown in Figure A4.4a, **PEtG-MMT** undergoes end-cap cleavage and complete depolymerization over ~48 days in the presence of 510 mM acetic acid, and with a slightly slower rate in 340 mM acetic acid. In the absence of acetic acid only ~18% depolymerization was observed over this time period. Furthermore, the addition of 510 mM acetic acid to **PEtG-control** did not lead to any significant depolymerization over 48 days. These results are consistent with our recent studies on PEtG coatings where it was found that nonirradiated PEtG with a UV light-responsive end-cap was highly stable at pH 3 for weeks³⁹. Although PEtG is a polyacetal, these acetals are not sensitive to mildly acidic conditions as the adjacent electron-withdrawing ester groups make them less susceptible to acidic cleavage in comparison with other polyacetals and polyketals.^{66,67,70,71}

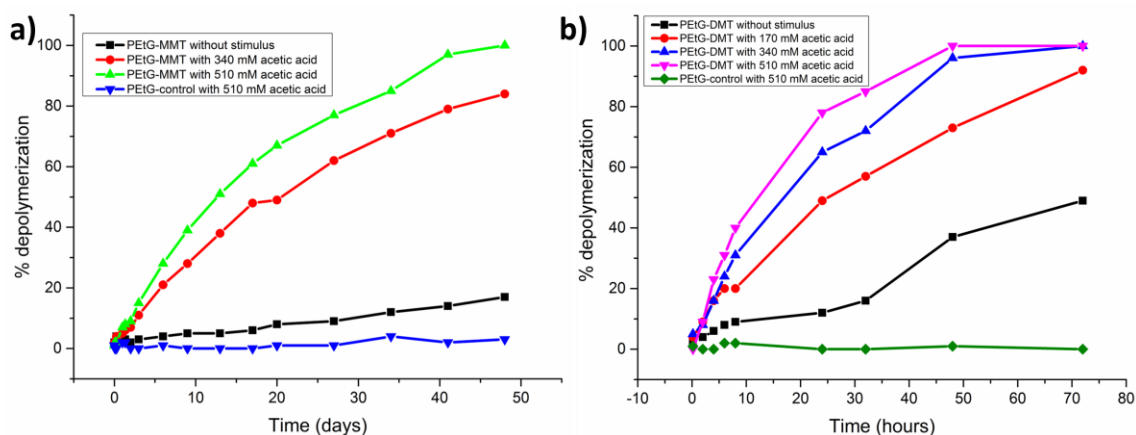


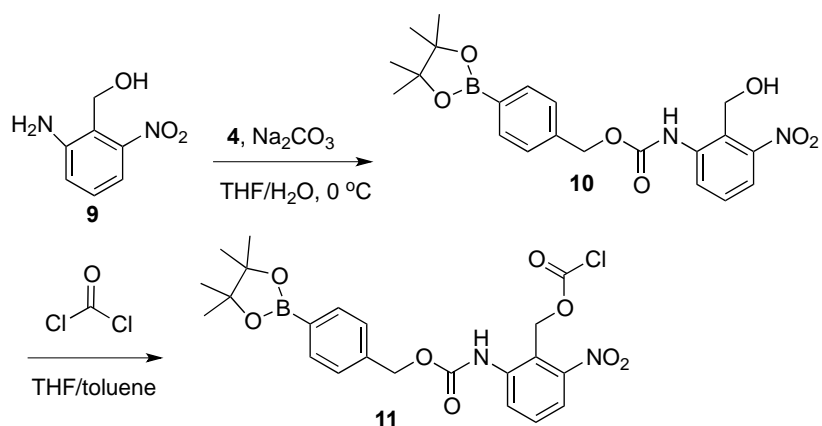
Figure 4.4 Percent depolymerization versus time for a) PEtG-MMT and b) PEtG-DMT in the absence and presence of varying concentrations of acetic acid.

The presence of two methoxy groups in the end-cap of PEtG-DMT was expected to lead to more rapid cleavage and subsequent depolymerization under acidic conditions and indeed this was the case. As shown in Figure 4.4b, complete end-cap cleavage and depolymerization occurred over only 2 days in the presence of 340 mM or 510 mM acetic acid and with a slightly slower rate in the presence of 170 mM acetic acid. However, ~50% depolymerization also occurred for PEtG-DMT without added acetic acid. This observation is characteristic of the typical trade-off with pH-sensitive groups where faster cleavage at mildly acidic pH is commonly accompanied by faster cleavage under neutral conditions. Nevertheless, the results show that pH-sensitive PEtGs can indeed be prepared and that the rate of triggering can be tuned by altering the chemical structure of the end-cap.

4.3.3 Development of a multi-responsive end-cap

While the above work demonstrates that diverse stimuli can be used to trigger PEtG depolymerization, for some applications of PEtG or other end-to-end-depolymerizable polymers, it may be beneficial to develop a versatile end-capping strategy that allows the polymer to respond to multiple stimuli, either individually or simultaneously. To prepare an end-cap responsive to multiple stimuli, the previously reported compound **9**⁵⁰ was reacted with chloroformate **4** in the presence of Na₂CO₃ in THF/H₂O at 0 °C to

functionalize the aniline group selectively, affording compound **10**. The benzylic alcohol of **10** was then reacted with phosgene to provide the chloroformate-activated end-cap **11**. The *o*-nitrobenzyl moiety on this end-cap provides sensitivity to UV light,⁷² but also to the presence of Zn/acetic acid⁷³ (Scheme A4.1). At the same time, the phenylboronic acid pinacol ester is responsive to H₂O₂. After fragmentation via the mechanism shown in Figure 4.2a, the resulting aniline can undergo a 1,4-elimination to release the PEtG, triggering depolymerization (Scheme A4.1). In addition, using this simple synthetic route, it should be possible to replace chloroformate **4** with other chloroformates such as **5** and **6**, such that this route can be used to prepare PEtG responsive to UV light, Zn/acetic acid and one other stimulus, provided a chloroformate responsive to that stimulus can be prepared. Chloroformate **11** was used to cap PEtG as described above (Scheme 4.2), providing **PEtG-multi**, having an M_n of 41 kg/mol and *D* of 1.6 (Table 4.1). TGA confirmed that the polymer had been well end-capped and that its thermal properties were similar to those of other PEtGs.



Scheme 4.3 Synthesis of multi-responsive end-cap **11**.

The depolymerization behaviour of this multi-responsive PEtG was also studied in the presence and absence of the relevant stimuli in 9:1 CD₃CN:D₂O. As shown in Figure 4.5, irradiation of **PEtG-multi** for 20 min with UV light followed by incubation in the solvent mixture resulted in ~50% depolymerization over 2 days. The addition of 100 mM H₂O₂ alone led to slightly more rapid depolymerization, and the combination treatment of 20 min of UV light irradiation and 130 mM H₂O₂ appeared to result in even slightly faster

depolymerization. However, when replicate runs were performed, it was determined that these three samples were not significantly different given the standard deviations on the measurements. While the result using UV light as a stimulus is similar to that observed for previously reported polyglyoxylates with a photoresponsive 6-nitroveratryl end-cap,²⁶ the rate of depolymerization using H₂O₂ is significantly slower for **PEtG-multi** than that observed for **PEtG-boronate** (Figure 4.3b). Following oxidative cleavage of the phenylboronic acid pinacol ester in **PEtG-multi** by H₂O₂, the molecule must undergo a 1,6-elimination, loss of CO₂, 1,4-elimination, and finally a second loss of CO₂ prior to the release of the hemiacetal-terminated PEtG for depolymerization (Scheme A4.1). On the other hand, **PEtG-boronate** only requires a single sequence of 1,6-elimination and loss of CO₂. While such elimination reactions can be very rapid under fully aqueous conditions, as the solvent polarity is decreased (such as through addition of CD₃CN), these reactions are known to be significantly slowed and may limit the rate of complete end-cap cleavage and thus the overall depolymerization rate of **PEtG-multi**.^{62,74} Another possible explanation is that the reactive quinone methides or azaquinone methides generated upon end-cap fragmentation can be trapped by the hydroxyl terminus of depolymerizing PEtG (Scheme A4.2). This would generate benzyl ether-capped polymers that can still undergo elimination to continue depolymerization, but at a slower rate. This would explain the initial rapid phase of depolymerization, followed by the slower phase of depolymerization.

The addition of Zn (250 mM) and acetic acid (700 mM), conditions previously reported for triggering dendrimer degradation⁷³ afforded ~80% depolymerization within 6 h. A control experiment where **PEtG-multi** was not exposed to any stimuli showed that less than 5% depolymerization occurred over 8 days. Furthermore, **PEtG-control** also underwent less than 5% depolymerization when exposed to Zn (250 mM) and acetic acid (700 mM) over the same time period. Control experiments described above and previously reported²⁶ have already confirmed the stability of **PEtG-control** in the presence of UV light and H₂O₂. Overall, these results demonstrate that PEtG can be designed to respond to multiple different stimuli through careful engineering of the end-cap, but that the requirement for multiple sequential reactions can slow the initiation of depolymerization.

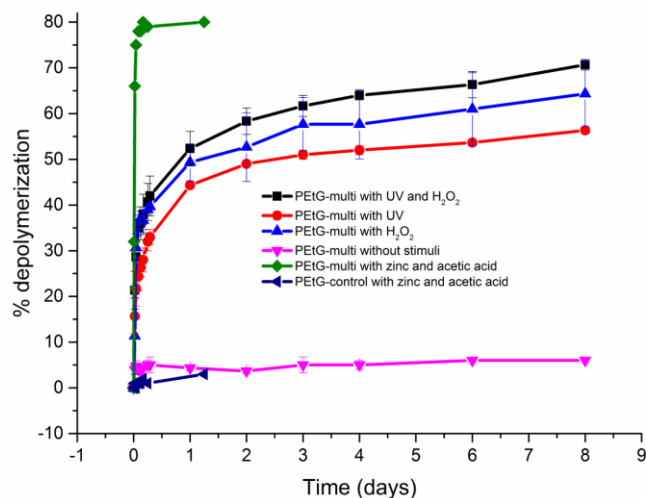
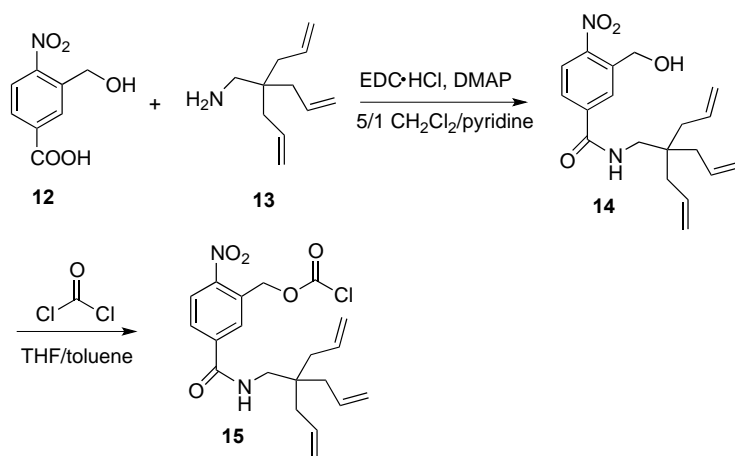


Figure 4.5 Depolymerization versus time for PETG-multi following exposure to UV light, H₂O₂, Zn/acetic acid, and combinations of these stimuli.

4.3.4 Development of a cross-linkable end-cap

Polyglyoxylates are of significant interest as coating materials as they undergo depolymerization through a surface erosion mechanism with the depolymerization time tunable based on the coating thickness.³⁹ In order to cure the coating and tune its physical properties, it was desirable to develop a curing process for the polymer. Thus, an end-cap that would allow for cross-linking was sought. Thiol-ene reactions have been extensively used to prepare cross-linked polymer networks in recent years,^{75,76} so it was envisioned that an end-cap bearing a stimuli-responsive moiety as well as multiple alkenes would be ideal for subsequent cross-linking using a multivalent thiol. Synthesis of the end-cap began from the previously reported benzoic acid derivative **12**⁵¹ and amine **13**,⁵² which were coupled using *N*-(3-dimethylaminopropyl)-*N'*-ethylcarbodiimide hydrochloride (EDC·HCl) in the presence of 4-(dimethylamino)pyridine (DMAP) to afford the amide **14**. This amide was then activated using phosgene in THF/toluene to provide the chloroformate **15** (Scheme 4.4). PETG was synthesized and end-capped using **15** as described above to afford **PEtG-trialkene** (Scheme 4.2) with the slight modification that due to the sterically bulky nature of this end-cap it was necessary to keep the end-capping conditions at -20 °C for 6

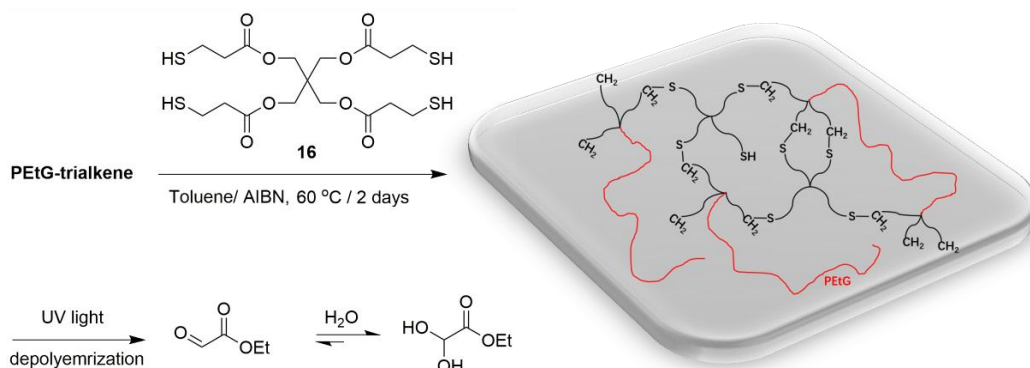
h instead immediately allowing the solution to gradually warm to room temperature. This ensured that the polymer had sufficient time to be end-capped at $-20\text{ }^{\circ}\text{C}$ as it would otherwise depolymerize when warmed to room temperature. The M_n of **PEtG-trialkene** was 11 kg/mol ($\mathcal{D} = 1.7$), which is lower than that of the other polymers. However, thermal analyses showed that it was well end-capped and had a T_g similar to that of the other PEtGs.



Scheme 4.4 Synthesis of cross-linkable end-cap **15**.

The cross-linking of **PEtG-trialkene** was performed using (pentaerythritol tetrakis(3-mercaptopropionate)) (**16**) in toluene at $60\text{ }^{\circ}\text{C}$ using 2,2'-azobis(2-methylpropionitrile) (AIBN) as an initiator to provide **PEtG-cross-linked** (Scheme 4.5). After the reaction, unreacted polymer and small molecules were removed by extracting the gel 3 times with CH_2Cl_2 . The resulting gel content was 72%. Infrared spectroscopy was used to confirm the reaction, as the peak at 1660 cm^{-1} corresponding to the $\text{C}=\text{C}$ stretch of the alkene almost entirely disappeared after cross-linking (Figure A4.50). In addition, the cross-linking resulted in an increase in the T_g from $-7\text{ }^{\circ}\text{C}$ for **PEtG-trialkene** to $5\text{ }^{\circ}\text{C}$ for **PEtG-cross-linked**. The end-cap of **PEtG-trialkene** contains an *o*-nitrobenzyl moiety enabling it to respond to UV light irradiation, so the depolymerization of the network in response to UV light was explored. The network **PEtG-cross-linked** was immersed in 9:1 $\text{CD}_3\text{CN}:\text{D}_2\text{O}$, then irradiated with UV light (2.8 mW/cm^2). Prior to irradiation, only peaks corresponding to CD_2HCN and DOH were observed in the ^1H NMR spectrum, as the network was completely insoluble. After 5 h of UV irradiation, although the network had not yet completely solubilized, peaks corresponding to the expected depolymerization product EtGH were clearly observed, confirming that depolymerization of the network could be

triggered (Figure 4.6). Thus, PEtG can be both incorporated into polymer networks to tune its properties and can also be depolymerized within network structures. It is anticipated that the structure and properties of the cross-linked networks can be optimized for different applications by varying the structure and ratio of the thiol cross-linking agent.



Scheme 4.5 Cross-linking of PEtG-trialkene and UV light triggered depolymerization of the resulting PEtG-cross-linked.

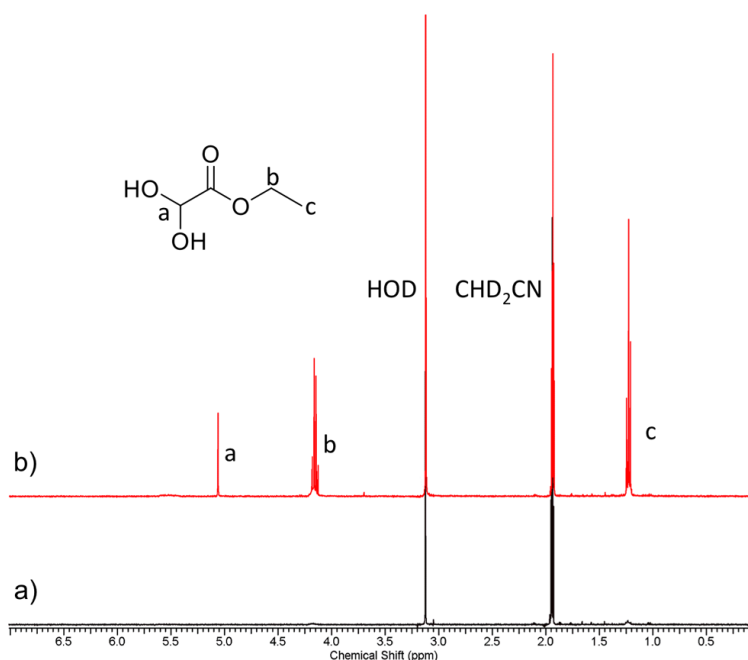


Figure 4.6 ¹H NMR spectrum (400 MHz, 9:1 CD₃CN:D₂O) of PEtG-cross-linked a) before and b) after UV irradiation. Note that peaks corresponding to derivatized

cross-linker 16 are not visible because assuming a 1:1 ratio of PEtG:16 in the network, there would be >100 EtGH molecules per derivatized 16.

4.3.5 Mechanically triggered depolymerization of PEtG

It was recently demonstrated that high molar mass poly(*o*-phthalaldehyde) could be cleaved by the mechanical force induced by ultrasound.²⁹ Unlike the conventional polymer control poly(methyl acrylate), that simply underwent chain scission to produce lower molar mass polymers, chain cleavage of poly(*o*-phthalaldehyde) induced end-to-end depolymerization resulting in the conversion of polymers to monomers. Although not technically an end-capping strategy, we sought to determine whether this mechanism of chain scission would also apply to high molar mass PEtG.

In order to evaluate this, the response of high molar mass **PEtG-disulfide-a** ($M_n = 250$ kg/mol) and lower molar mass **PEtG-disulfide-b** ($M_n = 26$ kg/mol) to ultrasound was studied and compared. Dilute (1 mg/mL) solutions of the polymers in THF were prepared in order to avoid polymer chain entanglement and then pulsed ultrasound was applied at -20 °C (1 s on, 0.5 s off). The solutions were removed at various time points and analyzed by SEC. After 5 min, the M_n of **PEtG-disulfide-a** had decreased from 250 kg/mol to 113 kg/mol (Figure 4.7a and c). With additional sonication over 60 min the molar mass continued to decrease to 46 kg/mol and the intensity of the refractive index (RI) signal in SEC decreased to almost baseline values suggesting that the polymer had almost completely depolymerized. Over this time period, the reduction in M_n and RI signal intensity arose from the continual cleavage of high molar mass polymers by ultrasound in addition to the depolymerization of these cleaved chains to small molecules. On the other hand, neither the molar mass or RI signal intensity in SEC changed for **PEtG-disulfide-b** over 60 min of pulses ultrasound (Figure 4.7b and c). This is consistent with the previously reported molecular weight threshold of 30 kg/mol for polystyrene chain cleavage by ultrasonication.⁸⁴

Unlike most mechanically induced chain scissions that involve the generation of macroradicals,⁸⁵ poly(*o*-phthalaldehyde) was demonstrated by trapping experiments to

undergo heterolytic bond cleavage prior to depolymerization²⁹. Because PEtG also has a polyacetal backbone, it was proposed to follow a similar mechanism. To confirm this, ultrasound was applied to PEtG-disulfide-a, as described above, but in the presence of *tert*-butyldimethylsilyl chloride, an electrophilic trapping agent capable of reacting with the nucleophilic terminus of heterolytically cleaved PEtG. Depolymerization was significantly slowed in comparison to without the trapping agent, suggesting that a heterolytic cleavage mechanism also applied to PEtG (Figure A4.53 and A4.54).

These results confirm that mechanical triggering with ultrasound is an additional stimulus that can be applied to initiate the depolymerization of PEtG. This should apply to PEtG with any end-cap, provided the molar mass is sufficiently high. Ultrasound is of particular interest for biomedical applications as ultrasonic radiation is routinely applied for medical imaging and there has been substantial interest in the development of drug delivery systems that are responsive to ultrasound.^{77,78}

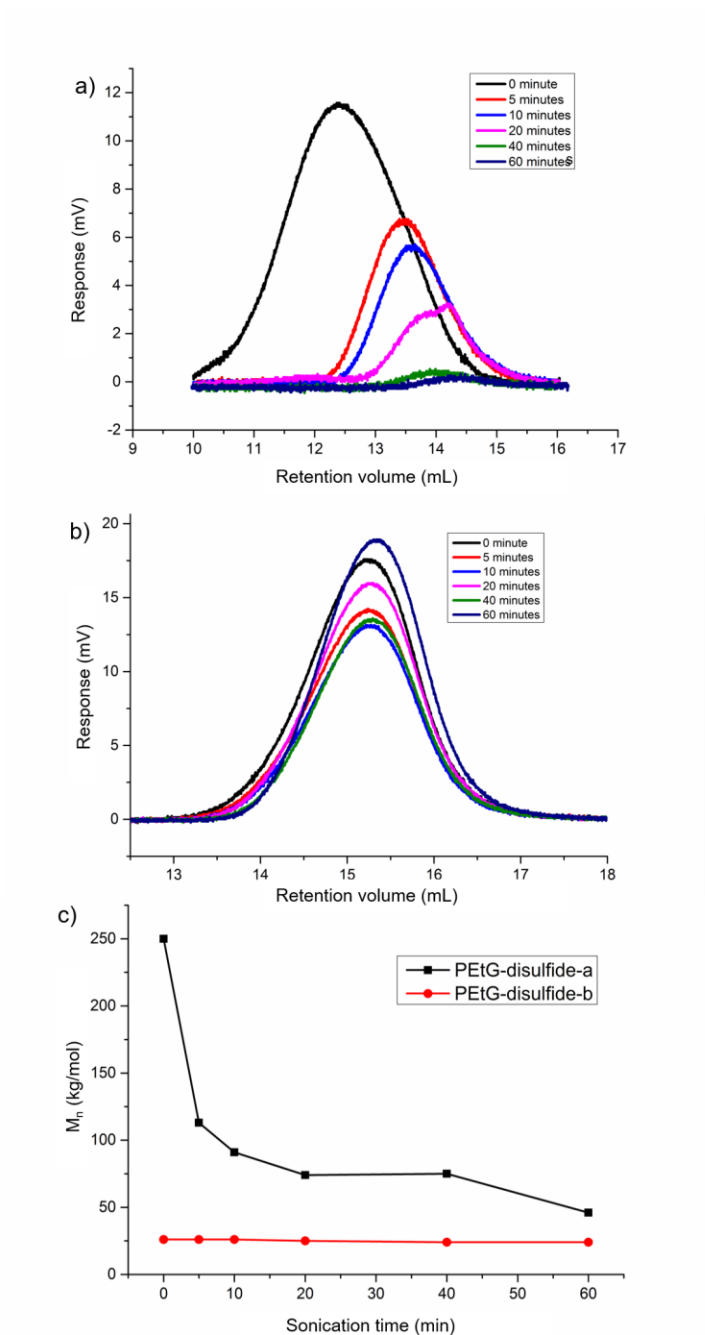


Figure 4.7 a-b) SEC traces (RI detection) for a) PETG-disulfide-a and b) PETG-disulfide-b following different sonication times; c) Changes in M_n for PETG-disulfide-a and PETG-disulfide-b following different sonication times.

4.4 Conclusions

It was demonstrated that a phenylboronic acid pinacol ester, disulfide, and azobenzene could be converted into chloroformates and used to end-cap PEG. This allowed PEG to undergo depolymerization in response to H_2O_2 and DTT, while the non-responsive **PEG-control** was very stable under these conditions. Relatively high concentrations of H_2O_2 and DTT were required due to the partial trapping of these nucleophilic stimuli by the depolymerization product ethyl glyoxylate. It is possible that this drawback will be mitigated in fully aqueous conditions, where water will be present at 10-fold higher concentration than in 9:1 $\text{CD}_3\text{CN}:\text{D}_2\text{O}$, but testing this will require the synthesis of water-soluble polyglyoxylates or water-dispersible block copolymers. It was also shown that acid-sensitive end-caps could be introduced to PEG by endcapping with triphenylmethylchlorides and that the sensitivity to acid could be tuned by adjusting the number of electron donating methoxy substituents on the phenyl ring. Next, a new end-cap that was responsive to multiple stimuli including UV light, H_2O_2 , and Zn/acetic acid was developed. It is envisioned that the backbone and synthetic method for this molecule can be applied to introduce other stimuli-responsive groups, providing a versatile strategy towards multi-responsive end-caps for end-to-end depolymerizable polymers. Furthermore, it was demonstrated that a cross-linkable trialkene could be incorporated into a photo-responsive end-cap, allowing cross-linked networks of PEG to be formed. Finally, the backbone of high molar mass PEG could also be cleaved mechanically, thereby initiating depolymerization. Overall, these new end-caps significantly expand the utility of PEG, by expanding the available stimuli from UV light to many other conditions, some of which are relevant to the physiological environments associated with disease states such as cancer and inflammation. It is also anticipated that these end-caps and triggering mechanisms will be useful for the growing field of stimuli-responsive backbone cleavable and end-to-end depolymerizable materials. Current work is focused on the incorporation of these triggering mechanisms into PEG block copolymers and the study of their assemblies in aqueous solution.

4.5 References

- (1) Tschan, M. J.-L.; Brulé, E.; Haquette, P.; Thomas, C. M. Synthesis of biodegradable polymers from renewable resources. *Polym. Chem.* **2012**, *3*, 836-851.
- (2) Hwang, S. W.; Song, J. K.; Huang, X.; Cheng, H.; Kang, S. K.; Kim, B. H.; Kim, J. H.; Yu, S.; Huang, Y.; Rogers, J. A. High-performance biodegradable/transient electronics on biodegradable polymers. *Adv. Mater.* **2014**, *26*, 3905-3911.
- (3) Siracusa, V.; Rocculi, P.; Romani, S.; Dalla Rosa, M. Biodegradable polymers for food packaging: A review. *Trends Food Sci. Tec.* **2008**, *19*, 634-643.
- (4) Nicolas, J.; Mura, S.; Brambilla, D.; Mackiewicz, N.; Couvreur, P. Design, functionalization strategies and biomedical applications of targeted biodegradable/biocompatible polymer-based nanocarriers for drug delivery. *Chem. Soc. Rev.* **2013**, *42*, 1147-1235.
- (5) Woodruff, M. A.; Hutmacher, D. W. The return of a forgotten polymer-polycaprolactone in the 21st century. *Prog. Polym. Sci.* **2010**, *35*, 1217-1256.
- (6) Anderson, J. M.; Shive, M. S. Biodegradation and biocompatibility of PLA and PLGA microspheres. *Adv. Drug Delivery Rev.* **2012**, *64*, 72-82.
- (7) Pitt, G.; Gratzl, M.; Kimmel, G.; Surles, J.; Sohindler, A. Aliphatic polyesters II. The degradation of poly(D,L-lactide), poly(ϵ -caprolactone), and their copolymers *in vivo*. *Biomaterials* **1981**, *2*, 215-220.
- (8) Li, S. Hydrolytic degradation characteristics of aliphatic polyesters derived from lactic and glycolic acids. *J. Biomed. Mater. Res.* **1999**, *48*, 342-353.
- (9) Hakkarainen, M.; Höglund, A.; Odelius, K.; Albertsson, A.-C. Tuning the release rate of acidic degradation products through macromolecular design of caprolactone-based copolymers. *J. Am. Chem. Soc.* **2007**, *129*, 6308-6312.
- (10) Källrot, M.; Edlund, U.; Albertsson, A.-C. Covalent grafting of poly(L-lactide) to tune the *in vitro* degradation rate. *Biomacromolecules* **2007**, *8*, 2492-2496.
- (11) Roth, M. E.; Green, O.; Gnaim, S.; Shabat, D. Dendritic, oligomeric, and polymeric self-immolative molecular amplification. *Chem. Rev.* **2015**, *116*, 1309-1352.
- (12) Fan, B.; Gillies, E. R. Self-immolative polymers. *Encycl. Polym. Sci. Technol.* **2015**, 1-35.

- (13) Phillips, S. T.; DiLauro, A. M. Continuous Head-to-tail depolymerization: An emerging concept for imparting amplified responses to stimuli-responsive materials. *ACS Macro Lett.* **2014**, *3*, 298-304.
- (14) Wong, A. D.; DeWit, M. A.; Gillies, E. R. Amplified release through the stimulus triggered degradation of self-immolative oligomers, dendrimers, and linear polymers. *Adv. Drug Delivery Rev.* **2012**, *64*, 1031-1045.
- (15) Alouane, A.; Labruere, R.; Le Saux, T.; Schmidt, F.; Jullien, L. Self-immolative spacers: Kinetic aspects, structure-property relationships, and applications. *Angew. Chem., Int. Ed.* **2015**, *54*, 7492-7509.
- (16) Sagi, A.; Weinstain, R.; Karton, N.; Shabat, D. Self-immolative polymers. *J. Am. Chem. Soc.* **2008**, *130*, 5434-5435.
- (17) DeWit, M. A.; Gillies, E. R. A cascade biodegradable polymer based on alternating cyclization and elimination reactions. *J. Am. Chem. Soc.* **2009**, *131*, 18327-18334.
- (18) Liu, G.; Zhang, G.; Hu, J.; Wang, X.; Zhu, M.; Liu, S. Hyperbranched self-immolative polymers (h-SIPs) for programmed payload delivery and ultrasensitive detection. *J. Am. Chem. Soc.* **2015**, *137*, 11645-11655.
- (19) McBride, R. A.; Gillies, E. R. Kinetics of self-immolative degradation in a linear polymeric system: demonstrating the effect of chain length. *Macromolecules* **2013**, *46*, 5157-5166.
- (20) Chen, E. K.; McBride, R. A.; Gillies, E. R. Self-immolative polymers containing rapidly cyclizing spacers: Toward rapid depolymerization rates. *Macromolecules* **2012**, *45*, 7364-7374.
- (21) DeWit, M. A.; Beaton, A.; Gillies, E. R. A reduction sensitive cascade biodegradable linear polymer. *J. Polym. Sci., Part A: Polym. Chem.* **2010**, *48*, 3977-3985.
- (22) Olah, M. G.; Robbins, J. S.; Baker, M. S.; Phillips, S. T. End-capped poly(benzyl ethers): Acid and base stable polymers that depolymerize rapidly from head-to-tail in response to specific applied signals. *Macromolecules* **2013**, *46*, 5924-5928.
- (23) Seo, W.; Phillips, S. T. Patterned plastics that change physical structure in response to applied chemical signals. *J. Am. Chem. Soc.* **2010**, *132*, 9234-9235.
- (24) DiLauro, A. M.; Robbins, J. S.; Phillips, S. T. Reproducible and scalable synthesis of

end-cap-functionalized depolymerizable poly(phthalaldehydes). *Macromolecules* **2013**, *46*, 2963-2968.

(25) DiLauro, A. M.; Lewis, G. G.; Phillips, S. T. Self-immolative poly(4,5-dichlorophthalaldehyde) and its applications in multi-stimuli-responsive macroscopic plastics. *Angew. Chem., Int. Ed.* **2015**, *127*, 6298-6303.

(26) Fan, B.; Trant, J. F.; Wong, A. D.; Gillies, E. R. Polyglyoxylates: A versatile class of triggerable self-immolative polymers from readily accessible monomers. *J. Am. Chem. Soc.* **2014**, *136*, 10116-10123.

(27) Kaitz, J. A.; Moore, J. S. Functional phthalaldehyde polymers by copolymerization with substituted benzaldehydes. *Macromolecules* **2013**, *46*, 608-612.

(28) Kaitz, J. A.; Moore, J. S. Copolymerization of *o*-phthalaldehyde and ethyl glyoxylate: Cyclic macromolecules with alternating sequence and tunable thermal properties. *Macromolecules* **2014**, *47*, 5509-5513.

(29) Diesendruck, C. E.; Peterson, G. I.; Kulik, H. J.; Kaitz, J. A.; Mar, B. D.; May, P. A.; White, S. R.; Martínez, T. J.; Boydston, A. J.; Moore, J. S. Mechanically triggered heterolytic unzipping of a low-ceiling-temperature polymer. *Nat. Chem.* **2014**, *6*.

(30) Liu, G.; Wang, X.; Hu, J.; Zhang, G.; Liu, S. Self-immolative polymersomes for high-efficiency triggered release and programmed enzymatic reactions. *J. Am. Chem. Soc.* **2014**, *136*, 7492-7497.

(31) de Gracia Lux, C.; McFearin, C. L.; Joshi-Barr, S.; Sankaranarayanan, J.; Fomina, N.; Almutairi, A. Single UV or near-IR triggering event leads to polymer degradation into small molecules. *ACS Macro Lett.* **2012**, *1*, 922-926.

(32) Li, Y.; Liu, G.; Wang, X.; Hu, J.; Liu, S. Enzyme-responsive polymeric vesicles for bacterial-strain-selective delivery of antimicrobial agents. *Angew. Chem., Int. Ed.* **2016**, *128*, 1792-1796.

(33) Lewis, G. G.; Robbins, J. S.; Phillips, S. T. Point-of-care assay platform for quantifying active enzymes to femtomolar levels using measurements of time as the readout. *Anal. Chem.* **2013**, *85*, 10432-10439.

(34) Lewis, G. G.; Robbins, J. S.; Phillips, S. T. Phase-switching depolymerizable poly(carbamate) oligomers for signal amplification in quantitative time-based assays.

Macromolecules **2013**, *46*, 5177-5183.

(35) Lewis, G. G.; Robbins, J. S.; Phillips, S. T. A prototype point-of-use assay for measuring heavy metal contamination in water using time as a quantitative readout. *Chem. Commun.* **2014**, *50*, 5352-5354.

(36) Yeung, K.; Kim, H.; Mohapatra, H.; Phillips, S. T. Surface-accessible detection units in self-immolative polymers enable translation of selective molecular detection events into amplified responses in macroscopic, solid-state plastics. *J. Am. Chem. Soc.* **2015**, *137*, 5324-5327.

(37) Zhang, H.; Yeung, K.; Robbins, J. S.; Pavlick, R. A.; Wu, M.; Liu, R.; Sen, A.; Phillips, S. T. Self-powered microscale pumps based on analyte-initiated depolymerization reactions. *Angew. Chem., Int. Ed.* **2012**, *51*, 2400-2404.

(38) Kim, H.; Mohapatra, H.; Phillips, S. T. Rapid, on-command debonding of stimuli-responsive cross-linked adhesives by continuous, sequential quinone methide elimination reactions. *Angew. Chem., Int. Ed.* **2015**, *54*, 13063-13067.

(39) Fan, B.; Trant, J. F.; Yardley, R. E.; Pickering, A. J.; Laguné-Labarthe, F.; Gillies, E. R. Photocontrolled degradation of stimuli-responsive poly(ethyl glyoxylate): Differentiating features and traceless ambient depolymerization. *Macromolecules* **2016**.

(40) Kim, H.; Baker, M. S.; Phillips, S. T. Polymeric materials that convert local fleeting signals into global macroscopic responses. *Chem. Sci.* **2015**, *6*, 3388-3392.

(41) Esser-Kahn, A. P.; Sottos, N. R.; White, S. R.; Moore, J. S. Programmable microcapsules from self-immolative polymers. *J. Am. Chem. Soc.* **2010**, *132*, 10266-10268.

(42) DiLauro, A. M.; Abbaspourrad, A.; Weitz, D. A.; Phillips, S. T. Stimuli-responsive core-shell microcapsules with tunable rates of release by using a depolymerizable poly(phthalaldehyde) membrane. *Macromolecules* **2013**, *46*, 3309-3313.

(43) Baker, M. S.; Kim, H.; Olah, M. G.; Lewis, G. G.; Phillips, S. T. Depolymerizable poly(benzyl ether)-based materials for selective room temperature recycling. *Green Chem.* **2015**, *17*, 4541-4545.

(44) Brasch, M.; Voets, I. K.; Koay, M. S.; Cornelissen, J. J. Phototriggered cargo release from virus-like assemblies. *Faraday Discuss.* **2013**, *166*, 47-57.

(45) Belloncle, B.; Bunel, C.; Menu-Bouaouiche, L.; Lesouhaitier, O.; Burel, F. Study of

the degradation of poly(ethyl glyoxylate): biodegradation, toxicity and ecotoxicity Assays. *J. Polym. Environ.* **2012**, *20*, 726-731.

(46) Brachais, C.; Huguet, J.; Bunel, C. Synthesis, characterization and stabilization of poly(methyl glyoxylate). *Polymer* **1997**, *38*, 4959-4964.

(47) Brachais, C.; Huguet, J.; Bunel, C.; Brachais, L. *in vitro* degradation of poly(methyl glyoxylate) in water. *Polymer* **1998**, *39*, 883-890.

(48) Henne, W. A.; Kularatne, S. A.; Ayala-López, W.; Doorneweerd, D. D.; Stinnette, T. W.; Lu, Y.; Low, P. S. Synthesis and activity of folate conjugated didemnin B for potential treatment of inflammatory diseases. *Bioorg. Med. Chem. Lett.* **2012**, *22*, 709-712.

(49) Wong, A. D.; Prinzen, A. L.; Gillies, E. R. Poly(ester amide)s with pendant azobenzenes: multi-responsive self-immolative moieties for modulating polymer assemblies. *Polym. Chem.* **2016**, *7*, 1871-1881.

(50) Ida, Y.; Matsubara, A.; Nemoto, T.; Saito, M.; Hirayama, S.; Fujii, H.; Nagase, H. Synthesis of quinolinomorphinan derivatives as highly selective δ -opioid receptor ligands. *Bioorg. Med. Chem.* **2012**, *20*, 5810-5831.

(51) Aujard, I.; Benbrahim, C.; Gouget, M.; Ruel, O.; Baudin, J. B.; Neveu, P.; Jullien, L. *o*-Nitrobenzyl photolabile protecting groups with red-shifted absorption: syntheses and uncaging cross-sections for one-and two-photon excitation. *Chem. Eur. J.* **2006**, *12*, 6865-6879.

(52) Wood, M. C.; Leitch, D. C.; Yeung, C. S.; Kozak, J. A.; Schafer, L. L. Chiral neutral zirconium amidate complexes for the asymmetric hydroamination of alkenes. *Angew. Chem., Int. Ed.* **2007**, *46*, 354-358.

(53) Huo, M.; Yuan, J.; Tao, L.; Wei, Y. Redox-responsive polymers for drug delivery: from molecular design to applications. *Polym. Chem.* **2014**, *5*, 1519-1528.

(54) Lallana, E.; Tirelli, N. Oxidation-responsive polymers: which groups to use, how to make them, what to expect from them (biomedical applications). *Macromol. Chem. Phys.* **2013**, *214*, 143-158.

(55) Mura, S.; Nicolas, J.; Couvreur, P. Stimuli-responsive nanocarriers for drug delivery. *Nat. Mater.* **2013**, *12*, 991-1003.

(56) Saito, G.; Swanson, J. A.; Lee, K. D. Drug delivery strategy utilizing conjugation via

reversible disulfide linkages: role and site of cellular reducing activities. *Adv. Drug Delivery Rev.* **2003**, *55*, 199-215.

(57) Kuppusamy, P.; Li, H.; Ilangovan, G.; Cardounel, A. J.; Zweier, J. L.; Yamada, K.; Krishna, M. C.; Mitchell, J. B. Noninvasive imaging of tumor redox status and its modification by tissue glutathione levels. *Cancer Res.* **2002**, *62*, 307-312.

(58) Gough, D. R.; Cotter, T. G. Hydrogen peroxide: A jekyll and hyde signalling molecule. *Cell Death Dis.* **2011**, *2*, e213.

(59) Lo, L.-C.; Chu, C.-Y. Development of highly selective and sensitive probes for hydrogen peroxide. *Chem. Commun.* **2003**, 2728-2729.

(60) Dewit, M. A.; Beaton, A.; Gillies, E. R. A reduction sensitive cascade biodegradable linear polymer. *J. Polym. Sci., Part A: Poly. Chem.* **2010**, *48*, 3977-3985.

(61) Jain, A. K.; Machhindra, G. G.; Desai, D. C.; Borhade, N.; Senthilkumar, S. P.; Dhiman, M.; Mangu, N. K.; Mali, S. V.; Dubash, N. P.; Halder, S.; Satyam, A. Mutual prodrugs containing bio-cleavable and drug releasable disulfide linkers. *Bioorg. Chem.* **2013**, *49*, 40-48.

(62) Wong, A. D.; GÜngör, T. M.; Gillies, E. R. Multiresponsive azobenzene end-cap for self-immolative polymers. *ACS Macro Lett.* **2014**, *3*, 1191-1195.

(63) Fina, N. J.; Edwards, J. O. The alpha effect. A review. *Int. J. Chem. Kinet.* **1973**, *5*, 1-26.

(64) Olejniczak, J.; Huu, V. A. N.; Lux, J.; Grossman, M.; He, S.; Almutairi, A. Light-triggered chemical amplification to accelerate degradation and release from polymeric particles. *Chem. Commun.* **2015**, *51*, 16980-16983.

(65) Liu, J.; Huang, Y.; Kumar, A.; Tan, A.; Jin, S.; Mozhi, A.; Liang, X. J. pH-Sensitive nano-systems for drug delivery in cancer therapy. *Biotechnol. Adv.* **2014**, *32*, 693-710.

(66) Hefferman, M. J.; Murthy, N. Polyketal nanoparticles: A new pH-sensitive biodegradable drug delivery vehicle. *Bioconjugate Chem.* **2005**, *16*, 1340-1342.

(67) Jain, R.; Standley, S. M.; Fréchet, J. M. J. Synthesis and degradation of pH-sensitive linear poly(amidoamine)s. *Macromolecules* **2007**, *40*, 452-457.

(68) Gillies, E. R.; Jonsson, T. B.; Fréchet, J. M. J. Stimuli-responsive supramolecular assemblies of linear-dendritic copolymers. *J. Am. Chem. Soc.* **2004**, *126*, 11936-11943.

- (69) Wuts, P. G. M.; Greene, T. W. *Protective Groups in Organic Synthesis. 4th Ed.*; Wiley and Sons Inc: Hoboken, New Jersey, 2007.
- (70) Yang, S. C.; Bhide, M.; Crispe, I. N.; Pierce, R. H.; Murthy, N. Polyketal copolymers: A new acid-sensitive delivery vehicle for treating acute inflammatory diseases. *Bioconjugate Chem.* **2008**, *19*, 1164-1169.
- (71) Rickerby, J.; Prabhakar, R.; Ali, M.; Knowles, J.; Brocchini, S. Water-soluble polyacetals derived from diphenols. *J. Mater. Chem.* **2005**, *15*, 1849-1856.
- (72) Bochet, C. G. Photolabile protecting groups and linkers. *J. Chem. Soc., Perkin Trans. I* **2002**, 125-142.
- (73) Warnecke, A.; Kratz, F. 2, 4-Bis(hydroxymethyl) aniline as a building block for oligomers with self-eliminating and multiple release properties. *J. Org. Chem.* **2008**, *73*, 1546-1552.
- (74) Robbins, J. S.; Schmid, K. M.; Phillips, S. T. Effects of electronics, aromaticity, and solvent polarity on the rate of azaquinone–methide-mediated depolymerization of aromatic carbamate oligomers. *J. Org. Chem.* **2013**, *78*, 3159-3169.
- (75) Kade, M. J.; Burke, D. J.; Hawker, C. J. The power of thiol-ene chemistry. *J. Polym. Sci., Part A: Polym. Chem.* **2010**, *48*, 743-750.
- (76) Hoyle, C. E.; Bowman, C. N. Thiol-ene click chemistry. *Angew. Chem., Int. Ed.* **2010**, *49*, 1540-1573.
- (77) Sirsi, S. R.; Borden, M. A. State-of-the-art materials for ultrasound-triggered drug delivery. *Adv. Drug Delivery Rev.* **2014**, *72*, 3-14.
- (78) Liu, H. L.; Fan, C. H.; Ting, C. Y.; Yeh, C. K. Combining microbubbles and ultrasound for drug delivery to brain tumors: current progress and overview. *Theranostics* **2014**, *4*, 432-444.
- (79) Chung, C.; Srikun, D.; Lim, C. S.; Chang, C. J.; Cho, B. R. A Two-photon fluorescent probe for ratiometric imaging of hydrogen peroxide in live tissue. *Chem. Commun.* **2011**, *47*, 9618-9620.
- (80) Wong, A. D.; Güngör, T. M.; Gillies, E. R. Multiresponsive azobenzene end-cap for self-immolative polymers. *ACS Macro Lett.* **2014**, *3*, 1191-1195.
- (81) Aujard, I.; Benbrahim, C.; Gouget, M.; Ruel, O.; Baudin, J. B.; Neveu, P.; Jullien, L.

o-Nitrobenzyl photolabile protecting groups with red-shifted absorption: syntheses and uncaging cross-sections for one-and two-photon excitation. *Chem. Eur. J.* **2006**, *12*, 6865-6879.

(82) Wood, M. C.; Leitch, D. C.; Yeung, C. S.; Kozak, J. A.; Schafer, L. L. Chiral neutral zirconium amidate complexes for the asymmetric hydroamination of alkenes. *Angew. Chem., Int. Ed.* **2007**, *46*, 354-358.

(83) Ida, Y.; Matsubara, A.; Nemoto, T.; Saito, M.; Hirayama, S.; Fujii, H.; Nagase, H. Synthesis of quinolinomorphinan derivatives as highly selective δ -opioid receptor ligands. *Bioorg. Med. Chem.* **2012**, *20*, 5810-5831.

(84) Nguyen, T. Q.; Liang, Q. Z.; Kausch, H.-H. Kinetics of ultrasonic and transient elongational flow degradation: a comparative study. *Polymer* **1997**, *38*, 3783-3793.

(85) Caruso, M. M.; Davis, D. A.; Shen, Q.; Odom, S. A.; Sottos, N. R.; White, S. R.; Moore, J. S. Mechanically-induced chemical changes in polymeric systems. *Chem. Rev.* **2009**, *109*, 5755-5798.

Chapter 5

5 Poly(ethyl glyoxylate)-poly(ethylene glycol) nanoparticles: Stimuli-responsive drug release via end-to-end polyglyoxylate depolymerization

The content of this chapter has been published in “B. Fan, E. R. Gillies, *Mol. Pharmaceutics*, **2017**, *14*, 2548–2559”

5.1 Introduction

Amphiphilic block copolymers can self-assemble in aqueous solution to form a wide range of morphologies including spherical micelles, cylindrical micelles, and vesicles.¹⁻³ Such assemblies have been of significant interest in recent years for the encapsulation and controlled release of drugs.⁴⁻⁶ These delivery vehicles can enhance the water-dispersibility of hydrophobic drugs and selectively target them to sites of action such as tumors *via* the enhanced permeation and retention effect or using active targeting groups.⁷⁻⁹ Ideally, the assembly would be stable in the blood stream, but selectively release its payload at the target site. To achieve this, polymer assemblies responsive to the conditions associated with various disease states have been developed. For example, systems responsive to the acidic pH encountered in tumor tissue or within the endosomal compartments of cells have been introduced.¹⁰⁻¹³ Reducing conditions, associated with the intracellular environment and hypoxic tumor tissue, have also been used to disrupt polymer assemblies.¹⁴⁻¹⁶ Furthermore, polymer systems responsive to reactive oxygen species such as H₂O₂, associated with inflammation and cancer have also been developed.^{17,18} Most of these systems require the action of the stimulus at many sites along the polymer backbone in order to change the properties of the polymer, resulting in drug release.

Over the past decade, a new class of degradable polymers that undergoes end-to-end depolymerization in response to the cleavage of a stimuli-responsive end-cap from the polymer terminus was introduced. Often termed “self-immolative polymers”, these macromolecules require the action of a single stimulus to completely depolymerize the polymer.¹⁹⁻²¹ This provides the potential for signal amplification at low stimulus

concentrations. End-caps responsive to stimuli such as light²²⁻²⁴, H₂O₂^{25,26}, thiols^{24,27}, and mildly acidic conditions²⁸ have been reported and have been used in applications such as sensors^{25,29,30} and responsive coatings or plastics³¹⁻³³. The incorporation of a second polymer block has provided amphiphilic copolymers that self-assembled to form nanoparticles such as micelles and vesicles.^{22,30,34} However, the potential of these systems for drug delivery has been explored only to a very limited extent. In addition, these examples involved depolymerization to species such as quinone methides and aza-quinone methides, which are likely toxic.³⁵

Our group reported poly(ethyl glyoxylate) (PEtG) as a self-immolative polymer.^{22,28,33} As shown in Figure 5.1, the depolymerization products are ultimately ethanol and glyoxylic acid, a metabolic intermediate that can be processed in the liver.³⁶ Studies have suggested that this depolymerization product should exhibit low toxicity both to mammals and the environment,³⁷ making PEtG a promising polymer for drug delivery and other applications. Using a UV light-responsive linker end-cap, we prepared amphiphilic block copolymers of PEtG and poly(ethylene glycol) (PEG) that self-assembled to form light-responsive nanoparticles.²² In addition, we recently reported end-caps responsive to H₂O₂, thiols, weak acids, and multiple stimuli.²⁸ However, these PEtG homopolymers were not water-soluble and the depolymerization was studied only in 9:1 CD₃CN:D₂O. This chapter describes the development of linker end-caps responsive to biologically relevant stimuli, and their application for the preparation of PEG-PEtG-PEG block copolymers. These block copolymers are self-assembled to form nanoparticles and the response of these nanoparticles to stimuli is studied. It is demonstrated that very low amounts of stimulus are sufficient to disrupt the assemblies. Furthermore, by simply changing the linker end-cap, these nanoparticles can be easily tuned to release drug molecules such as doxorubicin (Dox) and curcumin (Cur) using different stimuli such as light, thiols, and H₂O₂.

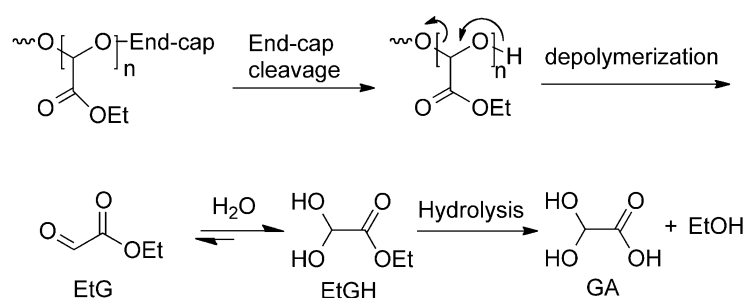


Figure 5.1 Depolymerization of PEtG to ethyl glyoxylate (EtG), hydration to form ethyl glyoxylate hydrate (EtGH), and hydrolysis to glyoxylic acid (GA) and ethanol.

5.2 Experimental section

General materials and procedures. Compounds **1**,²⁸ **2**,²² **5**,²² **9**,²⁸ azide-terminated PEG (PEG-N₃),³⁸ thiol-terminated PEG (PEG-SH),³⁹ and polymers **PEtG-nitrobenzyl**,²² **PEtG-disulfide**,²⁸ and **PEtG-nitrobenzyl-PEG**²² were previously reported and the same batches were used. Ethyl glyoxylate (EtG) in toluene solution (50% w/w) and dithiothreitol (DTT) were obtained from Alfa Aesar (Canada). Hydrogen peroxide solution (50 wt%) in water, tin(II) chloride dihydrate, Nile red and phosgene solution (15 wt. % in toluene) were purchased from Sigma-Aldrich (USA). Triethylamine, pyridine, and dichloromethane were distilled from CaH₂ before use. Anhydrous THF was obtained from a solvent purification system using Al₂O₃ columns. All the other chemicals were of reagent grade and used without further purification. ¹H NMR spectra were obtained in CDCl₃ at 400 MHz or 600 MHz on Varian Inova instruments. NMR chemical shifts (δ) are reported in ppm and are calibrated against residual solvent signals of CDCl₃ (δ 7.27), CD₃CN (δ 1.94), DMSO-*d*₆ (δ 2.50) or D₂O (δ 4.75). Fourier transform infrared (FT-IR) spectra were obtained using a Bruker tensor 27 instrument with films drop cast from CH₂Cl₂ on KBr plates. High-resolution mass spectrometry (HRMS) was performed using a Finnigan MAT 8400 electron impact (EI) mass spectrometer or Bruker microOTOF 11 electrospray mass spectrometer (ESI). Ultrapure water was obtained from a Barnstead EASYpure II system. SEC was performed in THF at 1.0 mL/min using a Viscotek GPC Max VE2001 solvent module equipped with a Viscotek VE3580 RI detector operating at 30 °C, two Agilent Polypore (300 x 7.5mm) columns, and a Polypore guard column (50 x 7.5mm). A calibration curve

was obtained using poly(methyl methacrylate) standards. Thermogravimetric analysis (TGA) was performed on Q50 from TA Instruments with a heating rate of 10 °C/min from 35-800 °C under nitrogen. Spectra/Por regenerated cellulose membranes were used for dialyses. Dynamic light scattering (DLS) was performed using a Zetasizer Nano ZS instrument from Malvern Instruments at 25 °C at a concentration of 0.8 mg/mL of polymer assemblies. TEM imaging was done using a Phillips CM10 microscope operating at an acceleration voltage of 80 kV. 3.0 µL of micelle suspension (0.3 mg / mL) was placed onto a copper grid. The resulting sample was air-dried for 24 h before imaging. At least 30 particles were measured to obtain the mean particle diameters. Fluorescence spectra were obtained using a QM-4 SE spectrometer from Photon Technology International (PTI) equipped with double excitation and emission monochromators. UV-visible spectra were obtained on a Varian UV/VIS Cary 300 spectrophotometer.

Synthesis of compound 6. Compound **5**²² (630.0 mg, 2.9 mmol, 1.0 equiv.) and tin(II) chloride dihydrate (4.2 g, 14.4 mmol, 5.0 equiv.) were dissolved in 39 mL of 10:3 THF: water and stirred at 70 °C under an Ar atmosphere for 30 min. After cooling to room temperature, the solution was poured into 50 mL of cold water and adjusted to pH 8.0 by addition of 1 M Na₂CO₃. The mixture was extracted with ethyl acetate (3 × 60.0 mL), and the resulting organic phase was washed with brine once, dried over anhydrous MgSO₄, filtered and the solvent was removed under reduced pressure to yield 450 mg of compound **6** (450.0 mg, 83%) as a yellow solid. ¹H NMR (400 MHz, DMSO-*d*₆): δ 8.61 (t, *J* = 5.3 Hz, 1H), 7.12 (d, *J* = 7.6 Hz, 1H), 7.08 (d, *J* = 1.8 Hz, 1H), 6.98 (dd, *J* = 7.6 Hz, 1.8 Hz, 1H), 5.08 (t, *J* = 5.3 Hz, 1H), 5.04 (s, 2H), 4.37 (d, *J* = 5.3 Hz, 1H), 3.98 (dd, *J* = 5.3 Hz, 2.4 Hz, 2H), 3.05 (t, *J* = 2.4 Hz, 1H). ¹³C NMR (100 MHz, DMSO-*d*₆): δ 166.3, 145.7, 133.1, 128.4, 126.7, 114.2, 113.4, 81.4, 72.3, 60.3, 28.1. HRMS (EI) calc'd. for [M]⁺ C₁₁H₁₂N₂O₂: 204.0899; found: 204.0901.

Synthesis of compound 8. Compound **6** (430.0 mg, 2.3 mmol, 1.0 equiv.) was dissolved in 12 mL of THF and 8 mL of saturated Na₂CO₃ solution was added. After the mixture was cooled to 0 °C, chloroformate **7**⁵⁸ (738.0 mg, 2.5 mmol, 1.1 equiv.) in 4.0 mL THF, and 4.0 mL saturated sodium carbonate solution were added into the system dropwise at the same

time. After stirring at room temperature for 1 h, the mixture was diluted with 50.0 mL ethyl acetate, the organic phase was collected, washed with brine once, dried over anhydrous MgSO_4 , filtered and then the solvent was removed under reduced pressure. The product was further purified by column with 1:1 ethyl acetate:hexane as the eluent to yield compound **8** (766.0 mg, 73%) as a yellow solid. ^1H NMR (400 MHz, $\text{DMSO-}d_6$): δ 9.08 (s, 1H), 8.68 (t, $J = 5.1$ Hz, 1H), 7.96 (s, 1H), 7.69 (d, $J = 8.2$ Hz, 1H), 7.60 (dd, $J = 1.6$ Hz, 8.2 Hz, 1H), 7.46 (d, $J = 7.8$ Hz, 2H), 7.42 (d, $J = 7.8$ Hz, 2H), 5.44 (t, $J = 5.5$ Hz, 1H), 5.17 (s, 2H), 4.54 (d, $J = 5.5$ Hz, 2H), 4.00 (dd, $J = 5.5$ Hz, 2.3 Hz, 2H), 3.10 (t, $J = 2.3$ Hz, 1H), 1.28 (s, 12H). ^{13}C NMR (100 MHz, $\text{DMSO-}d_6$): δ 166.0, 154.3, 140.5, 135.7, 135.0, 133.3, 127.5, 126.1, 123.5, 109.9, 84.1, 81.8, 73.9, 73.2, 66.1, 60.3, 28.9, 25.1. HRMS (ESI) calc'd. for $[\text{M}+\text{Na}]^+$ $\text{C}_{25}\text{H}_{29}\text{BN}_2\text{O}_6\text{Na}$: 487.2016; found: 487.2023.

Synthesis of chloroformate 3. Compound **8** (400.0 mg, 0.9 mmol, 1.0 equiv.) was dissolved in THF (4.0 mL). The resulting solution was then added dropwise into a phosgene solution (15wt. % in toluene, 1.8 mL, 2.6 mmol, 3.0 equiv.) under an Ar atmosphere at room temperature and was stirred for 16 h. The residual phosgene and solvent were then removed by high vacuum to yield compound **3** (432.0 mg 95%) as a yellow solid. Phosgene collected in the liquid nitrogen-cooled trap was then quenched with methanol (10.0 mL) and saturated sodium hydroxide solution (10.0 mL) (**Caution! Phosgene is toxic**). ^1H NMR (600 MHz, CDCl_3): δ 8.15 (s, 1H), 7.86 (d, $J = 8.2$ Hz, 2H), 7.65 (dd, $J = 8.2$ Hz, 1.8 Hz, 1H), 7.47 (d, $J = 8.2$ Hz, 1H), 7.42 (d, $J = 8.2$ Hz, 2H), 7.18 (d, $J = 8.2$ Hz, 1H) 7.12 (s, 1H), 6.38 (s, 1H), 5.33 (s, 2H), 5.25 (s, 2H), 4.24 (dd, $J = 5.3$ Hz, 2.4 Hz, 2H), 2.29 (t, $J = 2.4$ Hz, 1H), 1.36 (s, 12H). ^{13}C NMR (100 MHz, CDCl_3): δ 166.0, 153.8, 151.1, 138.5, 136.7, 135.1, 131.2, 129.0, 127.4, 125.3, 124.1, 83.9, 79.2, 72.0, 69.6, 67.5, 29.8, 24.8. HRMS (ESI) calc'd. for $[\text{M}+\text{Na}]^+$ $\text{C}_{26}\text{H}_{28}\text{BCIN}_2\text{O}_7\text{Na}$: 549.1576; found: 549.1588.

Synthesis of compound 10. Compound **6** (740.0 mg, 3.9 mmol, 1.0 equiv.) was dissolved in 30.0 mL of THF and 15.0 mL saturated Na_2CO_3 solution was then added. After the mixture was cooled to 0 $^\circ\text{C}$, chloroformate **9**²⁸ (1.9 g, 3.9 mmol, 1.0 equiv.) in 60.0 mL of CH_2Cl_2 and 30.0 mL saturated Na_2CO_3 solution were added into the system dropwise at

the same time. After stirring at room temperature for 1 h, the mixture was diluted with 300.0 mL of ethyl acetate, the organic phase was collected, washed with brine once, dried over anhydrous MgSO_4 , filtered and the solvent was removed under reduced pressure. The product was further purified by column chromatography using 1:1 ethyl acetate:hexane as the eluent to yield compound **10** (1.0 g, 39%) as a yellow solid. ^1H NMR (600 MHz, CDCl_3): δ 8.59 (s, 1H), 8.34 (s, 1H), 8.15 (s, 2H), 7.78 (d, $J = 7.6$ Hz, 2H), 7.67 (d, $J = 7.6$ Hz, 1H), 7.54 (t, $J = 7.6$ Hz, 1H), 7.45 (dd, $J = 7.6$ Hz, 1.8 Hz, 1H), 7.43 (d, $J = 7.6$ Hz, 2H), 7.12 (d, $J = 7.6$ Hz, 1H) 6.55 (s, 1H), 5.46 (s, 2H), 5.27 (s, 2H), 4.67 (s, 2H) 4.21 (dd, $J = 5.3$ Hz, 2.4 Hz, 2H), 2.27 (t, $J = 2.4$ Hz, 1H), 1.35 (s, 12H). ^{13}C NMR (100 MHz, CDCl_3): δ 166.7, 153.9, 153.6, 150.7, 138.6, 136.7, 134.8, 133.8, 132.5, 130.0, 128.6, 127.1, 124.7, 122.4, 120.1, 118.7, 115.2, 83.7, 79.2, 74.8, 71.6, 67.0, 63.3, 29.4, 24.6. HRMS (ESI) calc'd. for $[\text{M}+\text{Na}]^+$ $\text{C}_{33}\text{H}_{35}\text{BN}_4\text{O}_{10}\text{Na}$: 681.2344; found: 681.2361.

Synthesis of chloroformate 4. Compound **10** (900.0 mg, 1.4 mmol, 1.0 equiv.) was dissolved in THF (16.0 mL). The resulting solution was then added dropwise into a phosgene solution (15wt. % in toluene, 2.0 mL, 2.7 mmol, 2.0 equiv.) under an Ar atmosphere at room temperature and was stirred for 16 h. The residual phosgene and solvent was then removed by high vacuum to yield compound **4** (952.0 mg, 96%) as a yellow solid. Phosgene collected in the liquid nitrogen-cooled trap was then quenched with methanol (10.0 mL) and saturated sodium hydroxide solution (10.0 mL) (**Caution! Phosgene is toxic**). ^1H NMR (600 MHz, CDCl_3): δ 8.59 (s, 1H), 8.17 (s, 1H), 8.01 (s, H), 7.81 (d, $J = 8.2$ Hz, 2H), 7.70 (d, $J = 7.6$ Hz, 1H), 7.55 (t, $J = 8.2$ Hz, 1H), 7.48 (d, $J = 8.2$ Hz, 1H), 7.42 (d, $J = 8.2$ Hz, 2H), 7.18 (d, $J = 7.6$ Hz, 1H), 6.36 (s, 1H), 5.49 (s, 2H), 5.28 (s, 2H), 4.27 (s, 2H) 4.25 (dd, $J = 5.3$ Hz, 2.4 Hz, 2H), 2.29 (t, $J = 2.4$ Hz, 1H), 1.35 (s, 12H). Due to the poor solubility of this compound, no ^{13}C NMR spectrum was obtained. HRMS (ESI) calc'd. for $[\text{M}+\text{Na}]^+$ $\text{C}_{34}\text{H}_{34}\text{BCIN}_4\text{O}_{11}\text{Na}$: 743.1903; found: 743.1928.

Synthesis of PEtG-boronate. Ethyl glyoxylate (EtG) in toluene solution (20.0 mL) was distilled under vacuum (55 °C, 125 mbar) over P_2O_5 to remove toluene and trace water in the first, discarded fraction. The residue was then distilled twice successively over P_2O_5 at atmospheric pressure under argon at 130 °C to obtain the highly pure monomer. Purified

EtG (5.0 mL, 50.0 mmol, 1.0 equiv.) was then dissolved in CH₂Cl₂ (5.0 mL) and Et₃N (3.5 μL, 25.0 μmol, 0.0005 equiv.) was added. The solution was stirred for 1 h at -20 °C. Chloroformate 3 (0.5 g, 950.0 μmol, 0.019 equiv.) and Et₃N (130.0 μL, 730.0 μmol, 0.019 equiv.) were added at -20 °C to end-cap the polymer. The solution was gradually warmed to room temperature and then stirred for 24 h. The crude product was precipitated into methanol. After decanting the excess methanol, the residue was dried *in vacuo* for 48 h to provide 2.6 g of a white, sticky polymer. Yield = 52%. ¹H NMR (600 MHz, CDCl₃): δ 5.46-5.78 (m, 593H), 5.24 (s, 4H), 4.10-4.33 (m, 1274H), 1.36 (s, 12H), 1.21-1.44 (m, 1958H). FT-IR (KBr, thin film): 2986, 1750, 1467, 1447, 1376, 1297, 1139, 1217, 1017, 965, 733 cm⁻¹. SEC: M_n = 48 kg/mol, M_w = 72 kg/mol, Đ = 1.5. T_g = -1 °C.

Synthesis of PEtG-multi. Purified EtG (prepared as described above for **PEtG-boronate**) (5.0 mL, 50.0 mmol, 1.0 equiv.) was dissolved in CH₂Cl₂ (5.0 mL) and Et₃N (3.5 μL, 25.0 μmol, 0.0005 equiv.) was added. The solution was stirred for 1 h at -20 °C. Chloroformate 4 (1.0 g, 1.4 mmol, 0.028 equiv.) and Et₃N (190.0 μL, 1.4 mmol, 0.028 equiv.) were added at -20 °C to end-cap the polymer. The solution was allowed to slowly warm to room temperature and was stirred for 24 h at room temperature. The polymer was purified by dialysis against 1:1 acetone:methanol for 24 h (300.0 mL, 3 solvent changes) using a 6000-8000 g/mol MWCO membrane. The product was dried *in vacuo* for 48 h to provide **PEtG-multi** (0.8 g, 16%) as a white solid. ¹H NMR (600 MHz, CDCl₃): δ 7.76-7.84 (m, 2H), 7.64-7.71 (m, 2H), 7.36-7.45 (m, 2H), 5.46-5.78 (m, 111H), 5.26 (s, 4H), 4.10-4.33 (m, 256 H), 2.24-2.30 (m, 2 H), 1.21-1.44 (m, 407H). FT-IR (KBr, thin film): 2984, 2942, 1748, 1536, 1446, 1467, 1374, 1296, 1214, 1139, 961, 856 cm⁻¹. SEC: M_n = 6 kg/mol, M_w = 10 kg/mol, Đ = 1.6. T_g = 8 °C.

Synthesis of PEtG-disulfide-PEG. 2000 g/mol PEG-SH⁵⁹ (150.0 mg, 75.0 μmol, 6.0 equiv.) and **PEtG-disulfide** (0.3 g, 12.5 μmol, 1.0 equiv.) were dissolved in DMF (5.0 mL). The reaction mixture was placed under an Ar atmosphere and stirred at room temperature for 24 h. It was then transferred to a 50 kg/mol molecular weight cut-off (MWCO) membrane and dialyzed against deionized water for 16 h (1.0 L, 2 solvent changes) to remove DMF and most free PEG. The dialyzed material was then lyophilized,

washed 3 times with water to further remove free PEG, and dried to afford the product (760.0 mg, 89% yield) as a white, rubbery material. ^1H NMR (400 MHz, CDCl_3): δ 5.43-5.75 (m, 565H), 4.13-4.36 (m, 1154H), 3.65 (s, 364H), 3.39 (s, 6H), 1.18-1.42 (m, 1709H). ^{13}C NMR (150 MHz, CDCl_3): δ 164.7-166.8, 90.6-94.8, 71.8, 70.5, 62.0, 13.8. FT-IR (KBr, thin film): 2985, 2941, 2908, 1750, 1446, 1467, 1376, 1297, 1215, 1138, 1094, 1016, 960, 856, 734, 700 cm^{-1} . SEC: $M_n = 29$ kg/mol, $M_w = 43$ kg/mol, PDI = 1.4. $T_g = -9$ °C.

Synthesis of PEtG-boronate-PEG. 2000 g/mol PEG- N_3^5 (43.0 mg, 21.0 μmol , 3.0 equiv.) and **PEtG-boronate** (500.0 mg, 7.1 μmol , 1.0 equiv.) were dissolved in DMF (5.0 mL) and placed under an Ar atmosphere. CuSO_4 (4.0 mg, 25.0 μmol , 3.5 equiv.) and sodium ascorbate (5.0 mg, 25.0 μmol , 3.5 equiv.) were added and the reaction mixture was stirred at 40 °C for 16 h. It was then transferred into a regenerated cellulose membrane with a 50 kg/mol MWCO and dialyzed against deionized water for 16 h (1.0 L, 2 solvent changes) to remove DMF and most free PEG. The dialyzed material was then lyophilized, washed 3 times with water to further remove free PEG, and then dried to afford the product (520.0 mg, 98% yield) as a white, rubbery material. ^1H NMR (400 MHz, CDCl_3): δ 5.49-5.76 (m, 506 H), 4.12-4.31 (m, 1026 H), 3.65 (s, 364 H), 3.39 (s, 6 H), 1.15-1.43 (m, 1553 H). ^{13}C NMR (150 MHz, CDCl_3): δ 164.7-166.5, 90.3-93.9, 71.8, 70.5, 62.0, 13.7. FT-IR (KBr, thin film): 2985, 1752, 1468, 1448, 1375, 1298, 1217, 1139, 1094, 1017, 964, 855, 737 cm^{-1} . SEC: $M_n = 49$ kg/mol, $M_w = 87$ kg/mol, $D = 1.7$. $T_g = -3$ °C.

Synthesis of PEtG-multi-PEG. 750 g/mol PEG- N_3^5 (51.0 mg, 69.0 μmol , 2.4 equiv.) and **PEtG-multi** (200.0 mg, 29.0 μmol , 1.0 equiv.) were dissolved in DMF (5.0 mL) and placed under an Ar atmosphere. CuSO_4 (4.0 mg, 25.0 μmol , 0.9 equiv.) and sodium ascorbate (5.0 mg, 25.0 μmol , 0.9 equiv.) were added, and the mixture was stirred at 40 °C for 16 h. It was transferred to a 6-8 kg/mol MWCO membrane and dialyzed against deionized water for 16 h (1.0 L, 2 solvent changes) to remove DMF and most free PEG. The dialyzed material was then lyophilized, washed 3 times with water to further remove free PEG, and dried to afford the product (220.0 mg, 91%) as a white, rubbery material. ^1H NMR (600 MHz, CDCl_3): δ 7.74-7.89 (m, 4 H), 7.60-7.72 (m, 3 H), 7.48-7.58 (m, 3 H), 7.34-7.44 (m, 3H), 5.48-5.79 (m, 51 H), 5.15-5.30 (m, 5 H), 4.06-4.43 (m, 112 H), 3.65 (s, 136 H), 3.39

(s, 6 H), 1.16-1.51 (m, 173 H). ^{13}C NMR (150 MHz, CDCl_3): δ 164.4-166.7, 90.2-94.7, 70.5, 62.0, 13.9. FT-IR (KBr, thin film): 2983, 2874, 1753, 1659, 1583, 1534, 1467, 1448, 1374, 1349, 1296, 1217, 1093, 1018, 962, 855, 770, 735, 703, 654 cm^{-1} . SEC: $M_n = 7$ kg/mol, $M_w = 11$ kg/mol, PDI = 1.5. $T_g = -4$ °C.

Nanoparticle preparation. 8.0 mg of block copolymer was dissolved in 1.0 mL of DMSO with stirring overnight. 0.1 mL of the solution was injected quickly into 0.9 mL of rapidly stirring deionized water. After stirring for 0.5 h, the suspension was dialyzed using a 3 kg/mol molecular weight cut-off (MWCO) membrane against deionized water (1.0 L, 24 h, water changed once at ~12 h) to remove DMSO. Each nanoparticle system was prepared in triplicate.

Measurement of the critical aggregation concentration (CAC). A 5.0 mg/mL suspension of nanoparticles was prepared by the self-assembly procedure described in the manuscript with dialysis in deionized water (higher polymer concentration was used to obtain 5.0 mg/mL). 29.0 μL of a 0.1 mg/mL solution of Nile red in CH_2Cl_2 was added to each of a series of vials and then the solvent was evaporated to provide a thin film of Nile red. Next, 13 serial dilutions of the polymer suspension ranging from 2.5×10^{-4} to 1.0 mg/mL were added to the vials. The vials were gently shaken overnight then the fluorescence emission spectra (560-700 nm) of each vial was measured using an excitation wavelength of 540 nm. The CAC was then determined as the intercept of the two linear regions of the graph of fluorescence intensity vs. $\log(\text{copolymer concentration})$.

Nanoparticle degradation studied by DLS. Nanoparticles were prepared as above, except that the suspensions were dialyzed against either 100 mM, pH 7.4 phosphate buffer or 100 mM, pH 5.0 citrate buffer (1.0 L, 24 h, water changed once at ~12 h). The polymer concentration was ~ 0.8 mg/mL. The count rate was measured by DLS while fixing the attenuator at 7. DTT or H_2O_2 were added at concentrations ranging from 0.05 – 10 mM or not added in the case of controls. Irradiation with UV light was performed in an ACE Glass photochemistry cabinet containing a mercury light source (450 W bulb, 2.8 mW/cm^2 of UVA radiation) for 20 min. After applying the stimuli, the samples were incubated at 37

°C in the dark and the DLS count rate was measured at selected time points. **PEtG-nitrobenzyl-PEG** and **PEtG-multi-PEG** were studied in triplicate.

Nanoparticle depolymerization studied by NMR spectroscopy. 16.0 mg of copolymer was dissolved in 0.8 mL of DMSO-*d*₆. 0.2 mL of the resulting solution was rapidly injected into 1.0 mL of 100 mM, pH 7.4 phosphate- or 100 mM, pH 5.0 citrate-buffered D₂O. After stirring for 0.5 h, the nanoparticle suspension was transferred into NMR tubes, and initial ¹H NMR spectra were obtained. The corresponding stimuli were applied as described above for the DLS study. The samples were incubated at 37 °C and NMR spectra were obtained at time points over 1 or 2 days. The integration of the PEG peak at 3.6 ppm was set to 364 for the PEG 2000 g/mol conjugates or 136 for the 750 g/mol conjugate. The integration of the peaks at 1.0-1.2 ppm corresponding to the CH₃ group on released EtGH and its ethanol hydrolysis product was measured ($I_{\text{CH}_3 \text{ aq}}$) and compared its value in CDCl₃ ($I_{\text{CH}_3 \text{ CDCl}_3}$) (it corresponds to the CH₃ of the ethyl group on PEtG in this case) where both blocks are fully soluble, with the integration of the PEG peak set to 364 or 136. The extent of depolymerization is determined as follows: % depolymerization = $(I_{\text{CH}_3 \text{ aq}} / I_{\text{CH}_3 \text{ CDCl}_3}) \times 100\%$.

Study of nanoparticle stability in mouse serum. 4.0 mg of block copolymer was dissolved in 0.1 mL of DMSO with stirring overnight. 0.1 mL of the resulting solution was rapidly injected into 0.9 mL of rapidly stirring deionized water. After stirring for 0.5 h, the suspension was dialyzed using a 3 kg/mol MWCO membrane against 100 mM, pH 7.4 phosphate buffer (1 L, 24 h, water changed once at ~12 h) to remove DMSO. The particle solution was then diluted 10 times by mouse serum (Novex Normal mouse serum, Life technologies, USA). Specifically, 40 μL of solution was diluted with 360 μL mouse serum. The mixture was then added to low-volume cuvette and sealed. Subsequently, the samples were incubated at 37 °C in the dark and the DLS count rate was measured at selected time points. The attenuator was fixed at 7.

Loading and release of Nile red. Nanoparticles were prepared as described above in 100 mM, pH 7.4 phosphate buffer or 100 mM, pH 5.0 citrate buffer (1.0 L, 24 h, water changed once at ~12 h) at 0.8 mg/mL of polymer. 29.0 μL of a 0.1 mg/mL solution of Nile red in

CH₂Cl₂ was added to each of a series of vials and then the solvent was evaporated to provide a thin film of Nile red. To each vial, 1.5 mL of nanoparticle suspension was added, and the vials were gently shaken for 16 h to incorporate Nile red into the nanoparticles. Using an excitation wavelength of 540 nm, the initial emission intensity of Nile red was measured at 600 nm. Stimuli were then applied as described above for the DLS study and the samples were incubated at 37 °C in the dark. The emission intensity at 600 nm was measured at selected time points.

Loading and release of Dox. 10.0 mg of Dox (17.2 μmol) and 1.7 mg of triethylamine (17.2 μmol) were dissolved in 2.0 mL DMSO and stirred for 10 min, then 16.0 mg of **PEtG-nitrobenzyl-PEG** was added and the solution was stirred for 5 h. It was then injected quickly into 18.0 mL of deionized water and stirred for 15 min. The suspension was dialyzed against water (1.0 L, 48 h, water changed every ~12 h) using a 3500 g/mol MWCO membrane to remove free Dox and DMSO. To calculate the Dox content and loading efficiency, a portion of the suspension was lyophilized, then a measured mass of the product was dissolved in DMF. The absorbance of the DMF solution was measured by UV-vis spectroscopy at 500 nm and the Dox concentration was calculated based on a Dox calibration curve ($\epsilon = 46820 \text{ L/g}\cdot\text{cm}$). Loading efficiency = (mass of loaded drug/mass of actual drug used)×100%. Drug content = (mass of loaded drug/mass of nanoparticles with drug)×100%. Dox release was measured in 100 mM, pH 5.0 citrate or 100 mM, pH 7.4 phosphate buffer at polymer concentrations of 0.8 and 0.2 mg/mL respectively. 5.0 mL sample was irradiated with UV light as described above but for 3 h, while another 5.0 mL was kept in the dark. At each pH, the initial absorption was measured at 500 nm. Each sample was then transferred into a dialysis membrane (3500 g/mol MWCO) and dialyzed in the dark against the corresponding buffer solutions (1.0 L, 48 h, water changed every ~12 h) at 37 °C. The absorbance of the samples inside the dialysis membrane were measured at selected times over 2 or 4 days to quantify the percentage of released drug.

Loading and release of Cur. 10.0 mg of **PEtG-boronate-PEG**, **PEtG-disulfide-PEG**, or **PEtG-nitrobenzyl-PEG** (control) and 2.0 mg of Cur were dissolved in 1.0 mL DMF and stirred overnight. The solution was then injected into 9.0 mL of stirring deionized water

and stirred for an additional 1 min. The suspension was then dialyzed against 100 mM, pH 7.4 phosphate buffer (1.0 L, 16 h, buffer changed at ~8 h) using a 3500 g/mol MWCO membrane. It was then filtered through a 0.45 μm syringe filter (Acrodisc Syringe Filter Non-Pyrogenic 13 mm, Pall Life Science) to remove any unencapsulated and precipitated drug. 50.0 μL of the resulting nanoparticle suspension was diluted into 2.0 mL of DMF to fully dissolve the copolymer and Cur and the absorbance at 428 nm was used to calculate the Cur concentration ($\epsilon = 5740 \text{ L/g}\cdot\text{cm}$). This was used to calculate the loading efficiency and drug content as above for Dox. To measure the Cur release, the relevant stimuli (H_2O_2 or DTT; 0.5 or 5 mM) were added (or not added for controls) to the resulting nanoparticles in buffer (5.0 mL per sample) and they were incubated in the dark at 37 $^\circ\text{C}$. At selected time points, ~0.2 mL of the suspension was removed and filtered through a 0.45 μm syringe filter to remove the released Cur. 50.0 μL of the filtered suspension was then diluted into 2.0 mL of DMF, resulting in full dissolution. The absorbance of the DMF solution at 428 nm was measured to determine the percentage of drug remaining in the nanoparticles.

5.3 Results and discussion

5.3.1 Synthesis of stimuli-responsive PEG-PEG triblock copolymers

In this chapter, UV light, reducing conditions (i.e., thiols), H_2O_2 and combinations of these stimuli were targeted as triggers for initiating the depolymerization of PEG-PEtG-PEG assemblies for the release of drugs. As described above, thiols and H_2O_2 are stimuli that are relevant to pathological conditions such as inflammation and cancer.^{40,41} Light is a stimulus that can be easily applied in the laboratory with good spatiotemporal control, and can potentially be extended to two-photon processes for application *in vivo*.⁴² Based on previous work, chloroformates can effectively end-cap PEtG,²² so end-caps containing a chloroformate along with the stimuli-responsive group and a site for the conjugation of the PEG block were designed.

The structures of the linker end-caps employed in the current work are shown in Figure 5.2. We have previously reported end-caps **1**²⁸ and **2**²². End-cap **1** contains a disulfide, which can serve both as a site for the conjugation of PEG *via* thiol exchange and as a reduction-sensitive site. Reaction with a thiol trigger releases a thiol on the end-cap that cyclizes, releasing uncapped PEtG (Scheme A5.1a). End-cap **2** contains an alkyne for conjugation of the PEG block using a Cu(I)-assisted azide-alkyne cycloaddition (CuAAC) and a light-responsive *o*-nitrobenzyl moiety, that cleaves at the benzylic site to release uncapped PEtG (Scheme A5.1b). End-cap **3** contains an alkyne for CuAAC and a phenylboronate that is sensitive to H₂O₂. In the presence of H₂O₂, the boronate is cleaved. This releases the phenol, that undergoes a 1,6-elimination-decarboxylation, followed by a 1,4-elimination-decarboxylation to release uncapped PEtG (Scheme A5.1c). Finally, end-cap **4** contains an alkyne as well as both the boronate and *o*-nitrobenzyl groups, allowing it to release uncapped PEtG in response to either H₂O₂ or UV light by a series of elimination-decarboxylation reactions (Scheme A5.1d).

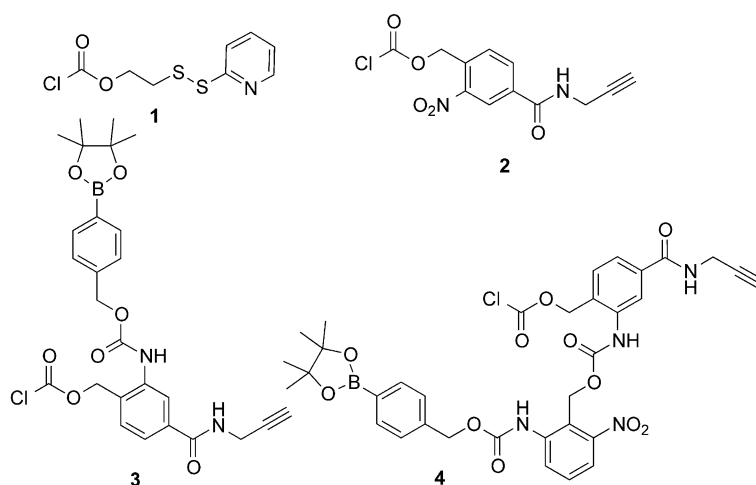
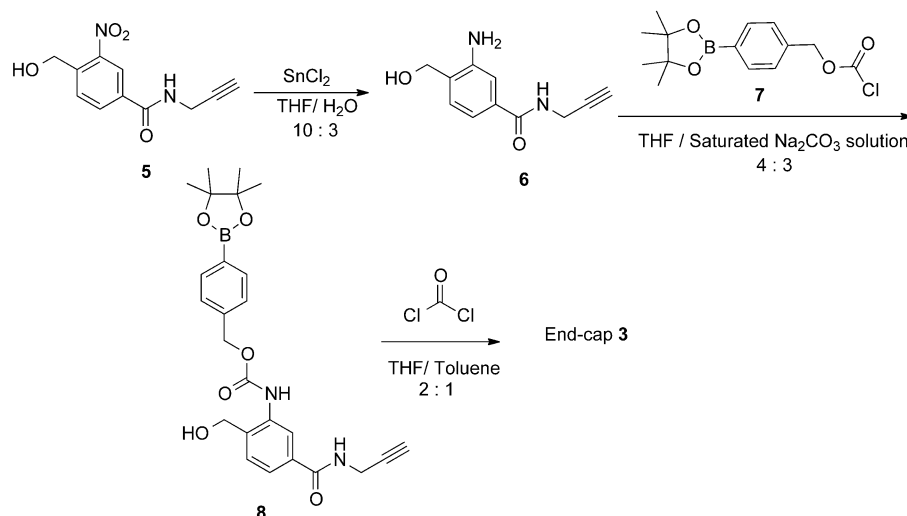


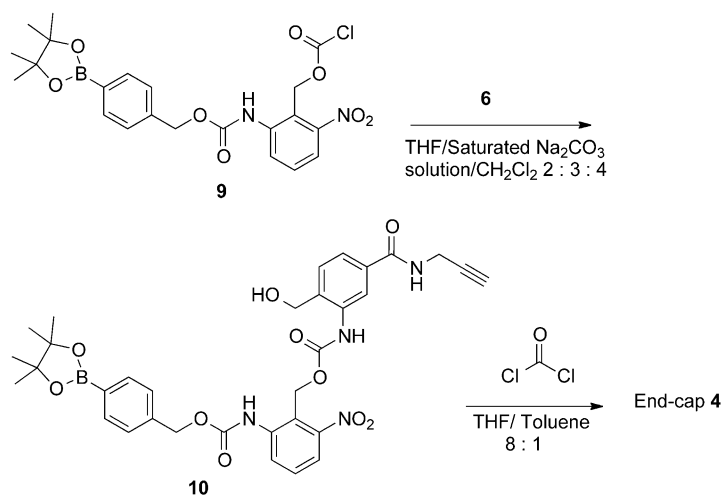
Figure 5.2 Chemical structures of linker end-caps each containing a chloroformate, one or more stimuli-responsive moieties, and a site for conjugation of PEG.

End-caps **1**²⁸ and **2**²² were prepared as previously reported. The preparation of end-cap **3** began with reduction of the nitro group in the *o*-nitrobenzyl alcohol **5**²² using SnCl₂ to afford the aniline **6** (Scheme 5.1). Selective reaction of the chloroformate **7**⁴³ with the aniline group in **6** provided compound **8**. Finally, activation with phosgene in THF/toluene

provided end-cap **3**. Recently, we reported chloroformate **9** as an end-cap that was responsive to both UV light and H₂O₂.²⁸ **9** was reacted selectively with the aniline group in compound **6** to afford compound **10**, which was then activated with phosgene to provide end-cap **4** (Scheme 5.2).



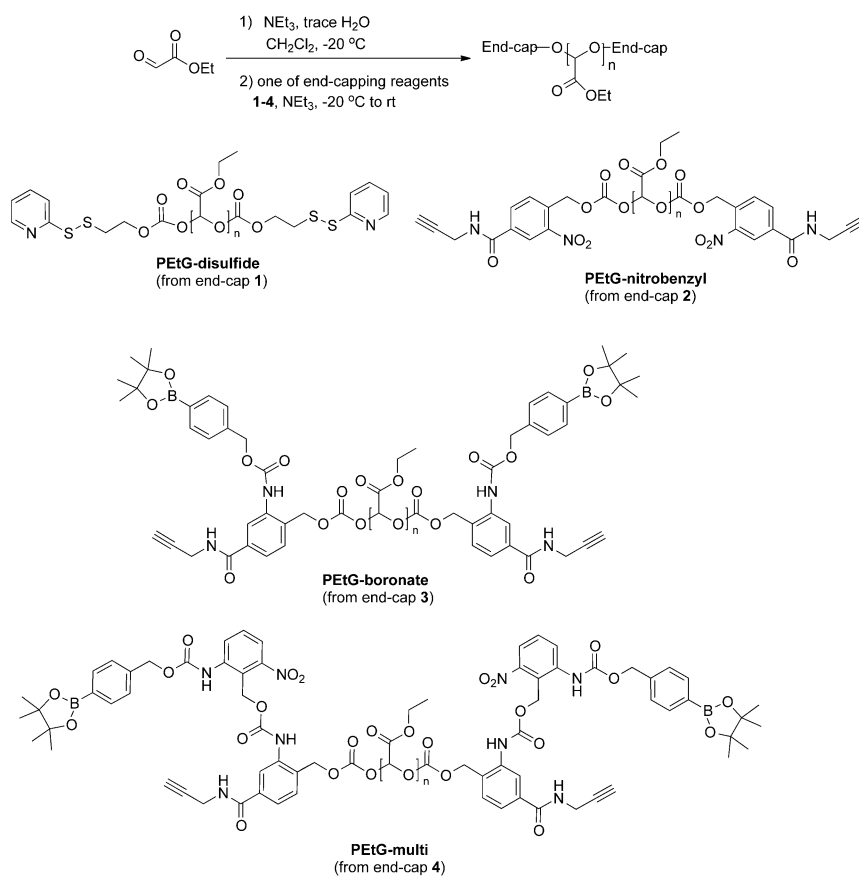
Scheme 5.1 Synthesis of end-cap 3.



Scheme 5.2 Synthesis of end-cap 4.

Following the previously reported procedure, PEtG was synthesized by the polymerization of freshly distilled ethyl glyoxylate in CH₂Cl₂ at -20 °C in the presence of catalytic NEt₃ (Scheme 5.3).²² End-cap and additional NEt₃ were then added at -20 °C to end-cap the

polymer and then the reaction was gradually warmed to room temperature. Capping with compounds **1**, **2**, **3**, and **4**, provided **PEtG-disulfide**,²⁸ **PEtG-nitrobenzyl**,²² **PEtG-boronate**, and **PEtG-multi** respectively. The polymers have end-caps at each terminus because EtGH generated from trace H₂O still present in the monomer after distillation initiates the polymerization. The PEtGs were purified by precipitation in methanol, except for **PEtG-multi**, which did not precipitate in methanol and was instead purified by dialysis.



Scheme 5.3 Synthesis of end-capped PEtGs.

The polymers were characterized by ¹H NMR spectroscopy, SEC, and TGA. NMR spectra were consistent with the proposed structures, although it was difficult to detect the end-cap peaks due to the high degrees of polymerization. Based on SEC analysis relative to PMMA standards, the molar masses of **PEtG-disulfide**, **PEtG-nitrobenzyl**, and **PEtG-boronate** ranged from 26-48 kg/mol and the dispersities (*D*) ranged from 1.4-2.1 (Table 5.1). **PEtG-multi** had a somewhat lower *M_n* of 6.3 kg/mol, likely due to the poor solubility of end-cap

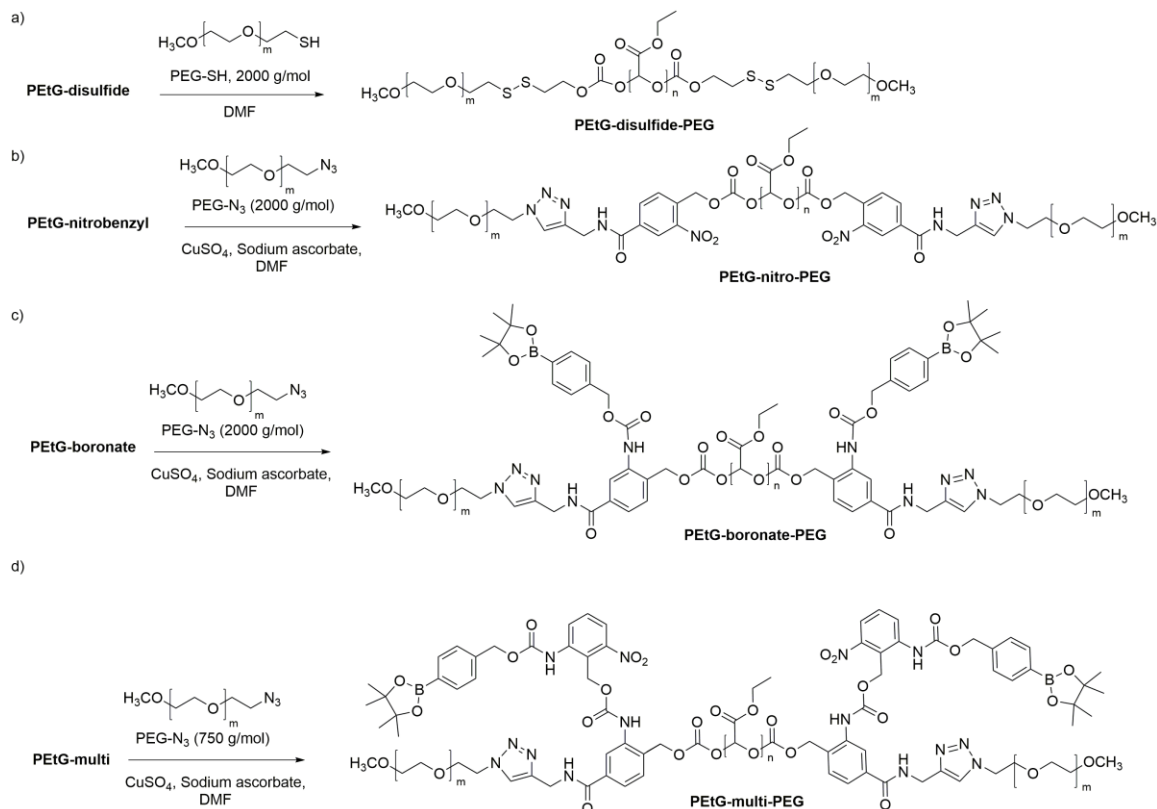
4 as well as high steric hindrance. It is possible that some depolymerization occurred before complete end-capping could be achieved. TGA showed that all of the polymers were quite thermally stable with onset degradation temperatures (T_o) greater than 160 °C. This confirmed complete end-capping of the isolated polymers as uncapped PEtG is thermally unstable and begins depolymerizing almost immediately upon heating.²²

Table 5.1 Properties of PEtG with different linker end-caps and PEG-PEtG-PEG copolymers. ^aThese polymers have been previously reported.²²

Polymer	M_n (SEC) (kg/mol)	\bar{D}	T_o (°C)
PEtG-disulfide^a	26	1.4	191
PEtG-nitrobenzyl^a	42	2.1	200
PEtG-boronate	48	1.5	165
PEtG-multi	6.3	1.6	204
PEtG-disulfide-PEG	29	1.4	179
PEtG-nitrobenzyl-PEG^a	40	2.1	203
PEtG-boronate-PEG	49	1.7	181
PEtG-multi-PEG	7.7	1.5	164

The next step was the conjugation of PEG to the reactive functional groups on the end-caps. PEG was selected as the hydrophilic block because it can be easily functionalized at its terminus and provides good water-dispersibility and biocompatibility in drug delivery applications.^{44,45} In previous work, small spherical nanoparticles were formed from a PEG-PEtG-PEG triblock copolymer with a hydrophilic mass fraction (f) of 0.10, where $f = \text{mass of PEG} / (\text{mass of PEG} + \text{mass of PEtG})$.²² Therefore, similar f values were targeted for the current work. While vesicles or larger particles would often be expected at such a low f values,^{1,46} this was attributed to the hydrophilicity of PEtG in comparison with other common hydrophobic blocks such as polybutadiene and polycaprolactone. **PEtG-disulfide** was coupled with PEG-SH *via* a disulfide exchange reaction in DMF to afford **PEtG-disulfide-PEG** (Scheme 5.4). **PEtG-nitrobenzyl** and **PEtG-boronate** were coupled to 2000 g/mol PEG-N₃ by CuAAC in DMF to afford **PEtG-nitrobenzyl-PEG** and **PEtG-boronate-PEG** respectively. Because of its lower initial M_n , **PEtG-multi** was coupled

with 750 g/mol PEG-N₃ to provide **PEtG-multi-PEG**. In each case, the excess PEG was removed by dialysis and washing with water.



Scheme 5.4 Synthesis of PEG-PEtG-PEG copolymers a) **PEtG-disulfide-PEG**, b) **PEtG-nitro-PEG**, c) **PEtG-boronate-PEG**, and d) **PEtG-multi-PEG**.

The purified block copolymers were characterized by ¹H NMR spectroscopy, SEC, and TGA. Removal of uncoupled PEG was confirmed by SEC as no peaks corresponding to free PEG were observed (Figures A5.15-A5.17). Only small increases in the M_ns for the block copolymers relative to the starting PEtGs were observed and there were no significant changes in their *D* values. Based on the integrations of the PEG peak relative to those of the PEtG in the ¹H NMR spectra, the CuAAC provided full conversion of the terminal alkynes to triazoles (Figure A5.13-A5.14). The *f* values for these polymers were calculated as 0.09 and 0.08 for **PEtG-nitrobenzyl-PEG** and **PEtG-boronate-PEG** respectively (Table 5.2). **PEtG-multi-PEG** had a higher *f* value of 0.20 due to the much lower initial M_n of the PEtG block. On the other hand, the disulfide exchange reaction

resulted in only ~50% conversion of the dithiopyridyl groups (Figure A5.12). This was deemed sufficient for nanoparticle formation as **PEtG-disulfide-PEG** had an f value of 0.08, very similar to that of the other copolymers. The T_o values for the block copolymers were similar to those of PEtG, although a 2-step degradation process was observed, with the first phase corresponding to PEtG and the second corresponding to PEG (Figures A5.19).

Table 5.2 Hydrophilic mass fractions (f) of the block copolymers and corresponding characterization of self-assembled nanoparticles by DLS and CAC measurement. Errors on the measurements correspond to the standard deviations.

Copolymer	f	Mean diameter measured by TEM (nm)	Z-average diameter (nm)	PDI	CAC ($\mu\text{g/mL}$)
PEtG-disulfide-PEG	0.08	55 ± 16	83 ± 1	0.19 ± 0.02	40
PEtG-nitrobenzyl-PEG	0.10	53 ± 17	82 ± 2	0.17 ± 0.03	32
PEtG-boronate-PEG	0.08	64 ± 26	85 ± 11	0.22 ± 0.05	32
PEtG-multi-PEG	0.20	47 ± 7	47 ± 9	0.18 ± 0.05	25

5.3.2 Self-assembly of PEtG-PEG triblock copolymers in aqueous solution

Self-assembly of each triblock copolymer was achieved by dissolving the polymer in DMSO and then injecting this solution into rapidly stirring water. The DMSO was then removed by dialysis. The diameters and polydispersity indices (PDIs) of the resulting nanoparticles were measured by DLS (Figures A5.20-A5.23). The Z-average hydrodynamic diameters of the nanoparticles ranged from 47 nm to 83 nm (Table 5.2). **PEtG-multi-PEG** formed the smallest assemblies, likely due to its relatively short block lengths and higher f value, while all other assemblies were of similar size. The PDIs ranged from 0.17 to 0.22, suggesting that the nanoparticles had reasonably narrow size distributions. TEM confirmed that the assemblies were solid, spherical particles (Figure 5.3). The mean diameters measured from the TEM images were smaller than those measured by DLS (Table 5.2) This can be attributed to the particles being in the dry rather

than hydrated state. Furthermore, an even small fraction of larger particles can significantly influence the Z-average diameter in DLS, due to the size dependence of the scattered light intensity. The critical aggregation concentrations (CACs) of the block copolymers were determined through the incorporation of the fluorescent probe Nile red.⁴⁷ The CAC values were all similar, ranging from 25 - 40 $\mu\text{g/mL}$. We also investigated the stabilities of the assemblies in mouse serum. Each system was stable for 24 h, and only the PEtG-boronate-PEG nanoparticles underwent some degradation over 96 h, with a $\sim 30\%$ reduction in count rate measured by DLS (Figure A5.24).

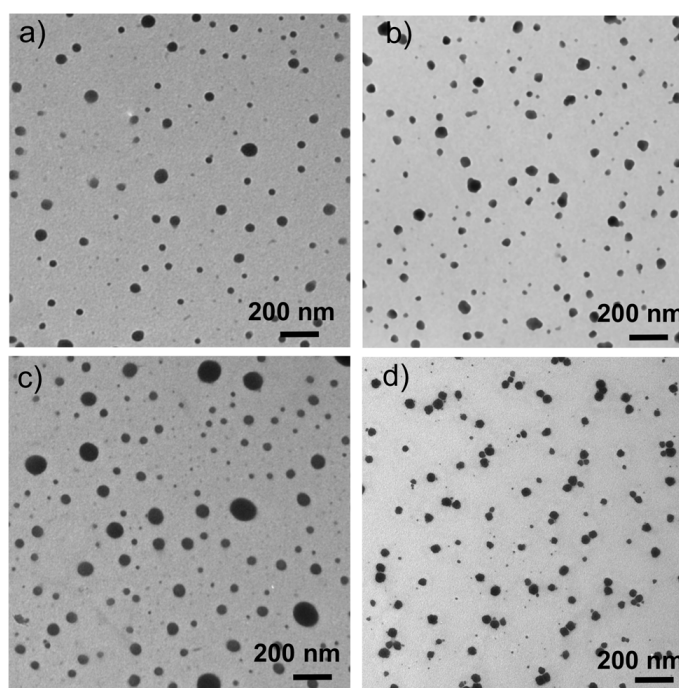


Figure 5.3 TEM images of nanoparticles formed from a) PEtG-disulfide-PEG, b) PEtG-nitrobenzyl-PEG, c) PEtG-boronate-PEG, and d) PEtG-multi-PEG.

5.3.3 Stimuli-responsive properties of the nanoparticles

Depolymerization of the nanoparticles in response to stimuli was studied using DLS and NMR spectroscopy. For DLS, the nanoparticles were prepared as described above and were dialyzed into 100 mM, pH 7.4 phosphate buffer unless otherwise indicated. After introduction of the stimulus, the nanoparticles were incubated at 37 $^{\circ}\text{C}$. DLS can provide

an indication of nanoparticle disintegration because the scattered light intensity, measured as the mean count rate, is proportional to the number of scattering species and their sizes. Disintegration of the micelles was expected to result in a decrease in the mean count rate. ^1H NMR spectroscopy was used to confirm that the disassembly of the nanoparticles was induced by the depolymerization of the PEtG block. For this experiment, the assemblies were prepared by injection of a DMSO- d_6 solution of the polymer into pH 7.4 phosphate- or pH 5.0 citrate-buffered D_2O ($\text{D}_2\text{O}:\text{DMSO-}d_6 = 5:1$). For practical reasons, the DMSO- d_6 was not removed. Prior to depolymerization, signals from the PEtG block were not observed in the NMR spectra because PEtG was packed into the nanoparticle core, resulting in very long relaxation times. However, upon depolymerization, peaks corresponding to the depolymerization product EtGH were observed and the percent depolymerization was measured based on the integration of peaks corresponding to this product relative to that of PEG.

The depolymerization of **PEtG-disulfide-PEG** nanoparticles was studied in the presence of varying concentrations of DTT, a commonly used thiol-based reducing agent. A reduction in count rate to less than 5% its initial value was observed in 3 h at 10 mM DTT (Figure 5.4a). The particle diameter remained constant over the first hour, then became multimodal and difficult to measure as the count rate became very low (Figure A5.25). The concentration of the thiol-based reducing agent glutathione has been reported to be as high as 15 mM in cancer cells,⁴⁸ so the nanoparticles exhibit responsive behavior at physiologically-relevant reducing agent concentrations. This is particularly significant because when depolymerization of the homopolymer **PEtG-disulfide** was studied in 9:1 $\text{CD}_3\text{CN}:\text{H}_2\text{O}$, 100 mM DTT was required because much of the DTT was trapped by reaction with ethyl glyoxylate.²⁸ The current results show that this trapping occurs to much less extent in the fully aqueous system where water competes more effectively as a nucleophile. However, it must also be noted that DTT is a stronger reducing agent than glutathione, so higher concentrations of glutathione would be required to achieve the same results as for DTT.⁴⁹ Below 10 mM DTT, the rate of nanoparticle degradation depended on the DTT concentration. At 1 mM DTT and below, the diameter did not change significantly as the count rate decreased over 48 h, suggesting that some assemblies were

still present (Figure A5.25). In the absence of DTT, the particles were stable for ~30 h, after which some degradation occurred, likely as a result of hydrolysis of the carbonate on the end-cap. As an additional control, **PEtG-nitro-PEG** nanoparticles, that were not designed to respond to DTT, were also exposed to 10 mM DTT. This system was stable for the first 10 h, after which slow degradation occurred. This degradation can arise from the cleavage of the carbonate, which may be assisted by nucleophilic DTT. However, the effect of 10 mM DTT on **PEtG-nitro-PEG** nanoparticles was clearly much less than on **PEtG-disulfide-PEG** nanoparticles. When the depolymerization was monitored by NMR spectroscopy at a concentration of 10 mM DTT, the rate was found to be similar to that observed by DLS (Figure 5.4b) and the depolymerization product was a mixture of EtGH and the DTT adduct that was characterized in our previous work²⁸ (Figure 5.4c).

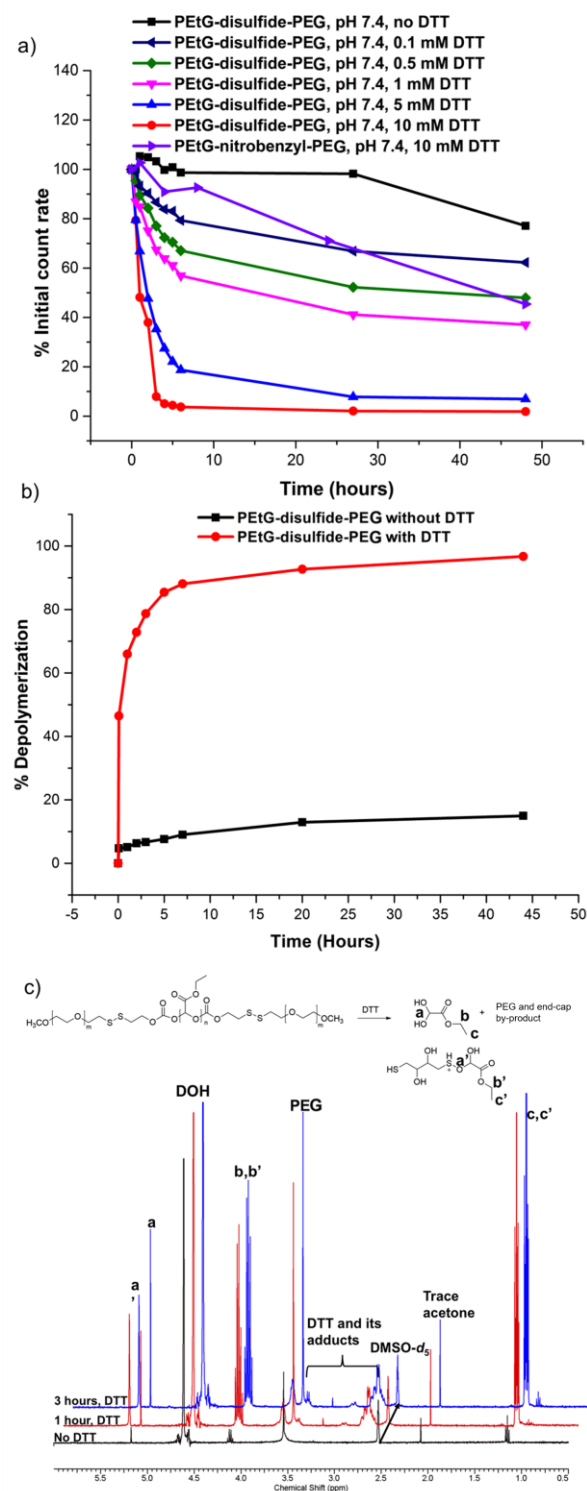


Figure 5.4 Stimuli-responsive properties of PEtG-disulfide-PEG nanoparticles: a) % Initial count rate versus time (measured by DLS) for nanoparticles exposed to varying

concentrations of DTT, b) % Depolymerization versus time for **PEtG-disulfide-PEG nanoparticles in 5:1 pH 7.4, phosphate buffered D₂O:DMSO-*d*₆ in the absence and presence of 10 mM DTT (measured by NMR spectroscopy). c) ¹H NMR spectra (400 MHz) of **PEtG-disulfide-PEG nanoparticles in the same solvent. Peaks corresponding to the depolymerization products EtGH and the DTT adduct appear after the addition of 10 mM DTT.****

We have previously studied the depolymerization of **PEtG-nitrobenzyl-PEG nanoparticles** at pH 7.4 by NMR spectroscopy, but we probed this in further detail here by DLS and also studied the depolymerization at pH 5.0 (100 mM citrate buffer). To cleave the nitrobenzyl linker end-cap, samples were irradiated with 2.8 mW/cm² of UVA light for 20 min. As shown in Figure 5.4b, after UV irradiation and incubation at 37 °C, a rapid decrease in the count rate was observed to less than 10% the initial value within 1 h at pH 7.4. The decrease was slower at pH 5.0, requiring 6 h to reach ~20% the initial value. This pH dependence arises because depolymerization occurs via hemiacetal breakdown, which can be catalyzed by acid or base, and exhibits a rate minimum at mildly acidic pH.⁵⁰ When **PEtG-nitrobenzyl-PEG nanoparticles** were not irradiated, there was no significant change in the count rate over 6 h. As an additional control experiment, non-light-sensitive **PEtG-disulfide-PEG assemblies** were also irradiated. No significant perturbations in count rate were observed. NMR spectroscopy in 5:1 D₂O:DMSO-*d*₆ showed that depolymerization of **PEtG-nitrobenzyl-PEG** to EtGH occurred following irradiation at a rate similar to that suggested by DLS (Figure A5.27). It also confirmed that the depolymerization was faster at pH 7.4 and that depolymerization did not occur to any significant extent without irradiation (Figures A5.27-A5.29). Overall, these results confirm that **PEtG-nitrobenzyl-PEG nanoparticles** can be selectively depolymerized by UV light.

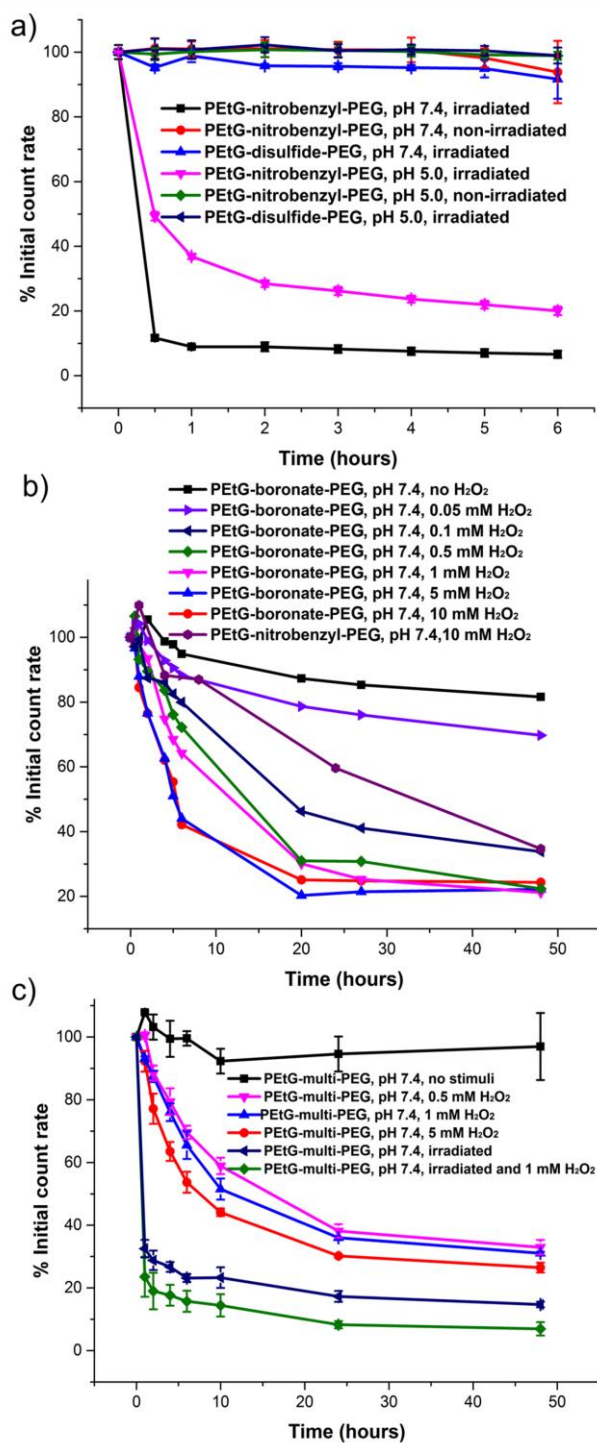


Figure 5.5 %Initial count rate, measured by DLS, versus time for nanoparticles and their corresponding controls with or without stimuli: a) PEtG-nitrobenzyl-PEG nanoparticles with UV light, b) PEtG-boronate-PEG with H₂O₂, c) PEtG-multi-PEG

with H₂O₂, UV light, or both. The study was carried out at pH 7.4, except for b) which was also performed at pH 5.0. The temperature was 37 °C. Error bars represent the standard deviation on 3 samples.

PEtG-boronate-PEG nanoparticles were studied in the presence of varying concentrations of H₂O₂. As shown in Figure 5.5b, even 0.05 mM H₂O₂ was able to induce an effect on the nanoparticles with a reduction in the count rate to ~70% its initial value over 48 h. This corresponds to less than 2 molar equiv. relative to the end-cap and less than 0.01 equiv. relative to monomer units in the polymer backbone. The ability of this system to respond to such low concentrations of H₂O₂ is a significant advance over previous work where a boronate-capped PEtG homopolymer in 9:1 CD₃CN:D₂O required ~100 mM H₂O₂ for complete depolymerization due to the trapping of nucleophilic H₂O₂ by EtG.²⁸ H₂O₂ is reported to be the most stable and highest concentration reactive oxygen species in living organisms, with concentrations varying significantly from 100 μM to 0.01 μM, depending on the stage of cell growth.^{51,52} It can be present even in healthy cells, but the highest concentrations are usually associated with unhealthy states such as inflammation or cell apoptosis. In the current system, the rate of particle degradation continued to increase with increasing H₂O₂ concentration up to ~5 mM H₂O₂. In the absence of H₂O₂, 80% of the initial count rate was retained over 48 h, with the small decrease likely resulting from non-specific cleavage as described above. As an additional control, the effect of 10 mM H₂O₂ on **PEtG-nitro-PEG** nanoparticles was investigated. Gradual degradation was observed for this control, suggesting that this concentration of nucleophilic H₂O₂ can induce some non-specific cleavage of the carbonate on the end-cap. However, the rate of degradation was still much slower than that resulting from the same concentration of H₂O₂ applied to **PEtG-boronate-PEG** nanoparticles. Study of the same system by NMR spectroscopy in 5:1 D₂O:DMSO-*d*₆ with and without 10 mM H₂O₂ confirmed that **PEtG-boronate-PEG** nanoparticles depolymerized at rates matching those observed by DLS and that the depolymerization product was EtGH, and small amount of the H₂O₂ adduct (Figure A5.30).

Finally, the response of **PEtG-multi-PEG** to UV light, H₂O₂ and a combination of these stimuli was studied. As shown from Figure 5.5c, almost immediate degradation of the

nanoparticles was observed after 20 min of UV irradiation. A slightly lower count rate was achieved using UV light and H₂O₂, which may result from the H₂O₂ being able to cleave a small amount of residual intact end-cap that remained after the irradiation. On the other hand, the degradation induced by H₂O₂ alone was significantly slower. As proposed in our previous work with PEtG homopolymers, this may arise from the requirement for multiple elimination reactions to initiate the depolymerization or from the trapping of reactive (azo)quinone methide species by depolymerizing PEtG.²⁸ In the absence of stimuli, **PEtG-multi-PEG** nanoparticles were stable during 48 h. NMR spectroscopy confirmed the depolymerization rate and that the expected products were produced (Figure A5.31-A5.32).

5.3.4 Encapsulation and triggered release of drugs and model drugs

To demonstrate the encapsulation and release abilities of the nanoparticles, the hydrophobic dye Nile red was first used as a model drug. It has strong fluorescence emission at ~600 nm when it is in hydrophobic environments such as the cores of polymer nanoparticles, but its fluorescence is quenched in aqueous environments due to aggregation.^{53,54} This allows its release from nanoparticles to be probed. Nanoparticles were incubated with a thin film of Nile red to load the dye into their cores then Nile red release in response to stimuli was probed. As shown in Figure 5.6a, **PEtG-disulfide-PEG** released Nile red at increasing rates with increasing concentrations of DTT in pH 7.4 phosphate buffer at 37 °C. The rates were in general agreement with the DLS and NMR studies described above. 0.5 mM DTT was the critical concentration required to provide a rapid release. Similar results were observed for **PEtG-boronate-PEG** nanoparticles, with 0.5 mM H₂O₂ being the critical concentration to trigger the release of a substantial fraction of the Nile red (Figure 5.6b).

Nile red-loaded **PEtG-nitrobenzyl-PEG** nanoparticles were triggered to release the dye by irradiation with UV light for 20 min. The release of Nile red at pH 7.4 was very rapid, with the fluorescence decreasing to less than 20% its initial value in 20 min (Figure 5.6c).

In agreement with the DLS and NMR studies, it was slightly slower at pH 5.0, reaching less than 60% of the initial fluorescence in 20 min. The photostability of Nile red under the irradiation conditions was confirmed to ensure that the decrease in fluorescence was a result of its release from the particles and not from photodegradation (Figure A5.33). The rapid release of Nile red from **PEtG-nitrobenzyl-PEG** nanoparticles confirms that depolymerization is very rapid following end-cap cleavage and that the slower rates in some of the DTT and H₂O₂ conditions can likely be attributed to end-cap cleavage being the rate-determining step.

The above results demonstrated that PEtG-based nanoparticles were capable of encapsulating and releasing cargo in response to their corresponding stimuli, so the next step was the loading and release of drug molecules. First, the encapsulation and release of Dox using **PEtG-nitrobenzyl-PEG** nanoparticles was investigated. Dox is a chemotherapeutic used in the treatment of a wide range of cancers.⁵⁵ It was encapsulated during self-assembly by co-dissolving it with the polymer in DMSO prior to nanoparticle formation. Unencapsulated drug was removed by dialysis. The Dox content was 13 wt% and the loading efficiency was ~23%. The release of Dox from the nanoparticles with and without UV irradiation was monitored at 37 °C at pH 7.4 and 5.0 using dialysis to separate encapsulated and released drug. As shown in Figure 5.7, UV irradiation triggered a burst release 65% and 80% of the Dox at pH 7.4 and pH 5.0 over the first 10 h. The increased release at pH 5.0, which contrasts with that observed for Nile red, can likely be attributed to increased protonation of Dox's primary amine group at pH 5. This increases its solubility in the aqueous medium outside the nanoparticle. In the absence of UV irradiation, the release was significantly slower at each pH.

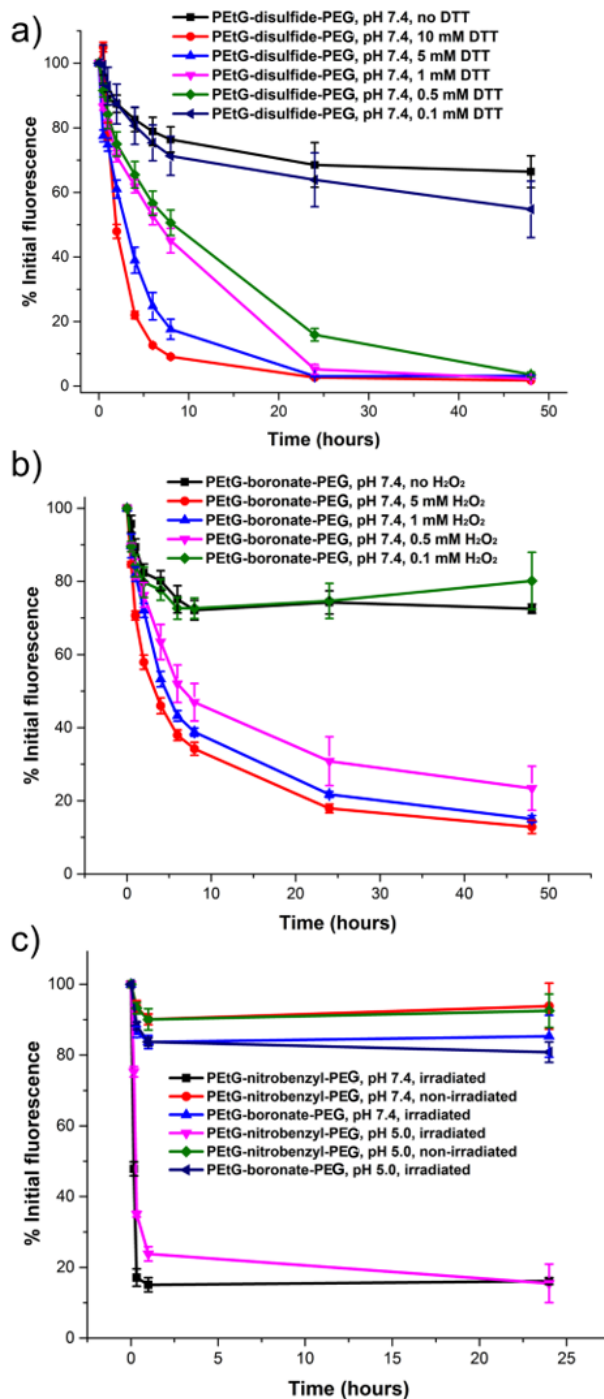


Figure 5.6 Change in Nile red fluorescence intensity as an indicator of its release from nanoparticles composed of a) PEtG-disulfide-PEG, b) PEtG-boronate-PEG, and c) PEtG-nitrobenzyl-PEG in the presence and absence of their corresponding stimuli. Error bars correspond to the standard deviation on three samples.

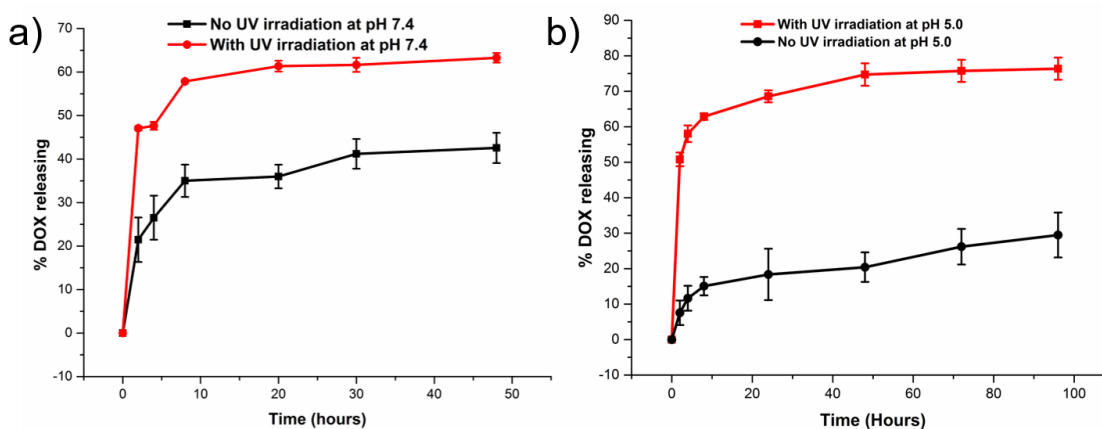


Figure 5.7 Release of Dox from PETG-nitrobenzyl-PEG nanoparticles with and without UV irradiation at a) pH 7.4 and b) pH 5.0.

While the stimulus-triggered release was demonstrated with Dox, the relatively rapid background release in the absence of stimulus was not ideal, so additional drugs were investigated. Curcumin (Cur) is a naturally-occurring polyphenol that has been shown to inhibit cancer cell survival and proliferation.⁵⁶ However, it suffers from poor solubility and bioavailability, so it would benefit significantly from an effective delivery system. As Cur is highly susceptible to photodegradation, **PETG-disulfide-PEG** and **PETG-boronate-PEG** were used with this drug, and **PETG-nitrobenzyl-PEG** was used as a control system that should not be triggered by DTT or H₂O₂. Cur was encapsulated by dissolving it with the copolymer in DMF, then adding this solution to buffer to induce self-assembly. The free drug was removed by dialysis and insoluble particles were removed by filtration. This resulted in drug contents of 7.8%, 11.0% and 12.4% and encapsulation efficiencies of 43%, 62% and 71% for **PETG-disulfide-PEG**, **PETG-boronate-PEG** and **PETG-nitrobenzyl-PEG** respectively. In initial studies, it was observed that the rapid release of Cur in the presence of the stimuli resulted in fast precipitation of the drug. Therefore, the analysis of released drug by a dialysis-based method was not used. Instead, the precipitated drug was separated by filtration, and the amount remaining in the nanoparticles was quantified by removing a small aliquot of the nanoparticle suspension, diluting it into DMF to provide complete dissolution, and measuring the absorbance of this solution at 428 nm.

Both 0.5 mM and 5 mM DTT triggered the release of more than 95% of Cur from **PEtG-disulfide-PEG** nanoparticles in the first hour (Figure 5.8a). In contrast, in the absence of DTT ~90% of the Cur was retained in the nanoparticles over 8 h. The effect of DTT on Cur release from **PEtG-nitrobenzyl-PEG** nanoparticles was also investigated as a control. ~90% of the drug was retained over 8 h in the presence of 0.5 mM DTT. At 5 mM DTT, the retention of curcumin in the nanoparticles dropped to ~50% over 8 h. This likely results from a direct reaction of DTT with Cur as thiols are known to undergo Michael addition reactions with Cur, disrupting π -conjugation and reducing its absorbance.⁵⁷ However, the effect of DTT on **PEtG-disulfide-PEG** nanoparticles at either concentration was still much greater than this background reaction, demonstrating the specificity of the triggering.

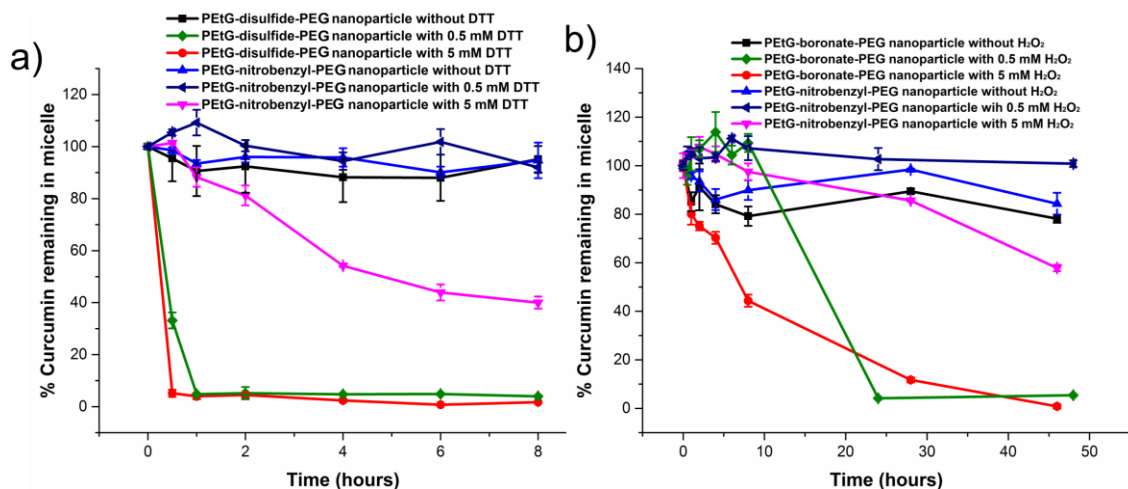


Figure 5.8 Curcumin retention in a) **PEtG-disulfide-PEG** and b) **PEtG-boronate-PEG** nanoparticles in the presence and absence of stimuli as well as their corresponding controls.

H₂O₂ triggered the release of Cur from **PEtG-boronate-PEG** micelles at concentrations of 0.5 or 5 mM. The release rate of Cur was faster at higher H₂O₂ concentrations due to faster cleavage of the end-cap. At 0.5 mM, a delay in the initiation of release for several hours was observed, suggesting that a critical amount of depolymerization is required to trigger the release. In the absence of H₂O₂, ~80% of the Cur was retained in the **PEtG-boronate-PEG** nanoparticles over 48 h. The response of Cur-loaded **PEtG-nitrobenzyl-PEG**

nanoparticles to H₂O₂ was also investigated as a control experiment. As for DTT, it was found that 0.5 mM H₂O₂ did not result in any significant change in the encapsulated Cur. However, 5 mM H₂O₂ resulted in a slow decrease, reaching ~60% the initial value after 48 h. This could arise from the non-specific action of H₂O₂ on the **PEtG-nitrobenzyl-PEG** nanoparticles, as was observed in the DLS study. It could also arise from the reaction of Cur with H₂O₂ as Cur is well known to exhibit antioxidant activity by scavenging reactive oxygen species.⁵⁷ Nevertheless, there was again a large difference between the specific triggering of **PEtG-boronate-PEG** nanoparticles compared to the background reaction of **PEtG-nitrobenzyl-PEG** nanoparticles.

5.4 Conclusions

In conclusion, two previously developed and two new linker end-caps were used to prepare a series of amphiphilic PEG-PEtG-PEG copolymers responsive to thiols, UV light, H₂O₂, and combinations of these stimuli. These copolymers were self-assembled to form nanoparticles in aqueous solution with hydrodynamic diameters ranging from 46-83 nm. Their depolymerization was induced by the respective stimuli and was studied by DLS and NMR spectroscopy. For DTT and H₂O₂, depolymerization occurred at a rate dependent on the stimulus concentration, and degradation of the nanoparticles could be detected at concentrations corresponding to less than 2 equiv. relative to the end-cap and less than 0.01 equiv. relative to the polymerization monomer. This confirmed that single end-cap cleavage events could be translated to afford large changes in the systems through depolymerization. The encapsulation and triggered release capabilities of the nanoparticles were also probed using Nile red, Dox, and Cur. In each case, the stimulus was capable of selectively releasing the payload. Furthermore, it was demonstrated that the system is highly tunable as the stimulus to which the system responds can be changed by changing only the small molecule linker end-cap between the two blocks. These properties make this new platform highly promising for drug delivery applications. Future work will focus on the *in vitro* and *in vivo* evaluation of these nanoparticles.

5.5 References

- (1) Mai, Y.; Eisenberg, A. Self-assembly of block copolymers. *Chem. Soc. Rev.* **2012**, *41*, 5969-5985.
- (2) Kim, J. K.; Yang, S. Y.; Lee, Y.; Kim, Y. Functional nanomaterials based on block copolymer self-assembly. *Prog. Polym. Sci.* **2010**, *35*, 1325-1349.
- (3) Albert, J. N.; Epps, T. H. Self-assembly of block copolymer thin films *Mater. Today* **2010**, *13*, 24-33.
- (4) Tyrrell, Z. L.; Shen, Y.; Radosz, M. Fabrication of micellar nanoparticles for drug delivery through the self-assembly of block copolymers. *Prog. Polym. Sci.* **2010**, *35*, 1128-1143.
- (5) Rösler, A.; Vandermeulen, G. W. M.; Klok, H.-A. Advanced drug delivery devices via self-assembly of amphiphilic block copolymers. *Adv. Drug Delivery Rev.* **2012**, *64*, 270-279.
- (6) Movassaghian, S.; Merkel, O. M.; Torchilin, V. P. Applications of polymer micelles for imaging and drug delivery. *Wiley Interdiscip. Rev.: Nanomed. Nanobiotechnol.* **2015**, *7*, 691-707.
- (7) Prabhakar, U.; Maeda, H.; Jain, R. K.; Sevick-Muraca, E. M.; Zamboni, W.; Farokhzad, O. C.; Barry, S. T.; Gabizon, A.; Grodzinski, P.; Blakey, D. C. Challenges and key considerations of the enhanced permeability and retention effect for nanomedicine drug delivery in oncology. *Cancer Res.* **2013**, *73*, 2412-2417.
- (8) Maeda, H.; Nakamura, H.; Fang, J. The EPR effect for macromolecular drug delivery to solid tumors: improvement of tumor uptake, lowering of systemic toxicity, and distinct tumor imaging *in vivo*. *Adv. Drug Delivery Rev.* **2013**, *65*, 71-79.
- (9) Nicolas, J.; Mura, S.; Brambilla, D.; Mackiewicz, N.; Couvreur, P. Design, functionalization strategies and biomedical applications of targeted biodegradable/biocompatible polymer-based nanocarriers for drug delivery. *Chem. Soc. Rev.* **2013**, *42*, 1147-1235.
- (10) Bachelder, E. M.; Beaudette, T. T.; Broaders, K. E.; Dashe, J.; Fréchet, J. M. Acetal-derivatized dextran: an acid-responsive biodegradable material for therapeutic applications. *J. Am. Chem. Soc.* **2008**, *130*, 10494-10495.

- (11) Chen, W.; Meng, F.; Li, F.; Ji, S.-J.; Zhong, Z. pH-Responsive biodegradable micelles based on acid-labile polycarbonate hydrophobe: synthesis and triggered drug release. *Biomacromolecules* **2009**, *10*, 1727-1735.
- (12) Liu, Y.; Wang, W.; Yang, J.; Zhou, C.; Sun, J. pH-Sensitive polymeric micelles triggered drug release for extracellular and intracellular drug targeting delivery. *Asian J. Pharm. Sci.* **2013**, *8*, 159-167.
- (13) Liu, J.; Huang, Y.; Kumar, A.; Tan, A.; Jin, S.; Mozhi, A.; Liang, X. J. pH-Sensitive nano-systems for drug delivery in cancer therapy. *Biotechnol. Adv.* **2014**, *32*, 693-710.
- (14) Ganta, S.; Devalapally, H.; Shahiwala, A.; Amiji, M. A Review of stimuli-responsive nanocarriers for drug and gene delivery. *J. Controlled Release* **2008**, *126*, 187-204.
- (15) Cheng, R.; Feng, F.; Meng, F.; Deng, C.; Feijen, J.; Zhong, Z. Glutathione-responsive nano-vehicles as a promising platform for targeted intracellular drug and gene delivery. *J. Controlled Release* **2011**, *152*, 2-12.
- (16) Ding, J.; Chen, J.; Li, D.; Xiao, C.; Zhang, J.; He, C.; Zhuang, X.; Chen, X. Biocompatible reduction-responsive polypeptide micelles as nanocarriers for enhanced chemotherapy efficacy *in vitro*. *J. Mater. Chem. B* **2013**, *1*, 69-81.
- (17) Liu, B.; Wang, D.; Liu, Y.; Zhang, Q.; Meng, L.; Chi, H.; Shi, J.; Li, G.; Li, J.; Zhu, X. Hydrogen peroxide-responsive anticancer hyperbranched polymer micelles for enhanced cell apoptosis. *Polym. Chem.* **2015**, *6*, 3460-3471.
- (18) de Gracia Lux, C.; Joshi-Barr, S.; Nguyen, T.; Mahmoud, E.; Schopf, E.; Fomina, N.; Almutairi, A. Biocompatible polymeric nanoparticles degrade and release cargo in response to biologically relevant levels of hydrogen peroxide. *J. Am. Chem. Soc.* **2012**, *134*, 15758-15764.
- (19) Phillips, S. T.; DiLauro, A. M. Continuous head-to-tail depolymerization: an emerging concept for imparting amplified responses to stimuli-responsive materials. *ACS Macro Lett.* **2014**, *3*, 298-304.
- (20) Fan, B.; Gillies, E. R. Self-immolative polymers. *Encycl. Polym. Sci. Technol.* **2015**, 1-35.
- (21) Wong, A. D.; DeWit, M. A.; Gillies, E. R. Amplified release through the stimulus triggered degradation of self-immolative oligomers, dendrimers, and linear polymers. *Adv.*

Drug Delivery Rev. **2012**, *64*, 1031-1045.

(22) Fan, B.; Trant, J. F.; Wong, A. D.; Gillies, E. R. Polyglyoxylates: A versatile class of triggerable self-immolative polymers from readily accessible monomers. *J. Am. Chem. Soc.* **2014**, *136*, 10116-10123.

(23) de Gracia Lux, C.; McFearin, C. L.; Joshi-Barr, S.; Sankaranarayanan, J.; Fomina, N.; Almutairi, A. Single UV or near-IR triggering event leads to polymer degradation into small molecules. *ACS Macro Lett.* **2012**, *1*, 922-926.

(24) Liu, G.; Wang, X.; Hu, J.; Zhang, G.; Liu, S. Self-immolative polymersomes for high-efficiency triggered release and programmed enzymatic reactions. *J. Am. Chem. Soc.* **2014**, *136*, 7492-7497.

(25) Lewis, G. G.; Robbins, J. S.; Phillips, S. T. Point-of-Care assay platform for quantifying active enzymes to femtomolar levels using measurements of time as the readout. *Anal. Chem.* **2013**, *85*, 10432-10439.

(26) Lewis, G. G.; Robbins, J. S.; Phillips, S. T. Phase-switching depolymerizable poly(carbamate) oligomers for signal amplification in quantitative time-based assays. *Macromolecules* **2013**, *46*, 5177-5183.

(27) DeWit, M. A.; Beaton, A.; Gillies, E. R. A reduction sensitive cascade biodegradable linear polymer. *J. Polym. Sci., Part A: Polym. Chem.* **2010**, *48*, 3977-3985.

(28) Fan, B.; Trant, J. F.; Gillies, E. R. End-capping strategies for triggering the end-to-end depolymerization of polyglyoxylates. *Macromolecules* **2017**, *49*, 9309-9319.

(29) Sagi, A.; Weinstain, R.; Karton, N.; Shabat, D. Self-immolative polymers. *J. Am. Chem. Soc.* **2008**, *130*, 5434-5435.

(30) Liu, G.; Zhang, G.; Hu, J.; Wang, X.; Zhu, M.; Liu, S. Hyperbranched self-immolative polymers (h-SIPs) for programmed payload delivery and ultrasensitive detection. *J. Am. Chem. Soc.* **2015**, *137*, 11645-11655.

(31) Seo, W.; Phillips, S. T. Patterned plastics that change physical structure in response to applied chemical signals. *J. Am. Chem. Soc.* **2010**, *132*, 9234-9235.

(32) Kim, H.; Mohapatra, H.; Phillips, S. T. Rapid, on-command debonding of stimuli-responsive cross-linked adhesives by continuous, sequential quinone methide elimination reactions. *Angew. Chem., Int. Ed.* **2015**, *54*, 13063-13067.

- (33) Fan, B.; Trant, J. F.; Yardley, R. E.; Pickering, A. J.; Laguné-Labarthe, F.; Gillies, E. R. Photocontrolled degradation of stimuli-responsive poly(ethyl glyoxylate): differentiating features and traceless ambient depolymerization. *Macromolecules* **2016**, *49*, 7196-7203.
- (34) DeWit, M. A.; Gillies, E. R. A cascade biodegradable polymer based on alternating cyclization and elimination reactions. *J. Am. Chem. Soc.* **2009**, *131*, 18327-18334.
- (35) Monks, T. J.; Jones, D. C. The metabolism and toxicity of quinones, quinonimines, quinone methides, and quinone-thioethers. *Curr. Drug Metab.* **2002**, *3*, 425-438.
- (36) Baker, P. R. S.; Cramer, S. D.; Kennedy, M.; Assimos, D. G.; Holmes, R. P. Glycolate and glyoxylate metabolism in hepg2 cells. *Am. J. Physiol. Cell Physiol.* **2004**, *287*, C1359-1365.
- (37) Belloncle, B.; Bunel, C.; Menu-Bouaouiche, L.; Lesouhaitier, O.; Burel, F. Study of the degradation of poly(ethyl glyoxylate): biodegradation, toxicity and ecotoxicity assays. *J. Polym. Environ.* **2012**, *20*, 726-731.
- (38) Nguyen, P. K.; Snyder, C. G.; Shields, J. D.; Smith, A. W.; Elbert, D. L. Clickable Poly(ethylene glycol)-microsphere-based cell scaffolds. *Macromol. Chem. Phys.* **2013**, *214*, 948-956.
- (39) Liu, Y.; Shipton, M. K.; Ryan, J.; Kaufman, E. D.; Franzen, S.; Feldheim, D. L. Synthesis, stability, and cellular internalization of gold nanoparticles containing mixed peptide-poly(ethylene glycol) monolayers. *Anal. Chem.* **2007**, *79*, 2221-2229.
- (40) Kuppusamy, P.; Li, H.; Ilangoan, G.; Cardounel, A. J.; Zweier, J. L.; Yamada, K.; Krishna, M. C.; Mitchell, J. B. Noninvasive imaging of tumor redox status and its modification by tissue glutathione levels. *Cancer Res.* **2002**, *62*, 307-312.
- (41) Gough, D. R.; Cotter, T. G. Hydrogen Peroxide: A jekyll and hyde signalling molecule. *Cell Death Dis.* **2011**, *2*, e213.
- (42) Gohy, J.-F.; Zhao, Y. Photo-responsive block copolymer micelles: design and behavior. *Chem. Soc. Rev.* **2013**, *42*, 7117.
- (43) Chung, C.; Srikun, D.; Lim, C. S.; Chang, C. J.; Cho, B. R. A two-photon fluorescent probe for ratiometric imaging of hydrogen peroxide in live tissue. *Chem. Commun.* **2011**, *47*, 9618-9620.

- (44) Harris, J. M.; Martin, N. E.; Modi, M. PEGylation: A novel process for modifying pharmacokinetics. *Clin. Pharmacokinet.* **2001**, *40*, 539-551.
- (45) Banerjee, S. S.; Aher, N.; Patil, R.; Khandare, J. Poly(ethylene glycol)-prodrug conjugates: Concept, design, and applications. *J. Drug Delivery* **2012**, *2012*, Article ID 103973.
- (46) Discher, D. E.; Eisenberg, A. Polymer vesicles. *Science* **2002**, *297*, 967-973.
- (47) Gillies, E. R.; Fréchet, J. M. A new approach towards acid sensitive copolymer micelles for drug delivery. *Chem. Commun.* **2003**, 1640-1641.
- (48) Montero, D.; Tachibana, C.; Winther, J. R.; Appenzeller-Herzog, C. Intracellular glutathione pools are heterogeneously concentrated. *Redox Biol.* **2013**, *1*, 508-513.
- (49) Rothwarf, D. M.; Scheraga, H. A. Equilibrium and kinetic constants for the thiol-disulfide interchange reaction between glutathione and dithiothreitol. *Proc. Natl. Acad. Sci.* **1992**, *89*, 7944-7948.
- (50) Funderburk, L. H.; Aldwin, L.; Jencks, W. P. Mechanisms of general acid and base catalysis of the reactions of water and alcohols with formaldehyde. *J. Am. Chem. Soc.* **1978**, *100*, 5444-5459.
- (51) Giorgio, M.; Trinei, M.; Migliaccio, E.; Pelicci, P. G. Hydrogen peroxide: A metabolic by-product or a common mediator of ageing signals? *Nat. Rev. Mol. Cell Biol.* **2007**, *8*, 722-728.
- (52) Forman, H. J.; Bernardo, A.; Davies, K. J. A. What is the concentration of hydrogen peroxide in blood and plasma? *Arch. Biochem. Biophys.* **2016**, *603*, 48-53.
- (53) Greenspan, P.; Mayer, E. P.; Fowler, S. D. Nile red: A selective fluorescent stain for intracellular lipid droplets. *J. Cell Biol.* **1985**, *100*, 965-973.
- (54) Krishna, M. M. G. Excited-state kinetics of the hydrophobic probe nile red in membranes and micelles. *J. Phys. Chem. A* **1999**, *103*, 3589-3595.
- (55) Tacar, O.; Sriamornsak, P.; Dass, C. R. Doxorubicin. *J. Pharm. Pharmacol.* **2012**, *65*, 157-170.
- (56) Salem, M.; Rohani, S.; Gillies, E. R. Curcumin, a promising anti-cancer therapeutic: a review of its chemical properties, bioactivity and approaches to cancer cell delivery. *RSC Adv.* **2014**, *4*, 10815-10829.

- (57) Priyadarsini, K. I. The chemistry of curcumin: from extraction to therapeutic agent. *Molecules* **2014**, *19*, 20091-20112.
- (58) Chung, C.; Srikun, D.; Lim, C. S.; Chang, C. J.; Cho, B. R. A two-photon fluorescent probe for ratiometric imaging of hydrogen peroxide in live tissue. *Chem. Commun.* **2011**, *47*, 9618-9620.
- (59) Liu, Y.; Shipton, M. K.; Ryan, J.; Kaufman, E. D.; Franzen, S.; Feldheim, D. L. Synthesis, stability, and cellular internalization of gold nanoparticles containing mixed peptide-poly(ethylene glycol) monolayers. *Anal. Chem.* **2007**, *79*, 2221-2229.

Chapter 6

6 Tuning the hydrophobic core of self-immolative polyglyoxylate assemblies

6.1 Introduction

Biodegradable polymers such as poly(lactic acid), poly(caprolactone) and poly(glycolic acid) have been extensively studied over the past few decades as replacements for traditional non-degradable polymers.¹⁻³ In particular, these biodegradable polymers are of significant interest as biomedical materials, such as sutures,⁴ tissue engineering scaffolds,² and drug delivery vehicles.⁵ Polyester nanoparticles have emerged as promising materials for the delivery of drugs, where they can address limitations of drugs such as poor water solubility, low stability, and toxic side effects.⁶⁻⁷ Thus far, several examples of polyester-based nanoparticles loaded with anti-cancer drugs have been approved for clinical trials in different countries, and GenexolTM-PM, which is a formulation based on PEG-*b*-poly(D,L-lactic acid) with paclitaxel incorporated, has been approved by the FDA.^{6, 8} However, the degradation of polyesters and the release of drugs from these systems are challenging to control and cannot be precisely controlled or “turned on” when needed.⁹⁻¹⁰

Stimuli-responsive polymers that can respond to external stimuli through degradation have been proposed as potential alternatives to polyesters.¹¹⁻¹² Systems responsive to changes in pH¹³⁻¹⁴ or temperature,¹⁵ oxidation,¹⁶ reduction,¹⁷ light¹⁸ and other stimuli have been explored and promising results have been achieved, particularly in the area of drug delivery. Over the past decade, a new class of stimuli-responsive polymers, often referred to as “self-immolative polymers” (SIPs) has emerged.¹⁹⁻²¹ SIPs are composed of a polymer backbone with stimuli-responsive end-caps at one or both termini. Cleavage of the end-cap results in a cascade of reactions leading to complete end-to-end depolymerization to small molecules. One advantage of SIPs is their ability to amplify signals, as one stimulus event can generate hundreds of small molecules. This has led to proof-of-concept applications of SIPs in molecular sensors,²² microcapsules,²³⁻²⁵ point-of-care assay devices,²⁶ and drug delivery.²⁷⁻²⁸ In addition, while traditional stimuli-responsive polymers require a substantial polymer redesign to change the stimulus to which the system responds, end-

caps responsive to different stimuli can easily be introduced to SIPs while retaining the same backbone.²⁹ This makes each backbone relatively versatile. Various backbones including polycarbamates,²² polycarbonates,³⁰⁻³¹ poly(benzyl ether)s³²⁻³³ and polyacetals³⁴⁻³⁵ have been reported and end-caps responsive to stimuli including light,^{27, 34, 36-37} redox agents,^{27, 29, 38} enzymes,^{22, 39} and changes in pH^{24, 29} or temperature⁴⁰⁻⁴¹ have been incorporated.

In Chapter 5, we demonstrated that self-immolative poly(ethyl glyoxylate) (PEtG) could be coupled with hydrophilic poly(ethylene glycol) (PEG) via stimuli-responsive linker end-caps to form amphiphilic block copolymers.²⁸ These copolymers were self-assembled into nanoparticles that could load and release drugs in response to low concentrations of stimuli. However, we found that the drug loading capabilities of PEtG-based particles were somewhat limited, ranging from 6.6 to 13 wt% depending on the drug. This limited drug loading was attributed to the relatively low hydrophobicity of PEtG. We hypothesized that it might be possible to tune the properties of the polyglyoxylate cores by the incorporation of more hydrophobic glyoxylate monomers. Therefore, in this Chapter we report the homopolymerization and copolymerization of *n*-butyl glyoxylate, L-menthyl glyoxylate, and chloral with ethyl glyoxylate to obtain new polyglyoxylates. These polyglyoxylates were incorporated into block copolymers and self-assembled to form particles. It is shown that these new assemblies have significantly improved drug loading capabilities, yet retain the important ability of SIPs to degrade and release drugs in response to external stimuli.

6.2 Experimental section

General materials and procedures. *n*-Butyl glyoxylate,³⁴ the linker end-cap,³⁴ PEG-N₃ (0.75, 2 and 5 kg/mol),⁴² and PEtG-PEG2000²⁸ (same batch used here) were synthesized as previously reported. Ethyl glyoxylate in toluene solution (50% w/w) and L-menthol were obtained from Alfa Aesar. Fumaryl chloride, dimethyl sulfide, chloral hydrate, and phosphorous pentoxide were purchased from Sigma-Aldrich. Celecoxib was purchased from Ontario Chemicals Inc. Penstrep, 10% fetal bovine serum (FBS), trypsin-EDTA (0.25%) and Dulbecco's modified Eagle medium (DMEM) with 4.5 g/L D-glucose and 110.0 mg/L sodium pyruvate were obtained from Gibco. Triethylamine, and

dichloromethane were distilled from CaH_2 before use. Anhydrous DMF was obtained from a solvent purification system using Al_2O_3 columns. Ethyl glyoxylate was purified as previously reported in Chapter 5. All the other chemicals were reagent grade and used without further purification unless otherwise noted. ^1H NMR spectra were obtained at 400 MHz or 600 MHz on Varian Inova instruments. NMR chemical shifts (δ) are reported in ppm and were calibrated against residual solvent signals of CDCl_3 (δ 7.27). Fourier transform infrared (FTIR) spectra were obtained in attenuated total reflectance mode using a PerkinElmer UATR Spectrum Two with films drop cast from CH_2Cl_2 on diamond. High-resolution mass spectrometry (HRMS) was performed with either a Thermo Scientific DFS (Double Focus Sector) mass spectrometer, using a reversed Nier Johnson geometry for electron impact (EI) ionization, or a Bruker microOTOF 11 for electrospray ionization (ESI). Size exclusion chromatography (SEC) was performed using a Viscotek GPC Max VE2001 solvent module. Samples were analyzed using a Viscotek VE3580 RI detector operating at 30 °C. The separation technique employed two Agilent Polypore (300 x 7.5mm) columns connected in series and to a Polypore guard column (50 x 7.5mm). Samples were dissolved in THF (glass distilled grade) at approximately 5.0 mg/mL and filtered through 0.22 μm syringe filters. Samples were injected using a 100 μL loop. The THF eluent was filtered and eluted at 1 mL/min for a total of 30 min. A calibration curve was obtained from poly(methyl methacrylate) (PMMA) standards with molar masses of 1540-1,126,000 g/mol. Differential scanning calorimetry (DSC) was performed using a Q2000 from TA Instruments (New Castle, DE). The heating/cooling rate was 10 °C /min from -60 to +100 °C or -60 to +150 °C. Glass transition temperatures (T_g) were obtained from the second heating cycle. Thermogravimetric analyses (TGA) were performed on a TGA Q50 from TA Instruments. The heating rate was 10 °C /min between 30-500 °C under N_2 . Dialyses were performed using Spectra/Por regenerated cellulose membranes with molecular weight cut-offs (MWCO) of either 2, 3.5, 6-8, 50 kg/mol. The hydrodynamic diameters of the polymer assemblies were measured by dynamic light scattering (DLS) using a Zetasizer Nano Series ZS instrument from Malvern Instruments with laser wavelength at 633 nm, at 25 °C in a 1 cm path length glass cuvette at a concentration of 1.0 mg/mL. TEM imaging was performed using a Phillips CM10 microscope operating at

an acceleration voltage of 80 kV. 3.0 μL of micelle suspension (0.1 mg/mL) was placed onto a copper grid. The resulting sample was air-dried overnight before imaging. At least 40 particles were measured to obtain the mean particle diameters. Ultraviolet light irradiation was performed using an ACE Glass photochemistry cabinet containing a mercury light source (450 W bulb, 1.5 mW/cm^2 of UVA radiation and 0.06 mW/cm^2 of UVB radiation).

Synthesis of L-menthyl fumarate. L-Menthol (32.0 g, 205.0 mmol, 2.2 equiv) and *N,N*-diisopropylethylamine (DIPEA) (48.7 mL, 280.0 mmol, 3.0 equiv) were dissolved in 400.0 mL of dry CH_2Cl_2 under a N_2 atmosphere in a flamed-dried flask equipped with a magnetic stir bar. The solution was cooled to 0 $^\circ\text{C}$, and then fumaryl chloride (10.0 mL, 93.0 mmol, 1.0 equiv) in 50.0 mL of CH_2Cl_2 was added dropwise into the solution. The reaction was then heated to 50 $^\circ\text{C}$, stirred for 4 h, and then quenched with water (10.0 mL). The CH_2Cl_2 phase was subsequently washed with saturated NaHCO_3 solution, brine, and then concentrated under reduced pressure. The crude material was then purified by flash chromatography (19 : 1 hexane : ethyl acetate) to provide 30.0 g product in 82% yield. ^1H NMR (400 MHz, CDCl_3): δ_{ppm} 6.83 (s, 2 H), 4.75-4.84 (m, 2 H), 1.99-2.04 (m, 2 H), 1.82-1.92 (m, 2 H), 1.66-1.75 (m, 4 H), 1.40-1.56 (m, 4 H), 0.84-0.95 (m, 18 H), 0.77 (d, $J = 7.0$ Hz, 6 H). ^{13}C NMR (100 MHz, CDCl_3): δ_{ppm} 164.6, 133.8, 75.3, 47.0, 40.7, 34.2, 31.4, 26.3, 22.0, 20.7, 16.3. MS (EI): Calc'd for $[\text{M}]^+$ ($\text{C}_{24}\text{H}_{40}\text{O}_4$): 392.29. Found: 392.25.

Synthesis of L-menthyl glyoxylate. Menthyl fumarate (25.0 g, 64.0 mmol, 1.0 equiv) was dissolved in 300.0 mL of CH_2Cl_2 , and the solution was cooled to -78 $^\circ\text{C}$ in a dry ice/acetone bath. Ozone was bubbled into the solution under stirring until the solution turned in blue, and then the solution was purged with oxygen. Dimethyl sulfide (5.6 mL, 76.8 mmol, 1.2 equiv) was then added dropwise to quench the system. After stirring for 5 h, the solution was warmed to room temperature, then the solvent and the residual dimethyl sulfide were removed by distillation at 70 $^\circ\text{C}$ under argon. A pale-yellow liquid (18.2 g, 67%) was obtained after distillation at 110 $^\circ\text{C}$ (0.2 mbar) over P_2O_5 . ^1H NMR (600 MHz, CDCl_3): δ_{ppm} 9.40 (s, 1 H), 4.84-4.90 (m, 1 H), 2.01-2.01 (m, 1 H), 1.82-1.89 (m, 1 H), 1.69-1.75 (m, 2 H), 1.49-1.57 (m, 2 H), 1.05-1.17 (m, 2 H), 0.92 (dd, $J = 6.7$ Hz, 16.4 Hz, 6 H), 0.76

(d, $J = 7.0$ Hz, 3 H). ^{13}C NMR (100 MHz, CDCl_3): δ_{ppm} 184.3, 159.2, 77.5, 46.7, 40.4, 34.0, 31.4, 26.2, 23.3, 21.9, 20.6, 16.2. HRMS (EI): Calc'd for $[\text{M}+\text{H}]^+$ ($\text{C}_{12}\text{H}_{21}\text{O}_3$): 213.1491. Found: 213.1492.

Synthesis of poly[(ethyl glyoxylate)-*co*-chloral] (PEtGC). First, chloral hydrate was converted to chloral. Chloral hydrate (10.0 g, 60.0 mmol, 1.0 equiv.) and P_2O_5 (8.5 g, 30.0 mmol, 0.5 equiv.) were mixed together under an N_2 atmosphere in a flamed-dried flask equipped with a magnetic stir bar. The flask was then heated in an oil bath, and the chloral hydrate started to melt when temperature reached $90\text{ }^\circ\text{C}$, resulting in its dehydration by P_2O_5 . The resulting pale-yellow liquid (5.6 g, 64%) was collected using a short path distillation head when the temperature was $\sim 110\text{ }^\circ\text{C}$ at ambient pressure. The identity of the product was confirmed by ^1H NMR spectroscopy in CDCl_3 ($\delta = 9.05$, s, 1H).⁴³ The purified chloral was then used for polymerization immediately. For the copolymer synthesis, purified ethyl glyoxylate (5.0 mL, 50.0 mmol, 1.0 equiv.) and chloral (1.0 mL, 9.5 mmol, 0.2 equiv.) were dissolved in CH_2Cl_2 (10.0 mL) and Et_3N (3.5 μL , 25.0 mol, 0.0005 equiv.) was added. The solution was stirred for 1 h at $-20\text{ }^\circ\text{C}$. Linker end-cap³⁴ (0.3 g, 1.0 mmol, 0.02 equiv.) suspended in CH_2Cl_2 (10.0 mL) and Et_3N (0.2 mL, 1.5 mmol, 0.03 equiv.) was added at $-20\text{ }^\circ\text{C}$ to end-cap the polymer. The solution was gradually warmed to room temperature and then stirred for 16 h. The solution was then precipitated into methanol and the solvent was decanted. The resulting residue was dried in vacuo to provide a white sticky polymer (2.1 g, 35%). ^1H NMR (400 MHz, CDCl_3): δ 5.48-6.26 (m, 1.0 H), 4.15-4.31 (m, 1.9 H), 1.23-1.36 (m, 2.9 H). FTIR: 3058, 2986, 1756 cm^{-1} . SEC: $M_n = 37\text{ kg/mol}$, $M_w = 55\text{ kg/mol}$, $D = 1.5$.

Synthesis of PEtBuG. Purified ethyl glyoxylate (3.0 mL, 30.0 mmol, 1.0 equiv.) and *n*-butyl glyoxylate (3.0 mL, 23.0 mmol, 0.8 equiv.) were dissolved in CH_2Cl_2 (6.0 mL) and Et_3N (2.0 μL , 15.0 μmol , 0.0005 equiv.) was added. The solution was stirred for 1 h at $-20\text{ }^\circ\text{C}$. The linker end-cap (0.3 g, 1.0 mmol, 0.033 equiv.) suspended in CH_2Cl_2 (6.0 mL) and Et_3N (0.2 mL, 1.5 mmol, 0.05 equiv.) were added at $-20\text{ }^\circ\text{C}$ to end-cap the polymer. The solution was gradually warmed to room temperature and then stirred for 16 h. Purification was achieved by dialysis of the polymer solution against 1:1 acetone:methanol (2 x 1.0 L,

6-8 kg/mol MWCO). The residue was dried *in vacuo* to provide 3.0 g (50% yield) of the polymer as a white, sticky solid. $^1\text{H NMR}$ (400 MHz, CDCl_3): δ 5.45-5.75 (m, 1.0 H), 3.99-4.32 (m, 2.1 H), 1.60-1.71 (m, 0.6 H), 1.34-1.44 (m, 0.6 H), 1.23-1.34 (m, 2.1 H), 0.87-0.97 (m, 1.1 H). FTIR: 2963, 2876, 1751, 1538 cm^{-1} . SEC: $M_n = 30$ kg/mol, $M_w = 63$ kg/mol, $D = 2.1$.

Synthesis of PMenG. Menthyl glyoxylate (3.0 mL, 14.0 mmol, 1.0 equiv.) was dissolved in CH_2Cl_2 (5.0 mL) and Et_3N (1.0 μL , 7.0 μmol , 0.0005 equiv.) was added. The solution was stirred for 2 h at -20 $^\circ\text{C}$. The linker end-cap (0.30 g, 1.0 mmol, 0.07 equiv.) suspended in CH_2Cl_2 (10.0 mL) and Et_3N (0.2 mL, 1.5 mmol, 0.11 equiv.) were added at -20 $^\circ\text{C}$ to end-cap the polymer. The solution was gradually warmed to room temperature and then stirred for 16 h. Purification was achieved by dialysis of the polymer solution against 1:1 acetone:methanol for 16 h (2 x 1.0 L, 2 kg/mol MWCO). The residue was dried *in vacuo* to provide 0.3 g (10% yield) of the polymer as a white solid. $^1\text{H NMR}$ (400 MHz, CDCl_3): δ 7.67-8.84 (m, 6 H), 5.42-5.85 (m, 10 H), 4.62-4.90 (m, 14 H), 4.11-4.34 (m, 4 H), 1.85-2.11 (m, 26 H), 1.59-1.75 (m, 30 H), 1.26-1.59 (m, 31 H), 0.96-1.11 (m, 26 H), 0.80-0.94 (m, 103 H), 0.67-0.79 (m, 49 H). FT-IR: 2957, 2928, 2871, 1751, 1669, 1536 cm^{-1} . SEC: $M_n = 2.0$ kg/mol, $M_w = 2.2$ kg/mol, $D = 1.1$.

Synthesis of PEtMenG. Purified ethyl glyoxylate (2.0 mL, 20.0 mmol, 1.0 equiv.) and menthol glyoxylate (2.0 mL, 9.4 mmol, 0.5 equiv.) were dissolved in CH_2Cl_2 (5.0 mL) and Et_3N (1.0 μL , 10.0 μmol , 0.0005 equiv.) was added. The solution was stirred for 2 h at -20 $^\circ\text{C}$. Linker end-cap (0.3 g, 1.0 mmol, 0.05 equiv.) suspended in CH_2Cl_2 (10.0 mL) and Et_3N (0.2 mL, 1.5 mmol, 0.075 equiv.) were added at -20 $^\circ\text{C}$ to end-cap the polymer. The solution was gradually warmed to room temperature and then stirred for 16 h. The resulting polymer was purified by dialysis against 1:1 acetone:methanol for 16 h (2 x 1.0 L, 6-8 kg/mol MWCO) to provide 0.4 g (10% yield) of a the polymer as a white powder. $^1\text{H NMR}$ (400 MHz, CDCl_3): δ 7.67-8.84 (m, 6 H), 5.62 (br s, 72 H), 4.72 (br s, 32 H), 4.23 (br s, 127 H), 1.85-2.11 (m, 74 H), 1.59-1.75 (m, 117 H), 1.37-1.53 (m, 77 H), 1.16-1.37 (m, 198 H), 0.96-1.11 (m, 68 H), 0.80-0.94 (m, 214 H), 0.67-0.79 (m, 75 H). FT-IR: 2957, 2871, 1750, 1673, 1536 cm^{-1} . SEC: $M_n = 34$ kg/mol, $M_w = 48$ kg/mol, $D = 1.4$.

Synthesis of PEtGC-PEG2000. 2 kg/mol PEG-N₃ (97.0 mg, 48.6 μ mol, 6.0 equiv.) and **PEtGC** (300.0 mg, 8.1 μ mol, 1.0 equiv.) were dissolved in DMF (5.0 mL) and then placed under an Ar atmosphere. CuSO₄ (4.0 mg, 28.0 μ mol, 3.5 equiv.) and sodium ascorbate (5.0 mg, 28.0 μ mol, 3.5 equiv.) were then added and the mixture was stirred at 40 °C for 16 h. The reaction mixture was then transferred into a regenerated cellulose membrane (50 kg/mol MWCO) and dialyzed against deionized water for 16 h (1.0 L, 2 solvent changes) to remove DMF and most free PEG. The dialyzed material was then lyophilized, washed 3 times with water to further remove free PEG, and then dried to afford 300.0 mg (90% yield) of the product as a white rubbery solid. ¹H NMR (600 MHz, CDCl₃): δ 5.42-5.97 (m, 340 H), 4.10-4.30 (m, 697 H), 3.62 (s, 364 H), 3.36 (s, 5 H), 1.20-1.34 (m, 1054 H). FTIR: 3058, 2986, 2944, 2874, 1751, 1755 cm⁻¹. SEC: M_n = 41 kg/mol, M_w = 53 kg/mol, *D* = 1.3.

Synthesis of PEtGC-PEG5000. The polymer was synthesized by the same procedure as **PEtGC-PEG2000**, except that 5000 g/mol PEG-N₃ were used. The yield was 73%. ¹H NMR (600 MHz, CDCl₃): δ 5.45-5.92 (m, 261 H), 4.10-4.30 (m, 583 H), 3.62 (s, 909 H), 3.36 (s, 4 H), 1.20-1.34 (m, 922 H). FT-IR (thin film): 2984, 2907, 2944, 2874, 1751, 1753 cm⁻¹. SEC: M_n = 36 kg/mol, M_w = 47 kg/mol, PDI = 1.3.

Synthesis of PEtBuG-PEG2000. The polymer was synthesized by the same procedure as **PEtGC-PEG2000**, except that **PEtBuG** was used. The yield was 42%. ¹H NMR (400 MHz, CDCl₃): δ 5.47-5.75 (m, 202 H), 4.07-4.33 (m, 411 H), 3.65 (s, 364 H), 3.39 (s, 6 H), 1.61-1.71 (m, 134 H), 1.34-1.44 (m, 129 H), 1.21-1.33 (m, 414 H), 0.87-0.97 (m, 217 H). FTIR: 2962, 2936, 2914, 2875, 1751, 1533 cm⁻¹. SEC: M_n = 36 kg/mol, M_w = 68 kg/mol, *D* = 1.9.

Synthesis of PEtBuG-PEG5000. The polymer was synthesized by the same procedure as **PEtGC-PEG2000**, except that **PEtBuG** and 5 kg/mol PEG-N₃ were used. The yield was >99%. ¹H NMR (400 MHz, CDCl₃): δ 5.45-5.70 (m, 171 H), 4.08-4.31 (m, 352 H), 3.65 (s, 909 H), 3.36 (s, 4 H), 1.59-1.72 (m, 216 H), 1.33-1.44 (m, 115 H), 1.24-1.34 (m, 363 H), 0.87-0.96 (m, 186 H). FT-IR (thin film): 2959, 2878, 1751 cm⁻¹. SEC: M_n = 42 kg/mol, M_w = 80 kg/mol, PDI = 1.9.

Synthesis of PMenG-PEG750. The polymer was synthesized by the same procedure as **PEtGC-PEG2000**, except that **PMenG** and 750 g/mol PEG-N₃ were used. The yield was 58%. ¹H NMR (400 MHz, CDCl₃): δ 7.62-8.77 (m, 6 H), 5.36-5.91 (m, 6 H), 4.58-4.97 (m, 12 H), 4.38-4.58 (m, 4 H), 3.65(s, 141 H), 3.38(s, 5 H), 1.84-2.16 (m, 16 H), 1.59-1.81 (m, 28 H), 1.33-1.55 (m, 20 H), 0.96-1.13 (m, 16 H), 0.80-0.97 (m, 74 H), 0.67-0.80 (m, 38 H). FT-IR (thin film): 2955, 2922, 2868, 2107, 1751, 1665, 1531 cm⁻¹. SEC: M_n = 5.9 kg/mol, M_w = 4.2 kg/mol, PDI = 1.2.

Synthesis of PEtMenG-PEG2000. The polymer was synthesized by the same procedure as **PEtGC-PEG2000**, except that **PEtMenG** was used. The yield was 50%. ¹H NMR (400 MHz, CDCl₃): δ 5.45-5.70 (m, 165 H), 4.61-4.79 (m, 51 H), 4.10-4.30 (m, 256 H), 3.62 (s, 364 H), 3.36 (s, 7 H), 1.82-2.10 (m, 128 H), 1.63-1.75 (m, 132 H), 1.37-1.51 (m, 123 H), 1.23-1.37 (m, 427 H), 0.97-1.14 (m, 115 H), 0.81-0.96 (m, 415 H), 0.69-0.80 (m, 183 H). FT-IR (thin film): 2955, 2933, 2870, 1751, 1538 cm⁻¹. SEC: M_n = 35 kg/mol, M_w = 53 kg/mol, PDI = 1.5.

Polymer self-assembly. 10.0 mg of block copolymer was dissolved in 1.0 mL of DMSO with stirring overnight. 0.1 mL of the resulting solution was then rapidly injected into 0.9 mL of rapidly stirring deionized water. After stirring for 5 min, the suspension was dialyzed against deionized water for 24 h (2 x 1.0 L) using a 3.5 kg/mol MWCO membrane to remove DMSO.

Measurement of the critical aggregation concentration (CAC). A 1.0 mg/mL suspension of polymer assemblies was prepared as described above. 29.0 μL of a 0.1 mg/mL solution of Nile red in CH₂Cl₂ was added to each of a series of vials and then the solvent was evaporated to provide a thin film of Nile red. Next, 13 serial dilutions of the polymer suspension ranging from 1 to 2.5 x 10⁻⁴ mg/mL were added to the vials (1.5 mL/vial). The vials were then incubated at 37 °C overnight. Fluorescence emission spectra (520-700 nm) of each suspension were then measured using a QM-4 SE spectrometer from Photon Technology International (PTI) equipped with double excitation and emission monochromators. The excitation wavelength was 485 nm and the emission intensity at λ_{max}

was record. The CAC was determined as the intercept of the two linear regions of the graph of fluorescence intensity vs. $\log(\text{copolymer concentration})$.

Particle degradation studied by DLS. Polymer assemblies were prepared as described above, except that the suspensions were dialyzed against 100 mM, pH 7.4 phosphate buffer for 24 h (2 x 1.0 L) instead of deionized water. The resulting polymer concentration was ~ 1.0 mg/mL. The count rate was measured by DLS while fixing the attenuator at 7. Then, the solution was divided in two. One half was kept in dark, while the other half was irradiated with UV light for 30 min. The samples were then incubated at 37 °C in the dark and the DLS count rate was measured at selected time points.

Loading of celecoxib. 10.0 mg of block copolymer and 3.0 mg of celecoxib were dissolved in 0.5 mL of DMF and stirred for 4 h. The solution was then rapidly injected into 9.5 mL of stirring deionized water and the resulting suspension was stirred for an additional 1 min at speed of 700 rpm. The suspension was then dialyzed against 100 mM, pH 7.4 phosphate buffer (2 x 1.0 L) for 16 h using a 3.5 kg/mol MWCO membrane. It was then filtered through glass pipette containing a cotton filter to remove any unencapsulated and precipitated drug. 100.0 μL of the resulting particle suspension was diluted into 1.6 mL of acetonitrile to fully dissolve the copolymer and celecoxib, then the solution was filtered through a 0.20 μm syringe filter (Acrodisc Syringe Filter Non-Pyrogenic 13 mm, Pall Life Science) to remove any buffer salts. The absorbance at 250 nm was measured using a Varian UV/VIS Cary 300 spectrophotometer to calculate the celecoxib concentration ($\epsilon = 22884 \text{ L/mol}\cdot\text{cm}$). This experiment was performed in triplicate and was used to calculate the loading efficiency and drug content, where:

Loading efficiency = (mass of loaded drug/mass of actual drug used) \times 100%.

Drug content = (mass of loaded drug/mass of nanoparticles with drug) \times 100%.

For analysis of the drug-loaded particles by TEM, the same procedure was used except that the particle suspension was dialyzed against deionized water instead of buffer.

Triggered release of celecoxib. 10.0 mL of drug-loaded polymer particle suspension (~1.0 mg/mL) was prepared as described above in pH 7.4 buffer, then was divided into two (5.0 mL) samples. One sample was irradiated for 30 min, and the other was kept in dark. They were then incubated in the dark at 37 °C. At selected time points, ~0.2 mL of the suspension was removed and filtered through a glass pipette containing a cotton filter to remove the released and precipitated celecoxib. 100.0 µL of the filtered suspension was then diluted into 1.6 mL of acetonitrile and the resulting suspension was filtered through a 0.20 µm syringe filter (Acrodisc Syringe Filter Non-Pyrogenic 13 mm, Pall Life Science) to remove any buffer salts. The absorbance of the acetonitrile solution at 250 nm was measured to determine the percentage of drug remaining in the assemblies. Each time point was measured in triplicate to calculate standard deviations.

***In vitro* cell toxicity assay.** Polymer particles were prepared for the assay at a concentration of 10.0 mg/mL in deionized water using the procedure as described above, except at 10-fold higher polymer concentration. The suspension was then either irradiated with UV light for 30 min or not irradiated. It was diluted 10-fold with Dulbecco's modified eagle medium (DMEM) containing 10% FBS and 100 units/mL of Penstrep to 1.0 mg/mL and then serial 2-fold dilutions were performed using the same medium. MDA-MB-231 cells were cultured in DMEM with 10% FBS and 100 units/mL of Penstrep in an atmosphere of 5% CO₂ at 37 °C. The cells were seeded in a 96 well plate (Corning Flat Bottom Plate) at a density of 5,000 cells/well and allowed to adhere for 24 h. The medium was then aspirated and replaced with various concentrations of particles, 0.2-0.05 mg/mL sodium dodecyl sulfate (positive control) or medium (negative control). The cells were incubated at 37 °C for 48 h. The medium was then aspirated and replaced with 100.0 µL of fresh medium containing 0.5 mg/mL (3-(4,5-dimethylthiazol-2-yl)-2,5-diphenyltetrazolium bromide) (MTT) reagent and the cells were incubated. After 4 h the plate was removed and the MTT reagent solution was aspirated. 50.0 µL of DMSO was added to each well to solubilize the formazan metabolic product of MTT. The plate was then placed in a plate reader (Tecan Infinite M1000 Pro) and the absorbance at 540 nm was measured to quantify the relative metabolic activities of the cells.

6.3 Results and discussion

6.3.1 Polymer synthesis

In addition to ethyl glyoxylate (**EtG**), three other aldehyde monomers were studied (Figure 6.1). *n*-Butyl glyoxylate (**BuG**) is an analog of ethyl glyoxylate, but with a longer aliphatic chain, making it more hydrophobic. L-Menthyl glyoxylate (**MenG**) is another hydrophobic analog but is derived from a chiral and bioactive alcohol, making it of interest.⁴⁴ Chloral (**C**) is not a glyoxylate, but has three chloro groups α to the aldehyde, making it susceptible to polymerization while at the same time being hydrophobic.⁴⁵ **EtG** was purchased and purified as previously reported.⁴⁰ **C** was purchased as its hydrate and then distilled over P₂O₅ to afford the aldehyde. **BuG** was synthesized as previously reported.³⁴ **MenG** was synthesized via ozonolysis of its corresponding fumarate derivative (Scheme A6.1).

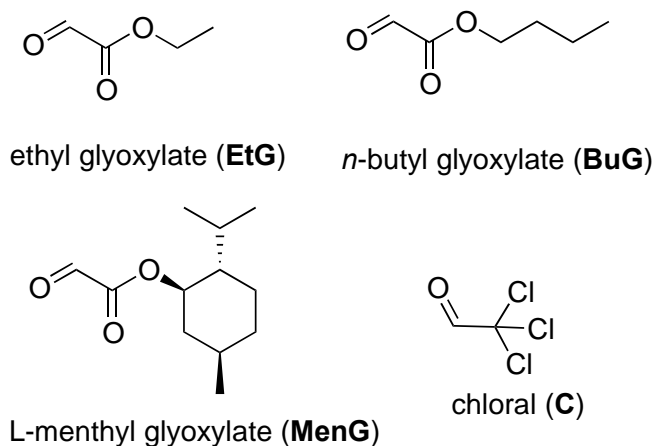
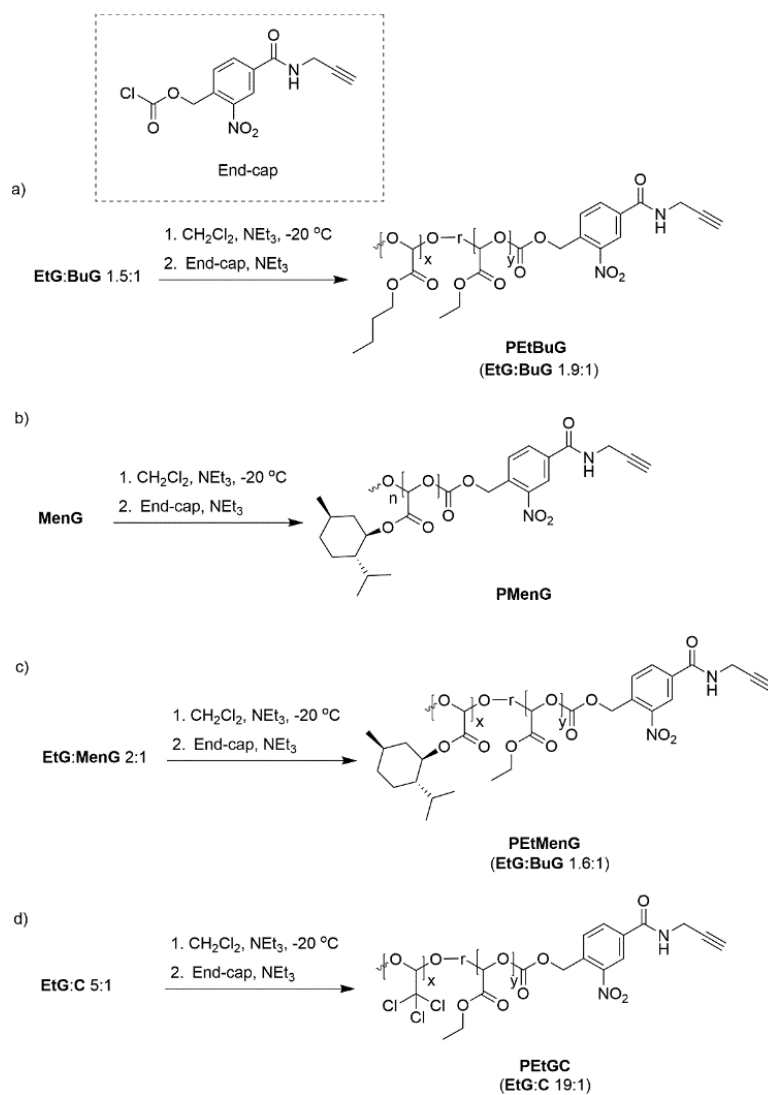


Figure 6.1 Chemical structure of the monomers used in this chapter

Next, the polymerization of the monomers was investigated. The polymerization reactions were conducted at -20 °C with trace NEt₃ and EtG hydrate as an initiator (Scheme 6.1, Table 6.1). After polymerization, the polymers were end-capped *in situ* with a UV light-responsive *o*-nitrobenzyl chloroformate derivative having an alkyne functional handle for subsequent conjugation of the PEG block.³⁴ The resulting polymers were isolated by precipitation in methanol or dialysis against 1:1 acetone:methanol. Poly(ethyl glyoxylate) (**PEtG**) was synthesized as previously reported.²⁸ We have previously reported that

homopolymerization of **BuG** gave low molar mass polymers, but that copolymerization with **EtG** afforded high molar masses with good incorporation of **BuG**.³⁴ Here we copolymerized **EtG** and **BuG** in a 1.5:1 molar ratio (Scheme 6.1a). Based on ¹H NMR spectroscopy, the resulting copolymer **PEtBuG** had a 1.9:1 mole ratio of the monomers, in reasonable agreement with the feed ratio. The number average molar mass (M_n) was 30 kg/mol and the dispersity (D) was 2.1 as measured by SEC in THF relative to PMMA standards. **MenG** was homopolymerized to afford **PMenG** with an M_n of 2.0 kg/mol and a D of 1.3 (Scheme 6.1b), but copolymerization of a 2:1 ratio of **EtG:MenG** provided the copolymer **PEtMenG** with an M_n of 34 kg/mol, D of 1.4 and a 1.6:1 ratio of **EtG:MenG** (Scheme 6.1c). It is known that the homopolymerization of chloral leads to predominately an isotactic 4/1-helical structure in the crystalline state, and it is insoluble in all solvents.⁴⁶ Therefore, we initially attempted the polymerization of a 1:1 ratio of **EtG:C**. The resulting copolymer precipitated from solution and could not be re-dissolved for analysis. Subsequently, we reduced the molar ratio to 3:1 **EtG:C**, but the resulting copolymer still had poor solubility in organic solvents such as CH₂Cl₂ and DMSO. Therefore, we polymerized a 5:1 ratio of **EtG:C**. The resulting copolymer **PEtGC** had an M_n of 37 kg/mol, D of 1.5, and a 19:1 ratio of **EtG:C**. The chloral content was much lower than that expected based on the monomer feed ratios, suggesting that the aldehyde of the **C** monomer was much less susceptible to polymerization than that of **EtG**, perhaps due to the quaternary carbon adjacent to the aldehyde.



Scheme 6.1 Synthesis of polymers: a) PEtBuG; b) PMenG; c) PEtMenG; d) PEtGC.

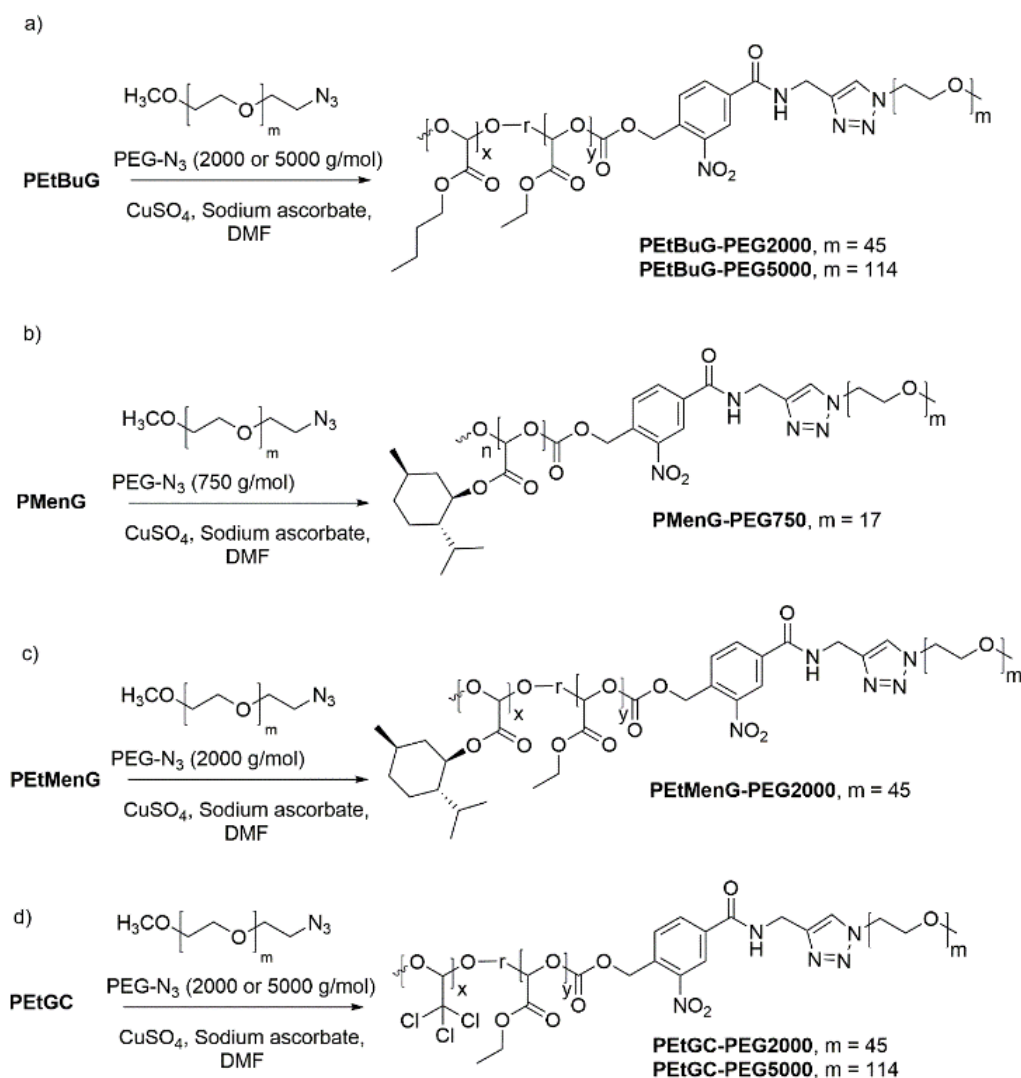
Table 6.1 SEC and thermal analysis results for the polymers. ^aFrom SEC; ^bFrom TGA; ^cFrom DSC; ^dFrom previously published work.

Polymers	M_n (kg/mol) ^a	D^a	T_o (°C) ^b	T_g (°C) ^c
PEtG^d	42	2.1	200	-5
PEtBuG	30	2.1	226	-11
PMenG	2.0	1.3	235	58
PEtMenG	34	1.4	230	24 ($T_m = 60$)
PEtGC	37	1.5	133	3

The thermal properties of the polymers were studied by TGA and DSC (Table 6.1, Figures A6.17-A6.22). Complete end-capping of the isolated polymers was confirmed by the fact that all of the polymers had onset degradation temperatures (T_o) higher than 100 °C. We have previously observed that non-capped polyglyoxylates began depolymerizing below 100 °C.³⁴ The T_o values for **PEtG**, **PEtBuG**, **PEtMenG**, and **PMenG** ranged from 200 to 235 °C while **PEtGC** had a T_o of 133 °C. This suggests that the chloral component of the polymer substantially reduced the thermal stability. As all of the polymers had the same end-cap, this suggests that introduction of the trichloromethyl moiety introduces a thermal labile bond along the backbone that can initiate degradation upon cleavage. **PEtG** had a T_g of -5 °C, while **PEtBuG** had a T_g of -11 °C due to the introduction of flexible side chains. **PMenG** had a T_g of 57 °C, while **PEtMenG** had a T_g of 24 °C. The increase in T_g for the menthyl-functionalized polymers can be attributed to the rigid cyclic structure of the menthyl moiety. **PEtMenG** also had a T_m of 60 °C. L-Menthol is a crystalline solid with a melting point of 41-44 °C, so crystallinity of the polymer likely arose from the menthyl moieties. It is possible that **PMenG** also had a T_m that was out of the range of the analysis (-60 – 150 °C, limited by the thermal stability of the polymers). **PEtGC** had a T_g of 3 °C, indicating that incorporation of the chloral moiety decreased segmental motion in the polymer, even at low monomer ratios.

Next, the polymers were converted to amphiphilic block copolymers by the conjugation of PEG to the alkyne moieties on the end-caps. PEG has been widely used as hydrophilic polymer for biomedical applications due to its high biocompatibility in various applications.⁴⁷ The coupling reactions were conducted via copper-assisted alkyne-azide cycloaddition reactions in DMF using azide-terminated PEG (PEG-N₃) (Scheme 6.2). It should be noted that because the polymerization was initiated with the glyoxylate hydrate, there were end-caps on both termini and consequently the coupling resulted in the formation of triblock copolymers (PEG-polyglyoxylate-PEG). In order to study the influence of different hydrophilic mass fractions (f), **PEtBuG** and **PEtGC** were each coupled with 2 and 5 kg/mol PEGs to afford **PEtBuG-PEG2000**, **PEtBuG-PEG5000**, **PEtGC-PEG2000** and **PEtGC-PEG5000** (Table 6.2). **PEtMenG** was coupled with 2

kg/mol PEG to afford **PEtMenG-PEG2000**. Because of its short hydrophobic block length, **PMenG** was coupled with 750 g/mol PEG to afford **PMenG-PEG750**. In all cases, the excess of PEGs were removed by dialysis and water washes. The purified block copolymers were characterized by ^1H NMR spectroscopy and SEC. Removal of uncoupled PEG was confirmed by SEC as no peaks corresponding to free PEG were observed (Figure A6.23-A6.28) and the expected fractions of PEG were observed in NMR spectroscopy (Figure A6.11-A6.16). The f values ranged from 0.11 – 0.39.



Scheme 6.2 Synthesis of block copolymers via coupling of PEG-N₃ with a) **PEtBuG**; b) **PMenG**; c) **PEtMenG**; d) **PEtGC**.

Table 6.2 Characterization data for the amphiphilic block copolymers and their resulting assemblies. ^aPreviously reported; ^bFrom SEC; ^cMeasured at 1 mg/mL of copolymer.

Block copolymer	M_n^b (kg/mol)	D^b	f	CAC (mg/L)	Nile red λ_{max} (nm) ^c
PEtG-PEG2000^a	40	2.1	0.10	79	598
PEtBuG-PEG2000	36	1.9	0.11	47	595
PEtBuG-PEG5000	42	1.9	0.24	64	597
PMenG-PEG750	5.9	1.2	0.39	64	600
PEtMenG-PEG2000	35	1.5	0.11	52	586
PEtGC-PEG2000	41	1.4	0.10	40	591
PEtGC-PEG5000	36	1.3	0.28	62	594

Self-assembly was performed via nanoprecipitation. Specifically, 0.1 mL of 10.0 mg/mL polymer solution in DMSO was injected into 0.9 mL of rapidly stirring water. After stirring for 5 min, the assemblies were dialyzed against water to remove DMSO. The critical aggregation concentrations (CACs) of these assemblies were determined by encapsulation of Nile red. The CACs of all assemblies were very similar, ranging from 40 to 79 mg/L. However, as expected the assemblies with higher f values also had higher CACs (Table 6.2). In addition, for very similar f values of 0.10-0.11, the CACs were lower for the more hydrophobic polymers such as **PEtBuG-PEG2000**, **PEtMenG-PEG2000**, and **PEtGC-PEG2000** than for the previously reported **PEtG-PEG2000**. The maximum emission wavelength (λ_{max}) of encapsulated Nile red can also serve as an indicator of the polarity of the environment at the core of the assembly, with a shift to shorter λ_{max} indicative of a more polar environment. At an assembly concentration of 1.0 mg/mL, λ_{max} ranged from 586-600 nm, with the assemblies having a lower CAC values, such as **PEtMenG-PEG2000**,

PEtGC-PEG2000, and **PEtBuG-PEG2000**, also having lower λ_{\max} . Overall, these results suggest that it was possible to tune the hydrophobicity of the assembly cores.

The assemblies were also characterized by dynamic light scattering (DLS) and transmission electron microscopy (TEM) (Figure 6.2, Figures A6.36-A6.42). Based on DLS, the hydrodynamic diameters ranged from 82-173 nm, with polydispersity indices (PDI) of 0.12-0.37 (Table 6.3). Based on TEM (Figure 6.2 and Figure A6.42), all of these assemblies were solid-core particles with average diameters ranging from 37-157 nm. The diameters measured by TEM were generally smaller than those measured by DLS, which can result from differences between the hydrated and dried states, and possible aggregation of assemblies in the suspensions used for DLS measurements. While longer PEG chains and higher f values would be expected to more effectively stabilize the assemblies, TEM images showed that the particles with longer PEG blocks aggregated to form larger particles. This was reproducible across multiple experiments, and might be attributed to interactions of particle coronas during drying. As there appeared to be no significant advantages of having the longer PEG block based on TEM or DLS, further studies focused on the 2 kg/mol PEG copolymers.

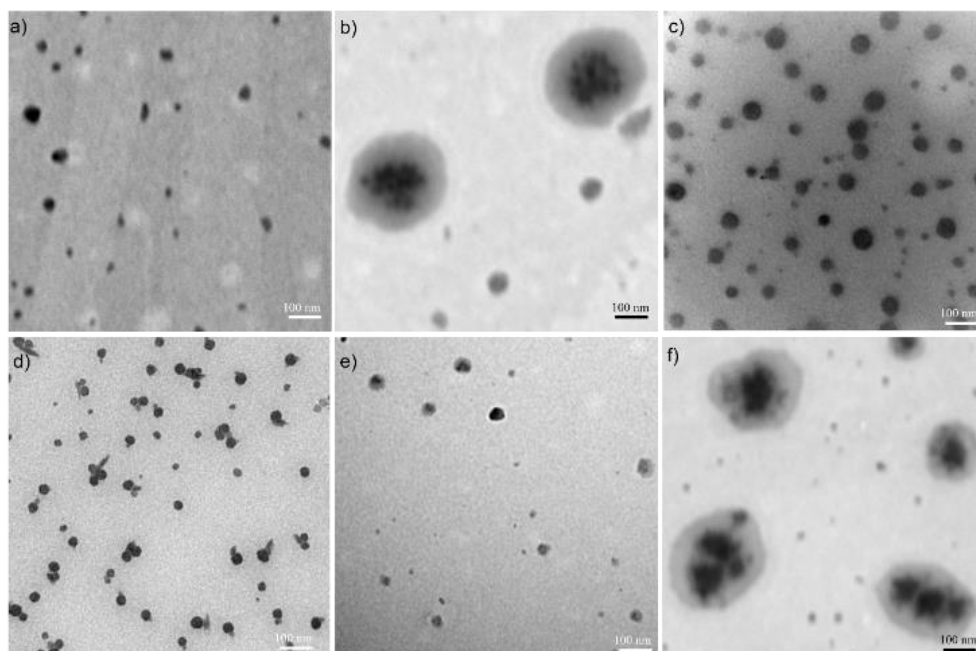


Figure 6.2 TEM images of particles formed from a) PEtBuG-PEG2000; b) PEtBuG-PEG5000; c) PEtMenG-PEG2000; d) PMenG-PEG750; e) PEtGC-PEG2000; f) PEtGC-PEG5000.

Table 6.3 Characterization data for the block copolymer assemblies. ^aPreviously reported.

Block copolymer	Mean diameter from TEM (nm)	Z-average diameter from DLS (nm)	PDI (from DLS)
PEtG-PEG2000^a	53 ± 17	82 ± 2	0.17 ± 0.03
PEtBuG-PEG2000	37 ± 11	105 ± 23	0.12 ± 0.01
PEtBuG-PEG5000	91 ± 107	110 ± 14	0.17 ± 0.02
PMenG-PEG750	39 ± 7	173 ± 17	0.37 ± 0.09
PEtMenG-PEG2000	38 ± 12	127 ± 26	0.25 ± 0.03
PEtGC-PEG2000	31 ± 16	139 ± 142	0.13 ± 0.02
PEtGC-PEG5000	157 ± 95	118 ± 21	0.19 ± 0.01

Due to the presence of the UV light-responsive linker end-cap in each block copolymer, the hydrophobic blocks were expected to depolymerize upon irradiation with UV light, resulting in disassembly of the particles. In order to verify this, the particles were suspended in pH 7.4 phosphate buffer at a concentration of 1.0 mg/mL, then irradiated with 1.5 mW/cm² of UVA light for 30 min. Controls consisted of non-irradiated particles. Particle disassembly was monitored based on the DLS count rate, which is proportional to particle number and particle mass when the attenuator is fixed at constant value. Thus, depolymerization would be expected to result in a decrease in the count rate. As shown in Figure 6.3, without UV irradiation all of the particles were relatively stable in pH 7.4 at 37 °C for 24 h, with less than 20% reduction in count rate. However, after irradiation the particles disassembled almost immediately, leading to more than a 70% reduction in count rate over the first 2 h. Thus, the particles were indeed responsive to the light stimulus.

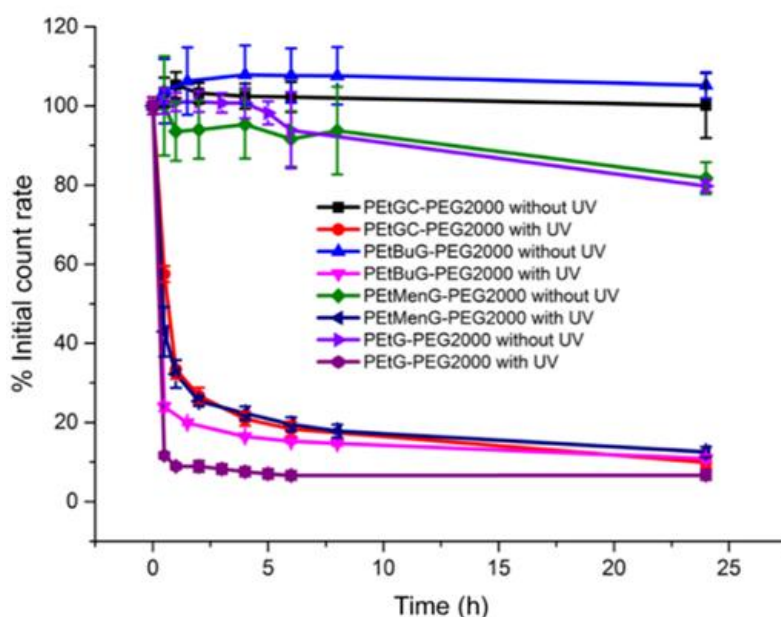


Figure 6.3 Depolymerization of particles following UV light irradiation (or no light for controls), monitored by DLS based on count rate.

6.3.2 Celecoxib loading and release

Celecoxib is anti-inflammatory drug that is used in the treatment of arthritis, and has also shown potential as a chemotherapeutic.⁴⁸ However, it is limited by adverse side effects and

low solubility (less than 3.3 mg/L), suggesting it could benefit from a drug delivery system. Therefore, celecoxib was loaded into the polymer assemblies. Drug loading was performed during the self-assembly process, with celecoxib co-dissolved in the organic phase with the polymer prior to nanoprecipitation. In contrast to the assemblies without drug where DMSO performed best as the organic solvent, DMF was found to be the best solvent for preparing celecoxib-loaded assemblies with diameters less than 100 nm and high drug loading.

Table 6.4 Size characterization and celecoxib loading data for the block copolymer assemblies containing drug.

Block copolymers	Mean diameter from TEM (nm)	Z-average diameter from DLS (nm)	PDI (from DLS)	Drug loading content (%)	Drug loading efficiency (%)
PEtG-PEG2000	19 ± 8	63 ± 1	0.16 ± 0.01	10.0 ± 2.6	37.4 ± 10.8
PEtBuG-PEG2000	20 ± 10	51 ± 1	0.14 ± 0.01	15.0 ± 3.2	59.0 ± 15.1
PEtMenG-PEG2000	39 ± 12	52 ± 9	0.15 ± 0.09	15.1 ± 5.2	60.0 ± 23.3
PEtGC-PEG2000	34 ± 31	97 ± 2	0.16 ± 0.01	5.9 ± 3.9	21.2 ± 15.1

As shown in Table 6.4, there were significant differences between the celecoxib content and loading efficiency for the different block copolymer assemblies. **PEtBuG-PEG2000** and **PEtMenG-PEG2000** assemblies had the highest celecoxib content at ~15 wt%, corresponding to a loading efficiency of ~60%. This suggests that the incorporation of hydrophobic comonomers improved the loading of hydrophobic drugs, likely because the assembly cores became more hydrophobic. **PEtGC-PEG2000** assemblies had the lowest celecoxib loading of only 6 wt%, corresponding to a loading efficiency of 21%. Although the cores of these assemblies were relatively hydrophobic based on the CAC values and the Nile red λ_{\max} , it is likely that the chloride groups on the chloral monomer did not enhance the compatibility with celecoxib. **PEtG-PEG2000** assemblies had an intermediate drug content of 10 wt% and a loading efficiency of 37%, which was significantly higher than **PEtGC-PEG2000** and significantly lower than **PEtBuG-PEG2000** and **PEtMenG-**

PEG2000. To confirm that the f value didn't have a significant influence on the drug content, celecoxib was also loaded into **PEtBuG-PEG5000** assemblies. The resulting celecoxib content was ~14 wt%, and not significantly different from that of **PEtBuG-PEG2000**. Thus, the chemical structure of the core block, rather than the block ratios dominates the loading efficiency.

The drug-loaded assemblies were also characterized by TEM and DLS. TEM indicated that the **PEtG-PEG-2000**, **PEtBuG-PEG2000**, and **PEtMenG-PEG2000** assemblies remained as spherical particles after drug encapsulation (Figure A6.47). **PEtGC-PEG2000** assemblies were somewhere irregularly shaped, suggesting that the morphology was altered by celecoxib incorporation (Figure A6.47d). This may be related to the poor compatibility between celecoxib and the hydrophobic block, which was also reflected in the low drug loading content. The Z-average diameters measured by DLS were all lower than those for the non-loaded assemblies and ranged from 51-97 nm.

Next, the stimulus-mediated release of celecoxib from the particles was studied. Drug-loaded assemblies suspended in pH 7.4 phosphate buffer were either stored in the dark to serve as controls or were irradiated for 30 min. Upon release from the assemblies, celecoxib precipitated due to its low aqueous solubility. At each time point, the precipitated drug was removed by filtration and the percentage of drug remaining suspended in the assemblies was measured.

All of these particles released celecoxib much more rapidly following irradiation with UV light than without irradiation (Figure 6.4). **PEtG-PEG2000** and **PEtMenG-PEG2000** released more than 70% of the celecoxib over the first 3 h. **PEtBuG-PEG2000** and **PEtGC-PEG2000** had more gradual release profiles, with ~40% and 50% respectively of the drug released over 3 h. The DLS results had indicated that all the particles disassembled very rapidly after irradiation. Therefore, the different apparent rates of drug release may be related to the drug crystallization process. For the cases where rapid celecoxib release was measured, it was observed that large celecoxib crystals were formed. This precipitate sedimented, resulting in a clear solution containing the PEG block and water-soluble small molecule depolymerization products. For the cases with apparent slow release of drug, the

solution turbidity increased dramatically after irradiation, suggesting the formation of small celecoxib crystals that did not sediment. Based on the filtration process employed in our release assay, the larger drug crystals would have been filtered off more efficiently, whereas the smaller crystals would have remained, appearing as non-released drug until they formed larger aggregates. It is known that the presence of small molecules in solution can influence the size of celecoxib crystals,⁴⁹⁻⁵⁰ so differences in depolymerization products may have influenced the crystallization and consequently the precipitation of the drug. Nevertheless, after 24 h, all of the triggered systems had released ~80% of the celecoxib.

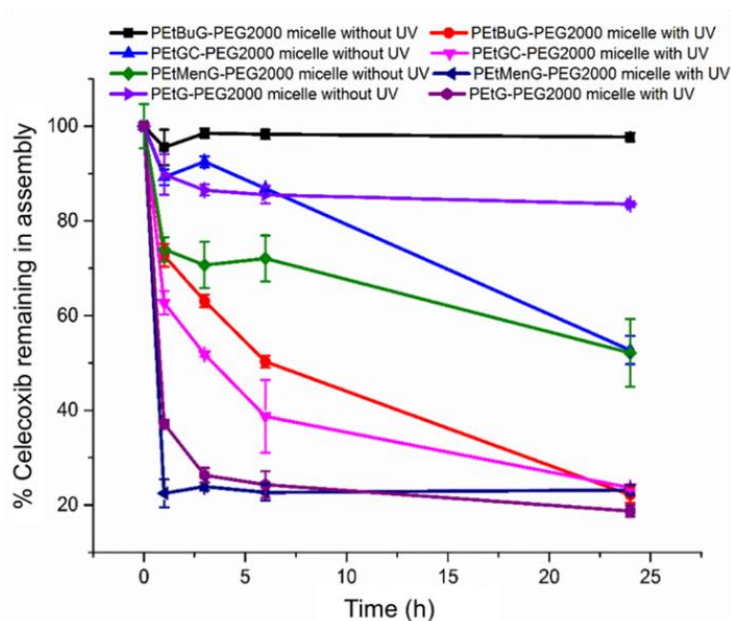


Figure 6.4 Release of celecoxib over time for assemblies irradiated with UV light and for the corresponding systems stored in the dark.

Non-triggered systems that were stored in the dark released celecoxib more slowly. **PEtBuG-PEG2000** most effectively retained the drug, with less than 5% released over 24 h. This suggests that the flexible hydrophobic butyl chains likely were not only favorable for obtaining high drug loadings, but also for retaining the drug in the absence of stimulus. Non-triggered **PEtG-PEG2000** assemblies released ~20% of their celecoxib over 24 h, while **PEtMenG-PEG2000** and **PEtGC-PEG2000** released ~45%. These rates were much

slower than the analogous irradiated systems, but suggest that the chemical structure of the core-forming block has a significant influence on the retention of drug.

6.3.3 *In vitro* toxicity studies

The toxicity of each of the non-loaded assemblies was investigated using MDA-MB-231 human breast cancer cells. Each system was evaluated in its irradiated and non-irradiated form following a 48 h incubation with the cells. In the absence of irradiation, **PEtMenG-PEG2000** and **PMenG-PEG750** assemblies showed minimal toxicity, with a high cell metabolic activity of >80% relative to control cells even at a concentration 1.0 mg/mL (Figure 6.5). Non-triggered **PEtG-PEG2000**, **PEtBuG-PEG2000**, **PEtBuG-PEG5000** assemblies had similar effects on cells, with 60% metabolic activity at a concentration of 1.0 mg/mL. **PEtGC-PEG2000** and **PEtGC-PEG5000** assemblies showed higher toxicity with only ~30% metabolic activity remaining at 1.0 mg/mL.

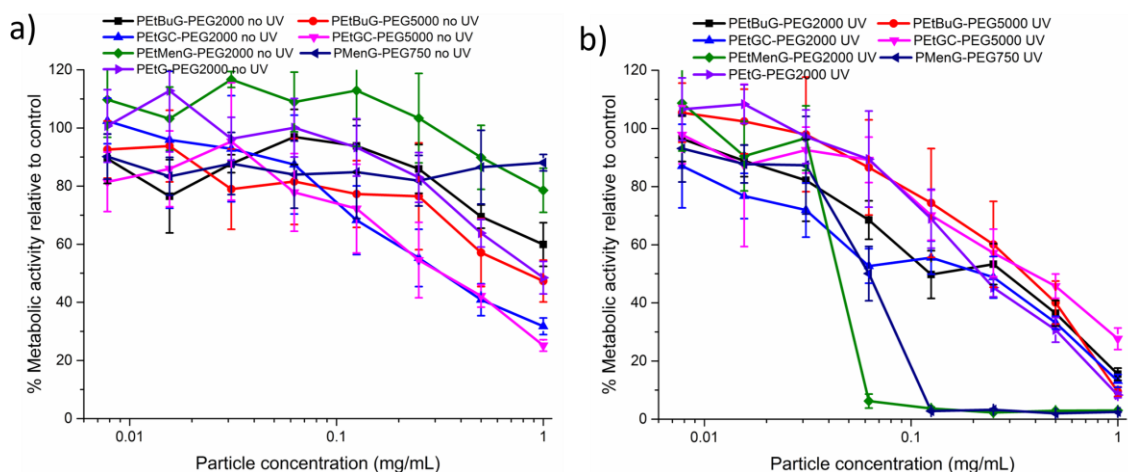


Figure 6.5 Metabolic activities, measured by MTT assays of a) particles before UV irradiation and b) after UV irradiation.

After irradiation, all of the assemblies exhibited higher toxicities compared to the non-triggered particles. Irradiation-induced depolymerization would produce the corresponding glyoxylate and chloral monomers, which would be rapidly hydrated and hydrolyzed to glyoxylate or chloral hydrate and ethanol, *n*-butanol or L-menthol. Glyoxylate and ethanol can be metabolized in the liver but not in this cancer cell line.⁵¹⁻⁵² This may explain why

some toxicity was observed in this assay ($IC_{50} \sim 250.0 \mu\text{g/mL}$), but not in whole organism studies previously reported.⁵³ Like ethanol, *n*-butanol occurs in a number of alcoholic beverages is considered have relatively low toxicity.⁵⁴ It is also metabolized by alcohol dehydrogenase in the liver. Chloral hydrate is used as a sedative for dental or medical treatments and has been administered to humans in gram-scale doses.⁵⁵ However, it is metabolized to trichloroethanol and trichloroethanol glucuronide in red blood cells and in plasma,⁵⁶ which would likely not happen in the current cell line and may explain why some toxicity to cells was observed. Interestingly, **PEtMenG-PEG2000** and **PMenG-PEG750** assemblies, which were the least toxic in their non-irradiated form were markedly more toxic than the other assemblies after irradiation, with an IC_{50} value on the order of 50 $\mu\text{g/mL}$. Although L-menthol is generally considered safe and is widely used as a cooling agent in various products from cold medications to toothpaste, exposure to high doses can lead to toxic effects.⁵⁷⁻⁵⁸ Indeed the IC_{50} value we obtained for the triggered polymers is in reasonable agreement with those determined in previous *in vitro* toxicity assays of menthol (50-120.0 $\mu\text{g/mL}$).⁵⁹ This toxicity was attributed to menthol's ability to cause the deterioration and induce leakage of mitochondrial membranes. Our assemblies therefore appear to be capable of depolymerizing and releasing biologically active menthol in response to stimuli. Given the interest in menthol as an analgesic, antifungal, antibacterial, and in other areas, the ability to release it in response to stimuli may prove useful for biomedical applications. Because of the complexities in the metabolic activity profiles of the different systems before and after irradiation, we chose to not evaluate the celecoxib-loaded particles in this assay.

6.4 Conclusions

In conclusion, we have successfully synthesized polyglyoxylates containing hydrophobic co-monomers including *n*-butyl glyoxylate, L-menthyl glyoxylate, and chloral. These polymers were end-capped with UV light-responsive linker, which allowed for their coupling with hydrophilic PEG to form amphiphilic block copolymers. The block copolymers were self-assembled into particles with diameters ranging from 82-173 nm in solution, and with cores having variable chemical structures and hydrophobicities, as

indicated by measurements of their CAC values and the λ_{\max} of encapsulated Nile red dye. All of the particles had similar triggerable disassembly capabilities based on DLS. The drug loading content for the hydrophobic drug celecoxib ranged from 6 wt% for **PEtGC-PEG2000** to 15 wt% for of **PEtBuG-PEG2000** and **PEtMenG-PEG2000**, suggesting that some cores were more compatible with celecoxib than others. All systems released celecoxib more rapidly when triggered with UV light as a stimulus than when not triggered, but differences in the precipitation of the drug and in drug retention were observed for the different systems. Finally, *in vitro* toxicity studies were performed on MDA-MB-231 cancer cells and it was found that the toxicity depended on the structure of the polymer and whether degradation had been triggered. Thus, it is possible to tune the self-assembly, drug loading, release, and toxicity of the polyglyoxylate assembly platform through simple tuning of the monomer polymer structures while retaining the essential stimuli-responsive properties. Future work will focus on the loading and release of different hydrophobic drugs, and on further *in vitro* and *in vivo* studies aimed at optimizing these systems for drug delivery applications.

6.5 References

- (1) Pitt, G.; Gratzl, M.; Kimmel, G.; Surlis, J.; Sohindler, A. Aliphatic polyesters II. The degradation of poly(D,L-lactide), poly(ϵ -caprolactone), and their copolymers *in vivo*. *Biomaterials* **1981**, *2*, 215-220.
- (2) Webb, A. R.; Yang, J.; Ameer, G. A. Biodegradable polyester elastomers in tissue engineering. *Expert Opin. Biol. Ther.* **2004**, *4*, 801-812.
- (3) Gunatillake, P.; Mayadunne, R.; Adhikari, R. Recent developments in biodegradable synthetic polymers. *Biotechnol. Annu. Rev.* **2006**, *12*, 301-347.
- (4) Hughes, S. C.; Stott, P. M.; Hearnden, A. J.; Ripley, L. G. A new and effective tension-band braided polyester suture technique for transverse patellar fracture fixation. *Injury* **2007**, *38*, 212-222.
- (5) Nicolas, J.; Mura, S.; Brambilla, D.; Mackiewicz, N.; Couvreur, P. Design, functionalization strategies and biomedical applications of targeted biodegradable/biocompatible polymer-based nanocarriers for drug delivery. *Chem. Soc. Rev.* **2013**, *42*, 1147-1235.
- (6) Varela-Moreira, A.; Shi, Y.; Fens, M. H.; Lammers, T.; Hennink, W. E.; Schiffelers, R. M. Clinical application of polymeric micelles for the treatment of cancer. *Mater. Chem. Front.* **2017**, *1*, 1485-1501.
- (7) Petros, R. A.; DeSimone, J. M. Strategies in the design of nanoparticles for therapeutic applications. *Nat. Rev. Drug Discovery* **2010**, *9*, 615.
- (8) Cabral, H.; Kataoka, K. Progress of drug-loaded polymeric micelles into clinical studies. *J. Controlled Release* **2014**, *190*, 465-476.
- (9) Hakkarainen, M.; Höglund, A.; Odellius, K.; Albertsson, A.-C. Tuning the release rate of acidic degradation products through macromolecular design of caprolactone-based copolymers. *J. Am. Chem. Soc.* **2007**, *129*, 6308-6312.
- (10) Källrot, M.; Edlund, U.; Albertsson, A.-C. Covalent grafting of poly (L-lactide) to tune the *in vitro* degradation rate. *Biomacromolecules* **2007**, *8*, 2492-2496.
- (11) Cabane, E.; Zhang, X.; Langowska, K.; Palivan, C. G.; Meier, W. Stimuli-responsive polymers and their applications in nanomedicine. *Biointerphases* **2012**, *7*:9.

- (12) Mura, S.; Nicolas, J.; Couvreur, P. Stimuli-responsive nanocarriers for drug delivery. *Nat. Mater.* **2013**, *12*, 991-1003.
- (13) Huh, K. M.; Kang, H. C.; Lee, Y. J.; Bae, Y. H. pH-sensitive polymers for drug delivery. *Macromol. Res.* **2012**, *20*, 224-233.
- (14) Liu, J.; Huang, Y.; Kumar, A.; Tan, A.; Jin, S.; Mozhi, A.; Liang, X. J. pH-sensitive nano-systems for drug delivery in cancer therapy. *Biotechnol. Adv.* **2014**, *32*, 693-710.
- (15) Agut, W.; Brûlet, A.; Schatz, C.; Taton, D.; Lecommandoux, S. pH and temperature responsive polymeric micelles and polymersomes by self-assembly of poly[2-(dimethylamino) ethyl methacrylate]-*b*-poly(glutamic acid) double hydrophilic block copolymers. *Langmuir* **2010**, *26*, 10546-10554.
- (16) de Gracia Lux, C.; Joshi-Barr, S.; Nguyen, T.; Mahmoud, E.; Schopf, E.; Fomina, N.; Almutairi, A. Biocompatible polymeric nanoparticles degrade and release cargo in response to biologically relevant levels of hydrogen peroxide. *J. Am. Chem. Soc.* **2012**, *134*, 15758-15764.
- (17) Lee, Y.; Mo, H.; Koo, H.; Park, J.-Y.; Cho, M. Y.; Jin, G.-w.; Park, J.-S. Visualization of the degradation of a disulfide polymer, linear poly(ethylenimine sulfide), for gene delivery. *Bioconjugate Chem.* **2007**, *18*, 13-18.
- (18) Olejniczak, J.; Huu, V. A. N.; Lux, J.; Grossman, M.; He, S.; Almutairi, A. Light-triggered chemical amplification to accelerate degradation and release from polymeric particles. *Chem. Commun.* **2015**, *51*, 16980-16983.
- (19) Fan, B.; Gillies, E. R. Self-Immolative Polymers. *Encycl. Polym. Sci. Technol.* **2015**, 1-35.
- (20) Roth, M. E.; Green, O.; Gnaim, S.; Shabat, D. Dendritic, oligomeric, and polymeric self-immolative molecular amplification. *Chem. Rev.* **2015**, *116*, 1309-1352.
- (21) Phillips, S. T.; DiLauro, A. M. Continuous head-to-tail depolymerization: an emerging concept for imparting amplified responses to stimuli-responsive materials. *ACS Macro Lett.* **2014**, *3*, 298-304.
- (22) Sagi, A.; Weinstain, R.; Karton, N.; Shabat, D. Self-immolative polymers. *J. Am. Chem. Soc.* **2008**, *130*, 5434-5435.

- (23) DiLauro, A. M.; Abbaspourrad, A.; Weitz, D. A.; Phillips, S. T. Stimuli-responsive core-shell microcapsules with tunable rates of release by using a depolymerizable poly(phthalaldehyde) membrane. *Macromolecules* **2013**, *46*, 3309-3313.
- (24) Esser-Kahn, A. P.; Sottos, N. R.; White, S. R.; Moore, J. S. Programmable microcapsules from self-immolative polymers. *J. Am. Chem. Soc.* **2010**, *132*, 10266-10268.
- (25) Tang, S.; Yourdkhani, M.; Possanza Casey, C. M.; Sottos, N. R.; White, S. R.; Moore, J. S. Low Ceiling Temperature Polymer Microcapsules with Hydrophobic Payloads via Rapid Emulsion-Solvent Evaporation. *ACS Appl. Mater. Interfaces* **2017**, *9*, 20115-20123.
- (26) Lewis, G. G.; Robbins, J. S.; Phillips, S. T. A prototype point-of-use assay for measuring heavy metal contamination in water using time as a quantitative readout. *Chem. Commun.* **2014**, *50*, 5352-5354.
- (27) Liu, G.; Wang, X.; Hu, J.; Zhang, G.; Liu, S. Self-immolative polymersomes for high-efficiency triggered release and programmed enzymatic reactions. *J. Am. Chem. Soc.* **2014**, *136*, 7492-7497.
- (28) Fan, B.; Gillies, E. R. Poly(ethyl glyoxylate)-Poly(ethylene oxide) Nanoparticles: Stimuli-Responsive Drug Release via End-to-End Polyglyoxylate Depolymerization. *Mol. Pharmaceutics* **2017**, *14*, 2548-2559
- (29) Fan, B.; Trant, J. F.; Gillies, E. R. End-Capping Strategies for Triggering End-to-End Depolymerization of Polyglyoxylates. *Macromolecules* **2016**, *49*, 9309-9319.
- (30) Gnaim, S.; Shabat, D. Self-Immolative Chemiluminescence Polymers: Innate Assimilation of Chemiexcitation in a Domino-like Depolymerization. *J. Am. Chem. Soc.* **2017**, *139*, 10002-10008.
- (31) Chen, E. K.; McBride, R. A.; Gillies, E. R. Self-immolative polymers containing rapidly cyclizing spacers: toward rapid depolymerization rates. *Macromolecules* **2012**, *45*, 7364-7374.
- (32) Baker, M. S.; Kim, H.; Olah, M. G.; Lewis, G. G.; Phillips, S. T. Depolymerizable poly(benzyl ether)-based materials for selective room temperature recycling. *Green Chem.* **2015**, *17*, 4541-4545.
- (33) Ergene, C.; Palermo, E. F. Cationic poly(benzyl ether) s as self-immolative antimicrobial polymers. *Biomacromolecules* **2017**, *18*, 3400-3409.

- (34) Fan, B.; Trant, J. F.; Wong, A. D.; Gillies, E. R. Polyglyoxylates: a versatile class of triggerable self-immolative polymers from readily accessible monomers. *J. Am. Chem. Soc.* **2014**, *136*, 10116-10123.
- (35) DiLauro, A. M.; Phillips, S. T. End-capped poly(4, 5-dichlorophthalaldehyde): a stable self-immolative poly(aldehyde) for translating specific inputs into amplified outputs, both in solution and the solid state. *Polym. Chem.* **2015**, *6*, 3252-3258.
- (36) de Gracia Lux, C.; McFearin, C. L.; Joshi-Barr, S.; Sankaranarayanan, J.; Fomina, N.; Almutairi, A. Single UV or Near IR triggering event leads to polymer degradation into small molecules. *ACS Macro Lett.* **2012**, *1*, 922-926.
- (37) Fan, B.; Trant, J. F.; Yardley, R. E.; Pickering, A. J.; Lagugné-Labarthe, F.; Gillies, E. R. Photocontrolled Degradation of Stimuli-Responsive Poly(ethyl glyoxylate): Differentiating Features and Traceless Ambient Depolymerization. *Macromolecules* **2016**, *49*, 7196-7203.
- (38) DeWit, M. A.; Beaton, A.; Gillies, E. R. A reduction sensitive cascade biodegradable linear polymer. *J. Polym. Sci., Part A: Polym. Chem.* **2010**, *48*, 3977-3985.
- (39) Zhang, H.; Yeung, K.; Robbins, J. S.; Pavlick, R. A.; Wu, M.; Liu, R.; Sen, A.; Phillips, S. T. Self-Powered Microscale Pumps Based on Analyte-Initiated Depolymerization Reactions. *Angew. Chem., Int. Ed.* **2012**, *51*, 2400-2404.
- (40) Fan, B.; Trant, J. F.; Hemery, G.; Sandre, O.; Gillies, E. R. Thermo-responsive self-immolative nanoassemblies: direct and indirect triggering. *Chem. Commun.* **2017**, *53*, 12068-12071.
- (41) Peterson, G. I.; Church, D. C.; Yakelis, N. A.; Boydston, A. J. 1, 2-oxazine linker as a thermal trigger for self-immolative polymers. *Polymer* **2014**, *55*, 5980-5985.
- (42) Nguyen, P. K.; Snyder, C. G.; Shields, J. D.; Smith, A. W.; Elbert, D. L. Clickable Poly(ethylene glycol)-Microsphere-Based Cell Scaffolds. *Macromol. Chem. Phys.* **2013**, *214*, 948-956.
- (43) Fenneteau, J.; Vallerotto, S.; Ferrié, L.; Figadère, B. Liebeskind–Srogl cross-coupling on γ -carboxyl- γ -butyrolactone derivatives: application to the side chain of amphoteric C and F. *Tetrahedron Lett.* **2015**, *56*, 3758-3761.

- (44) Oertling, H.; Reckziegel, A.; Surburg, H.; Bertram, H.-J. Applications of menthol in synthetic chemistry. *Chem. Rev.* **2007**, *107*, 2136-2164.
- (45) Rosen, I.; Hudgin, D.; Sturm, C.; McCain, G.; Wilhelm, R. Poly(chloroaldehydes). I. Polychloral stabilization. *J. Polym. Sci., Part A: Polym. Chem.* **1965**, *3*, 1535-1543.
- (46) Elias, H.-G., *Macromolecules*. Springer Science & Business Media: 2012; Vol. 1.
- (47) Zalipsky, S. Functionalized poly(ethylene glycols) for preparation of biologically relevant conjugates. *Bioconjugate Chem.* **1995**, *6*, 150-165.
- (48) Jendrossek, V., Exploiting celecoxib in cancer therapy. In *Mitochondria: The anti-cancer target for the third millennium*, Neuzil, J.; Pervaiz, S.; Fulda, S., Eds. Springer: Dordrecht, 2014; pp 105-133.
- (49) Bhatt, V.; Shete, G.; Bansal, A. K. Mechanism of generation of drug nanocrystals in celecoxib: mannitol nanocrystalline solid dispersion. *Int. J. Pharm.* **2015**, *495*, 132-139.
- (50) Zhang, S.-W.; Brunskill, A. P.; Schwartz, E.; Sun, S. Celecoxib–Nicotinamide Cocrystal Revisited: Can Entropy Control Cocrystal Formation? *Cryst. Growth Des.* **2017**, *17*, 2836-2843.
- (51) Baker, P. R.; Cramer, S. D.; Kennedy, M.; Assimos, D. G.; Holmes, R. P. Glycolate and glyoxylate metabolism in HepG2 cells. *Am. J. Physiol.: Cell Physiol.* **2004**, *287*, C1359-C1365.
- (52) Wanders, R. J.; Waterham, H. R. Biochemistry of mammalian peroxisomes revisited. *Annu. Rev. Biochem.* **2006**, *75*, 295-332.
- (53) Belloncle, B.; Bunel, C.; Menu-Bouaouiche, L.; Lesouhaitier, O.; Burel, F. Study of the degradation of poly(ethyl glyoxylate): biodegradation, toxicity and ecotoxicity assays. *J. Polym. Environ.* **2012**, *20*, 726-731.
- (54) Greim, H., *The MAK-Collection for Occupational Health and Safety*. Wiley-VCH: 2012.
- (55) Wilson, S.; Easton, J.; Lamb, K.; Orchardson, R.; Casamassimo, P. A retrospective study of chloral hydrate, meperidine, hydroxyzine, and midazolam regimens used to sedate children for dental care. *Pediatric Dentistry* **2000**, *22*, 107-112.
- (56) Abbas, R.; Fisher, J. W. A physiologically based pharmacokinetic model for trichloroethylene and its metabolites, chloral hydrate, trichloroacetate, dichloroacetate,

trichloroethanol, and trichloroethanol glucuronide in B6C3F1 mice. *Toxicol. Appl. Pharmacol.* **1997**, *147*, 15-30.

(57) Kumar, A.; Baitha, U.; Aggarwal, P.; Jamshed, N. A fatal case of menthol poisoning. *Int. J. Appl. Basic Med. Res.* **2016**, *6*, 137.

(58) Kamatou, G. P.; Vermaak, I.; Viljoen, A. M.; Lawrence, B. M. Menthol: a simple monoterpene with remarkable biological properties. *Phytochemistry* **2013**, *96*, 15-25.

(59) Bernson, V. S.; Pettersson, B. The toxicity of menthol in short-term bioassays. *Chem.-Biol. Interact.* **1983**, *46*, 233-246.

Chapter 7

7 Thermo-responsive self-immolative nanoassemblies: Direct and indirect triggering

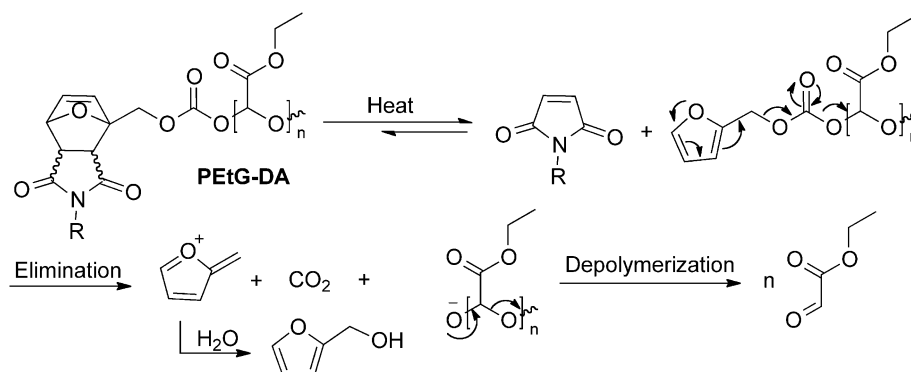
The content of this chapter has been published in “B. Fan, J. F. Trant, G. Hemery, O. Sandre, E. R. Gillies *Chem. Commun.* **2017**, 53, 12068–12071”

7.1 Introduction

Nanoassemblies are of great interest due to their ability to mimic biological nanostructures and their capacity to perform diverse functions such as controlled release¹, catalysis,² and templating of inorganic structures.³ Stimuli-responsive macromolecular assemblies have attracted significant attention,⁴ due to their ability to undergo morphological or functional changes in response to stimuli. Assemblies responsive to stimuli such as light,⁵ heat,⁶ and pH⁷ have been reported. Heat is particularly attractive as it can be easily applied either directly with good spatiotemporal control, or indirectly through photothermal⁸ or magnetothermal effects⁹. Many examples of thermo-responsive polymer assemblies employing polymers such as poly(*N*-isopropylacrylamide) that undergo solubility changes in response to temperature have been reported.¹⁰ There are very few examples involving thermally-initiated bond cleavage.¹¹

Over the last decade, a new class of stimuli-responsive polymers, often termed self-immolative polymers (SIPs), has been developed. These polymers can be triggered to depolymerize from end-to-end upon the cleavage of a stimulus-responsive end-cap from the terminus.¹² The propagating depolymerization mechanism amplifies the stimulus-mediated event. Various backbones including polycarbamates,¹³ poly(benzyl ether)s,¹⁴ and polyaldehydes¹⁵⁻¹⁷ have been reported. A single SIP backbone can respond to different signals by simply changing the end-cap.¹⁸ SIPs responsive to stimuli including light,¹⁹ oxidizing or reducing agents,²⁰ and enzymes¹³ have been reported. Assemblies such as vesicles¹⁹ and micelles²¹ have been prepared from SIPs and shown to undergo disintegration and payload release in response to stimuli.

Thus far, one thermo-responsive SIP end-cap was reported.²² This 1,2-oxazine end-cap underwent cyclo-reversion to an unstable carbamoylnitroso intermediate that hydrolyzed and decarboxylated to initiate depolymerization. However, the end-capping was challenging, as it required generation of the unstable nitroso species to perform the cyclo-addition. Furthermore, the end-cap cleavage and depolymerization were very slow, occurring over tens of days. Here we report that simple Diels-Alder (DA) adducts of furan and maleimides can serve as thermo-responsive end-caps. Upon heating, a retro-Diels Alder reaction occurs, revealing a furan.²³ Based on the known instability of similarly substituted furan derivatives,²⁴ it is proposed that the released furfuryl carbonate undergoes an elimination reaction to release an uncapped poly(ethyl glyoxylate) (PEtG) SIP for depolymerization (Scheme 7.1). Exploiting the easy synthetic modification of this end-cap, amphiphilic block copolymers can be prepared, and self-assembled into thermo-responsive vesicles and micelles. Furthermore, indirect triggering of SIP nanoassemblies is demonstrated for the first time using the magnetothermal effect with iron oxide nanoparticles (IONPs) under an alternating magnetic field.



Scheme 7.1 Proposed end-cap cleavage and depolymerization mechanism of PETG end-capped with a DA adduct (PEtG-DA).

7.2 Experimental section

General materials and procedures. **Micelle-control**¹⁵ and **PEtG-control**²⁵ were previously reported and the same batches were used here. Ethyl glyoxylate in toluene solution (50% w/w), 2-(hydroxymethyl)furan, diisopropylethylamine were obtained from

Alfa Aesar (Canada). Nile red and phosgene solution (15 wt. % in toluene) were purchased from Sigma-Aldrich (USA). Iron dichloride tetra-hydrate powder ($\text{FeCl}_2 \cdot 4\text{H}_2\text{O}$), iron trichloride hexahydrate 45% solution ($\text{FeCl}_3 \cdot 6\text{H}_2\text{O}$), diethylene glycol, *N*-methyl-diethanolamine, nitric acid were obtained from Sigma-Aldrich (France). Beycostat NE was obtained from CECA chemicals (France). Triethylamine, pyridine, and dichloromethane were distilled from calcium hydride before use. Anhydrous tetrahydrofuran, acetonitrile were obtained from a solvent purification system using aluminum oxide columns. All the other chemicals were of reagent grade and used without further purification. ^1H NMR spectra were obtained at 400 MHz or 600 MHz on Varian Inova instruments. NMR chemical shifts (δ) are reported in ppm and were calibrated against residual solvent signals of CDCl_3 (δ 7.27), CD_3CN (δ 1.94), or D_2O (δ 4.75). Fourier transform infrared (FT-IR) spectra were obtained in attenuated total reflectance (ATR) mode using a PerkinElmer UATR Spectrum Two with films drop cast from CH_2Cl_2 on diamond. High-resolution mass spectrometry (HRMS) was performed with either a Thermo Scientific DFS (Double Focus Sector) mass spectrometer, using a reversed Nier Johnson geometry for electron impact (EI) ionization, or a Bruker microOTOF 11 for electrospray ionization (ESI). The SEC instrument was equipped with a Viscotek GPC Max VE2001 solvent module. Samples were analyzed using the Viscotek VE3580 RI detector operating at 30 °C. The separation technique employed two Agilent Polypore (300×7.5 mm) columns connected in series and to a Polypore guard column (50×7.5 mm). Samples were dissolved in THF (glass distilled grade) at approximately 5.0 mg/mL and filtered through 0.22 μm syringe filters. Samples were injected using a 100 μL loop. The THF eluent was filtered and eluted at 1.0 mL/min for a total of 30 min. A calibration curve was obtained from PMMA samples with molecular weight ranges of 1,540-1,126,000/mol. Thermogravimetric analyses (TGA) were performed on a TGA Q50 from TA Instruments. The heating rate was 10 °C/min between 30-500 °C under N_2 . Ultrapure water was obtained from a Barnstead EASYpure II system. Dialyses were performed using Spectra/Por regenerated cellulose membranes with 3500 g/mol molecular weight cut-off. The hydrodynamic diameters of the polymer assemblies were measured by dynamic light scattering (DLS) using a Zetasizer Nano Series ZS instrument from Malvern Instruments,

at room temperature (25 °C) in a 1 cm path length glass cuvette at a concentration of 0.8 mg/mL suspension of polymer assemblies. Fluorescence spectra were obtained using a QM-4 SE spectrometer from Photon Technology International (PTI) equipped with double excitation and emission monochromators. TEM imaging was performed using a Phillips CM10 microscope operating at an acceleration voltage of 80 kV. 3.0 μ L of micelle suspension (0.08 mg/mL) was placed onto a copper grid. The resulting sample was air-dried overnight before imaging. TEM for IONPs and IONPs loaded micelles was performed on a Hitachi H7650 microscope operated at 80 kV on samples deposited at \sim 1.0 mg/mL onto copper grids by a lab-made spraying tool.

Synthesis of Compound 3a. *N*-benzyl maleimide²⁸ (2.0 g, 10.7 mmol) and 2-(hydroxymethyl) furan (931.0 μ L, 1.1 g, 10.7 mmol) were dissolved in anhydrous acetonitrile under a nitrogen atmosphere in a flame-dried flask equipped with a magnetic stirring-bar. The reaction was stirred at 35 °C for 14 h. When TLC indicated the reaction had reached equilibrium, the solvent was removed, and the reaction was concentrated under reduced pressure for 1 h. NMR spectroscopy of the unpurified reaction product indicated a ratio of (1:0.4:0.3) of *endo*-*exo*-unreacted maleimide. The crude material was then purified by flash chromatography (6:4 to 4:6 hexanes-ethyl acetate) to provide 2.3 g of a mixture of the *endo* and *exo* in a 70:30 ratio and a 75 % isolated yield. A small amount of material was purified further by preparative TLC (8:2 hexanes-ethyl acetate, 7 elutions) to provide analytical samples of both the *endo* and *exo* products. Due to the inherent thermal instability, the material is stored at -20 °C until needed. **3a-endo** ¹H NMR (600 MHz, CDCl₃): δ_{ppm} 7.31-7.26 (m, 5H), 6.15 (dd, *J* = 5.8, 1.5 Hz, 1H), 6.06 (d, *J* = 5.8 Hz, 1H), 5.26 (dd, *J* = 5.5, 1.6 Hz, 1H), 4.47 (s, 2H), 4.25 (d, *J* = 12.2 Hz, 1H), 4.15 (d, *J* = 12.2 Hz, 1H), 3.63 (dd, *J* = 7.6, 5.5 Hz, 1H), 3.40 (d, *J* = 7.6 Hz, 1H), 2.11 (s, 1H); ¹³C NMR (100 MHz, CDCl₃): δ_{ppm} 174.8, 174.4, 135.31, 135.28, 134.5, 129.0, 128.4, 128.0, 92.1, 79.5, 61.4, 47.9, 46.0, 42.3; HRMS (ESI): Calc'd for [M]⁺ (C₁₆H₁₅NO₄): 285.1001; Found: 285.1012. **3a-exo** ¹H NMR (600 MHz, CDCl₃): δ_{ppm} 7.33-7.26 (m, 5H), 6.61 (d, *J* = 5.7 Hz, 1H), 6.54 (dd, *J* = 5.7, 1.5 Hz, 1H), 5.28 (d, *J* = 1.7 Hz, 1H), 4.66 (s, 2H), 4.09 (dd, *J* = 12.2, 8.8 Hz, 1H), 4.03 (dd, *J* = 12.2, 6.3 Hz, 1H), 3.02 (d, *J* = 6.5 Hz, 1H), 2.99 (d, *J* = 6.5 Hz, 1H), 2.76 (bt, *J* = 7.4 Hz, 1H); ¹³C NMR (100 MHz, CDCl₃): δ_{ppm} 175.7, 175.6,

138.3, 136.9, 135.2, 128.6, 128.0, 127.8, 91.4, 80.8, 60.7, 50.0, 48.1, 42.5; HRMS (ESI): Calc'd for $[M]^+$ ($C_{16}H_{15}NO_4$): 285.1001; Found: 285.0993.

Synthesis of compound 4a. Compound **3a** (500.0 mg, 1.8 mmol, 1.0 equiv.) was dissolved in THF (10.0 mL). The resulting solution was then added dropwise into a phosgene solution (15 wt% in toluene, 3.8 mL, 5.3 mmol, 3.0 equiv.) under an argon atmosphere at room temperature and was stirred for 24 h. The residual phosgene and solvent were then removed under high vacuum to yield chloroformate **4a** (590.0 mg, 97%) as white gel. Phosgene collected in the liquid nitrogen-cooled trap was then quenched with methanol (20.0 mL) and saturated sodium hydroxide solution (20.0 mL). (**Caution! Phosgene is highly toxic.**) 1H NMR (400 MHz, $CDCl_3$): δ_{ppm} 7.33-7.19 (m, 5H), 6.59 (dd, $J = 5.5, 1.2$ Hz, 2H), 6.44 (d, $J = 5.5$ Hz, 2H), 6.15 (dd, $J = 5.9, 1.6$ Hz, 1H), 5.98 (d, $J = 5.9$ Hz, 1H), 5.29 (d, $J = 1.6$ Hz, 2H), 5.26 (dd, $J = 5.5, 1.6$ Hz, 1H), 5.03-4.94 (m, 3H), 4.80-4.68 (m, 3H) 4.62 (s, 4H), 4.44 (s, 2H), 3.63 (dd, $J = 7.8, 5.5$ Hz, 1H), 3.34 (d, $J = 7.8$ Hz, 1H), 2.99-2.89 (m, 4H); ^{13}C NMR (100 MHz, $CDCl_3$): δ_{ppm} 174.9, 173.6, 150.5, 138.0, 135.9, 135.0, 128.9, 128.6, 127.9, 127.8, 125.2, 88.8, 81.2, 49.7, 48.4, 46.2, 42.3; HRMS (EI) calc'd. for $[M]^+$ ($C_{17}H_{14}ClNO_5$): 347.0561; Found: 347.0573.

Synthesis of compound 3b. *N*-propargyl maleimide²⁹ (1.7 g, 12.6 mmol, 1.0 equiv.) and 2-(hydroxymethyl)furan (1.1 mL, 1.2 g, 12.6 mmol, 1.0 equiv.) were dissolved in anhydrous acetonitrile (10.0 mL) under a nitrogen atmosphere in a flame-dried flask equipped with a magnetic stirring-bar. The reaction was stirred at 35 °C for 14 h. When TLC indicated the reaction had reached equilibrium, the solvent was removed, and the reaction was concentrated under reduced pressure for 1 h. NMR spectroscopy of the unpurified product indicated a ratio of (3.7:0.7:1.0) of *endo-exo*-unreacted maleimide. The crude material was then purified by flash chromatography (1:1 to 4:6 hexanes-ethyl acetate) to provide 2.1 g of a mixture of the *endo* and *exo* in an 80:20 ratio and a 72% isolated yield. A small amount of material was purified further by preparative TLC (7:3 hexanes-ethyl acetate, 4 elutions) to provide analytical samples of both the *endo* and *exo* products. Due to the inherent thermal instability, the material is stored at -20 °C until needed. **3b-endo** 1H NMR (600 MHz, $CDCl_3$): δ_{ppm} 6.43 (dd, $J = 5.8, 1.6$ Hz, 1H), 6.31 (d, $J = 5.8$ Hz, 1H), 5.31 (dd, $J = 5.5, 1.6$ Hz, 1H), 4.26 (d, $J = 12.8$ Hz, 1H), 4.17 (d, $J =$

12.8 Hz, 1H), 4.06 (d, $J = 2.5$ Hz, 2H), 3.67 (dd, $J = 7.6, 5.5$ Hz, 1H), 3.48 (d, $J = 7.6$ Hz, 1H), 2.16 (t, $J = 2.5$ Hz, 1H), 2.10 (bs, 1H); ^{13}C NMR (100 MHz, CDCl_3): δ_{ppm} 173.8, 173.4, 135.6, 134.7, 92.3, 79.7, 76.0, 71.4, 61.4, 50.1, 48.2, 27.6; HRMS (ESI): Calc'd for $[\text{M}]^+$ ($\text{C}_{12}\text{H}_{11}\text{NO}_4$): 233.0688. Found: 233.06824. **3b-exo** ^1H NMR (400 MHz, CDCl_3): δ_{ppm} 6.62 (d, $J = 5.7$ Hz, 1H), 6.55 (dd, $J = 5.7, 1.6$ Hz, 1H), 5.29 (d, $J = 1.7$ Hz, 1H), 4.25 (d, $J = 2.5$ Hz, 2H), 4.10 (d, $J = 1.8$ Hz, 2H), 3.68 (dd, $J = 7.6, 5.5$ Hz, 1H), 3.48 (d, $J = 7.6$ Hz, 1H), 2.21 (t, $J = 2.5, 2.5$ Hz, 1H), 1.64 (bs, 1H); ^{13}C NMR (100 MHz, CDCl_3): δ_{ppm} 174.5, 174.4, 138.3, 137.0, 91.5, 80.9, 76.2, 71.7, 60.5, 50.1, 48.1, 27.9; ESI (MS): Calc'd for $[\text{M}]^+$ ($\text{C}_{12}\text{H}_{11}\text{NO}_4$): 233.0688; Found: 233.06892.

Synthesis of compound 4b. Compound **3b** (500.0 mg, 2.2 mmol, 1.0 equiv.) was dissolved in THF (10.0 mL). The resulting solution was then added dropwise into a phosgene solution (15 wt% in toluene, 4.6 mL, 6.4 mmol, 3.0 equiv.) under an argon atmosphere at room temperature and was stirred for 24 h. The residual phosgene and solvent were then removed by high vacuum to yield chloroformate **4b** (610.0 mg, 97%) as a white gel. Phosgene collected in the liquid nitrogen-cooled trap was then quenched with methanol (20.0 mL) and saturated sodium hydroxide solution (20.0 mL). (**Caution! Phosgene is highly toxic.**) ^1H NMR (600 MHz, CDCl_3): δ_{ppm} 6.66 (d, $J = 5.3$ Hz, 2 H), 6.53 (d, $J = 5.3$ Hz, 1 H), 6.50 (d, $J = 5.9$ Hz, 2 H), 6.34 (d, $J = 5.9$ Hz, 1 H), 5.39 (d, $J = 4.1$ Hz, 1H), 5.35 (s, 2 H), 5.09-5.05 (m, 3 H), 4.88 (d, $J = 12.3$ Hz, 1H), 4.78 (d, $J = 12.9$ Hz, 2H), 4.25 (d, $J = 2.9$ Hz, 4 H), 4.11 (d, $J = 2.4$ Hz, 3 H), 3.73 (dd, $J = 5.3, 2.4$ Hz, 1H), 3.46 (d, $J = 7.6$ Hz, 1H), 3.08 (d, $J = 6.5$ Hz, 2 H), 3.00 (d, $J = 6.5$ Hz, 2 H), 2.21 (t, $J = 2.4$ Hz, 1H), 2.19 (t, $J = 2.4$ Hz, 1H); ^{13}C NMR (150 MHz, CDCl_3): δ_{ppm} 174.0, 172.8, 150.9, 138.4, 136.4, 133.7, 129.2, 128.4, 125.5, 89.3, 81.5, 76.2, 71.9, 68.1, 50.2, 48.8, 46.7, 28.3, 27.9; HRMS (EI) calc'd. for $[\text{M}]^+$ $\text{C}_{13}\text{H}_{10}\text{ClNO}_5$: 295.0248; Found: 295.0257.

Synthesis of PEtG-DA-Bn and typical procedure for synthesis of end-capped PEtG.

Ethyl glyoxylate in toluene solution (20.0 mL) was distilled under vacuum (25 °C, 0.3 mbar) over P_2O_5 to remove toluene and trace water in the first, discarded fraction. The residue was then distilled twice successively over P_2O_5 at atmospheric pressure under argon at 130 °C to obtain the highly pure monomer. Purified ethyl glyoxylate (2.0 mL, 20.0

mmol, 1.0 equiv.) was dissolved in CH₂Cl₂ (2.0 mL) and Et₃N (1.0 μL, 10.0 μmol, 0.0005 equiv.) was added. The solution was stirred for 1 h at -20 °C. Compound **4a** (0.1 g, 280.0 μmol, 0.014 equiv.) and Et₃N (38.0 μL, 280.0 μmol, 0.014 equiv.) were added at -20 °C to end-cap the polymer. The solution was gradually warmed to room temperature and then stirred for 16 h. Purification was achieved by precipitation of the crude reaction mixture into methanol. After decanting the excess methanol, the residue was dried *in vacuo* to provide 1.1 g of a white, sticky polymer in 55% yield. ¹H NMR (600 MHz, CDCl₃): δ 7.28-7.32 (m, 10 H), 5.48-5.73 (m, 239 H), 4.15-4.31 (m, 449 H), 1.23-1.36 (m, 658 H). FT-IR: 2985, 1748, 1468, 1447, 1376, 1297, 1214, 1137, 1094, 1015, 989, 856, 675 cm⁻¹. SEC: M_n = 33 kg/mol, M_w = 59 kg/mol, *D* = 1.8.

Synthesis of PEtG-DA-alkyne. The polymer is synthesized by the same procedure described for **PEtG-DA-Bn** except that compound **4b** was used as the end-cap. The yield was 60%. ¹H NMR (600 MHz, CDCl₃): δ 5.47-5.76 (m, 630 H), 4.14-4.29 (m, 1184 H), 1.24-1.40 (m, 1754 H). FTIR: 2985, 1748, 1468, 1447, 1376, 1297, 1214, 1138, 1094, 1016, 962, 857, 675 cm⁻¹. SEC: M_n = 63 kg/mol, M_w = 130 kg/mol, *D* = 2.0.

Synthesis of Block Copolymer PEtG-DA-PEG750. 750 g/mol PEG-N₃ (36.0 mg, 48.0 μmol, 6.0 equiv.) and **PEtG-DA-alkyne** (500.0 mg, 8.0 μmol, 1.0 equiv.) were dissolved in DMF (5.0 mL). After removing the air and refilling with argon, CuSO₄ (4.0 mg, 28.0 μmol, 3.5 equiv.) and sodium ascorbate (5.0 mg, 28.0 μmol, 3.5 equiv.) were added into the solution, and the mixture was stirred at 40 °C for 16 h. The reaction mixture was then transferred into a regenerated cellulose membrane (50 kg/mol MWCO) and dialyzed against deionized water for 16 h (1.0 L, 2 solvent changes) to remove DMF and most free PEG. The dialyzed material was then lyophilized, washed 3 times with water to further remove free PEG, and then dried to afford 500.0 mg of the product as a white, rubber-like, polymer in 98% yield. ¹H NMR (600 MHz, CDCl₃): δ 5.47-5.75 (m, 341 H), 4.07-4.33 (m, 704 H), 3.63 (s, 136 H), 3.37 (s, 6 H), 1.13-1.42 (m, 1075 H). ¹³C NMR (150 MHz, CDCl₃): δ 164.7-166.3, 90.3-94.7, 70.7, 62.3, 14. FTIR: 2985, 1750, 1468, 1447, 1376, 1298, 1216, 1138, 1017, 1095, 964, 857, 677 cm⁻¹. SEC: M_n = 59 kg/mol, M_w = 111 kg/mol, *D* = 1.9.

Synthesis of PEtG-DA-PEG5000. The polymer was synthesized by the same procedure described above for the synthesis of **PEtG-DA-PEG750**, except that 5000 g/mol PEG-N₃ was used. The yield was 98 %. ¹H NMR (600 MHz, CDCl₃): δ 5.45-5.70 (m, 670 H), 4.10-4.30 (m, 1399 H), 3.62 (s, 909 H), 3.36 (s, 3 H), 1.20-1.34 (m, 2110 H). ¹³C NMR (150 MHz, CDCl₃): δ 164.6-166.7, 90.8-93.9, 70.5, 62.0, 13.8. FT-IR (thin film): 2985, 2874, 1750, 1468, 1448, 1376, 1298, 1216, 1136, 1095, 1018, 962, 856, 680 cm⁻¹. SEC: M_n = 35 kg/mol, M_w = 71 kg/mol, *D* = 2.0.

Synthesis of Vesicle-control. The polymer was synthesized by the same procedure as **Micelle-control**^{1a}, except that 750 g/mol PEG-N₃ was used. The yield was 86%. ¹H NMR (600 MHz, CDCl₃): δ 5.47-5.77 (m, 553 H), 4.07-4.36 (m, 1040 H), 3.65 (s, 136 H), 3.39 (s, 9 H), 1.13-1.47 (m, 1573 H). ¹³C NMR (150 MHz, CDCl₃): δ 164.0-166.5, 90.0-94.2, 70.5, 62.0, 13.8. FT-IR (thin film): 2985, 2874, 1752, 1467, 1448, 1376, 1297, 1217, 1140, 1096, 1018, 965, 855, 732 cm⁻¹. SEC: M_n = 77 kg/mol, M_w = 177 kg/mol, *D* = 2.3.

Study of PEtG-DA-Bn Depolymerization in Solution and Representative Procedure for Studying Depolymerization by NMR Spectroscopy. **PEtG-DA-Bn** (15.0 mg) was dissolved in a 9:1 mixture of CD₃CN: D₂O (1.2 mL) at ambient temperature (22 °C). The solution was then divided between two NMR tubes. One tube was incubated at 75 °C in an oven, while the other one was stored at room temperature (22 °C). ¹H NMR spectra were recorded at defined intervals to monitor the depolymerization of the materials. At the same time, benzyl chloroformate end-capped PEtG (**PEtG-control**) was also subjected to the same procedure and its depolymerization was monitored by NMR spectroscopy as non-triggerable control. The extent of depolymerization was calculated as % depolymerization = 100 – x, where x is the integration of the peak at 5.5 ppm, when the integration of the peak at 4.2 ppm was set to 200 (which remained constant as it corresponds to the CH₃CH₂O- in both polymer and the depolymerization product).

Self-assembly of PEtG-PEG Block Copolymers. 8.0 mg of block copolymer was fully dissolved in 1.0 mL of organic solvent by stirring overnight (THF for **PEtG-DA-PEG750** and **Vesicle-control** and DMSO for **PEtG-DA-PEG5000** and **Micelle-control**). For vesicles, 0.9 mL deionized water was added slowly into 0.1 mL of copolymer in THF with

gentle stirring. For micelles, 0.1 mL of the copolymer in DMSO was injected quickly into 0.9 mL of rapidly stirring deionized water. After stirring for 10 min, the suspension was then dialyzed against deionized water for 16 h (1.0 L, 2 solvent changes) to remove THF or DMSO, affording an aqueous suspension of assemblies.

Study of Assembly Decomposition by DLS. The assemblies were formed by the procedure described above, except that the assemblies suspension was dialyzed against 100 mM pH 7.4 phosphate buffer solution. The assemblies were then transferred into plastic cuvettes and the count rate (CR) was measured by DLS while fixing the attenuator. Samples were then incubated either at 75 °C in an oven or at room temperature (22 °C). CR changes were recorded at defined intervals to monitor the decomposition of assemblies.

Study of Nile Red Release. A stock of copolymer assembly solution at a concentration of 0.8 mg/mL was prepared by the above standard self-assembly procedure in pH 7.4 phosphate buffer. 29.0 μ L of a 0.1 mg/mL solution of Nile red in CH_2Cl_2 was added to each of a series of vials and then the solvent was evaporated to provide a thin film of Nile red. To each vial, 1.5 mL of assembly suspension was added, and the vials were gently shaken for 16 h to incorporate Nile red into the nanoparticles. After the initial fluorescence emission (600 nm) of the micelle suspension was measured using an excitation wavelength of 540 nm. Some samples were stored in an oven at 75 °C, with others were stored at room temperature (22 °C). The fluorescence emission was recorded at defined intervals to monitor the decomposition of assemblies.

Study of Assembly Depolymerization by ^1H NMR Spectroscopy. 10.0 mg of block copolymer was fully dissolved in 0.4 mL of $\text{DMSO-}d_6$. 0.2 mL of the resulting solution was rapidly injected into 1.0 mL of 100 mM, pH 7.4 phosphate buffered D_2O . After stirring for 10 min, the micelle suspension was divided between two NMR tubes. One tube was incubated in an oven at 75 °C, while the other one was kept at room temperature. ^1H NMR spectra were recorded at defined intervals to monitor the depolymerization of the materials. At the same time, **Micelle-control** was subjected to the same procedure. Percent depolymerization was determined using the sum of the integration of the methyl peaks corresponding to EtGH and ethanol (1.0-1.2 ppm), which plateaued at a very similar (1872)

value to that of the methyl peak at 1.17-1.45 ppm in the block copolymer taken in CDCl_3 (integration 2111) when setting the PEG peak integral to 909. The % polymer remaining was calculated as $100 - (\text{sum of integration from 1.0-1.2 ppm}/1872) \times 100$.

“Polyol” Synthesis of Iron Oxide Nanoparticles³⁰. 1.1 g (4.0 mmol) of $\text{FeCl}_3 \cdot 6\text{H}_2\text{O}$ and 398.0 mg (2.0 mmol) of $\text{FeCl}_2 \cdot 4\text{H}_2\text{O}$ were dissolved in a mixture of 40.0 g of di(ethylene glycol) (DEG) and 40.0 g of *N*-methyldiethanolamine (NMDEA). Meanwhile, 640.0 mg (16.0 mmol) of NaOH was dissolved in a mixture of 20.0 g of DEG and 20.0 g of NMDEA. Both solutions were stirred overnight under nitrogen flux to prevent the oxidation of Fe^{2+} species. The solutions were then mixed and stirred for 3 h, before heating the mixture to 210 °C with an oil bath, reflux set-up and mechanical agitation. The set-up was open and a flux of nitrogen helped to remove traces of water before temperature reaches 210 °C. Once a temperature of 210 °C was reached, the set-up was closed, and 1.0 mL of water was injected in the system with a syringe through a septum, leading to a burst of nuclei. The formation of nanoparticles was carried on for 30 min, then the system was cooled to room temperature. The black sediment was separated magnetically and washed with a mixture of ethanol and ethyl acetate (1:1 v/v) 3 times. Possible iron hydroxides were removed by treatment with 10% nitric acid. The nanoparticles were then washed 2 times with acetone and 2 times with diethyl ether before being dispersed in water.

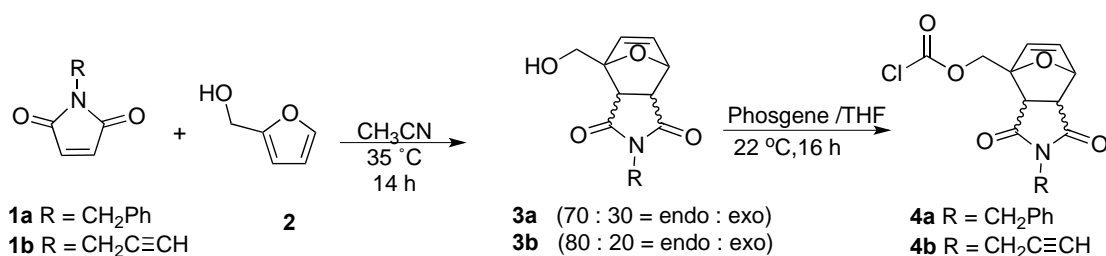
Coating of IONPs. 113.0 mg of BeycoStat NE was deposited in a 50.0 mL beaker. 15.0 mL of water was added and the solution was stirred with a mechanical agitator. 2.5 mL of a ferrofluid with an iron oxide concentration of 18.0 g/L (45.0 mg of iron oxide in solution) was added to the surfactant. Then 2.6 mL of a 69 % w/w HNO_3 solution was added to reach a final HNO_3 concentration of 2.0 M. The solution was heated to 60 °C for 30 min with a water bath. The nanoparticles were then sedimented over a permanent magnet and washed 3 times with 50.0 mL of methanol, before being dispersed in 45.0 mL of dichloromethane or tetrahydrofuran (THF). The iron oxide content of this dispersion was estimated by dissolving 50.0 μL of solution in 5.0 mL of 5.0 M HCl M with the help of a sonication bath. The absorption at 350 nm corresponding to the peak of the $[\text{Fe}(\text{Cl})_6]^{3-}$ complex was compared to a calibration curve. The final concentration was estimated at 6.0 g/L of Fe_2O_3 .

Loading of IONPs into Micelles. 1.0 mg of **PEtG-DA-PEG5000** or **Micelle-control** was dissolved in 0.2 mL of THF, meanwhile IONPs (dispersed in THF with a concentration of 6.0 mg/mL) were mixed at different feed weight ratios (FWR) as needed with the polymer solution. This mixture was then added dropwise to 1.8 mL water via a micro-syringe while magnetically stirring. THF was allowed to evaporate by leaving the vials open for 24 h.

Dynamic Light Scattering Coupled with Magnetic Field Hyperthermia. The combined DLS-MFH set-up based on a remote DLS setup VASCO Flex™ from Cordouan Technologies (Pessac, France) has been previously reported³¹ and is shown in Fig. A7.40. Micelles loaded with 35 mass % IONPs were studied by DLS-MFH. The sample was heated up to the desired external temperature by a water bath. The temperature of the sample was measured with an optical fiber probe. After 1 h equilibration at the target temperature, the alternating magnetic field was applied at the maximum available amplitude of 10.2 kA/m and frequency of 755 kHz. Meanwhile, DLS was operating continuously at a backscattering angle of 165° to measure the sample diameter (Z-average), polydispersity index (PDI) and signal intensity changes during this period.

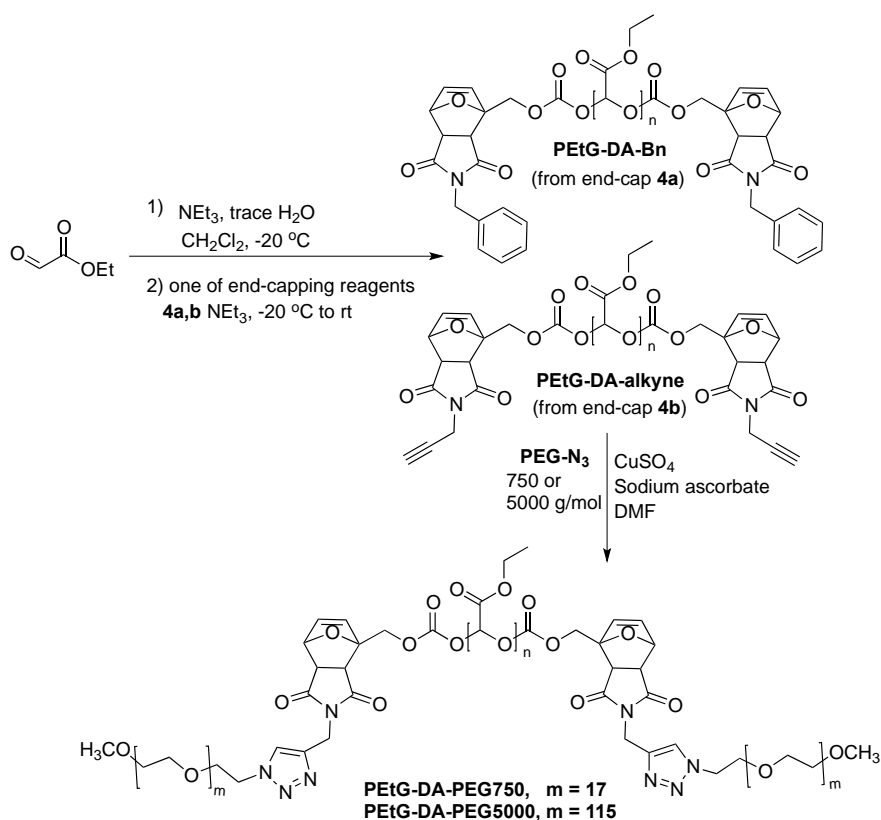
7.3 Results and discussion

To test the proposed concept, we capped PEtG with the DA adduct and evaluated its thermo-responsiveness. First, *N*-benzylmaleimide (**1a**) was reacted with furfuryl alcohol (**2**) in a DA reaction to obtain **3a** as a 70:30 mixture of *endo:exo* diastereomers (Scheme 7.2). **3a** was then activated as the chloroformate **4a**. Polymerization of ethyl glyoxylate was conducted at -20 °C,¹⁵ and the resulting PEtG was end-capped *in situ* by reaction with **4a** to afford **PEtG-DA-Bn** (Scheme 7.3). The number average molecular weight (M_n) was 33 kg/mol and the dispersity (\mathcal{D}) was 1.8 based on size exclusion chromatography (SEC). Successful end-capping was confirmed by thermogravimetric analysis as the capped polymer was stable to > 165 °C in the solid state, whereas uncapped polymer depolymerized below 100 °C¹⁵ (Fig. A7.28, Table A7.1).



Scheme 7.2 Synthesis of end-caps **4a** and **4b**.

To test the thermo-responsiveness of **PEtG-DA-Bn**, the polymer was dissolved in 9:1 CD₃CN:D₂O and incubated at different temperatures. A non-responsive PEtG end-capped by benzyl chloroformate (**PEtG-control**, Scheme A7.1)²⁵ was also examined. The depolymerization was monitored by ¹H NMR spectroscopy. Initially, the spectrum of **PEtG-DA-Bn** consisted of broad peaks attributable to the polymer (Fig. 7.1). When the polymer was heated, a sharp peak at 5.1 ppm corresponding to the depolymerization product ethyl glyoxylate hydrate (EtGH) emerged. The extent of depolymerization was quantified based on the integrations of polymer and EtGH peaks. Over 24 h, 85% depolymerization occurred at 75 °C, 53 % at 60 °C, and 8% at 40 °C (Figs. 7.2a, A7.22). In contrast, **PEtG-DA-Bn** at 22 °C and **PEtG-control** at 75 °C underwent less than 10% depolymerization even after 4 days (Figs. 7.2a, A7.21, A7.23). Overall, the rate of end-cap cleavage and depolymerization was much faster for **PEtG-DA-Bn** than that of the previously reported oxazine system,²² which required several days, resulting in substantial background degradation of the controls. Thus, DA adducts can provide rapid and selective thermo-responsive depolymerization.



Scheme 7.3 Synthesis of end-capped PEtG and its block copolymers.

To prepare thermally-responsive assemblies from amphiphilic block copolymers, end-cap **4b** with a propargyl group was synthesized (Scheme 7.2). **4b** was installed on PEtG to afford **PEtG-DA-alkyne** with an M_n of 63 kg/mol and a D of 2.0 (Scheme 7.3). This polymer underwent depolymerization at rates very similar to those of **PEtG-DA-Bn** (Figs. 7.2a, A7.24-A7.25). It was then coupled with two different lengths of azide-functionalized poly(ethylene glycol) (PEG-N₃; 750 and 5000 g/mol) to give copolymers **PEtG-DA-PEG750** and **PEtG-DA-PEG5000**. The success of the couplings was confirmed by SEC (Figs. A7.30-A7.31) and ¹H NMR and ¹³C NMR spectroscopy (Figs. A7.15-A7.18).

Assemblies were prepared by nanoprecipitation involving the addition of H₂O into THF for **PEtG-DA-PEG750** and DMSO into H₂O for **PEtG-DA-PEG5000**. Based on dynamic light scattering (DLS), the Z-average diameters of the assemblies were 480 ± 80 nm for **PEtG-DA-PEG750** and 87 ± 3 nm for **PEtG-DA-PEG5000** (Figs. A7.33-A7.34).

Transmission electron microscopy (TEM) showed that **PEtG-DA-PEG750** formed vesicles, while **PEtG-DA-PEG5000** formed solid spherical nanoparticles (Fig. 7.3).

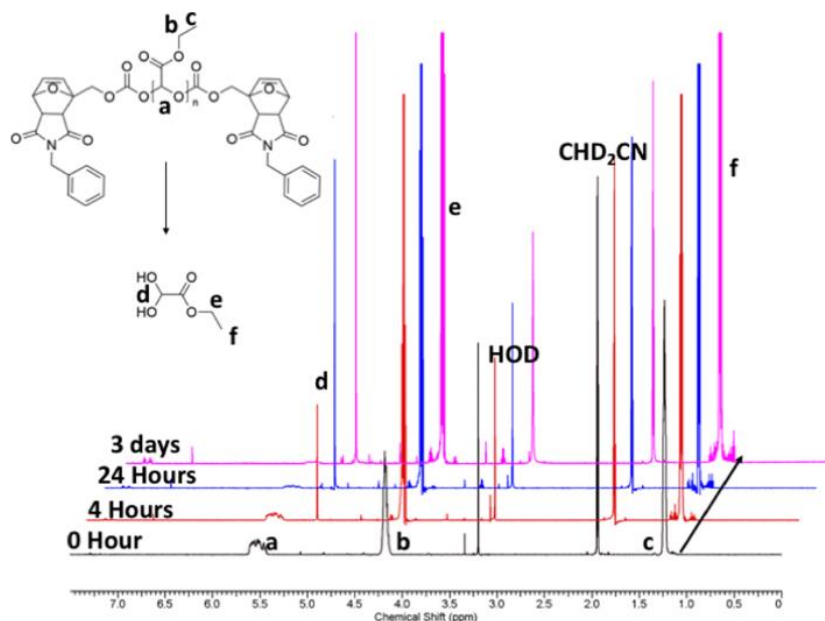


Figure 7.1 ^1H NMR spectra of **PEtG-DA-Bn** incubated in 9:1 $\text{CD}_3\text{CN}:\text{D}_2\text{O}$ at 75°C . Spectra are offset to allow the progression over time to be clearly observed.

After incubation of the assemblies at 75°C for 16 h, no remaining assemblies were detected by TEM (Fig. A7.37). This suggests that depolymerization of the PEtG resulted in disassembly. This disassembly was further probed using DLS by fixing the detector attenuation factor and recording the mean count rate (CR), which is proportional to the number and molar mass of the scattering species. Both the thermo-responsive vesicles and micelles prepared from **PEtG-DA-PEG750** and **PEtG-DA-PEG5000** showed an 80% decrease in CR when incubated at 75°C for 10 h (Fig. 7.2b). In contrast, when these systems were incubated at 22°C less than a 20% change in CR was observed. To ensure that the depolymerization at 75°C did not arise from non-specific thermal bond cleavage, we prepared additional vesicle and micelle controls (**Vesicle-control** and **Micelle-control**) from previously reported PEtG-PEG block copolymers containing a photocleavable nitrobenzyl end-cap/linker, that should not be thermo-responsive (Scheme A7.1).¹⁵ For

both of these systems, the CR initially increased, which could be attributed to some aggregation, but it remained within 20% of its initial value.

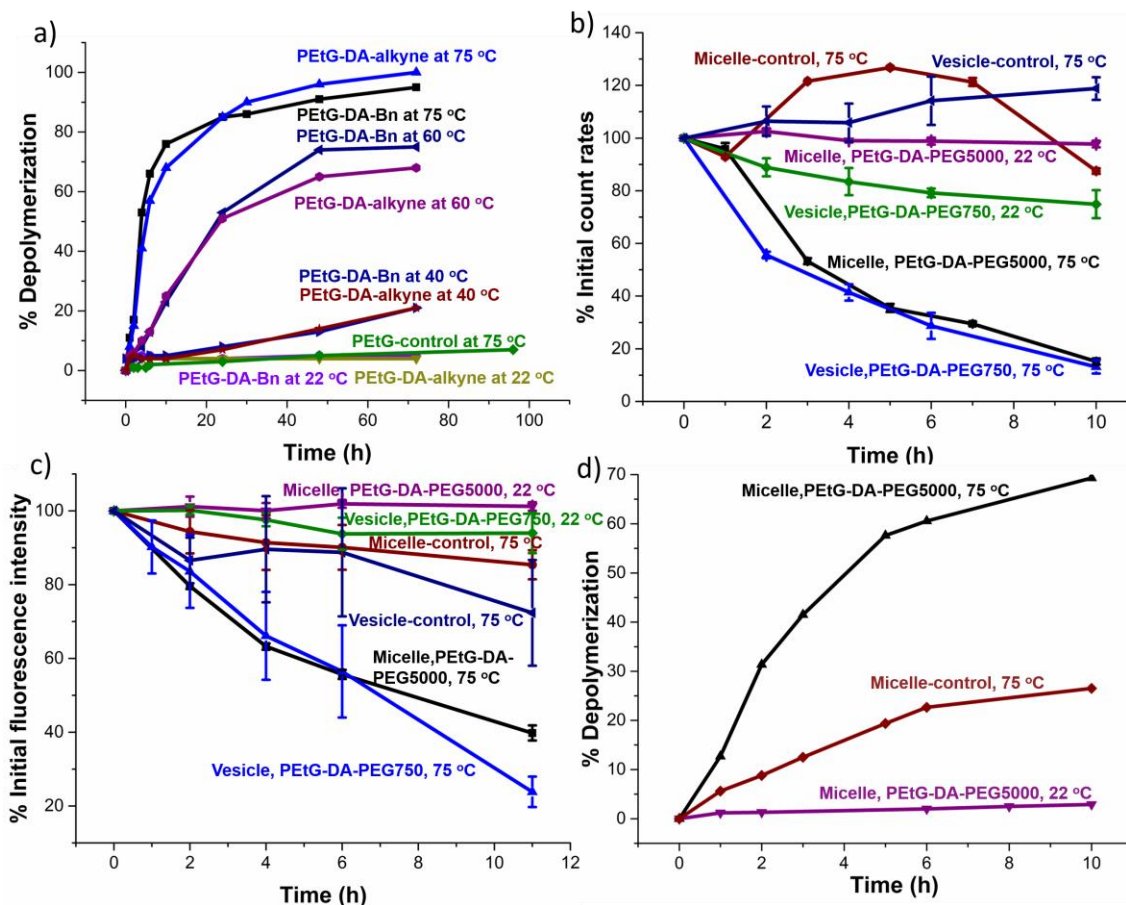


Figure 7.2 a) Depolymerization of polymers in 9:1 CD₃CN:D₂O monitored by NMR spectroscopy; Assembly degradation in pH 7.4 phosphate buffer monitored by b) DLS count rate changes, c) Nile red fluorescence changes, and d) NMR spectroscopy.

The release of cargo from the vesicles and micelles was also explored. Nile red is a hydrophobic dye with strong fluorescence emission in a hydrophobic environment, but greatly reduced fluorescence due to quenching in hydrophilic environments such as water. Nile red was incorporated into the responsive vesicles and micelles as well as their corresponding controls. When the thermo-responsive assemblies were incubated at 75 °C, the fluorescence intensity of Nile red decreased by 60-70% over 11 h (Fig.7.2c), consistent with its release into the aqueous environment. However, for either the same assemblies

incubated at 22 °C or the non-thermo-responsive controls incubated at 75 °C, only ~10-20% intensity decrease was observed after 11 h.

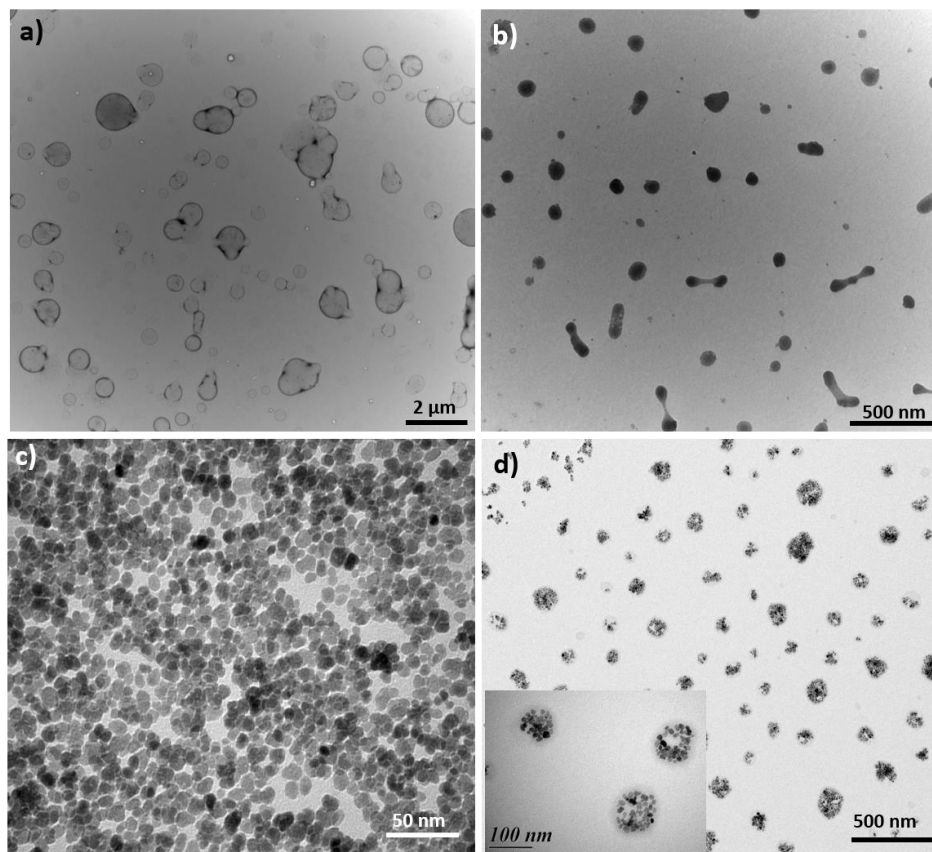


Figure 7.3 TEM images of a) PETG-DA-PEG750 vesicles, b) PETG-DA-PEG5000 micelles, c) unloaded IONPs, d) IONP-loaded PETG-DA-PEG5000 micelles.

To confirm that breakdown of the assemblies was induced by the depolymerization of the PETG blocks, the depolymerization of **PETG-DA-PEG5000** micelles was studied by ^1H NMR spectroscopy. In this case, the assemblies were prepared by nanoprecipitation of the polymer in $\text{DMSO-}d_6$ into pH 7.4 phosphate buffered D_2O ($\text{DMSO-}d_6$: D_2O = 1:5). Only the peak corresponding to the PEG block was observed initially, consistent with self-assembly of PETG at the particle cores (Fig. A7.26). However, after 1 h at 75 °C, peaks corresponding to EtGH appeared, confirming depolymerization. As shown in Fig. 7.2d, ~65% depolymerization had occurred over 10 h at 75 °C, whereas less than 5% depolymerisation occurred at 22 °C. For **Micelle-control**, at 75 °C, there was only about

20% depolymerization, which could be induced by nonspecific hydrolysis of the carbonate group of the end-cap. Combined, these data support that the thermo-responsive assemblies can degrade in response to external heat, and that this is due to the thermally responsive end-cap.

For some applications, direct bulk heating to trigger depolymerization can be a viable process. However, in other cases, it would be necessary to apply a more selective and localized heating. Therefore, we also explored the incorporation of IONPs into the micelle core and the use of magnetic field hyperthermia (MFH) to obtain localized heating around the IONPs. This magnetothermal effect has previously been shown to enable a similar cleavage of bonds at the IONP surface.²⁶

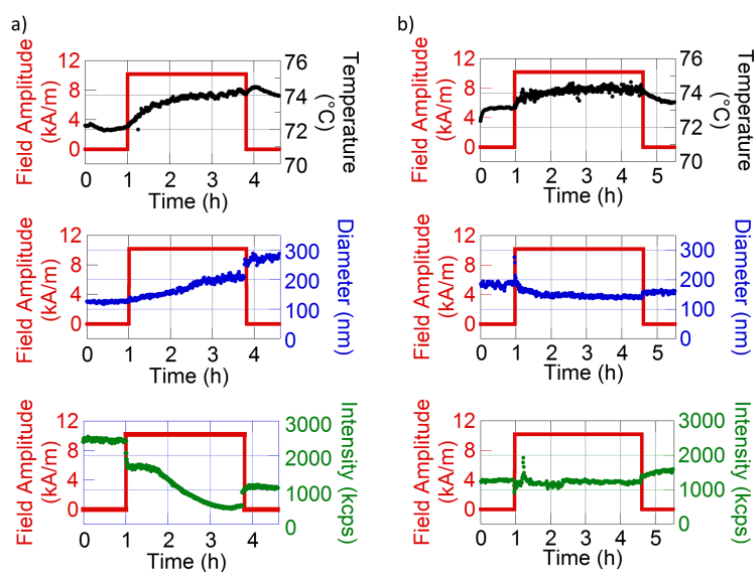


Figure 7.4 Bulk temperature, particle diameter, and count rate measured before, during, and after magnetic hyperthermia using an *in situ* DLS for 35 mass% IONP-loaded a) PEtG-DA-PEG5000 micelles and b) Micelle-control.

Hydrophobic IONPs were synthesized via the “polyol” process (11.2 ± 1.9 nm diameter, Fig. 7.3c),⁸ and then coated with Beycostat NE surfactant to be incorporated into the micelle cores via nanoprecipitation of co-assembled IONPs and **PEtG-DA-PEG5000** from a THF solution into water.²⁷ The pure micelle solution was transparent and colorless. When

the IONPs were introduced, the colloidal suspension became brown and darkened as the concentration of iron increased (Fig. A7.39). However, even at 35 mass % of IONP relative to polymer, the suspension was still transparent, confirming the IONPs were well dispersed and not precipitating. TEM showed that the IONPs were aggregated in spherical shapes with dimensions of ~ 100 nm (Fig. 7.3d).

Samples with the highest IONP content of 35 mass%, theoretically able to produce the largest increases of temperature, were studied. **Micelle-control** was also loaded with IONPs. The samples were first heated to 72 °C and equilibrated for 1 h. The Z-average particle diameter and scattering CR were measured using an *in situ* MFH-DLS setup as previously reported (Fig. A7.40).⁹ No changes in CR or diameter were observed during the initial 1 h, suggesting that the composite structure may stabilize the assemblies. Then, magnetic field oscillations at maximum amplitude of 10.2 kA m⁻¹ and 755 kHz were applied. Heat generated by the IONP-loaded micelles led to only a slight increase in temperature of ~ 2 °C for the bulk suspension. Nevertheless, the MFH had a rapid effect on the magnetic micelles, leading to an increase in diameter and large decrease in the CR. Normally, an increase in diameter would be expected to lead to an increase in CR. However, based on the experiments carried out on non-magnetic micelles, we hypothesize that upon application of MFH, the polymer depolymerized, leading to an overall reduction of the concentration of scattering species and reduced CR. The resulting unstabilized hydrophobic IONPs then aggregated, resulting in an increased diameter. In the case of the control IONP-loaded **Micelle-control**, a similar elevation of temperature was recorded, but diameters and intensities remained relatively constant. The experiment was also conducted at lower initial temperatures (53 °C) for the IONP-loaded thermo-responsive micelles but no significant changes were observed by DLS over the same time period (Fig. A7.41). Thus, while elevated initial temperatures were required for the MFH effect, these experiments demonstrate the ability to indirectly and selectively trigger the disassembly of the thermo-responsive micelles. A complementary small angle neutron scattering (SANS) study confirmed the thermo-induced degradation of the assemblies, both for pure and IONP-loaded **PEtG-DA-PEG5000** micelles heated at 80 °C for 30 min (Fig. A7.42).

7.4 Conclusions

In conclusion, this chapter showed that a simple DA adduct of a furan and maleimide could serve as a new thermo-responsive end-cap for SIPs. It was readily functionalized to enable conjugation of PEG, forming block copolymers. Thermo-responsive PEtG-PEG copolymers with different PEG weight fractions were prepared and self-assembled to form micelles or vesicles. These nanoassemblies were triggered to disassemble upon heating as demonstrated by TEM, DLS, release of Nile red, and NMR spectroscopy. Furthermore, MFH was used as an indirect stimulus to trigger the degradation of IONP-loaded micelles. Future work will involve the tuning of the structures of the end-caps and the assemblies to enable them to respond to heat stimuli both directly and indirectly at lower temperatures.

7.5 References

- (1) Ganta, S.; Devalapally, H.; Shahiwala, A.; Amiji, M. A review of stimuli-responsive nanocarriers for drug and gene delivery. *J. Controlled Release* **2008**, *126*, 187-204.
- (2) Ge, J.; Huynh, T.; Hu, Y.; Yin, Y. Hierarchical magnetite/silica nanoassemblies as magnetically recoverable catalyst-supports. *Nano Lett.* **2008**, *8*, 931-934.
- (3) Wang, Y.; Angelatos, A. S.; Caruso, F. Template synthesis of nanostructured materials via layer-by-layer assembly. *Chem. Mater.* **2007**, *20*, 848-858.
- (4) Zhuang, J.; Gordon, M. R.; Ventura, J.; Li, L.; Thayumanavan, S. Multi-stimuli responsive macromolecules and their assemblies. *Chem. Soc. Rev.* **2013**, *42*, 7421-7435.
- (5) Katz, J. S.; Burdick, J. A. Light-responsive biomaterials: development and applications. *Macromol. Biosci.* **2010**, *10*, 339-348.
- (6) Agut, W.; Brûlet, A.; Schatz, C.; Taton, D.; Lecommandoux, S. pH and temperature responsive polymeric micelles and polymersomes by self-assembly of poly[2-(dimethylamino) ethyl methacrylate]-*b*-poly(glutamic acid) double hydrophilic block copolymers. *Langmuir* **2010**, *26*, 10546-10554.
- (7) Liu, J.; Huang, Y.; Kumar, A.; Tan, A.; Jin, S.; Mozhi, A.; Liang, X. J. pH-sensitive nano-systems for drug delivery in cancer therapy. *Biotechnol. Adv.* **2014**, *32*, 693-710.
- (8) Huang, X.; El-Sayed, I. H.; Qian, W.; El-Sayed, M. A. Cancer cell imaging and photothermal therapy in the near-infrared region by using gold nanorods. *J. Am. Chem. Soc.* **2006**, *128*, 2115-2120.
- (9) Hemery, G.; Garanger, E.; Lecommandoux, S.; Wong, A. D.; Gillies, E. R.; Pedrono, B.; Bayle, T.; Jacob, D.; Sandre, O. Thermosensitive polymer-grafted iron oxide nanoparticles studied by in situ dynamic light backscattering under magnetic hyperthermia. *J. Phys. D: Appl. Phys.* **2015**, *48*, 494001-494014.
- (10) Qin, S.; Geng, Y.; Discher, D. E.; Yang, S., Temperature-controlled assembly and release from polymer vesicles of poly(ethylene oxide)-block-poly(N-isopropylacrylamide). *Adv. Mater.* **2006**, *18*, 2905-2909.
- (11) Jackson, A. W.; Fulton, D. A., Making polymeric nanoparticles stimuli-responsive with dynamic covalent bonds. *Polym. Chem.* **2013**, *4*, 31-45.

- (12) Roth, M. E.; Green, O.; Gnaim, S.; Shabat, D. Dendritic, oligomeric, and polymeric self-immolative molecular amplification. *Chem. Rev.* **2015**, *116*, 1309-1352.
- (13) Sagi, A.; Weinstain, R.; Karton, N.; Shabat, D. Self-immolative polymers. *J. Am. Chem. Soc.* **2008**, *130*, 5434-5435.
- (14) Olah, M. G.; Robbins, J. S.; Baker, M. S.; Phillips, S. T. End-capped poly(benzyl ethers): acid and base stable polymers that depolymerize rapidly from head-to-tail in response to specific applied signals. *Macromolecules* **2013**, *46*, 5924-5928.
- (15) Fan, B.; Trant, J. F.; Wong, A. D.; Gillies, E. R. Polyglyoxylates: a versatile class of triggerable self-immolative polymers from readily accessible monomers. *J. Am. Chem. Soc.* **2014**, *136*, 10116-10123.
- (16) DiLauro, A. M.; Abbaspourrad, A.; Weitz, D. A.; Phillips, S. T. Stimuli-responsive core-shell microcapsules with tunable rates of release by using a depolymerizable poly(phthalaldehyde) membrane. *Macromolecules* **2013**, *46*, 3309-3313.
- (17) Knoll, A. W.; Pires, D.; Coulembier, O.; Dubois, P.; Hedrick, J. L. Probe-based 3-D nanolithography using self-amplified depolymerization polymers. *Adv. Mater.* **2010**, *22*, 3361-3365.
- (18) Fan, B.; Trant, J. F.; Gillies, E. R. End-Capping Strategies for Triggering End-to-End Depolymerization of Polyglyoxylates. *Macromolecules* **2016**, *49*, 9309-9319.
- (19) Liu, G.; Wang, X.; Hu, J.; Zhang, G.; Liu, S. Self-immolative polymersomes for high-efficiency triggered release and programmed enzymatic reactions. *J. Am. Chem. Soc.* **2014**, *136*, 7492-7497.
- (20) Liu, G.; Zhang, G.; Hu, J.; Wang, X.; Zhu, M.; Liu, S. Hyperbranched self-immolative polymers (h-SIPs) for programmed payload delivery and ultrasensitive detection. *J. Am. Chem. Soc.* **2015**, *137*, 11645-11655.
- (21) Fan, B.; Gillies, E. R. Poly(ethyl glyoxylate)-Poly(ethylene oxide) Nanoparticles: Stimuli-Responsive Drug Release via End-to-End Polyglyoxylate Depolymerization. *Mol. Pharmaceutics* **2017**, *14*, 2548.
- (22) Peterson, G. I.; Church, D. C.; Yakelis, N. A.; Boydston, A. J. 1, 2-oxazine linker as a thermal trigger for self-immolative polymers. *Polymer* **2014**, *55*, 5980-5985.

- (23) Gandini, A., The furan/maleimide Diels-Alder reaction: A versatile click-unclick tool in macromolecular synthesis. *Prog. Polym. Sci.* **2013**, *38*, 1-29.
- (24) Zanetti, J. E.; Bashour, J. T., α -Furfuryl bromide (2-bromomethylfuran). *J. Am. Chem. Soc.* **1939**, *61*, 2249-2251.
- (25) Fan, B.; Trant, J. F.; Yardley, R. E.; Pickering, A. J.; Lagugne-Labarthet, F. O.; Gillies, E. R., Photocontrolled degradation of stimuli-responsive poly(ethyl glyoxylate): Differentiating features and traceless ambient depolymerization. *Macromolecules*, **2016**, *49*, 7196-7203.
- (26) N'Guyen, T. T.; Duong, H. T.; Basuki, J.; Montembault, M. R.; Davis, T. P., Functional iron oxide magnetic nanoparticles with hyperthermia-induced drug release ability by using a combination of orthogonal click reactions. *Angew. Chem., Int. Ed.* **2013**, *52*, 14152-14156.
- (27) Agut, W.; Brulet, A.; Taton, D.; Sandre, O.; Lecommandoux, S., Depletion induced vesicle-to-micelle transition from self-assembled rod-coil diblock copolymers with spherical magnetic nanoparticles. *Soft Matter*. **2011**, *7*, 9744-9750.
- (28) Sortino, M.; Cechinel Filho, V.; Corrêa, R.; Zacchino, S. N-Phenyl and N-phenylalkyl-maleimides acting against *Candida* spp.: Time-to-kill, stability, interaction with maleamic acids. *Bioorg. Med. Chem.* **2008**, *16*, 560-568.
- (29) Link, M.; Li, X.; Kleim, J.; Wolfbeis, O. S. Click Chemistry Based Method for the Preparation of Maleinimide-Type Thiol-Reactive Labels. *Eur. J. Org. Chem.* **2010**, *2010*, 6922-6927.
- (30) Hemery, G.; Keyes Jr, A. C.; Garaio, E.; Rodrigo, I.; Garcia, J. A.; Plazaola, F.; Garanger, E.; Sandre, O. Tuning Sizes, Morphologies, and Magnetic Properties of Monocore Versus Multicore Iron Oxide Nanoparticles through the Controlled Addition of Water in the Polyol Synthesis. *Inorg. Chem.* **2017**, *56*, 8232-8243.
- (31) Hemery, G.; Garanger, E.; Lecommandoux, S.; Wong, A. D.; Gillies, E. R.; Pedrono, B.; Bayle, T.; Jacob, D.; Sandre, O. Thermosensitive polymer-grafted iron oxide nanoparticles studied by in situ dynamic light backscattering under magnetic hyperthermia. *J. Phys. D: Appl. Phys.* **2015**, *48*, 494001-494014.

Chapter 8

8 Temperature-dependent depolymerization of trityl end-capped poly(ethyl glyoxylate): potential applications in smart packaging

8.1 Introduction

Stimuli-responsive polymers, which respond to stimuli with changes in chemical or physical properties, have been intensively researched over the past couple of decades.¹ Their unique behavior relative to conventional non-responsive polymers has inspired their use in a wide variety of applications including biosensors,² smart coatings,³ drug delivery vehicles,⁴⁻⁵ as well as self-healing and shape-memory materials.⁶⁻⁷ However, conventional stimuli-responsive polymers that contain many responsive moieties along the polymer backbone usually require a large number of stimuli-mediated events to bring about significant changes in properties.⁸⁻⁹ This may result in limitations for some applications.

Self-immolative polymers (SIPs), are a recently developed class of stimuli-responsive polymers that consist of a polymer backbone and a stimuli-responsive end-cap at one or both polymer termini.⁹⁻¹⁰ Upon detection of an external signal that can cleave the end-cap, complete collapse of the polymer backbone via end-to-end depolymerization occurs. Compared with traditional stimuli-responsive polymers, SIPs can be easily modified to achieve responsiveness to different stimuli via alterations of the end-cap rather than complete re-engineering of the polymer backbone. Using this strategy, SIPs that respond to stimuli including light,¹¹⁻¹⁴ heat,¹⁵⁻¹⁶ changes in pH,¹⁷⁻¹⁸ oxidation,¹⁹ and reduction²⁰⁻²² have been developed. In addition, the response mechanism of SIPs allows signal amplification, as one equivalent of stimulus can lead to complete polymer depolymerization and generation of many monomers or degradation products. In the past several years, SIPs including polycarbamates,²³⁻²⁴ polycarbonates,^{21, 25-26} poly(benzyl ether)s,²⁷⁻²⁹ and polyacetals³⁰⁻³⁵ have been reported.

We reported polyglyoxylates as a class of polyacetal-based SIPs in 2014.¹¹ They can be prepared from commercial monomers including ethyl glyoxylate and degrade to environmentally benign products such as glyoxylic acid and ethanol.³⁶⁻³⁷ Unlike other SIPs, they also depolymerize to volatile products (e.g., ethyl glyoxylate) as demonstrated in chapter 3, so they undergo rapid depolymerization in the solid state.³³ We also reported the polymerization of different glyoxylate monomers that enable the properties of the polymers to be tuned and also the incorporation of different end-caps that enable poly(ethyl glyoxylate) (PEtG) to respond to different stimuli in chapter 4.¹⁷ As part of this work, we reported 4-methoxytriphenylmethyl (MMT) end-capped PEtG that was responsive to acid in aqueous-organic solvents and the rate of end-cap cleavage could be increased by the introduction of additional electron-donating methoxy groups to the aromatic ring (e.g., in dimethoxytriphenylmethyl, DMT) (Figure 8.1). While **PEtG-DMT** and **PEtG-MMT** were stable for days to weeks in aqueous-organic solvent mixtures in the absence of acid, we unexpectedly found that these polymers disappeared into the air when cast as films and stored in the dry state in the absence of any acid, even for a few days. This result contrasted with our previous work on PEtG films with UV light-responsive end-caps which only depolymerized when their end-caps had been actively cleaved off.³³ This chapter describes our exploration of this interesting phenomenon and the potential application of four different triphenylmethyl (trityl) end-capped PEtGs in smart packaging. To the best of our knowledge, this is the first observation of this type of behavior for the well-known trityl group and the first example of SIPs applied in this manner.

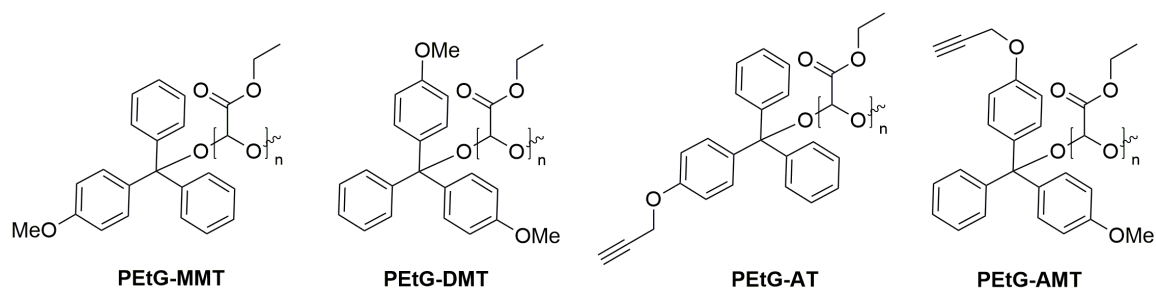


Figure 8.1 Structures of trityl end-capped PEtG.

8.2 Experimental section.

General materials and procedures. **PEtG-DMT** ($M_n = 21$ kg/mol, $D = 1.3$), **PEtG-MMT** ($M_n = 29$ kg/mol, $D = 1.5$) and **PEtG-control** ($M_n = 35$ kg/mol, $D = 1.4$) were previously reported in Chapter 4 and the same batches were used here. Ethyl glyoxylate in toluene solution (50% w/w), imidazole, 4-bromophenol, benzophenone, 4-methoxybenzophenone, and propargyl bromide solution in toluene (80 wt. %) were obtained from Alfa Aesar. Nile red (Technical grade), IR-780 iodide, *n*-BuLi in hexane (2.5 M), tetrabutylammonium fluoride solution in THF (1.0 M), acetyl chloride were purchased from Sigma-Aldrich. Triethylamine and CH_2Cl_2 were distilled from CaH_2 before use. Anhydrous tetrahydrofuran, DMF were obtained from a solvent purification system equipped with aluminum oxide columns. All the other chemicals were of reagent grade and used without further purification. ^1H NMR spectra were obtained at 400 MHz or 600 MHz on Varian Inova instruments. NMR chemical shifts (δ) are reported in ppm and calibrated against residual solvent signals of CDCl_3 (δ 7.27), C_6D_6 (δ 7.16), $\text{DMSO-}d_6$ (δ 2.50), or CD_3CN (δ 1.94). Fourier transform infrared (FT-IR) spectra were obtained in attenuated total reflectance (ATR) mode using a PerkinElmer UATR Spectrum Two with films drop cast from CH_2Cl_2 on diamond. High-resolution mass spectrometry (HRMS) was performed with a Thermo Scientific DFS (Double Focus Sector) mass spectrometer, using a reversed Nier Johnson geometry for electron impact (EI) ionization. The SEC instrument was equipped with a Viscotek GPC Max VE2001 solvent module. Samples were analyzed using the Viscotek VE3580 RI detector operating at 30 °C. The separation technique employed two Agilent Polypore (300 × 7.5mm) columns connected in series and to a Polypore guard column (50 × 7.5mm). Samples were dissolved in THF (glass distilled grade) at approximately 5.0 mg/mL and filtered through 0.22 μm syringe filters. Samples were injected using a 100 μL loop. The THF eluent was filtered and eluted at 1.0 mL/min for a total of 30 min. A calibration curve was obtained from PMMA samples with molecular weight ranges of 1,540-1,126,000 g/mol. UV-visible spectra were obtained on a Varian UV/VIS Cary 300 spectrophotometer.

Synthesis of Compound 2. 4-Bromophenol (4.0 g, 23.0 mmol), *tert*-butyldimethylsilyl chloride (17.3 g, 115.0 mmol) and imidazole (9.4 g, 138.0 mmol) were dissolved in 50 mL of anhydrous DMF under an Ar atmosphere in a flame-dried flask equipped with a magnetic stirring-bar. The reaction was stirred at 22 °C for 2 h. When TLC indicated the reaction had reached equilibrium, the reaction was quenched with 200.0 mL of distilled water. The mixture was then extracted with ethyl acetate (3 x 100.0 mL), and the combined organic phase was washed with saturated NaHCO₃ solution (1 x 50.0 mL) and brine (1 x 50.0 mL), and then dried over anhydrous MgSO₄. The solvent was then removed under reduced pressure to yield the crude product, which was further purified by flash chromatography (5 : 1 = hexanes : ethyl acetate) to provide 6.0 g of clear liquid product in 91% yield. ¹H NMR (400 MHz, CDCl₃): δ 7.34 (d, *J* = 8.98 Hz, 2 H), 6.74 (d, *J* = 8.98 Hz, 2 H), 0.98 (s, 9 H), 0.20 (s, 6 H). Spectral data are consistent with published values.⁴²

Synthesis of Compound 3a. 3.4 mL of *n*-BuLi in hexane (2.5 M) was added to a solution of compound **2** (2.0 g, 7.0 mmol) in 10.0 mL of anhydrous THF at -78 °C. The solution was stirred for 30 min at -78 °C. Benzophenone (1.5 g, 8.2 mmol) dissolved in 10.0 mL of anhydrous THF was added dropwise to the above solution. The combined mixture was further stirred for 5 h at -78 °C, and then warmed back to room temperature by itself and stirred for overnight. The reaction was then quenched with 30.0 mL of distilled water, extracted with ethyl acetate (3 x 30.0 mL), and the combined organic phase was washed with distilled water (1 x 30.0 mL) and brine (1 x 30.0 mL). Finally, it was dried over anhydrous MgSO₄. The solvent was then removed under reduced pressure to provide 2.4 g of a viscous oil in 89% yield, and the product was used without further purification. ¹H NMR (400 MHz, CDCl₃): δ 7.20-7.34 (m, 10 H), 7.10 (d, *J* = 7.81 Hz, 2 H), 6.75 (d, *J* = 7.81 Hz, 2 H), 0.97 (s, 9 H), 0.18 (s, 6 H).

Synthesis of Compound 4a. 9.0 mL of tetrabutylammonium fluoride solution in THF (1.0 M) was added to compound **3a** (2.0 g, 5.1 mmol) in 20.0 mL THF. The mixture was stirred for 2 h at room temperature, then 20.0 mL distilled water was added to the reaction. The mixture was then extracted with ethyl acetate (3 x 30.0 mL), and the combined organic phase was washed with distilled water (1 x 30.0 mL) and brine (1 x 30.0 mL), then dried

over anhydrous MgSO_4 . The solvent was removed under reduced pressure to provide the crude product, which was further purified by flash chromatography (3:1= hexanes : ethyl acetate) to provide 1.1 g of yellow powder in 78% yield. ^1H NMR (400 MHz, CD_3CN): δ 7.20-7.34 (m, 10 H), 7.05 (d, $J = 8.59$ Hz, 2 H), 6.89 (s, 1 H), 6.75 (d, $J = 8.59$ Hz, 2 H), 4.15 (s, 1 H). ^{13}C NMR (100 MHz, CD_3CN): δ 157.2, 149.2, 140.3, 130.6, 129.1, 128.2, 115.7, 82.4. HRMS (EI) calc'd. for $[\text{M}]^+$ ($\text{C}_{19}\text{H}_{16}\text{O}_2$): 276.1150; Found: 276.1152.

Synthesis of Compound 5a. Propargyl bromide solution (0.5 mL, 4.0 mmol) in toluene (80 wt.%) and potassium carbonate (0.6 g, 4.0 mmol) was sequentially added to compound **4a** (1.0 g, 3.6 mmol) in 15.0 mL of acetone. The mixture was stirred for 16 h at 60 °C, then the solvent was removed under reduced pressure. 30.0 mL of distilled water was added to the mixture, which was then extracted with ethyl acetate (3 x 30.0 mL). The combined organic phase was washed with distilled water (1 x 30.0 mL) and brine (1 x 30.0 mL), then dried over anhydrous MgSO_4 . The solvent was removed under reduced pressure to provide the crude product, which was further purified by flash chromatography (2:1= hexanes : ethyl acetate) to provide 0.9 g of a viscous yellow oil in 82% yield. ^1H NMR (400 MHz, CDCl_3): δ 7.20-7.34 (m, 10 H), 7.17 (d, $J = 8.20$ Hz, 2 H), 6.89 (d, $J = 8.20$ Hz, 2 H), 4.66 (d, $J = 2.34$ Hz, 2 H), 2.50 (t, $J = 2.34$ Hz, 1 H). ^{13}C NMR (100 MHz, CDCl_3): δ 156.3, 146.6, 128.9, 127.5, 126.8, 113.8, 81.3, 78.2, 75.2, 55.4. HRMS (EI) calc'd. for $[\text{M}]^+$ ($\text{C}_{22}\text{H}_{18}\text{O}_2$): 314.1307; Found: 314.1301.

Synthesis of Compound 6a. Acetyl chloride (0.4 mL, 6.4 mmol) was added to compound **5a** (0.4 g, 1.3 mmol) in 10.0 mL toluene. The mixture was stirred and refluxed for 5 h, then the solvent was removed under reduced pressure to provide 0.4 g of a viscous pale yellow oil in 98% yield. ^1H NMR (400 MHz, CDCl_3): δ 7.23-7.33 (m, 10 H), 7.16 (d, $J = 8.98$ Hz, 2 H), 6.89 (d, $J = 8.98$ Hz, 2 H), 4.69 (d, $J = 2.34$ Hz, 2 H), 2.52 (t, $J = 2.34$ Hz, 1 H). ^{13}C NMR (100 MHz, CDCl_3): δ 156.9, 145.4, 138.4, 130.9, 129.6, 129.0, 127.7, 113.8, 81.3, 78.4, 75.7, 55.8. HRMS (EI) calc'd. for $[\text{M}]^+$ ($\text{C}_{22}\text{H}_{17}\text{ClO}$): 332.0968; Found: 332.0968.

Synthesis of Compound 3b. Compound **3b** was synthesized by the same procedure as compound **3a**, except that 4-methoxybenzophenone was used. The product was a colorless, viscous oil, obtained in 85% yield. ^1H NMR (400 MHz, CDCl_3): δ 7.20-7.34 (m, 5 H), 7.17

(d, $J = 8.59$ Hz, 2 H), 7.10 (d, $J = 8.59$ Hz, 2 H), 6.83 (d, $J = 8.59$ Hz, 2 H), 6.77 (d, $J = 8.59$ Hz, 2 H), 3.80 (s, 3 H) 0.97 (s, 9 H), 0.19 (s, 6 H).

Synthesis of Compound 4b. Compound **4b** was synthesized by the same procedure as compound **4a**. The product was an orange solid obtained in 87% yield. ^1H NMR (400 MHz, CD_3CN): δ 7.20-7.34 (m, 5 H), 7.13 (d, $J = 8.76$ Hz, 2 H), 7.04 (d, $J = 8.76$ Hz, 2 H), 6.87 (s, 1 H), 6.85 (d, $J = 8.76$ Hz, 2 H), 6.74 (d, $J = 8.76$ Hz, 2 H), 3.76 (s, 3 H). ^{13}C NMR (100 MHz, CDCl_3): δ 158.5, 155.2, 147.3, 139.1, 129.3, 127.8, 127.0, 113.8, 113.1, 81.5, 55.2. HRMS (EI) calc'd. for $[\text{M}]^+$ ($\text{C}_{20}\text{H}_{18}\text{O}_3$): 306.1256; Found: 306.1257.

Synthesis of Compound 5b. Compound **5b** was synthesized by the same procedure as compound **5a**. The product was a viscous orange oil, obtained in 96% yield. ^1H NMR (400 MHz, CDCl_3): δ 7.22-7.34 (m, 5 H), 7.20 (d, $J = 8.98$ Hz, 2 H), 7.17 (d, $J = 8.98$ Hz, 2 H), 6.91 (d, $J = 8.98$ Hz, 2 H), 6.83 (d, $J = 8.98$ Hz, 2 H), 4.67 (d, $J = 2.34$ Hz, 2 H), 3.79 (s, 3H), 2.51 (t, $J = 2.34$ Hz, 1 H). ^{13}C NMR (100 MHz, CDCl_3): δ 158.8, 156.8, 147.5, 140.6, 139.6, 129.4, 128.0, 127.3, 114.3, 113.4, 81.6, 78.8, 75.8, 56.0, 55.4. HRMS (EI) calc'd. for $[\text{M}]^+$ ($\text{C}_{23}\text{H}_{20}\text{O}_3$): 344.1412; Found: 344.1411.

Synthesis of Compound 6b. Compound **6b** was synthesized by the same procedure as compound **6a**. The product was a viscous orange oil, obtained in 98% yield. ^1H NMR (600 MHz, C_6D_6): δ 7.44 (d, $J = 8.76$ Hz, 2 H), 7.30 (d, $J = 8.76$ Hz, 2 H), 7.00-7.09 (m, 5 H), 6.72 (d, $J = 8.76$ Hz, 2 H), 6.63 (d, $J = 8.76$ Hz, 2 H), 4.13 (d, $J = 2.34$ Hz, 2 H), 3.25 (s, 3H), 1.95 (t, $J = 2.34$ Hz, 1 H). ^{13}C NMR (100 MHz, C_6D_6): δ 159.7, 157.6, 146.5, 139.3, 138.2, 131.6, 130.3, 114.3, 113.5, 82.3, 78.9, 75.9, 55.7, 54.9. HRMS (EI) calc'd. for $[\text{M}]^+$ ($\text{C}_{23}\text{H}_{19}\text{ClO}_2$): 362.1074; Found: 362.1068.

Synthesis of PEtG-AT and representative procedure for the synthesis of end-capped PEtG. Ethyl glyoxylate in toluene solution (20.0 mL) was distilled under vacuum (25 °C, 0.3 mbar) over P_2O_5 to remove toluene and trace water in the first, discarded fraction. The residue was then distilled twice successively over P_2O_5 at atmospheric pressure under argon at 130 °C to obtain the highly pure monomer. Freshly distilled CH_2Cl_2 (5.0 mL) and Et_3N (4.0 μL , 25.0 μmol , 0.0005 equiv.) were added to freshly distilled ethyl glyoxylate (5.0

mL, 50.0 mmol, 1.0 equiv.) under an Ar atmosphere in a flame-dried flask equipped with a magnetic stir bar. The solution was stirred for 1 h at -20 °C. Compound **6a** (0.2 g, 63.0 μ mol, 0.013 equiv.) and Et₃N (0.3 mL, 1.9 mmol, 0.038 equiv.) were added at -20 °C to end-cap the polymer. The solution was gradually warmed to room temperature over a period of 4 h, and then stirred for 16 h. Purification was achieved by precipitation of the crude reaction mixture into methanol containing 2 vol% Et₃N. After decanting the excess methanol, the residue was dried *in vacuo* to provide 3.2 g of a white, sticky polymer in 64% yield. ¹H NMR (600 MHz, CDCl₃): δ 7.20-7.47 (m, 19 H), 6.90 (s, 4 H), 5.45-5.79 (m, 272 H), 4.68 (s, 4 H), 4.04-4.47 (m, 620 H), 1.12-1.51 (m, 968H). FTIR: 2985, 2939, 2909, 1751, 1467, 1447, 1375, 1297, 1216, 1138, 1094, 1017, 964, 856, 735, 702 cm⁻¹. SEC: M_n = 19 kg/mol, M_w = 30 kg/mol, *D* = 1.6.

Synthesis of PEtG-AMT. The polymer was synthesized by the same procedure described for **PEtG-AT** except that compound **6b** was used as the end-cap. The yield was 70%. ¹H NMR (400 MHz, CDCl₃): δ 7.15-7.49 (m, 19 H), 6.89 (s, 4 H), 6.81 (s, 4 H), 5.47-5.76 (m, 341 H), 4.67 (s, 4 H), 4.14-4.29 (m, 700 H), 1.24-1.40 (m, 1093 H). FTIR: 2985, 2949, 2908, 1748, 1468, 1447, 1374, 1298, 1214, 1138, 1093, 1015, 962, 856, 735, 701, 667 cm⁻¹. SEC: M_n = 34 kg/mol, M_w = 81 kg/mol, *D* = 2.4.

Mass loss study. PEtG was dissolved in CH₂Cl₂ at a concentration of 90.0 mg/mL. The solution was drop cast onto pre-weighed glass slides. The solvent was evaporated by placing the coatings in a fumehood for 3 h. This provided coatings with masses of ~30.0 mg and surface areas of ~2.0 cm². The coatings were each accurately weighed, then then placed at different temperatures (fridge, oven, or ambient). At defined time points, the coatings were weighed to determine the percentage of the initial mass remaining. The experiment was performed in triplicate for each polymer and temperature.

Variable temperature ¹H NMR depolymerization study. PEtG-AMT was dissolved in DMSO-*d*₆ at a concentration of 10.0 mg/mL, then the solution was transferred into a quartz NMR tube and sealed with Teflon tape. After the first ¹H NMR spectrum was taken at 25 °C, the temperature of spectrometer was increased at intervals of 25 °C until it reached 125 °C. Each increment took ~15 min. The ¹H NMR spectra were recorded at each interval to

monitor polymer depolymerization. The same experimental procedure was also conducted on **PEtG-control**.

Color change study of trityl end-capped PEtG (and control) coatings containing Nile red. To prepare PEtG coatings with 0.1 wt.% Nile red, 0.1 mL of a 100.0 mg/mL polymer solution in CH₂Cl₂ was mixed with 10.0 μL of a 1.0 mg/mL Nile red solution in CH₂Cl₂. The solution was then drop cast on glass slide over a ~ 1.0 cm² surface area. After all the solvent was evaporated by placing the coating in a fumehood for 3 h, a digital picture of each coating was obtained. Then, the coatings were incubated in at 22 °C and new pictures were obtained at defined time points. The rectangular color patches are generated from the eyedropper function in Windows PowerPoint by sub-sampling from digital pixels of pictures to display color changes of the coating.

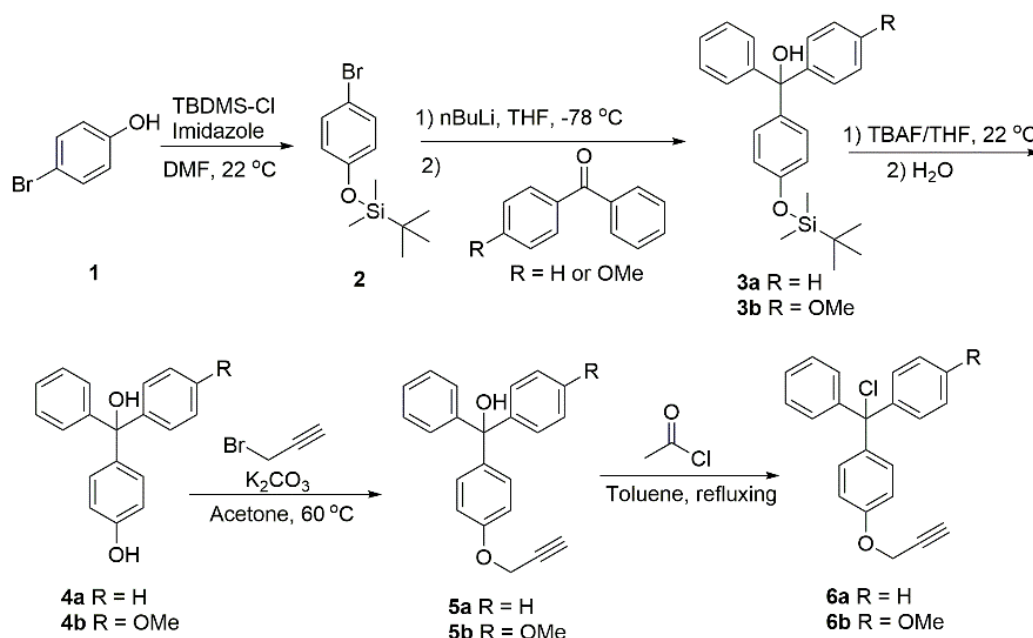
Color change study of trityl end-capped PEtG (and control) coatings containing IR-780. This experiment was performed by the same procedure as for Nile red except that a loading of 0.5 wt% was needed to obtain an obvious color change.

UV-Vis absorption measurement of PEtG coating. To prepare a **PEtG-AMT** coating containing 0.1 wt% Nile red, 0.2 mL of a 50.0 mg/mL polymer solution in toluene was mixed with 10.0 μL of 1.0 mg/mL Nile red in CH₂Cl₂. The solution was then drop cast on a glass slide over a ~ 9.0 cm² surface area. After all the solvent was evaporated by placing the coating in fumehood for 4 h, the initial absorption of the coating was measured in a UV-Vis spectrometer. Then, the coating was put in a 37 °C oven to incubate for 24 h, and then another absorption was measured. The same experiment was also conducted on **PEtG-control**.

8.3 Results and discussion.

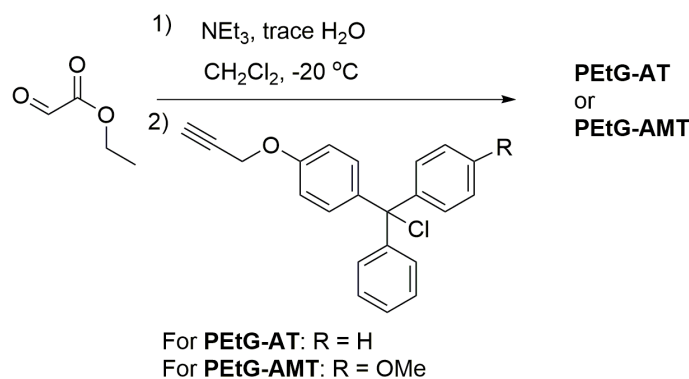
In addition to the previously reported MMT and DMT end-capped PEtG, we also synthesized and studied trityl end-caps containing a propargyl ether with zero or one methoxy groups (Scheme 8.1) and used these to prepare the corresponding trityl end-capped polymers **PEtG-AT** and **PEtG-AMT** (Figure 8.1). These polymers had initially been designed to provide an alkyne coupling site for the preparation of amphiphilic block

copolymers, but were included in the current study because of the subtle electronic effects that are introduced by the alkyne group. To synthesize these two new end-caps, the phenol group of 4-bromophenol **1** was first protected by reaction with *tert*-butyldimethylsilyl chloride (TBDMS-Cl) to afford the TBDMS-protected compound **2**. Next, reaction of compound **2** with *n*-BuLi followed by either benzophenone or 4-methoxybenzophenone provided compounds **3a** and **3b**, respectively. Subsequently, the TBDMS protecting group was removed by treatment with *tetra-n*-butylammonium fluoride (TBAF) to afford compounds **4a/b**. Alkylation with propargyl bromide provided compounds **5a/b**. Finally, reaction with acetyl chloride provided the target end-caps **6a** and **6b**.



Scheme 8.1 Synthesis of new trityl chloride based end-caps with alkynes and zero or one methoxy groups.

Polymerization and end-capping were performed at $-20\text{ }^{\circ}\text{C}$ in the presence of triethylamine and initiation by trace hydrate of the monomer as previously reported (Scheme 8.2).¹¹ Molar masses of the polymers ranged from 19 kg/mol to 34 kg/mol. **PEtG-control** (Figure 8.2)³³ was also used in the current study.



Scheme 8.2 Synthesis of PEtG-AT and PEtG-AMT.

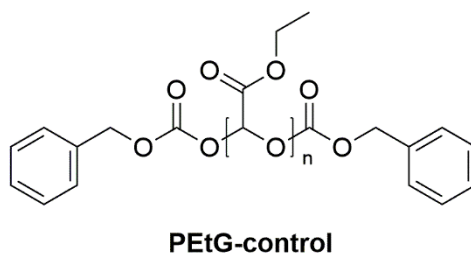


Figure 8.2 Chemical structure of PEtG-control.

To measure the solid-state depolymerization of the trityl end-capped PEtGs, the polymers were dissolved in CH_2Cl_2 and then drop-cast onto glass slides to form coatings. The coatings were then stored at different temperatures and their mass loss was measured. At $6\text{ }^\circ\text{C}$, all the polymer coatings were relatively stable for ~ 30 days (Figure 8.3). However, **PEtG-DMT** and **PEtG-AMT** began to depolymerize after 30 days. At $10\text{ }^\circ\text{C}$, **PEtG-DMT** began depolymerizing almost immediately and **PEtG-AMT** after ~ 5 days. This suggests that the DMT end-cap may be slightly less stable compared with the AMT end-cap. It is possible that the propargyl ether of the AMT is less electron-donating than the methoxy due to the modest electronegativity of the alkyne. **PEtG-MMT** and **PEtG-AT** were stable at $10\text{ }^\circ\text{C}$ for the first ~ 15 days and then began to depolymerize. At $22\text{ }^\circ\text{C}$, **PEtG-DMT** and **PEtG-AMT** lost $\sim 50\%$ of their mass over 5 days, while **PEtG-MMT** and **PEtG-AT** lost 50% of their mass over 15-20 days. Finally, at $30\text{ }^\circ\text{C}$ **PEtG-DMT** and **PEtG-AMT** rapidly

depolymerized, losing more than 50% of their mass over the first day and **PEtG-MMT** and **PEtG-AT** lost 50% of their mass over 3-5 days. We did not perform quantitative mass loss studies with a simple trityl end-capped having no electron-donating groups, but have not observed any depolymerization of this polymer over 20 days at room temperature in our lab. **PEtG-control** was also studied and did not undergo any significant mass loss at any of the studied temperatures over 35 days.

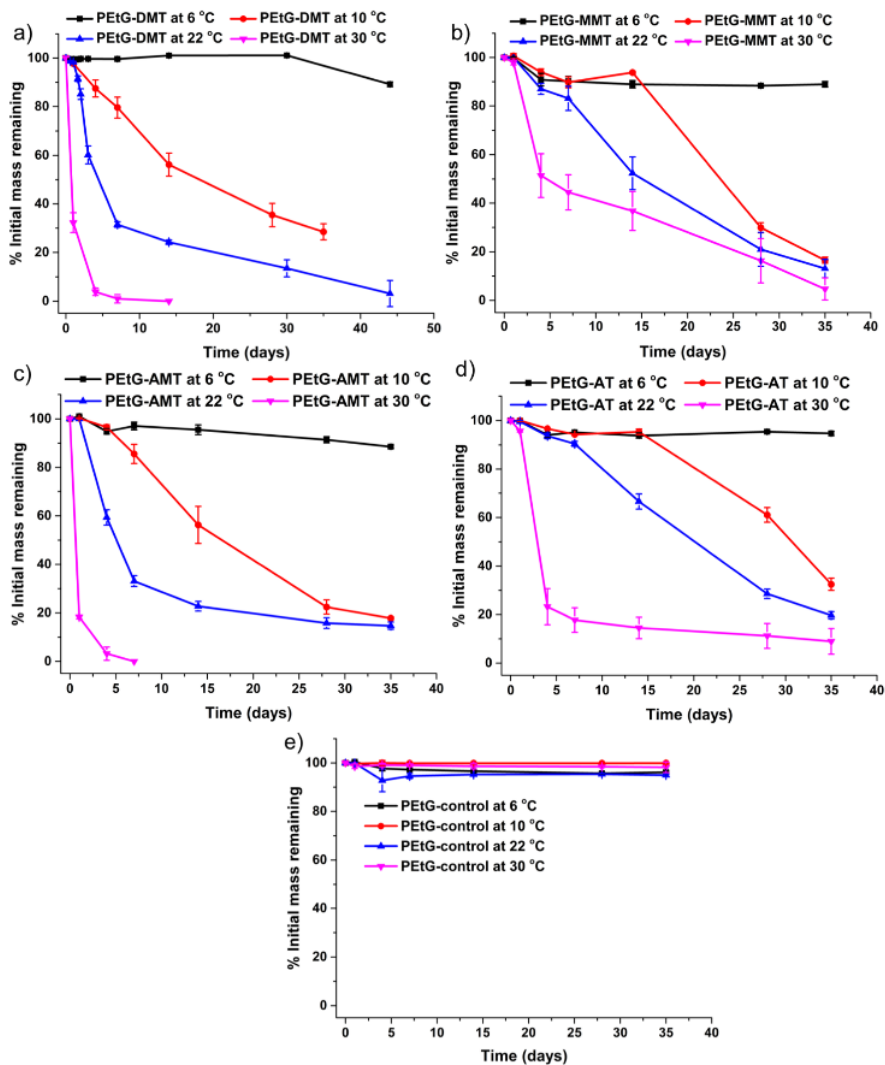


Figure 8.3 Mass loss profiles for end-capped PEtGs at different temperatures: a) PEtG-DMT; b) PEtG-MMT; c) PEtG-AMT; d) PEtG-AT; d) PEtG-control. In each experiment, the error bars represent the standard deviation of the measurements for three samples.

To further demonstrate the effect of temperature and confirm the depolymerization, **PEtG-AMT** and **PEtG-control** were dissolved in DMSO- d_6 and sealed in NMR tubes, then variable temperature ^1H NMR spectroscopy was performed. After the first spectrum was taken at 25 °C, the temperature was increased at intervals of 25 °C up to 125 °C. Each increment took ~15 min and ^1H NMR spectra were acquired at each temperature. Over the time period of the study, **PEtG-AMT** was relatively stable below 100 °C, as indicated by broad peaks corresponding to PEtG backbone and pendant esters (Figure 8.4a). However, when the temperature reached 100 °C, a singlet at 9.1 ppm emerged, indicating depolymerization to ethyl glyoxylate. With a further increase to 125 °C, the singlet at 9.1 ppm increased dramatically in intensity and the broad peak at 5.4 ppm corresponding to the PEtG backbone methine proton decreased in intensity. After 1 h at 125 °C, the peak at 5.4 ppm had almost completely disappeared, indicating complete depolymerization of **PEtG-AMT**. For **PEtG-control** carried through the same experimental conditions, only a small degree of depolymerization was observed (Figure 8.4b). This result demonstrates that the depolymerization of **PEtG-AMT** was induced by end-cap removal at elevated temperature.

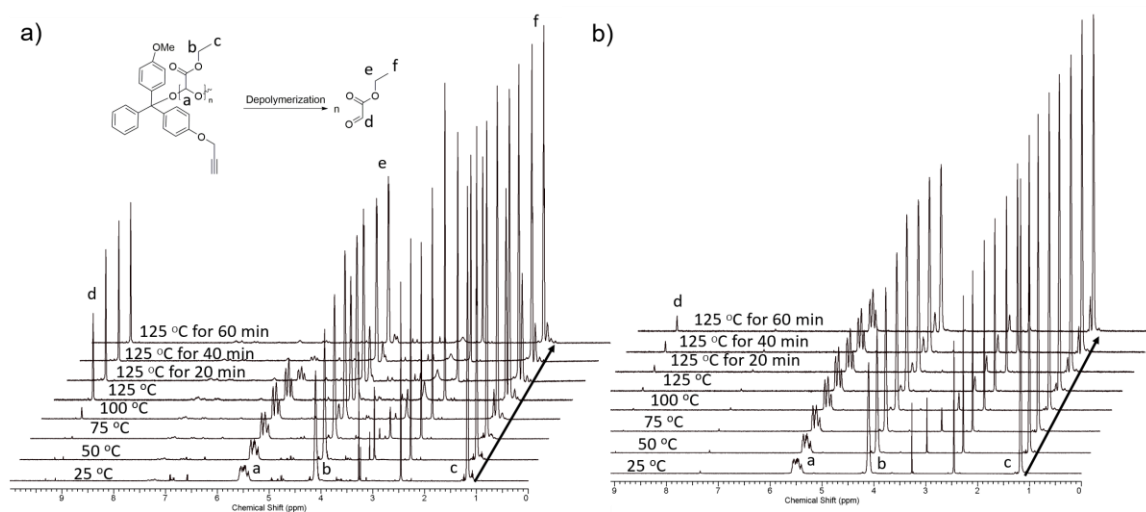


Figure 8.4 Variable temperature ^1H NMR spectra of a) **PEtG-AMT** and b) **PEtG-control** at different temperatures (15 min per temperature increment unless otherwise indicated). Spectra are offset to allow the progression over time to be clearly observed.

Overall, these studies showed that trityl end-capped PEtG underwent depolymerization in a temperature-dependent manner and that the rate of this depolymerization could be tuned based on the electronics of the specific trityl groups. In addition, this behavior was specific to the trityl end-caps compared to carbonate end-caps. We attribute it to an equilibrium existing between the capped and uncapped forms of the PEtG (Figure 8.5). The position of this equilibrium depends on the stability of the trityl cation, with electron-donating groups favoring the uncapped polymer. In the uncapped state, PEtG can depolymerize, releasing the volatile monomer ethyl glyoxylate (boiling point ~ 110 °C) and continually shifting the equilibria to the right, particularly for solid state samples. At higher temperatures, this depolymerization and monomer evaporation occurs more rapidly, and is also more highly favored thermodynamically due to the entropic contributions of depolymerization and evaporation. In contrast, in conventional small molecule chemistry involving trityl groups, the product is often not volatile and there are no onwards reactions driving the equilibrium to the right. Thus, the combination of factors leading to the observed thermal instability with the current system are quite unique and consequential.

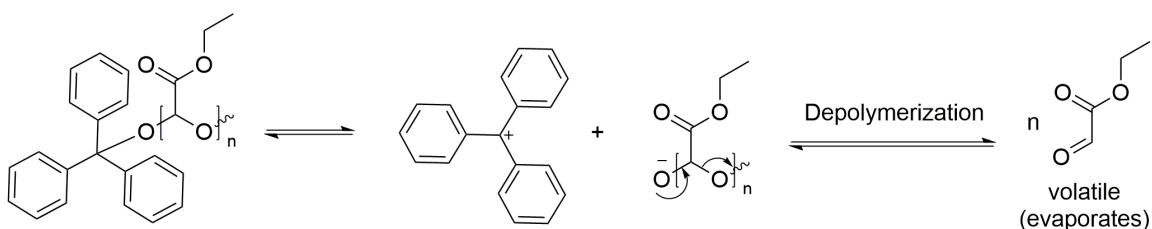


Figure 8.5 Mechanism for temperature dependent depolymerization of trityl-capped PEtG.

Based on the mass loss profiles, we envisioned that the temperature-dependent behavior of the trityl end-capped PEtGs could be harnessed for applications where the thermal history of the material is important. For example, storage temperatures are critical in the transport of food and other perishable materials. Thus far, there are two main classes of food quality sensors. One type can directly measure the quality of the food product inside the packaging by detecting the chemicals associated with food spoilage, such as amines, ethanol and hydrogen sulfide. This can be done by interaction of chemicals with pH sensitive dye,

proteins and enzymes, such as bromocresol green with volatile basic amine,³⁸ hydrogen sulfide with myoglobin,³⁹ and monoamine oxidase with biogenic amines.⁴⁰ Another type provides information on the conditions of the package exterior by integrating the temperature and time associated with food storage, and is more commonly used for fresh meat. This type of sensor is usually based on the polymerization or diffusion rate, chemical or enzymatic reactions.⁴¹ As the depolymerization of trityl end-capped PEtG is directly associated with storage temperature and time, this material has the potential to serve as a simple, low-cost component in smart packaging for food and other sensitive products. It will also serve as the first example of time and temperature sensor that based on the mechanism of depolymerization rate to open new possibility for the design of food quality sensor.

To use the depolymerization reaction of PEtG for smart packaging, it is critical to translate the depolymerization into a clear visual signal. To achieve this, we investigated the incorporation of hydrophobic dyes, whose optical properties can change, depending on their environments. First, Nile red was investigated as it can exhibit variable color from deep red to strong yellow-gold, depending on its environment. It was well mixed with the trityl end-capped PEtGs through co-dissolution in CH₂Cl₂, then solvent evaporation to form a deep pink coating containing 0.1 wt% of the dye (Figure 8.6a). After 24 h at 22 °C, the **PEtG-DMT** and **PEtG-AMT** coatings had changed from deep pink into deep purple with a noticeable loss of polymer. To clearly display this color change, squares corresponding to computer generated color samples that were sub-sampled from digital pixels of the pictures of PEtG coatings are included in Figure 8.6a. For **PEtG-MMT**, the color change occurred over ~4 days, and for **PEtG-AT** over ~6 days. In contrast, **PEtG-control** coatings didn't show any significant color change during their incubation at 22 °C for 6 days. To examine this change spectroscopically, thinner films of both **PEtG-AMT** and **PEtG-control** were prepared, then the absorptions of the films before and after incubation were measured. Before incubation, both films had Nile red absorptions centered at 544 nm with a bandwidth of ~85 nm (width at half-peak height) (Figure 8.6c-d). However, after incubation for 24 h, the baseline of the **PEtG-AMT** sample significantly increased, presumably due to scattering arising from Nile red aggregation after the

disappearance of the polymer. In addition, the bandwidth increased to ~ 115 nm (after subtraction of the base-line). This presumably results in the color change. **PEtG-control** didn't exhibit any significant change in the absorption profile.

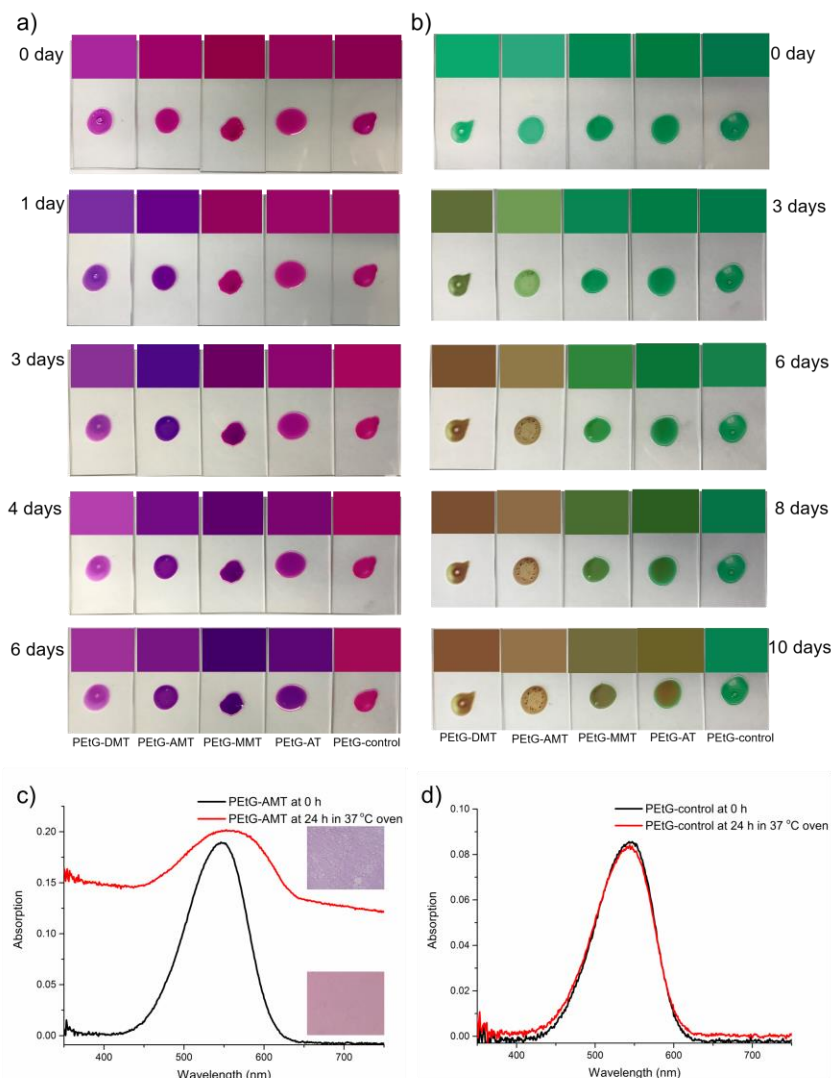


Figure 8.6 a) and b) Color changes of different PEtG coatings containing either a) 0.1 wt% Nile red or b) 0.5 wt% IR-780 incubated at 22 °C for different time periods. The rectangular color patches are computer generated color samples that were sub-sampled from digital pixels to display color changes of the coating. c) and d) UV-Vis spectra of c) PEtG-AMT and d) PEtG-control thin films containing 0.1 wt% Nile red before and after incubation at 37 °C for 24 h, the inserted pictures in c) are polymer coatings before and after incubation.

While incorporated Nile red underwent a color change upon depolymerization, it was subtle in some cases. Thus, the incorporation of another hydrophobic dye, IR-780, was also explored. This dye appeared as green when well dispersed in the hydrophobic polymer environment (Figure 8.6b). However, upon incubation at 22 °C, the coatings turned brown over 3-10 days, corresponding to dye aggregation. The time over which the color changed was again dependent on the specific trityl end-cap but overall it took longer than the Nile red color change as we observed that it occurred when some degree of the polymer had depolymerized and the monomer evaporated. Thus, the time for the response signal depends to some extent on the specific dye.

8.4 Conclusions.

In conclusion, we have demonstrated that PEtG with trityl end-caps having electron-donating groups undergo solid state depolymerization in a temperature-dependent manner. This process is driven by the evaporation of monomer under ambient conditions. The rate of depolymerization could be tuned based on the structures of the trityl groups. By mixing the polymer with trace amounts of hydrophobic dye, we showed proof-of-the-principle that these molecules can serve as smart coatings that can indicate the thermal history of materials. Using color matching, it is anticipated that such coatings could be read and analyzed directly by visual color changes or using an application on a hand-held device such as a cell phone. This would enable their use as simple smart packaging labels. This is the first concept to utilize the depolymerization rate of polymer as food storage history sensor, also the first application of this type for an SIP and capitalizes on the unique ability of PEtG to depolymerize to volatile products.

8.5 References.

- (1) Stuart, M. A. C.; Huck, W. T.; Genzer, J.; Müller, M.; Ober, C.; Stamm, M.; Sukhorukov, G. B.; Szleifer, I.; Tsukruk, V. V.; Urban, M. Emerging applications of stimuli-responsive polymer materials. *Nat. Mater.* **2010**, *9*, 101-113.
- (2) Holtz, J. H.; Asher, S. A. Polymerized colloidal crystal hydrogel films as intelligent chemical sensing materials. *Nature* **1997**, *389*, 829-832.
- (3) Nath, N.; Chilkoti, A. Creating “smart” surfaces using stimuli responsive polymers. *Adv. Mater.* **2002**, *14*, 1243-1247.
- (4) Mura, S.; Nicolas, J.; Couvreur, P. Stimuli-responsive nanocarriers for drug delivery. *Nat. Mater.* **2013**, *12*, 991-1003.
- (5) Cabane, E.; Zhang, X.; Langowska, K.; Palivan, C. G.; Meier, W. Stimuli-responsive polymers and their applications in nanomedicine. *Biointerphases* **2012**, *7*:9.
- (6) Meng, H.; Li, G. A review of stimuli-responsive shape memory polymer composites. *Polymer* **2013**, *54*, 2199-2221.
- (7) Habault, D.; Zhang, H.; Zhao, Y. Light-triggered self-healing and shape-memory polymers. *Chem. Soc. Rev.* **2013**, *42*, 7244-7256.
- (8) Fan, B.; Gillies, E. R. Self-Immolative Polymers. *Encycl. Polym. Sci. Technol.* **2015**, 1-35.
- (9) Roth, M. E.; Green, O.; Gnaim, S.; Shabat, D. Dendritic, oligomeric, and polymeric self-immolative molecular amplification. *Chem. Rev.* **2015**, *116*, 1309-1352.
- (10) Phillips, S. T.; DiLauro, A. M. Continuous head-to-tail depolymerization: an emerging concept for imparting amplified responses to stimuli-responsive materials. *ACS Macro Lett.* **2014**, *3*, 298-304.
- (11) Fan, B.; Trant, J. F.; Wong, A. D.; Gillies, E. R. Polyglyoxylates: a versatile class of triggerable self-immolative polymers from readily accessible monomers. *J. Am. Chem. Soc.* **2014**, *136*, 10116-10123.
- (12) Liu, G.; Wang, X.; Hu, J.; Zhang, G.; Liu, S. Self-immolative polymersomes for high-efficiency triggered release and programmed enzymatic reactions. *J. Am. Chem. Soc.* **2014**, *136*, 7492-7497.

- (13) de Gracia Lux, C.; McFearin, C. L.; Joshi-Barr, S.; Sankaranarayanan, J.; Fomina, N.; Almutairi, A. Single UV or Near IR triggering event leads to polymer degradation into small molecules. *ACS Macro Lett.* **2012**, *1*, 922-926.
- (14) Liu, G.; Zhang, G.; Hu, J.; Wang, X.; Zhu, M.; Liu, S. Hyperbranched self-immolative polymers (h-SIPs) for programmed payload delivery and ultrasensitive detection. *J. Am. Chem. Soc.* **2015**, *137*, 11645-11655.
- (15) Fan, B.; Trant, J. F.; Hemery, G.; Sandre, O.; Gillies, E. R. Thermo-responsive self-immolative nanoassemblies: direct and indirect triggering. *Chem. Commun.* **2017**, *53*, 12068-12071.
- (16) Peterson, G. I.; Church, D. C.; Yakelis, N. A.; Boydston, A. J. 1, 2-oxazine linker as a thermal trigger for self-immolative polymers. *Polymer* **2014**, *55*, 5980-5985.
- (17) Fan, B.; Trant, J. F.; Gillies, E. R. End-capping strategies for triggering end-to-end depolymerization of polyglyoxylates. *Macromolecules* **2016**, *49*, 9309-9319.
- (18) Esser-Kahn, A. P.; Sottos, N. R.; White, S. R.; Moore, J. S. Programmable microcapsules from self-immolative polymers. *J. Am. Chem. Soc.* **2010**, *132*, 10266-10268.
- (19) Lewis, G. G.; Robbins, J. S.; Phillips, S. T. A prototype point-of-use assay for measuring heavy metal contamination in water using time as a quantitative readout. *Chem. Commun.* **2014**, *50*, 5352-5354.
- (20) DeWit, M. A.; Beaton, A.; Gillies, E. R. A reduction sensitive cascade biodegradable linear polymer. *J. Polym. Sci., Part A: Polym. Chem.* **2010**, *48*, 3977-3985.
- (21) Chen, E. K.; McBride, R. A.; Gillies, E. R. Self-immolative polymers containing rapidly cyclizing spacers: toward rapid depolymerization rates. *Macromolecules* **2012**, *45*, 7364-7374.
- (22) Wong, A. D.; GÜngör, T. M.; Gillies, E. R. Multiresponsive azobenzene end-cap for self-immolative polymers. *ACS Macro Lett.* **2014**, *3*, 1191-1195.
- (23) Han, D.; Yu, X.; Chai, Q.; Ayres, N.; Steckl, A. J. Stimuli-responsive self-immolative polymer nanofiber membranes formed by coaxial electrospinning. *ACS Appl. Mater. Interfaces* **2017**, *9*, 11858-11865.
- (24) Sagi, A.; Weinstain, R.; Karton, N.; Shabat, D. Self-immolative polymers. *J. Am. Chem. Soc.* **2008**, *130*, 5434-5435.

- (25) Gnaim, S.; Shabat, D. Self-immolative chemiluminescence polymers: innate assimilation of chemiexcitation in a domino-like depolymerization. *J. Am. Chem. Soc.* **2017**, *139*, 10002-10008.
- (26) Gisbert-Garzaran, M.; Lozano, D.; Vallet-Regí, M.; Manzano, M. Self-immolative polymers as novel pH-responsive gate keepers for drug delivery. *RSC Adv.* **2017**, *7*, 132-136.
- (27) Yeung, K.; Kim, H.; Mohapatra, H.; Phillips, S. T. Surface-accessible detection units in self-immolative polymers enable translation of selective molecular detection events into amplified responses in macroscopic, solid-state plastics. *J. Am. Chem. Soc.* **2015**, *137*, 5324-5327.
- (28) Kim, H.; Mohapatra, H.; Phillips, S. T. Rapid, On-command debonding of stimuli-responsive cross-linked adhesives by continuous, sequential quinone methide elimination reactions. *Angew. Chem., Int. Ed.* **2015**, *54*, 13063-13067.
- (29) Ergene, C.; Palermo, E. F. Cationic Poly(benzyl ether)s as self-immolative antimicrobial polymers. *Biomacromolecules* **2017**, *18*, 3400-3409.
- (30) Schwartz, J. M.; Phillips, O.; Engler, A.; Sutlief, A.; Lee, J.; Kohl, P. A. Stable, high-molecular-weight poly(phthalaldehyde). *J. Polym. Sci., Part A: Polym. Chem.* **2017**, *55*, 1166-1172.
- (31) Kaitz, J. A.; Moore, J. S. Copolymerization of *o*-phthalaldehyde and ethyl glyoxylate: cyclic macromolecules with alternating sequence and tunable thermal properties. *Macromolecules* **2014**, *47*, 5509-5513.
- (32) Tang, S.; Yourdkhani, M.; Possanza Casey, C. M.; Sottos, N. R.; White, S. R.; Moore, J. S. Low ceiling temperature polymer microcapsules with hydrophobic payloads via rapid emulsion-solvent evaporation. *ACS Appl. Mater. Interfaces* **2017**, *9*, 20115-20123.
- (33) Fan, B.; Trant, J. F.; Yardley, R. E.; Pickering, A. J.; Lagugné-Labarthe, F. o.; Gillies, E. R. Photocontrolled degradation of stimuli-responsive poly(ethyl glyoxylate): differentiating features and traceless ambient depolymerization. *Macromolecules* **2016**, *49*, 7196-7203.

- (34) DiLauro, A. M.; Lewis, G. G.; Phillips, S. T. Self-immolative poly(4,5-dichlorophthalaldehyde) and its applications in multi-stimuli-responsive macroscopic plastics. *Angew. Chem., Int. Ed.* **2015**, *127*, 6298-6303.
- (35) Fan, B.; Gillies, E. R. Poly(ethyl glyoxylate)-poly(ethylene oxide) nanoparticles: stimuli-responsive drug release via end-to-end polyglyoxylate depolymerization. *Mol. Pharmaceutics* **2017**, *14*, 2548-2559
- (36) Belloncle, B.; Burel, F.; Oulyadi, H.; Bunel, C. Study of the *in vitro* degradation of poly(ethyl glyoxylate). *Polym. Degrad. Stabil.* **2008**, *93*, 1151-1157.
- (37) Belloncle, B.; Bunel, C.; Menu-Bouaouiche, L.; Lesouhaitier, O.; Burel, F. Study of the degradation of poly(ethyl glyoxylate): biodegradation, toxicity and ecotoxicity assays. *J. Polym. Environ.* **2012**, *20*, 726-731.
- (38) Pacquit, A.; Lau, K. T.; McLaughlin, H.; Frisby, J.; Quilty, B.; Diamond, D. Development of a volatile amine sensor for the monitoring of fish spoilage. *Talanta* **2006**, *69*, 515-520.
- (39) Smolander, M.; Hurme, E.; Latva-Kala, K.; Luoma, T.; Alakomi, H.-L.; Ahvenainen, R. Myoglobin-based indicators for the evaluation of freshness of unmarinated broiler cuts. *Innovative Food Sci. Emerging Technol.* **2002**, *3*, 279-288.
- (40) Lange, J.; Wittmann, C. Enzyme sensor array for the determination of biogenic amines in food samples. *Anal. Bioanal. Chem.* **2002**, *372*, 276-283.
- (41) Fuertes, G.; Soto, I.; Carrasco, R.; Vargas, M.; Sabattin, J.; Lagos, C. Intelligent packaging systems: sensors and nanosensors to monitor food quality and safety. *J. Sens.* **2016**, *2016*.
- (42) Kamino, B. A.; Castrucci, J.; Bender, T. P. Controlling the physical and electrochemical properties of arylamines through the use of simple silyl ethers: liquid, waxy and glassy arylamines. *Silicon* **2011**, *3*, 125.

Chapter 9

9 Conclusions and future perspectives

Overall, the work presented in this thesis serves to increase our understanding of and expand the utility of polyglyoxylate-based SIPs for various applications through the design, synthesis, and study of responsive end-caps and new polymer backbones.

Chapter 3 described a detailed study of the solid-state depolymerization of UV-sensitive PEtG under different conditions such as varying pH, temperature, and coating thickness. Several important fundamental differences between this class of polymers and conventional degradable polymers were revealed through this work. For example, polymer backbone cleavage and depolymerization exhibited different dependencies on pH, emphasizing the decoupling of these processes. Probing of the coating erosion mechanism illustrated an interesting combination of features from surface erosion and bulk degradation mechanisms that arise from the end-to-end depolymerization mechanism and further differentiate these polymers from conventional degradable polymers. It was also demonstrated that, unlike backbone cleavage, PEtG depolymerization did not exhibit a dependence on water and that PEtG could depolymerize back to the volatile monomer ethyl glyoxylate at ambient temperature and pressure. This unusual feature was utilized to perform facile polymer reprogramming/recycling via an irradiation-trapping-repolymerization sequence as well as polymer patterning by a simple irradiation-evaporation sequence. However, in order to apply this material for photo-lithography, nano-sized patterning should be demonstrated in the future to show its value over traditional materials. In addition, the physical properties of PEtG are not ideal for patterning as the polymer has a low T_g , and is therefore in its rubbery form at room temperature. Patterning of a higher T_g polyglyoxylate would afford patterns that can retain their form over longer time periods. This work also suggests the potential application of PGs as smart coatings.

Chapter 4 described work towards increasing the flexibility of the triggering stimuli initiating depolymerization by incorporating different end-caps capable of responding to

environmental cues other than UV light. For example, new end-caps that made polyglyoxylates respond to biologically relevant signals such as changes in the concentrations of oxidizing or reducing agents such as hydrogen peroxide and thiols respectively were introduced to PEtG. In addition, a novel multi-responsive end-cap that responded to very different stimuli including UV light, hydrogen peroxide, and reducing conditions simultaneously was developed. Furthermore, a cross-linker end-cap that allowed SIPs to form cross-linked networks while at the same time depolymerizing in response to external stimuli, such as UV light were developed. Finally, high molar mass PEtG was demonstrated to depolymerize by mechanical stimulation independent of the end-cap. It is anticipated that the versatility in end-capping strategies and potential depolymerization stimuli will not only expand PEtG's utility for different applications but will also be useful for other classes of end-to-end depolymerizable polymers.

Chapter 5 described the development of polyglyoxylate-based nano-assemblies via the design of new linker end-caps that allowed different stimuli-responsive PEtGs to form amphiphilic block copolymers. These amphiphilic block copolymers were self-assembled to form nanoparticles in aqueous solution. Based on the work in Chapter 4, the design and synthesis of H₂O₂-, reduction-, and dual-responsive (both UV light and H₂O₂) linker end-caps were described and applied. Cleavage of the linker end-caps was triggered by stimuli including a thiol reducing agent, UV light, H₂O₂, or combinations of these stimuli, resulting in nanoparticle disintegration. Low stimuli concentrations were effective in rapidly disrupting the nanoparticles showing that signal amplification could be achieved. Nile red, doxorubicin, and curcumin were encapsulated into the nanoparticles and were selectively released upon application of the appropriate stimuli. The ability to tune the stimuli-responsiveness simply by changing the linker end-cap makes this new platform highly attractive for applications in drug delivery.

Chapter 6 explored the incorporation of different monomers to increase the hydrophobicity of PG-based particles to improve the hydrophobic drug loading efficiency. Specifically, *n*-butyl glyoxylate, chloral and menthyl glyoxylate were homopolymerized or copolymerized with ethyl glyoxylate to obtain new polymers with higher hydrophobicity. These polymers

were incorporated into amphiphilic block copolymers with PEG using a UV light-responsive linker end-cap. The copolymers self-assembled to form nanoparticles in aqueous solution and the resulting nanoparticles were capable of significantly improved drug loading relative to PEG-PEtG-PEG. Initial *in vitro* studies revealed interesting differences between the toxicities of the different systems both before and after application of the stimulus.

Chapter 7 introduced the design and synthesis of a new generation of thermo-responsive end-caps based on a retro-Diels-Alder and subsequent furan elimination reaction, allowing SIPs to depolymerize in response to heat. Using block copolymers, thermo-responsive micelles and vesicles were prepared and shown to disassemble upon heating. It was also demonstrated that the thermal degradation of micelles could also be triggered indirectly by magnetic field hyperthermia after incorporation of iron oxide nanoparticles into the assemblies. It is anticipated that this end-cap can be used with other classes of SIPs and SRPs in general and that this system can serve as a platform for the development of heat-responsive materials.

Chapter 8 demonstrated that trityl end-capped PEtG could depolymerize and evaporate in a temperature-dependent manner at relatively low temperatures. Moreover, the responsiveness of PEtG was easily tuned by changing the substituents on the trityl group. Furthermore, by mixing the polymer with small amounts of hydrophobic dye, it was possible to translate this depolymerization into a visual signal. This suggests that these polymers have the potential to be used in smart packaging applications, where they can provide information on the combination of time and temperature during storage.

In summary, this thesis involved significant developments in the design and synthesis of new end-caps and monomers that endow PGs as self-immolative polymers to be responsive to a series of different stimuli, including light, reducing and oxidizing conditions, acids, heat, and multiple stimuli simultaneously or independently. The solid state polymer studies revealed the differentiating depolymerization properties of PG films and rare ambient traceless depolymerization. Moreover, this thesis developed proof-of-concept results

towards a number of applications for responsive PGs, including photo-patterning, smart coatings, drug delivery nanoparticles, and smart packaging sensor.

Future work should explore further development of these applications. Specifically, in Chapter 3, more work will be needed to investigate the potential of photo-responsive polyglyoxylates as micro- and nano-fabrication materials, and to optimize the aspect ratio of the obtained structures as well as their compatibility with other micro- and nano-fabrication steps. In addition, it would be ideal to increase the rate of pattern formation by increasing the pattern developing temperature or using a more volatile glyoxylate, such as methyl glyoxylate. For Chapter 4, further work can focus on kinetic depolymerization studies of each type of responsive polyglyoxoyate, and optimization of the synthesis of some of the end-caps and polymers to improve yields. Related to Chapter 5 and Chapter 6, future work will focus on the *in vitro* and *in vivo* studies of polyglyoxylate nanoparticles to testify their biocompatibilities and effectiveness as drug delivery vehicles. Cell viability assay should be performed on a range of cell lines both with and without stimuli. However, as the degradation products are metabolized in the liver, *in vivo* dose escalation toxicity studies will be needed to determine whether the polymers can potentially be applied for drug delivery. For Chapter 7, the future work should involve tuning of the structures of the end-caps to enable nanoassemblies to respond to heat stimuli both directly and indirectly at lower temperatures. This can be achieved by choosing dienophiles with extra electron-withdrawing groups, and dienes with increased bulkiness to prefer the forming of *endo* DA adduct. Lastly, Chapter 8 should increase the library of trityl end-caps to improve the range of temperature responsiveness for different types of temperature sensitive goods. Moreover, the tests with real foods or others should be conducted to promote the practical applications of this class of sensors.

Appendix 1: Permission to reuse copyrighted material in Chapter 1

2018/2/5

Rightslink® by Copyright Clearance Center



RightsLink®



Title: Polyglyoxylates: A Versatile Class of Triggerable Self-Immolative Polymers from Readily Accessible Monomers

Author: Bo Fan, John F. Trant, Andrew D. Wong, et al

Publication: Journal of the American Chemical Society

Publisher: American Chemical Society

Date: Jul 1, 2014

Copyright © 2014, American Chemical Society

Logged in as:
Bo Fan
Account #:
3000851023

[LOGOUT](#)

PERMISSION/LICENSE IS GRANTED FOR YOUR ORDER AT NO CHARGE

This type of permission/license, instead of the standard Terms & Conditions, is sent to you because no fee is being charged for your order. Please note the following:

- Permission is granted for your request in both print and electronic formats, and translations.
- If figures and/or tables were requested, they may be adapted or used in part.
- Please print this page for your records and send a copy of it to your publisher/graduate school.
- Appropriate credit for the requested material should be given as follows: "Reprinted (adapted) with permission from (COMPLETE REFERENCE CITATION). Copyright (YEAR) American Chemical Society." Insert appropriate information in place of the capitalized words.
- One-time permission is granted only for the use specified in your request. No additional uses are granted (such as derivative works or other editions). For any other uses, please submit a new request.

If credit is given to another source for the material you requested, permission must be obtained from that source.

Appendix 2: Permission to reuse copyrighted material in Chapter 2 and published chapters

2018/2/5

Rightslink® by Copyright Clearance Center



RightsLink®

[Home](#)
[Account Info](#)
[Help](#)


Title: Tunable Photocontrolled Motions Using Stored Strain Energy in Malleable Azobenzene Liquid Crystalline Polymer Actuators

Author: Xili Lu, Shengwei Guo, Xia Tong, Hesheng Xia, Yue Zhao

Publication: Advanced Materials

Publisher: John Wiley and Sons

Date: Jun 6, 2017

© 2017 WILEY-VCH Verlag GmbH & Co. KGaA, Weinheim

Logged in as:

Bo Fan

Account #:
3000851023

[LOGOUT](#)

Order Completed

Thank you for your order.

This Agreement between Bo Fan ("You") and John Wiley and Sons ("John Wiley and Sons") consists of your license details and the terms and conditions provided by John Wiley and Sons and Copyright Clearance Center.

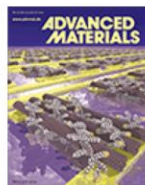
Your confirmation email will contain your order number for future reference.

2018/2/5

Rightslink® by Copyright Clearance Center



RightsLink®

[Home](#)
[Account Info](#)
[Help](#)


Title: Temperature Controlled Water/Oil Wettability of a Surface Fabricated by a Block Copolymer: Application as a Dual Water/Oil On-Off Switch

Author: Baolong Xue, Longcheng Gao, Yongping Hou, Zhiwen Liu, Lei Jiang

Publication: Advanced Materials

Publisher: John Wiley and Sons

Date: Oct 17, 2012

Copyright © 2013 WILEY-VCH Verlag GmbH & Co. KGaA, Weinheim

Logged in as:

Bo Fan

Account #:
3000851023

[LOGOUT](#)

Order Completed

Thank you for your order.

This Agreement between Bo Fan ("You") and John Wiley and Sons ("John Wiley and Sons") consists of your license details and the terms and conditions provided by John Wiley and Sons and Copyright Clearance Center.

2018/2/5

Rightslink® by Copyright Clearance Center



RightsLink®

[Home](#)
[Account Info](#)
[Help](#)


ACS Publications
Most Trusted. Most Cited. Most Read.

Title: Efficient Colorimetric pH Sensor Based on Responsive Polymer-Quantum Dot Integrated Graphene Oxide

Author: Kwanyeol Paek, Hyunseung Yang, Junhyuk Lee, et al

Publication: ACS Nano

Publisher: American Chemical Society

Date: Mar 1, 2014

Copyright © 2014, American Chemical Society

Logged in as:

Bo Fan

Account #:

3000851023

[LOGOUT](#)

PERMISSION/LICENSE IS GRANTED FOR YOUR ORDER AT NO CHARGE

2018/2/5

Rightslink® by Copyright Clearance Center



RightsLink®

[Home](#)
[Account Info](#)
[Help](#)


ACS Publications
Most Trusted. Most Cited. Most Read.

Title: CO₂-Responsive Polymer Single-Chain Nanoparticles and Self-Assembly for Gas-Tunable Nanoreactors

Author: Weizheng Fan, Xia Tong, Farhad Farnia, et al

Publication: Chemistry of Materials

Publisher: American Chemical Society

Date: Jul 1, 2017

Copyright © 2017, American Chemical Society

Logged in as:

Bo Fan

Account #:

3000851023

[LOGOUT](#)

PERMISSION/LICENSE IS GRANTED FOR YOUR ORDER AT NO CHARGE

2018/2/5

Rightslink® by Copyright Clearance Center



RightsLink®

[Home](#)
[Account Info](#)
[Help](#)


Title: Paclitaxel-conjugated PEG and arginine-grafted bioreducible poly (disulfide amine) micelles for co-delivery of drug and gene

Author: Kihoon Nam, Hye Yeong Nam, Pyung-Hwan Kim, Sung Wan Kim

Publication: Biomaterials

Publisher: Elsevier

Date: November 2012

Copyright © 2012 Elsevier Ltd. All rights reserved.

Logged in as:

Bo Fan

Account #:

3000851023

[LOGOUT](#)

Order Completed

Thank you for your order.

This Agreement between Bo Fan ("You") and Elsevier ("Elsevier") consists of your license details and the terms and conditions provided by Elsevier and Copyright Clearance Center.

2018/2/5

Rightslink® by Copyright Clearance Center



RightsLink®

[Home](#)[Account Info](#)[Help](#)ACS Publications
Most Trusted. Most Cited. Most Read.

Title: Biocompatible Polymeric Nanoparticles Degrade and Release Cargo In Response to Biologically Relevant Levels of Hydrogen Peroxide

Author: Caroline de Gracia Lux, Shivanjali Joshi-Barr, Trung Nguyen, et al

Publication: Journal of the American Chemical Society

Publisher: American Chemical Society

Date: Sep 1, 2012

Copyright © 2012, American Chemical Society

Logged in as:

Bo Fan

Account #:
3000851023[LOGOUT](#)**PERMISSION/LICENSE IS GRANTED FOR YOUR ORDER AT NO CHARGE**

2018/2/5

Rightslink® by Copyright Clearance Center



RightsLink®

[Home](#)[Account Info](#)[Help](#)ACS Publications
Most Trusted. Most Cited. Most Read.

Title: Fast Photodegradable Block Copolymer Micelles for Burst Release

Author: Dehui Han, Xia Tong, Yue Zhao

Publication: Macromolecules

Publisher: American Chemical Society

Date: Feb 1, 2011

Copyright © 2011, American Chemical Society

Logged in as:

Bo Fan

Account #:
3000851023[LOGOUT](#)**PERMISSION/LICENSE IS GRANTED FOR YOUR ORDER AT NO CHARGE**

2018/2/5

Rightslink® by Copyright Clearance Center



RightsLink®

[Home](#)[Account Info](#)[Help](#)ACS Publications
Most Trusted. Most Cited. Most Read.

Title: Kinetics of Self-Immolative Degradation in a Linear Polymeric System: Demonstrating the Effect of Chain Length

Author: Ryan A. McBride, Elizabeth R. Gillies

Publication: Macromolecules

Publisher: American Chemical Society

Date: Jul 1, 2013

Copyright © 2013, American Chemical Society

Logged in as:

Bo Fan

Account #:
3000851023[LOGOUT](#)**PERMISSION/LICENSE IS GRANTED FOR YOUR ORDER AT NO CHARGE**

2018/2/5

Rightslink® by Copyright Clearance Center



RightsLink®

Home

Account
Info

Help

ACS Publications
Most Trusted. Most Cited. Most Read.**Title:** Patterned Plastics That Change
Physical Structure in Response
to Applied Chemical Signals**Author:** Wanji Seo, Scott T. Phillips**Publication:** Journal of the American
Chemical Society**Publisher:** American Chemical Society**Date:** Jul 1, 2010

Copyright © 2010, American Chemical Society

Logged in as:

Bo Fan

Account #:

3000851023

LOGOUT

PERMISSION/LICENSE IS GRANTED FOR YOUR ORDER AT NO CHARGE

2018/2/5

Rightslink® by Copyright Clearance Center



RightsLink®

Home

Account
Info

Help

ACS Publications
Most Trusted. Most Cited. Most Read.**Title:** Stimuli-Responsive Core-Shell
Microcapsules with Tunable
Rates of Release by Using a
Depolymerizable
Poly(phthalaldehyde) Membrane**Author:** Anthony M. DiLauro, Alireza
Abbaspourrad, David A. Weitz,
et al**Publication:** Macromolecules**Publisher:** American Chemical Society**Date:** May 1, 2013

Copyright © 2013, American Chemical Society

Logged in as:

Bo Fan

Account #:

3000851023

LOGOUT

PERMISSION/LICENSE IS GRANTED FOR YOUR ORDER AT NO CHARGE

2018/2/5

Rightslink® by Copyright Clearance Center



RightsLink®

Home

Account
Info

Help

ACS Publications
Most Trusted. Most Cited. Most Read.**Title:** A Cascade Biodegradable
Polymer Based on Alternating
Cyclization and Elimination
Reactions**Author:** Matthew A. DeWit, Elizabeth R.
Gillies**Publication:** Journal of the American
Chemical Society**Publisher:** American Chemical Society**Date:** Dec 1, 2009

Copyright © 2009, American Chemical Society

Logged in as:

Bo Fan

Account #:

3000851023

LOGOUT

PERMISSION/LICENSE IS GRANTED FOR YOUR ORDER AT NO CHARGE

2018/2/5

Rightslink® by Copyright Clearance Center



RightsLink®

[Home](#)
[Account Info](#)
[Help](#)


Title: Self-Immolative Polymersomes for High-Efficiency Triggered Release and Programmed Enzymatic Reactions

Author: Guhuan Liu, Xiaorui Wang, Jinming Hu, et al

Publication: Journal of the American Chemical Society

Publisher: American Chemical Society

Date: May 1, 2014

Copyright © 2014, American Chemical Society

Logged in as:

Bo Fan

Account #:
3000851023

[LOGOUT](#)

PERMISSION/LICENSE IS GRANTED FOR YOUR ORDER AT NO CHARGE



RightsLink®

[Home](#)
[Account Info](#)
[Help](#)


Title: Photocontrolled Degradation of Stimuli-Responsive Poly(ethyl glyoxylate): Differentiating Features and Traceless Ambient Depolymerization

Author: Bo Fan, John F. Trant, Rebecca E. Yardley, et al

Publication: Macromolecules

Publisher: American Chemical Society

Date: Oct 1, 2016

Copyright © 2016, American Chemical Society

Logged in as:

Bo Fan

Account #:
3000851023

[LOGOUT](#)

PERMISSION/LICENSE IS GRANTED FOR YOUR ORDER AT NO CHARGE



RightsLink®

[Home](#)
[Account Info](#)
[Help](#)


Title: End-Capping Strategies for Triggering End-to-End Depolymerization of Polyglyoxylates

Author: Bo Fan, John F. Trant, Elizabeth R. Gillies

Publication: Macromolecules

Publisher: American Chemical Society

Date: Dec 1, 2016

Copyright © 2016, American Chemical Society

Logged in as:

Bo Fan

Account #:
3000851023

[LOGOUT](#)

PERMISSION/LICENSE IS GRANTED FOR YOUR ORDER AT NO CHARGE



RightsLink®

[Home](#)
[Account Info](#)
[Help](#)


ACS Publications Title:
Most Trusted. Most Cited. Most Read.

Poly(ethyl glyoxylate)-
Poly(ethylene oxide)
Nanoparticles: Stimuli-
Responsive Drug Release via
End-to-End Polyglyoxylate
Depolymerization

Author: Bo Fan, Elizabeth R. Gillies

Publication: Molecular Pharmaceutics

Publisher: American Chemical Society

Date: Aug 1, 2017

Copyright © 2017, American Chemical Society

Logged in as:

Bo Fan

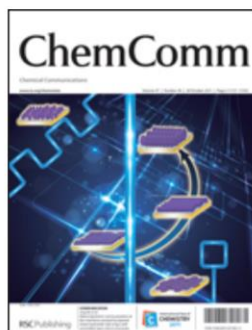
Account #:
3000851023

[LOGOUT](#)

PERMISSION/LICENSE IS GRANTED FOR YOUR ORDER AT NO CHARGE



RightsLink®

[Home](#)
[Account Info](#)
[Help](#)


Title: Thermo-responsive self-immolative nanoassemblies: direct and indirect triggering

Author: Bo Fan, John F. Trant, Gauvin Hemery, Olivier Sandre, Elizabeth R. Gillies

Publication: Chemical Communications (Cambridge)

Publisher: Royal Society of Chemistry

Date: Oct 6, 2017

Copyright © 2017, Royal Society of Chemistry

Logged in as:

Bo Fan

Account #:
3000851023

[LOGOUT](#)

Order Completed

Thank you for your order.

This Agreement between Bo Fan ("You") and Royal Society of Chemistry ("Royal Society of Chemistry") consists of your license details and the terms and conditions provided by Royal Society of Chemistry and Copyright Clearance Center.

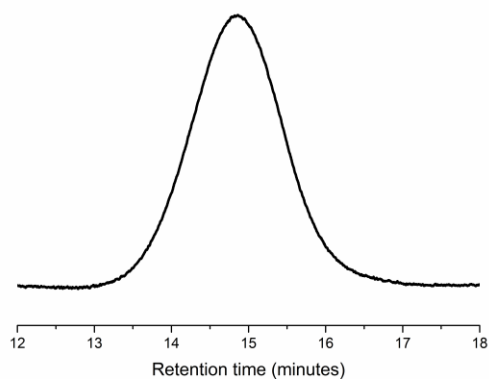


Figure A3.3. Size exclusion chromatogram of the **PEtG-NVOC** used in this study (refractive index detection).

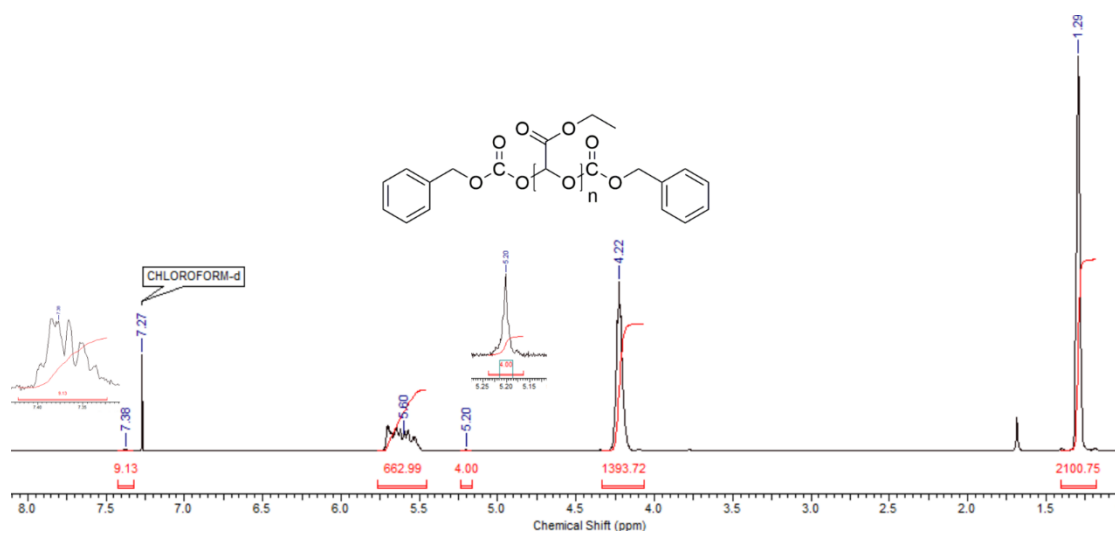


Figure A3.4. ¹H NMR spectrum of PETG end-capped by benzyl chloroformate used in this study (CDCl₃, 600 MHz). Zoom inset shows peaks corresponding to the end-cap.

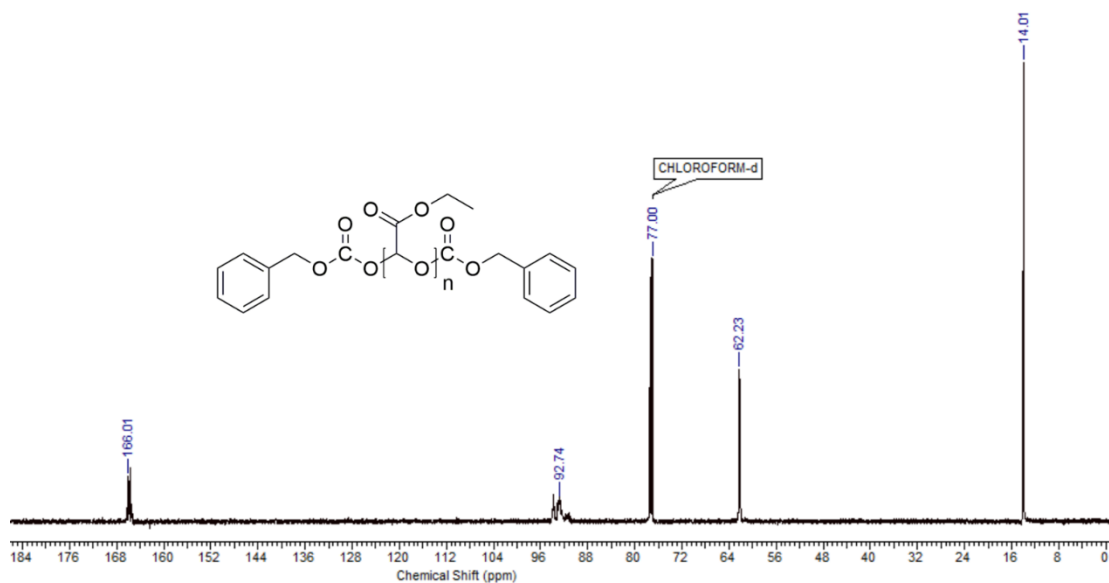


Figure A3.5. ^{13}C NMR spectrum of PEtG end-capped by benzyl chloroformate used in this study (CDCl_3 , 150 MHz).

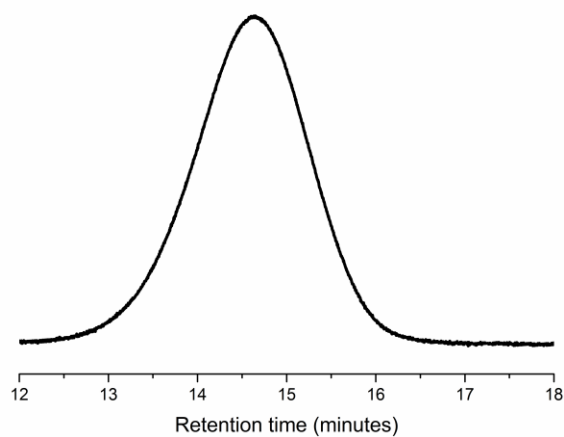


Figure A3.6. Size exclusion chromatogram of the PEtG end-capped by benzyl chloroformate used in this study (refractive index detection).

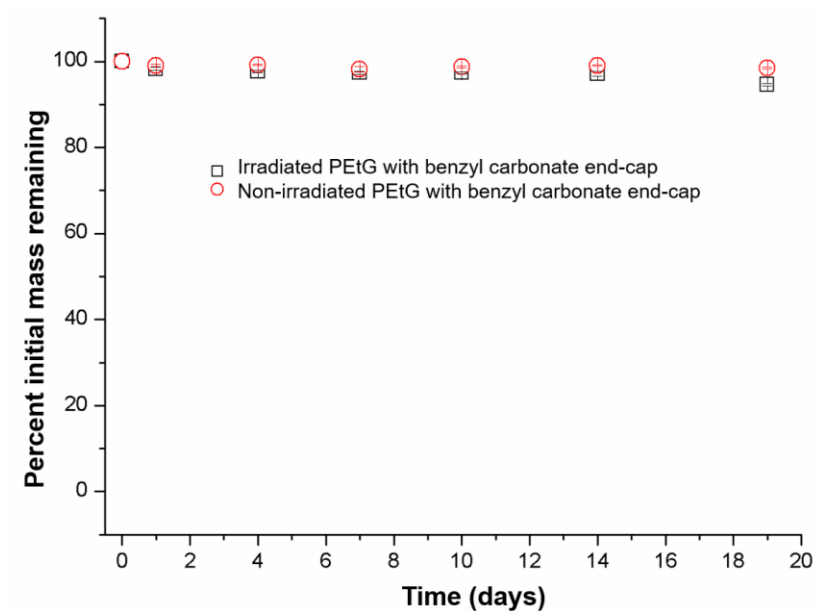


Figure A3.7. Mass loss profiles of coatings prepared PETG end-capped with a non-photo-responsive benzyl carbonate end-cap either with irradiation or without irradiation in 0.1 M, pH 7.0 phosphate buffer at 20 °C.

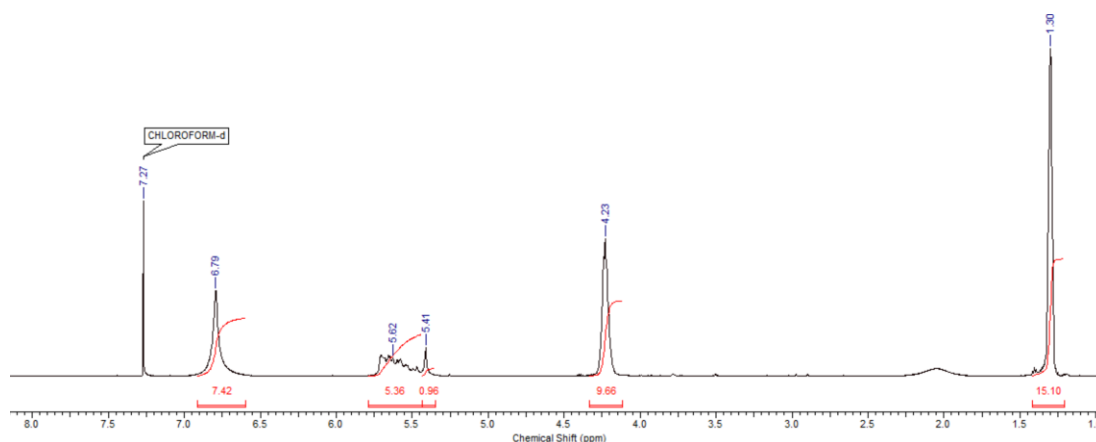


Figure A3.8. ¹H NMR spectrum (CDCl₃, 600 MHz) of residual coating material from a 150 μm-thick coating of irradiated **PEtG-NVOC** after 3 days of immersion in 0.1 M, pH 7 buffer at 20 °C. The spectrum shows the absence of end-cap peaks, confirming the complete removal of end-cap during the irradiation. In addition, peaks corresponding to ethyl glyoxylate hydrate (EtGH) are observed at 5.41 and 6.79 ppm. Assignment of the EtGH peak was made with reference to the previous depolymerization study in solution.¹ The high integration of the peak at 6.79 ppm is believed to result from bound H₂O, which can hydrogen bond to the hydrate. This is also consistent with the broadness and downfield shift of the H₂O peak at 2.1 ppm.

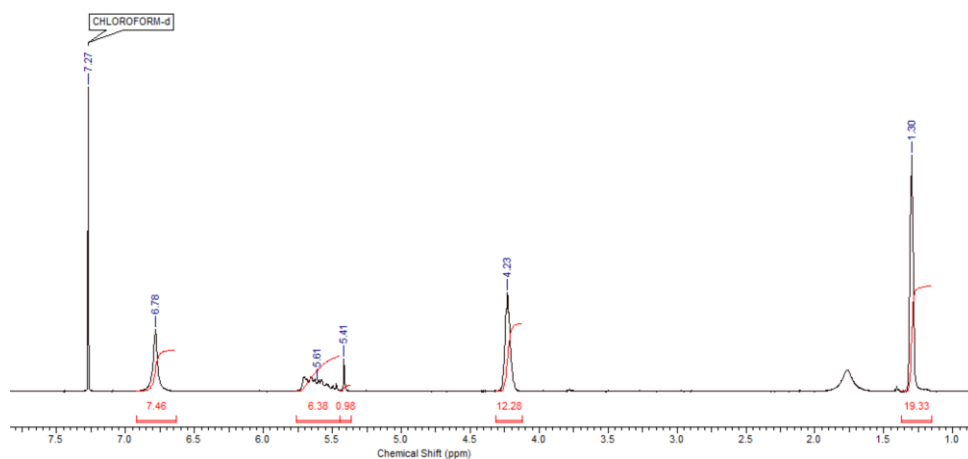


Figure A3.9. ¹H NMR spectrum (CDCl₃, 600 MHz) of residual coating material from a 150 μm coating of irradiated **PEtG-NVOC** after 6 days of immersion in 0.1 M, pH 7 buffer at 20 °C. The same discussion as for Figure A3.8 applies.

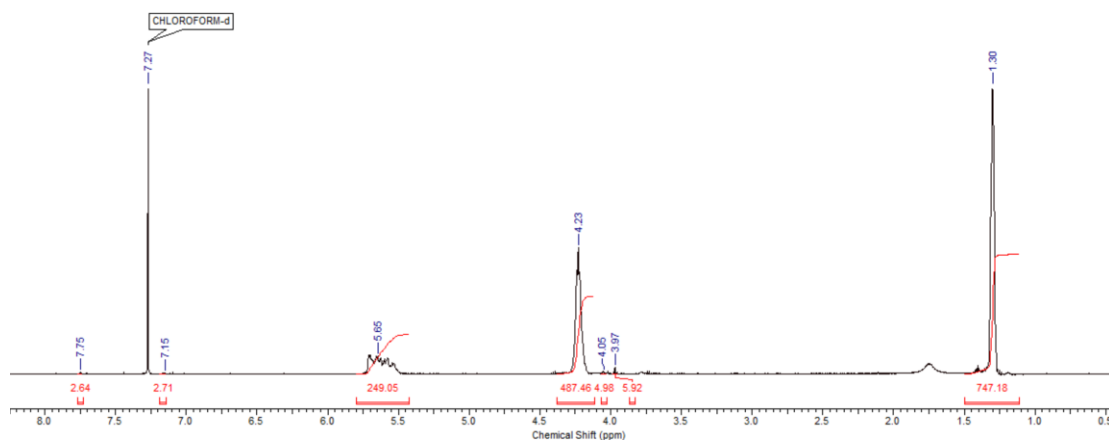


Figure A3.10. ¹H NMR spectrum (CDCl₃, 600 MHz) of residual coating material from a 150 μm coating of non-irradiated **PEtG-NVOC** after 8 days of immersion in 0.1 M, pH 7 buffer at 20 °C. Intact end-cap peaks are observed at ~4 ppm and 7-8 ppm and no depolymerization products are observed.

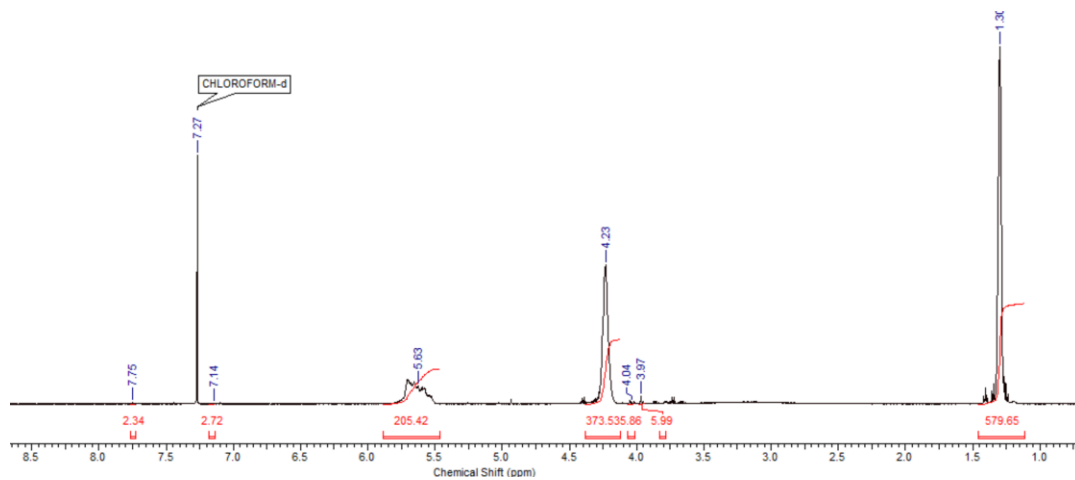
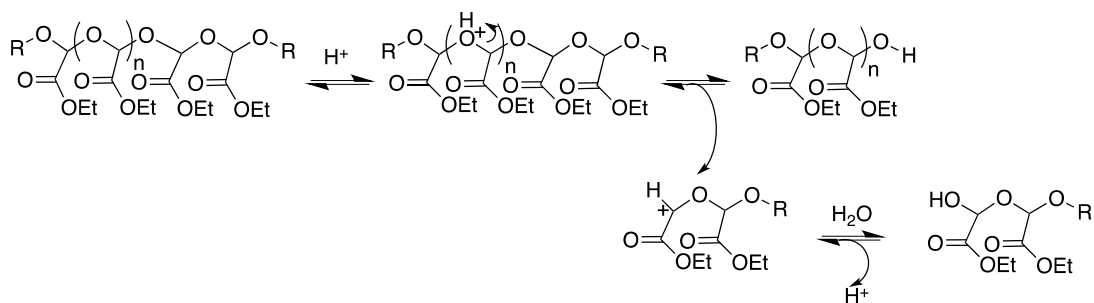
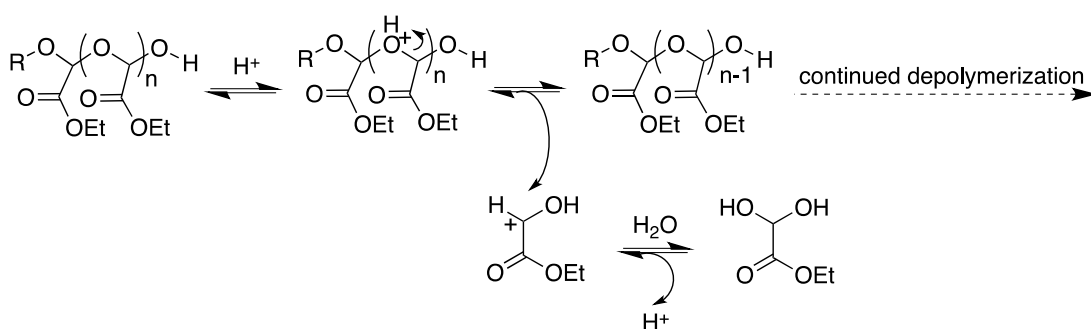


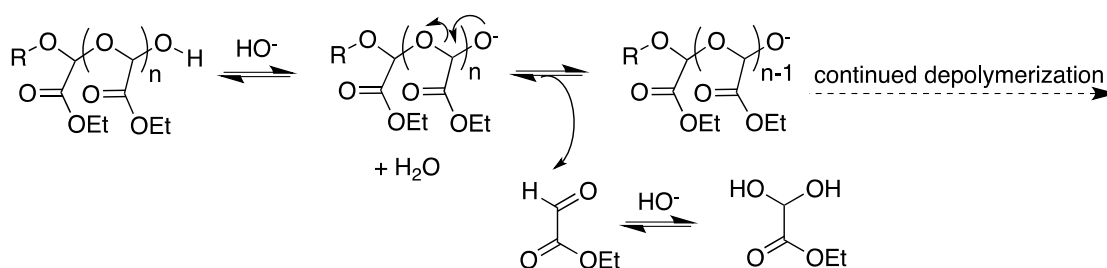
Figure A3.11. ¹H NMR spectrum (CDCl₃, 600 MHz) of residual coating material from a 150 μm coating of non-irradiated **PEtG-NVOC** after 38 days of immersion in 0.1 M, pH 7 buffer at 20 °C. The same comments as for Figure A3.10 apply.



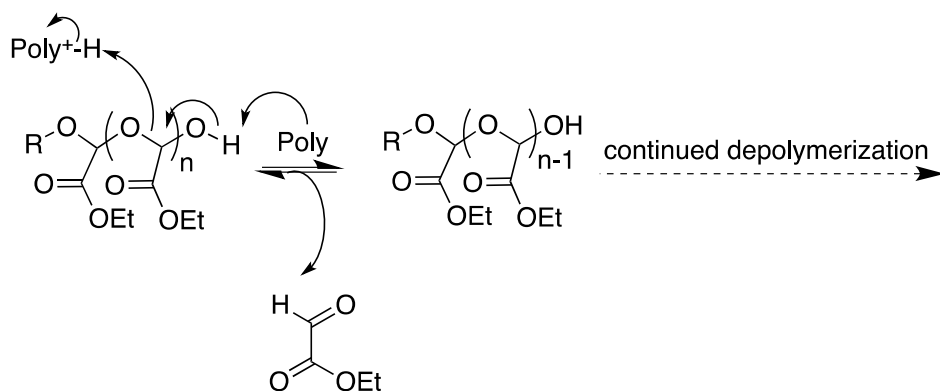
Scheme A3.1. Proposed acid-catalyzed cleavage of an acetal linkage in the PETg backbone. R represents the terminal group. The resulting hemiacetal-terminated polymers/oligomers can subsequently decompose via the mechanisms shown in Scheme A3.2-A3.3.



Scheme A3.2. Proposed PETg terminal hemiacetal cleavage and ethyl glyoxylate hydrate formation by an acid-catalyzed mechanism. R represents the terminal group.



Scheme A3.3. Proposed PETg terminal hemiacetal cleavage and ethyl glyoxylate hydrate formation by a base-catalyzed mechanism. R represents the terminal group. Note that a “water-catalyzed” reaction has been proposed to follow a similar mechanism, where H₂O rather than HO⁻ serves as the base.



Scheme A3.4. Mechanism proposed for the depolymerization of PEtG in the absence of water. Poly corresponds to the polymer matrix in the solid state.

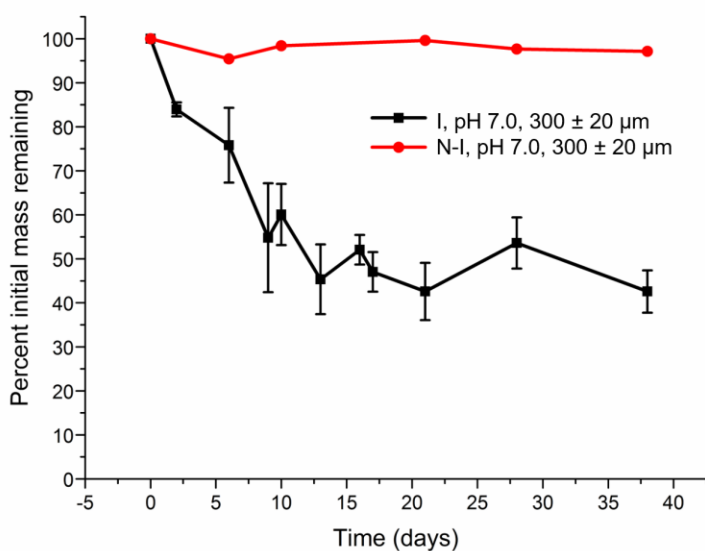


Figure A3.12. Mass loss profile for UV light irradiated (I) and non-irradiated (N-I) PEtG-NVOC immersed in pH 7.0 buffer at 20 °C pH 7.0. The film thickness was 300 μm. Incomplete depolymerization of the irradiated polymer is attributed to incomplete end-cap cleavage.

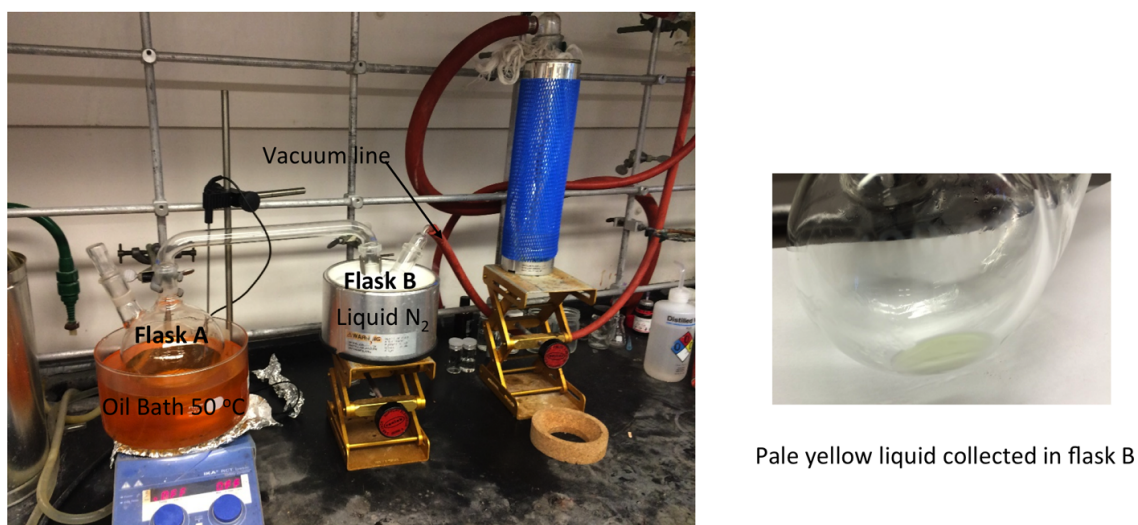


Figure A3.13. Experimental set-up for the collection of depolymerized ethyl glyoxylate.

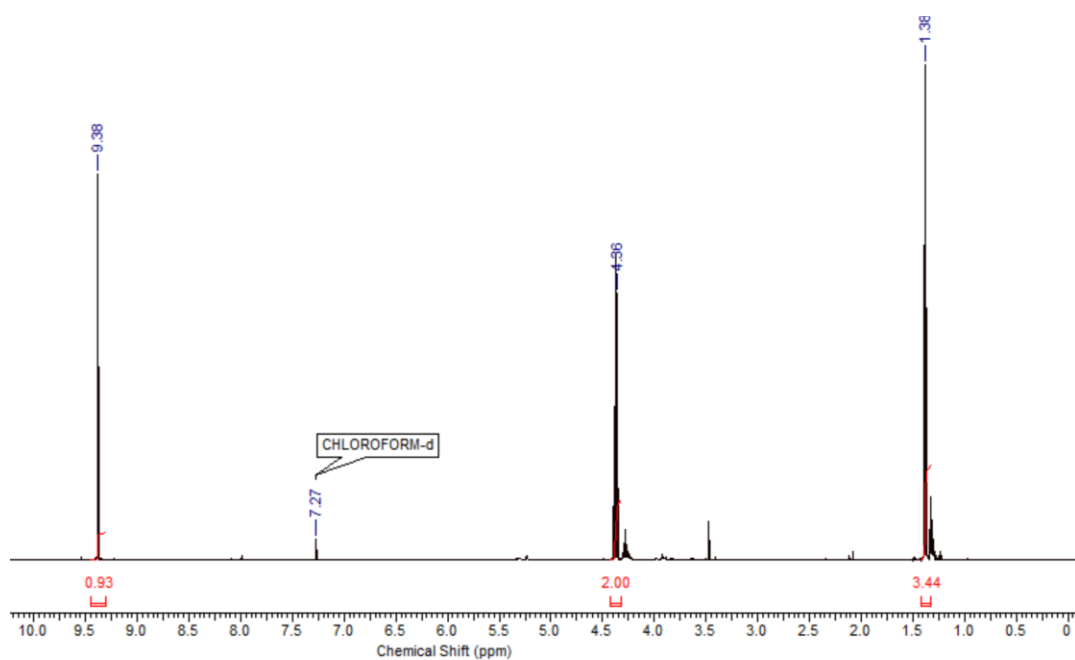


Figure A3.14. ¹H NMR spectrum (600 MHz, CDCl₃) of collected ethyl glyoxylate.

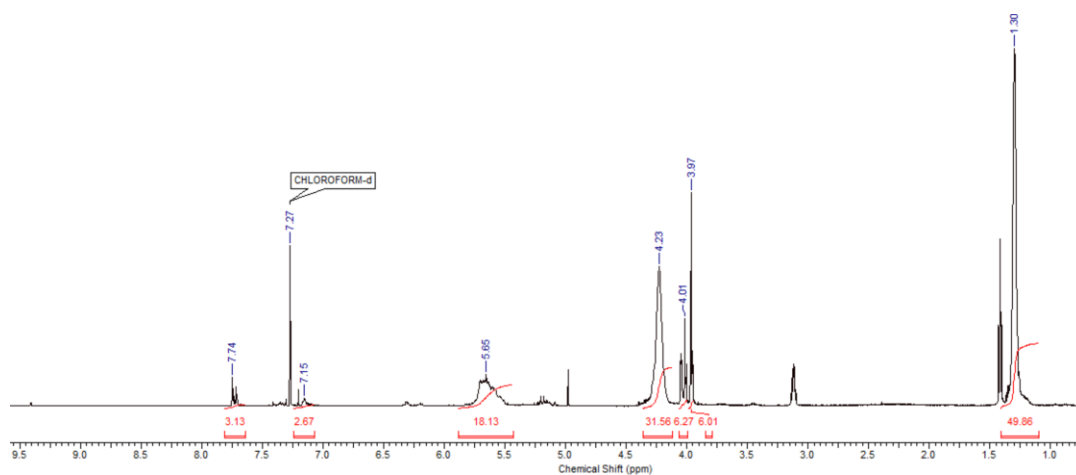


Figure A3.15. ^1H NMR spectrum (600 MHz, CDCl_3) of repolymerized PEtG-NVOC.

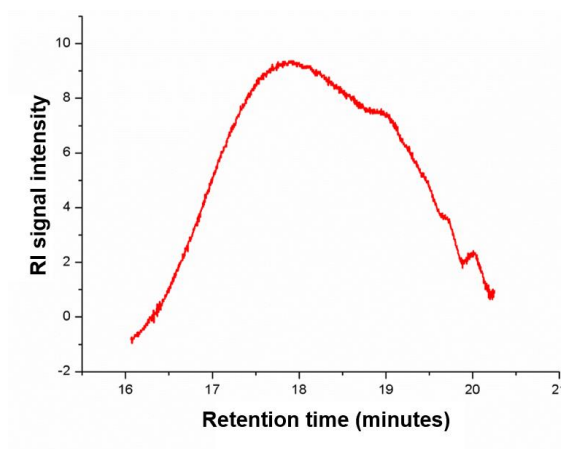


Figure A3.16. Size exclusion chromatogram of repolymerized PEtG-NVOC after depolymerization, monomer collection and repolymerization.

Appendix 4: Supporting information for Chapter 4

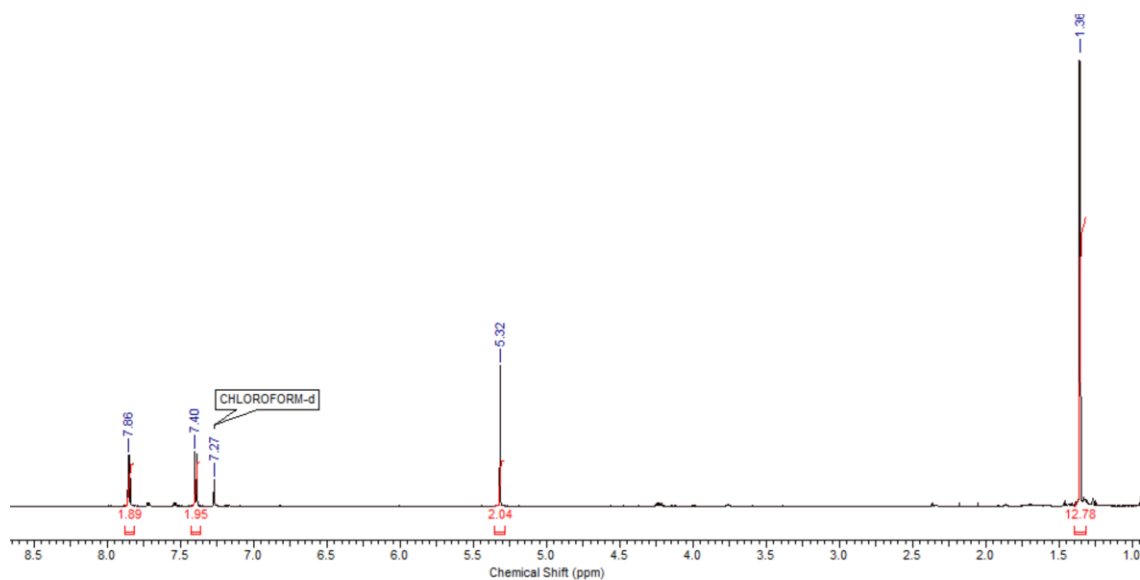


Figure A4.1. ^1H NMR spectrum of chloroformate **4** (CDCl_3 , 400 MHz).

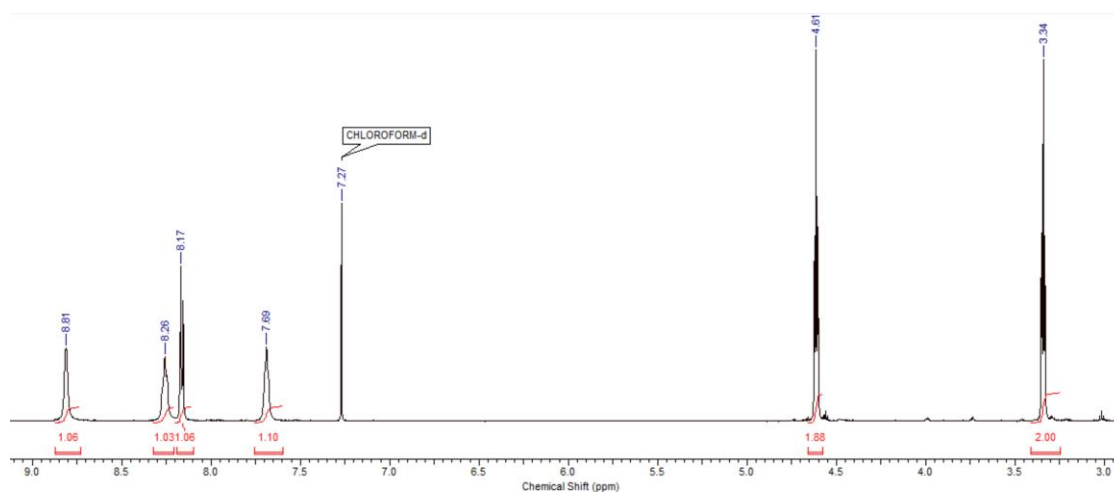


Figure A4.2. ^1H NMR spectrum of chloroformate **5** (CDCl_3 , 400 MHz).

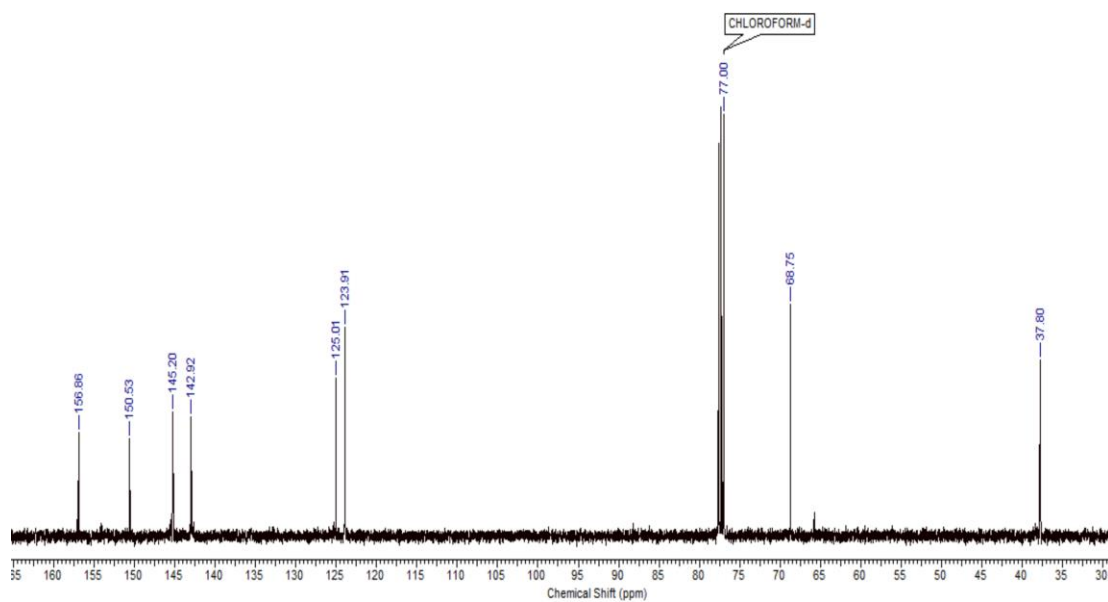


Figure A4.3. ^{13}C NMR spectrum of chloroformate **5** (CDCl_3 , 150 MHz).

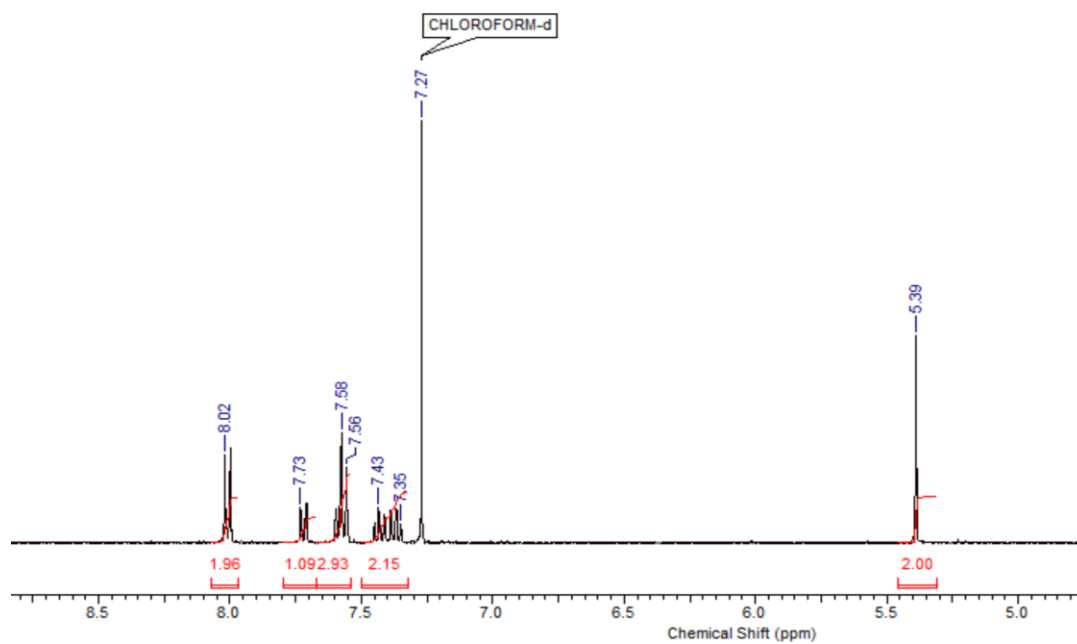


Figure A4.4. ^1H NMR spectrum of chloroformate **6** (CDCl_3 , 400 MHz).

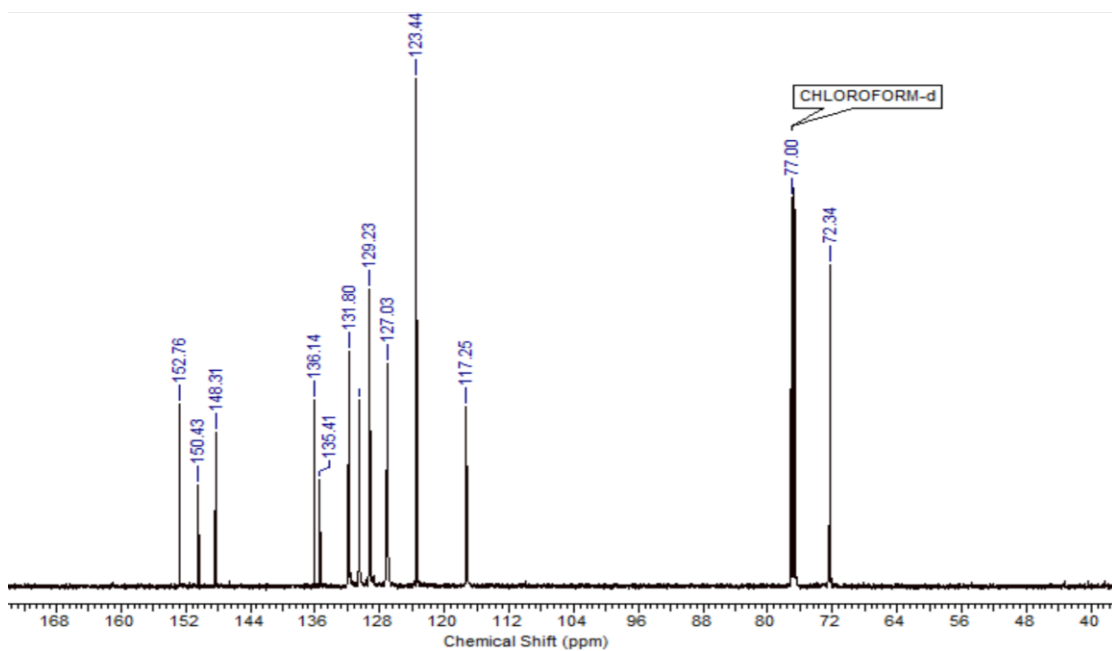


Figure A4.5. ^{13}C NMR spectrum of chloroformate **6** (CDCl_3 , 150 MHz).

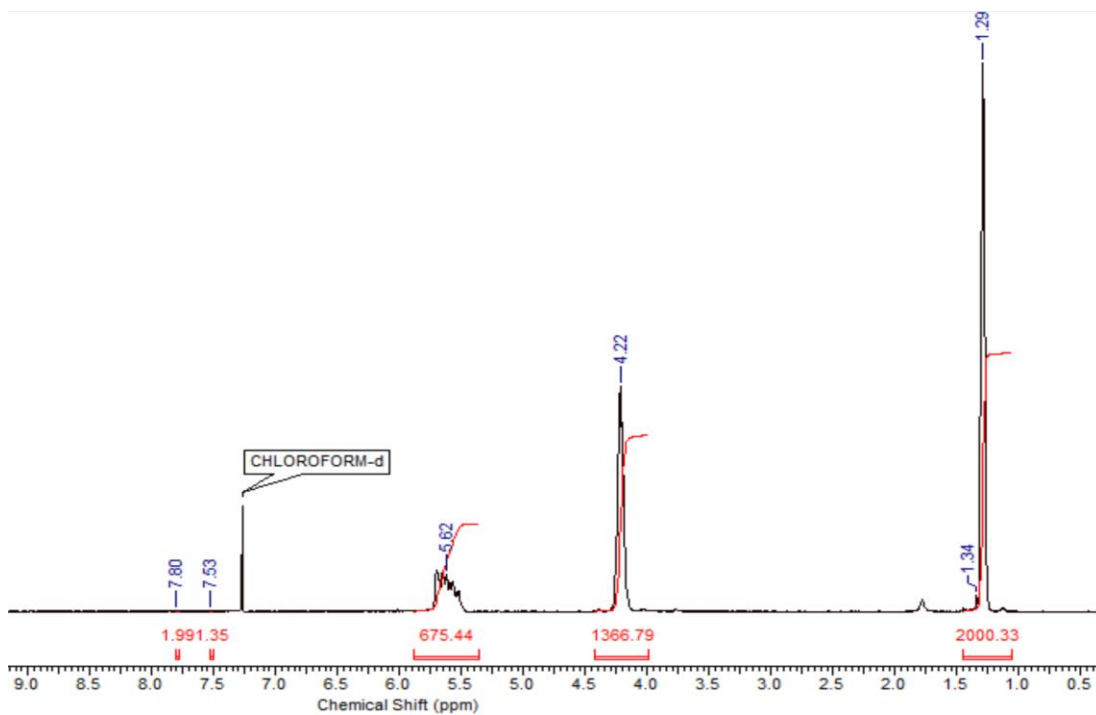


Figure A4.6. ^1H NMR spectrum of PEtG-boronate (CDCl_3 , 400 MHz).

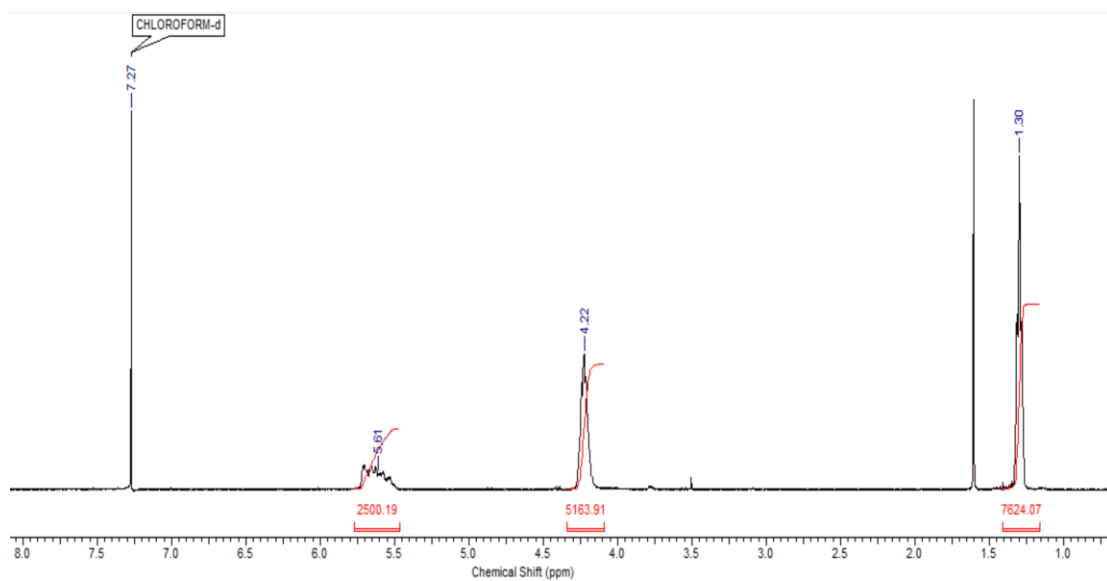


Figure A4.7. ¹H NMR spectrum of **PEtG-disulfide-a** (CDCl₃, 400 MHz).

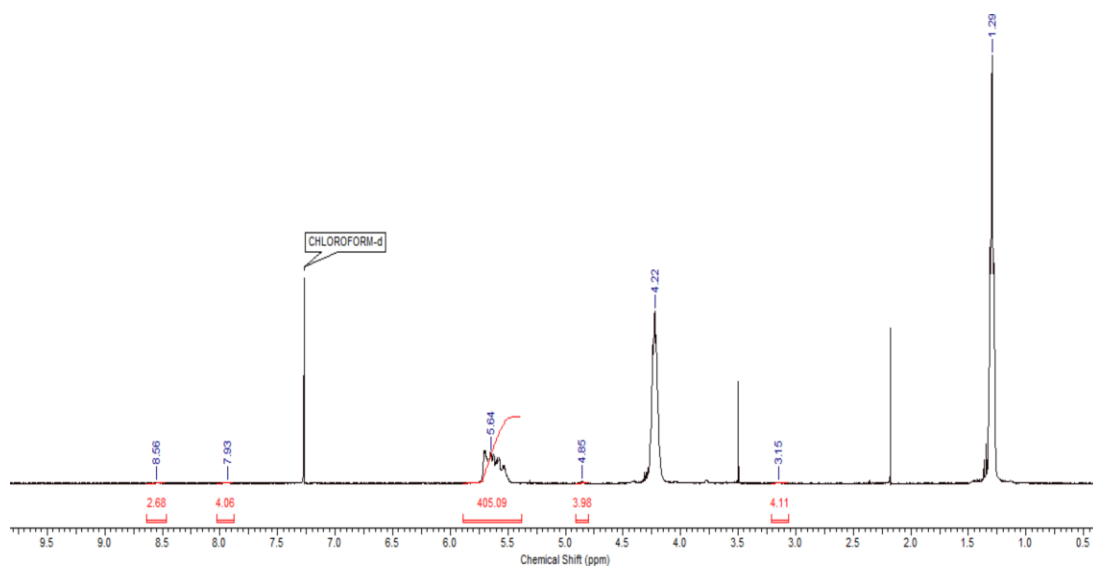


Figure A4.8. ¹H NMR spectrum of **PEtG-disulfide-b** (CDCl₃, 400 MHz).

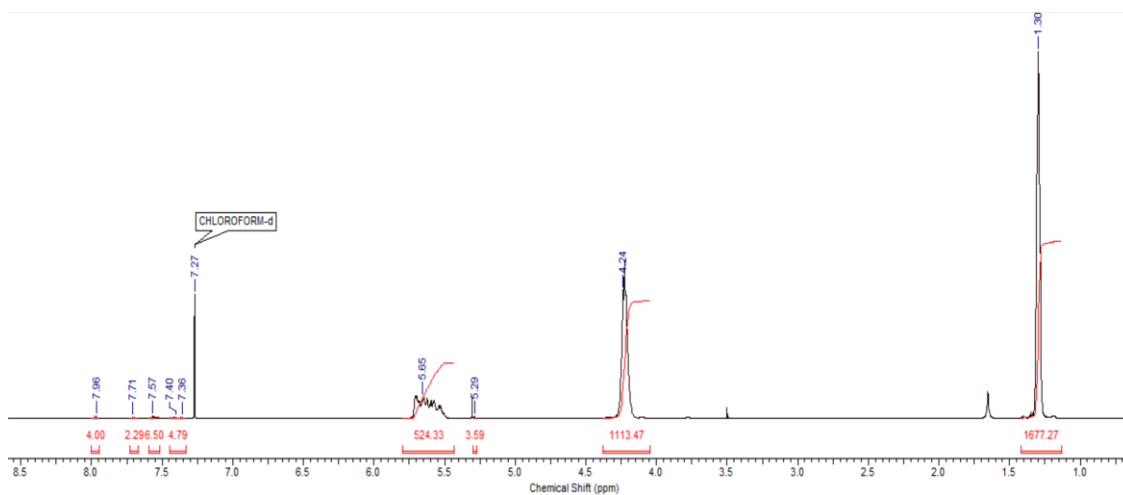


Figure A4.9. ^1H NMR spectrum of **PEtG-azobenzene** (CDCl_3 , 600 MHz).

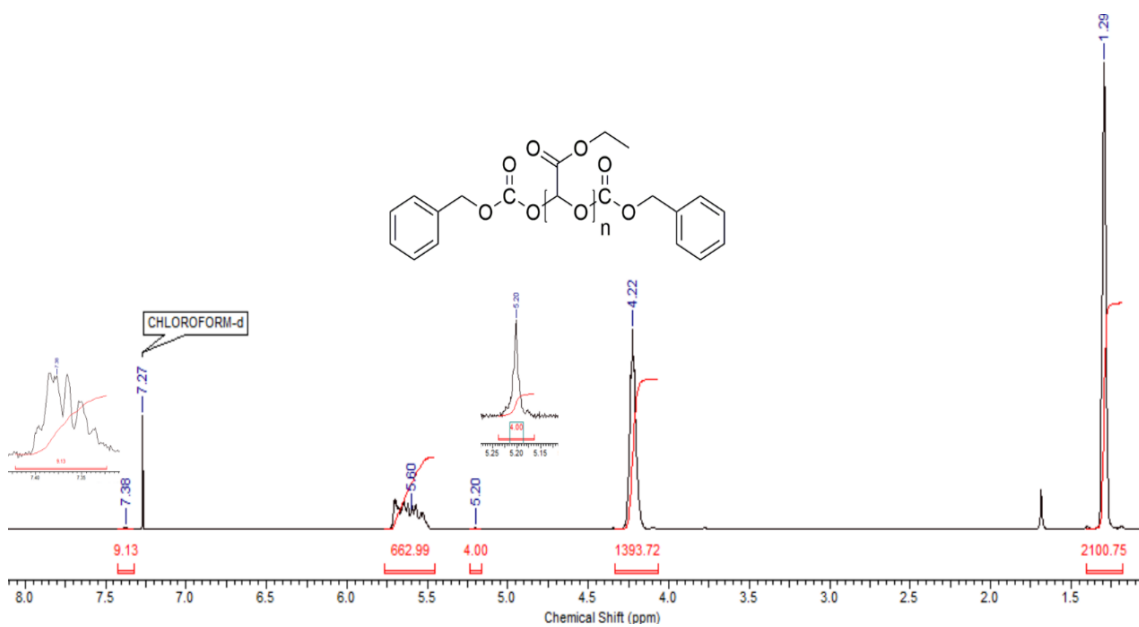


Figure A4.10. ^1H NMR spectrum of **PEtG-control** (CDCl_3 , 600 MHz).

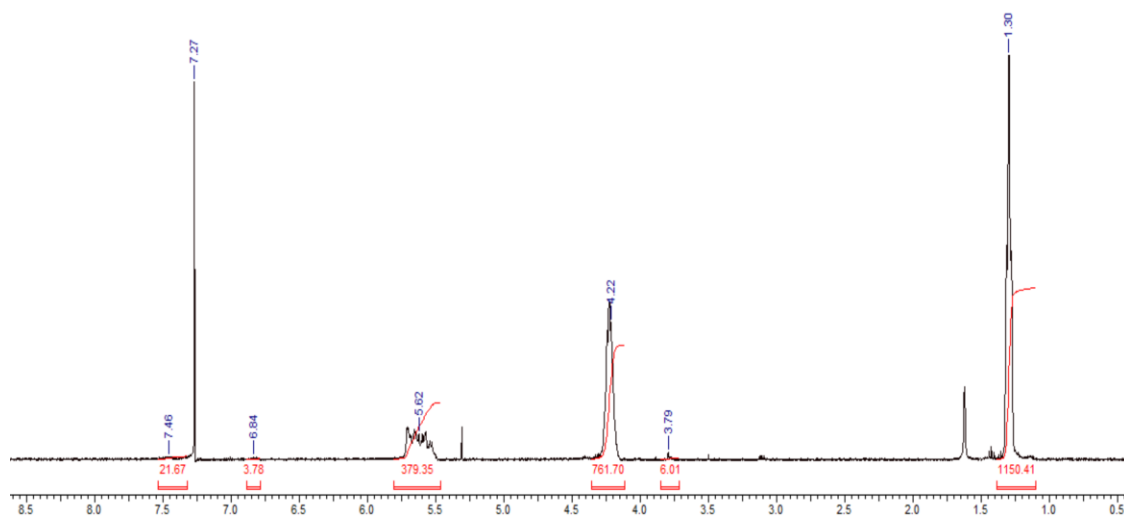


Figure A4.11. ^1H NMR spectrum of **PEtG-MMT** (CDCl_3 , 400 MHz).

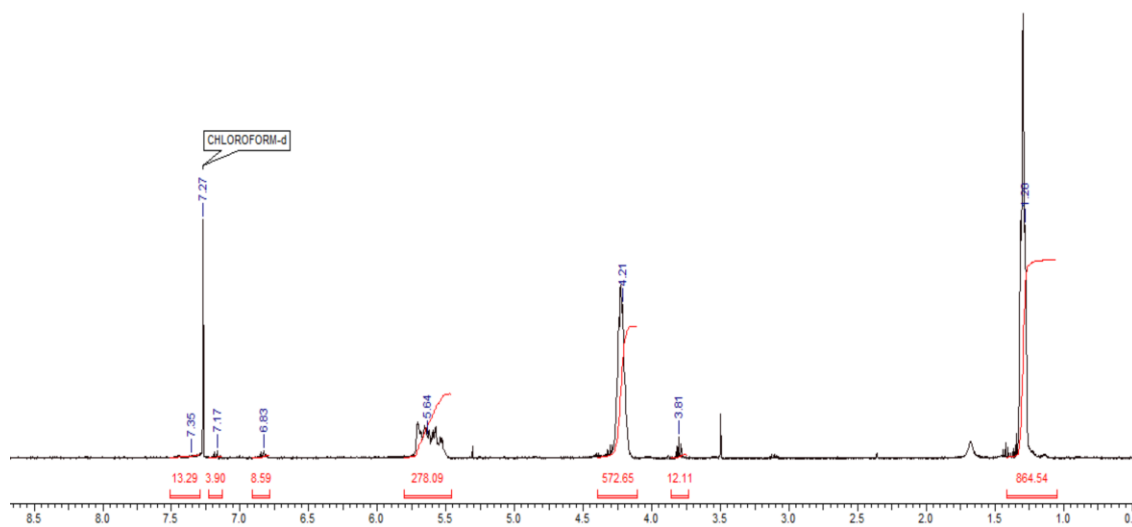


Figure A4.12. ^1H NMR spectrum of **PEtG-DMT** (CDCl_3 , 400 MHz).

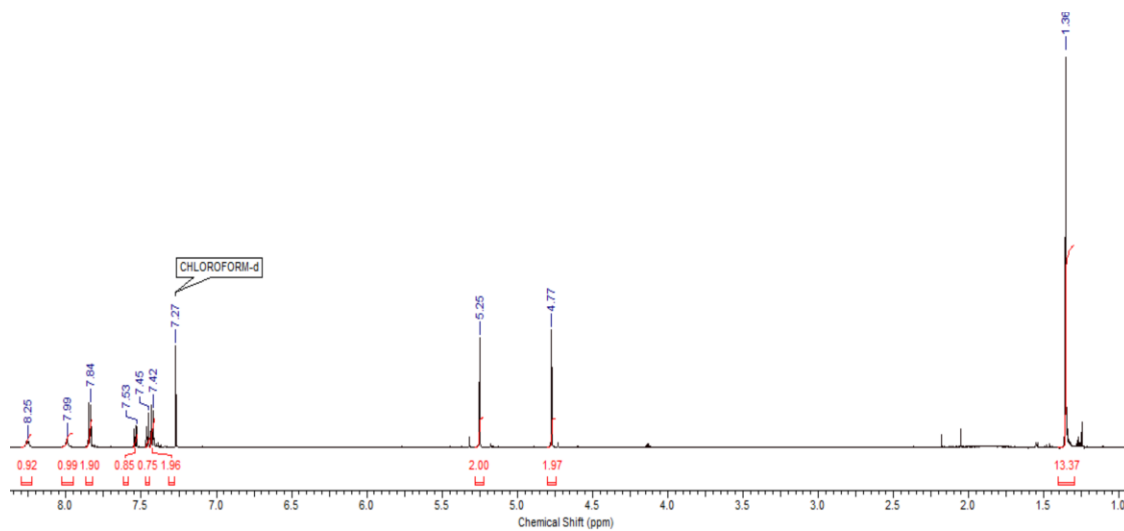


Figure A4.13. ¹H NMR spectrum of compound **10** (CDCl₃, 400 MHz)

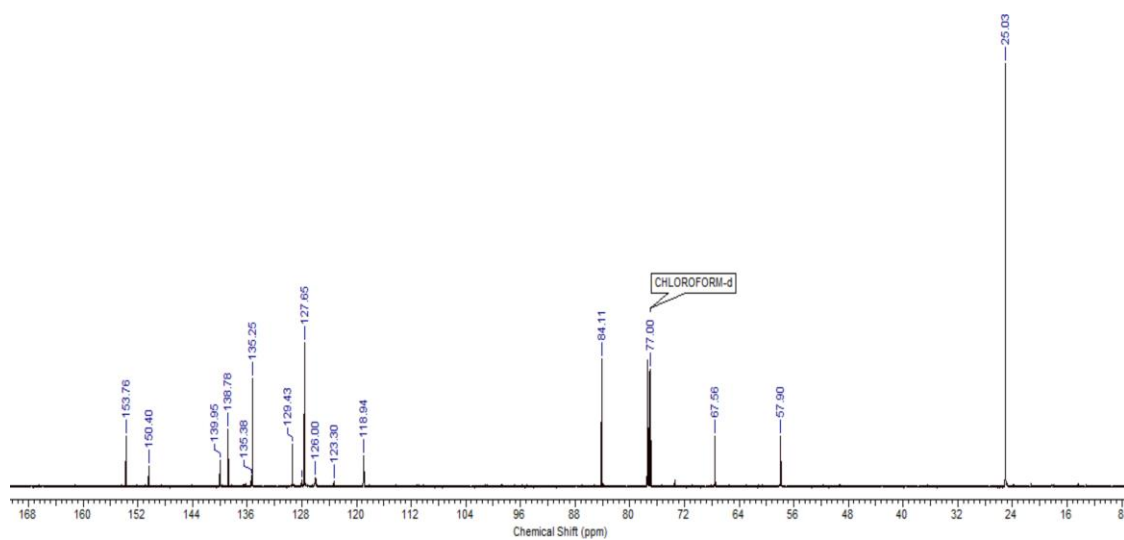


Figure A4.14. ¹³C NMR spectrum of compound **10** (CDCl₃, 150 MHz)

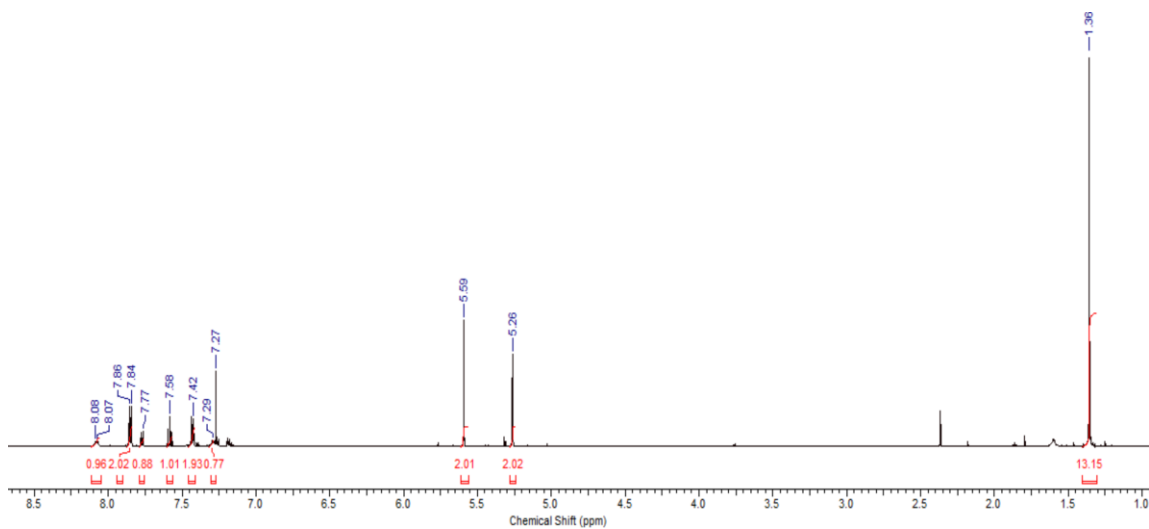


Figure A4.15. ¹H NMR spectrum of chloroformate **11** (CDCl₃, 600 MHz).

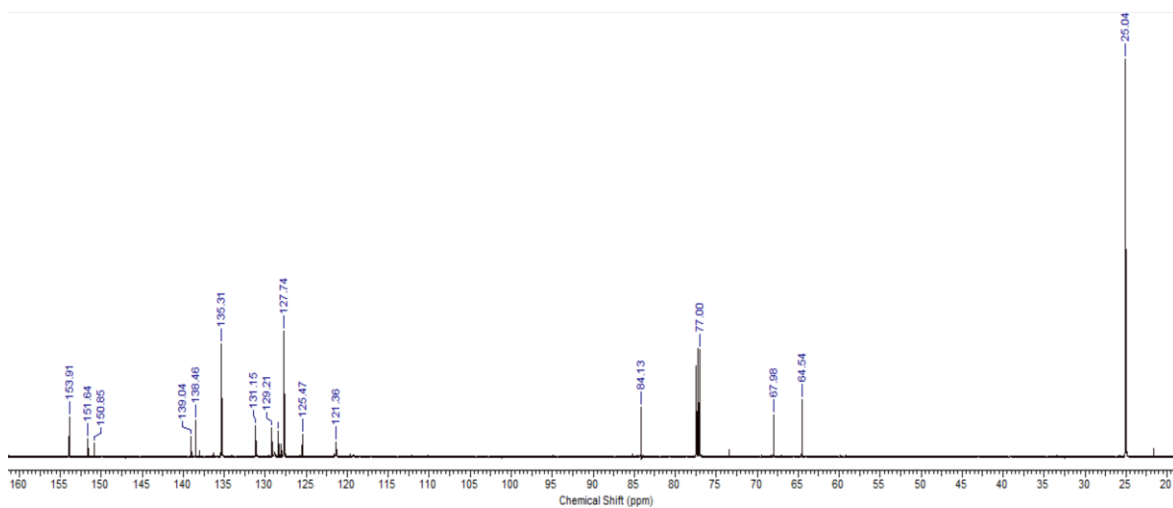


Figure A4.16. ¹³C NMR spectrum of chloroformate **11** (CDCl₃, 150 MHz).

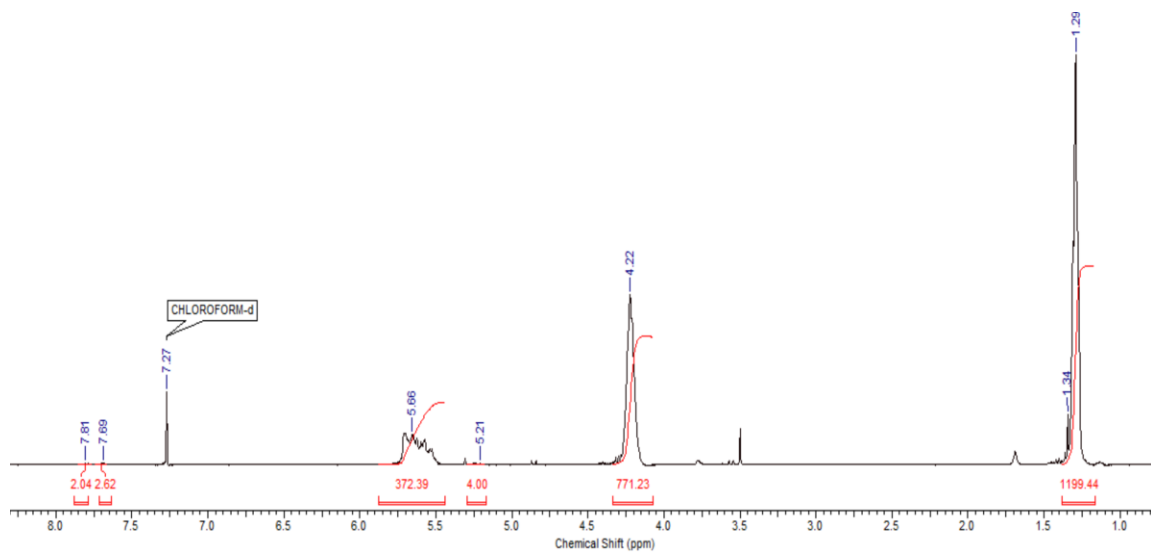


Figure A4.17. ¹H NMR spectrum of PEtG-multi (CDCl₃, 400 MHz).

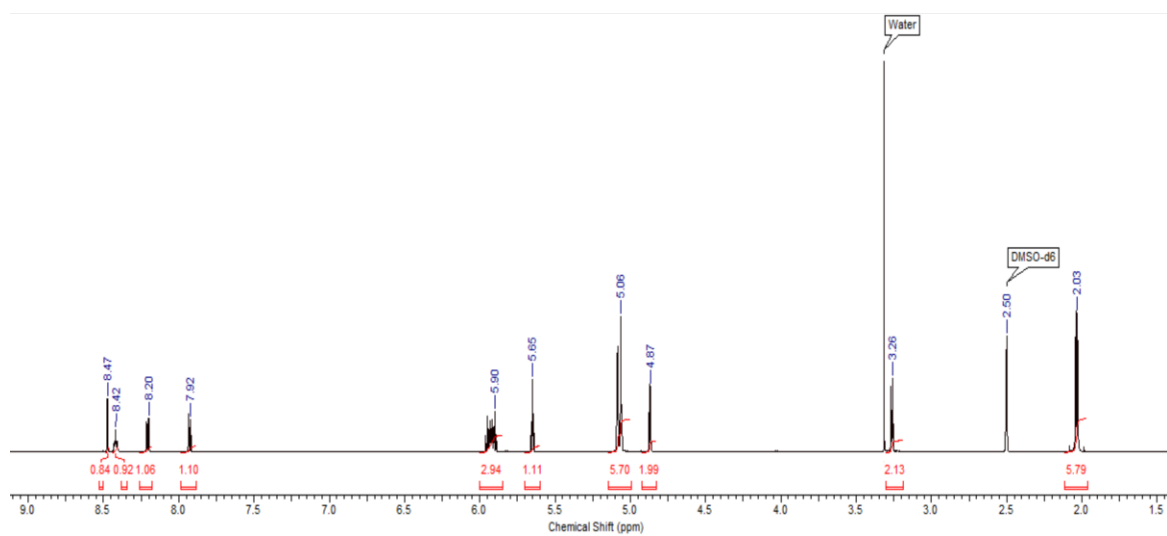


Figure A4.18. ¹H NMR spectrum of compound 14 (CDCl₃, 600 MHz).

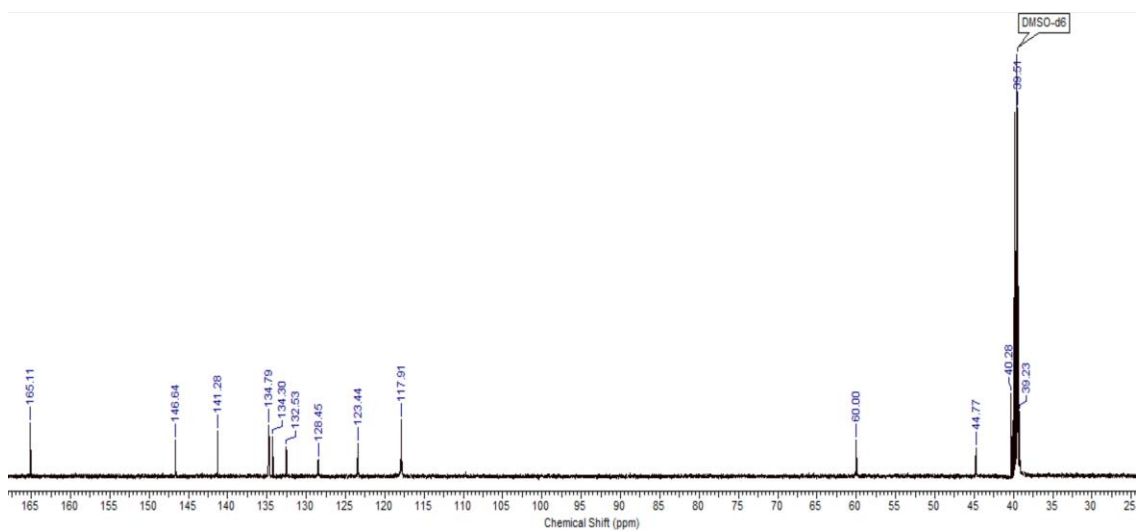


Figure A4.19. ^{13}C NMR spectrum of compound **14** (CDCl_3 , 150 MHz).

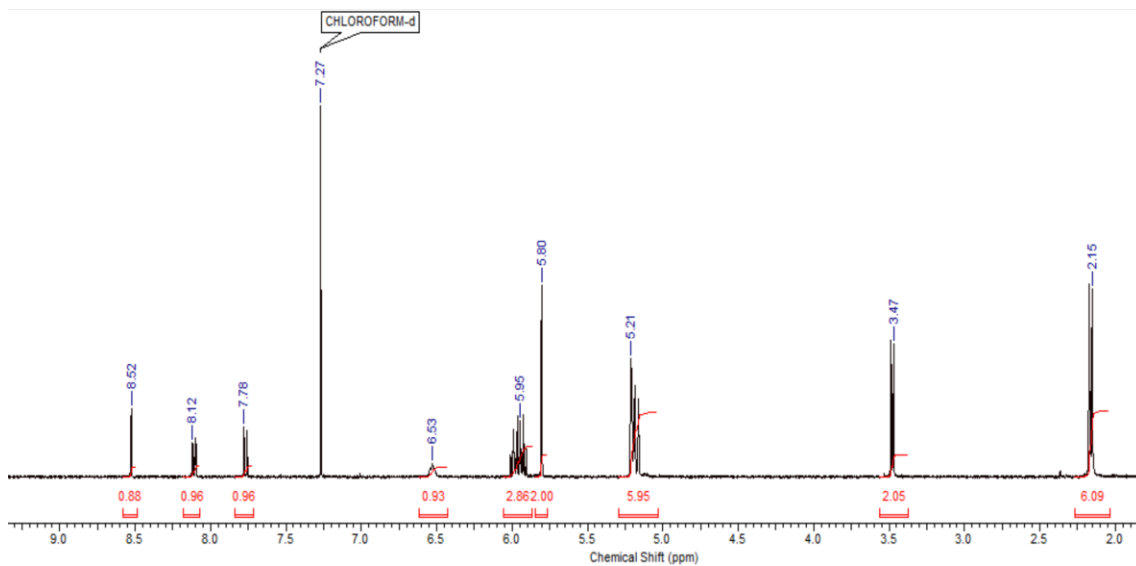


Figure A4.20. ^1H NMR spectrum of chloroformate **15** (CDCl_3 , 600 MHz).

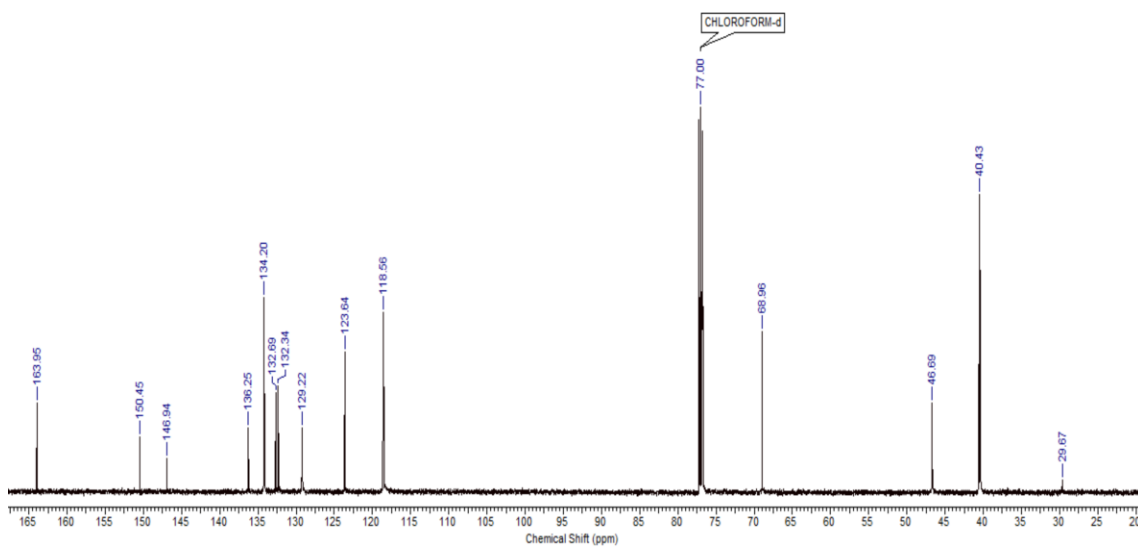


Figure A4.21. ^{13}C NMR spectrum of chloroformate **15** (CDCl_3 , 150 MHz).

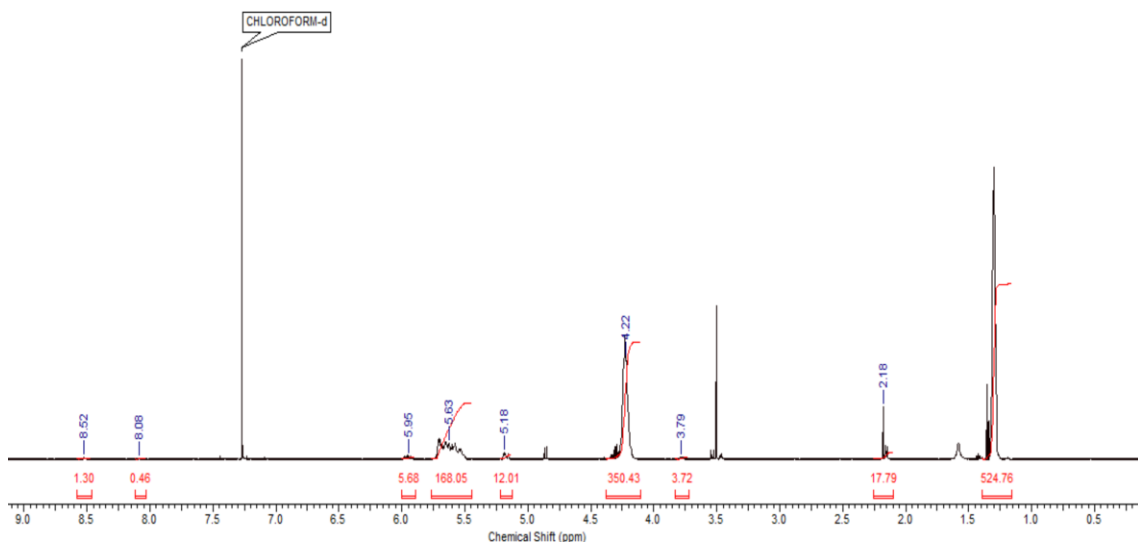


Figure A4.22. ^1H NMR spectrum of **PEtG-trialkene** (CDCl_3 , 600 MHz).

Reaction of ethyl glyoxylate with H₂O₂. 30 μ L of H₂O₂ (50 wt.% in water) (1.1 equivalent to ethyl glyoxylate) was dissolved in 1 mL of 9:1 CD₃CN:D₂O, then 50 mg of distilled ethyl glyoxylate. After 10 min, ¹H and ¹³C NMR spectra were obtained of the above solution (Figures A4.23-A4.24). HRMS was performed after solvents were removed under house vacuum (Figure A4.25). ¹H NMR (600 MHz, CDCl₃): δ 5.30 (s, 1H), 4.18-4.30 (m, 2H), 1.20-1.30 (m, 3H). ¹³C NMR (150 MHz, CDCl₃): δ 168.5, 96.8, 62.9, 14.4. HRMS (EI) calc'd. for [M]⁺ C₄H₉O₅:137.0450; found: 137.0453.

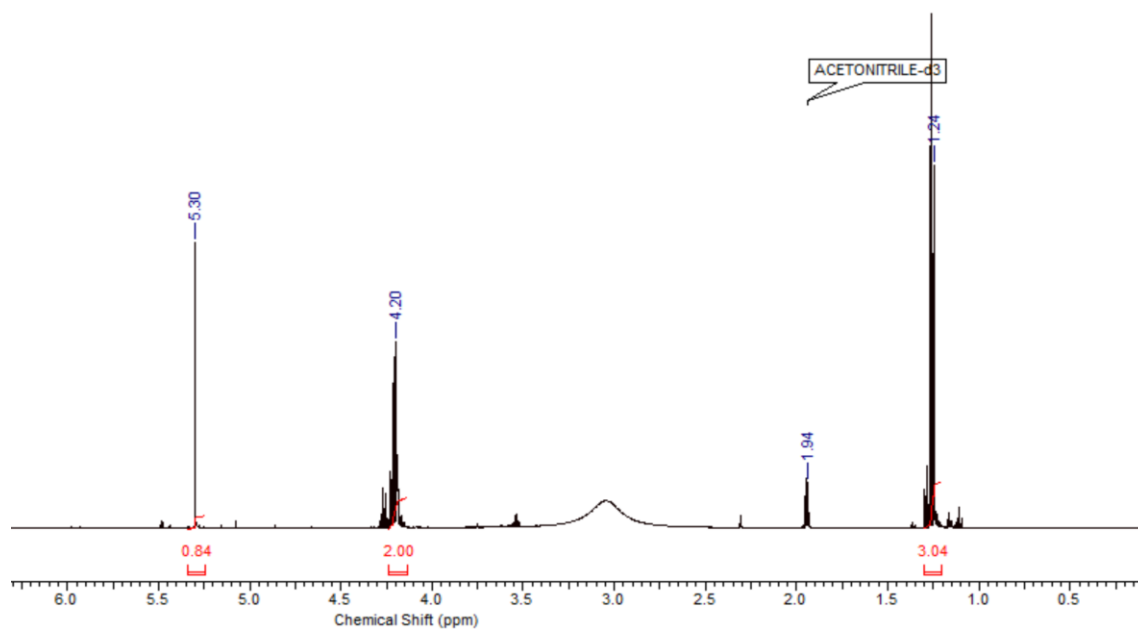


Figure A4.23. ¹H NMR spectrum of the peroxy hydrate reaction product of ethyl glyoxylate and H₂O₂ (9:1 CD₃CN:D₂O, 600 MHz).

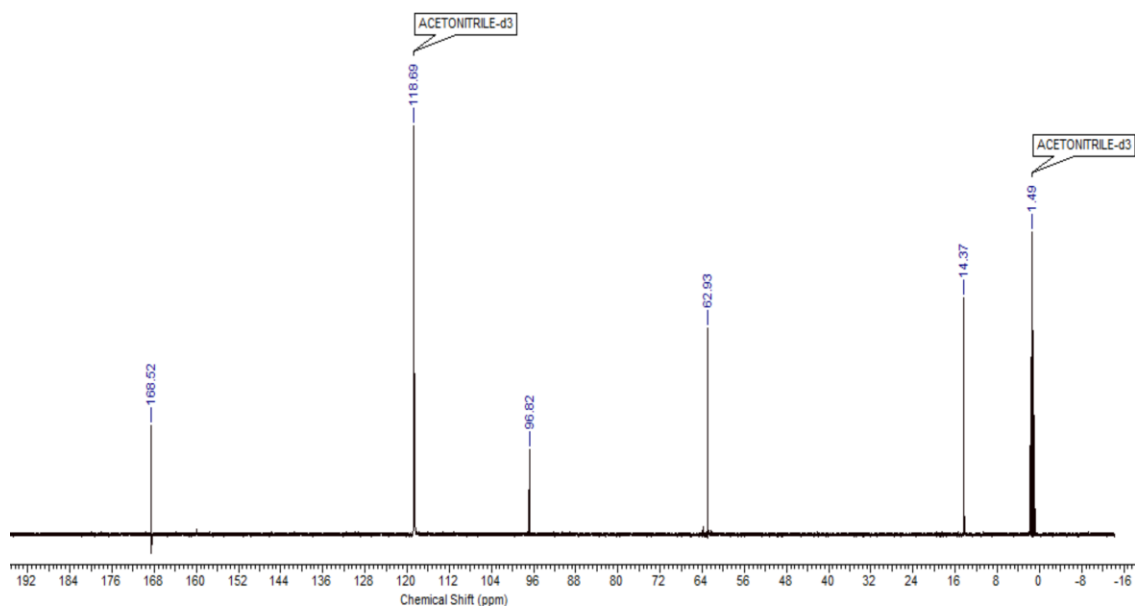


Figure A4.24. ^{13}C NMR spectrum of the peroxy hydrate reaction product of ethyl glyoxylate and H_2O_2 (9:1 $\text{CD}_3\text{CN}:\text{D}_2\text{O}$, 150 MHz).

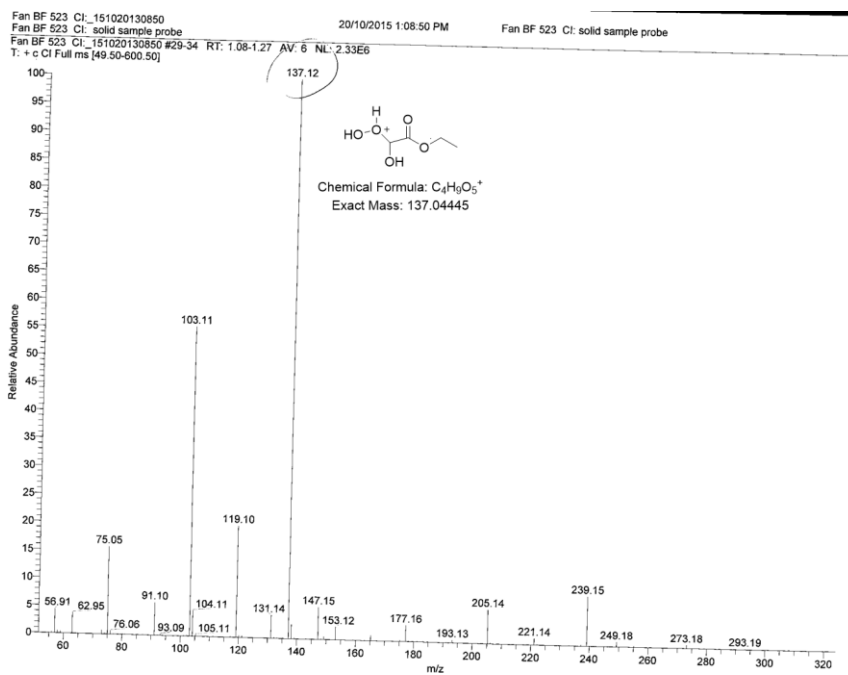


Figure A4.25. MS spectrum of the peroxy hydrate reaction product of ethyl glyoxylate and H_2O_2 .

Reaction of ethyl glyoxylate with DTT. 84 mg (1.1 equivalent to ethyl glyoxylate) DTT was dissolved in 1 mL of 9:1 CD₃CN:D₂O, then 50 mg ethyl glyoxylate was added. After 10 min, ¹H and ¹³C NMR spectra were obtained of the above solution (Figures A4.26-A4.27). HRMS was performed after solvents were removed under house vacuum (Figure A4.28). ¹H NMR (600 MHz, CDCl₃): δ 5.24 (s, 1 H), 4.17 (qua., *J* = 7.0 Hz, 2 H), 3.69-3.75 (m, 1 H), 3.51-3.61 (m, 1 H), 2.72-2.88 (m, 2 H), 2.53-2.62 (m, 2 H), 1.22 (t, *J* = 7.0 Hz, 3 H). ¹³C NMR (150 MHz, CDCl₃): δ 171.7, 74.4, 72.7, 63.0, 33.7, 28.0, 14.4. MS (EI) calc'd. for [M-H₂O]⁺ C₈H₁₅O₄S₂:239.0406; found: 239.0388.

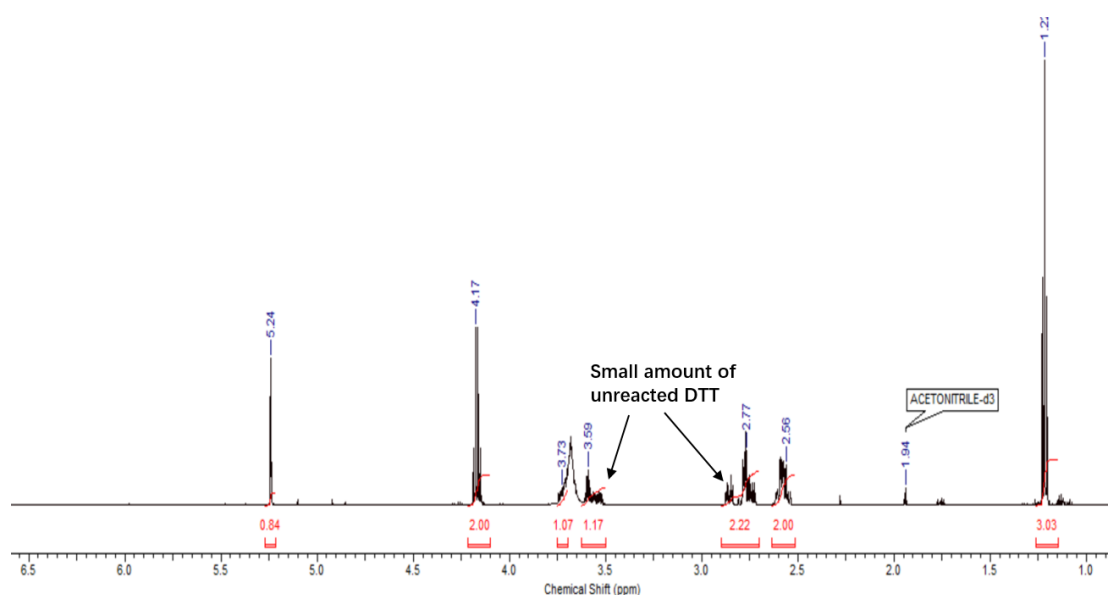


Figure A4.26. ¹H NMR spectrum of the reaction product of ethyl glyoxylate and DTT (9:1 CD₃CN:D₂O, 600 MHz). Residual unreacted DTT remains.

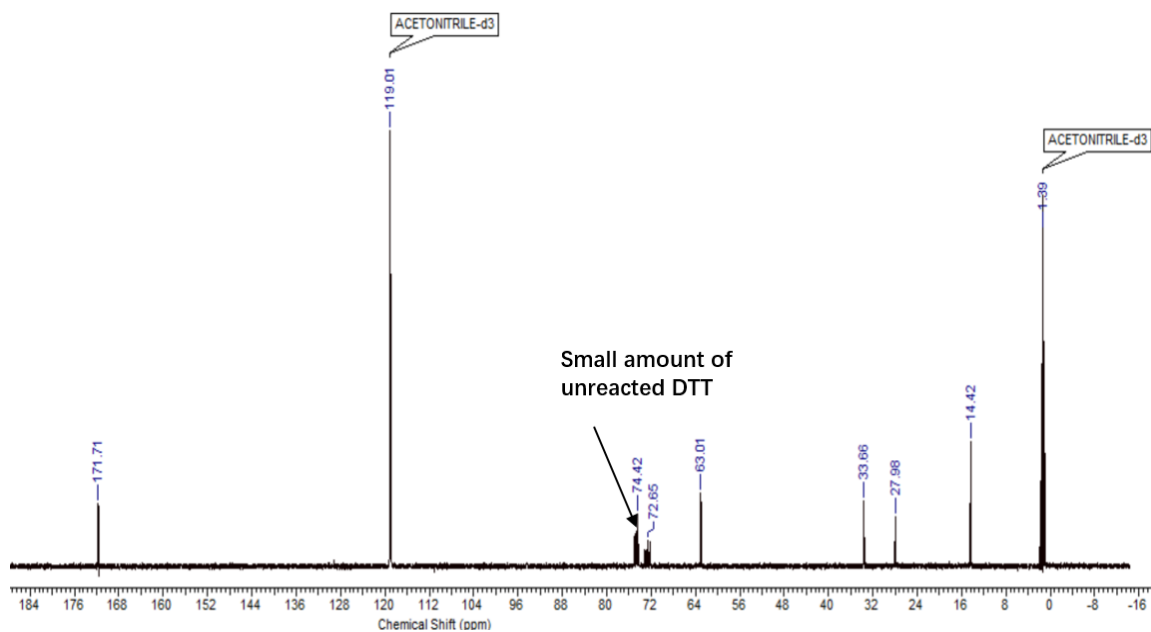


Figure A4.27. ^{13}C NMR spectrum spectrum of the reaction product of ethyl glyoxylate and DTT (9:1 $\text{CD}_3\text{CN}:\text{D}_2\text{O}$, 150 MHz). Residual unreacted DTT remains.

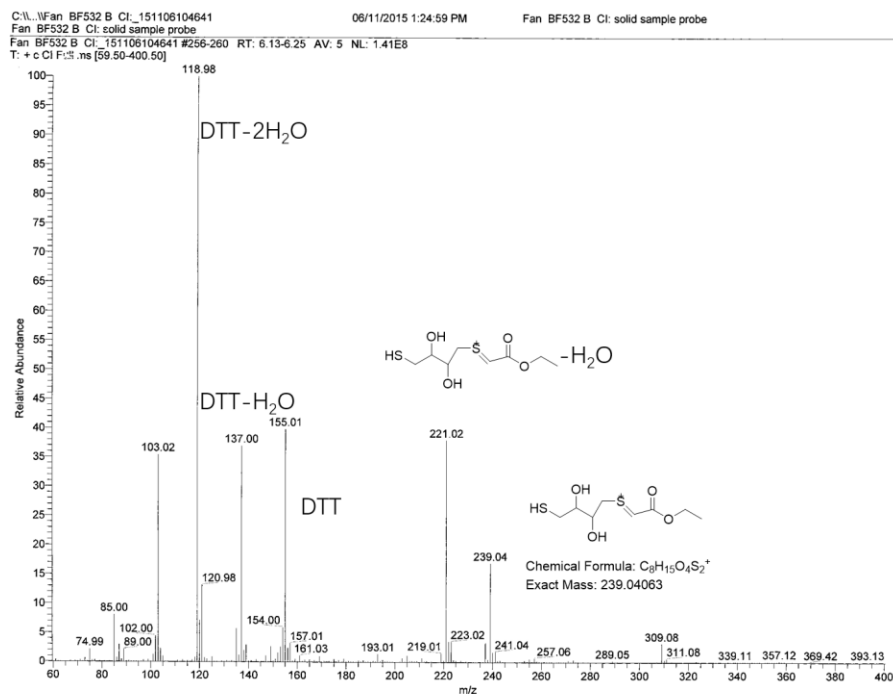


Figure A4.28. MS spectrum of the reaction product of ethyl glyoxylate and DTT.

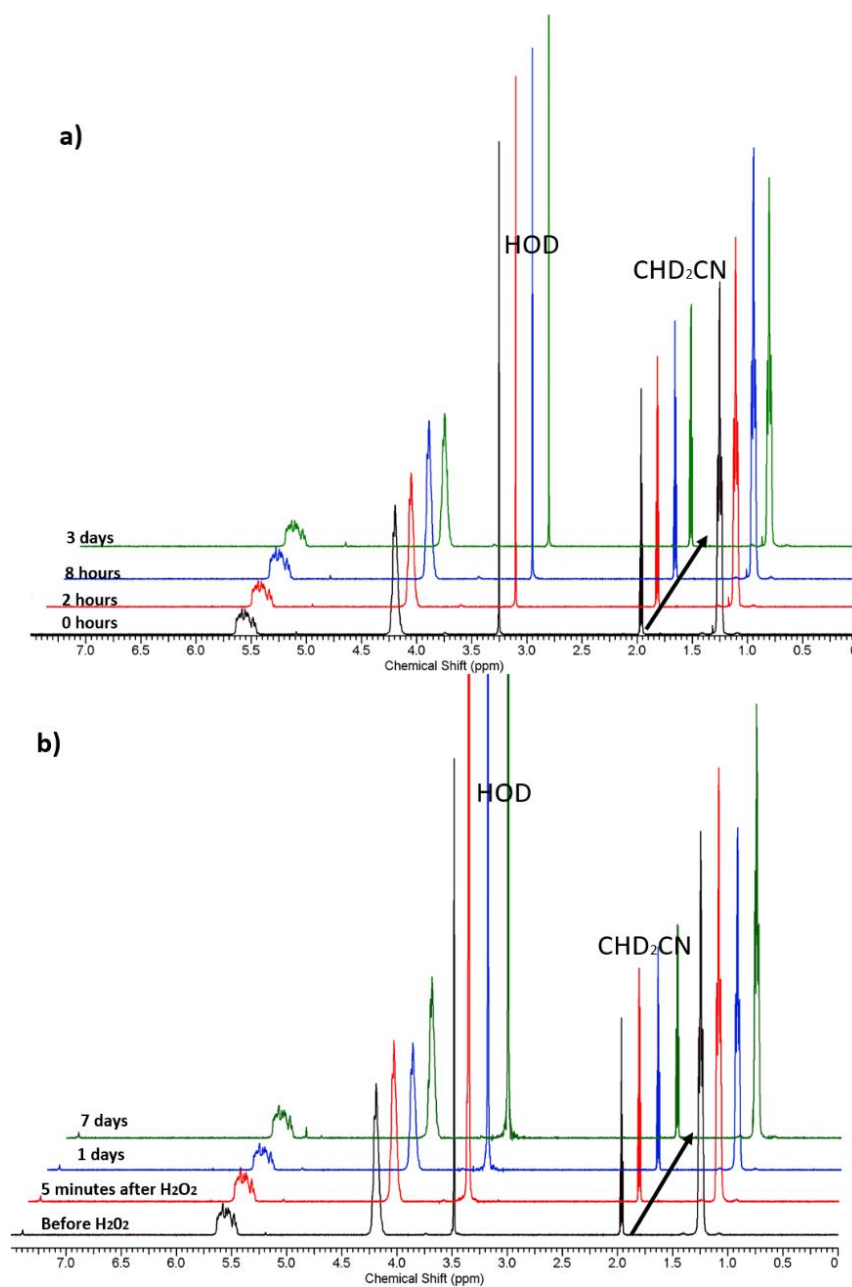


Figure A4.29. ^1H NMR spectra (400 MHz) of a) **PETG-boronate** dissolved in 9:1 $\text{CD}_3\text{CN}:\text{D}_2\text{O}$ without H_2O_2 and b) **PETG-control** dissolved in 9:1 $\text{CD}_3\text{CN}:\text{D}_2\text{O}$ with addition of H_2O_2 . Spectra are offset to allow the progression over time to be clearly observed. No changes were observed, indicating that the polymer is stable under these conditions and H_2O_2 does not cleave the polymer backbone.

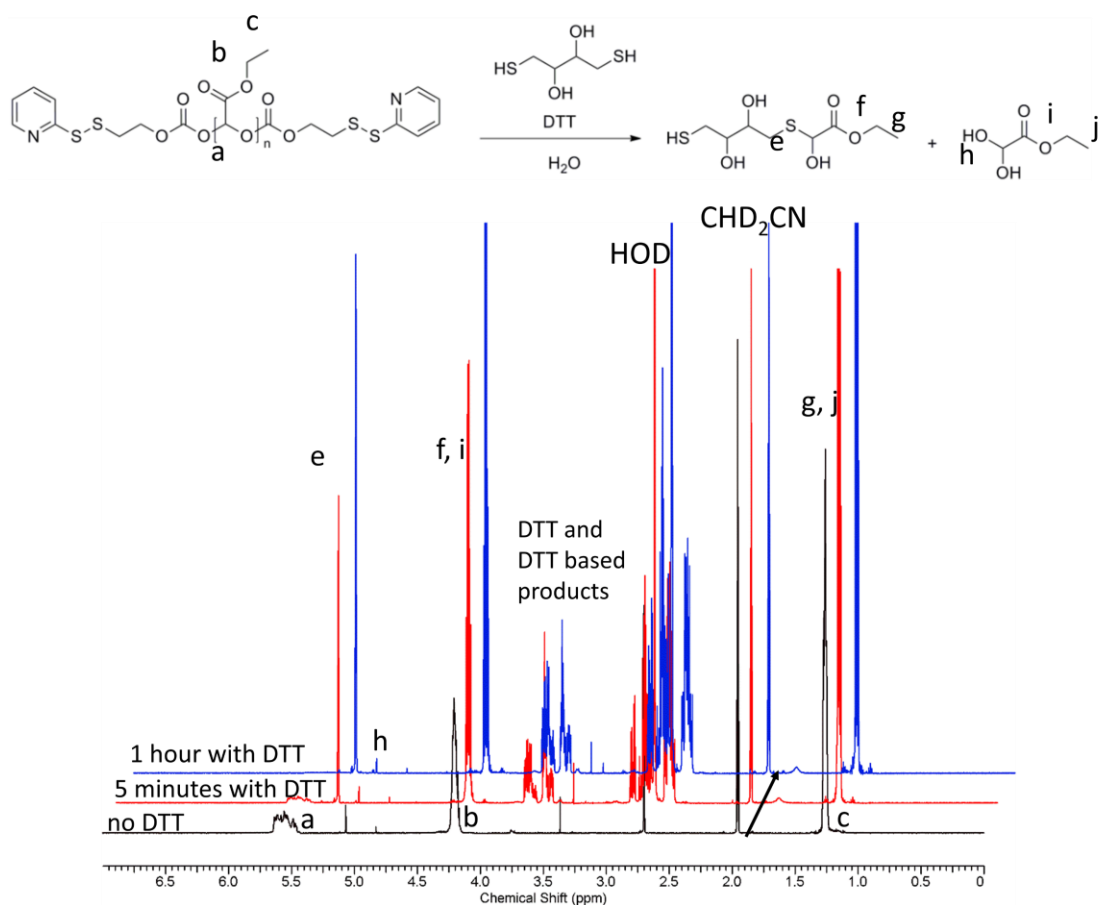


Figure A4.30. ^1H NMR spectra (400 MHz) of PETG-disulfide **a** in 9:1 $\text{CD}_3\text{CN}:\text{D}_2\text{O}$ before and after the addition of DTT. Spectra are offset to allow the progression over time to be clearly observed. Rapid disappearance of the peak at 5.5 ppm confirms rapid depolymerization and conversion into ethyl glyoxylate hydrate and the DTT adduct (see Figures A4.26-A4.28 for additional details on the adduct formation).

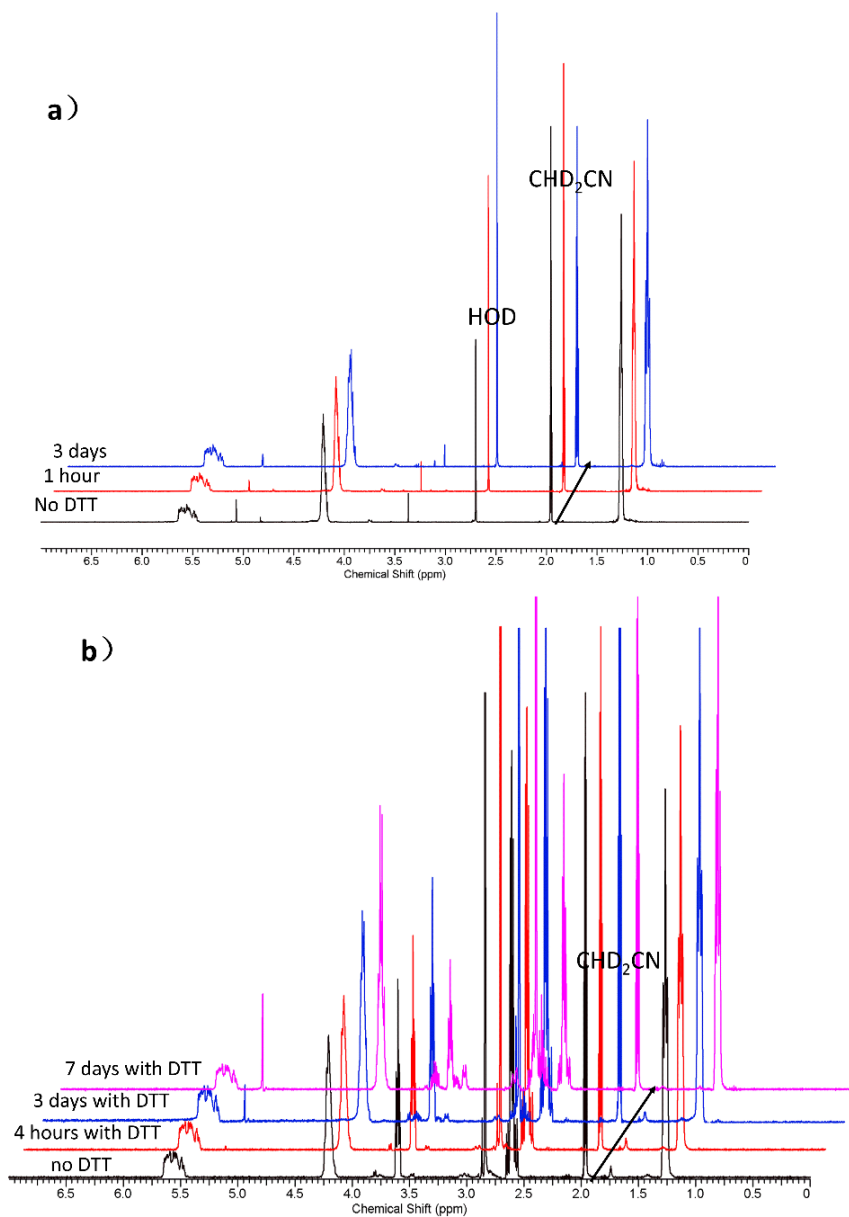


Figure A4.31. ^1H NMR spectra (400 MHz) of a) **PETG-disulfide a** dissolved in 9:1 $\text{CD}_3\text{CN}:\text{D}_2\text{O}$ without DTT and b) **PETG-control** dissolved in 9:1 $\text{CD}_3\text{CN}:\text{D}_2\text{O}$ with DTT added. Spectra are offset to allow the progression over time to be clearly observed. Very minimal changes in the peak at 5.5 ppm were observed, indicating that the polymers are quite stable under these conditions.

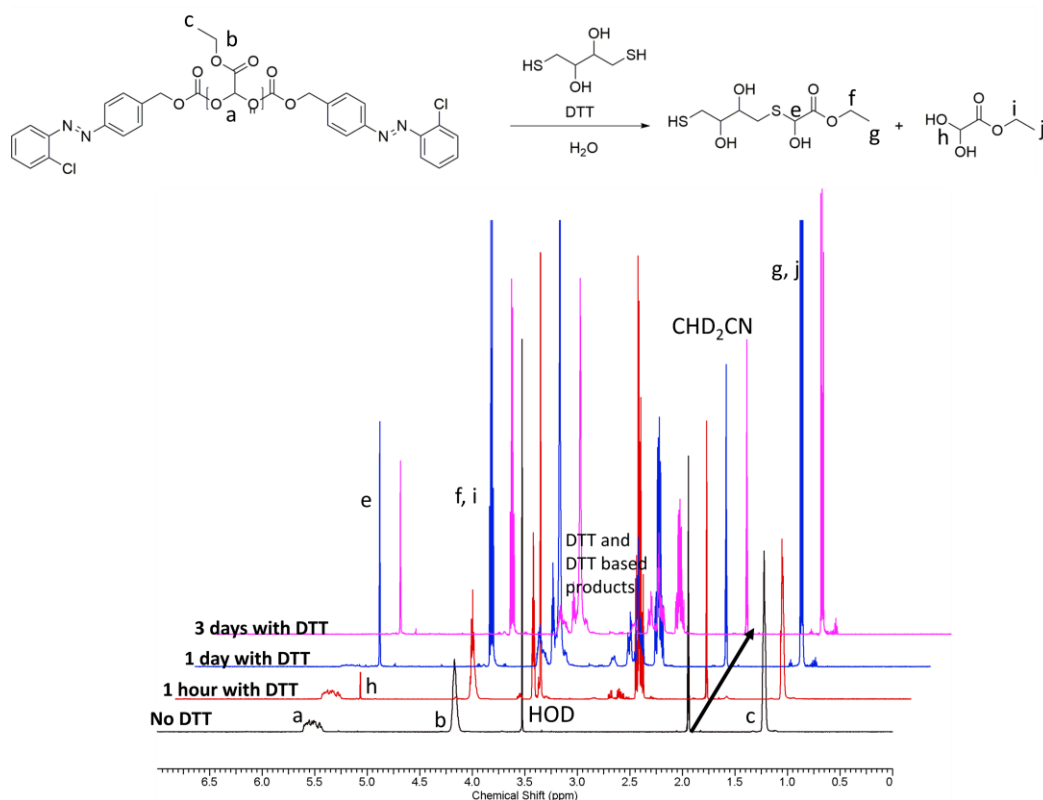


Figure A4.32. ¹H NMR spectra (600 MHz) of PEtG-azobenzene in 9:1 CD₃CN:D₂O before and after the addition of DTT. Spectra are offset to allow the progression over time to be clearly observed. Disappearance of the peak at 5.5 ppm confirms depolymerization and conversion into ethyl glyoxylate hydrate and the DTT adduct (see Figures A4.26- A4.28 for additional details on the adduct formation).

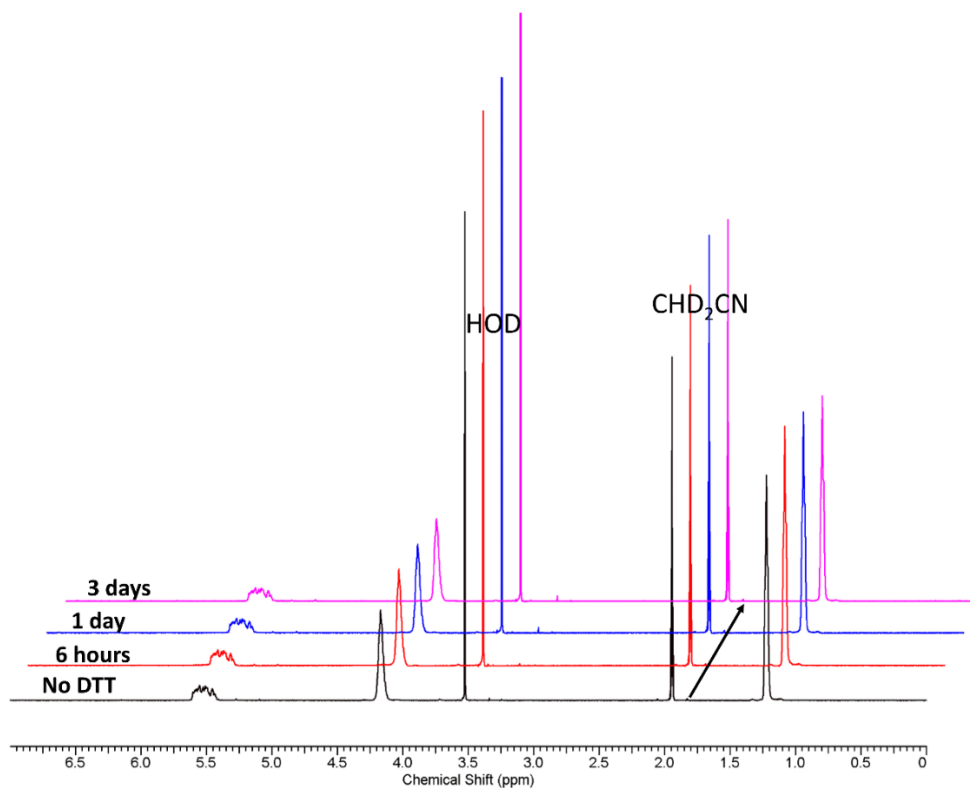


Figure A4.33. ^1H NMR spectra (600 MHz) of PEtG-azobenzene in 9:1 $\text{CD}_3\text{CN}:\text{D}_2\text{O}$ without the addition of DTT. Spectra are offset to allow the progression over time to be clearly observed. No changes were observed, indicating that the polymer is stable under these conditions.

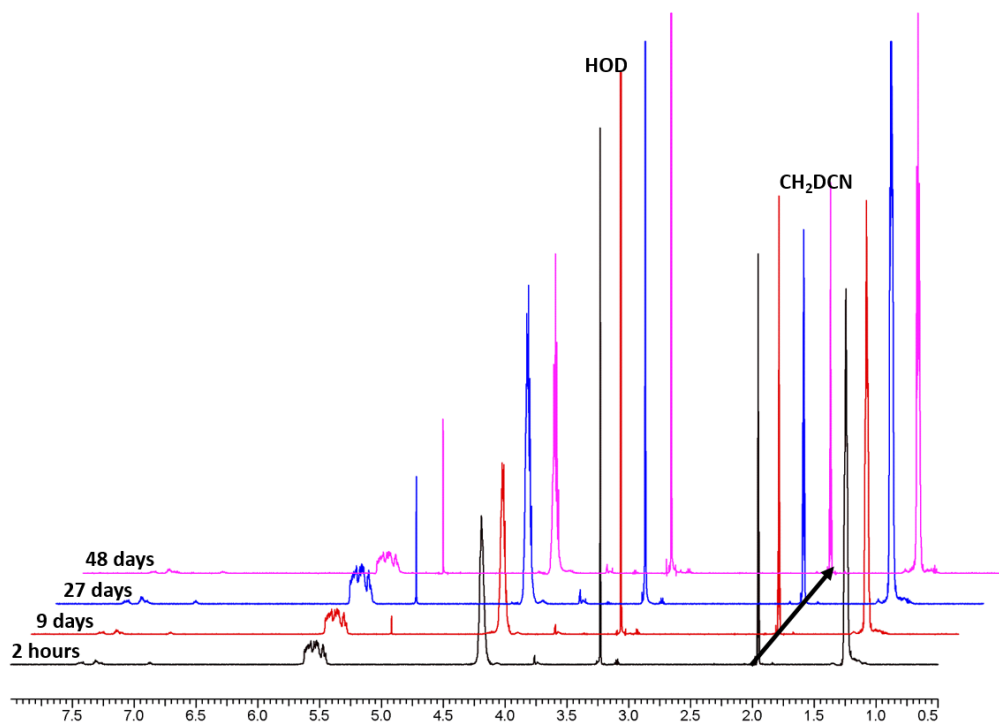


Figure A4.34. ¹H NMR spectra (600 MHz) of PETg-MMT in 9:1 CD₃CN:D₂O without the addition of acetic acid. Spectra are offset to allow the progression over time to be clearly observed. The gradual conversion of the broad peak at 5.5 ppm to a sharp peak at 5.1 ppm corresponding to ethyl glyoxylate hydrate indicates very slow depolymerization of the polymer under these conditions.

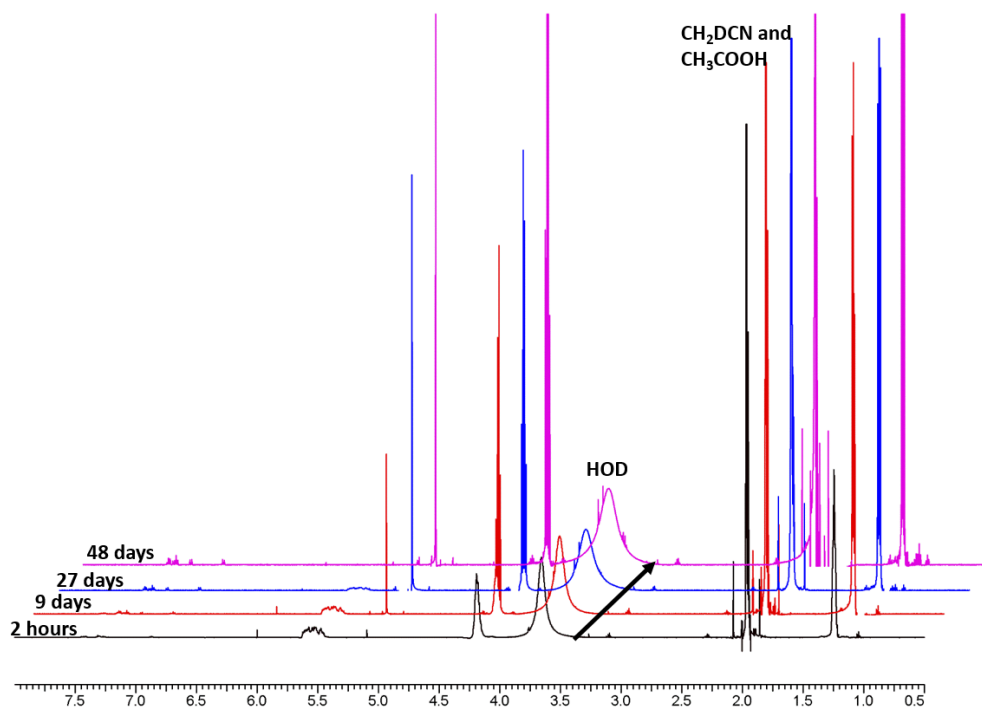


Figure A4.35. ¹H NMR spectra (600 MHz) of PEtG-MMT in 9:1 CD₃CN:D₂O with 510 mM acetic acid added. Spectra are offset to allow the progression over time to be clearly observed. Conversion of the broad peak at 5.5 ppm to a sharp peak at 5.1 ppm corresponding to ethyl glyoxylate hydrate indicates complete depolymerization of the polymer under these conditions.

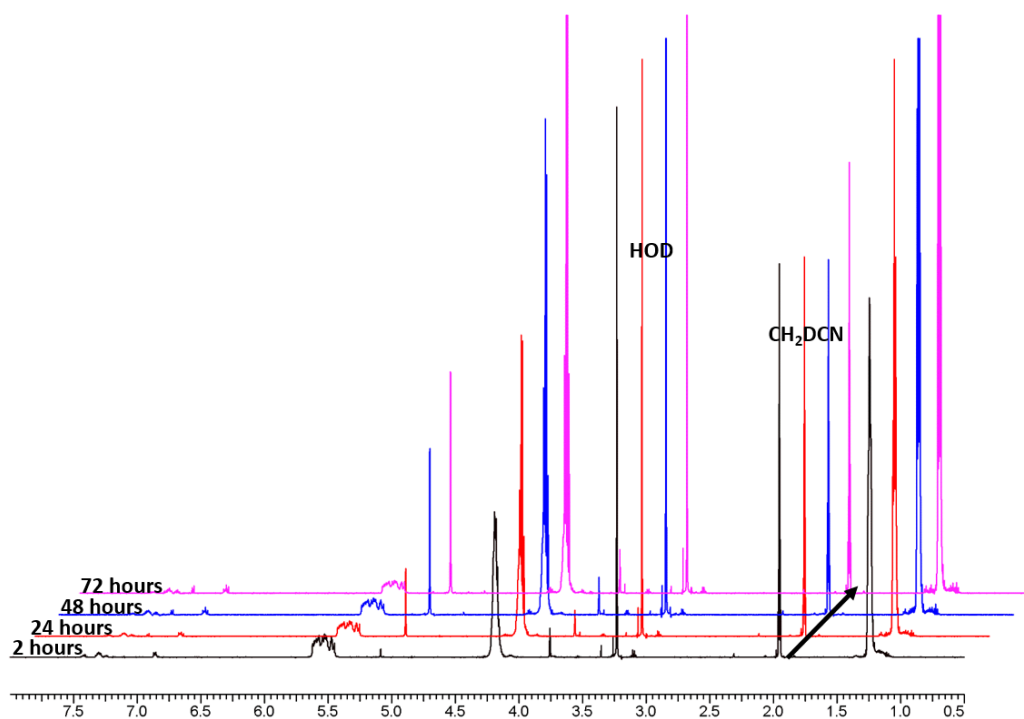


Figure A4.36. ¹H NMR spectra (600 MHz) of **PEtG-DMT** in 9:1 CD₃CN:D₂O without the addition of acetic acid. Spectra are offset to allow the progression over time to be clearly observed. The gradual conversion of the broad peak at 5.5 ppm to a sharp peak at 5.1 ppm corresponding to ethyl glyoxylate hydrate indicates slow depolymerization of the polymer under these conditions.

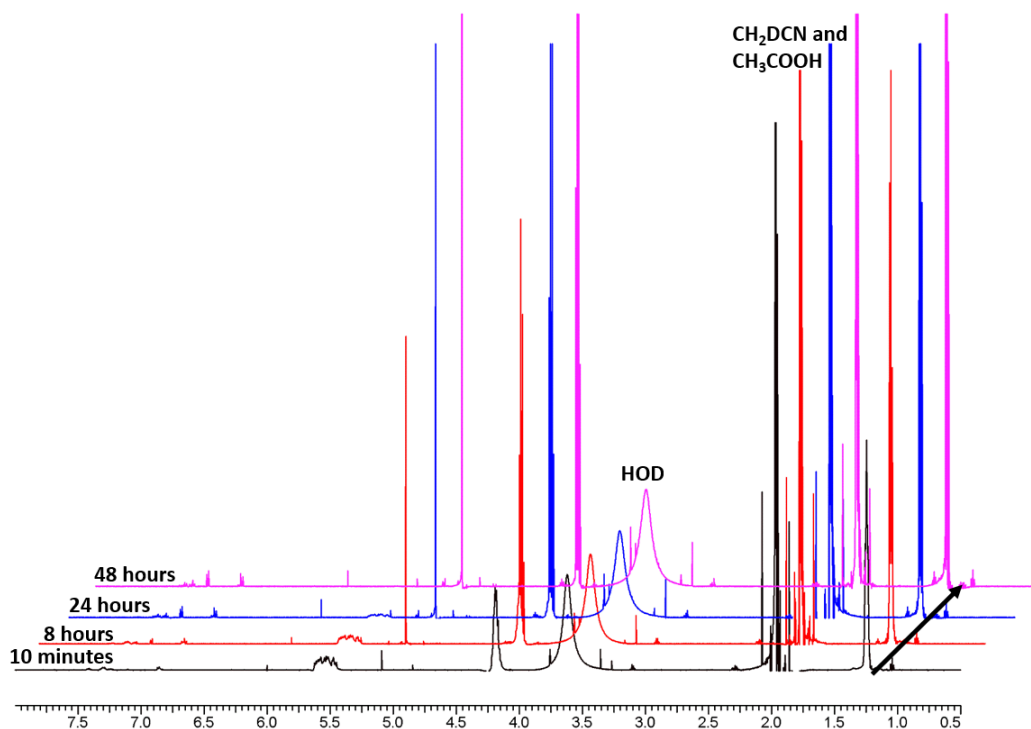


Figure A4.37. ¹H NMR spectra (600 MHz) of **PETG-DMT** in 9:1 CD₃CN:D₂O with 510 mM acetic acid added. Spectra are offset to allow the progression over time to be clearly observed. Conversion of the broad peak at 5.5 ppm to a sharp peak at 5.1 ppm corresponding to ethyl glyoxylate hydrate indicates complete depolymerization of the polymer under these conditions.

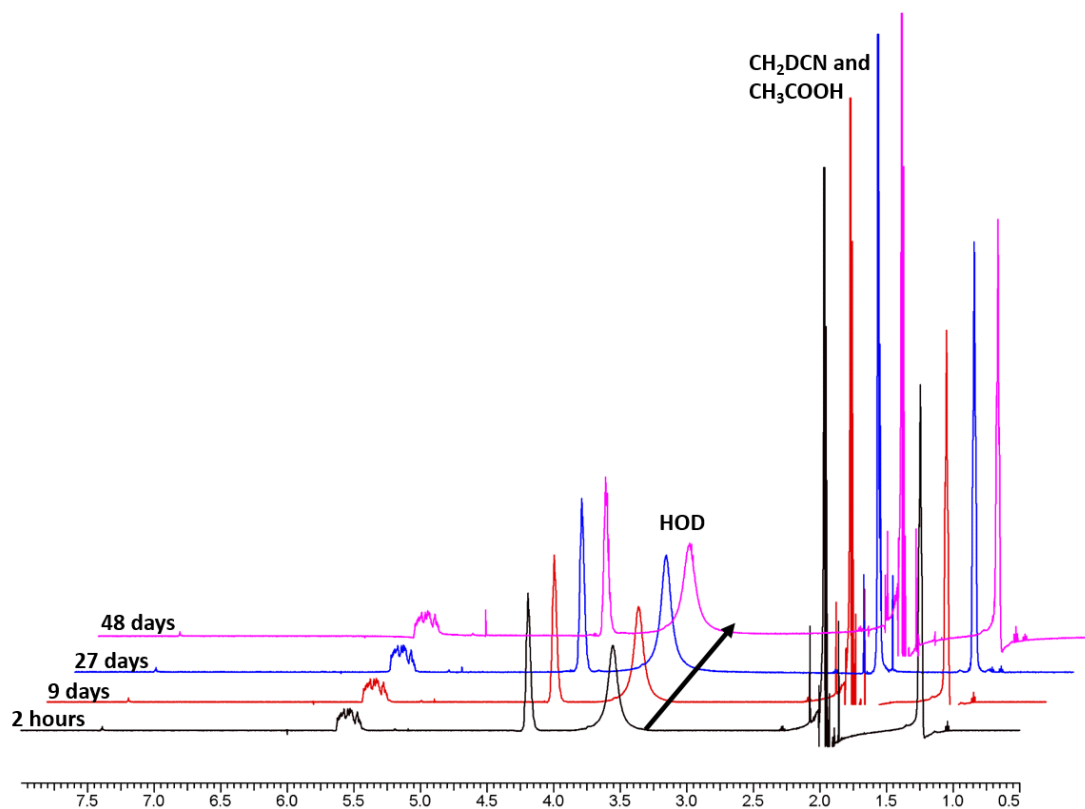


Figure A4.38. ¹H NMR spectra (600 MHz) of PEtG-control in 9:1 CD₃CN:D₂O with 510 mM acetic acid added. Spectra are offset to allow the progression over time to be clearly observed. Only very minimal conversion of the broad peak at 5.5 ppm to a sharp peak at 5.1 ppm corresponding to ethyl glyoxylate hydrate was observed, confirming that the polymer was quite stable under these conditions.

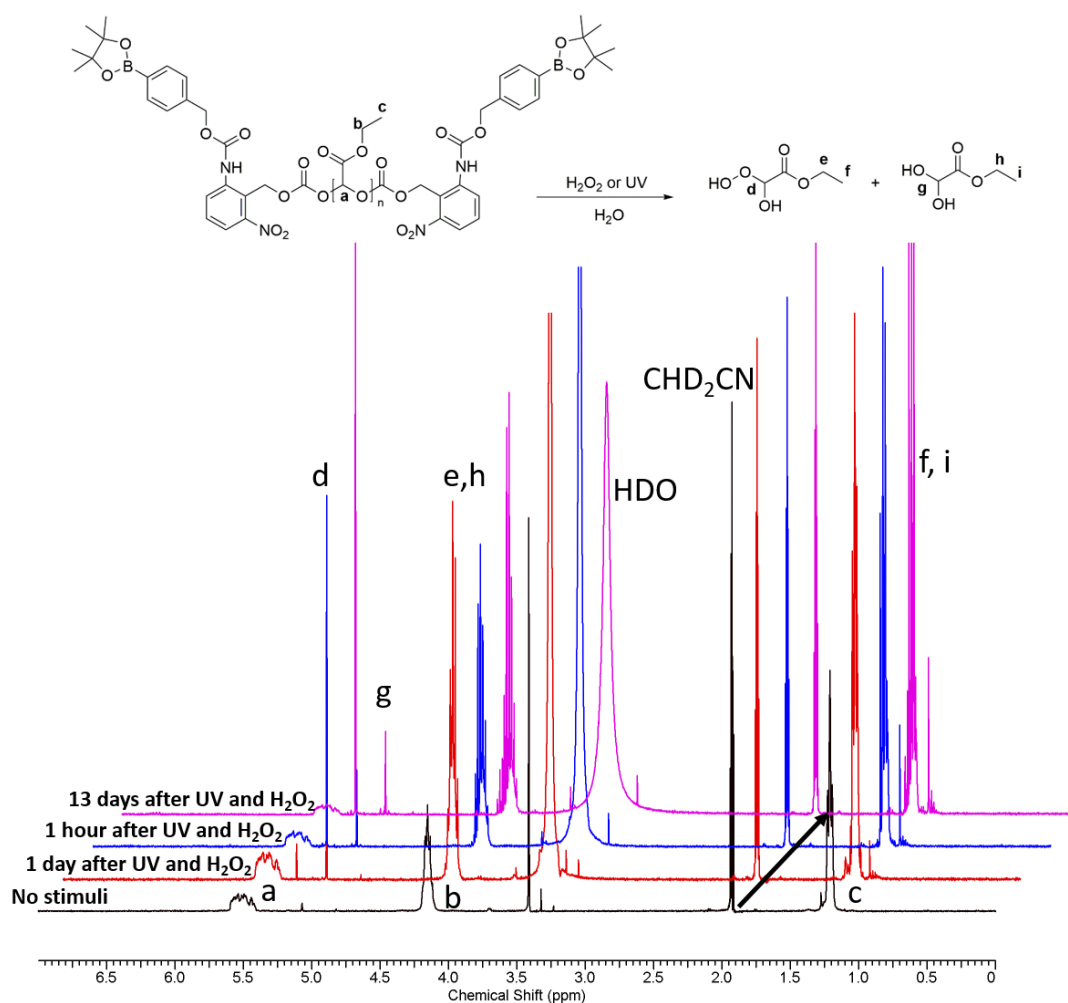


Figure A4.39. ¹H NMR spectra (400 MHz) of PETg-multi in 9:1 CD₃CN:D₂O with both UV irradiation and H₂O₂ added. Spectra are offset to allow the progression over time to be clearly observed. Conversion of the broad peak at 5.5 ppm to sharp peaks at 5.1 and 5.3 ppm confirms depolymerization to ethyl glyoxylate hydrate and the peroxy hydrate (for more details on the formation of the peroxy hydrate, please refer to Figures A4.23-A4.25).

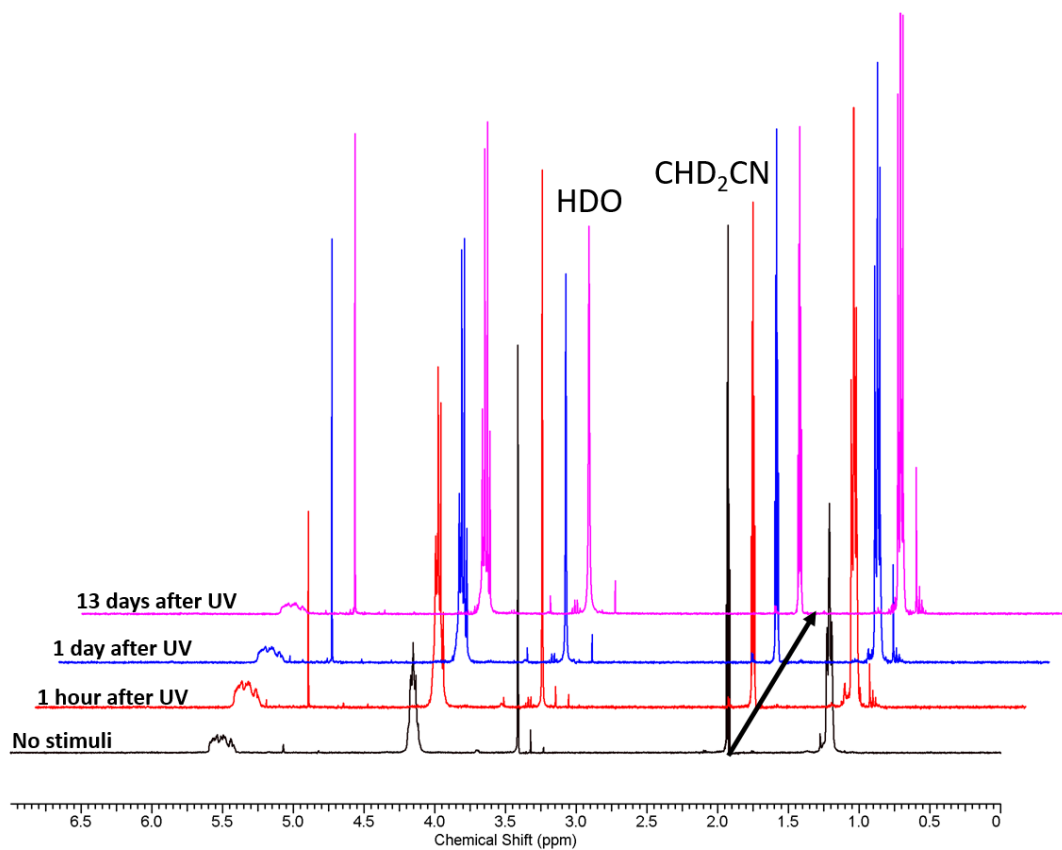


Figure A4.40. ¹H NMR spectra (400 MHz) of **PETG-multi** in 9:1 CD₃CN:D₂O with UV irradiation only. Spectra are offset to allow the progression over time to be clearly observed. Conversion of the broad peak at 5.5 ppm to a sharp peak at 5.1 ppm confirms depolymerization to ethyl glyoxylate hydrate.

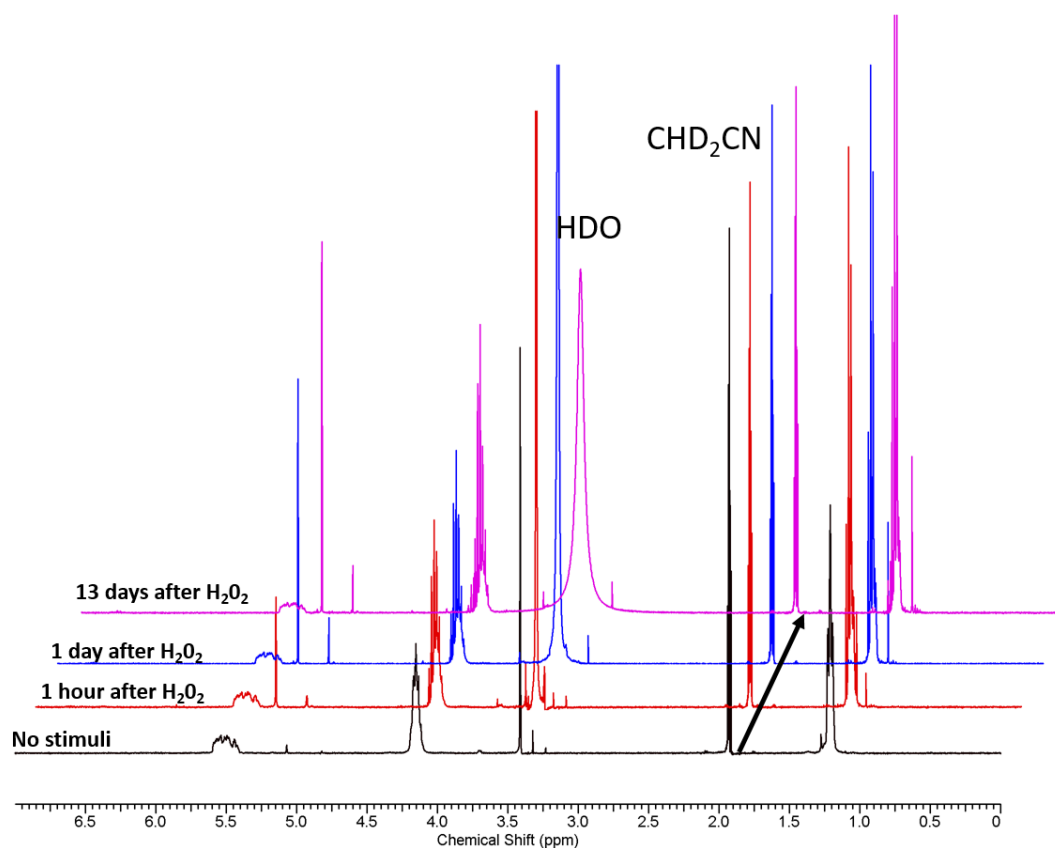


Figure A4.41. ^1H NMR spectra (400 MHz) of **PETG-multi** in 9:1 $\text{CD}_3\text{CN}:\text{D}_2\text{O}$ with H_2O_2 addition only. Spectra are offset to allow the progression over time to be clearly observed. Conversion of the broad peak at 5.5 ppm to sharp peaks at 5.1 and 5.3 ppm confirms depolymerization to ethyl glyoxylate hydrate and the peroxy hydrate (for more details on the formation of the peroxy hydrate, please refer to Figures A4.23-A4.25).

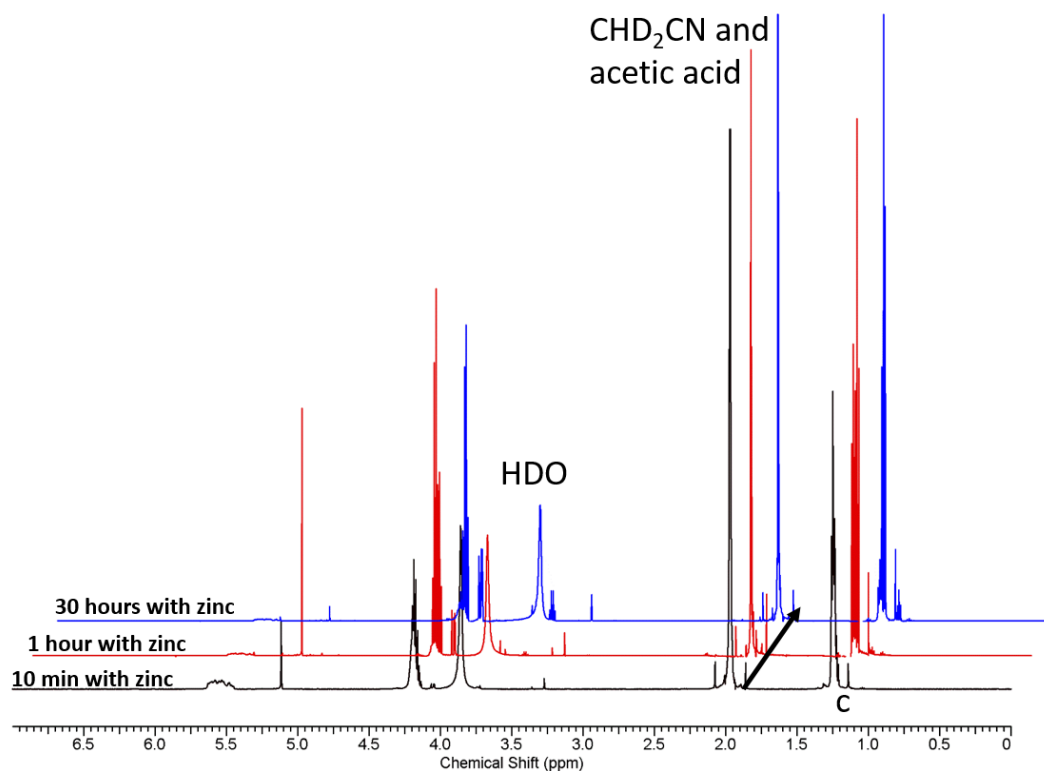


Figure A4.42. ¹H NMR spectra (600 MHz) of **PEtG-multi** in 9:1 CD₃CN:D₂O with Zn/acetic acid added. Spectra are offset to allow the progression over time to be clearly observed. Conversion of the broad peak at 5.5 ppm to a sharp peak at 5.1 confirms depolymerization to ethyl glyoxylate hydrate.

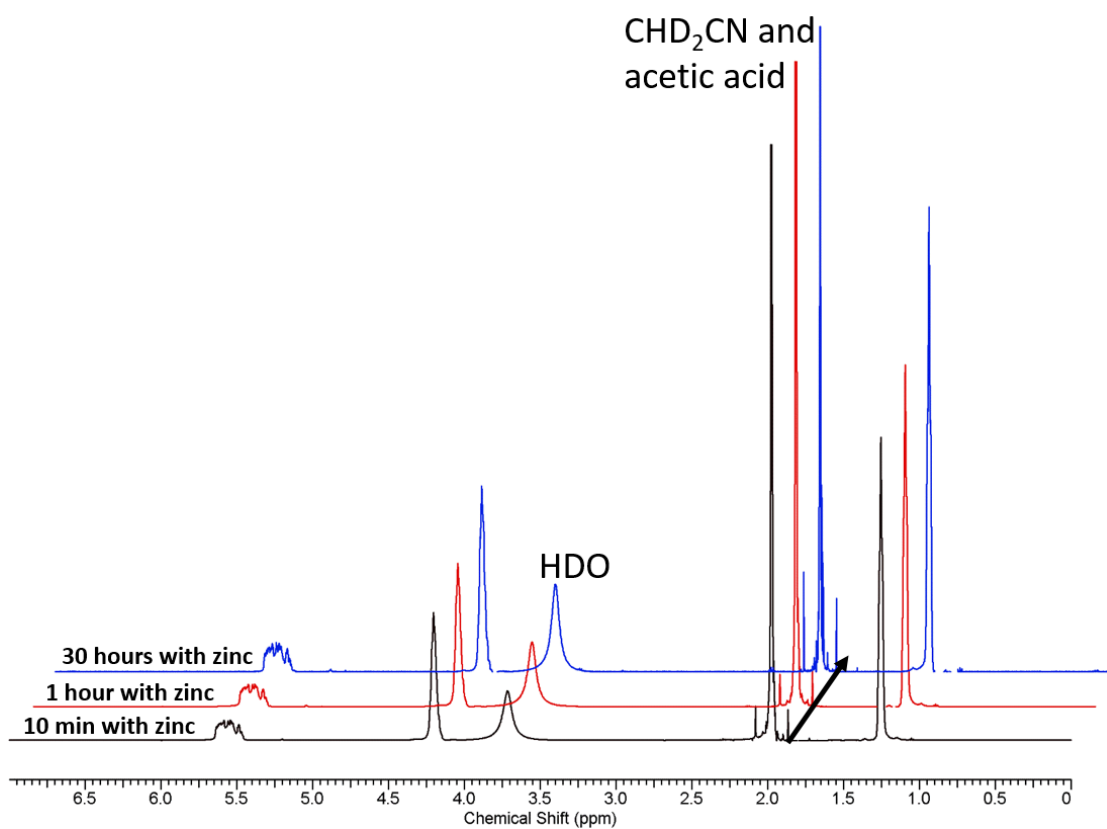


Figure A4.43. ¹H NMR spectra (600 MHz) of PEtG-control in 9:1 CD₃CN:D₂O with Zn/acetic acid added. Spectra are offset to allow the progression over time to be clearly observed. No changes in the spectra were observed, confirming that the polymer was stable under these conditions.

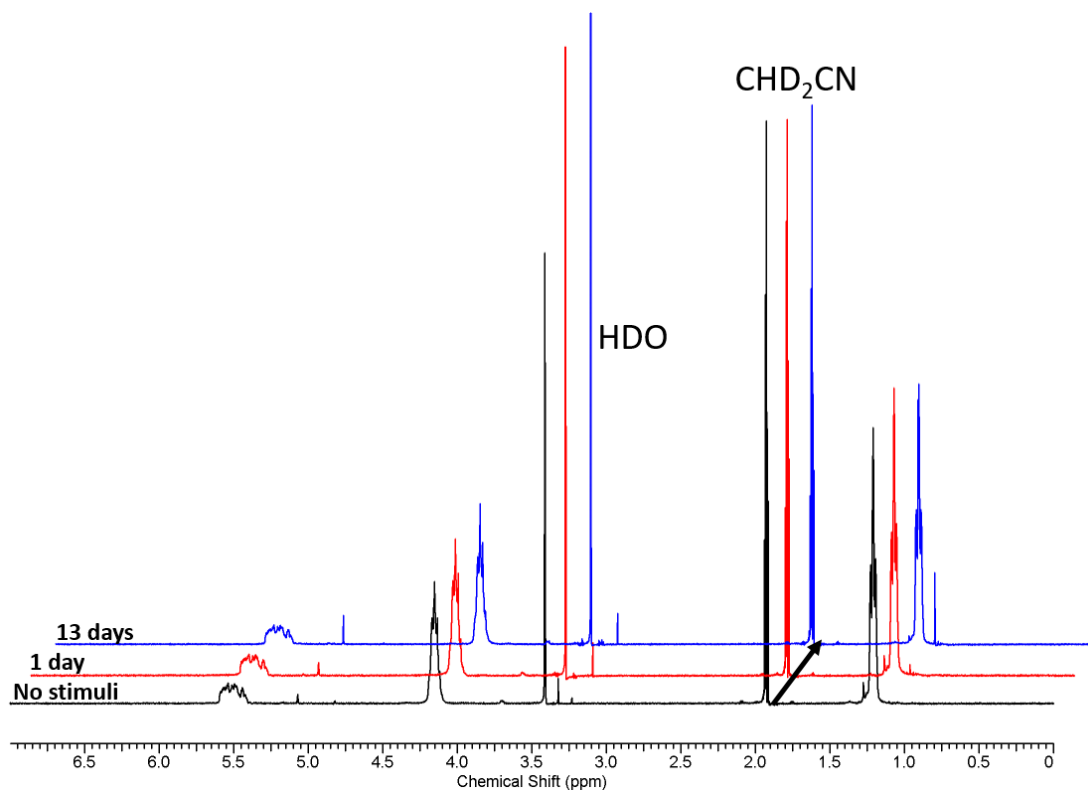


Figure A4.44. ¹H NMR spectra (400 MHz) of PEtG-multi in 9:1 CD₃CN:D₂O without stimuli. Spectra are offset to allow the progression over time to be clearly observed. Only very minimal conversion of the broad peak at 5.5 ppm to a sharp peak at 5.1 ppm corresponding to ethyl glyoxylate hydrate was observed, confirming that the polymer was quite stable under these conditions.

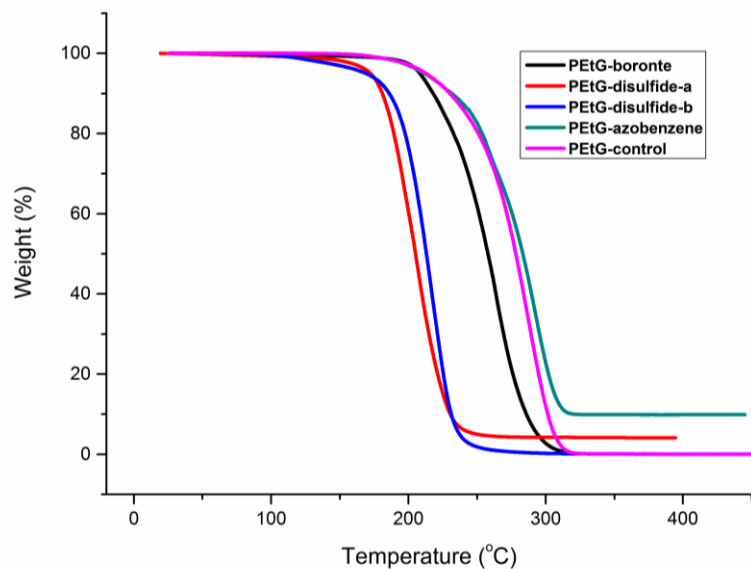


Figure A4.45. TGA curves of **PEtG-boronate**, **PEtG-disulfide**, **PEtG-azobenzene** **PEtG-control**.

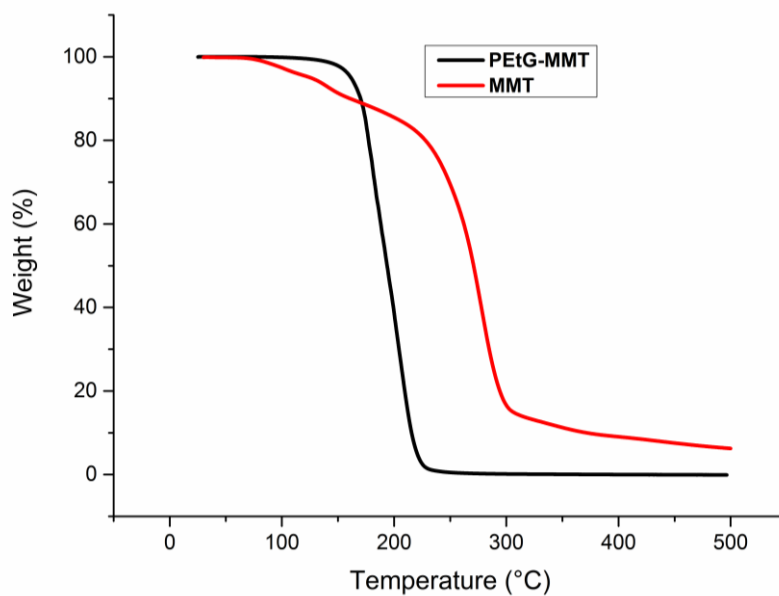


Figure A4.46. TGA curves of **PEtG-MMT** and the corresponding end-cap **MMT**.

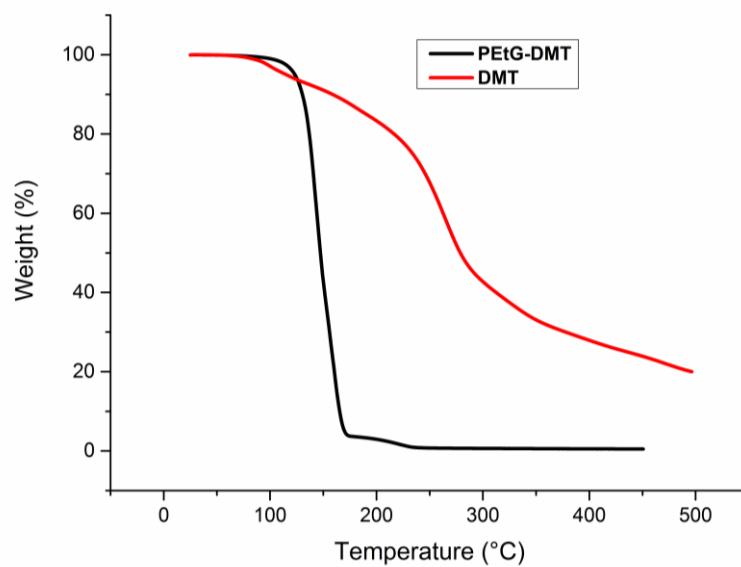


Figure A4.47. TGA curves of **PEtG-DMT** and its end-cap **DMT**.

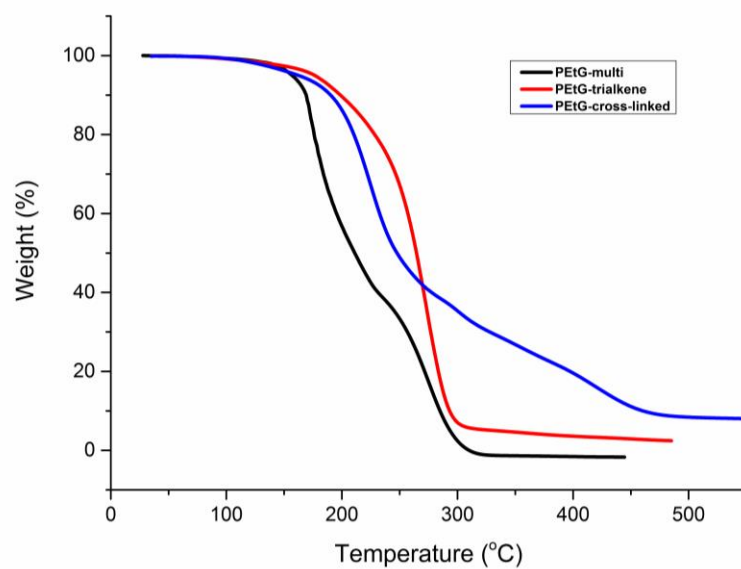


Figure A4.48. TGA curves of **PEtG-multi**, **PEtG-alkene**, **PEtG-cross-linked**.

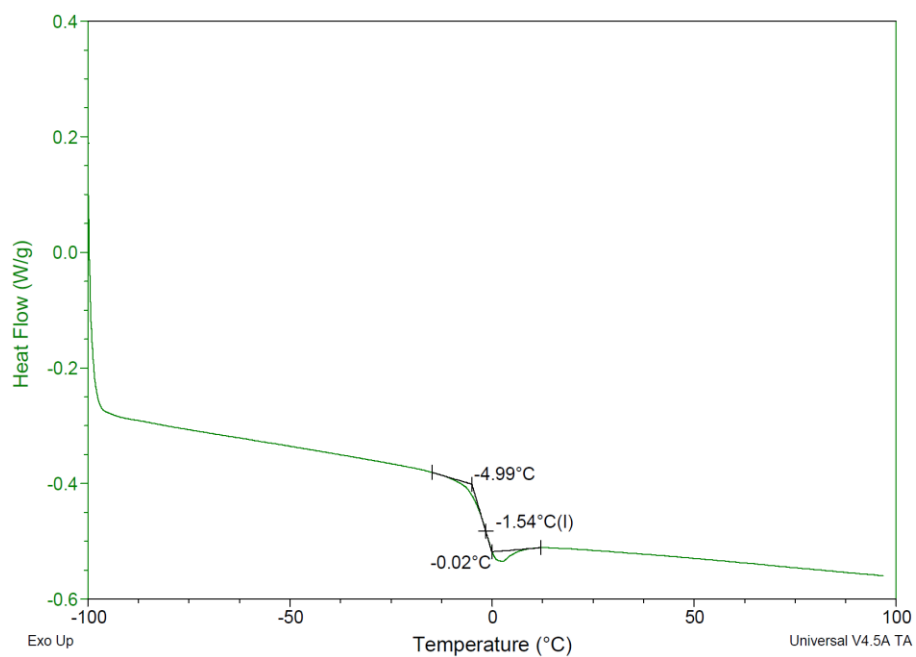


Figure A4.49. DSC curve of **PEtG-azobenzene**.

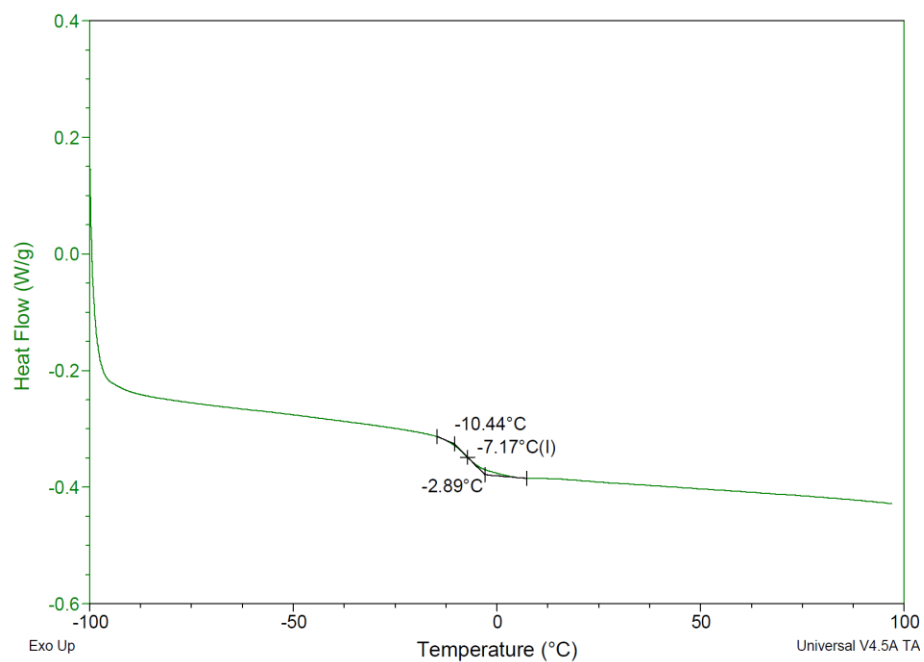


Figure A4.50. DSC curve of **PEtG-trialkene**.

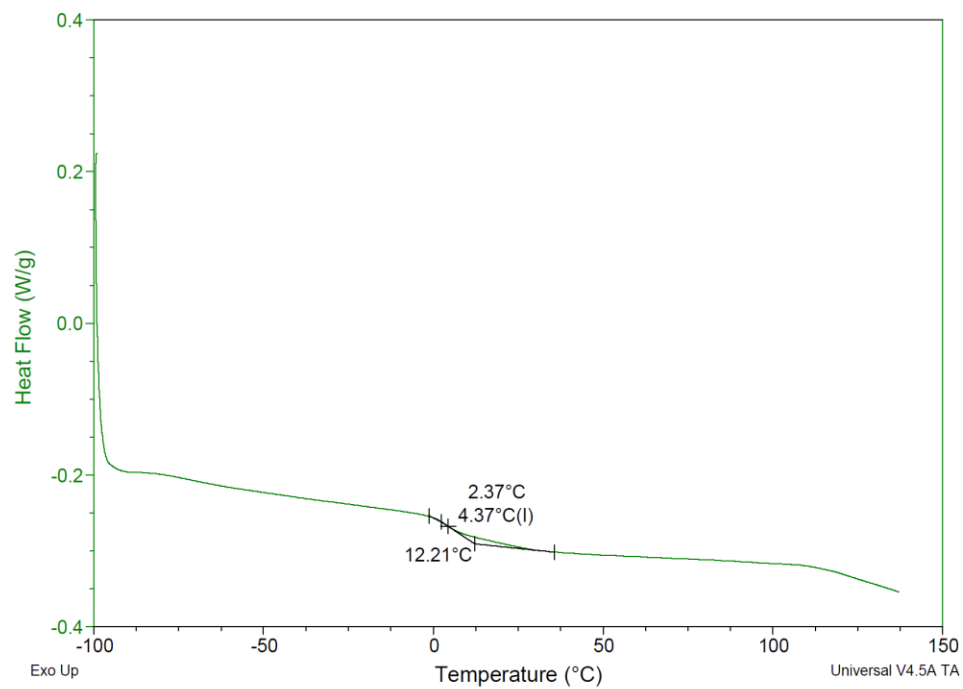


Figure A4.51. DSC curve of **PEtG-cross-linked**.

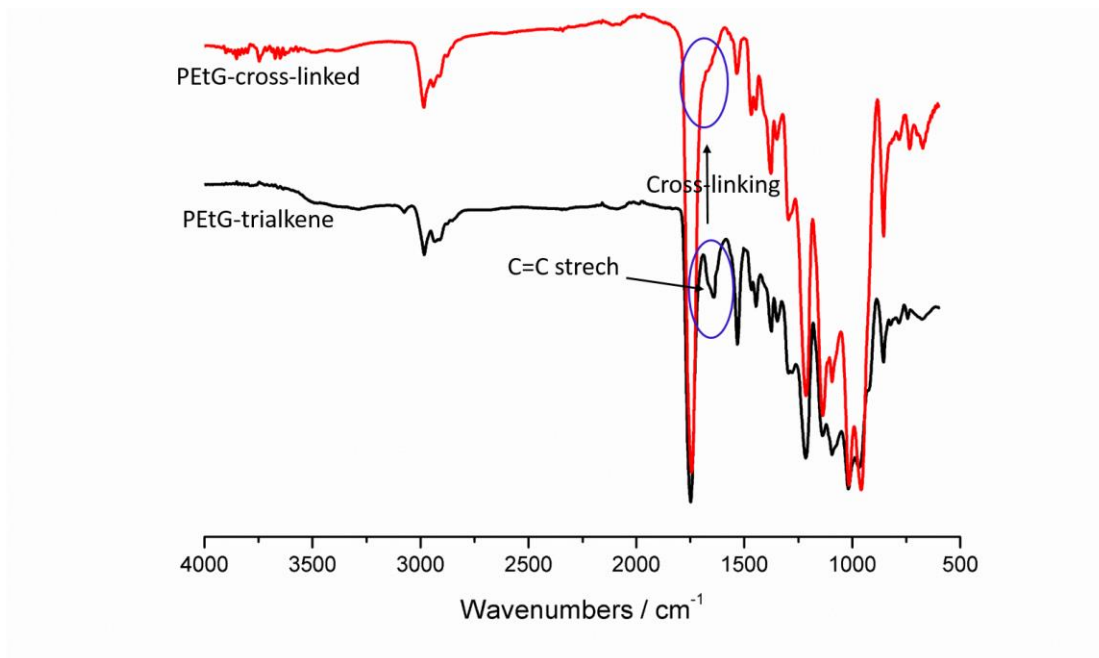
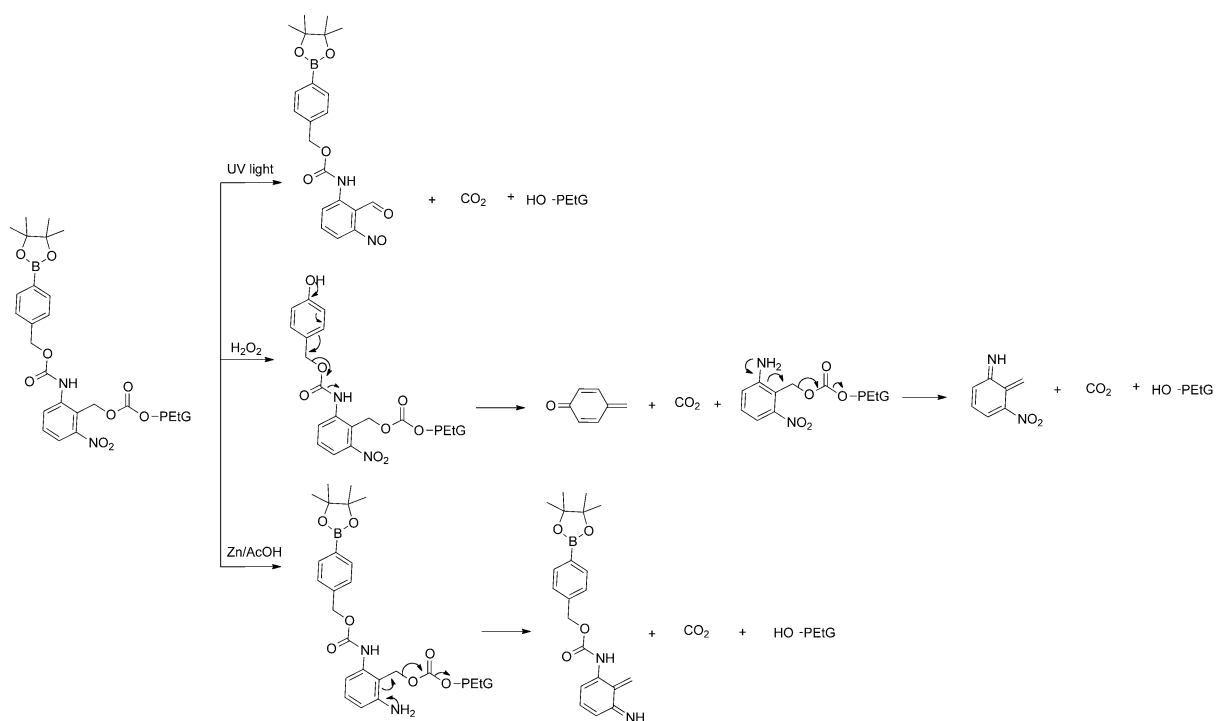
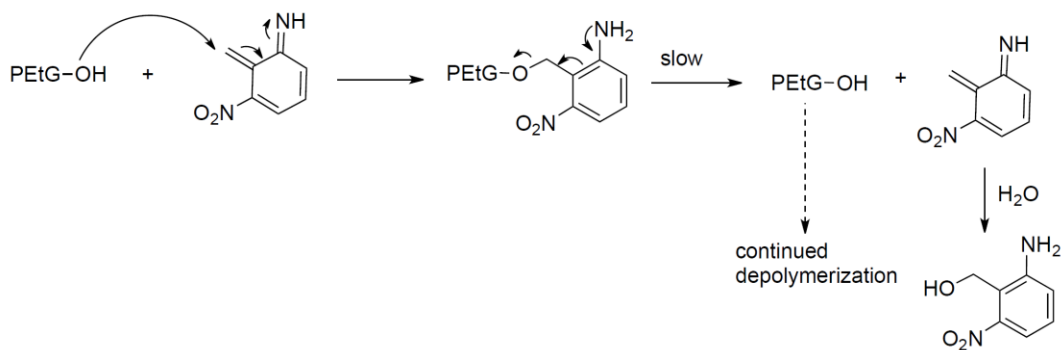


Figure A4.52. FT-IR spectra of **PEtG-trialkene** and **PEtG-cross-linked**, showing disappearance of the peak at 1660 cm^{-1} corresponding to the C=C stretch following cross-linking.



Scheme A4.1. Proposed mechanisms of decomposition of the multi-responsive end-cap **11** in response to different stimuli.



Scheme A4.2. Example of a possible trapping of depolymerizing PEtG by an azaquinone methide to generate a benzyl ether that subsequently undergoes slow elimination to continue depolymerization.

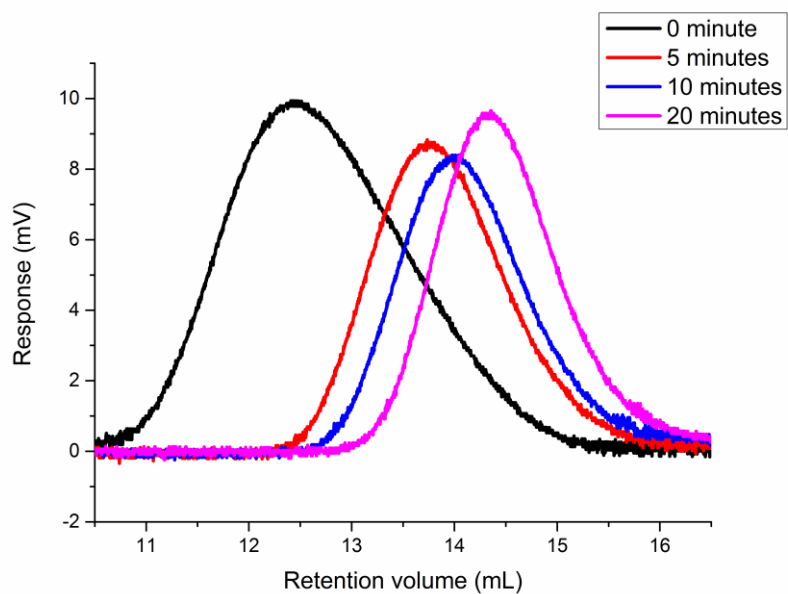


Figure A4.53. SEC traces (RI detection) for PEtG-disulfide-a following different sonication times in the presence of the trapping agent TBDMS-Cl.

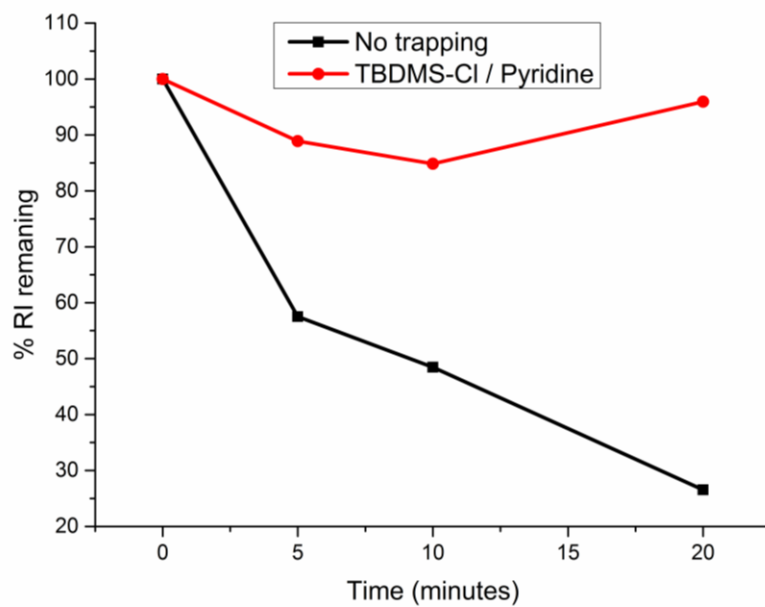
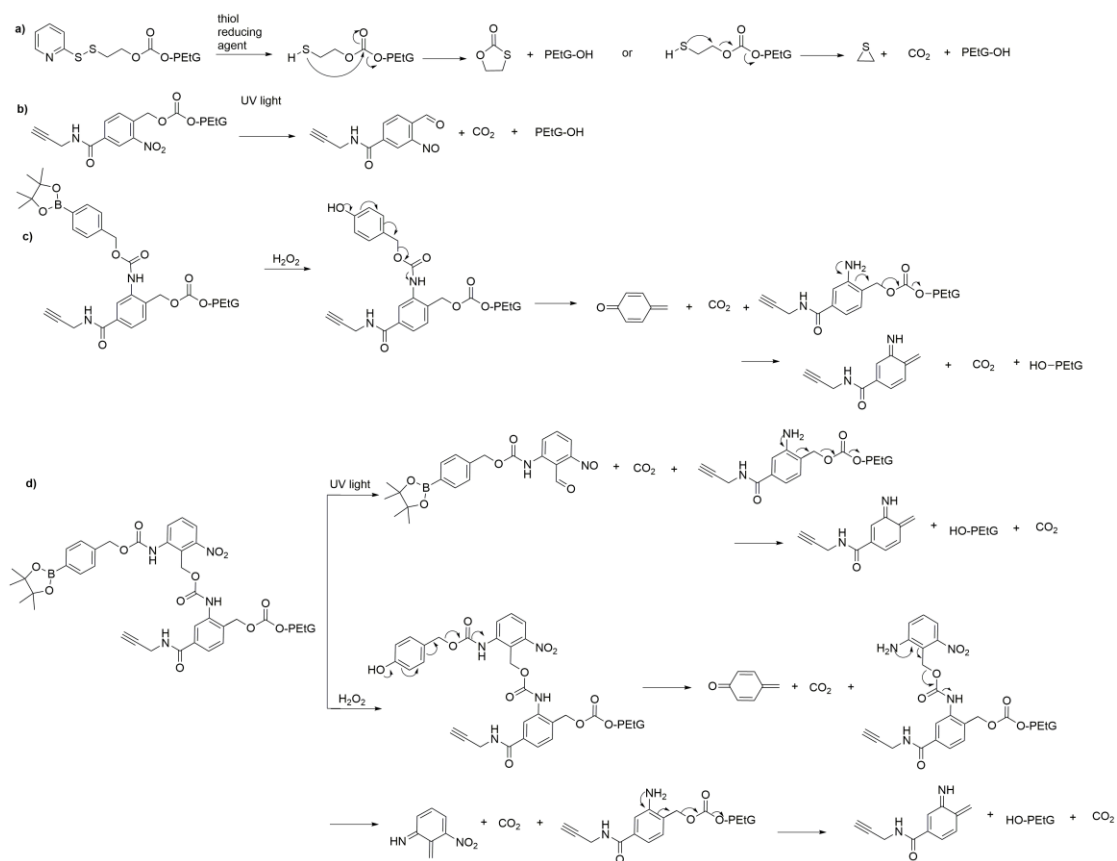


Figure A4.54. Percent initial SEC refractive index (RI) signal remaining for PEtG-disulfide-a following different sonication times in the presence of the trapping agent TBDMS-Cl.

Appendix 5: Supporting information for Chapter 5



Scheme A5.1. Degradation mechanisms of different end-caps in respond to stimuli.

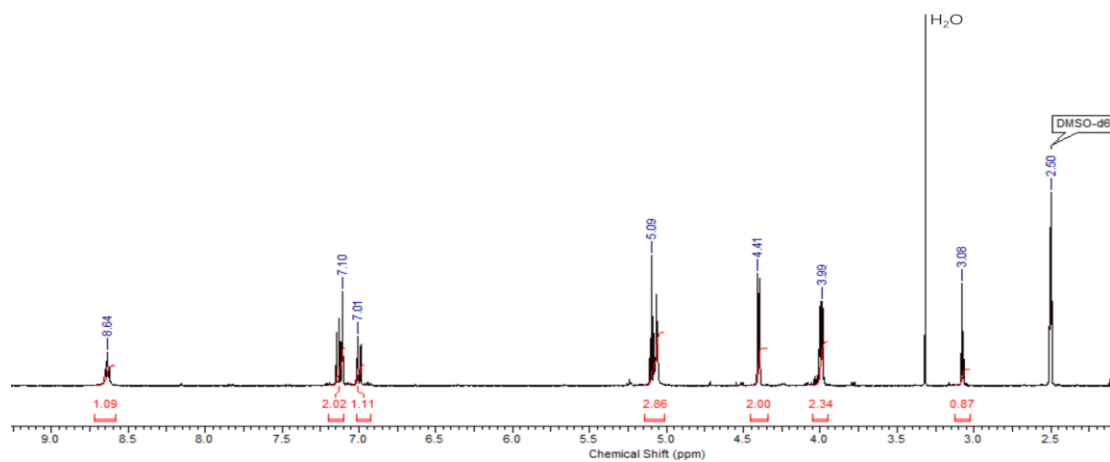


Figure A5.1. ^1H NMR spectrum of compound **6** ($\text{DMSO-}d_6$, 400 MHz).

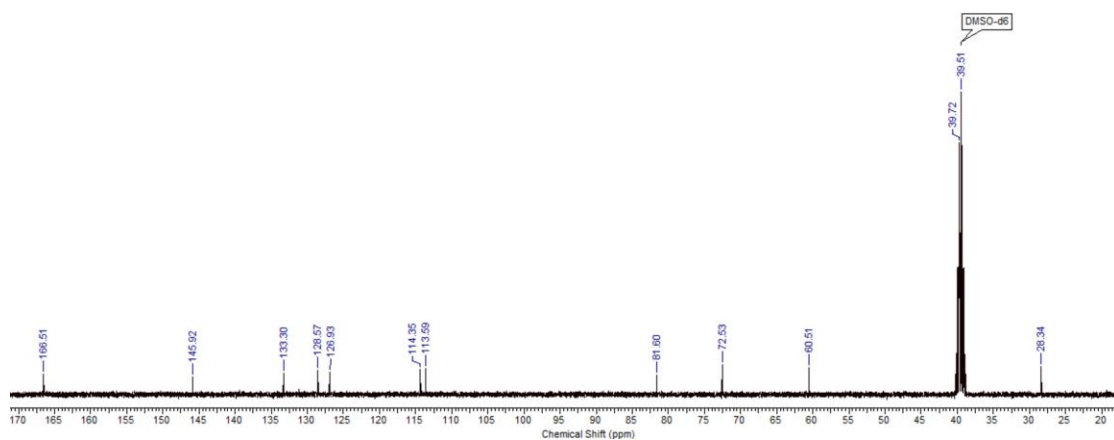


Figure A5.2. ^{13}C NMR spectrum of compound **6** ($\text{DMSO-}d_6$, 150 MHz).

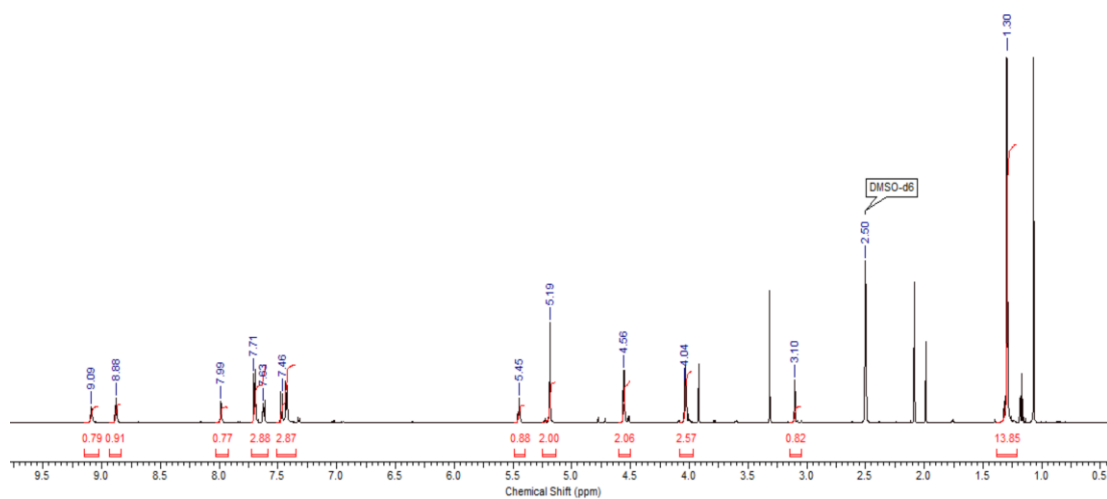


Figure A5.3. ^1H NMR spectrum of compound **8** ($\text{DMSO-}d_6$, 400 MHz) (trace acetone and ethyl acetate present).

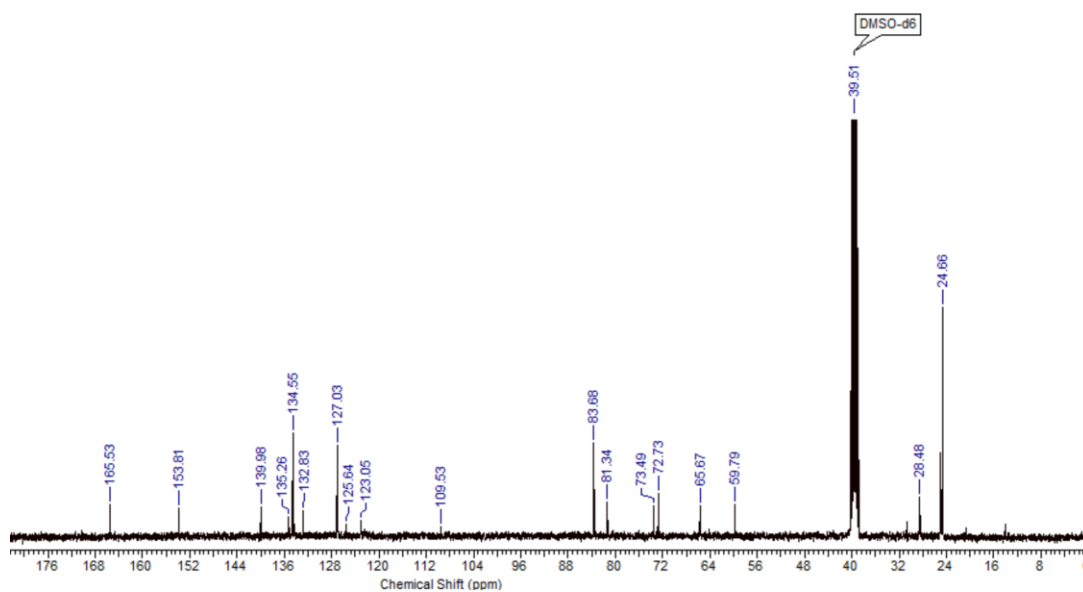


Figure A5.4. ^{13}C NMR spectrum of compound **8** ($\text{DMSO-}d_6$, 150 MHz).

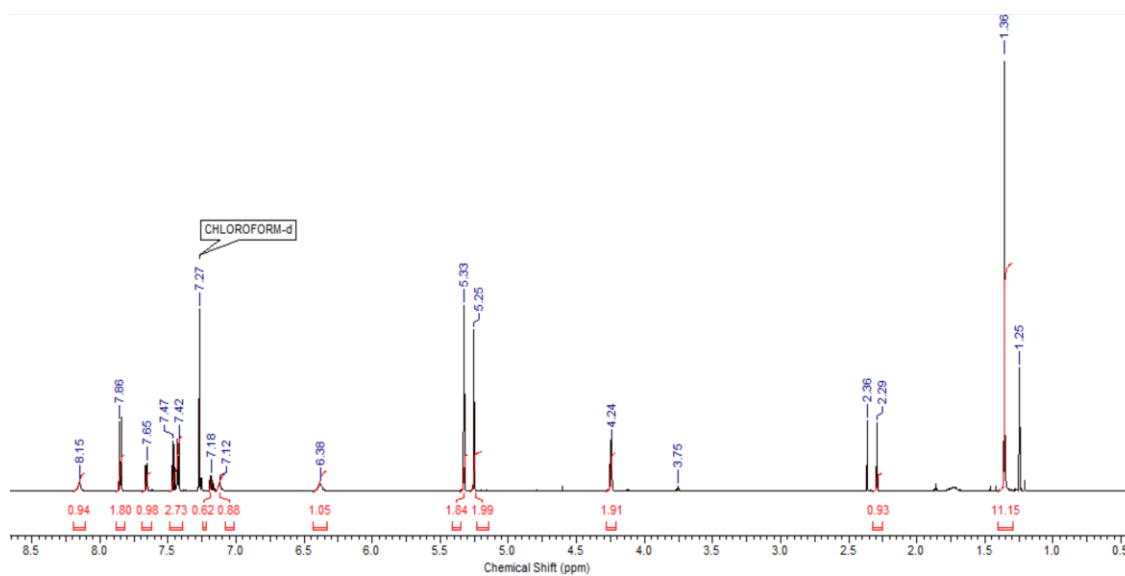


Figure A5.5. ^1H NMR spectrum of chloroformate **3** (CDCl_3 , 600 MHz) (trace toluene present).

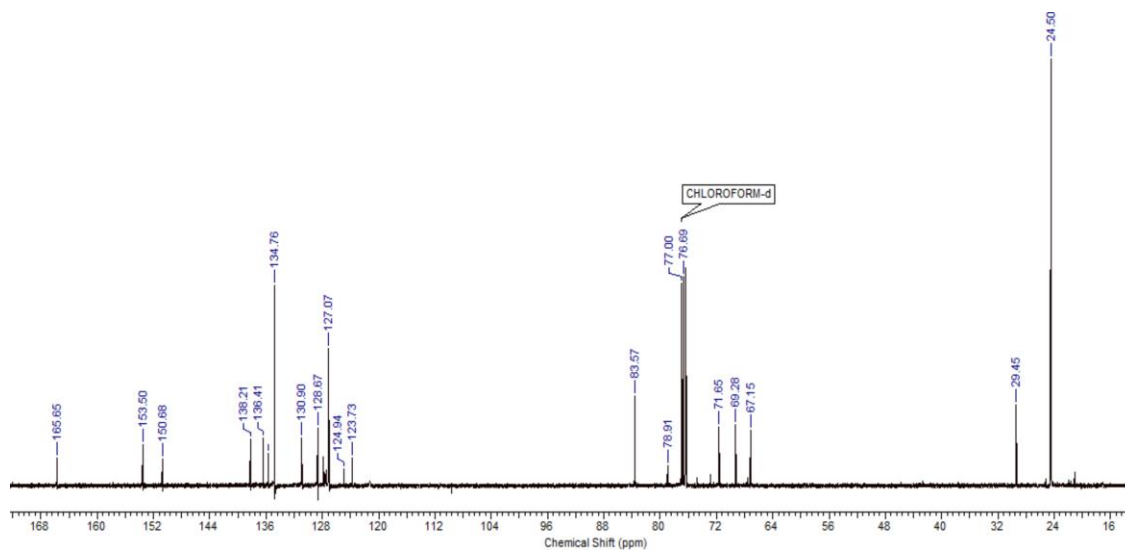


Figure A5.6. ^{13}C NMR spectrum of chloroformate **3** (CDCl_3 , 150 MHz).

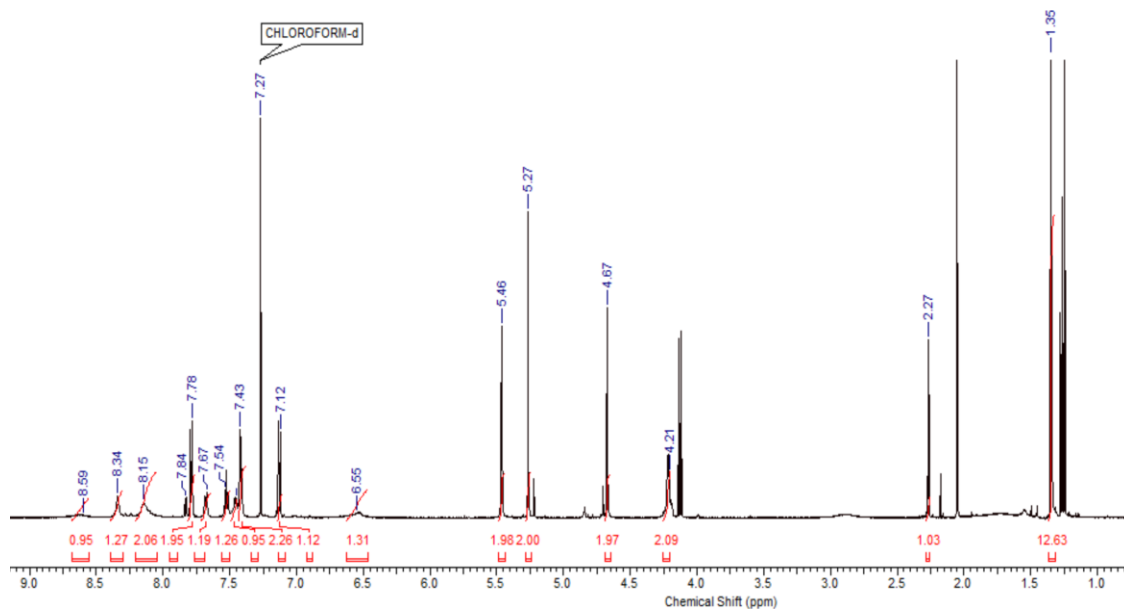


Figure A5.7. ^1H NMR spectrum of compound **10** (CDCl_3 , 600 MHz) (ethyl acetate present).

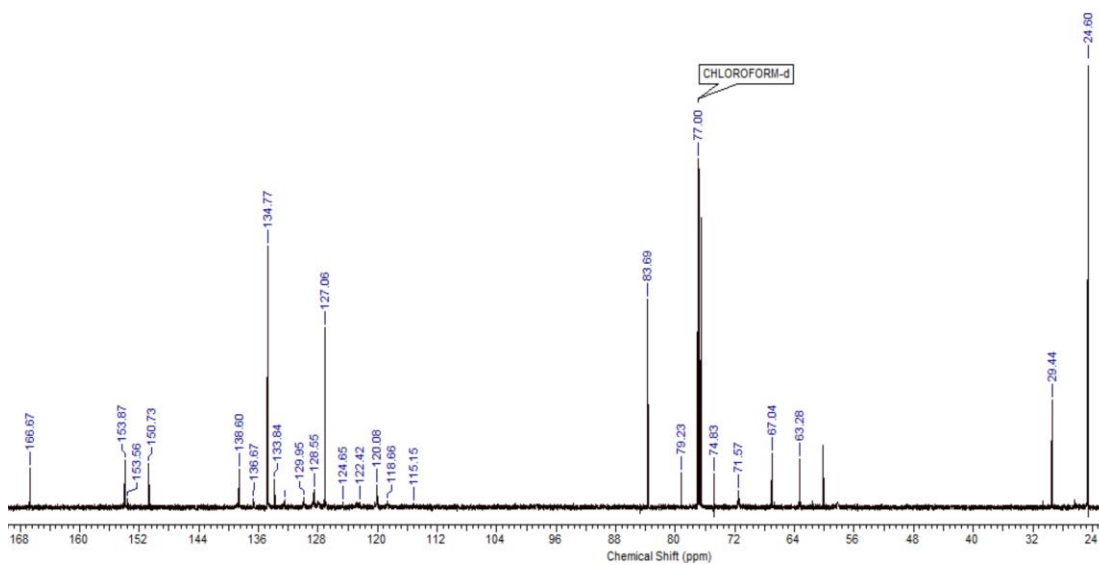


Figure A5.8. ^{13}C NMR spectrum of compound **10** (CDCl_3 , 100 MHz).

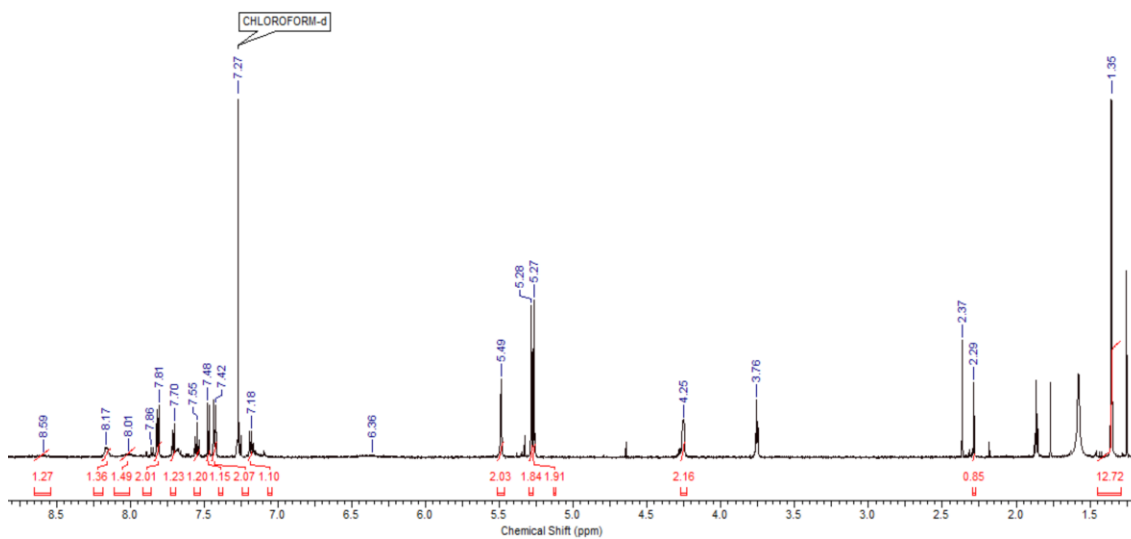


Figure A5.9. ^1H NMR spectrum of chloroformate **4** (CDCl_3 , 600 MHz) (trace toluene and THF present).

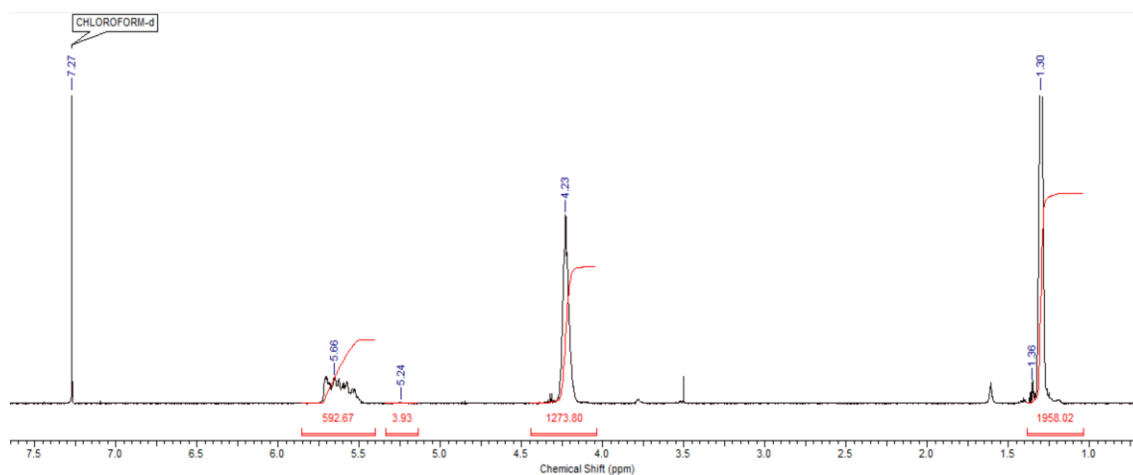


Figure A5.10. ¹H NMR spectrum of PEtG-boronate (CDCl₃, 600 MHz).

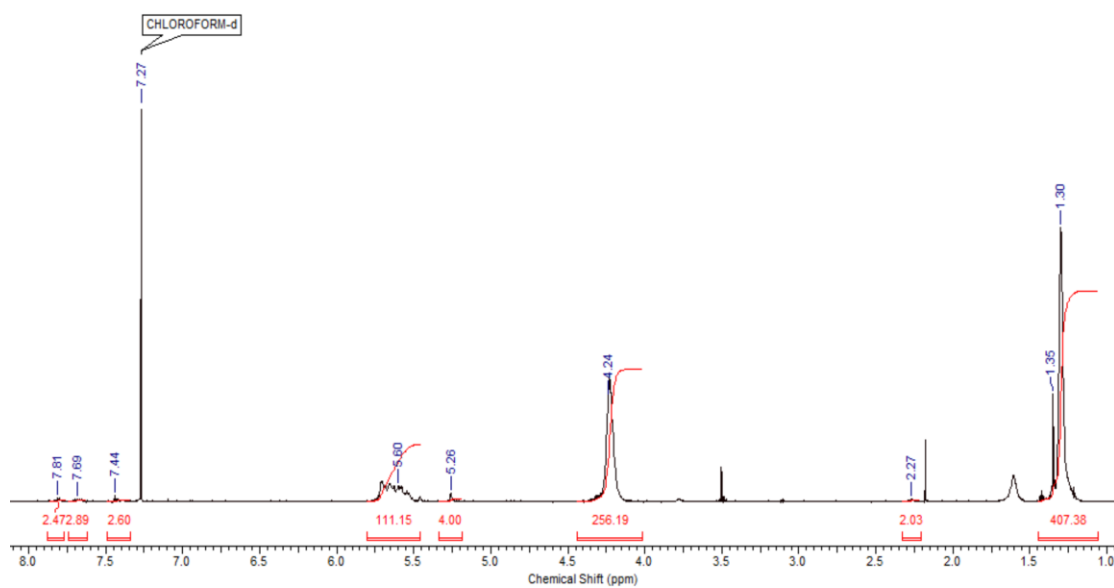


Figure A5.11. ¹H NMR spectrum of PEtG-multi (CDCl₃, 600 MHz).

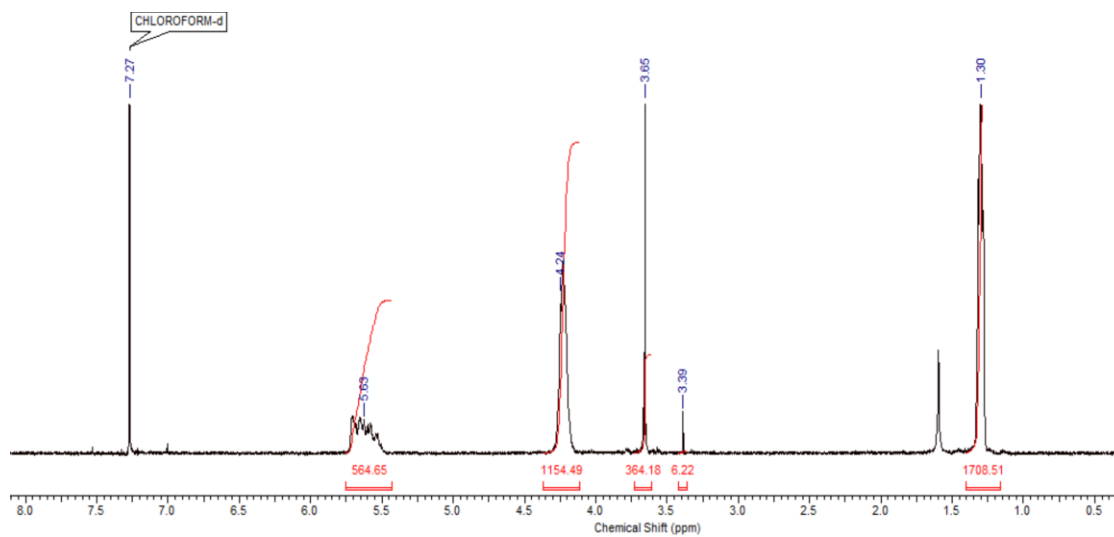


Figure A5.12. ^1H NMR spectrum of PEtG-disulfide-PEG (CDCl_3 , 400Hz)

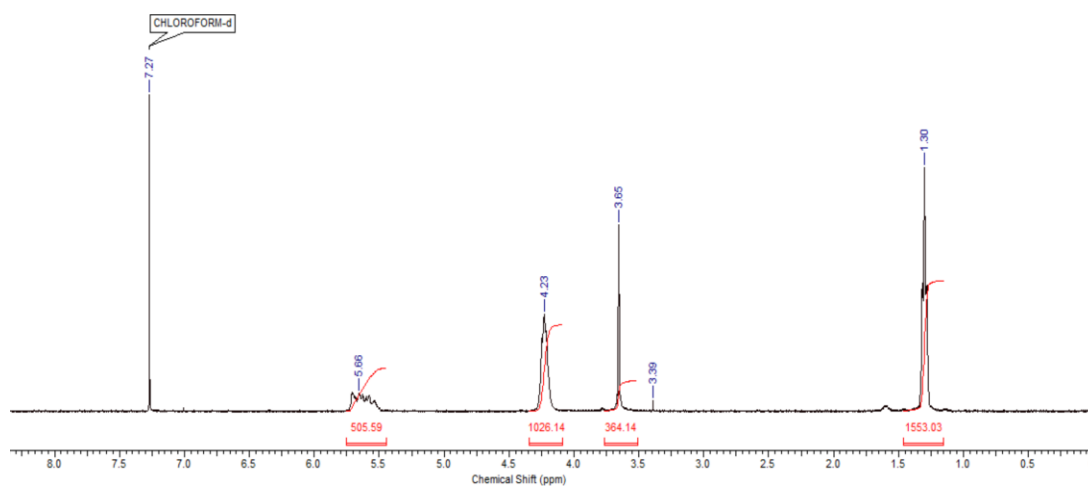


Figure A5.13. ^1H NMR spectrum of PEtG-boronate-PEG (CDCl_3 , 400 MHz).

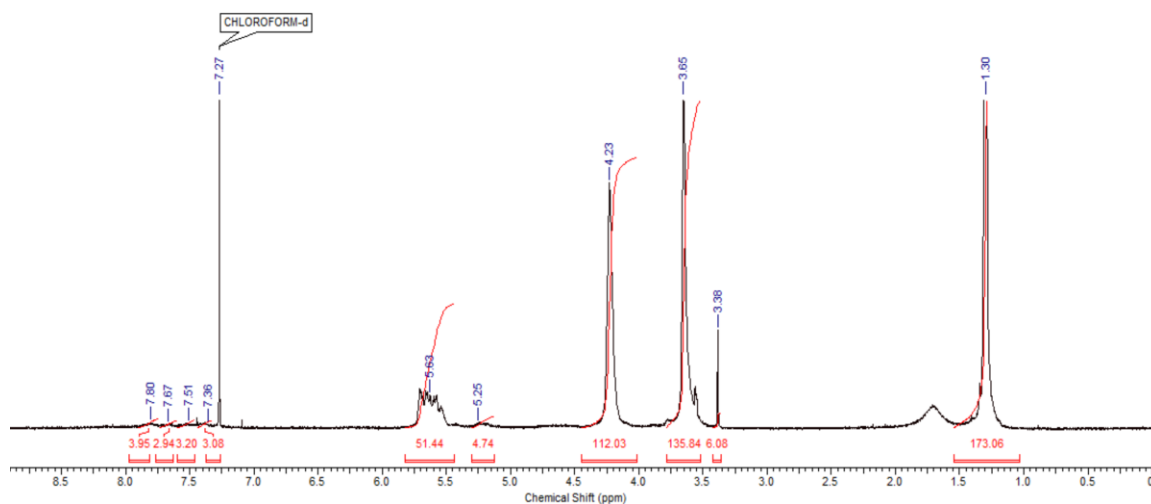


Figure A5.14. ^1H NMR spectrum of **PEtG-multi-PEG** (CDCl_3 , 600 MHz).

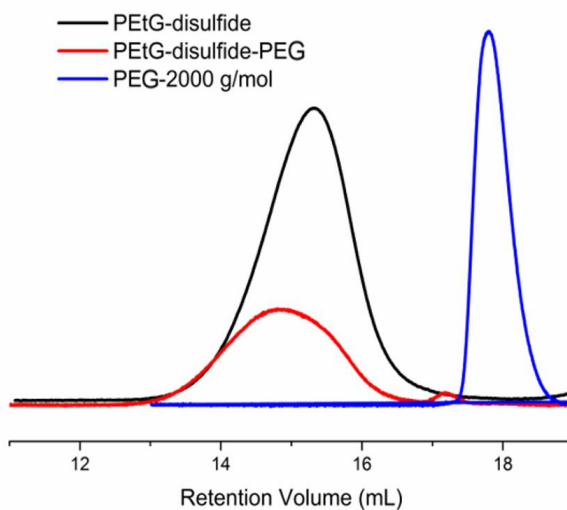


Figure A5.15. SEC traces of **PEtG-disulfide** before and after coupling with PEG (refractive index detection). The very small peak at 17.2 min likely corresponds to a small amount of dimerized PEG-SH that could not be removed by dialysis/washing.

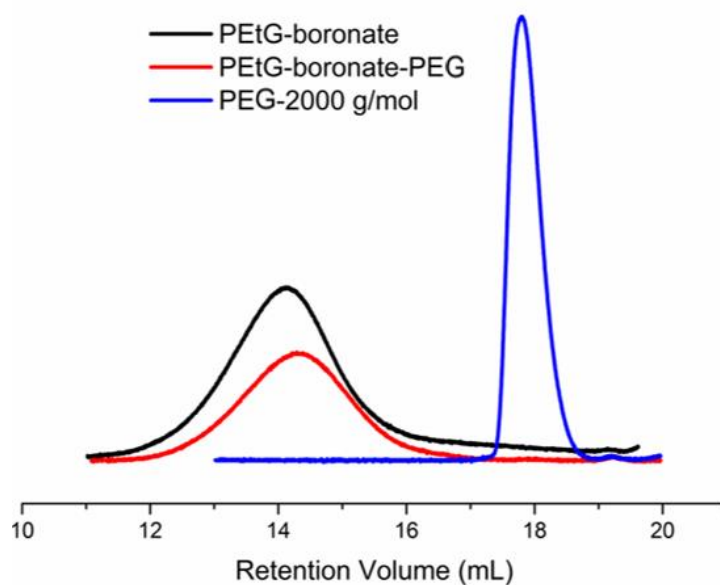


Figure A5.16. SEC traces of **PEtG-boronate** before and after coupling with PEG (refractive index detection).

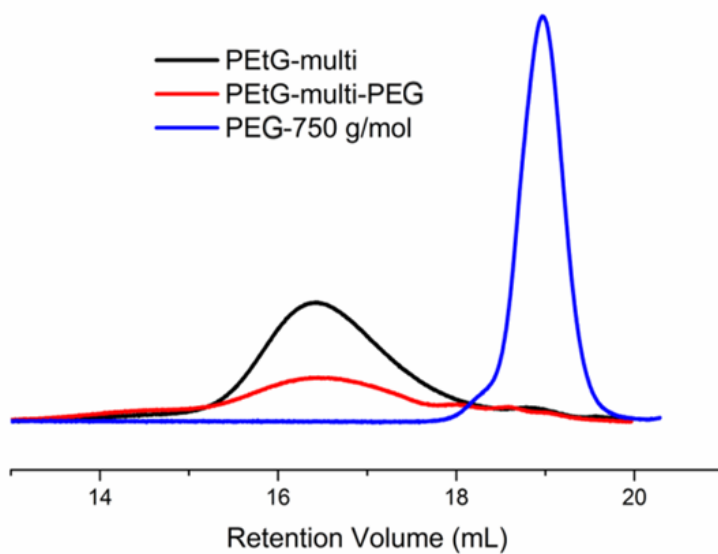


Figure A5.17. SEC traces of **PEtG-multi** before and after coupling with PEG (refractive index detection).

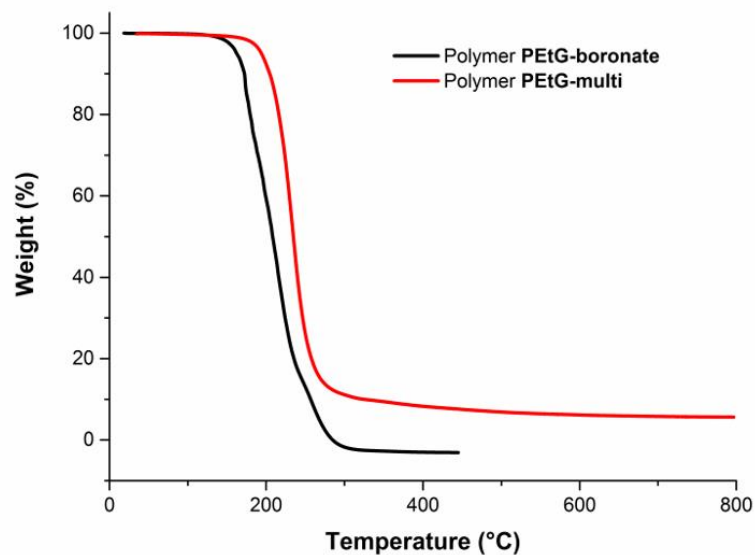


Figure A5.18. TGA curves of the new linker end-capped **PEtG**.

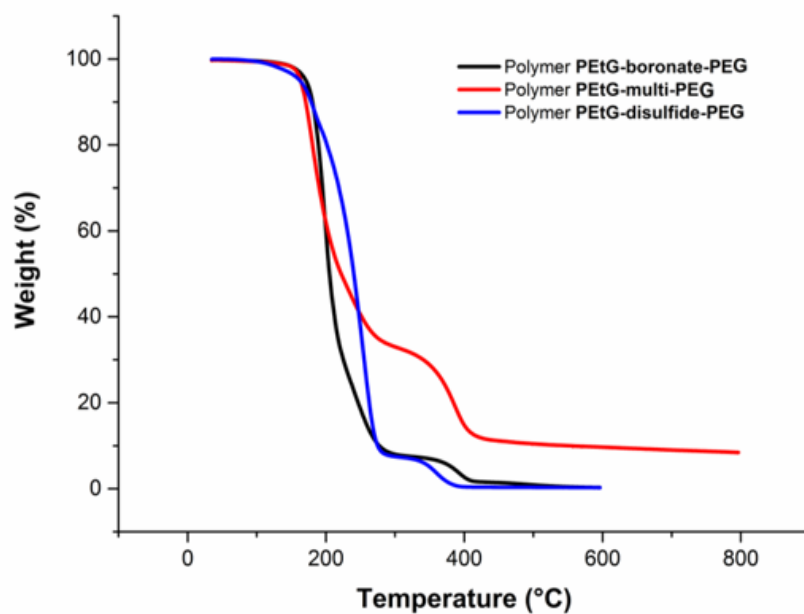


Figure A5.19. TGA curves of the new **PEG-PEtG-PEG** block copolymers.

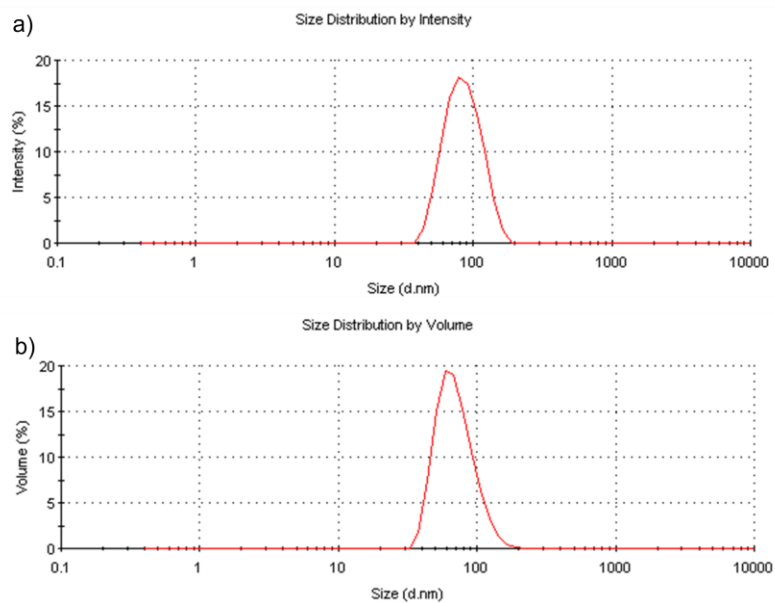


Figure A5.20. a) Intensity and b) Volume distribution of hydrodynamic diameters measured by DLS for nanoparticles prepared from **PEtG-disulfide-PEG**.

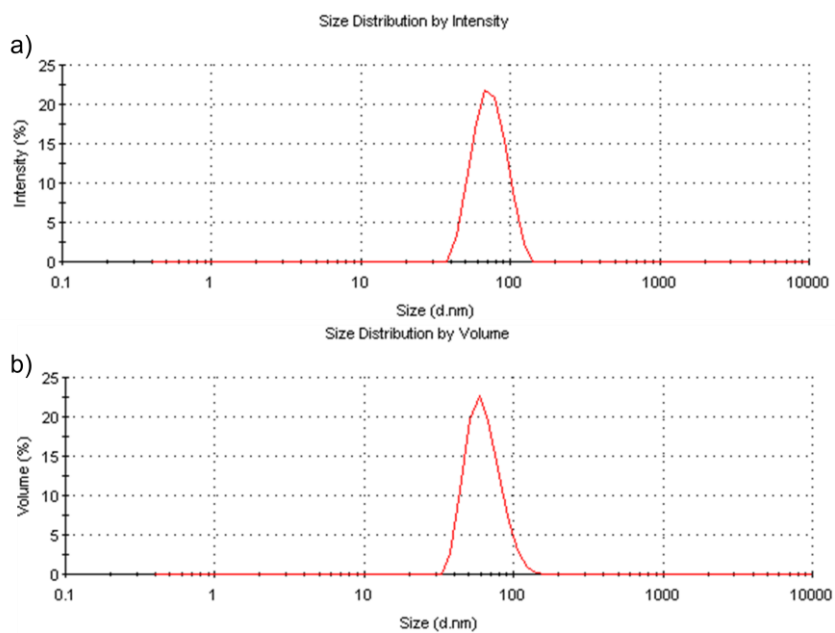


Figure A5.21. a) Intensity and b) Volume distribution of hydrodynamic diameters measured by DLS for nanoparticles prepared from **PEtG-nitrobenzyl-PEG**.

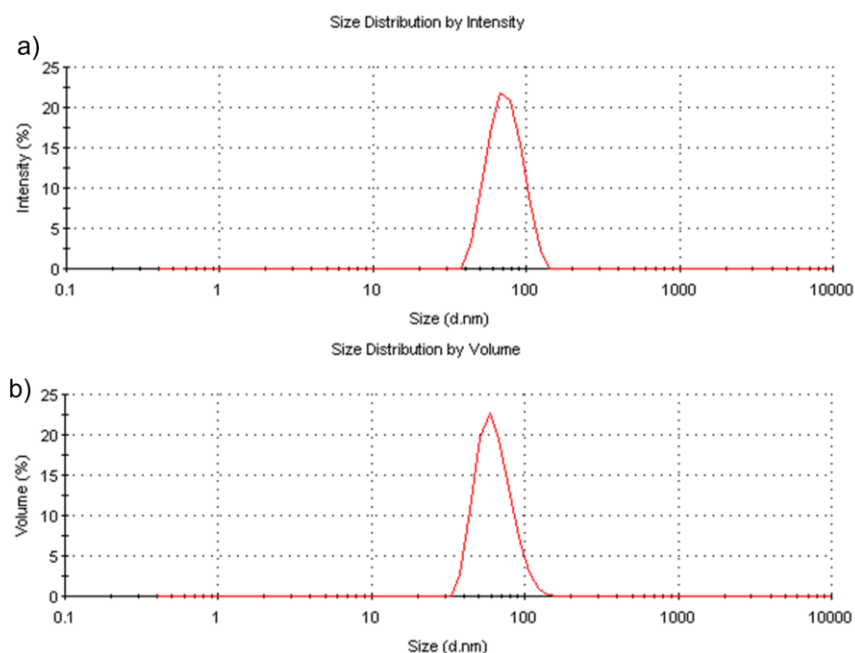


Figure A5.22. a) Intensity and b) Volume distribution of hydrodynamic diameters measured by DLS for nanoparticles prepared from **PEtG-boronate-PEG**.

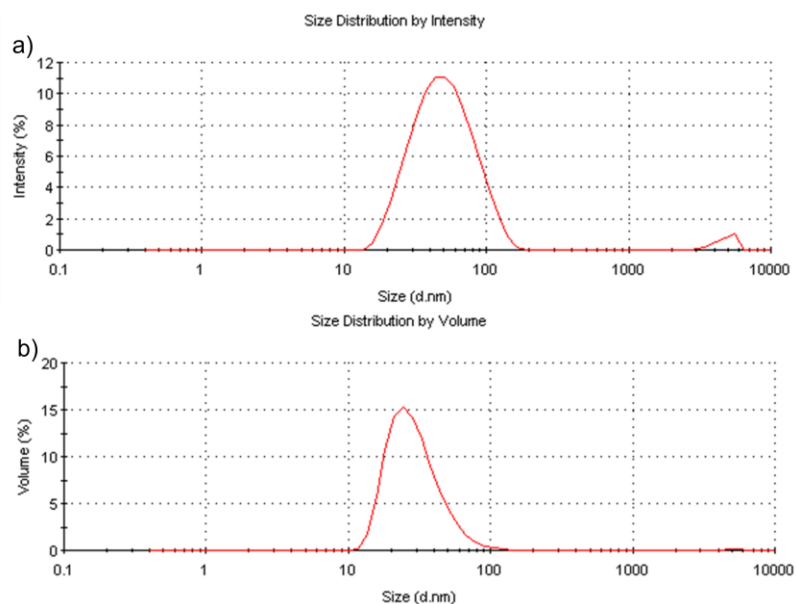


Figure A5.23. a) Intensity and b) Volume distribution of hydrodynamic diameters measured by DLS for nanoparticles prepared from **PEtG-multi-PEG**.

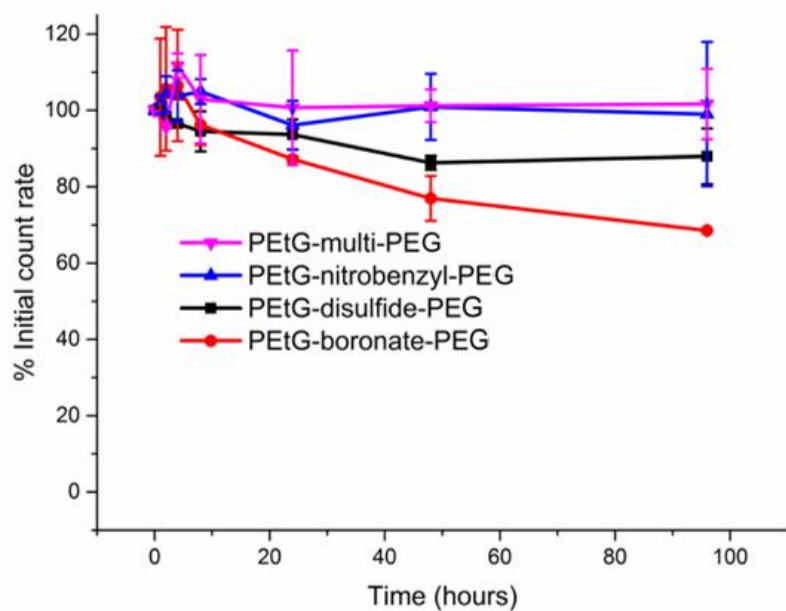


Figure A5.24. Nanoparticle stability in serum: % Initial count rate versus time in serum, measured by DLS.

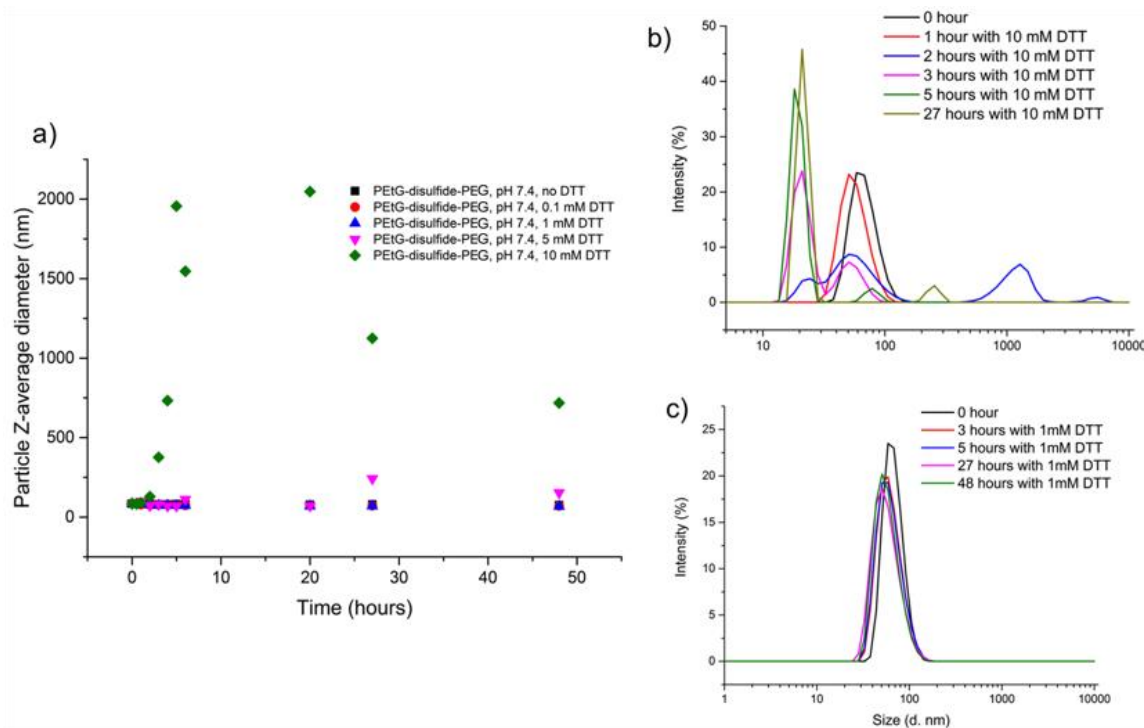


Figure A5.25. a) Evolution of assembly diameter as a function of time for **PEtG-disulfide-PEG** at different DTT concentrations. b) Representative intensity distributions measured for **PEtG-disulfide-PEG** assemblies in the presence of 10 mM DTT. Note that by 3 h, the count rate had dropped to less than 5% its initial value, so the measured diameters likely have little meaning (Figure 4). c) Representative intensity distributions measured for **PEtG-disulfide-PEG** assemblies in the presence of 1 mM DTT, showing that assemblies were likely present throughout the experiment even though the count rate had decreased to less than half its initial value.

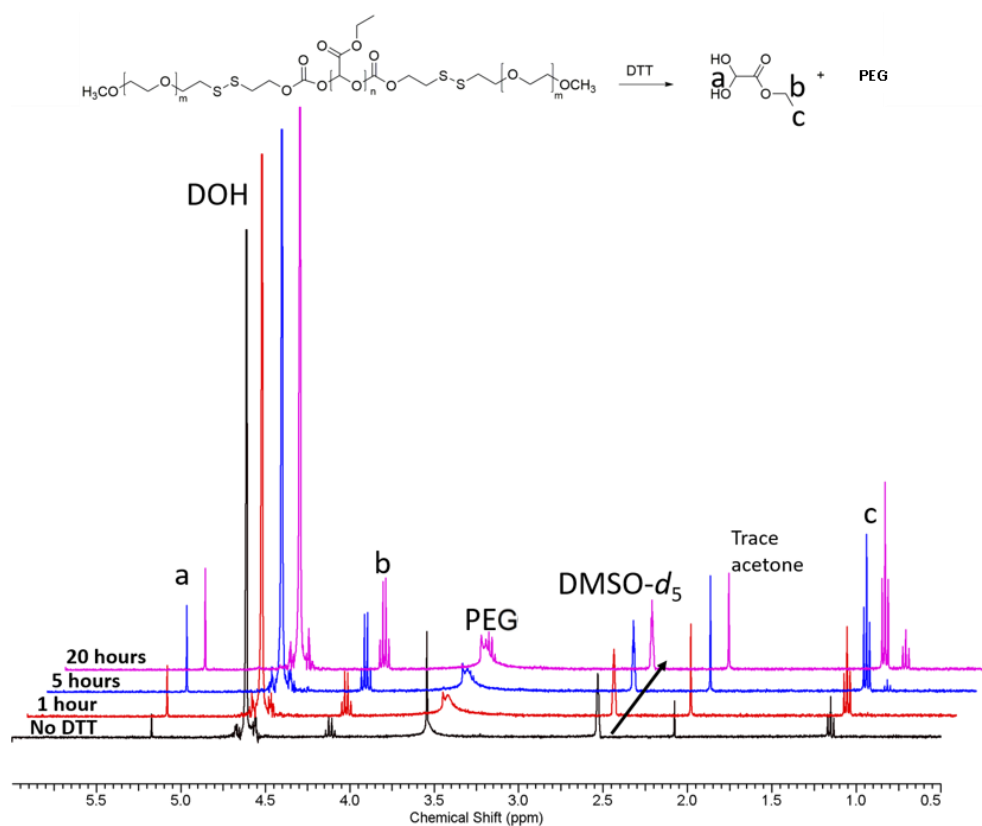


Figure A5.26. ^1H NMR spectra (400 MHz) of **PETG-disulfide-PEG** nanoparticles in 5:1 pH 7.4 phosphate buffered $\text{D}_2\text{O}:\text{DMSO-}d_6$ without the addition of DTT. Less than 20% depolymerization occurred over 20 h.

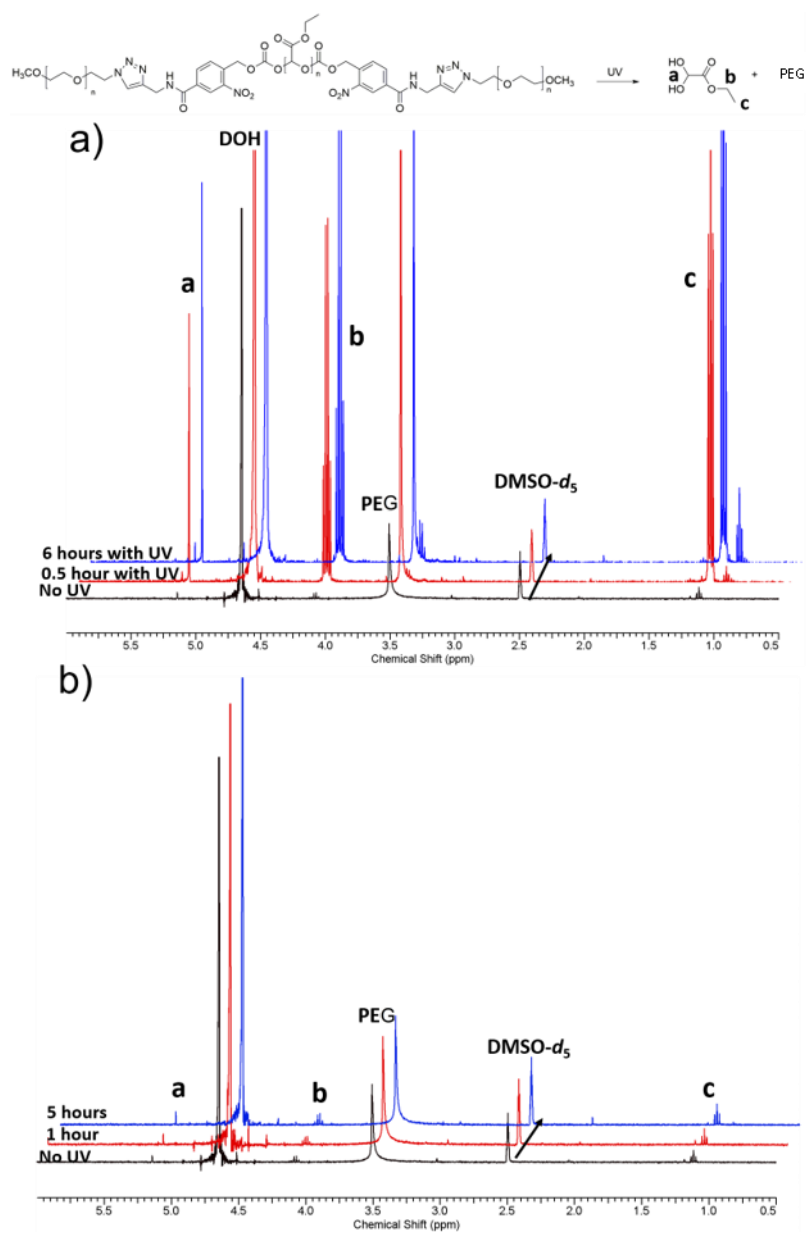


Figure A5.27. a) ^1H NMR spectra of **PETG-nitrobenzyl-PEG** nanoparticles in 5:1 pH 7.4 buffered $\text{D}_2\text{O}:\text{DMSO}-d_6$ (400 MHz) at different time periods after irradiation. b) ^1H NMR spectra of **PETG-nitrobenzyl-PEG** nanoparticles in 5:1 pH 7.4 buffered $\text{D}_2\text{O}:\text{DMSO}-d_6$ (400 MHz) at different time periods without irradiation. Peaks corresponding to the depolymerization product EtGH appear after irradiation whereas the non-irradiated nanoparticles do not undergo any significant depolymerization.

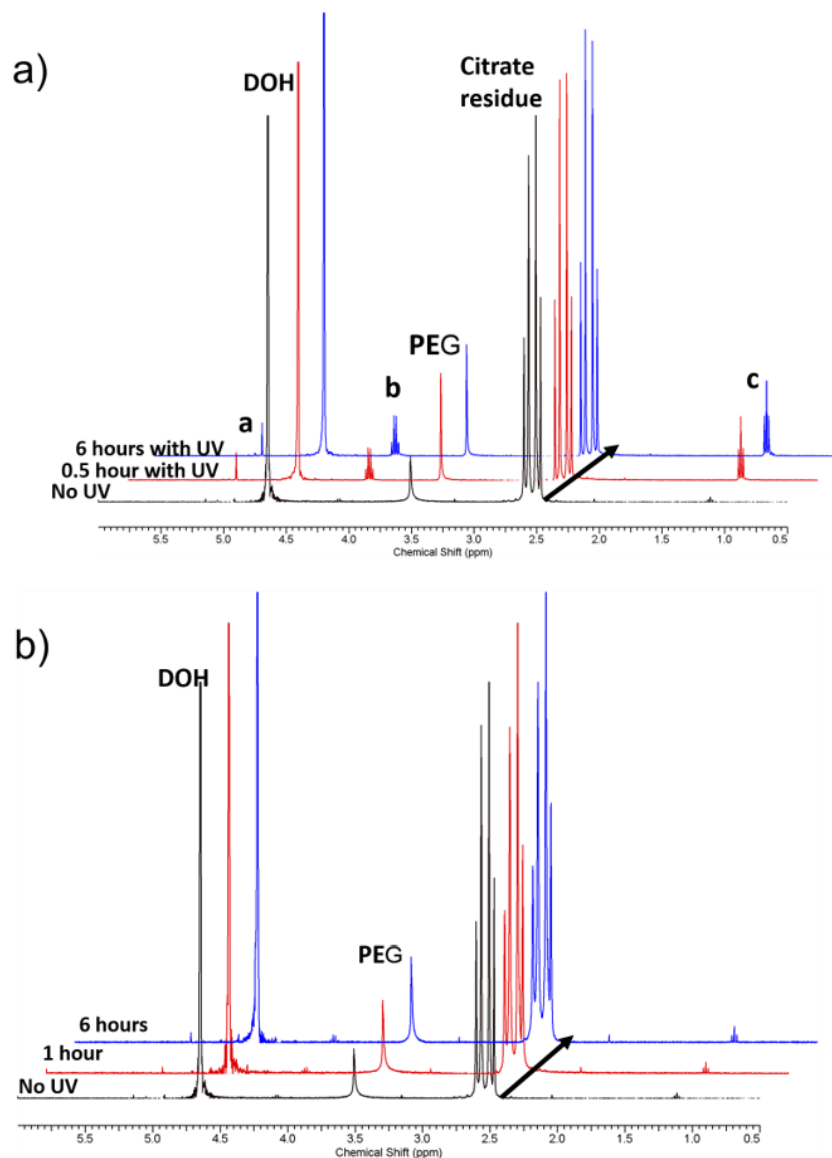


Figure A5.28. a) ^1H NMR spectra of **PETG-nitrobenzyl-PEG** nanoparticles in 5:1 pH 5.0 buffered $\text{D}_2\text{O}:\text{DMSO-}d_6$ (400 MHz) at different time periods after irradiation. b) ^1H NMR spectra of **PETG-nitrobenzyl-PEG** nanoparticles in 5:1 pH 5.0 buffered $\text{D}_2\text{O}:\text{DMSO-}d_6$ (400 MHz) at different time periods without irradiation. Peaks corresponding to the depolymerization product EtGH appear after irradiation whereas the non-irradiated nanoparticles do not undergo any significant depolymerization.

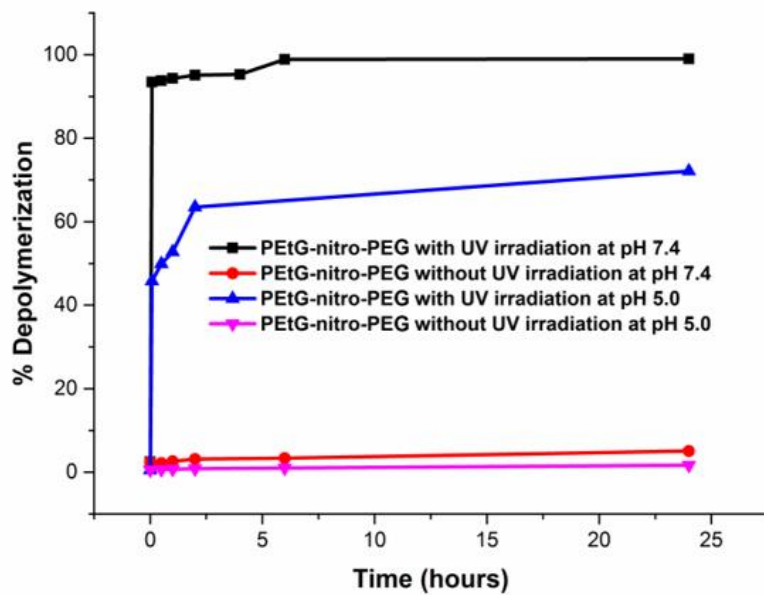


Figure A5.29. % Depolymerization versus time for **PEtG-nitrobenzyl-PEG** nanoparticles in 5:1 D₂O:DMSO-*d*₆ buffered to either pH 7.4 or pH 5.0 with and without UV irradiation as measured by NMR spectroscopy.

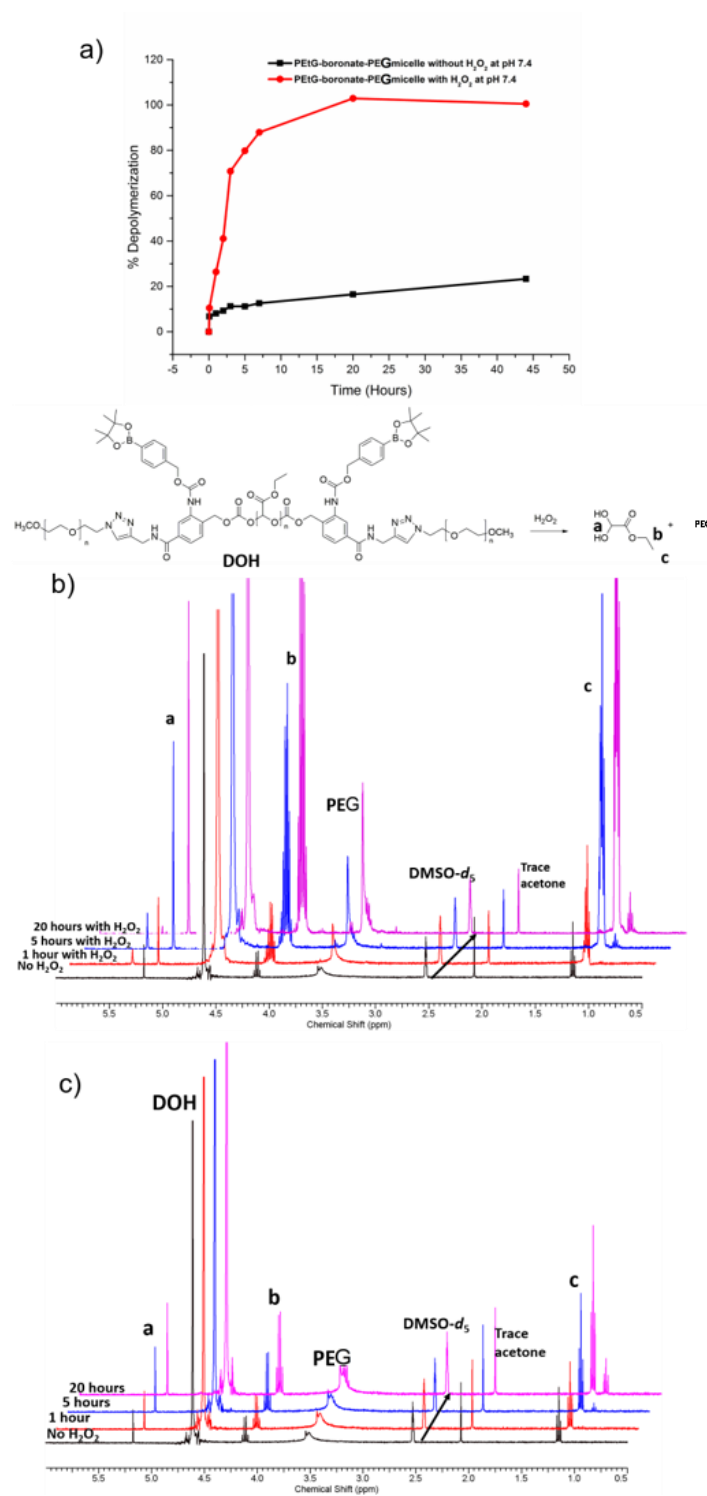
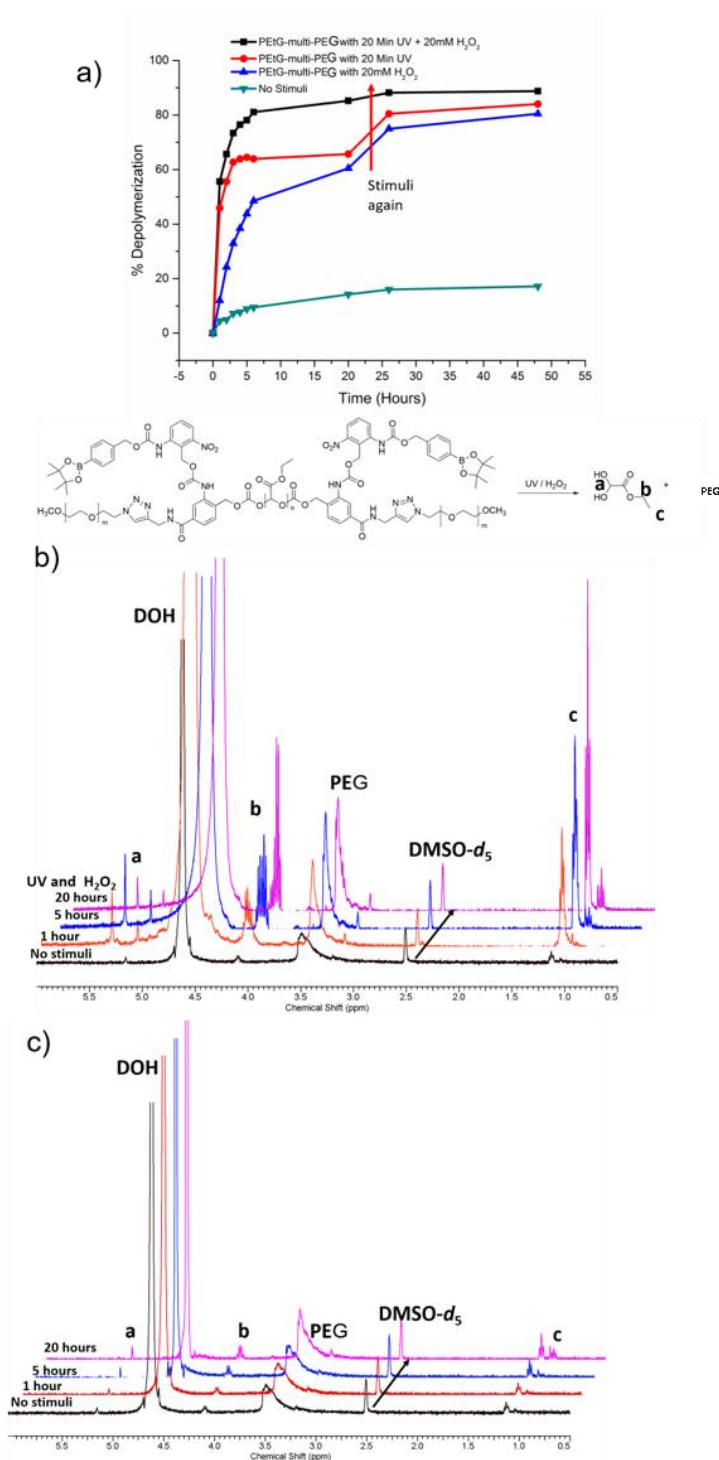


Figure A5.30. a) % Depolymerization versus time for **PEtG-boronate-PEG** nanoparticles in 5:1 pH 7.4 buffered D₂O:DMSO-*d*₆ with and without 10 mM H₂O₂ as

measured by NMR spectroscopy. b) ^1H NMR spectra of **PEtG-boronate-PEG** nanoparticles in 5:1 pH 7.4 buffered $\text{D}_2\text{O}:\text{DMSO-}d_6$ (400 MHz) at different time periods after addition of 10 mM H_2O_2 . c) ^1H NMR spectra of **PEtG-boronate-PEG** nanoparticles in 5:1 pH 7.4 buffered $\text{D}_2\text{O}:\text{DMSO-}d_6$ (400 MHz) at different time periods without H_2O_2 . Peaks corresponding to the depolymerization product EtGH appear after stimulus whereas the nanoparticles without stimulus undergo small amount of depolymerization.



buffered D₂O:DMSO-*d*₆ (400 MHz) at different time periods after addition of 10 mM H₂O₂ and UV irradiation. c) ¹H NMR spectra of **PEtG-multi-PEG** nanoparticles in 5:1 pH 7.4 buffered D₂O:DMSO-*d*₆ (400 MHz) at different time periods without stimuli. Peaks corresponding to the depolymerization product EtGH appear after stimulus (at longer time points, some hydrolysis of EtGH to glyoxylate was also observed) whereas the nanoparticles without stimulus do not undergo any significant depolymerization.

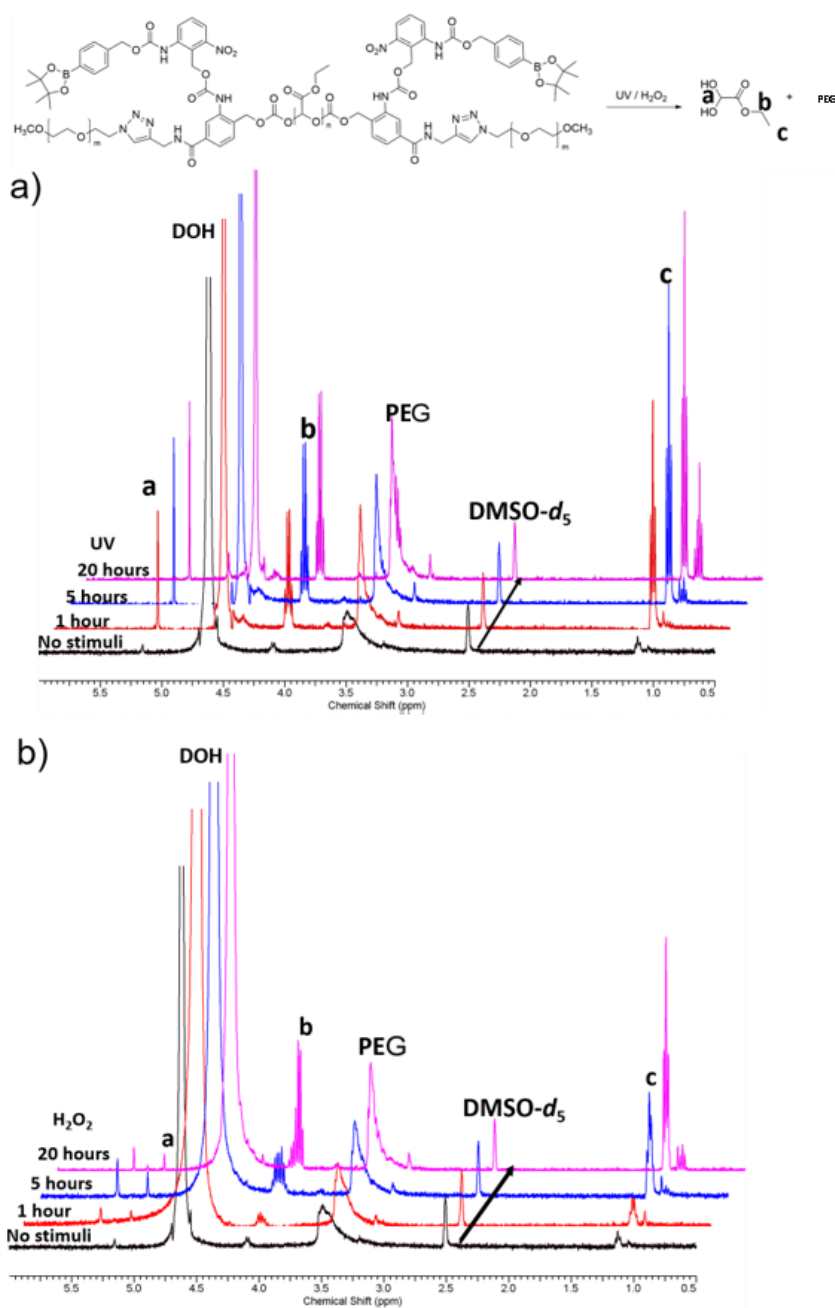


Figure A5.32. a) ¹H NMR spectra of **PETG-multi-PEG** nanoparticles in 5:1 pH 7.4 buffered D₂O:DMSO-*d*₆ (400 MHz) at different time periods after UV irradiation. b) ¹H NMR spectra of **PETG-multi-PEG** nanoparticles in 5:1 pH 7.4 buffered D₂O:DMSO-*d*₆ (400 MHz) at different time periods with addition of 10 mM H₂O₂. Peaks corresponding to the depolymerization product EtGH appear after the stimuli were applied. In this case, the stimuli were also re-applied after 24 h.

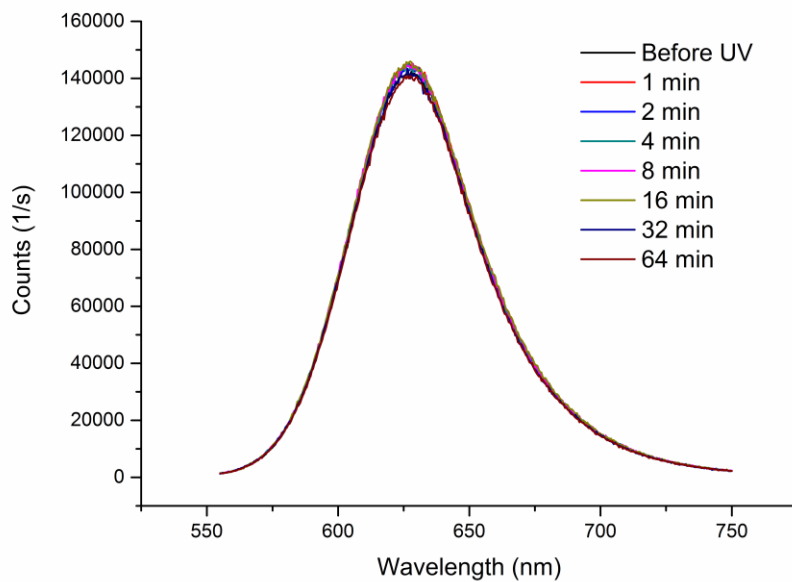
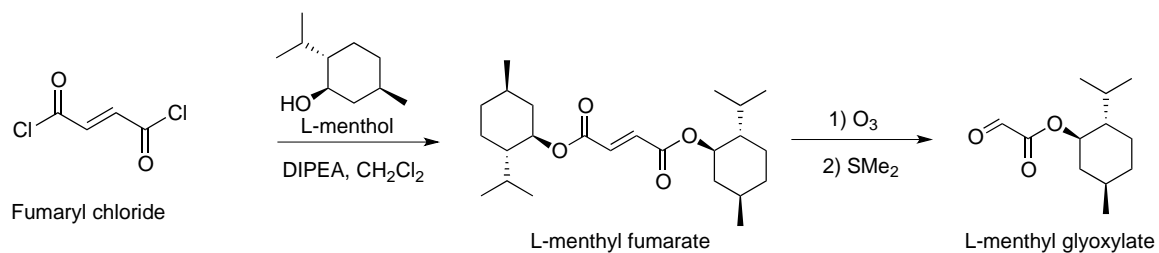


Figure A5.33. Fluorescence spectra of Nile red in ethanol following different UV irradiation times. No changes in Nile red fluorescence were observed, confirming the photostability of the dye.

Appendix 6: Supporting information for Chapter 6



Scheme A6.1. Synthesis of menthyl glyoxylate.

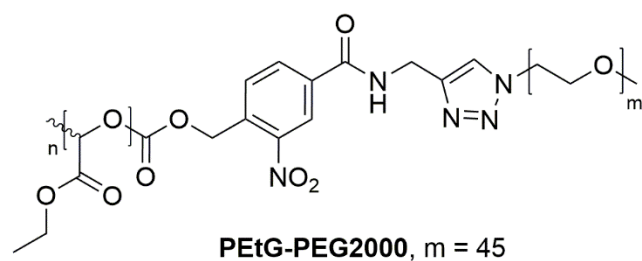


Figure A6.1. Structure of PEtG-PEG2000

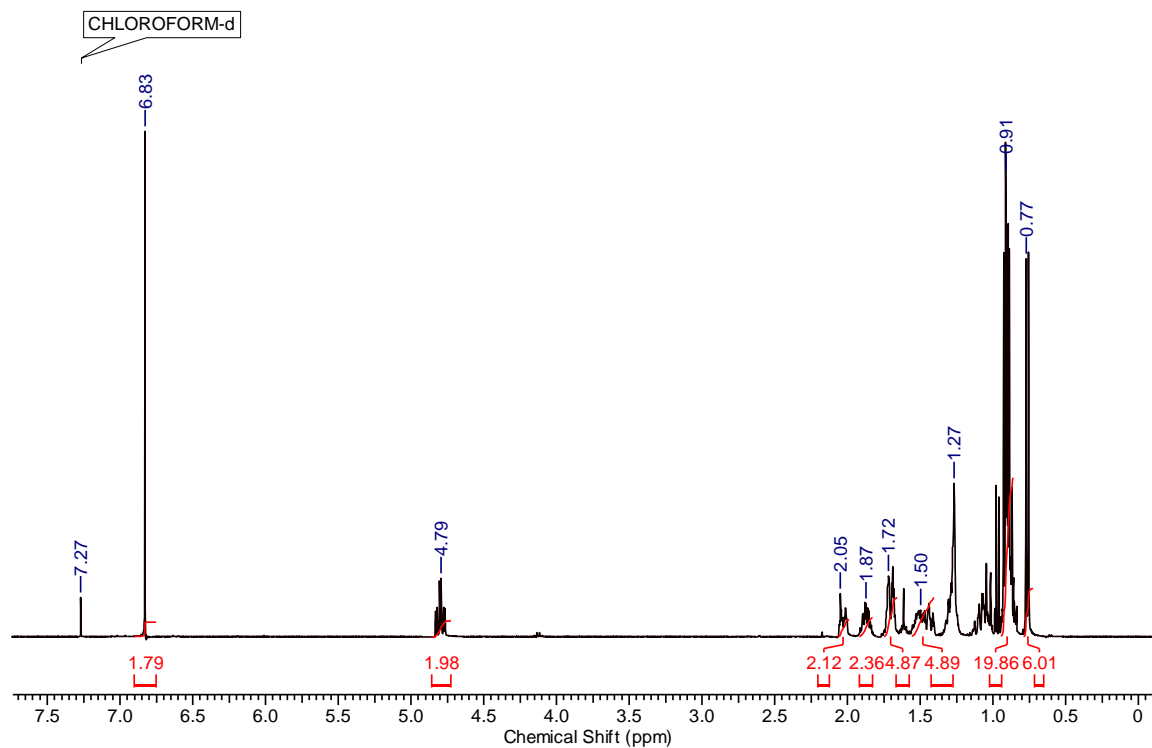


Figure A6.2. ^1H NMR spectrum of L-menthyl fumarate (CDCl_3 , 400Hz).

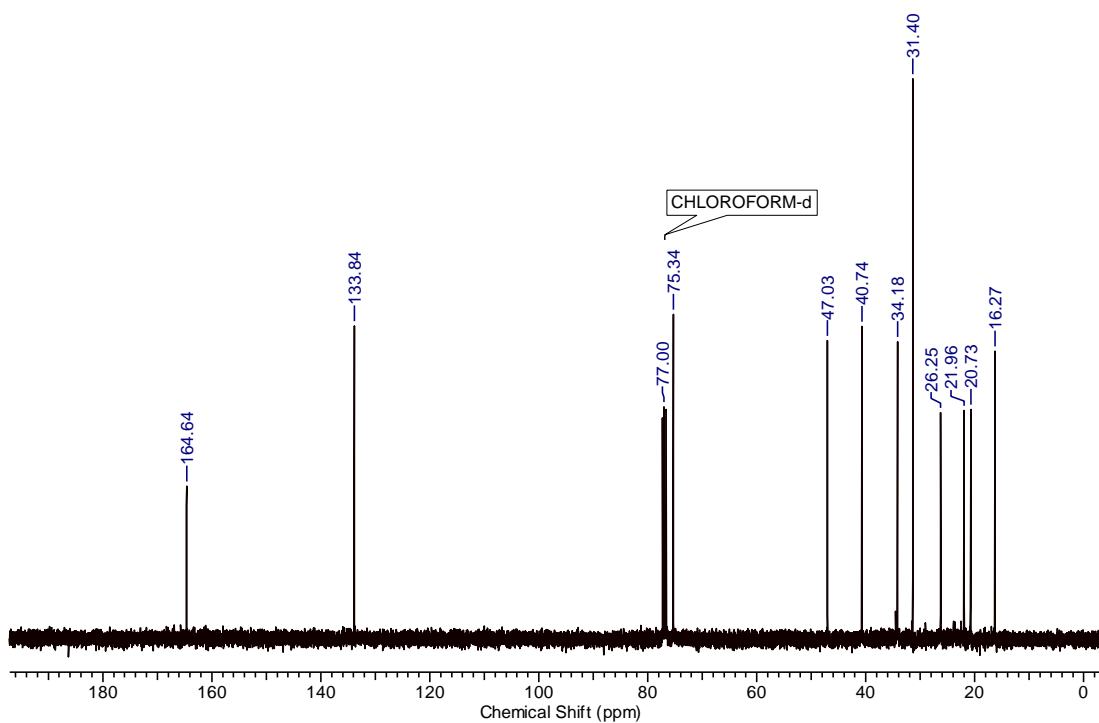


Figure A6.3. ^{13}C NMR spectrum of L-menthyl fumarate (CDCl_3 , 100Hz).

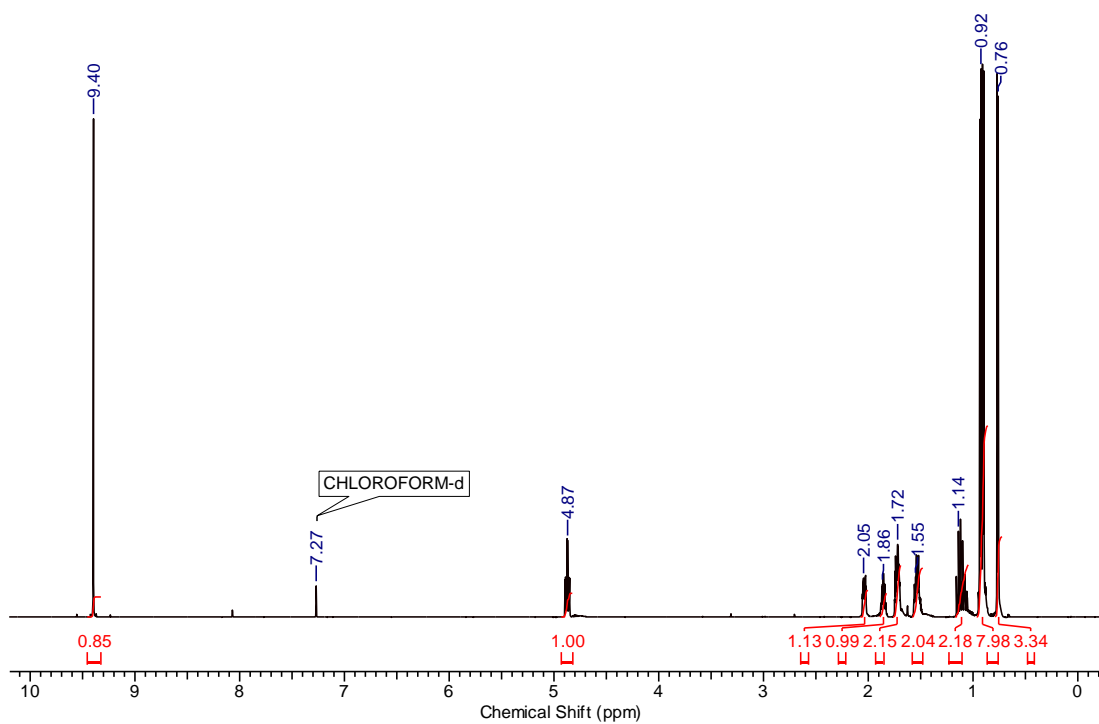


Figure A6.4. ^1H NMR spectrum of L-menthyl glyoxylate (CDCl_3 , 600Hz).

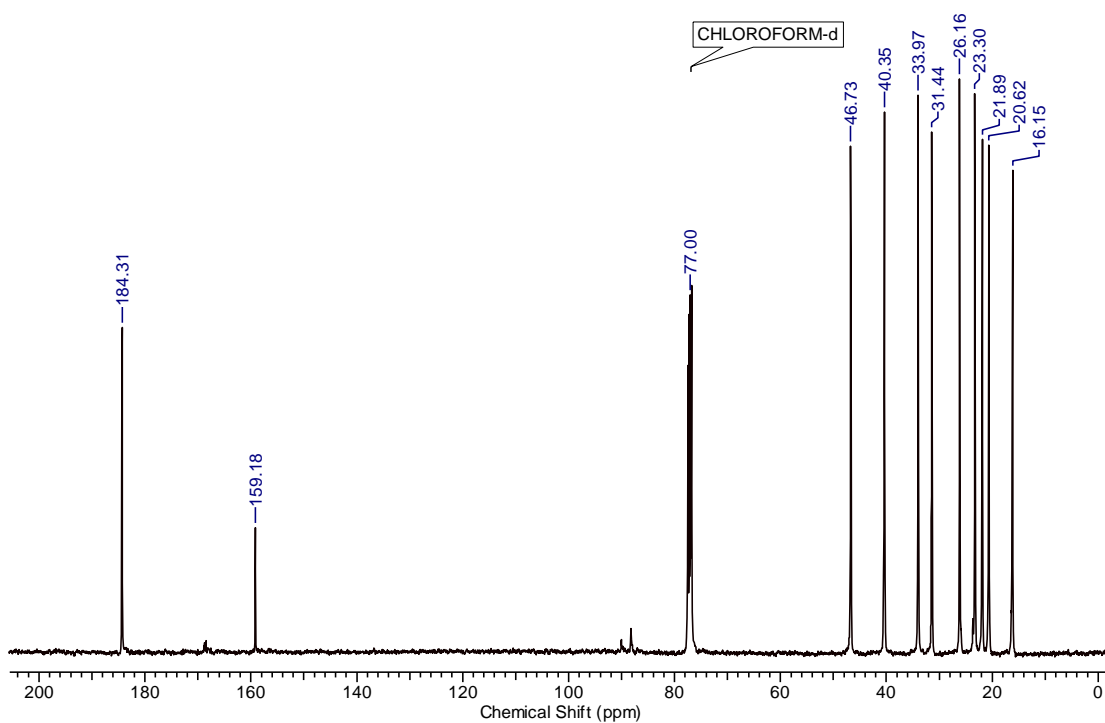


Figure A6.5. ¹³C NMR spectrum of L-menthyl glyoxylate (CDCl₃, 150Hz).

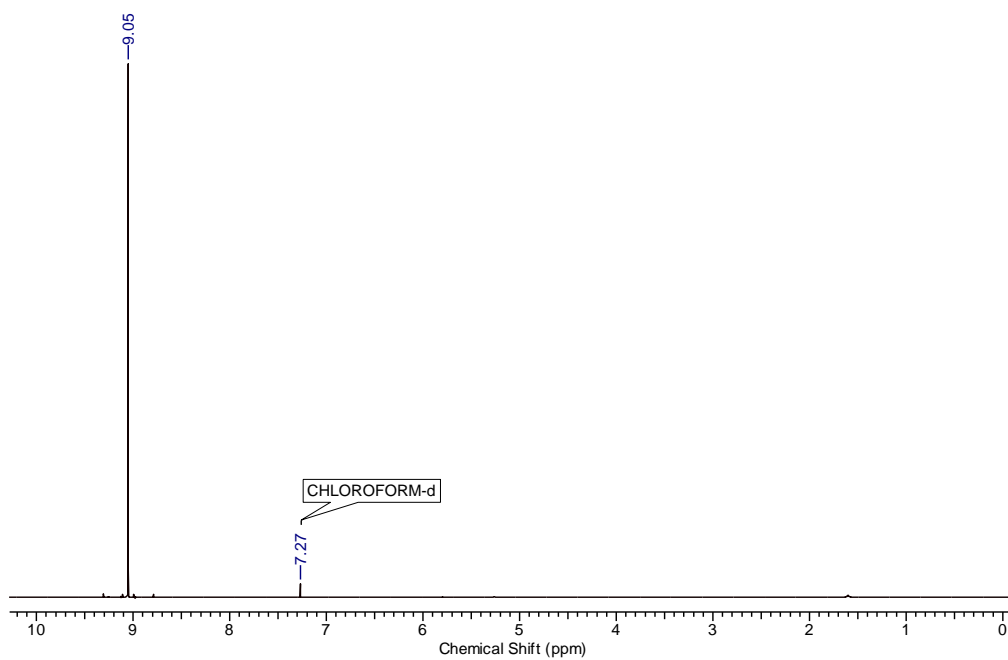


Figure A6.6. ¹H NMR spectrum of chloral (CDCl₃, 400Hz).

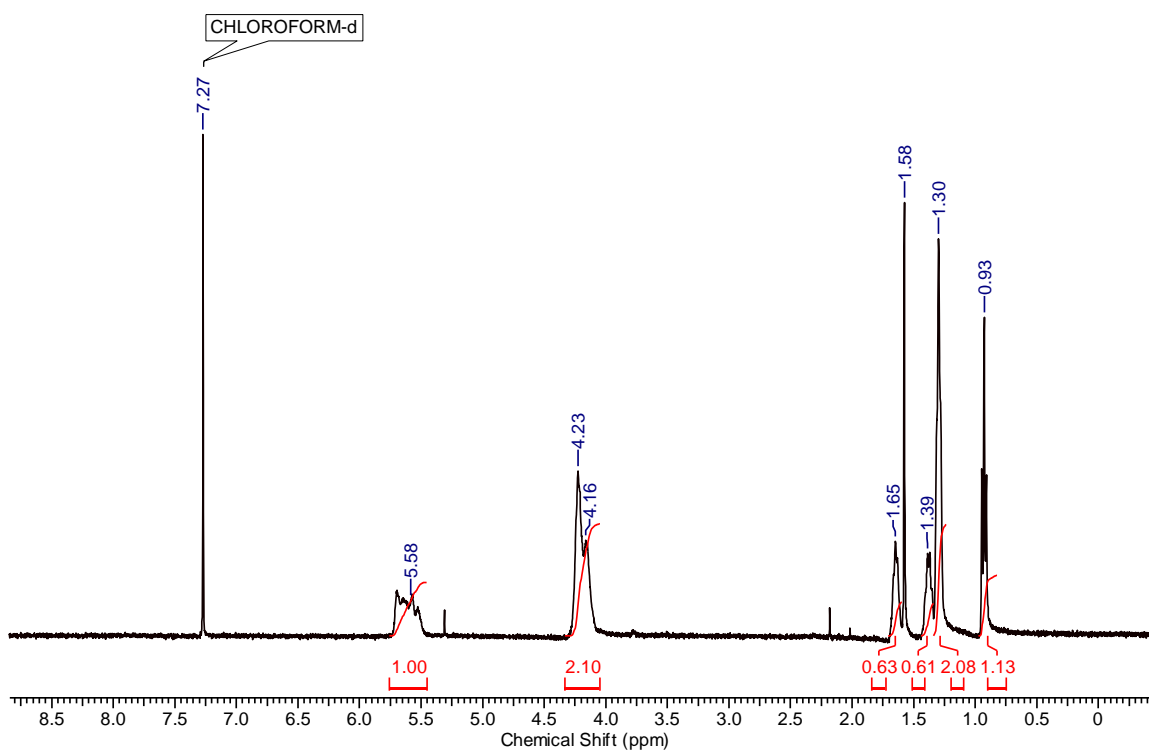


Figure A6.7. ^1H NMR spectrum of **PEtBuG** (CDCl_3 , 400Hz).

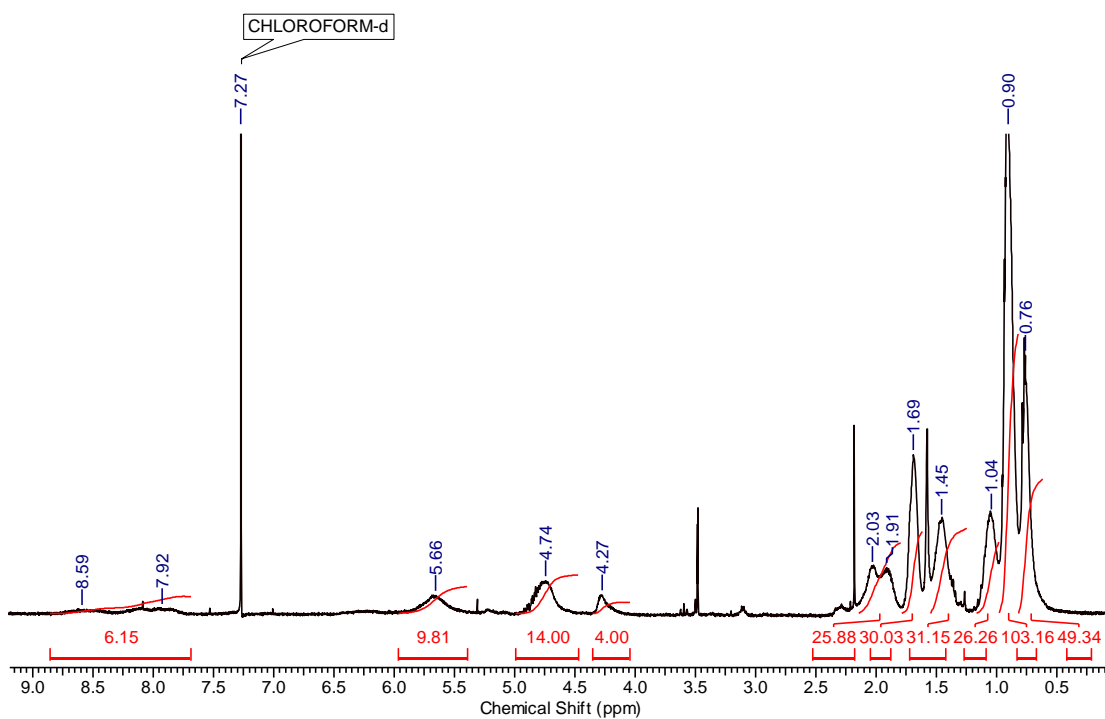


Figure A6.8. ^1H NMR spectrum of **PMenG** (CDCl_3 , 400Hz).

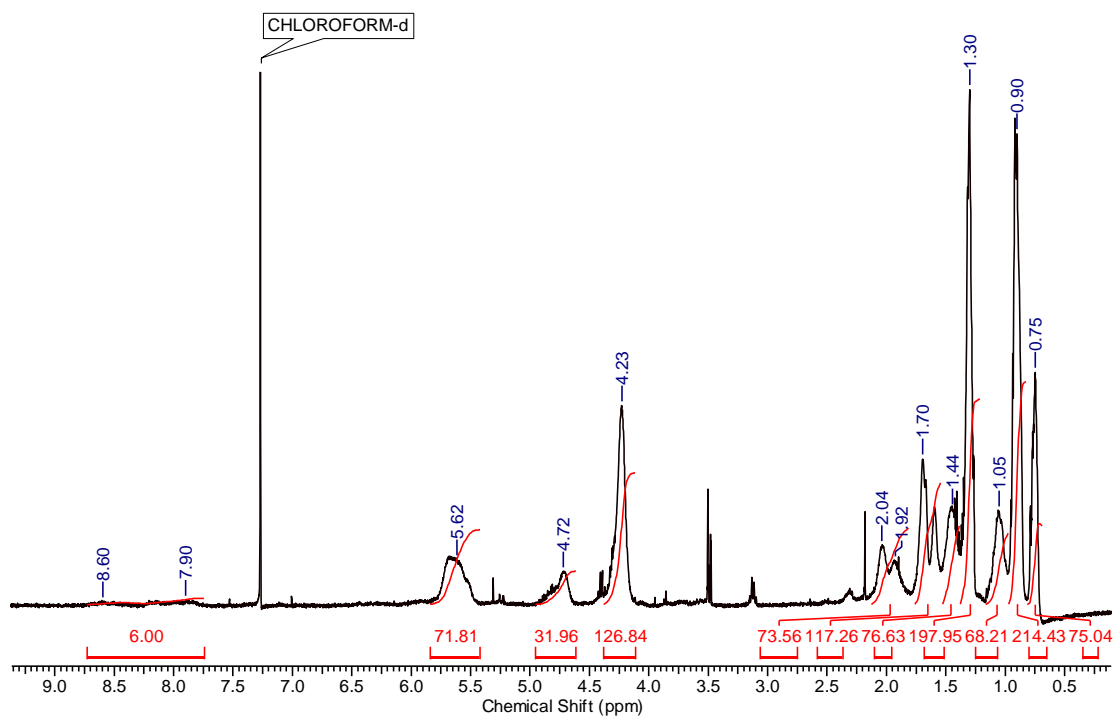


Figure A6.9. ^1H NMR spectrum of **PEtMenG** (CDCl_3 , 400Hz).

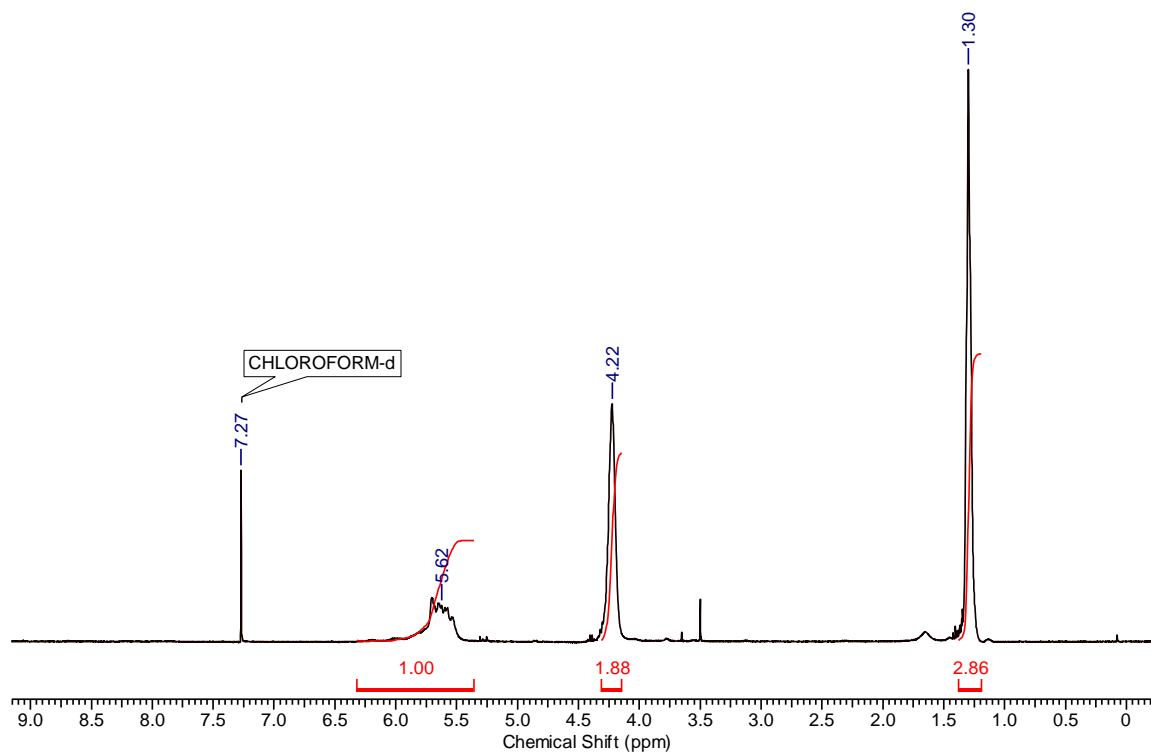


Figure A6.10. ^1H NMR spectrum of **PEtGC** (CDCl_3 , 400Hz).

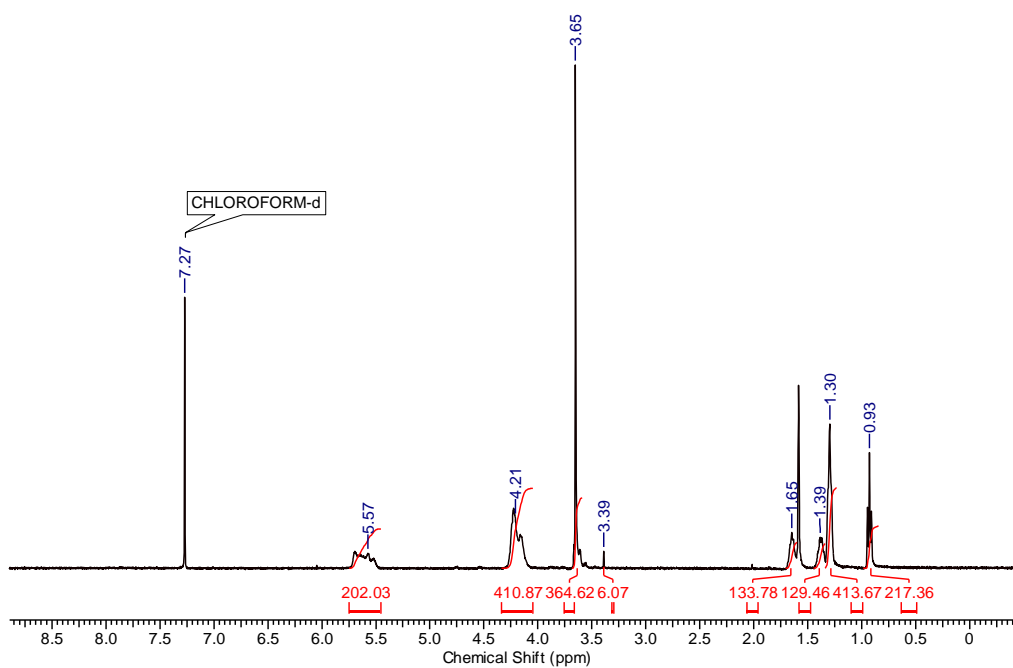


Figure A6.11. ^1H NMR spectrum of **PETbuG-PEG2000** (CDCl_3 , 400Hz).

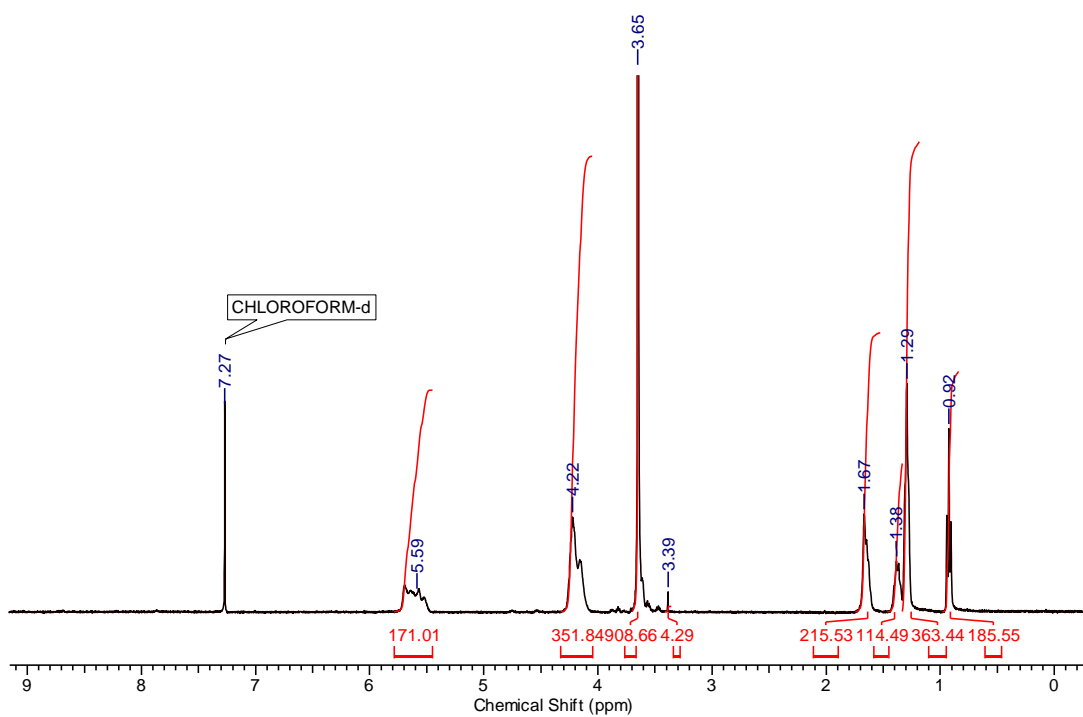


Figure A6.12. ^1H NMR spectrum of **PETbuG-PEG5000** (CDCl_3 , 400Hz).

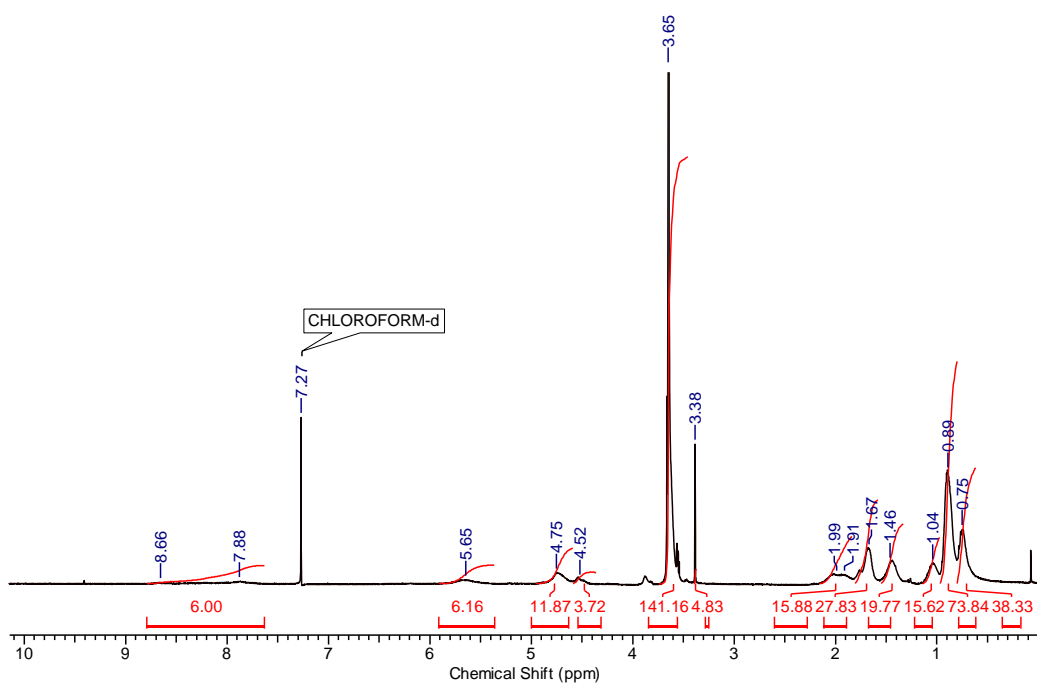


Figure A6.13. ^1H NMR spectrum of **PMenG-PEG750** (CDCl_3 , 400Hz).

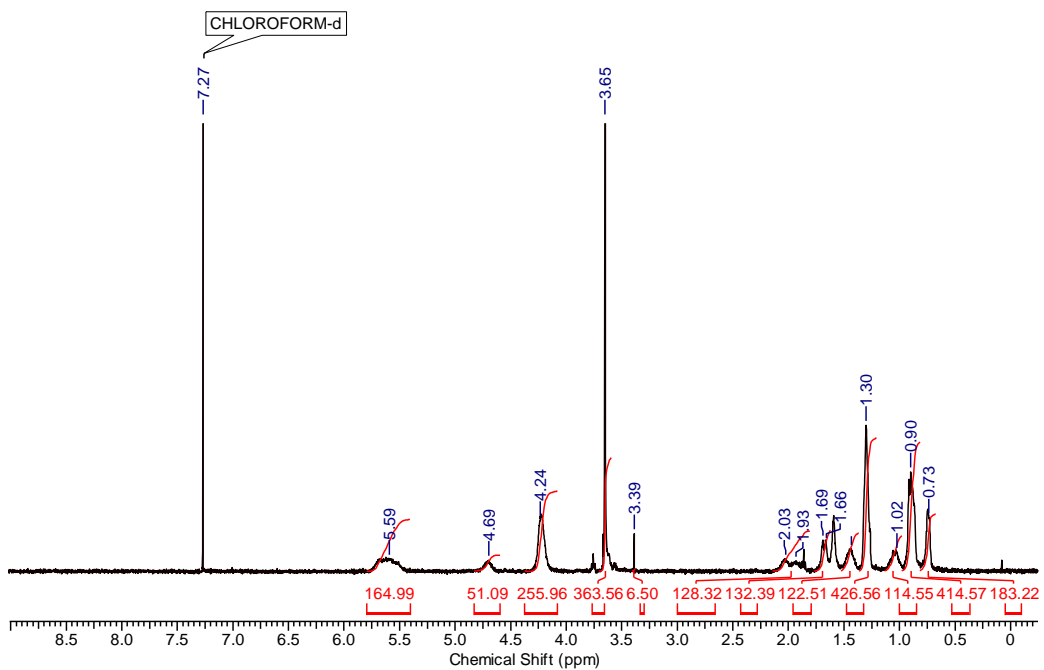


Figure A6.14. ^1H NMR spectrum of **PEtMenG-PEG2000** (CDCl_3 , 400Hz).

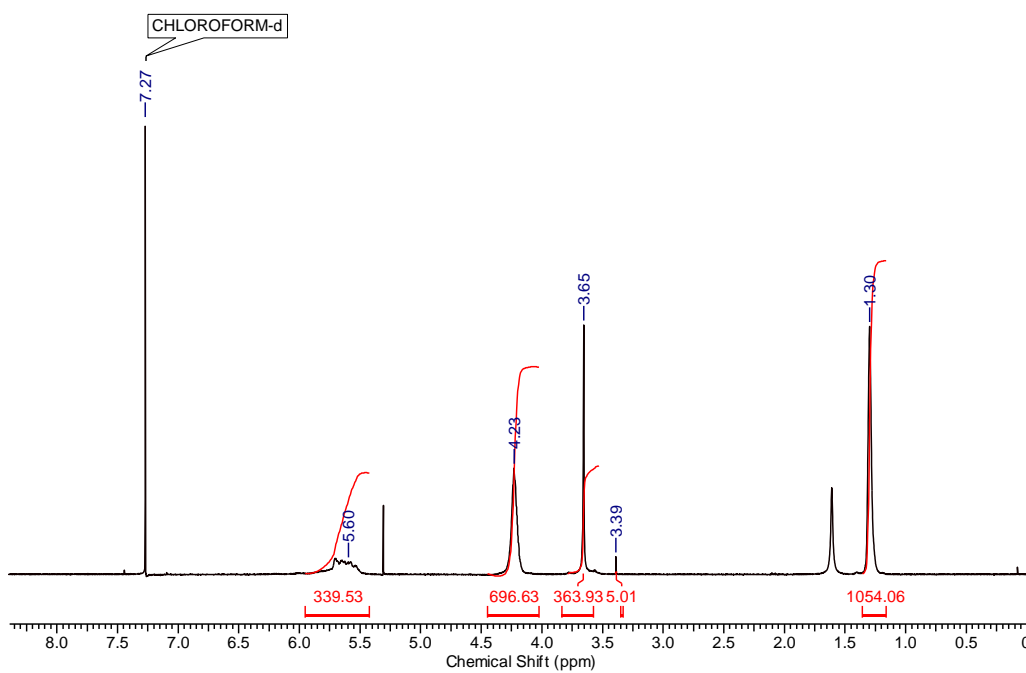


Figure A6.15. ^1H NMR spectrum of **PETGC-PEG2000** (CDCl_3 , 600Hz) with presence of trace dichloromethane.

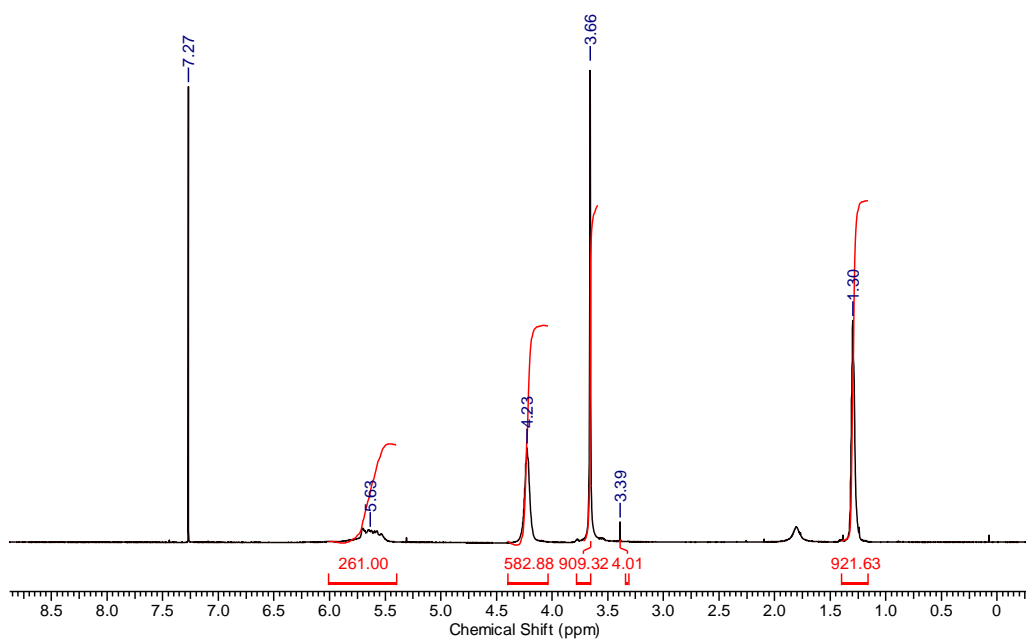


Figure A6.16. ^1H NMR spectrum of **PETGC-PEG5000** (CDCl_3 , 600Hz).

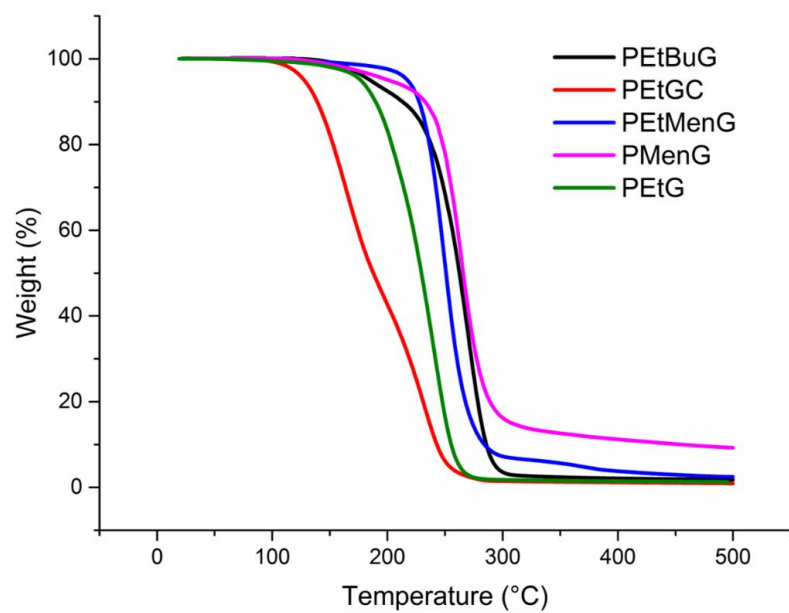


Figure A6.17. TGA curves of the polymers.

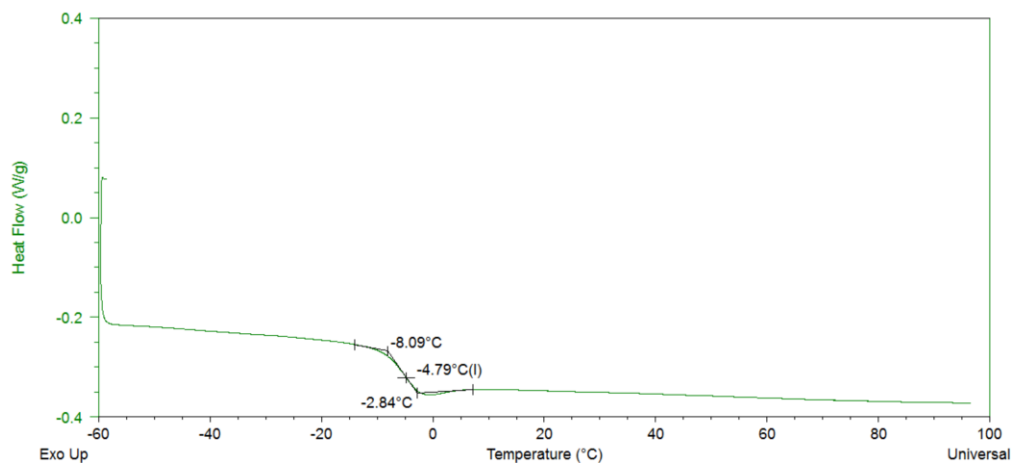


Figure A6.18. DSC trace for **PETG**.

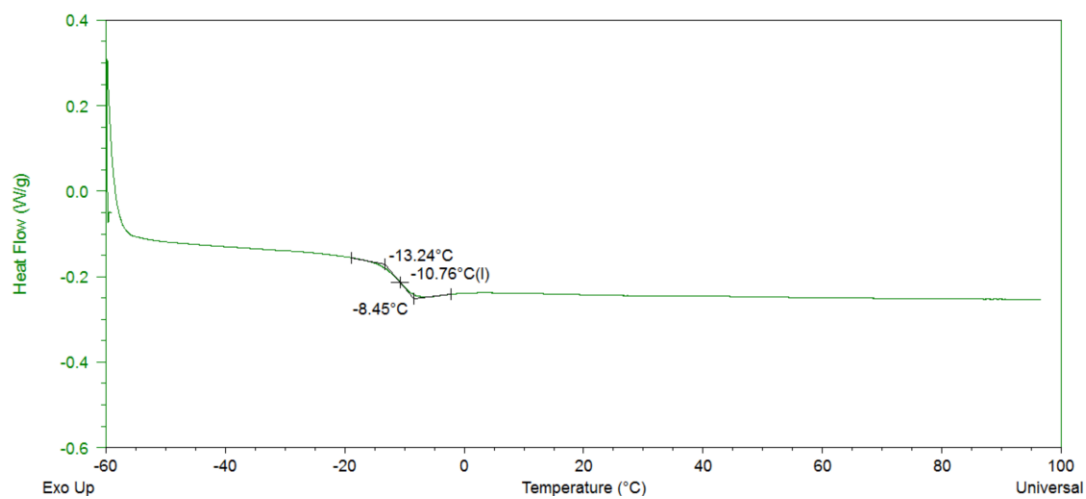


Figure A6.19. DSC trace for PEtBuG.

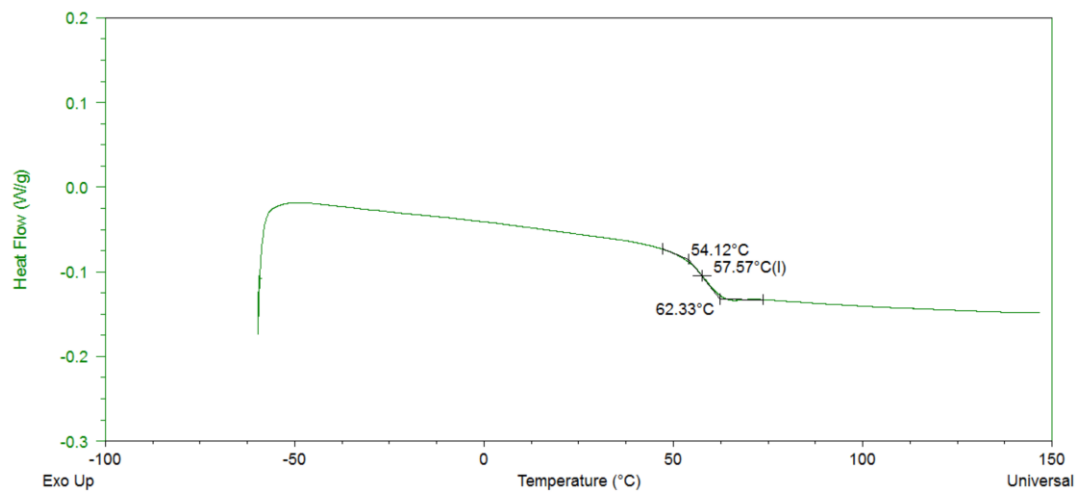


Figure A6.20. DSC trace for PMenG.

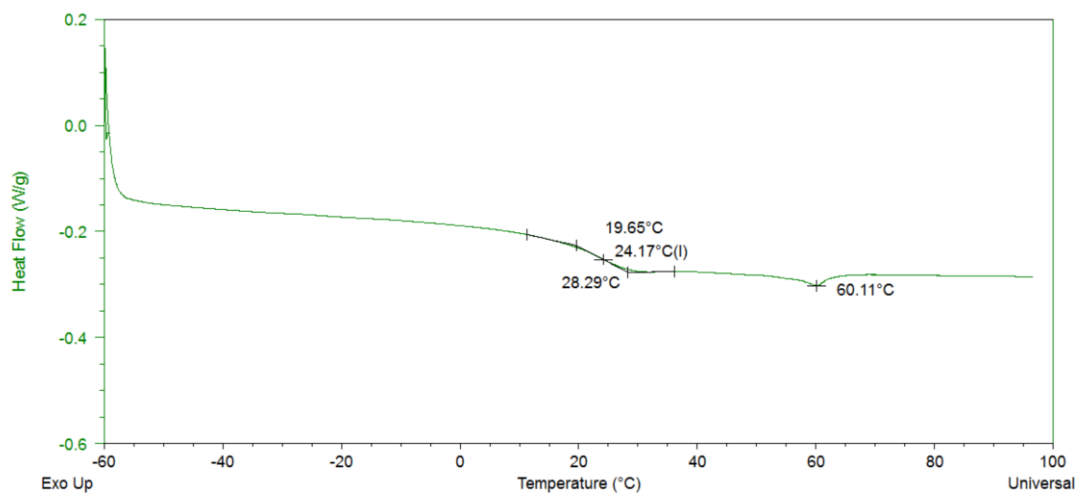


Figure A6.21. DSC trace for **PEtMenG**.

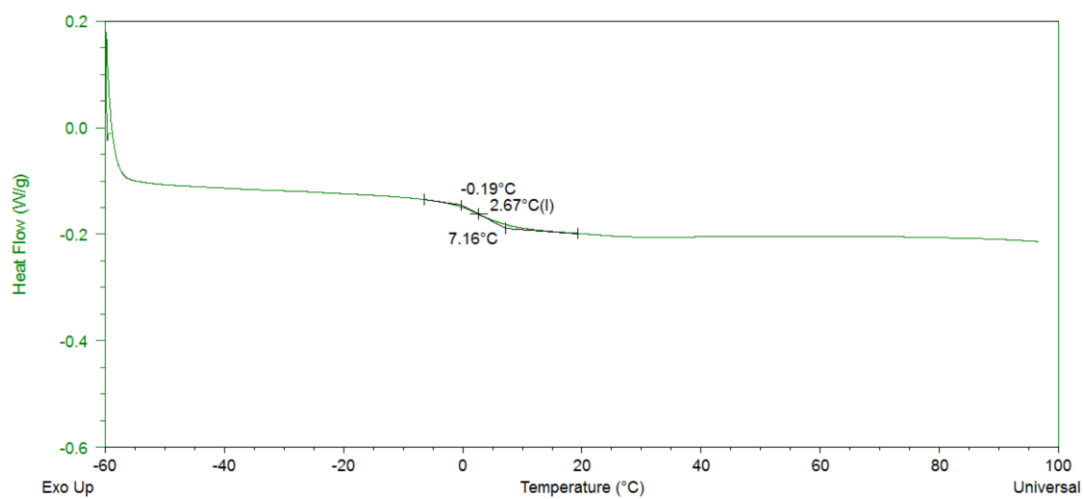


Figure A6.22. DSC trace for **PEtGC**.

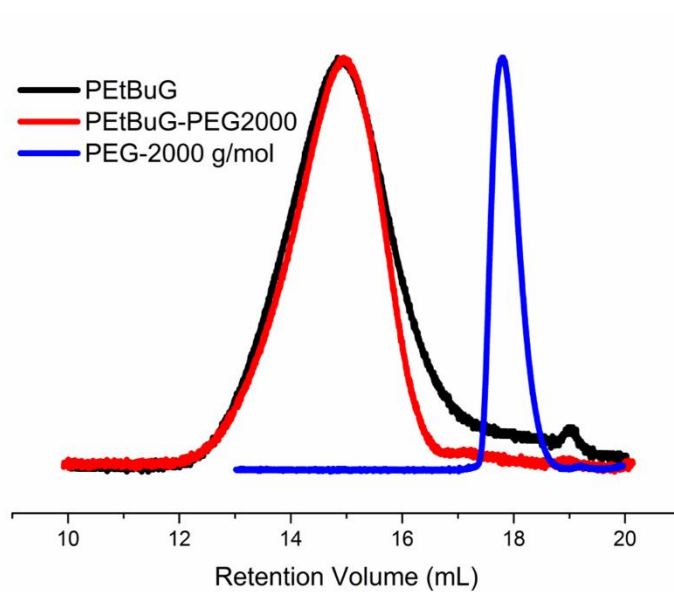


Figure A6.23. SEC traces of **PEtBuG** and **PEtBuG-PEG2000** (refractive index detection).

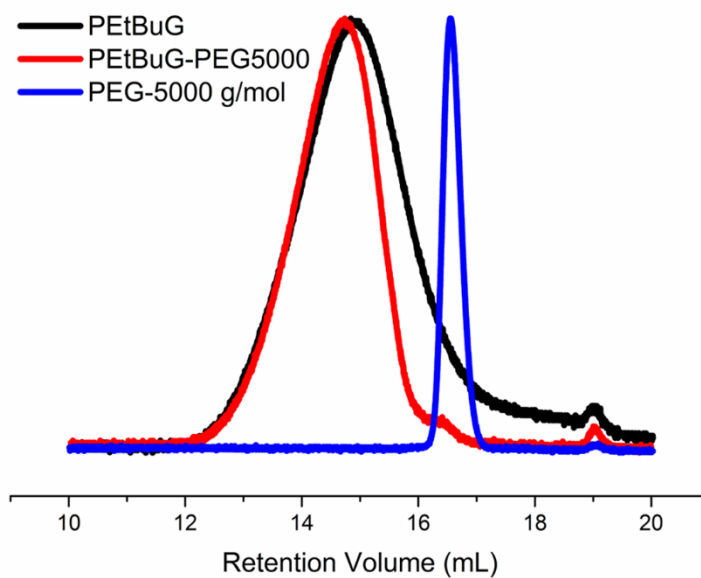


Figure A6.24. SEC traces of **PEtBuG** and **PEtBuG-PEG5000** (refractive index detection).

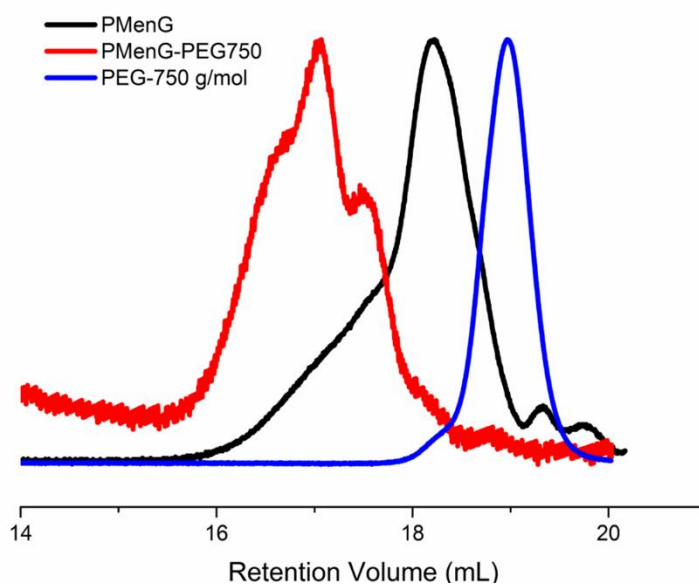


Figure A6.25. SEC traces of **PMenG** and **PMenG-PEG750** (refractive index detection).

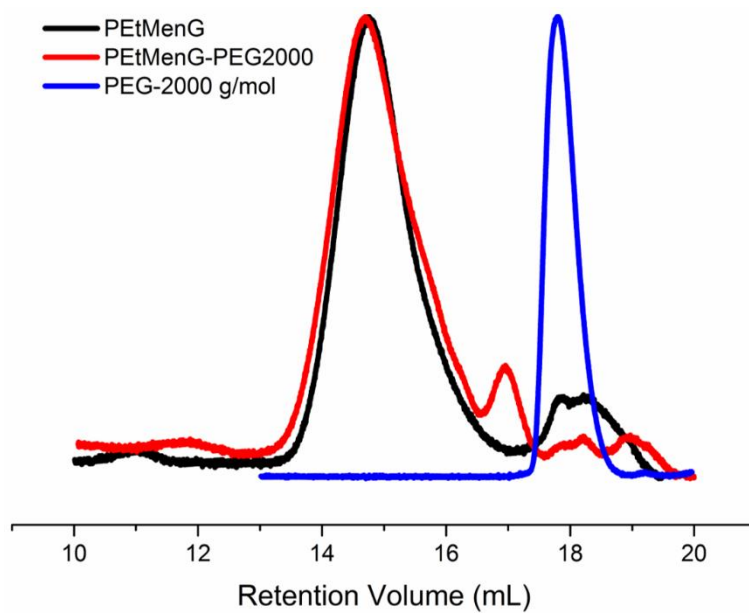


Figure A6.26. SEC traces of **PEtMenG** and **PEtMenG-PEG2000** (refractive index detection).

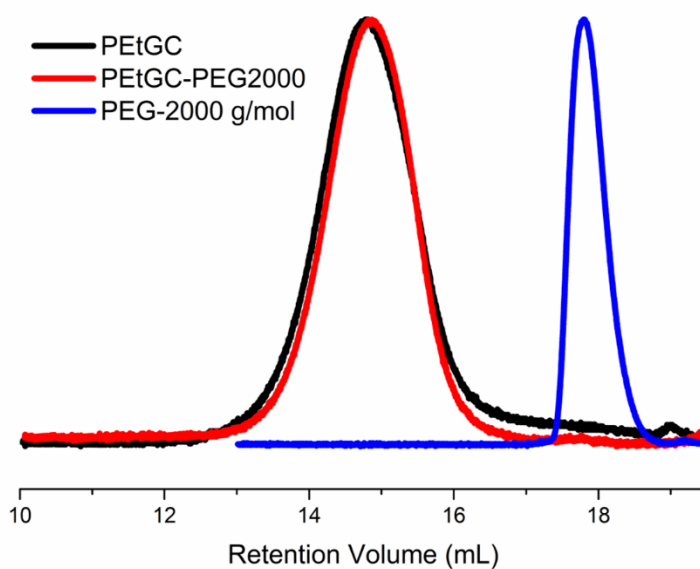


Figure A6.27. SEC traces of **PEtGC** and **PEtGC-PEG2000** (refractive index detection).

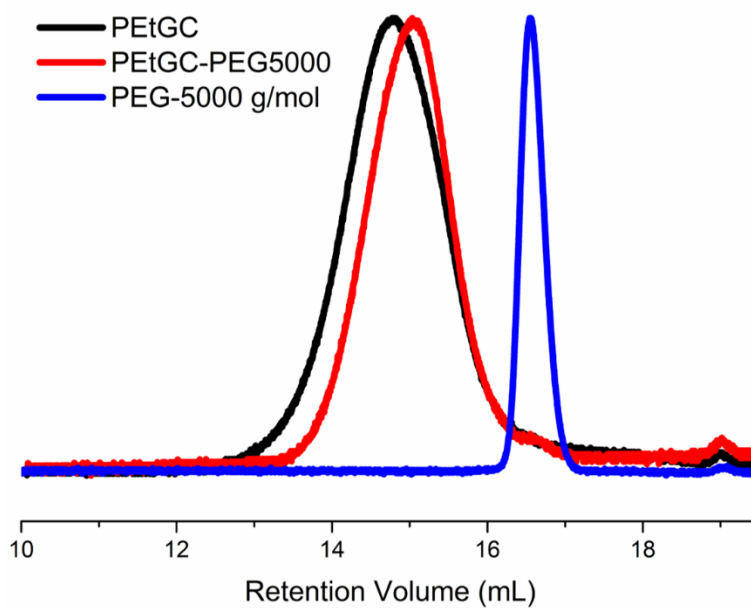


Figure A6.28. SEC traces of **PEtGC** and **PEtGC-PEG5000** (refractive index detection).

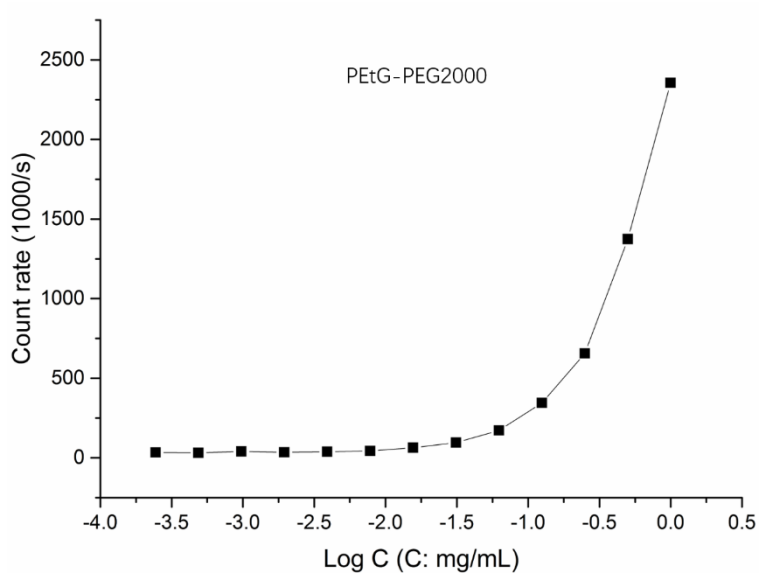


Figure A6.29. Nile red fluorescence intensity vs log(polymer concentration) for **PEtG-PEG2000**.

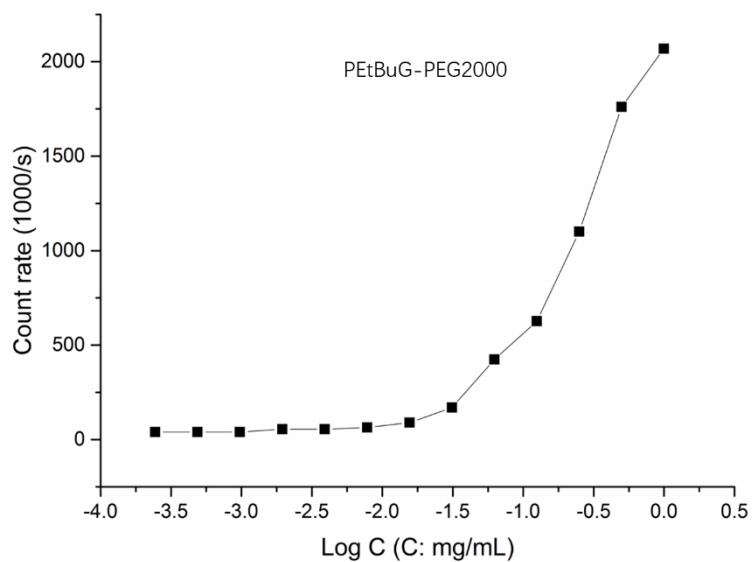


Figure A6.30. Nile red fluorescence intensity vs log(polymer concentration) for **PEtBuG-PEG2000**.

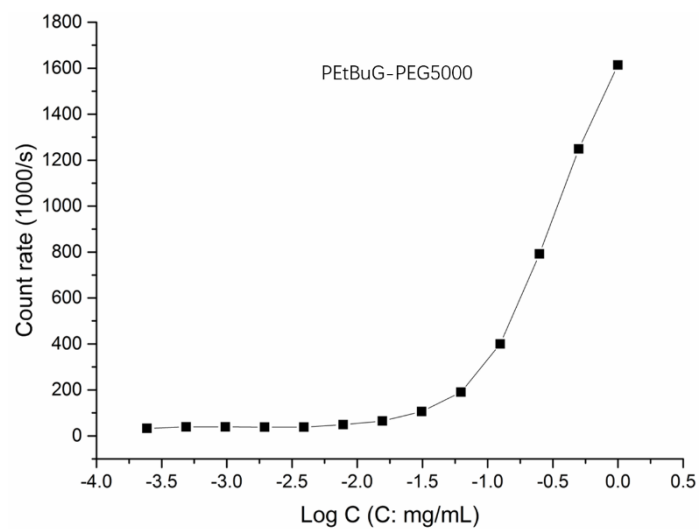


Figure A6.31. Nile red fluorescence intensity vs log(polymer concentration) for **PEtBuG-PEG5000**.

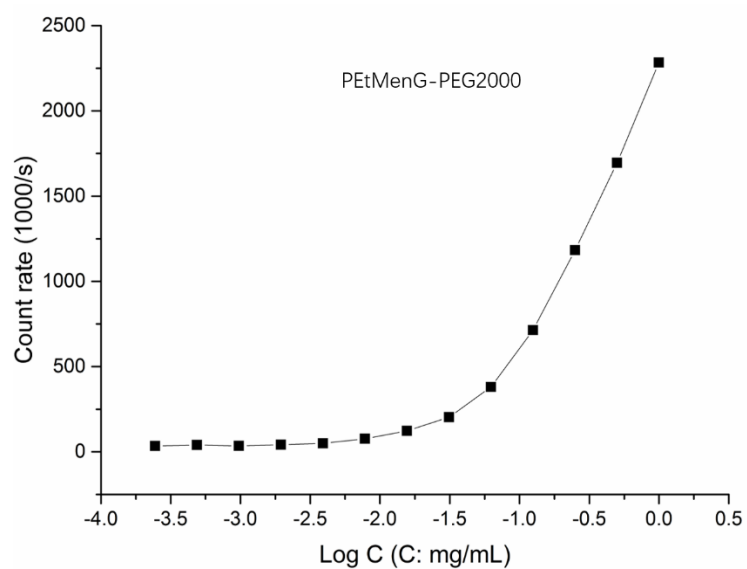


Figure A6.32. Nile red fluorescence intensity vs log(polymer concentration) for **PEtMenG-PEG2000**.

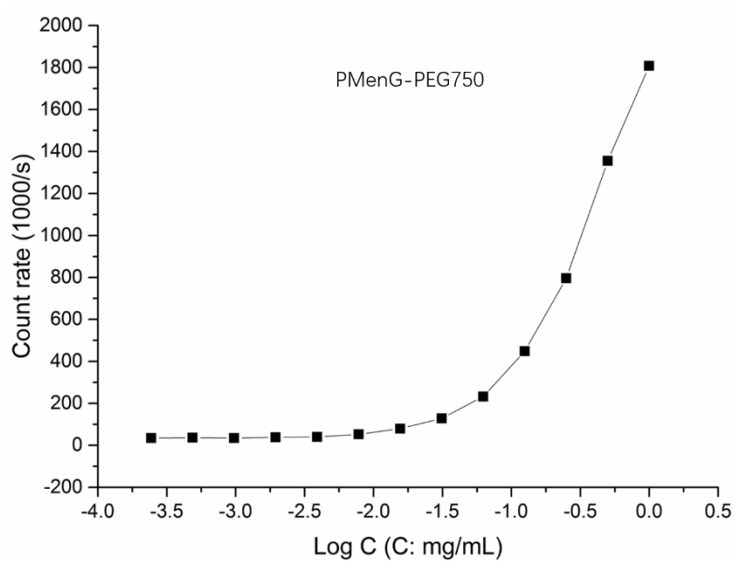


Figure A6.33. Nile red fluorescence intensity vs log(polymer concentration) for **PMenG-PEG750**.

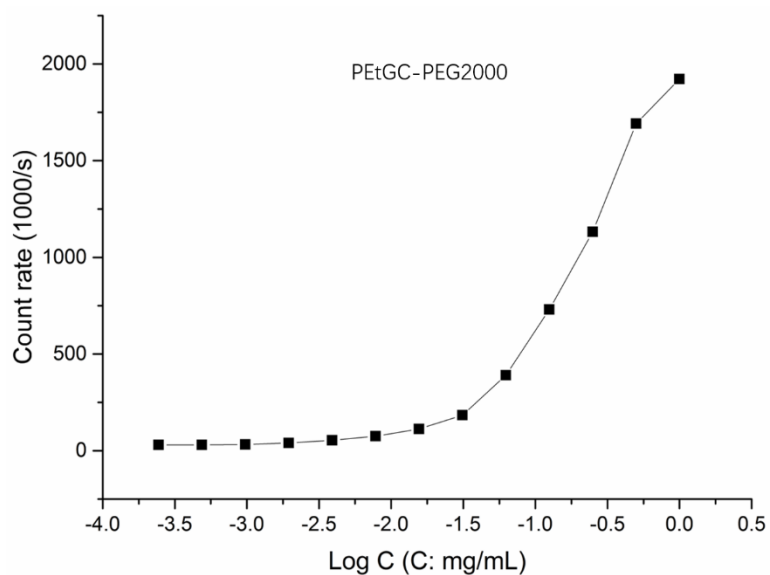


Figure A6.34. Nile red fluorescence intensity vs log(polymer concentration) for **PEtGC-PEG2000**.

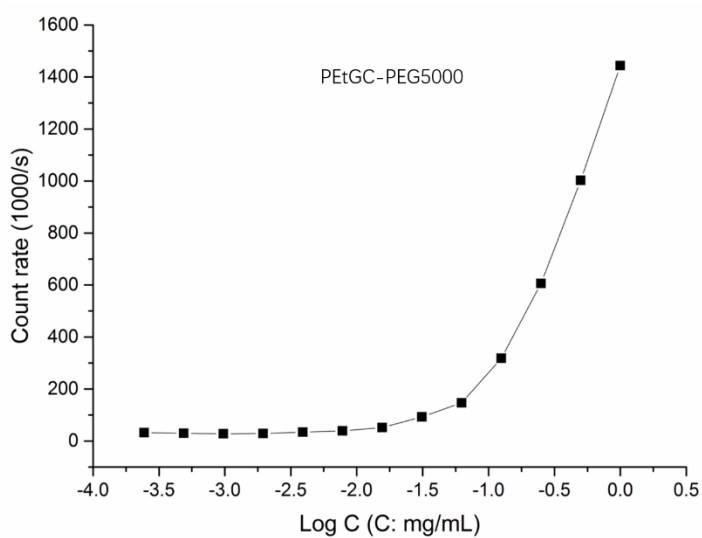


Figure A6.35. Nile red fluorescence intensity vs log(polymer concentration) for **PEtGC-PEG5000**.

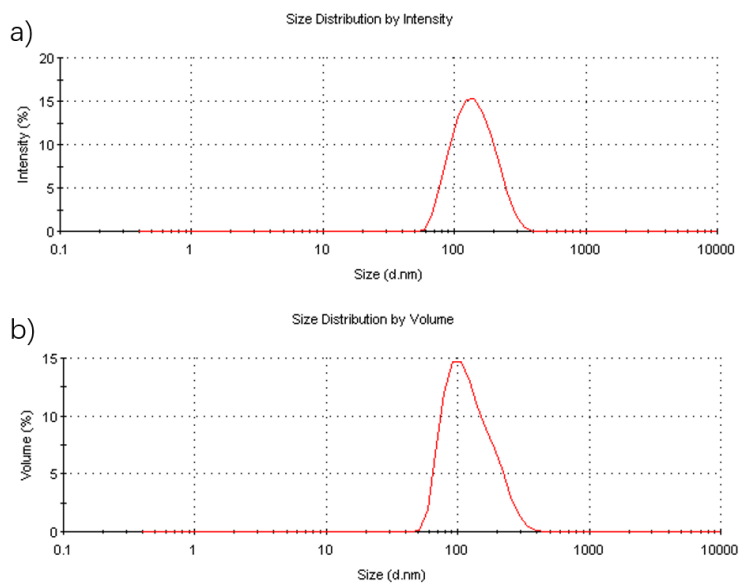


Figure A6.36. a) Intensity and b) Volume distributions of hydrodynamic diameters measured by DLS for assemblies prepared from **PEtBuG-PEG2000**.

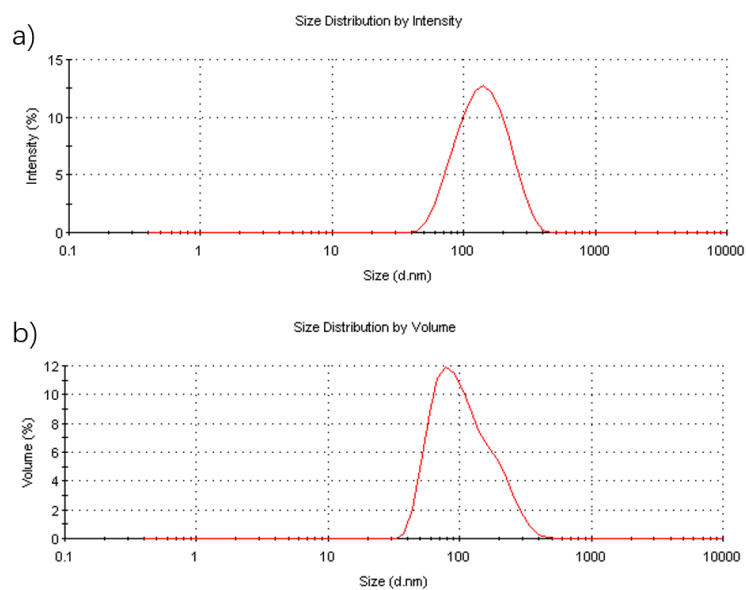


Figure A6.37. a) Intensity and b) Volume distributions of hydrodynamic diameters measured by DLS for assemblies prepared from **PEtBuG-PEG5000**.

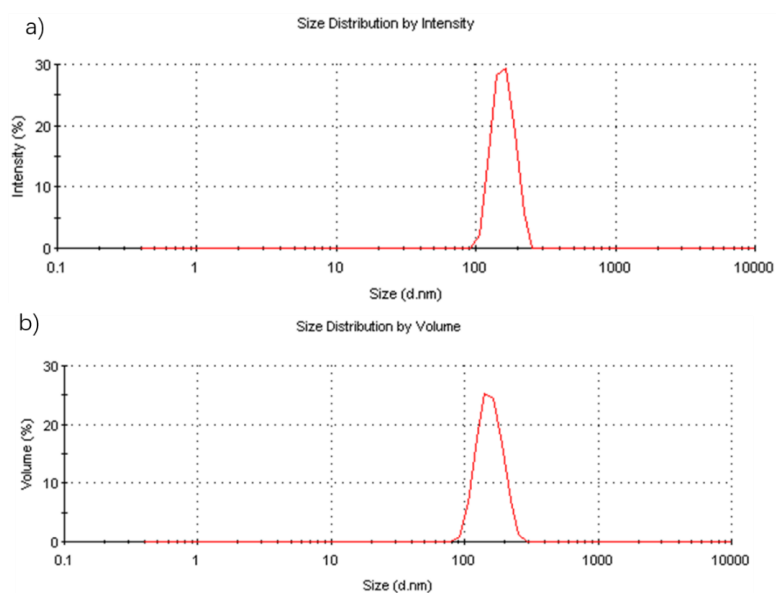


Figure A6.38. a) Intensity and b) Volume distributions of hydrodynamic diameters measured by DLS for assemblies prepared from **PMenG-PEG750**.

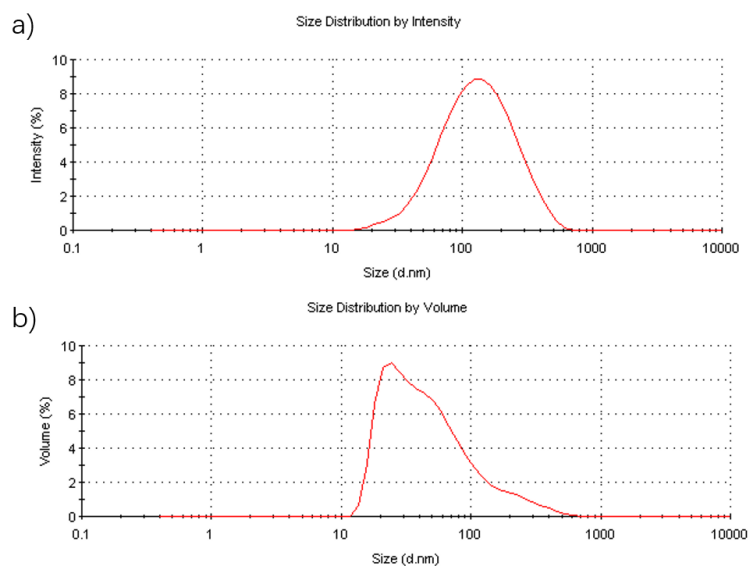


Figure A6.39. a) Intensity and b) Volume distributions of hydrodynamic diameters measured by DLS for assemblies prepared from **PEtMenG-PEG2000**.

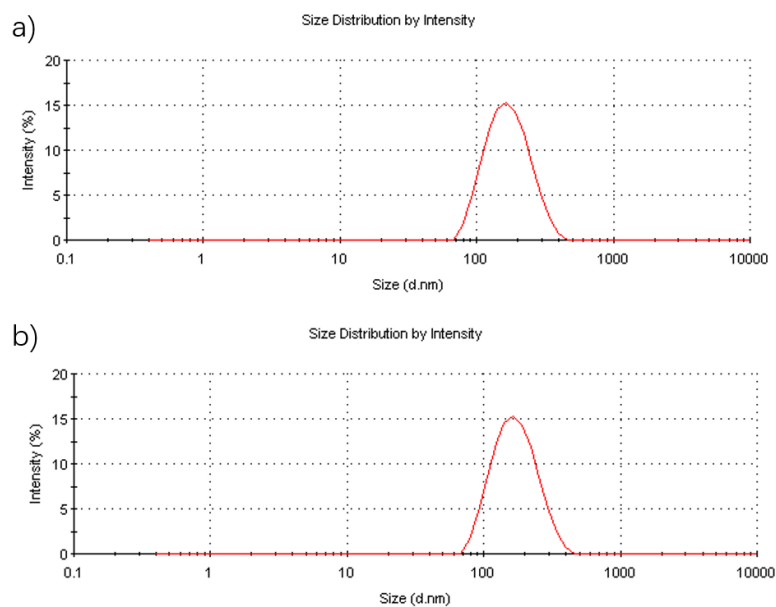


Figure A6.40. a) Intensity and b) Volume distributions of hydrodynamic diameters measured by DLS for assemblies prepared from **PEtGC-PEG2000**.

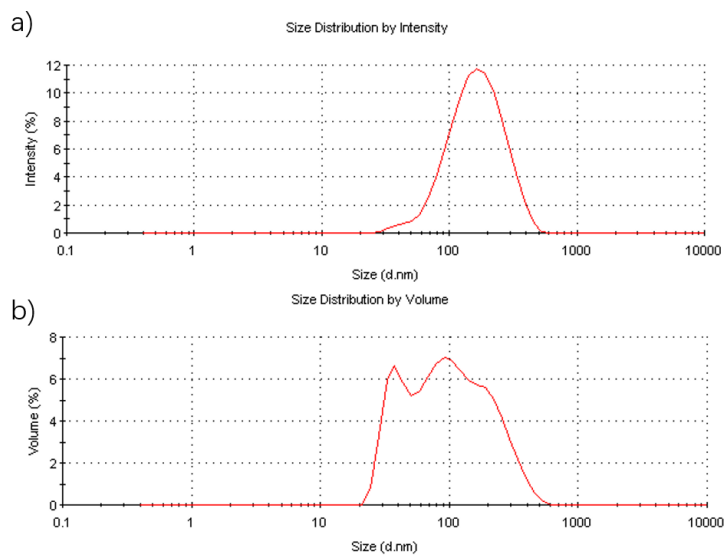


Figure A6.41. a) Intensity and b) Volume distributions of hydrodynamic diameters measured by DLS for assemblies prepared from **PEtGC-PEG5000**.

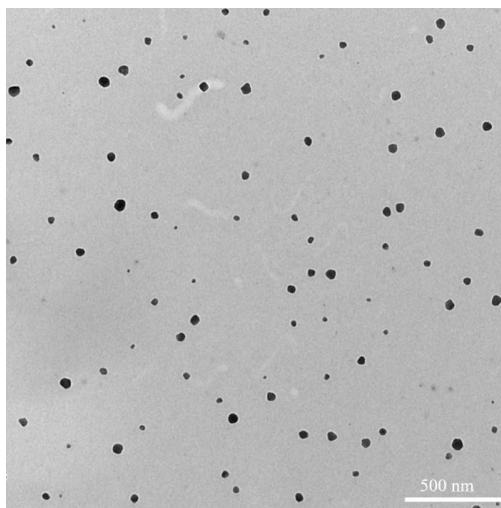


Figure A6.42. TEM images of particles formed from PEtG-PEG2000.

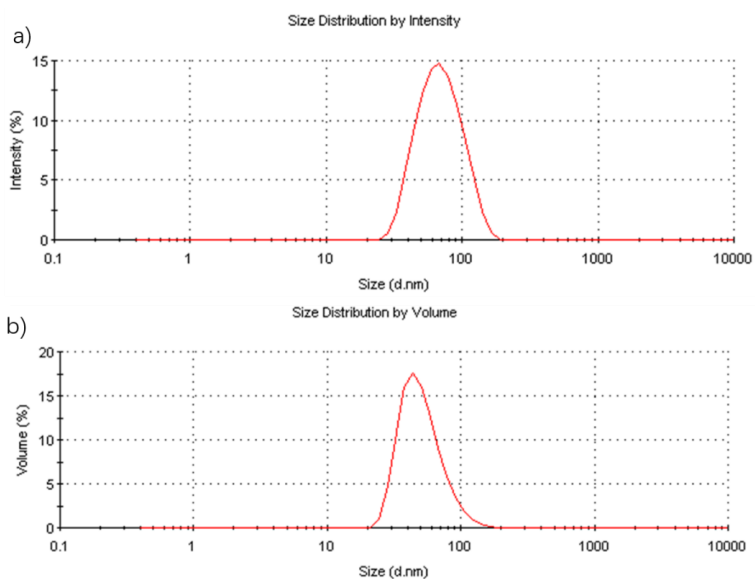


Figure A6.43. a) Intensity and b) Volume distributions of hydrodynamic diameters measured by DLS for assemblies loaded with celecoxib prepared from **PEtG-PEG2000**.

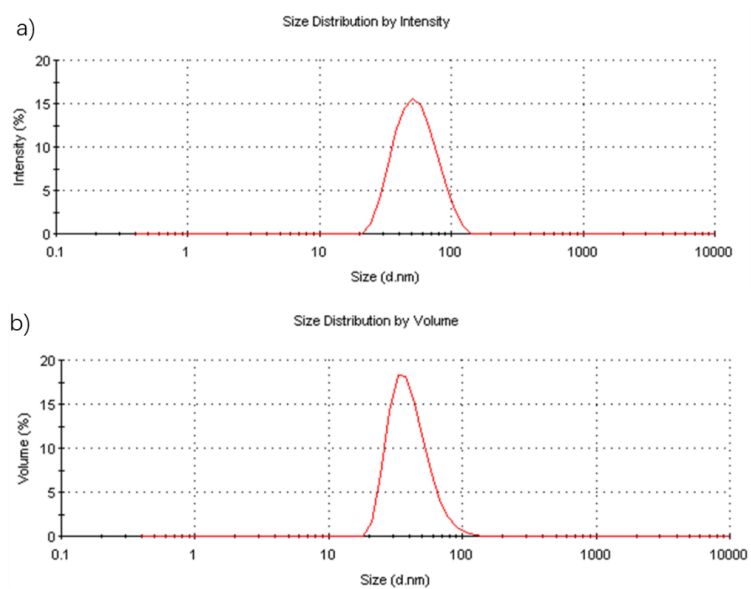


Figure A6.44. a) Intensity and b) Volume distribution of hydrodynamic diameters measured by DLS for assemblies loaded with celecoxib prepared from **PEtBuG-PEG2000**.

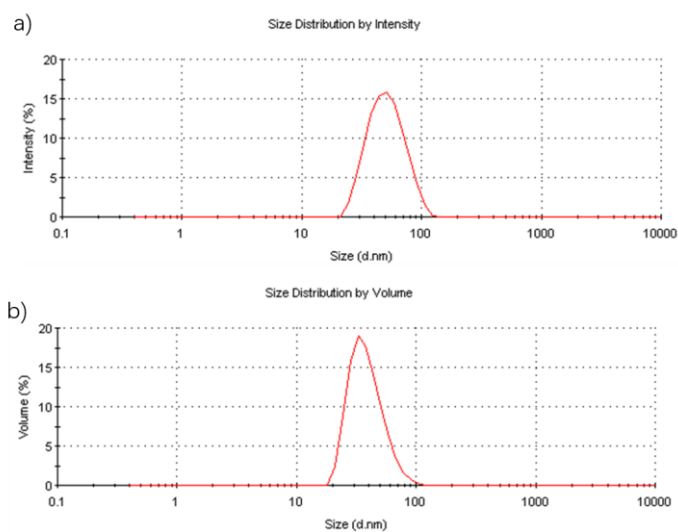


Figure A6.45. a) Intensity and b) Volume distributions of hydrodynamic diameters measured by DLS for assemblies loaded with celecoxib prepared from **PEtMenG-PEG2000**.

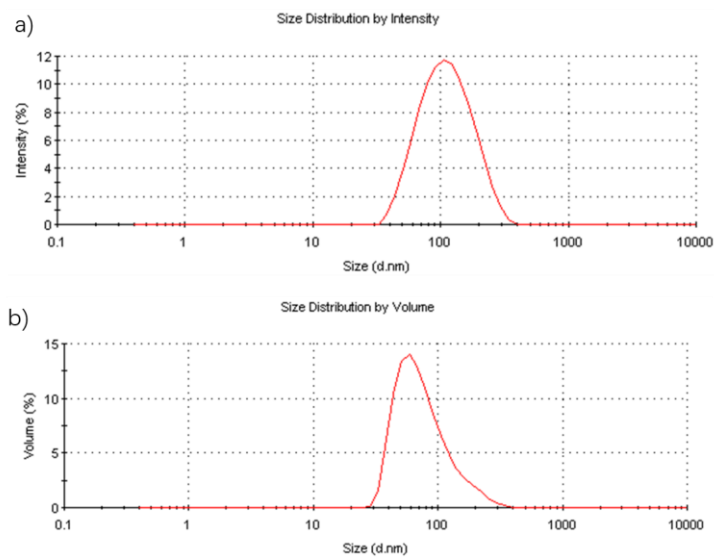


Figure A6.46. a) Intensity and b) Volume distributions of hydrodynamic diameters measured by DLS for assemblies loaded with celecoxib prepared from **PEtGC-PEG2000**.

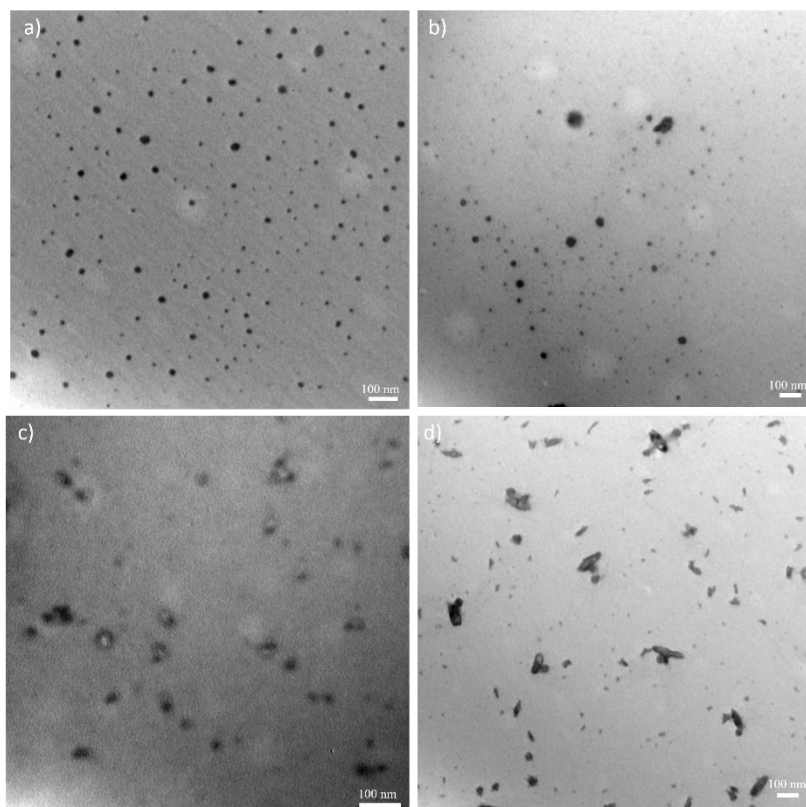


Figure A6.47. TEM images of a) **PEtG-PEG2000**, b) **PEtBuG-PEG2000**, c) **PEtMenG-PEG2000** and d) **PEtGC-PEG2000** particles loaded with celecoxib.

Appendix 7: Supporting information for Chapter 7

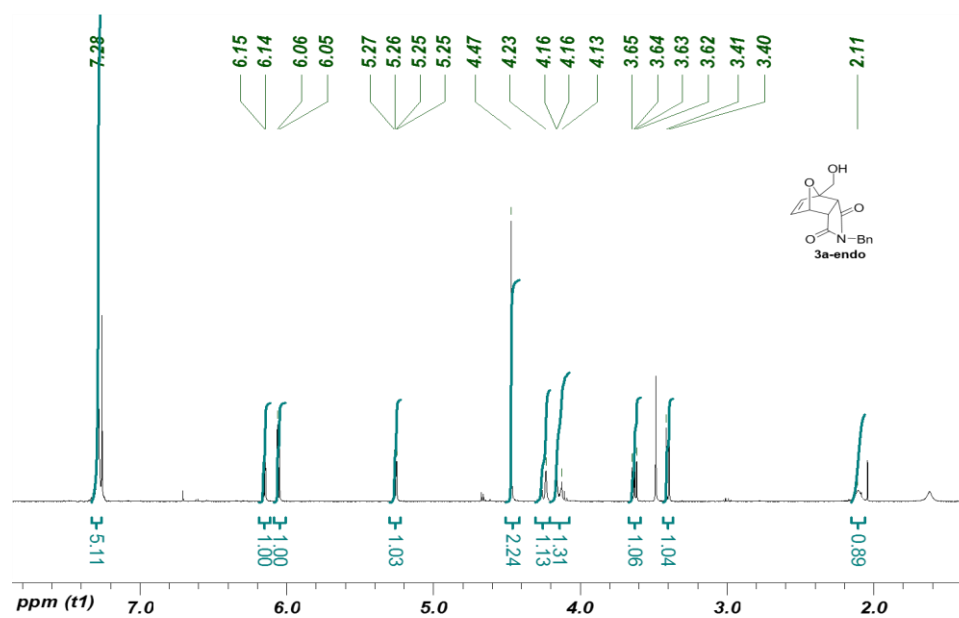


Figure A7.1. ¹H NMR spectrum of Compound **3a-endo** (CDCl₃, 600Hz).

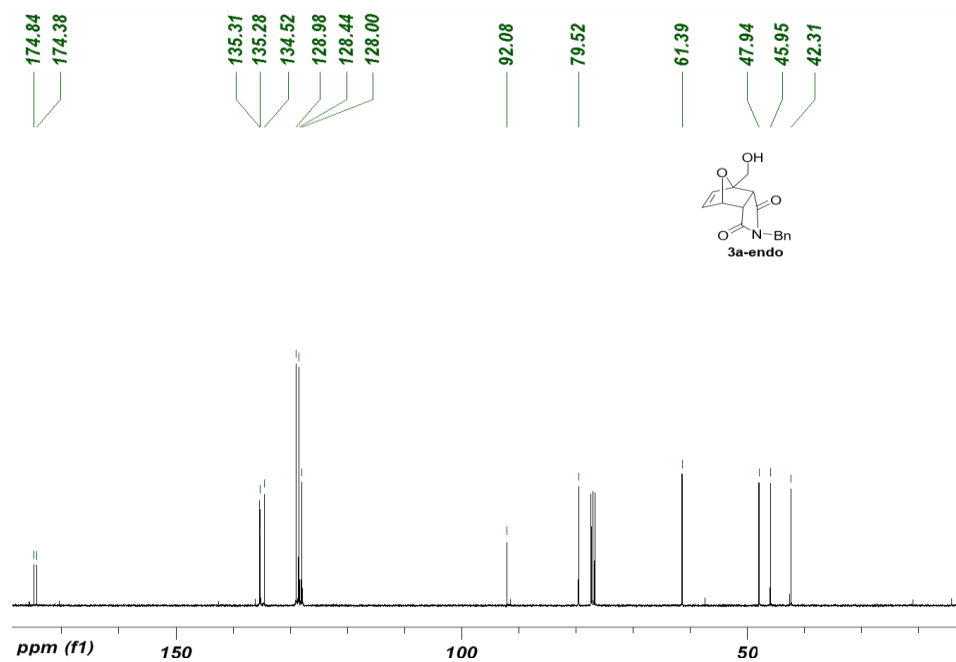


Figure A7.2. ¹³C NMR spectrum of Compound **3a-endo** (CDCl₃, 100Hz).

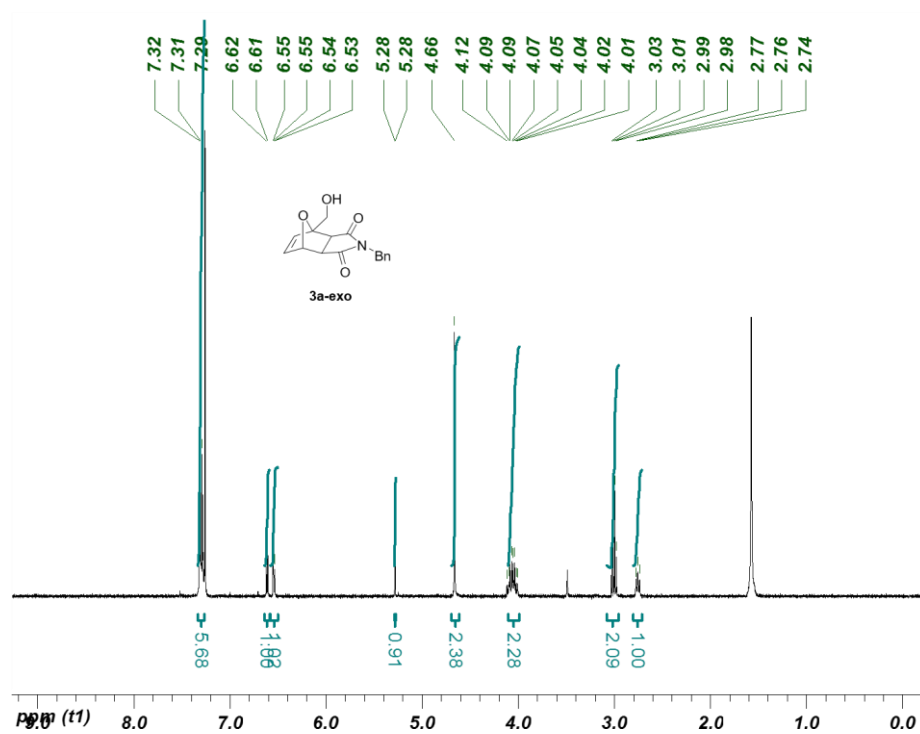


Figure A7.3. ^1H NMR spectrum of Compound **3a-exo** (CDCl_3 , 600Hz)

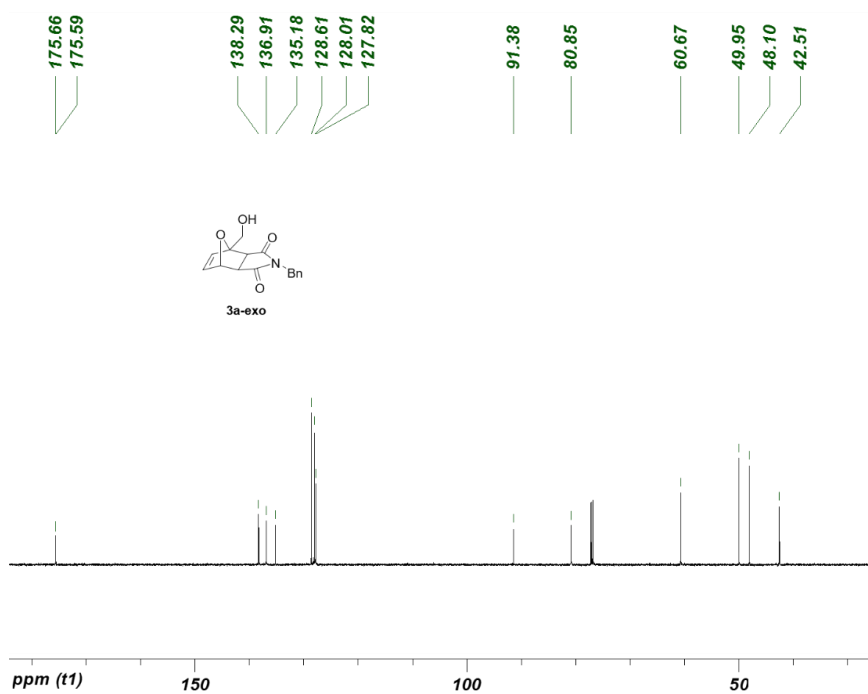


Figure A7.4. ^{13}C NMR spectrum of Compound **3a-exo** (CDCl_3 , 100Hz).

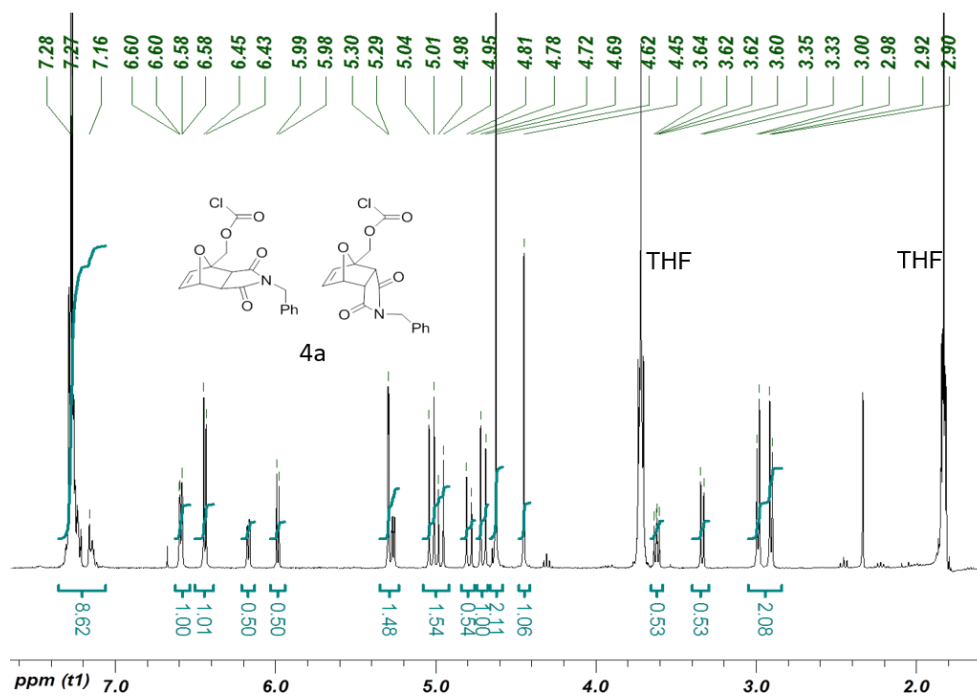


Figure A7.5. ^1H NMR spectrum of Chloroformate **4a** (CDCl_3 , 400Hz) (residual THF present).

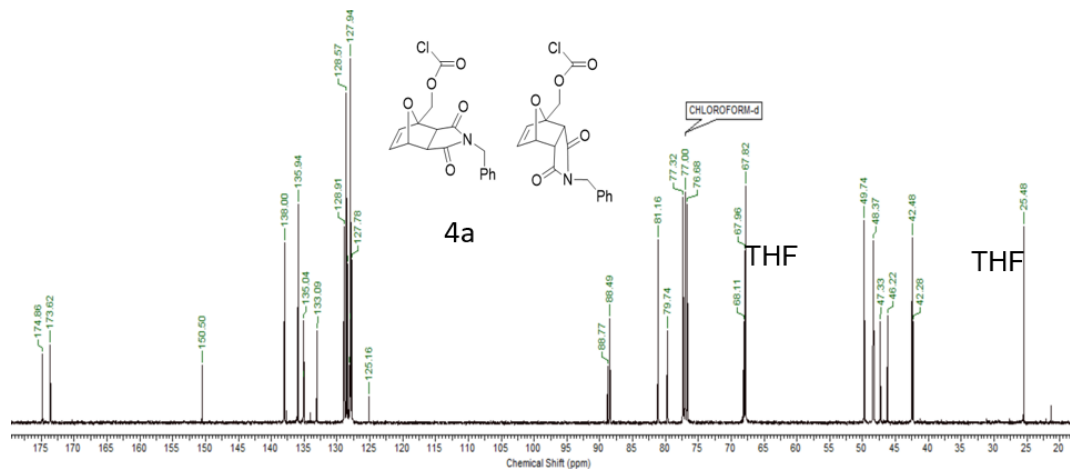


Figure A7.6. ^{13}C NMR spectrum of Chloroformate **4a** (CDCl_3 , 100Hz).

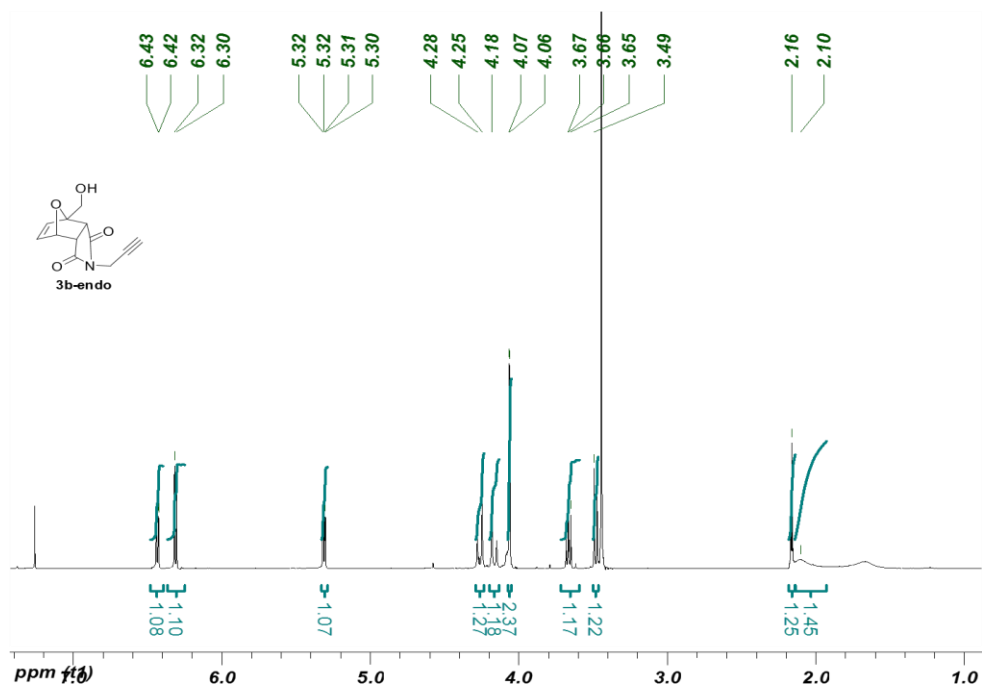


Figure A7.7. ¹H NMR spectrum of Compound **3b-endo** (CDCl₃, 600Hz).

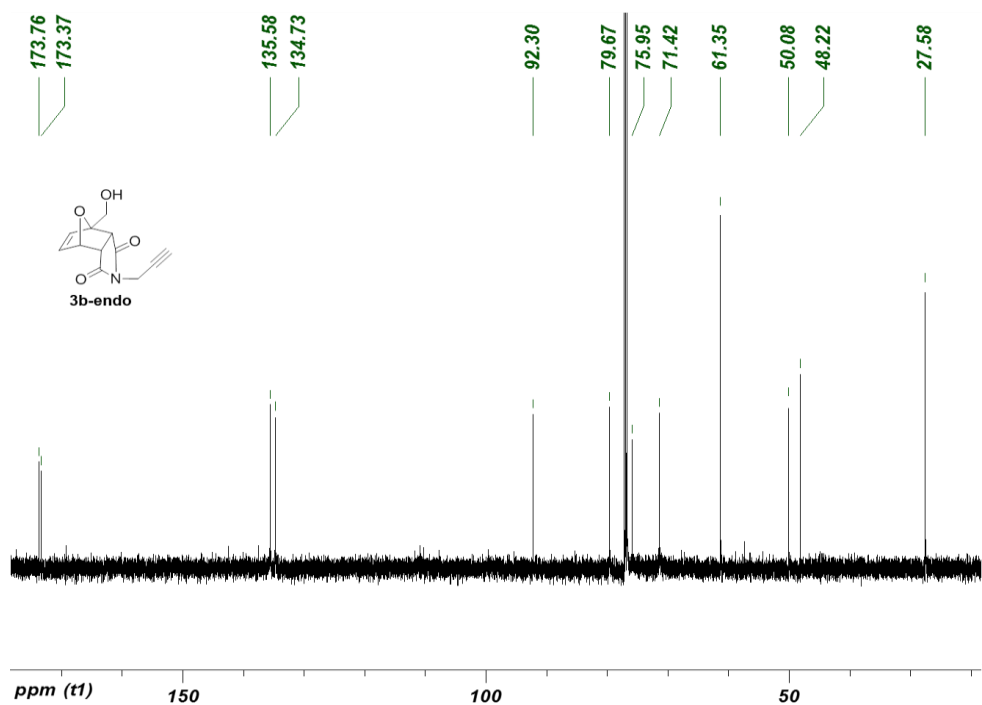


Figure A7.8. ¹³C NMR spectrum of Compound **3b-endo** (CDCl₃, 100Hz).

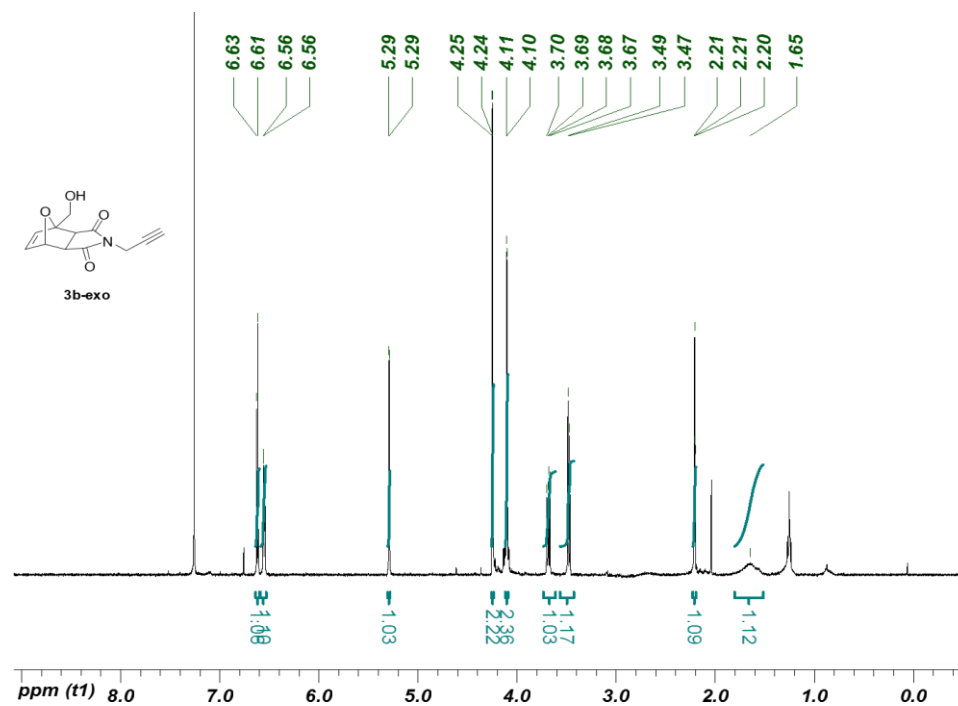


Figure A7.9. ¹H NMR spectrum of Compound **3b-exo** (CDCl₃, 400Hz).

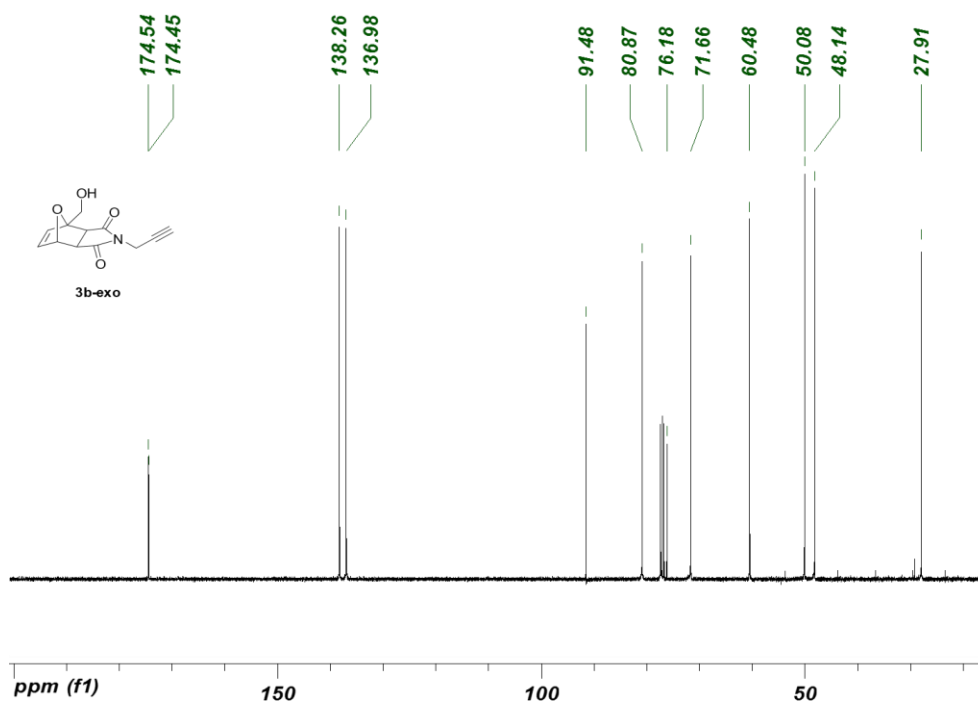


Figure A7.10. ¹³C NMR spectrum of Compound **3b-exo** (CDCl₃, 100Hz).

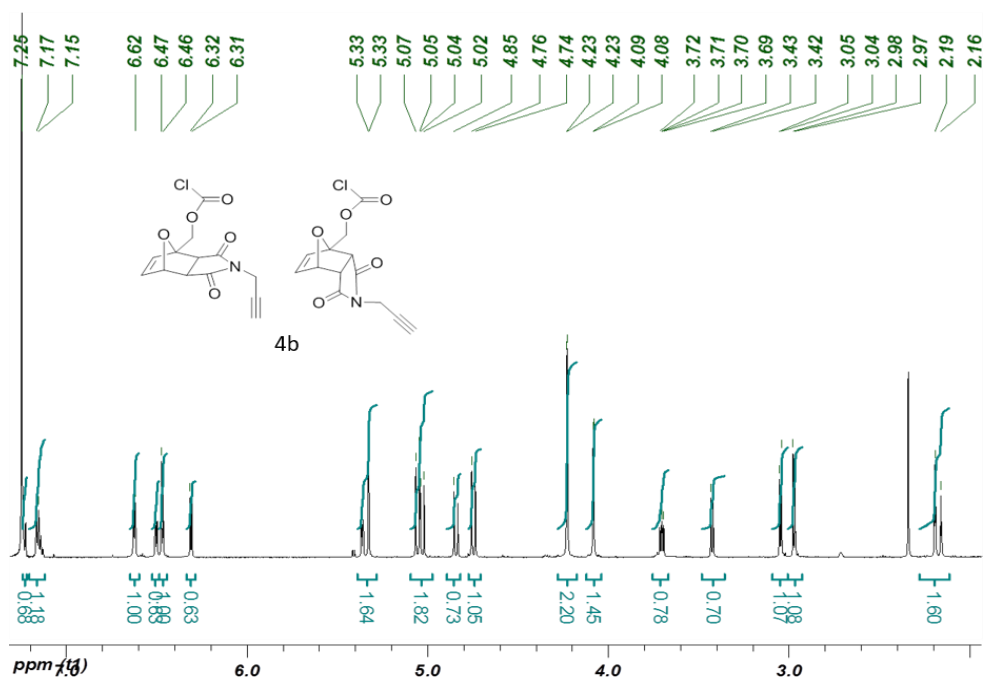


Figure A7.11. ¹H NMR spectrum of Chloroformate **4b** (CDCl₃, 400Hz).

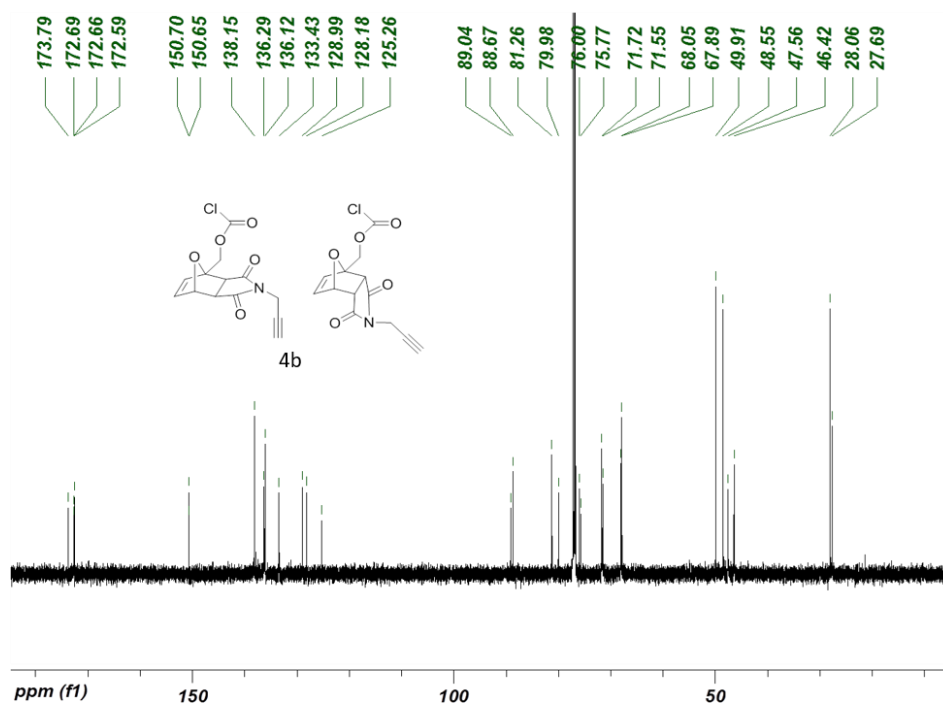


Figure A7.12. ¹³C NMR spectrum of Chloroformate **4b** (CDCl₃, 100Hz).

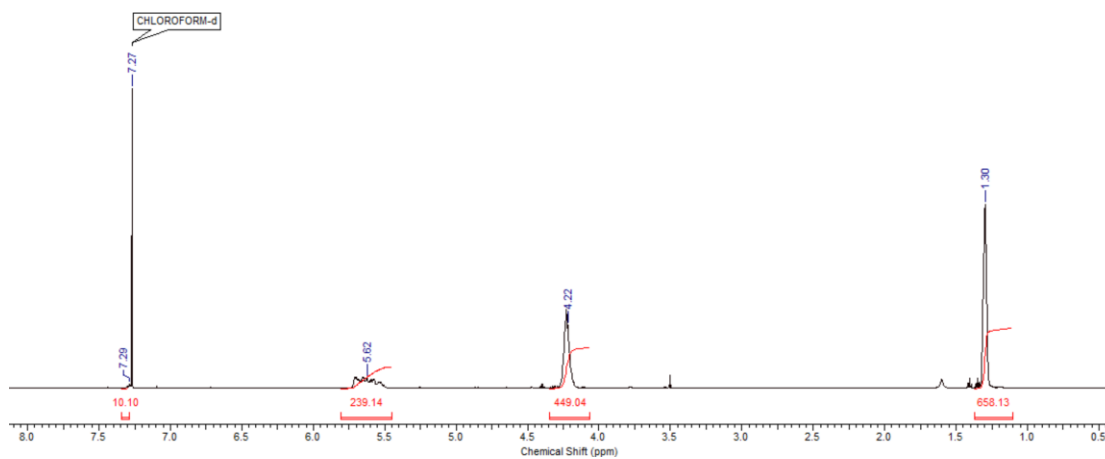


Figure A7.13. ^1H NMR spectrum of **PEtG-DA-Bn** (CDCl_3 , 600Hz).

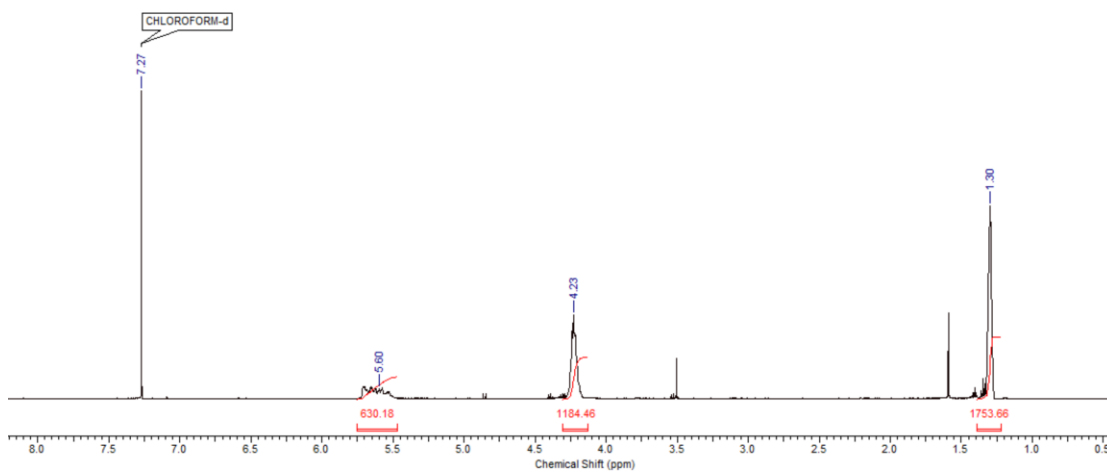


Figure A7.14. ^1H NMR spectrum of **PEtG-DA-alkyne** (CDCl_3 , 600Hz).

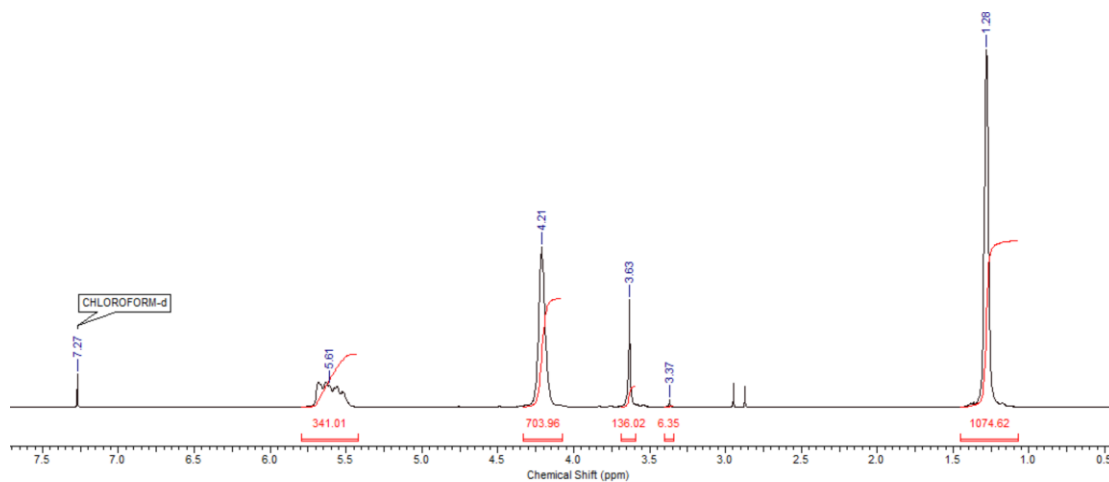


Figure A7.15. ^1H NMR spectrum of **PEtG-DA-PEG750** (CDCl_3 , 600Hz). The success of the PEG coupling is evidenced by the presence of the PEG peak at 3.6 ppm and its corresponding integration.

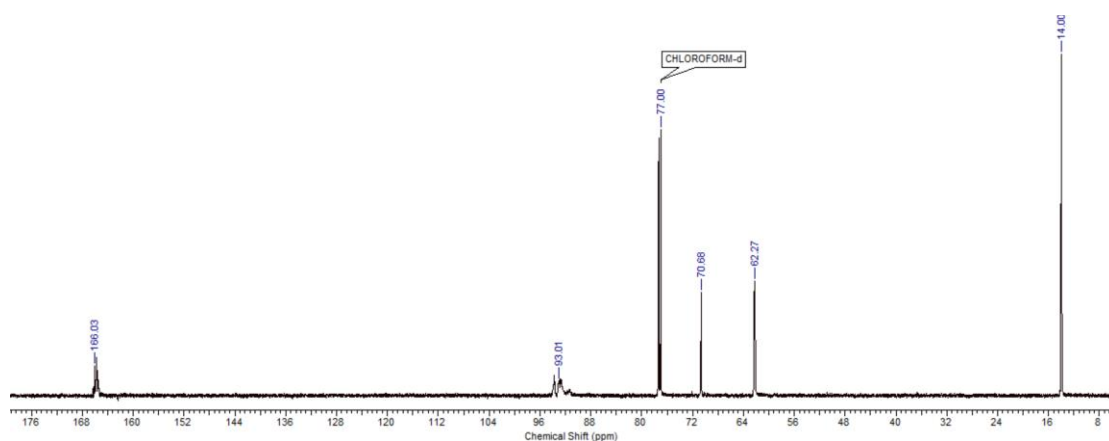


Figure A7.16. ^{13}C NMR spectrum of **PEtG-DA-PEG750** (CDCl_3 , 150Hz). The success of the PEG coupling is evidenced by the presence of the PEG peak at 70 ppm.

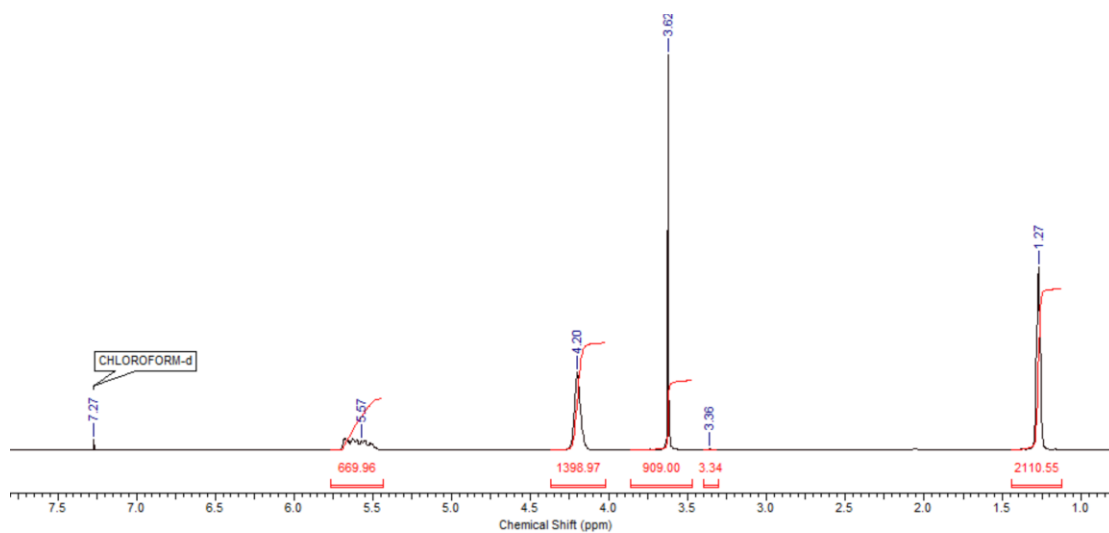


Figure A7.17. ^1H NMR spectrum of **PEtG-DA-PEG5000** (CDCl_3 , 600Hz). The success of the PEG coupling is evidenced by the presence of the PEG peak at 3.6 ppm and its corresponding integration.

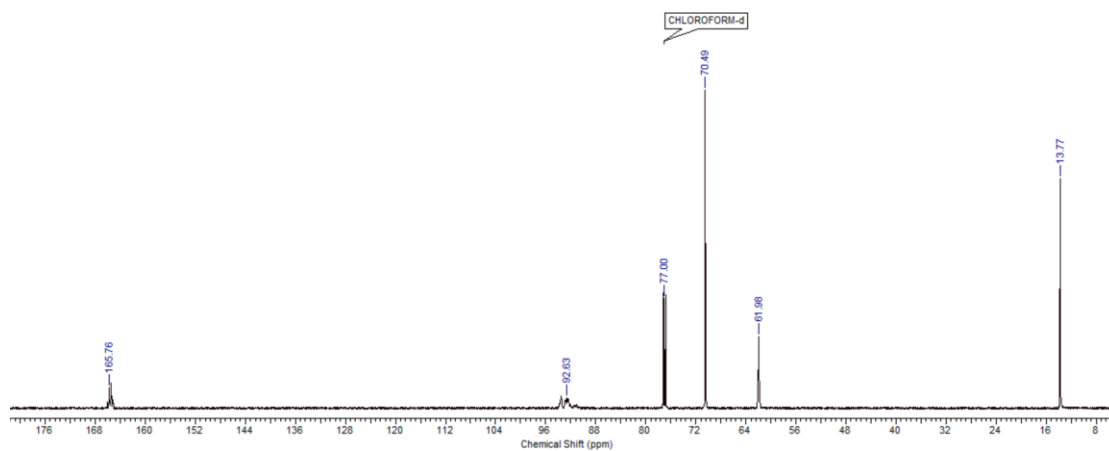


Figure A7.18. ^{13}C NMR spectrum of **PEtG-DA-PEG5000** (CDCl_3 , 150Hz). The success of the PEG coupling is evidenced by the presence of the PEG peak at 70 ppm.

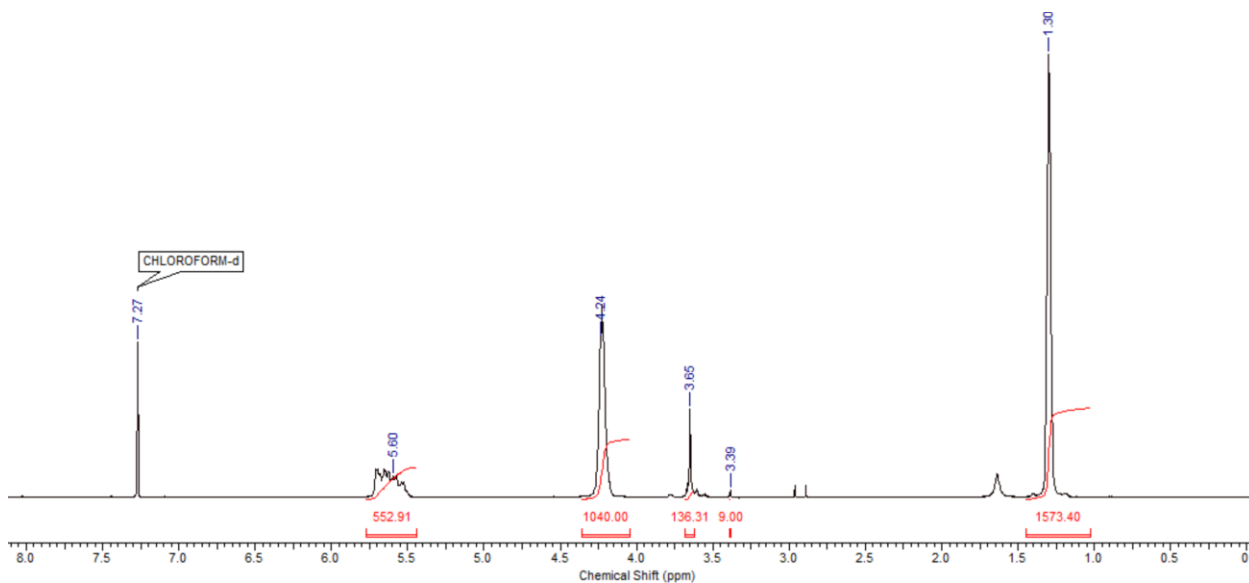


Figure A7.19. ^1H NMR spectrum of **Vesicle-control** (CDCl_3 , 600Hz). The success of the PEG coupling is evidenced by the presence of the PEG peak at 3.6 ppm and its corresponding integration.

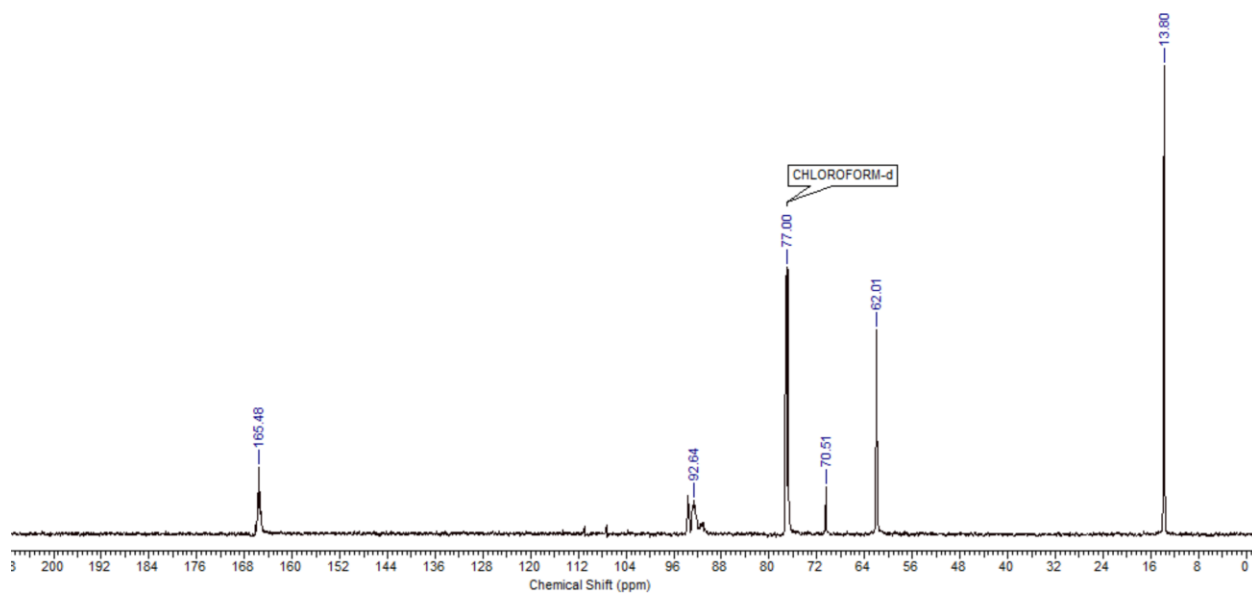


Figure A7.20. ^{13}C NMR spectrum of **Vesicle-control** (CDCl_3 , 150Hz). The success of the PEG coupling is evidenced by the presence of the PEG peak at 70 ppm.

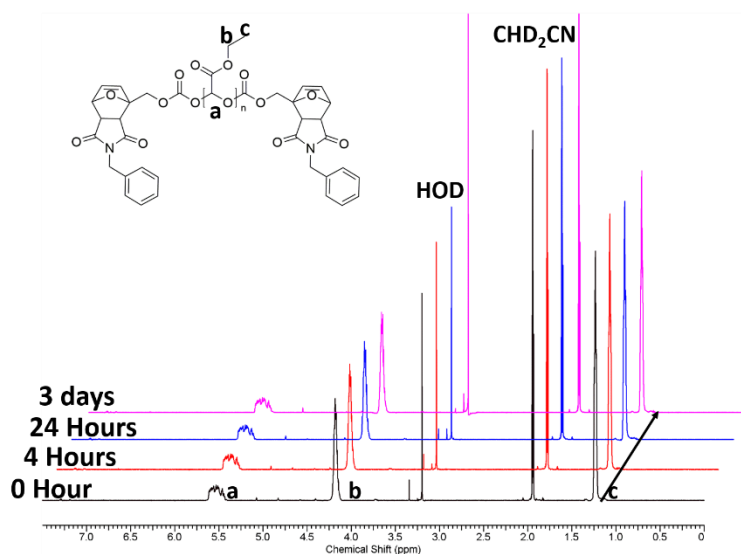


Figure A7.21. ^1H NMR spectra of **PETG-DA-Bn** incubated in 9:1 $\text{CD}_3\text{CN}:\text{D}_2\text{O}$ at 22 $^\circ\text{C}$ over time. Spectra are offset to allow the progression over time to be clearly observed.

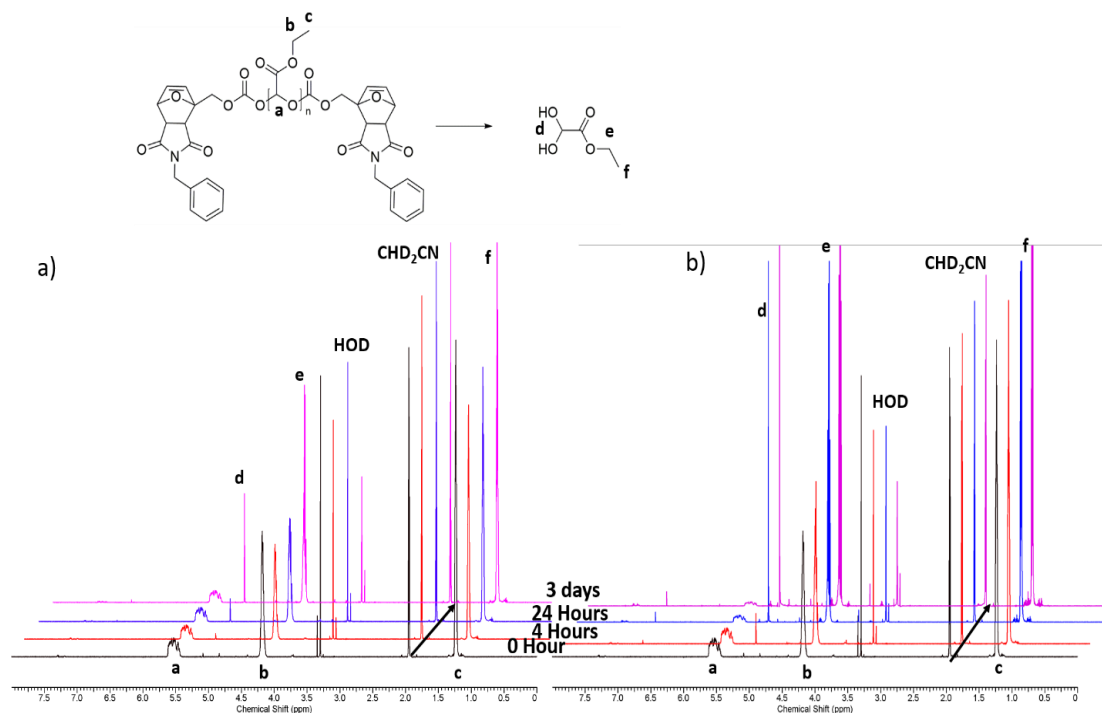


Figure A7.22. ^1H NMR spectra of **PETG-DA-Bn** incubated in 9:1 $\text{CD}_3\text{CN}:\text{D}_2\text{O}$ at a) 40 $^\circ\text{C}$ and b) 60 $^\circ\text{C}$. Spectra are offset to allow the progression over time to be clearly observed.

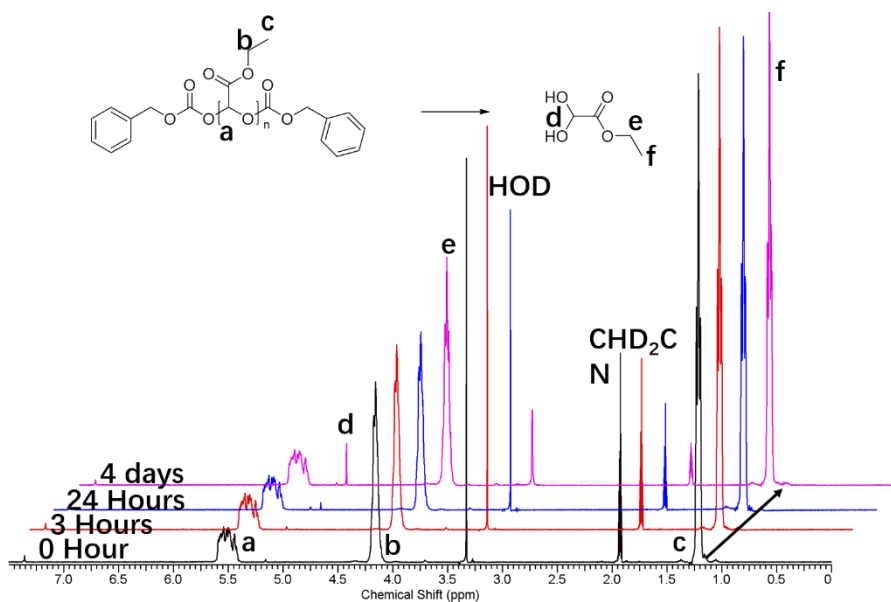


Figure A7.23. ^1H NMR spectra of **PEtG-control** incubated in 9:1 $\text{CD}_3\text{CN}:\text{D}_2\text{O}$ at 75°C . Spectra are offset to allow the progression over time to be clearly observed.

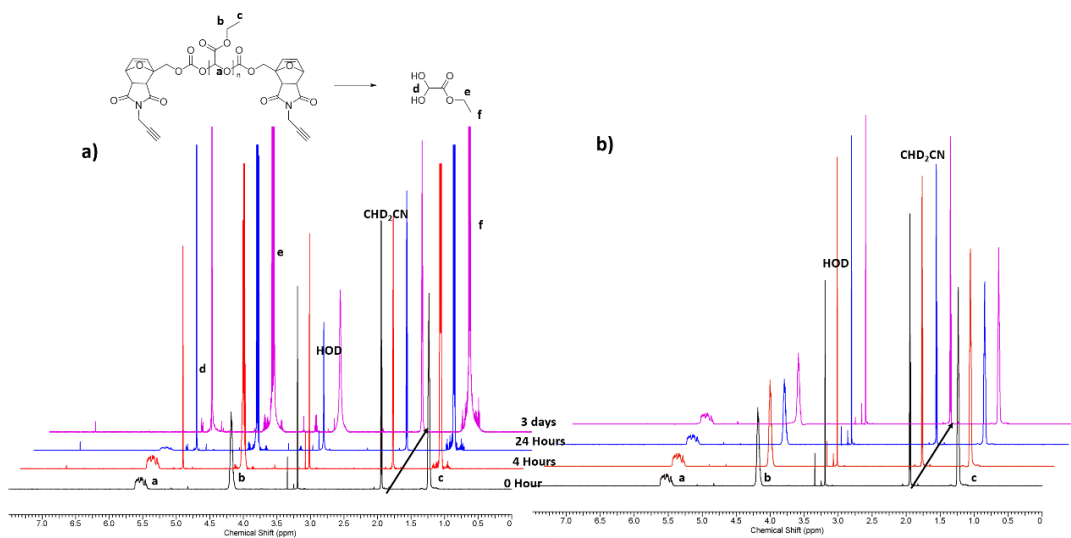


Figure A7.24. ^1H NMR spectra of **PEtG-DA-alkyne** incubated in 9:1 $\text{CD}_3\text{CN}:\text{D}_2\text{O}$ at a) 75°C and b) 22°C . Spectra are offset to allow the progression over time to be clearly observed.

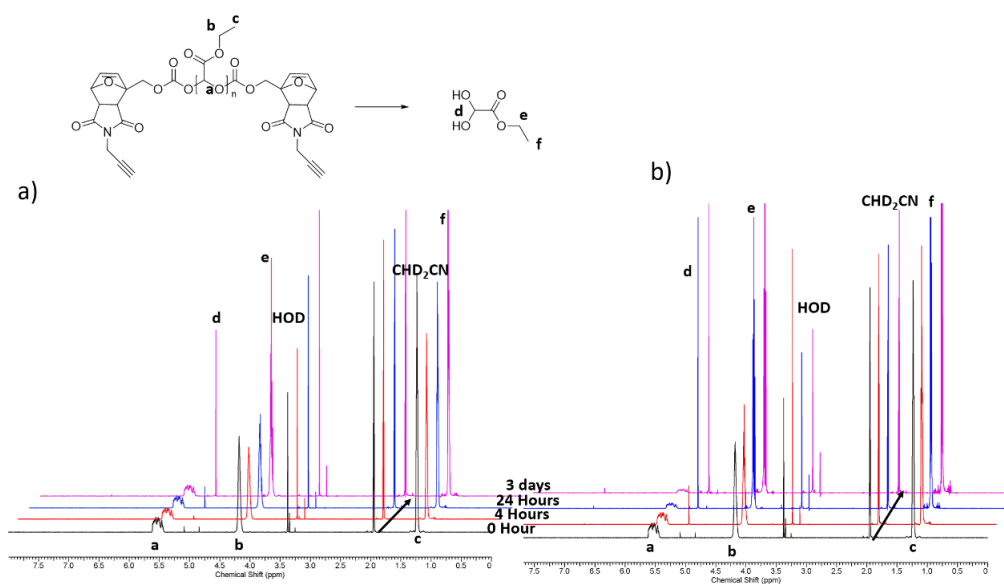


Figure A7.25. ^1H NMR spectra of **PETG-DA-alkyne** incubated in 9:1 $\text{CD}_3\text{CN}:\text{D}_2\text{O}$ at a) 40 °C and b) 60 °C. Spectra are offset to allow the progression over time to be clearly observed.

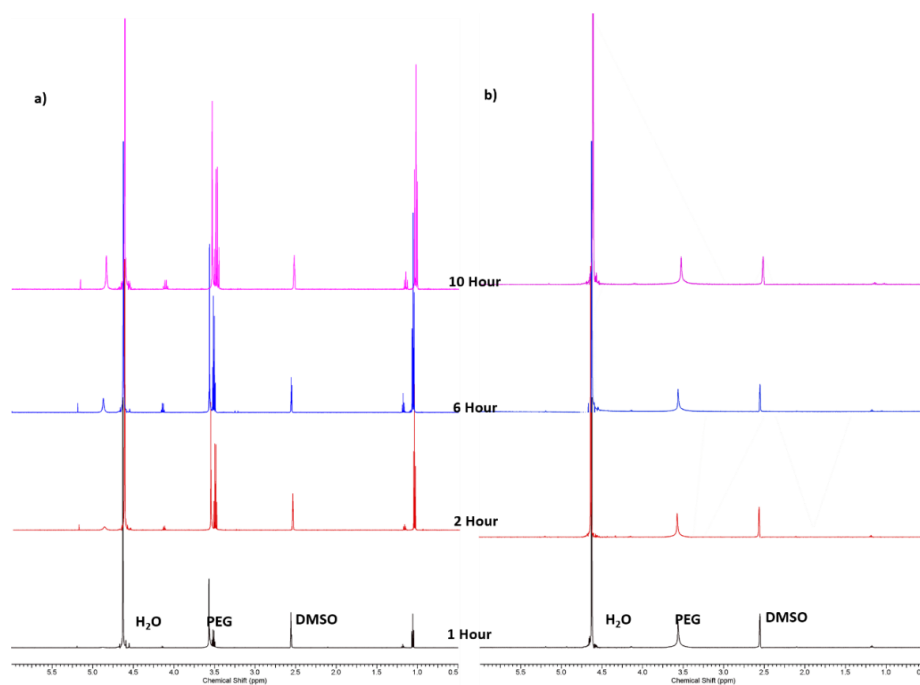


Figure A7.26. ^1H NMR spectra of **PETG-DA-PEG5000** micelles incubated in 5:1 $\text{DMSO-}d_6:\text{D}_2\text{O}$ at a) 75 °C and b) 22 °C.

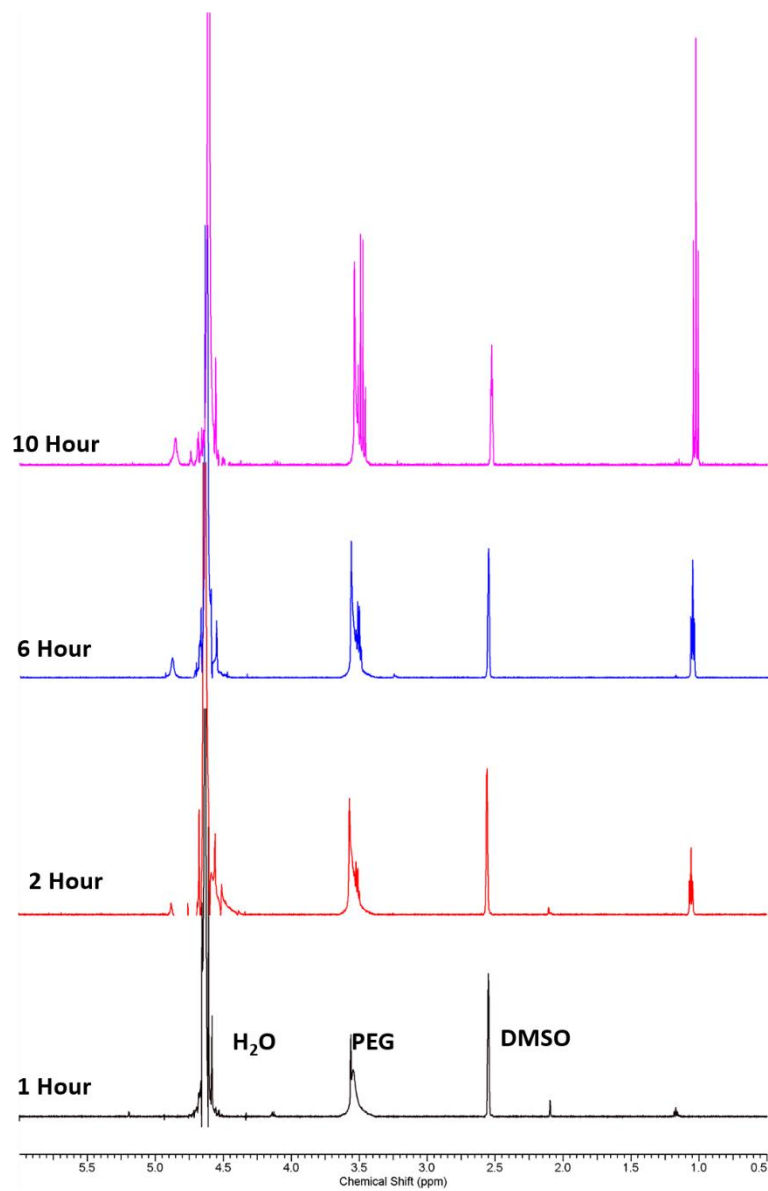


Figure A7.27. ^1H NMR spectra of **Micelle-control** incubated in 5:1 DMSO- d_6 :D $_2$ O at 75 °C.

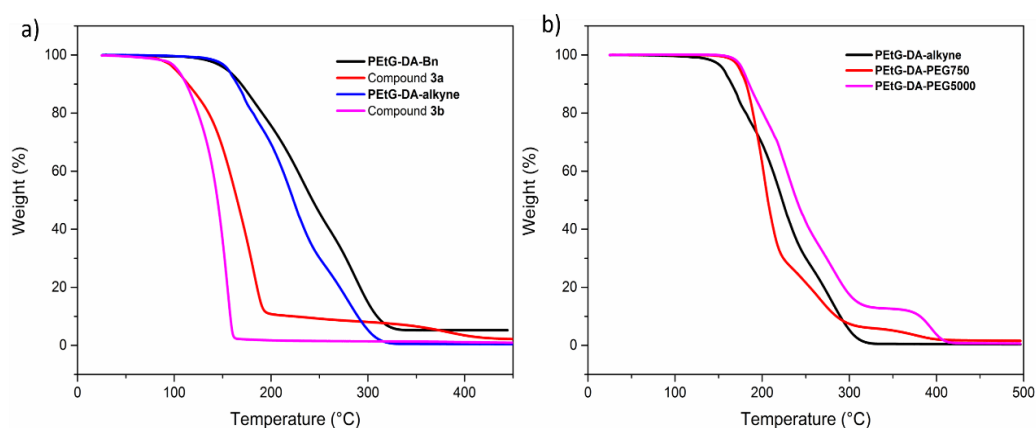


Figure A7.28. TGA curves of thermo-responsive a) end-caps and polymers; b) homopolymer PEtG compared with the PEtG-PEG block copolymers. It can be noted that the polymers were more thermally stable than the DA adduct itself (compound **3a** or **3b**), which depolymerized at ~ 100 °C. There are two possible explanations for this phenomenon: 1) the polymer may serve as a matrix to protect the end-cap decomposition; 2) the elimination reaction following the retro-DA reaction is the rate-limiting step for thermal depolymerization. In the block copolymers, the presence of a second decomposition step at 300 °C provides can be attributed to the PEG block.

Table A7.1. Molecular weights, measured by SEC in THF relative to PMMA standards, for the polymers, and thermal properties as measured by TGA. T_o = onset degradation temperature measured by TGA.

Polymer	M_n (SEC) (kg/mol)	Dispersity (D)	T_o (°C)
PEtG-DA-Bn	33	1.8	169
PEtG-control^{1b}	42	1.4	N/A
PEtG-DA-alkyne	63	2.0	154
PEtG-DA-PEG750	59	1.9	177
PEtG-DA-PEG5000	35	2.0	171
Micelle-control^{1a}	40	2.1	N/A
Vesicle-control	77	2.3	N/A

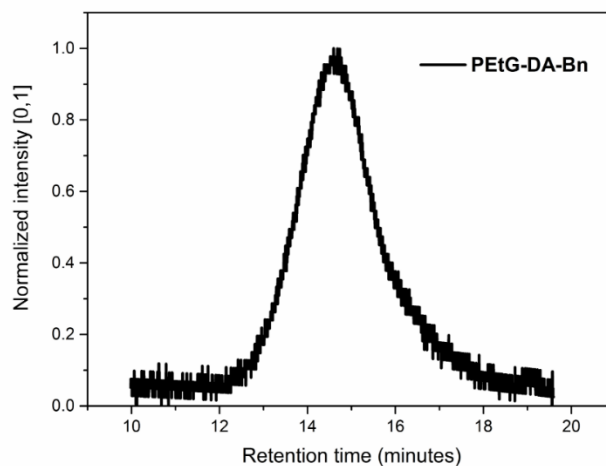


Figure A7.29. SEC curve of **PEtG-DA-Bn**.

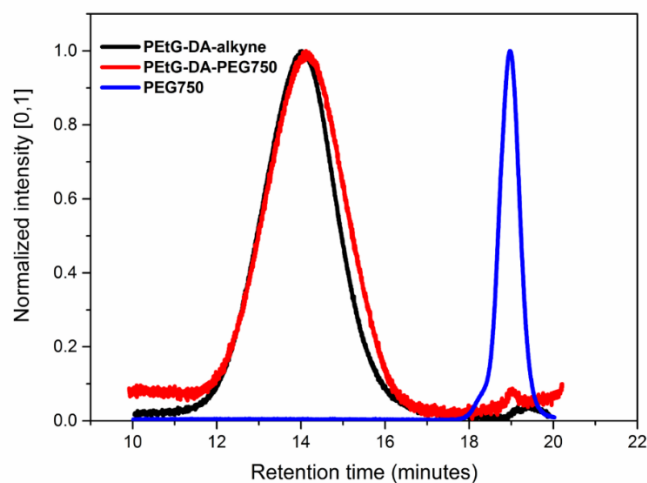


Figure A7.30. Comparison of SEC curves of **PEtG-DA-alkyne**, PEG 750 g/mol, and **PEtG-DA-PEG750**. No increase in molar mass was observed upon coupling of PEG, which is consistent with previous work and can be attributed to the small mass fraction of the PEG as well as possible conformational changes that would cancel the effects of the addition of mass.

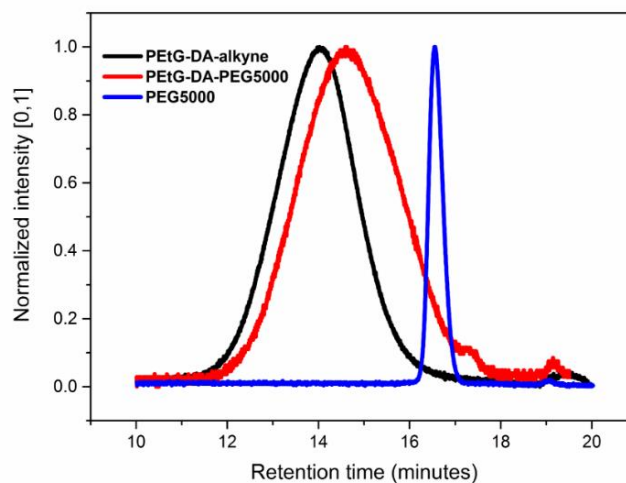


Figure A7.31. Comparison of SEC curves of **PETG-DA-alkyne**, PEG 750 g/mol, and **PETG-DA-PEG5000**. As THF is not an ideal solvent for PEG, after coupling with PEG5000, the hydrodynamic radius of **PEG-DA-PEG5000** decreased rather than increased likely due to some polymer chain collapse. However the absence of a free PEG peak combined its presence in the NMR spectra clearly confirmed the presence of PEG in the block copolymer.

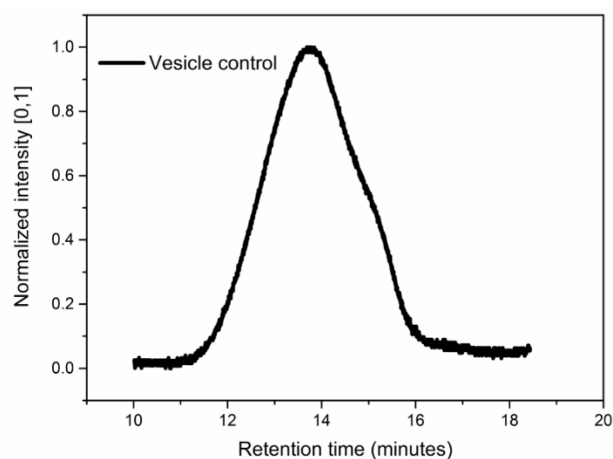


Figure A7.32. SEC curve of **Vesicle-control**.

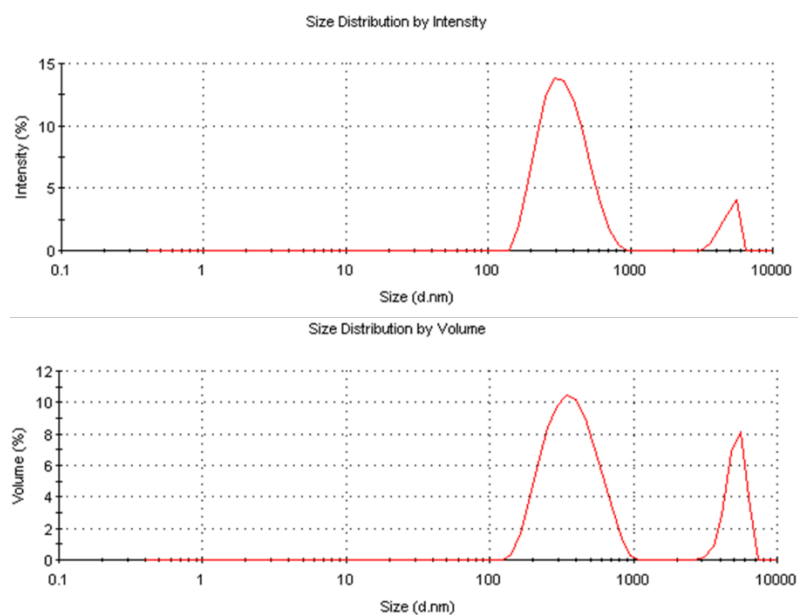


Figure A7.33. DLS intensity (top) and volume (bottom) distributions for **PEtG-DA-PEG750** vesicles.

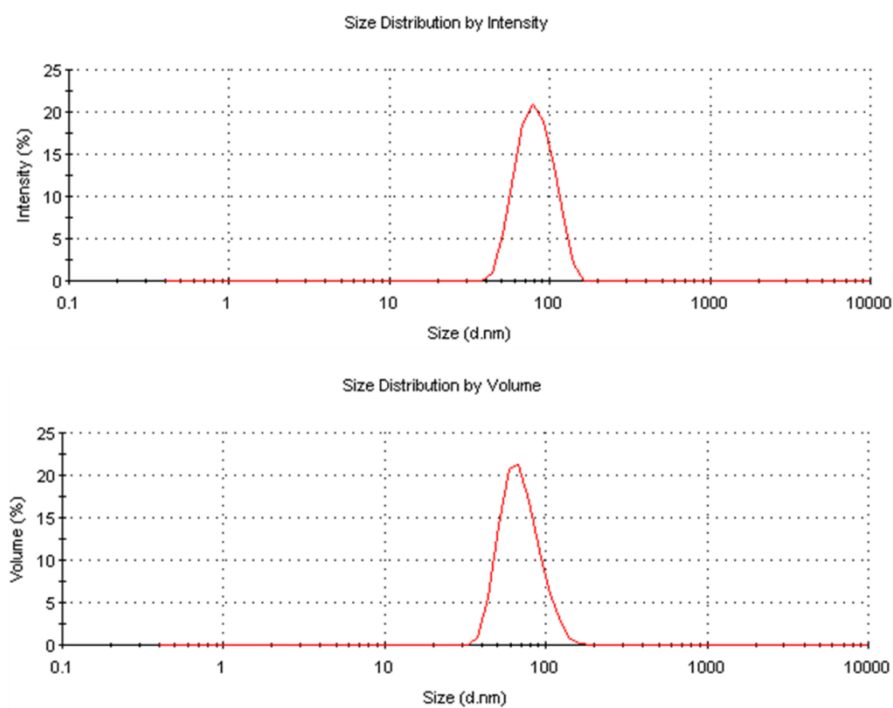


Figure A7.34. DLS intensity (top) and volume (bottom) distributions for **PEtG-DA-PEG5000** micelles.

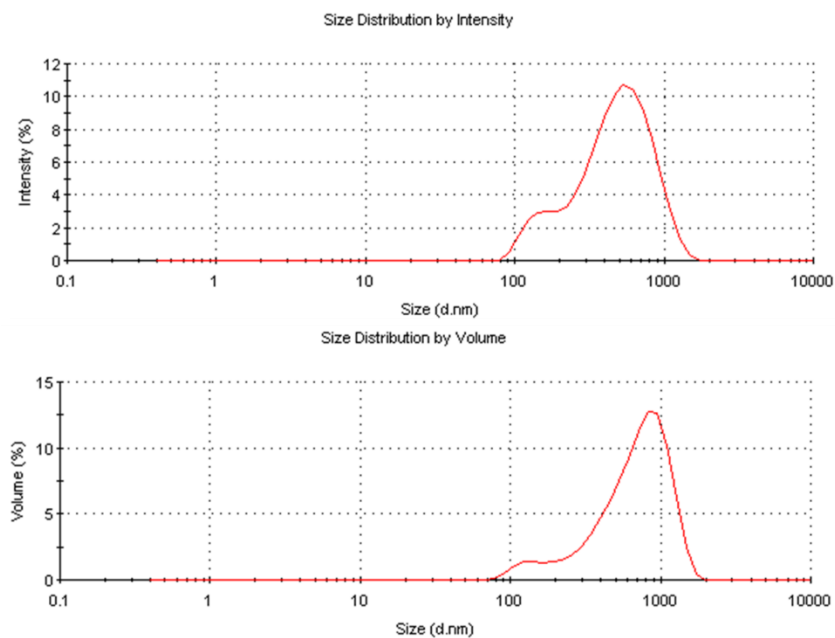


Figure A7.35. DLS intensity (top) and volume (bottom) distributions for **Vesicle-control**.

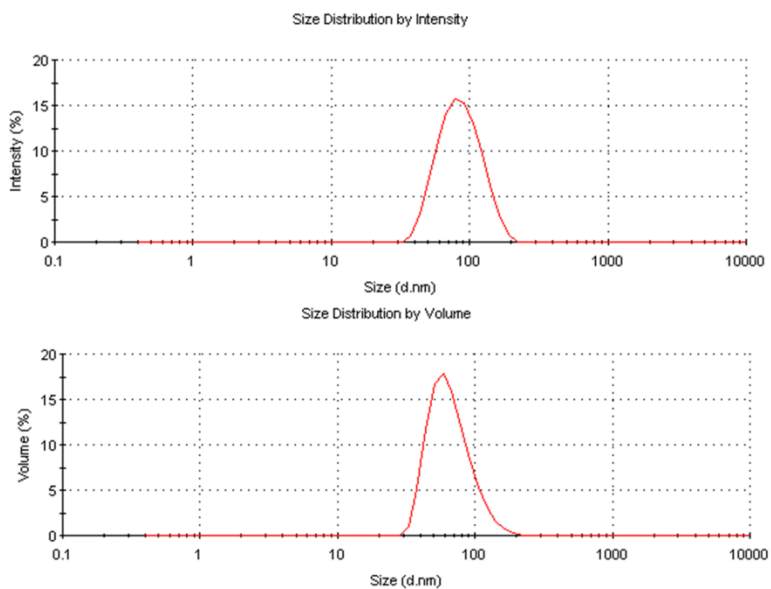


Figure A7.36. DLS intensity (top) and volume (bottom) distributions for **Micelle-control**.

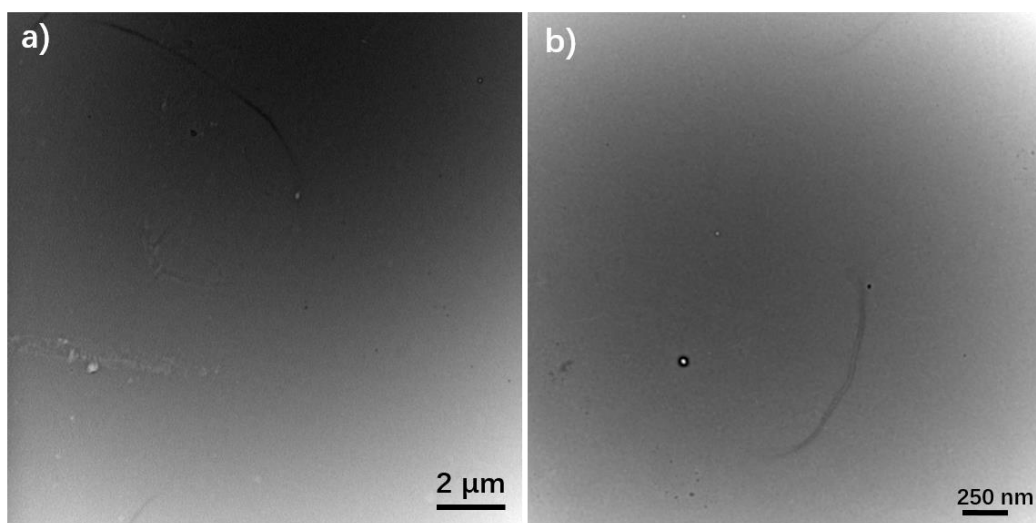


Figure A7.37. TEM images of a) **PEtG-DA-PEG750** vesicles and b) **PEtG-DA-PEG5000** micelles after incubation at 75 °C for 16 h. No assemblies were observed.

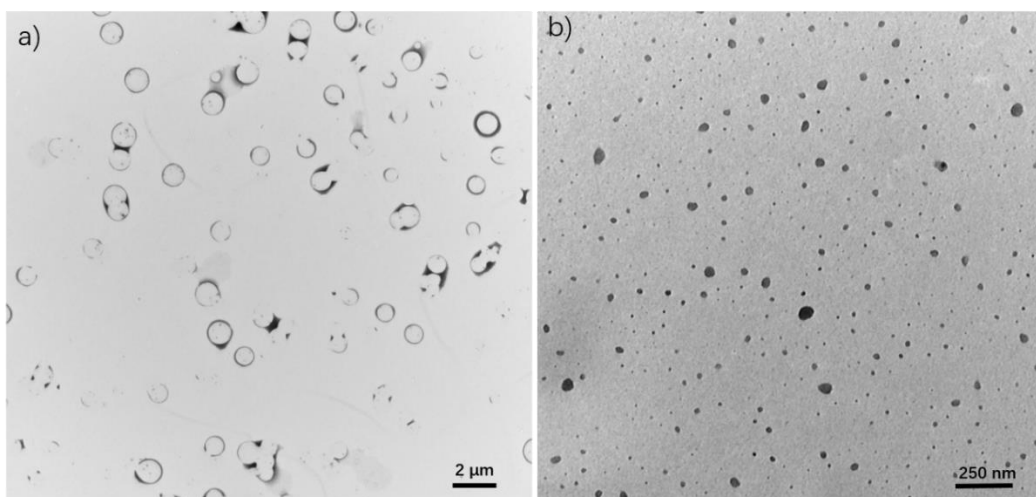


Figure A7.38. TEM images of a) **Vesicle-control** and b) **Micelle-control**.

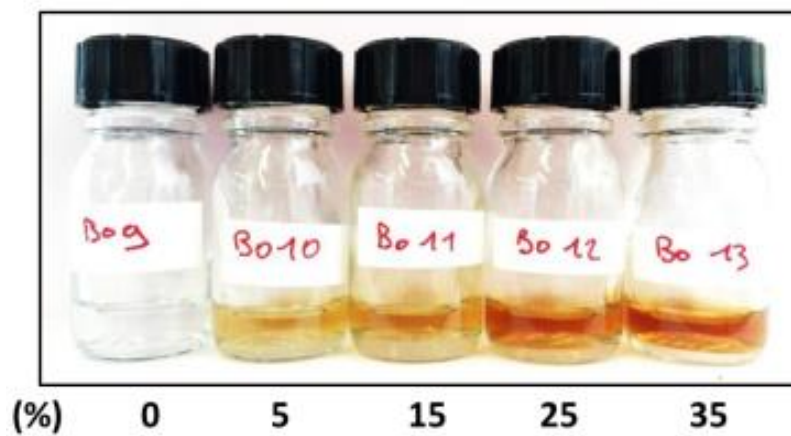


Figure A7.39. Photos of IONP-loaded **PEtG-DA-PEG5000** micelles with increasing mass % of IONP.

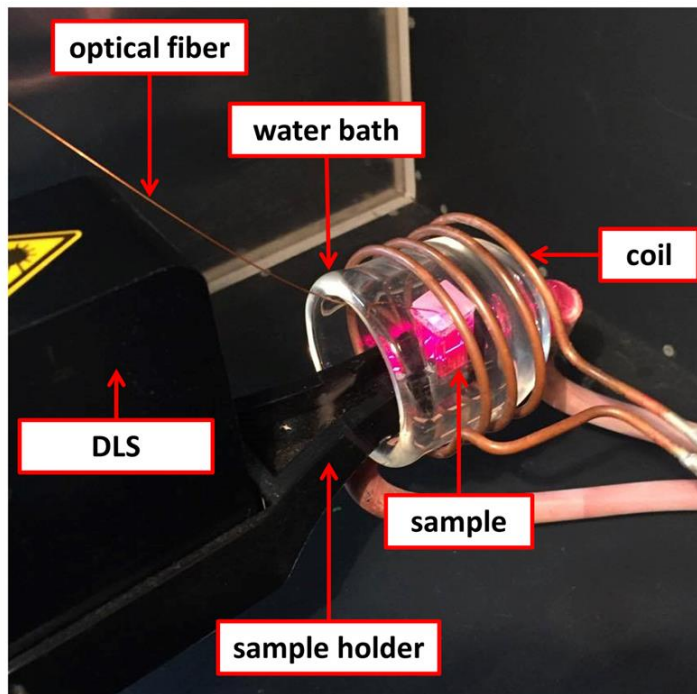


Figure A7.40. Photo of the dynamic light scattering magnetic hyperthermic set-up.

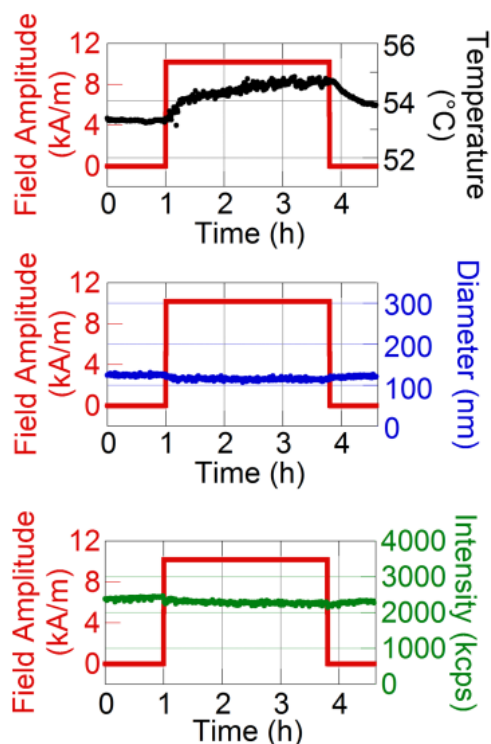


Figure A7.41. Bulk temperature, particle diameter, and count rate measured before, during, and after magnetic hyperthermia using an *in situ* DLS for IONP-loaded **PEtG-DA-PEG5000** with a bulk temperature of 53 °C.

Small angle neutron scattering (SANS) experiments were performed at the Orphée neutron facility of LLB-CEA (Saclay, France) on the PAXY spectrometer equipped with a 2D (anisotropic SANS) detector. Micelles were suspended at a concentration of $0.6 \text{ mg}\cdot\text{mL}^{-1}$ in pure D_2O , of neutron scattering length density $\text{SLD}(\text{D}_2\text{O})=6.40\times 10^{-6} \text{ \AA}^{-2}$. The calculated SLD of iron oxide and ethyl glyoxylate monomer are $\text{SLD}(\gamma\text{-Fe}_2\text{O}_3)=6.98\times 10^{-6} \text{ \AA}^{-2}$ and $\text{SLD}(\text{EtG})=1.31\times 10^{-6} \text{ \AA}^{-2}$, respectively. The neutron scattering contrast of the micelles in heavy water thus arises almost exclusively from the hydrophobic Poly(EtG) block of the polymer, the hydrophilic PEG block being highly hydrated, thus having negligible contribution to the neutron scattering contrast. Three beamline configurations were used to cover overlapping scattering vector (q) ranges of $1.92\times 10^{-3} - 2.84\times 10^{-2}$, $1.05\times 10^{-2} - 0.154$, and $3.19\times 10^{-2} - 0.427 \text{ \AA}^{-1}$, with the following values of sample-to-detector distance D and neutron wavelength λ : $D=7 \text{ m}$ and $\lambda=15 \text{ \AA}$, $D=3 \text{ m}$ and $\lambda=6 \text{ \AA}$, $D=1$

m and $\lambda=6 \text{ \AA}$. The scattering intensity curves were divided by the transmission factor and subtracted from the incoherent background, before normalizing by the flat signal of a cuvette filled with light water to correct the detector efficiency, yielding the absolute intensity in cm^{-1} .

Study of the thermal degradation by small angle neutron scattering. The thermal degradation of the thermosensitive micelles was also investigated by small-angle neutron scattering (SANS). Micelles loaded with IONPs were prepared as previously described, with few changes to adapt to this other characterization technique. The IONPs ($d_{\text{TEM}}=10.5 \text{ nm}$) and the polymer were mixed in deuterated THF, and nano-precipitated in deuterated water to improve the contrast between the micelles and their solvent. Pure **PEtG-DA-PEG5000** micelles (BO14) or magnetically loaded thermosensitive micelles (BO15, 35 mass% iron oxide relative to polymer) were prepared this way, at a concentration of $0.6 \text{ mg}\cdot\text{mL}^{-1}$. The effect of long heating on the structure of the micelles was evidenced by comparing the SANS curves (Fig. A7.42) before and after heating at $80 \text{ }^\circ\text{C}$ in an oven for 30 min. The curves of micelles before heating were well fitted by a polydisperse sphere form factor multiplied by a “sticky hard sphere” structure factor to take into account short-range attractions. The fitted radius and volume fraction of the micelles were respectively $R_0=10.9 \text{ nm}$ and $\phi=0.00028$ ($R_0=11.7 \text{ nm}$ and $\phi=0.00030$) for the unloaded micelles BO14 (respectively magnetically loaded micelles BO15) with a high dispersity $\sigma=0.4$ (Log-normal distribution) in both cases. The weight-average radius of the micelles that take into account this Log-normal dispersity can be calculated using $R_w = \langle R^4 \rangle / \langle R^3 \rangle = R_0 \cdot \exp(7\sigma^2/2)$, leading to $R_w=19.1 \text{ nm}$ for pure micelles and $R_w=20.5 \text{ nm}$ for magnetic ones. These SANS sizes are still much lower than the hydrodynamic radius of the micelles found around 50 nm . However, this can be explained by the relatively high hydration level of **PEtG** blocks compared to standard hydrophobic polymers, leading to a dominant contribution to the neutron scattering contrast from the dense dehydrated cores of the micelles compared to their hydrated shells. This is also why the fitted volume fractions around $0.03 \text{ vol}\%$ are about twice lower than expected from the 0.6 mg/mL total concentration in polymer.

The curves of the heat-treated micelles were not fitted by a model shape. Nonetheless, they can be interpreted by a drastic reduction of the volume fraction of suspended copolymer micelles, together with an increase of the size of the remaining objects (as ascribed to aggregation of the remaining IONPs). This SANS experiment thus brings another evidence of the thermosensitivity of **PEtG-DA-PEG5000** copolymer micelles that did not disappear when embedding IONPs in their core.

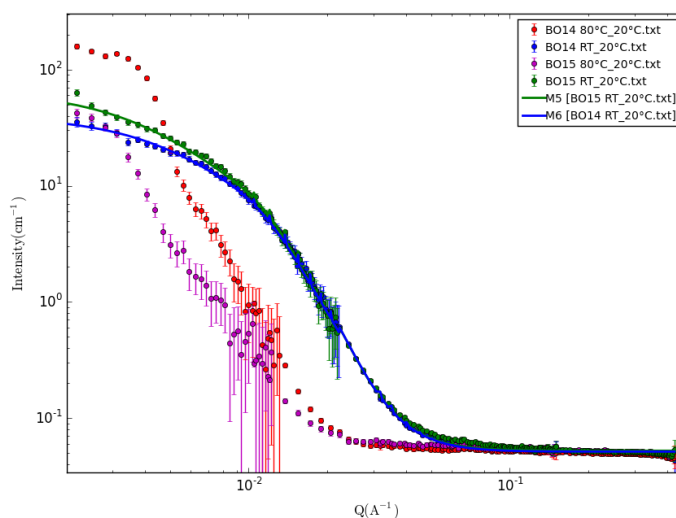
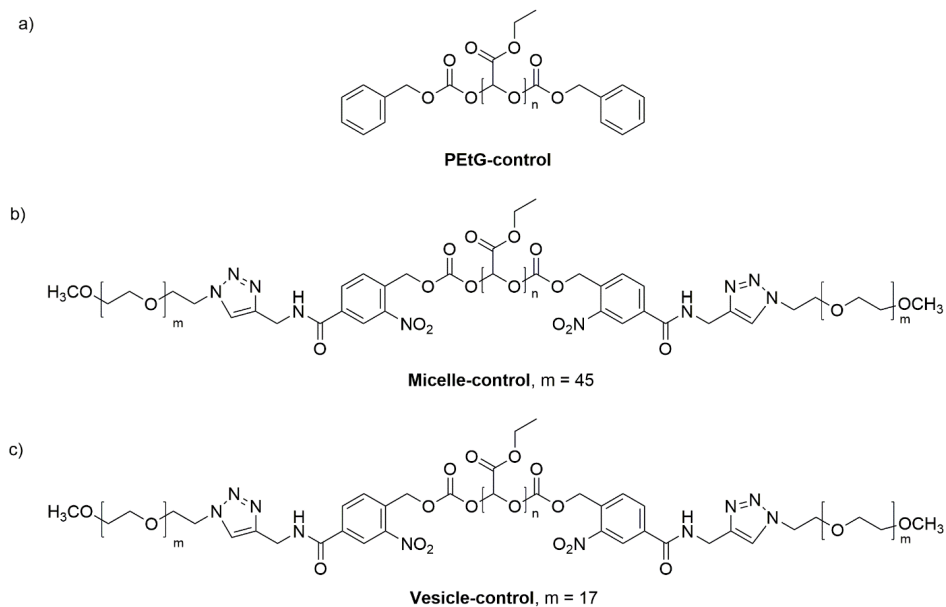
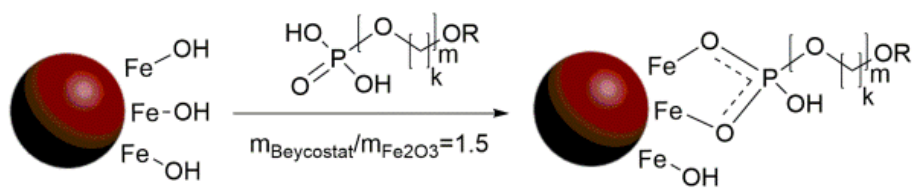


Figure A7.42. SANS curves of pure micelles BO14 and magnetically loaded micelles BO15 before and after treatment at 80°C for 30 min (the SANS curves being acquired afterwards, at 20°C). The curves of the untreated micelles were fitted by a polydisperse sphere form factor multiplied by a “sticky hard sphere” structure factor. Solid lines represent simulated curves using the SasView 3.1.2 software (<http://sasview.org>) with a polydisperse sphere form factor $P(q)$ multiplied by a “sticky hard sphere” structure factor $S(q)$ to take into account short-range attractive interactions between the micelles. In addition to the SLDs that were fixed to their theoretical values, the parameters of the polydisperse sphere form factor were the volume fraction ϕ , the incoherent background level, the median radius R_0 of the micelles and the width σ of the distribution of radii as described by a Log-normal law. Other fitting parameters of the sticky hard sphere structure factor $S(q)$ were the “stickiness” $\tau=0.047\pm 0.006$ (respectively $\tau=0.036\pm 0.0015$) and the

“perturbation distance” $\varepsilon=0.637\pm 0.019$ (respectively $\varepsilon=0.605\pm 0.012$) for the pure micelles BO14 (respectively magnetically loaded micelles BO15).



Scheme A7.1. Chemical structure of a) **PEtG-control**, b) **Micelle-control**, and c) **Vesicle control**.



Scheme A7.2. Coating of IONPs.

Appendix 8: Supporting information for Chapter 8

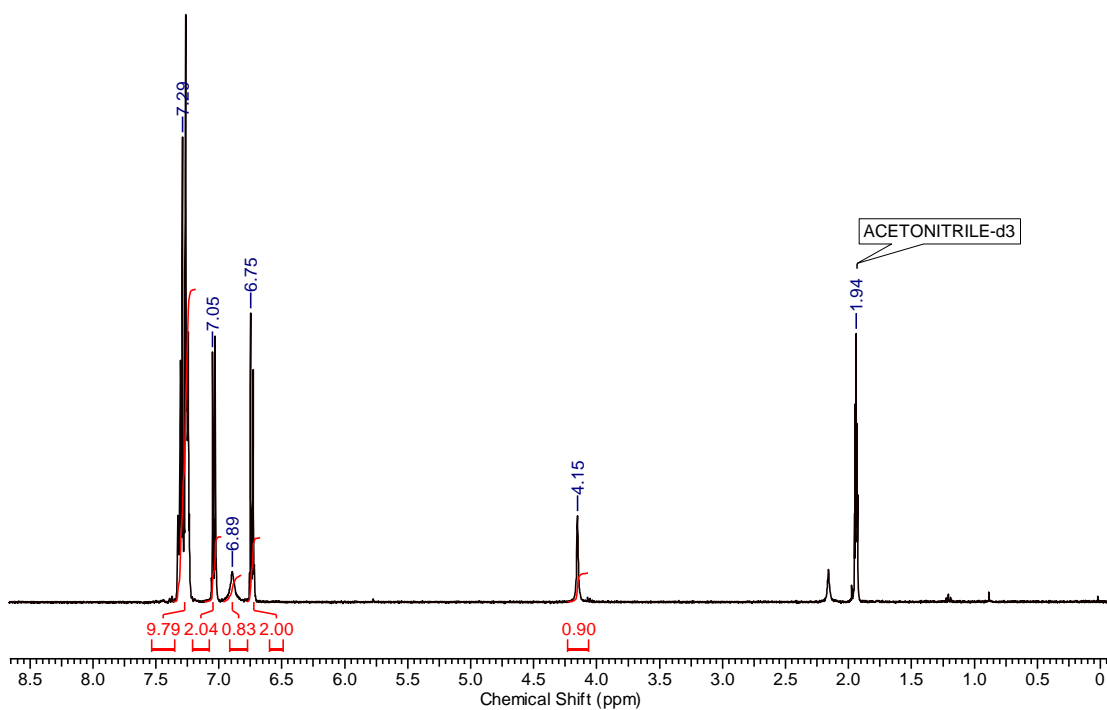


Figure A8.1. ¹H NMR (400 Hz, CD₃CN) spectrum of Compound **4a**.

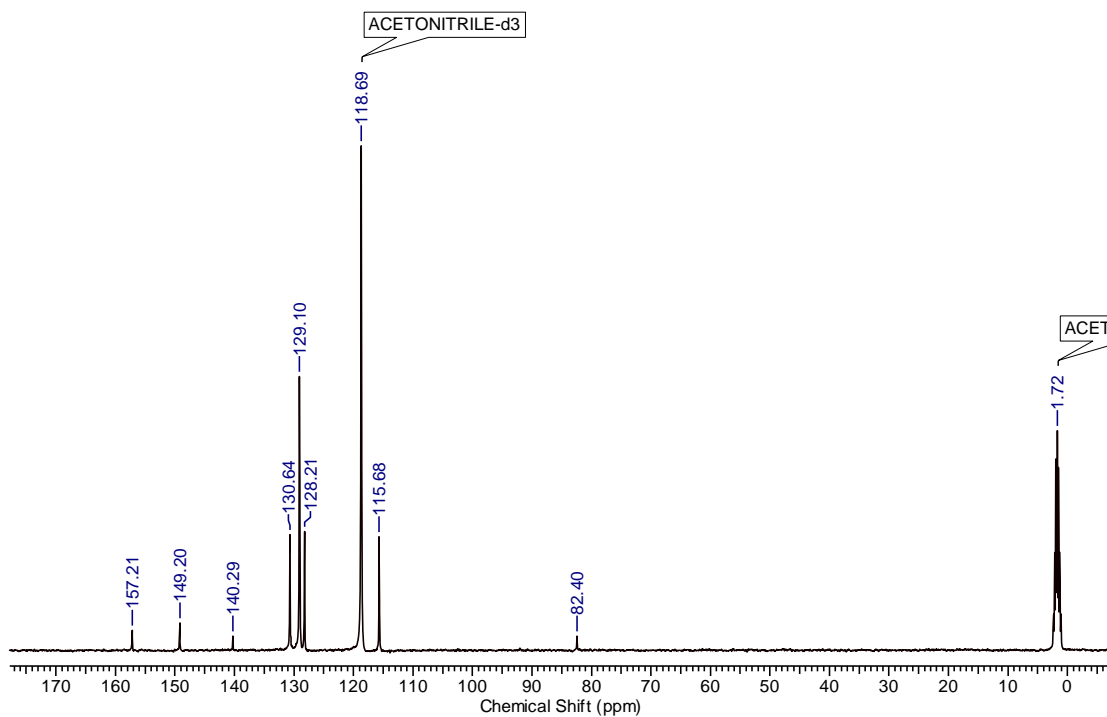


Figure A8.2. ¹³C NMR (100 Hz, CD₃CN) spectrum of Compound **4a**.

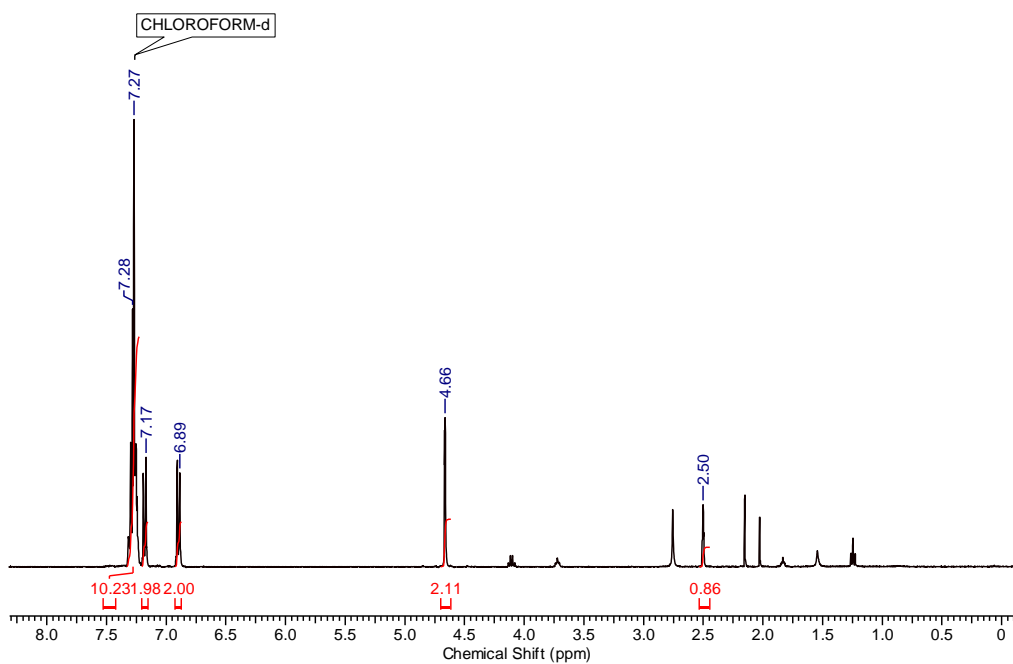


Figure A8.3. ¹H NMR (400 Hz, CDCl₃) spectrum of Compound 5a, with presence of trace ethyl acetate and acetone.

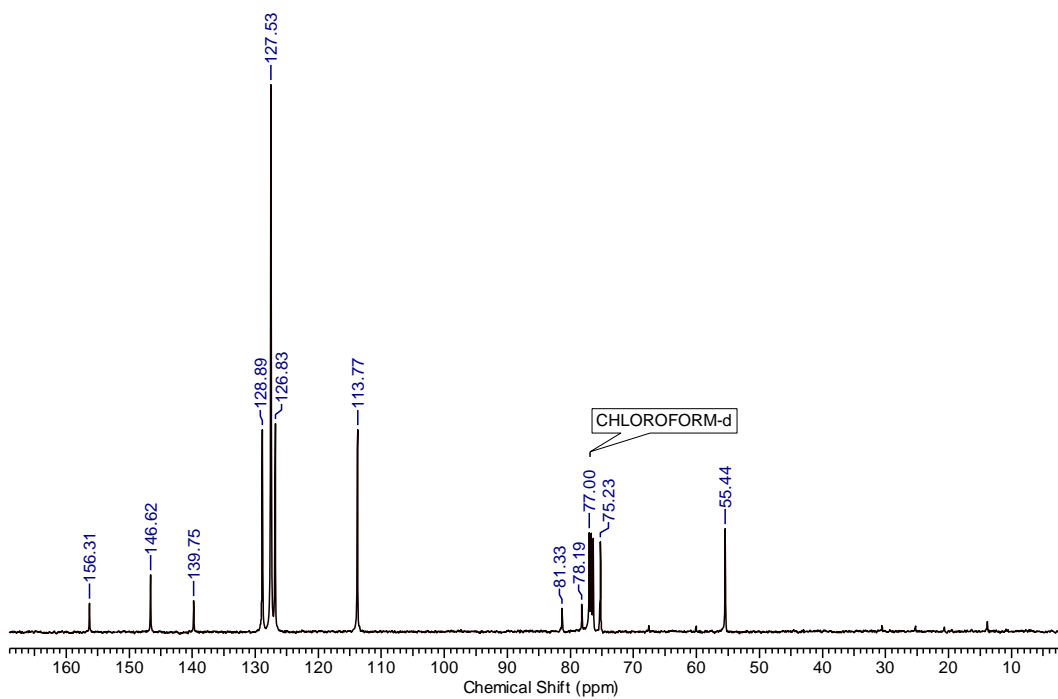


Figure A8.4. ¹³C NMR (100 Hz, CDCl₃) spectrum of Compound 5a.

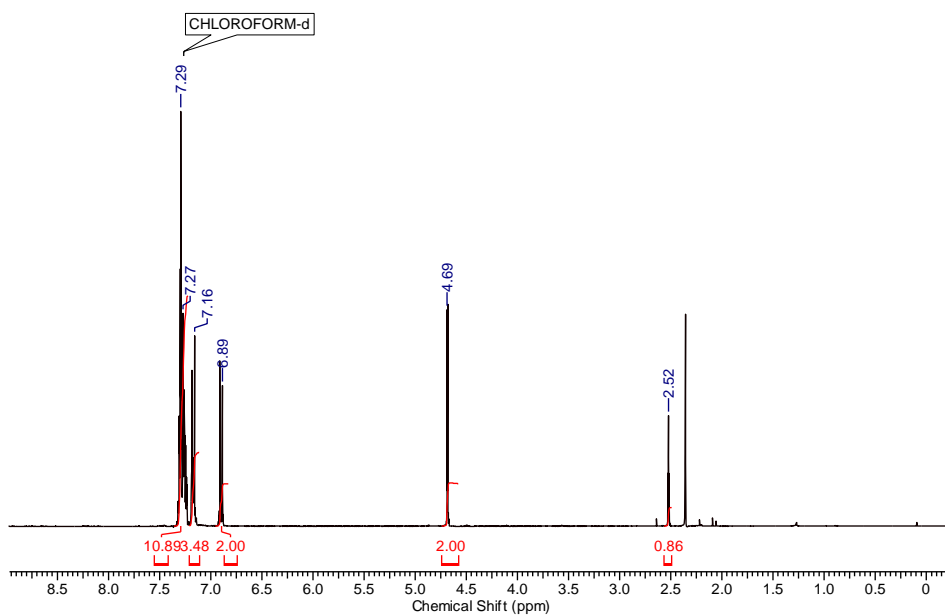


Figure A8.5. ^1H NMR (400 Hz, CDCl_3) spectrum of Compound **6a**, with presence of trace toluene.

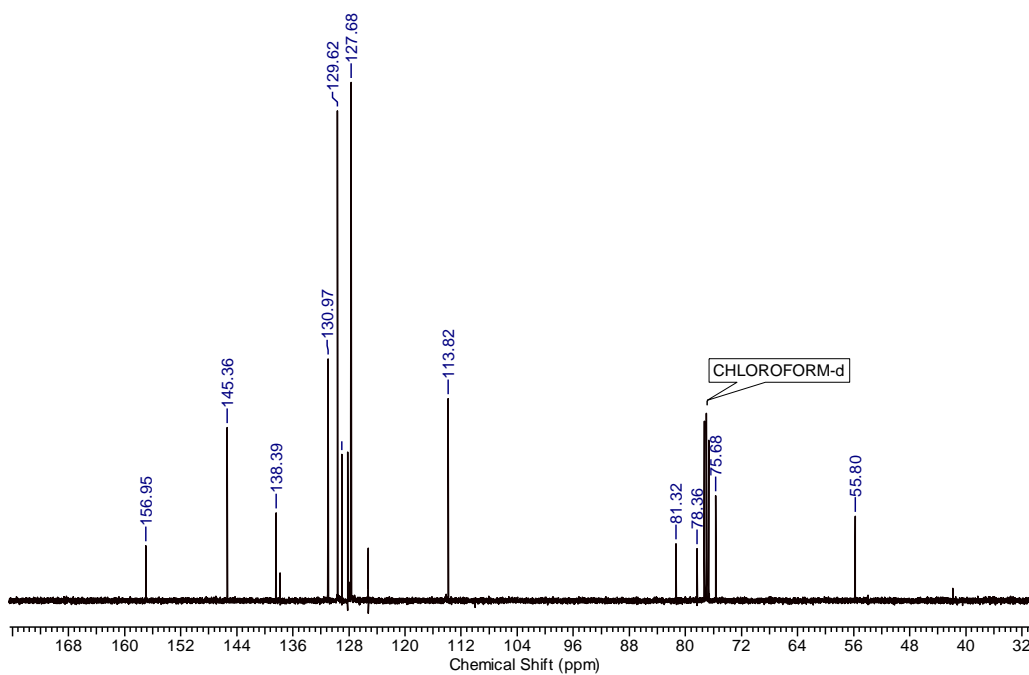


Figure A8.6. ^{13}C NMR (100 Hz, CDCl_3) spectrum of Compound **6a**, with presence of trace toluene.

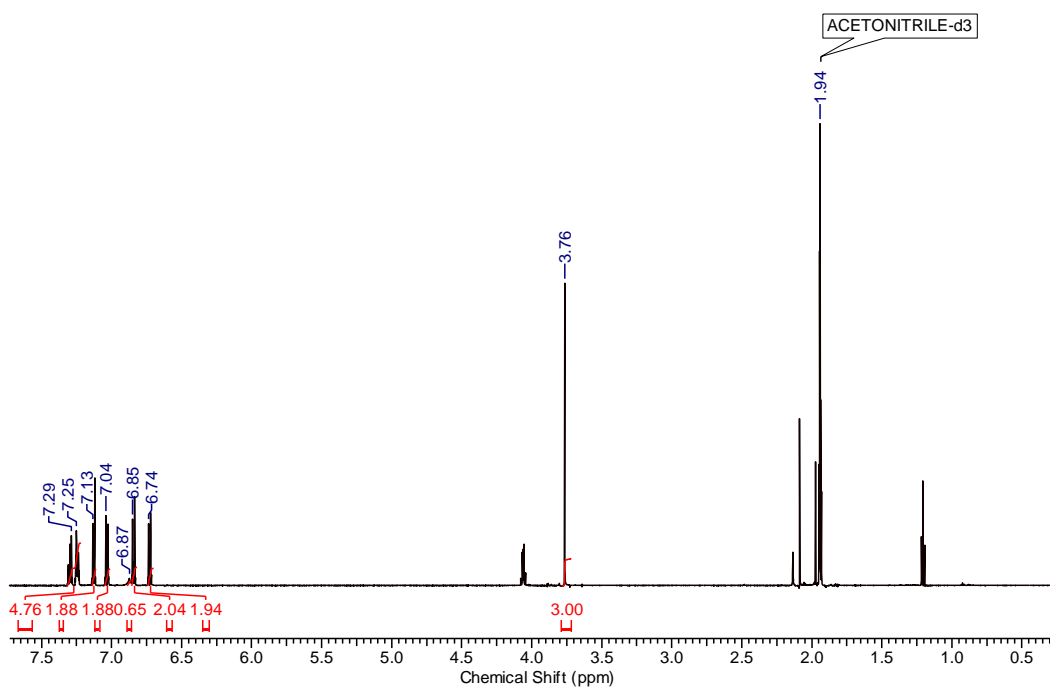


Figure A8.7. ^1H NMR (400 Hz, CD_3CN) spectrum of Compound **4b**, with presence of trace ethyl acetate.

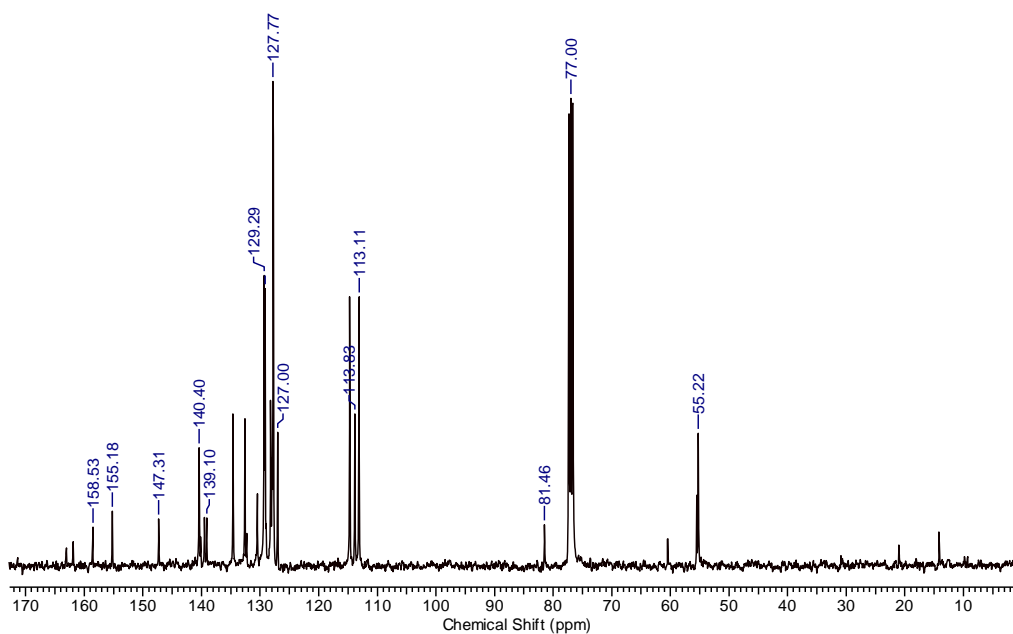


Figure A8.8. ^{13}C NMR (100 Hz, CD_3Cl) spectrum of Compound **4b**, with presence of trace ethyl acetate and impurity.

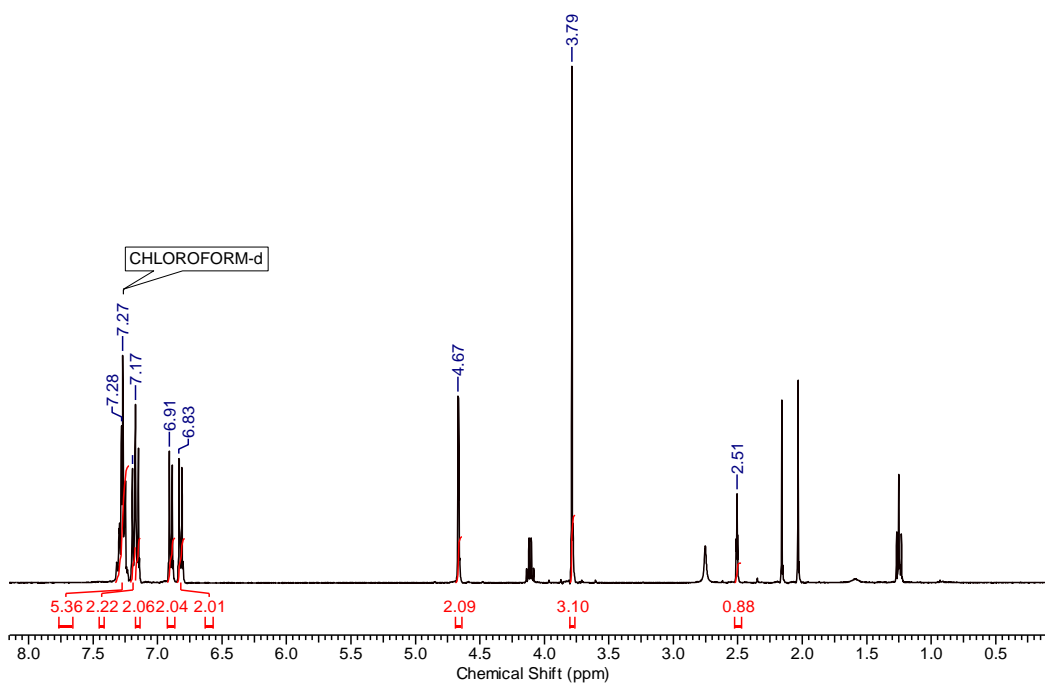


Figure A8.9. ^1H NMR (400 Hz, CD_3Cl) spectrum of Compound **5b**, with presence of trace ethyl acetate and acetone.

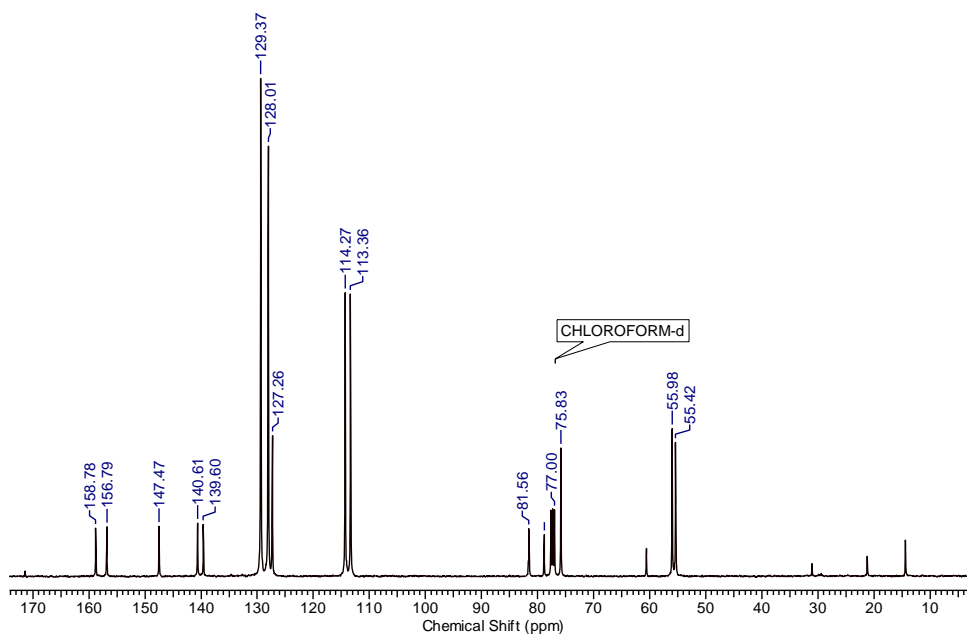


Figure A8.10. ^{13}C NMR (100 Hz, CD_3Cl) spectrum of Compound **5b**, with presence of trace ethyl acetate and acetone.

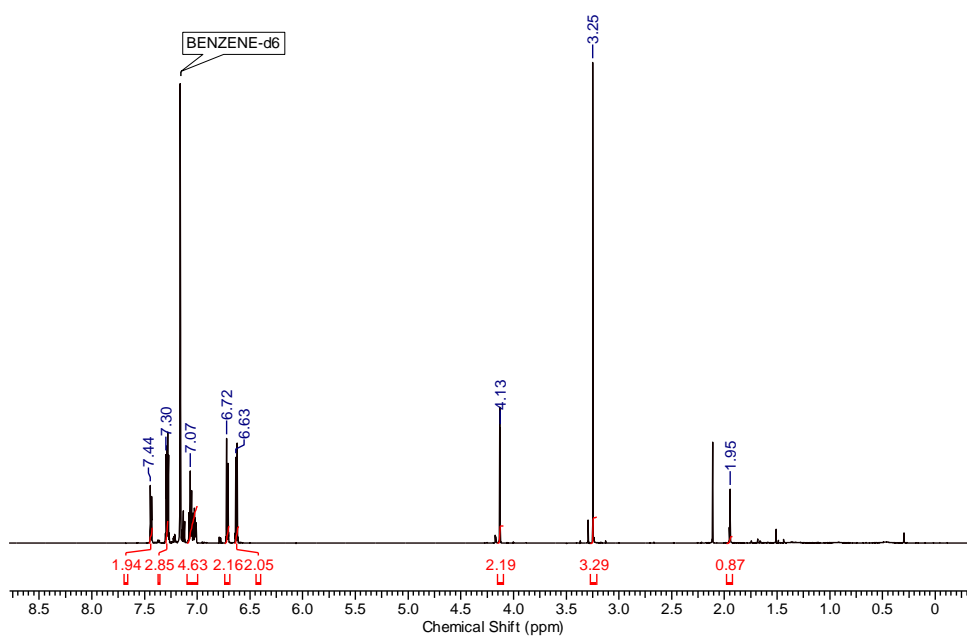


Figure A8.11. ^1H NMR (600 Hz, C_6D_6) spectrum of Compound **6b**, with presence of trace toluene.

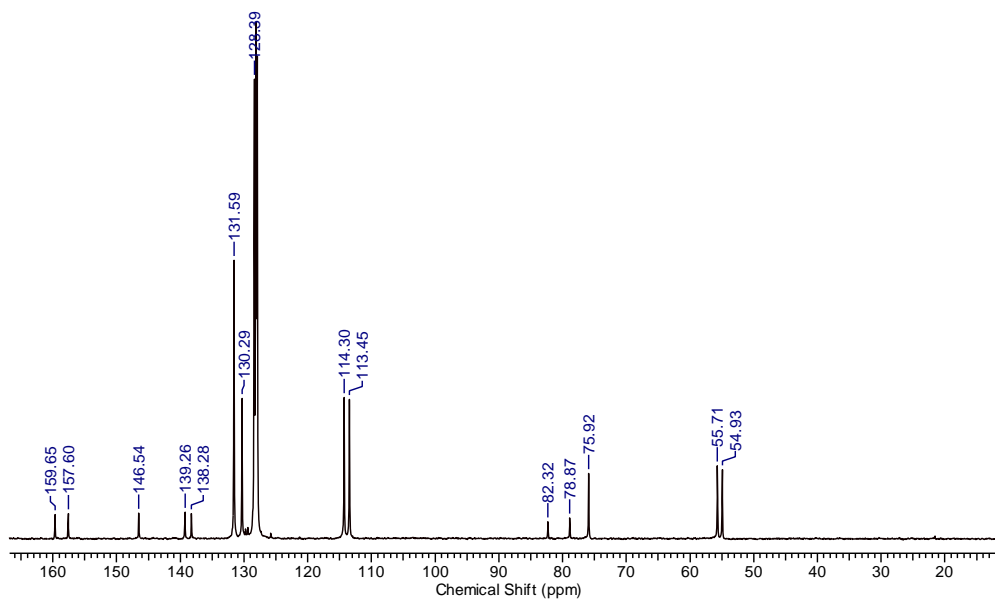


Figure A8.12. ^{13}C NMR (100 Hz, C_6D_6) spectrum of Compound **6b**.

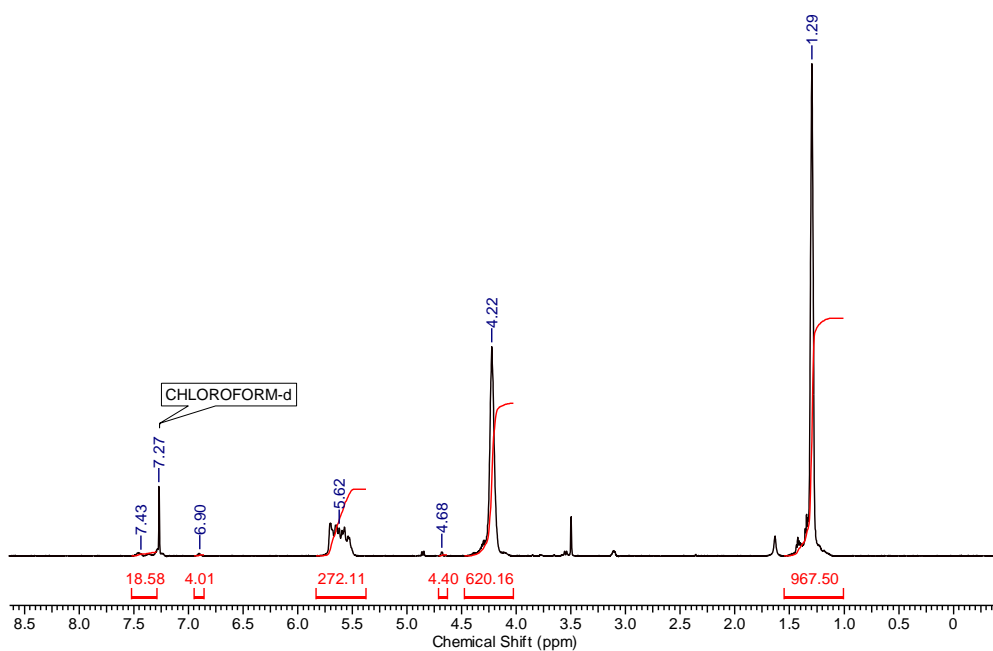


Figure A8.13. ^1H NMR (600 Hz, CD_3Cl) spectrum of **PEtG-AT**.

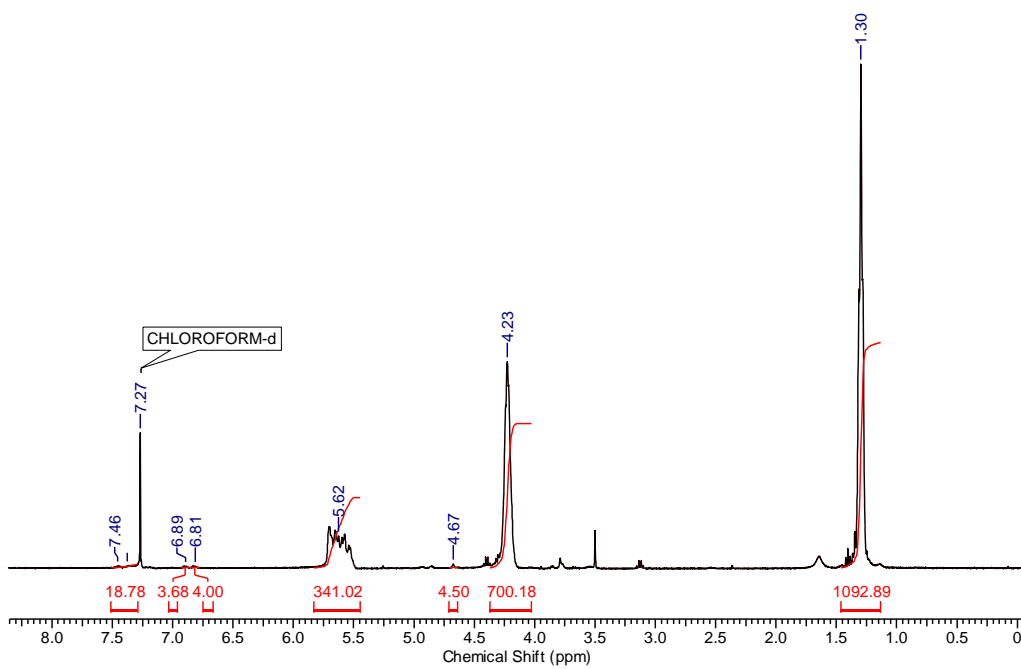


Figure A8.14. ^1H NMR (400 Hz, CD_3Cl) spectrum of **PEtG-AMT**.

Curriculum Vitae

Bo Fan

Education

- *Ph.D. Candidate*, The Department of Chemical and Biochemical Engineering
The University of Western Ontario, London, Ontario, Canada 2015.01-2018.04
 Thesis Supervisor: Prof. Elizabeth R. Gillies
- *Master of Chemistry*, The Department of Chemistry
The University of Western Ontario, London, Ontario, Canada 2013.01-2014.12
 Thesis Supervisor: Prof. Elizabeth R. Gillies
- *Bachelor of Engineering*, The Department of Polymer Materials and Engineering
Sichuan University, Chengdu, Sichuan, China 2008.09 -2012.06
 Thesis Supervisor: Prof. Guangsu Huang

Work Experience

➤ Graduate Research Assistant

The University of Western Ontario, London, Ontario, Canada 2013.01- Present

Job Description: Development and Applications of a New Generation of Controllable Degradable Polymer Materials.

So far, I have participated in more than 10 research projects, including and not limited to the synthesis of polyglyoxylates, end-capping strategies of polyglyoxylates, photo-controlled solid depolymerization of polyglyoxylates, multi-responsive nanoparticles for drug delivery, thermal-responsive assemblies, plants stimuli-responsive coating for fertilizer, food quality sensing materials and the like.

➤ Graduate Teaching Assistant

The University of Western Ontario, London, Ontario, Canada 2013.01- Present

Job Description: Undergraduate Class and Laboratory Teaching Assistant.

The work includes preparation of course-related materials, teaching and guidance of undergraduate basic chemistry experiments, such inorganic chemistry, organic chemistry, and biochemical engineering experiments. Extracurricular work includes preparation, marking of assignments, quizzes, experiment reports, and Q & A.

Honors & Awards

1. Western Graduate Research Scholarship (WGRS) 2013-Present.
2. Western Graduate Research Assistance (WGRA) 2013-Present.
3. Third prize for 3 Minutes Thesis Competition in the 2016 Western Engineering Heat, University of Western Ontario.

4. Master thesis project (Stimuli-responsive biodegradable polymers) was selected as advanced technology for 2015 Proteus Innovation Competition.
5. Third prize for social scholarship 2011 awarded by Shenzhen Senior Technology Material Co. LTD (Sichuan University).
6. Excellent Volunteer of Academic Year 2010-2011 (Sichuan University).
7. First prize Scholarship of Academic Year 2009-2010 (Sichuan University).
8. Second prize Scholarship of Academic Year 2008-2009 (Sichuan University).
9. Excellent Student Officer of Academic Year 2008-2009 (Sichuan University).

Publications & Patent

➤ Patent

1. Gillies, E. R.; Fan, B.; Trant, J. F.; Wong, A. D. "Polyglyoxylates, manufacture and use thereof" PCT Application (2015), No. 61/989,086. Chinese Patent publication number CN106536475A.

➤ Book Chapter

1. Fan, B; Gillies, E. R. "Self-immolative polymers" Encyc. Polym. Sci. & Eng. 2015, 1-35, Wiley.

➤ Research Papers

1. **Fan, B.;** Trant, J. F.; Wong, A. D.; Gillies, E. R. "Polyglyoxylates: A versatile class of triggerable self-immolative polymers from readily accessible monomers" **J. Am. Chem. Soc.** **2014**, 136, 10116-10123.
2. **Fan, B.;** Trant, J. F.; Yardley, R. E.; Pickering, A. J. Lagugne-Labarthe, F.; Gillies, E. R. "Photocontrolled degradation of stimuli-responsive poly(ethyl glyoxylate): differentiating features and traceless ambient depolymerization" **Macromolecules** **2016**, 49, 7196-7203.
3. **Fan, B.;** Trant, J. F.; Gillies, E. R. "End-capping strategies for triggering end-to-end depolymerization of polyglyoxylates" **Macromolecules** **2016**, 49, 9309-9319.
4. Trant, J. F.; Jain, N.; Mazzuca, D.M.; McIntosh, J.T.; **Fan, B.;** Mansour Haeryfar, S.M; Lecommandoux, S.; Gillies, E. R. "Synthesis, self-assembly, and immunological activity of α -galactose-functionalized dendron-lipid amphiphiles" **Nanoscale** **2016**, 8, 17694-17704.
5. **Fan, B.;** Gillies, E. R. "Poly(ethyl glyoxylate)-poly(ethylene oxide) nanoparticles: Stimuli responsive drug release via end-to-end polyglyoxylate depolymerization" **Mol. Pharmaceutics** **2017**, 14, 2548-2559. Invited article published in a special issue "Polymers in Drug Delivery: Chemistry and Applications".
6. **Fan, B.;** Trant, J. F.; Hemery, G.; Sandre, O.; Gillies, E. R. "Thermal-responsive self-immolative nanoassemblies: Direct and indirect triggering" **ChemComm.** **2017**, 53, 12068-12071. Highlighted in the front cover for that issue.

7. **Fan, B.;** Salazar, R.; Gillies, E. R. “Temperature-dependent depolymerization of trityl end-capped poly(ethyl glyoxylate): potential applications in smart packaging”, Prepared manuscript.
8. **Fan, B.;** Trant, J. F.; Yardley Rebecca; Gillies, E. R. “Tuning the hydrophobic cores of self-immolative polyglyoxylate assemblies”, Prepared manuscript.
9. Gambles, M. T.; **Fan, B.;** Borecki A.; Gillies, E. R. “Hybrid polyester-self-immolative polymer nanoparticles for controlled drug release”, Prepared manuscript.

Conference Presentations

1. **Fan, B.;** Gillies, E. R. “Polyglyoxylate: A new class of multi-responsive material for drug-delivery purpose” Nano Ontario, 2017, Poster Presentation
2. **Fan, B.;** Gillies, E. R. “Polyglyoxylate: A new class of multi-responsive material for drug-delivery purpose” 100th Canadian Chemistry Conference and Exhibition, 2017, Oral Presentation
3. MacDonald, J. P.; **Fan, B.;** Heuchan, S. M. E.; Bauman, L. A.; Henry, H. A. L; Gillies, E. R. “Stimuli-responsive coating for targeted release of fertilizer” 100th Canadian Chemistry Conference and Exhibition, 2017, Poster Presentation
2. Heuchan, S. M. E.; **Fan, B.;** MacDonald, J. P.; Henry, H. A. L; Gillies, E. R. “Plant stimuli-responsive biodegradable polymers for the use in timed release fertilizer coating” OE3C, 2017, Poster Presentation
3. **Fan, B.;** Gillies, E. R. “Poly(glyoxylates): a new class of depolymerizable materials with amplified response to stimuli and applications in drug delivery” 10th World Biomaterials Congress 2016, Oral Presentation.
4. Yardley, R.; Gillies, E. R.; **Fan, B.;** Trant, J.; Wong, A. D.; Gungor, T. “Stimuli-responsive supramolecular assemblies of amphiphilic self-immolative polymers” The International Chemical Congress of Pacific Basin Society 2015, Poster Presentation.
5. **Fan, B.;** Trant, J. F.; Wong, A. D.; Gillies, E. R. “Polyglyoxylate: A versatile class of triggerable self-immolative polymers from readily accessible monomers” Fallona Family Interdisciplinary showcase 2015, Poster Presentation.
6. **Fan, B.;** Trant, J. F.; Wong, A. D.; Gillies, E. R. “Polyglyoxylate: A versatile class of triggerable self-immolative polymers from readily accessible monomers” 36th Canadian High Polymer Forum, 2014, Poster Presentation.
7. Gillies, E. R.; Wong, A. D.; **Fan, B.;** Trant, J. F.; “Self-immolative linear polymers: New backbones, end-caps and assemblies” American Chemical Society Conference 2014, Oral Presentation.

Professional Development & Memberships

-Canadian Society for Chemistry (CSC) 2017

Graduate Courses

CBE 9180B	Instrumental Methods of Analysis	90
Chem 9653S	Polymers: Synthesis to Function	90
CBE 9170A	Mathematical Methods in Engineering	94
CBE 9450B	Adv. Chemical Reaction Engineering	80
CBE 9550A	Adv. Particle & Fluidization	92
CBE 9250B	Adv. Biomaterials Engineering	83
Chem 9663S	Adv. Polymer Chemistry	81
Chem 9553B	Mechanistic Organic Chemistry	88
Chem 9503S	Adv. NMR Spectroscopy	88
Chem 9621Q	Bioinorganic Chemistry Methods	83